Construction et évaluation de signatures hydrologiques pour le diagnostic et l'amélioration d'un modèle hydrologique distribué

Ivan Horner

Université Grenoble Alpes

THÈSE

Pour obtenir le grade de

DOCTEUR DE L'UNIVERSITÉ GRENOBLE ALPES

Spécialité : **Océan, Atmosphère, Hydrologie (CEOAH)**

Arrêté ministériel : 25 mai 2016

Présentée par

Ivan Horner

Thèse dirigée par **Flora Branger**
et co-encadrée par **Olivier Vannier**

préparé au sein de **l'Unité de Recherche RiverLy de l'Institut National de Recherche pour l'Agriculture, l'Alimentation et l'Environnement (Inrae), Lyon-Villeurbanne, France**
dans l'École Doctorale **Terre, Univers, Environnement**

Design and evaluation of hydrological signatures for the diagnosis and improvement of a process-based distributed hydrological model

Thèse soutenue publiquement le **16 juin 2020**,
devant le jury composé de :

M. Christophe Cudennec
Professeur, Agrocampus Ouest, Rennes, France, Rapporteur
M^me^ Hélène Roux
Maître de conférence, IMFT, Toulouse, France, Rapporteure
M^me^ Hilary McMillan
Associate Professor, SDSU, San Diego, USA, Examinatrice
M. Michel Estèves
Directeur de Recherche, IRD, Grenoble, France, Président
M. Fabrice Rodriguez
IDTPE, IFSTTAR, Nantes, Examinateur
M^me^ Flora Branger
ICPEF, Inrae, Lyon, France, Directrice de thèse
M. Olivier Vannier
Docteur Ingénieur, CNR, Lyon, France, Co-Encadrant de thèse, Invité

Contents

Acknowledgment

I undertook my PhD for the experience, the keen interest on the subject, the confidence I had in the environment it was to take place, the challenge, and many other motivations. And now, only a few weeks after my PhD defense, I can already see clearly how lucky I was to be so well surrounded during these three years and a half. There are many people that I wish to thank for making this experience not only successful but also enjoyable, exciting and rewarding.

I must start by thanking my outstanding supervisors for their trust, support, guidance and all the time they gave to this PhD. The three of you – Flora Branger, Olivier Vannier and Isabelle Braud – formed a well functioning supervision team and it was a pleasure for me to work with you.

Flora Branger, I am very grateful for you trust in my abilities to undertake this PhD and for your ever pertinent guidance as my PhD director. Your counsel at each step of my research, your encouragement to investigate ideas – both fruitful and fruitless – and the necessary cooling down of my enthusiasm when I got lost in endless explorations, the freedom you let me have and so many other things you did, were all very valuable to me and, I know, contributed most significantly to the success of my PhD. I must also acknowledge all the time you took to thoroughly read and correct every chapters of my PhD manuscript with so much precision and exigency.

Thank you to you also, Olivier Vannier, for accepting to supervise my PhD work and be so much available for our monthly meetings and reading/correcting all my writings. Particularly so when I know that your activities at Compagnie National du Rhône (CNR) were already so demanding and time consuming. Not only did you provide regular and very valuable guidance all along my PhD years, you also enabled this research to profit from a fruitful collaboration with CNR with freedom and many interactions, including these regular stays I did at CNR that I very much enjoyed. Both as a friend and supervisor, your contributions and encouragement were very precious to me and I know that more than once you contributed to build back my confidence when it failed.

Finally, although not officially part of my supervision – but clearly, in practice, you were part of it –, my gratitude and thanks go to you, Isabelle Braud, for counseling me so well from start to finish in this research. Thank you for all your valuable insights you contributed during our regular meetings on my progress or on my PhD manuscript you read and corrected so thoroughly. I appreciated greatly your availability even when I unexpectedly dropped by your office for some questions or discussion. During all these years, I also valued the confidence you had in my work and the choices I made.

My thanks also go to the members of my PhD committee – Sandrine Anquetin, Guillaume Thirel and Thomas Pelt – who met with my supervisors and myself each year to discuss my progress. Your attentive ears, your comments and questions were very helpful to take a step back and have fresh insights into my research to better grasp what I should undertake or focus on next.

My PhD jury – Michel Esteve, Fabrice Rodriguez, Hilary McMillan, Hélène Roux and Christophe Cudennec – also deserves my sincere thanks for accepting to evaluate my work at the end of this journey and for their benevolence and insightful comments and questions. Special thanks to you Hilary for waking up so early for my PhD defense and making the Zoom

Webinar license available to me.

My PhD would not have been possible without the funding from CNR as well as Agence de l'Eau RMC and BRGM who believed in this project and supported it accordingly. I greatly appreciate their support and thank them. My thanks also go to OZCAR who financed my stay in San Diego and enabled me to visit the Southern Sierra CZO sites. I must also acknowledge and thank the data providers which include EDF, SPC GD and IGE – thank you Guillaume Nord for providing the Claduègne catchment detailed data – as well as the university of JENA for providing J2000, JAMS and an access to their Forge – thank you Sven Kraelish for helping me with the OPTAS toolbox of JAMS; it was most useful in my research.

In the course of my PhD work, much help was provided by different persons and at different times that I must acknowledge as they brought key helps when needed. In particular, I would like to thank you Claire Lauvernet for taking so much time teaching me about sensitivity analysis and helping me choose the right approach and analyze the results. Your help has been very precious to me and, with no doubt, contributed to a significant shift in my research that proved to be very valuable. I would also like to sincerely thank you Hilary McMillan for your warm welcome at the San Diego State University during my short stay. I am very grateful, not only for all the time you took while I was there to guide me and discuss with me the Southern Sierra data, but also for all the time you took for reading and providing very useful and relevant feedback on my article that initiated during this stay in the US.

Thank you Michel Guilmore for helping me in visiting the Southern Sierra sites when (meteorological) conditions were far from ideal. Thank you Isabelle Gouttevin and Jean-Philip Vidal for pre-processing the hourly SAFRAN dataset and computing the reference evapotranspiration. Jean-Philip, I also very much appreciated these long conversations about my PhD and R and how best one should plot data or code efficiently for fast processing. Isabelle, I also remember our numerous conversations to get me started with J2000 at the beginning of my PhD. Because administrative stuff is far from being my cup of tea, I am most grateful for your help, Adeline, Marion, Véronique D., Hélène, Vanessa, Angélique, and all the research support team. Jean-Pierre, Frédéric and Claire, thank you for your frequent help in computer related stuff.

I also want to thank all my colleagues and friends both at Irstea/Inrae and CNR. Thank you Adrien for having been a so lively "co-bureau", always eager to debate and with whom I build this unique office indoor garden. Thank you Mattéo, Yassin and Alexandre for all these late conversations at the office when I was finishing my manuscript. Thank you Sophie, Laura, Emilie R., Lucie, Alexie, Eric, Anne-Laure, Maïlys, Maxime M., Quentin, etc. for all the good times spent with you in Lyon both at work and after work. My thanks also go to all my other collegues for all these little day-to-day life moments we shared Emeline, Peng, Remi, Nicolas D., Benjamin, Jérôme, Tariq, Jean, William, Jérémie, Guillaume, Sylvain, Fabien, Mickaël, Céline, Benoit, Lionel, Michel, Christine, Etienne, Sebastien, Maud, Oussayenou, Kadir, André, Nadia and Véronique.

Of course, I must not forget my friends who supported me during these 3 years and more. Thank you Martin and Clotaire for all the good times in Lyon including our regular pétanques and climbing sessions. Thank you Aymeric for these regular beers and discussions during our evenings in Lyon, it was a pleasure to have you nearby. Thank you to you Elisabeth – godmother

and friend – for our regular reunions in Lyon that I've always enjoyed. Thank you Camille, Vincent, Bérénice, Franklin, Noémie, Hélèna, Nicolas, Lamia, Chloé, Vincent, Sébastien and so many other for all our times together throughout these years; these were so refreshing! Among other things, I remember these New Year Holidays when I was so deep in my PhD writing and you made it possible for me to keep working and have a lot of fun at the same time. Thank you Olivia and JB for all these week-ends in Chambery, in the montains or in Lyon that were always great moments to breath. Thank you also to you Martin, Mumu, Caro, Violette, Maxou, Thibaut for these great moments during our yearly reunions or other times!

And last but not least, I deeply thank my family. Thank you dear mum and dad for you ever strong support! Thank you Aurélia and Vanina, and to you, Jorge and David! And of course, thank you to my wonderful new nephews Antoine and Marc that I am so happy to have welcomed in my life during these last years! And thank you Lucile for all you did to support me during this PhD adventure!

Abstract / Résumé

Abstract

The evaluation of hydrological models is typically based on comparisons of observed and simulated streamflow time series using performance metrics such as the Nash-Sutcliffe Efficiency. Although it provides relevant measures of the predictive performance of a model, this type of approach provides very little information on the reasons behind good or bad performance. Instead, Gupta et al. (2008) proposed to use hydrological signatures which are indicators that characterize catchment behaviors. Because they can be related to hydrological processes, using them when comparing observation with simulation enable the evaluation of the model while offering diagnostics, i.e. indications on the hydrological processes that are well or badly represented in the model.

In this PhD thesis, we focus on the interpretations and diagnostic power of hydrological signatures and how they can be used to guide the improvement of a distributed model. We present the building of a set of hydrological signatures, using only widely available data – precipitation, streamflow and air temperature – to characterize the hydrological functioning of 4 Ardèche sub-catchments (South East of France) and 10 snow dominated catchments of the Southern Sierra mountains (California, USA). Already existing and new hydrological signatures are selected and/or designed. Collectively, they can characterize catchment behavior in a wide variety of hydro-climatic contexts. We demonstrate the value of additional snow measurements to evaluate the information content of snow dedicated hydrological signatures. In the context of the Ardèche catchment, we set up the J2000 distributed model and use a sensitivity analysis to understand how the hydrological signatures are linked to the model parameters. This provides insights into how they are to be interpreted in the context of the J2000 Ardèche model and allows the assessment of their diagnostic power. Finally, combining the results of the sensitivity analysis with comparisons between observed and simulated hydrological signatures, we undertake an in-depth diagnostic of the model to provide and test recommendations for its improvement. Deficiencies of the model functioning are identified, mainly related to soil and groundwater storage and fluxes, highlighting issues in the spatial representation of soil and geological properties.

Résumé

L'évaluation des modèles hydrologiques est généralement basée sur des comparaisons des séries de débit observées et simulées à l'aide de critères de performance tels que l'efficience de Nash-Sutcliffe. Bien que cette approche fournisse des mesures pertinentes de la performance prédictive d'un modèle, elle ne fournit que très peu d'informations sur les raisons d'une bonne ou d'une mauvaise performance. Gupta et al. (2008) ont proposé d'utiliser plutôt des signatures hydrologiques, des indicateurs qui caractérisent le comportement d'un bassin versant. Les signatures hydrologiques pouvant être liées aux processus hydrologiques, la comparaison des signatures hydrologiques observées et simulées permet l'évaluation du modèle tout en offrant des diagnostics, i.e. des indications sur les processus hydrologiques qui y sont bien ou mal représentés.

Dans cette thèse de doctorat, nous nous concentrons sur l'interprétation et le pouvoir diagnostique des signatures hydrologiques et comment celles-ci peuvent être utilisées pour guider l'amélioration d'un modèle distribué. Nous présentons la construction d'un jeu de signatures hydrologiques, utilisant uniquement des données largement disponibles – précipitations, débit et température de l'air – pour caractériser le fonctionnement hydrologique de 4 sous-bassins versants de l'Ardèche (Sud-Est de la France) et 10 bassins versants de montagne à influence nivale (Southern Sierra, Californie, États-Unis). Des signatures hydrologiques existantes et des nouvelles sont sélectionnées et/ou développées. Conjointement, elles permettent de caractériser le comportement de bassins versants dans une grande variété de contextes hydro-climatiques. Des mesures de neige supplémentaires sont utilisées afin d'évaluer la pertinence des signatures hydrologiques dédiées aux processus nivaux. Par ailleurs, le modèle distribué J2000 est déployé sur le bassin versant de l'Ardèche et une analyse de sensibilité est réalisée afin de comprendre comment les signatures hydrologiques sont liées aux paramètres du modèle. Cela nous permet de déterminer la façon dont elles doivent être interprétées dans le contexte du modèle J2000 de l'Ardèche et permet l'évaluation de leur pouvoir diagnostique. Enfin, en combinant les résultats de l'analyse de sensibilité avec des comparaisons entre signatures observées et simulées, nous entreprenons un diagnostic approfondi du modèle afin de dériver et tester des recommandations pour son amélioration. Nous identifions des déficiences du modèle, principalement liées au flux et stockage de l'eau souterraine et des sols, mettant en évidence des problèmes de représentation spatiale des propriétés géologiques et pédologiques.

List of Figures

List of Tables

General introduction

Context

Water is an essential resources for ecosystems and humans. It is essentials for economical activities, energy production, drinking water and agriculture. Climate change is expected to significantly decrease the availability of water in many regions of the world which could lead to more frequent persistent severe droughts (Dai, 2010). The effects of climate change combined with the increasing pressure on water resources due to population growth and economic development leads to an uncertain future regarding the access of human societies to water[1]. This highlights the need and importance of sustainable water management practices. While human activities and the management of water resources impact the quality and quantity of available water, many aspects of social and economic development also depends on water and it is today well recognized that water availability and human activities are interdependent[1]. This is therefore not surprising that one of the main challenges for hydrological sciences that has been put forth by the International Association of Hydrological Sciences (IAHS) for the decade 2013-2022, through the "Panta Rhei" program, is to be able to account for this close relationship between human societies and water resources (Montanari et al., 2013).

Water scarcity is expected to become more common in Europe, particularly in Central and Southern Europe as a consequence of climate change[2]. For example, studying the effect of several climate change scenarios, Quintana-Seguí et al. (2011) suggested that low flows for catchments located in the South East of France, including the Rhône catchment, could decrease by 20%. In catchments affected by snow or glacier such as in the European Alps, a decrease in volume and a shift in timing of streamflow due to snow melt is expected, affecting among many other things, the potential for hydroelectricity production and agriculture (Gobiet et al., 2014). In the European context, Schmidt and Benítez-Sanz (2012) highlighted the main challenges that remain to be addressed by current policies in European countries. They listed recommendations to guide the development of better suited water management policies and mentioned the need to incresse our abilities to better forecast water availability and future water uses.

The high variability in space and time of precipitation and energy inputs and the effects of various anthropogenic water uses require specific tools to understand and predict the availability of water in space and time. Distributed hydrological models are valuable in that regard given their ability to explicitly account for (1) spatial variability of meteorological inputs, (2) spatial heterogeneity of physical characteristics such as vegetation or sub-surface characteristics (soils and geology) and (3) human activities such as water uptakes (for irrigation or drinking water) or dams. In addition, such models can simulate river flow not only at the outlet of a catchment – the main physical entity typically considered in these models – but along the entire river network as well as provide estimates of water content in the sub-surface i.e. in the soils or deeper aquifers, spatially, over the entire catchment.

An example of such a model is the J2000 model, originally developed at the University of Jena (Germany) for the assessment of water resources and water quality in the context of

[1] WWAP (World Water Assessment Program). 2012. *The United Nations World Water Development Report 4: Managing Water under Uncertainty and Risk.* Paris, UNESCO. http://www.unesco.org/new/en/natural-sciences/environment/water/wwap/wwdr/wwdr4-2012/

[2] Water Scarcity and Droughts Expert Network. 2007. *Drought Management Plan Report including agricultural, drought indicators and climate change aspects.* European Communities. https://ec.europa.eu/environment/water/quantity/pdf/dmp_report.pdf

the European Water Framework Directive (Krause et al., 2006). It is a process-based model which is distributed in space to explicitly account for the spatial heterogeneity of land-use, soil and geology. The J2000 model was adapted and extended for the building of the J2000-Rhône model developed at Irstea during the MDR project (2013-2016) (Branger et al., 2016). It is designed to represent the natural and human-influenced functioning of the entire Rhône catchment (100 000 km^2) one of the main french rivers. The J2000-Rhône model takes into account several human water uses: uptakes for irrigation, drinking water and dams.

The MDR project was funded by the Agence de l'Eau Rhône-Méditerrané-Corse and the Compagnie Nationale du Rhône (CNR), a company managing many hydropower plants along the Rhône river, to address the important issue of the possible and likely decrease of water availability in the Rhône catchment that could impact the well-being of local population, industries, agriculture and hydroelectricity production. The J2000-Rhône model is a valuable tool to address these concerns as demonstrated by Branger et al. (2016) who undertook a preliminary prospective study on the effect of climate change and different changes in water uses related to irrigation and drinking water uptakes.

The Rhône catchment spans a large diversity of hydro-climatic contexts from the Alpine catchments, heavily influenced by the seasonal effects of glacier and snow processes, the low land and forested catchments of the Saône river, to the Mediterranean catchments characterized by a long dry Summer and intense precipitation events mainly during Fall. The ambition of the J2000-Rhône model, which is to represent this large diversity of hydro-climatic contexts while accounting for human influences, faces many challenges. In particular, the specification of the parameters of the model requires tremendous efforts to specify parameter values that result in a good performance over the entire catchment, while remaining realistic. In their work to parameterize and improve the J2000-Rhône model, Branger et al. (2016) undertook an expert-based approach to gradually modify and improve the model. However, considering the Nash-Sutcliff Efficiency criterion to measure performance on a large set of Rhône sub-catchments, they were able to achieve only moderately good results and very different depending on the considered sub-catchment as illustrated in Figure A. Branger et al. (2016) also highlighted the limits and lack of reproducibility of the expert-based approach they followed.

The typical approach to parameterize a hydrological model is the use of a more or less sophisticated calibration procedure based on performance metrics and past observations of catchment response, typically streamflow at the catchment outlet. However, in the case of distributed models, the large number of parameters involved makes such an approach difficult. In addition, while it might lead to better performance it also often leads to less physical realism of the internal behavior of the model and to the loss of the interpretable link between the spatially distributed parameters and the physical characteristics of the catchments (McMillan et al., 2016). The J2000-Rhône model is dedicated to long term studies typically involving running simulations in conditions that are different than the past or present days. This requires that the parameters should be as much as possible independent of current climate conditions (if studying the effect of climate change) and that the interpretable links between parameters and catchment characteristics should not be lost (if studying, for example, the effect of land-use change). It is particularly important, for such models, to provide the right answers, for the

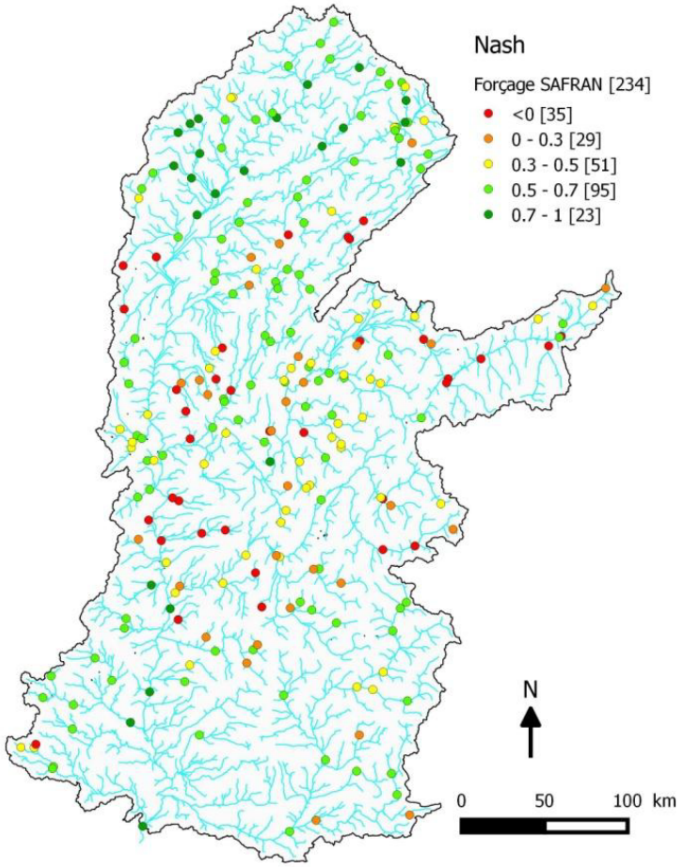

Figure A: Rhône catchment and associated river network. The dots indicate the localization of 234 control stations. The filling colors indicate the performance, measured by the Nash-Sutcliff Efficiency, obtained for the corresponding sub-catchments with the J2000-Rhône model over the 1987-2012 period. (taken from Branger et al. 2016)

right reasons (Kirchner, 2006) in order to have confidence in the results of prospective studies such as the ones the J2000-Rhône model is intended for.

A way forward to address the issue of evaluation and improvement of hydrological models and achieve better results for the right reasons is in the diagnostic-evaluation approach introduced by Gupta et al. (2008). Instead of performance metrics, they proposed to use process-based metrics that are called hydrological signatures. Hydrological signatures are indicators that describe the behavior of the catchment and that can be related to hydrological processes. Gupta et al. (2008) proposed to use them when comparing observed data with simulated data in order to compare their behaviors. In particular, since hydrological signatures can be related to the functioning of the catchment, this approach can enable the identification of what is well of badly represented in the model. This "diagnostic" capability of hydrological signatures can therefore be used to improve models in terms of hydrological processes representation.

Hydrological signatures are not new in hydrology as they can be seen as the results of any type of hydrological data analysis that are used to understand the functioning of catchments (e.g. McMillan et al. 2011, 2014) or characterize catchment response for various purposes (e.g. Clausen and Biggs 2000; Olden and Poff 2003; Shamir et al. 2005b,a). Since the work of Gupta et al. (2008), hydrological signatures have gained in popularity in the modeling community for the development, calibration and evaluation of hydrological models (e.g. Yilmaz et al. 2008; Westerberg et al. 2011; Euser et al. 2013; Clark et al. 2011b; Pokhrel et al. 2012). However, they

are most of the time used as mere additional metrics alongside traditional performance metrics with no in-depth analysis of the implications regarding model and catchment functioning. In addition, most studies focus on simple lumped models and only a few studies make use of them for the diagnostic and evaluation of distributed models (e.g. Yilmaz et al. 2008; McMillan et al. 2016; Höllering et al. 2018). We can also note that there is only a small diversity in the hydrological signatures that are currently used. The large majority of studies are based on the same ones, often derived only from the flow duration curve (e.g. Westerberg et al. 2011; Pokhrel et al. 2012; Guse et al. 2016a; Ley et al. 2016; Todorović et al. 2019). In addition, the choice, design and relevance of hydrological signatures is often not questioned by authors (McMillan et al., 2017) and the interpretations, in terms of hydrological processes, are most often only (if at all) hypothesized and not verified.

PhD objectives and thesis structure

This PhD thesis is dedicated to the choice, design and interpretation of hydrological signatures and their usefulness for the diagnostic and improvement of a distributed hydrological model. More specifically, the research presented in this manuscript has three main objectives that can be summarized as follows:

- create a set of hydrological signatures based only on widely available data (precipitation, streamflow and air temperature) combining commonly used ones and the design of new ones;
- evaluate the information content (regarding hydrological processes) and diagnostic power of hydrological signatures;
- explore how hydrological signatures can be used for the diagnostic and improvement of a distributed model.

This manuscript synthesizes the approach followed to address these objectives and the results obtained. It is structured in 6 chapters.

In Chapter 1, a brief overview of hydrological processes and modeling approaches is presented. It also summarizes the issue of model parameter identification and presents the diagnostic approach to model evaluation and the use of hydrological signatures in modeling contexts. An overview of existing hydrological signatures is proposed along the main current limitations regarding their selection, design and evaluation. This review of the literature eventually leads to the definition of the detailed objectives of this thesis and the presentation of the methodology followed to address them.

In Chapter 2, the studied catchments and the associated datasets are presented in details. It includes the presentation of the Ardèche catchment (a sub-catchment of the Rhône catchment) and of four of its subcatchments used as our main case study. The J2000 model and how it accounts for hydrological processes is presented in details along with its setup on the Ardèche catchment. A set of 10 snow dominated catchments located in the Southern Sierra mountains

(California, USA), used as our case study for snow dedicated hydrological signatures, is also presented.

Chapter 3 is an article published in *Hydrological Processes*. This article is based on the 10 Southern Sierra snow dominated catchments and a set of snow dedicated hydrological signatures based on streamflow, precipitation and air temperature. It focuses on the information content of these signatures and how their hypothesized interpretations can be verified using additional snow measurements.

Chapter 4 presents a set of hydrological signatures based only on precipitation and streamflow data. It includes existing hydrological signatures as well as new hydrological signatures. They are presented in the context of the Ardèche sub-catchments with a particular emphasis on their interpretation in terms of catchment functioning and their potential value for the diagnostic of the J2000 Ardèche model.

Chapter 5 presents a preliminary diagnostic of the J2000 Ardèche model which highlights the need for a better understanding of the link between hydrological signatures and model parameters. To address this limitation, a sensitivity analysis of the hydrological signatures to the model parameters is undertaken. The sensitivity analysis enable the identification of the links between hydrological signatures and model parameters. The hypothesized interpretations of the hydrological signatures are verified in the context of the J2000 model and results provide an evaluation of their diagnostic power, i.e. how well they can be related to model functioning and particular modeled processes and help in identifying model issues.

In Chapter 6, an in-depth diagnostic of the J2000 Ardèche model is detailed. Recommendations for its improvement are proposed, tested and evaluated. The improvement of the model is discussed and structural deficiencies of the model are highlighted. The diagnostic and improvement methodology is eventually discussed.

Finally, this research closes on a general conclusion where the main results are summarized and the implications and perspectives of this research are discussed.

Chapter 1

State-of-the-art: using hydrological signatures for more processes realism in hydrological modeling

Contents

1.1 Catchment hydrology: hydrological processes and modeling

1.1.1 An overview of hydrological processes

Catchment hydrology is the science that studies the journey of water within a catchment, a physical entity typically defined as the drainage area resulting from the surface topography (Wagener et al., 2007). This topographic definition of a catchment supposes that the crest line effectively divides the water that eventually reaches a given section in the river network (the catchment outlet) by different pathways either at the ground-surface, within the soils or through the bedrock, if not released to the atmosphere through evapotranspiration. It neglects possible movements of water below the ground surface that bypass the catchment river outlet and its boundaries, through, for example, complex geological structures e.g. large aquifers spanning multiple topographic catchments, karstic underground pathways, etc.

Catchment hydrology focuses on all *"the mechanisms of movement and storage of water"* (Wagener et al., 2007) occurring within the catchment boundaries. These mechanisms or hydrological processes are the results of interactions between water and various physical entities that constitute a catchment such as plants, soils and geology (Sivapalan, 2006). Large heterogeneity of catchments physical characteristics and large variability of climate inputs (precipitation, energy) around the world result in large differences in catchment hydrological behaviors. This supports the idea of *"uniqueness of places"* of Beven (2000) and makes the emergence of a *"unified theory"* of hydrology (Sivapalan, 2006; Kirchner, 2003) or a classification framework for catchments with respect to their physical characteristics and hydrological behavior (Wagener et al., 2007) particularly difficult. In addition, the vast majority of catchments is affected by various human influences changing their physical characteristics and behavior (Montanari et al., 2013) – agriculture, forest management, urbanization, dams, water uptake for irrigation, drinking water, etc. – which bring another layer of complexity (more heterogeneity and variability).

The various natural hydrological processes that control the catchment hydrological behavior occur within a large spectrum of spatial and temporal scales (Blöschl and Sivapalan, 1995; Woods, 2006; Sivapalan, 2006). Figure 1.1, taken from Blöschl and Sivapalan (1995), provides a synthetic overview of the main hydrological processes and their corresponding spatial and temporal scales. Figure 1.1 includes precipitation phenomena (from small cumulus convection to large front) that drive catchment response including fast (from minutes to days) and slow (from days to years) streamflow generation processes. The overland flow (i.e. at the ground surface) is a fast streamflow generation process, as such flows reach the river network quickly. Movement of water within soils often named inter-flow or subsurface flow is controlled by slower hydrological processes; such flows reach the river network more slowly. Slow hydrological processes are those controlling the movement of water in unsaturated soils, groundwater storage and aquifers.

The fast reaction of catchment to precipitation events has long been attributed to overland flow following the mechanism that was first described by Horton (1933). Horton (1933) argued that streamflow generated during a precipitation event at the outlet of a catchment is mostly caused by overland flow due to the limited capacity of soils to infiltrate water. In this theory, overland flow is due to precipitation rates exceeding the maximum infiltration rate capacity of

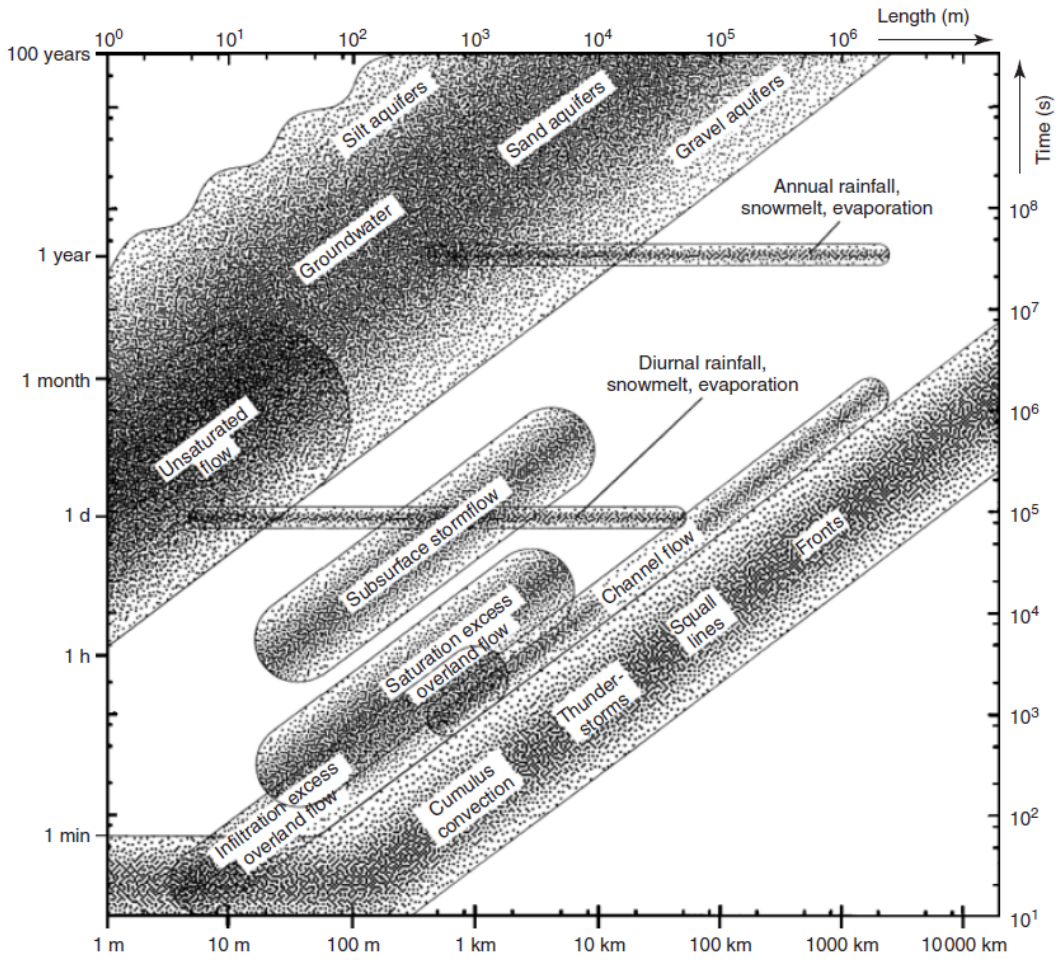

Figure 1.1: Schematic relationships between the spatial (x axis) and temporal (y axis) scales of many hydrological processes. (from Blöschl and Sivapalan (1995))

soils. Moreover, the maximum infiltration rate of soils decreases during a precipitation event due to soils wetness states and ground surface degradation; intense precipitation or large/heavy rain drops altering the ground surface and decreasing its permeability. This hydrological process, also called infiltration excess overland flow, is indeed found dominant in desert and semi-arid regions where infiltration rate of soils is often exceeded due to the lack of soil protection by plants and very low porosity of the top layers of soil (Freeze, 1974). However, in temperate and humid regions, it has been recognized to play only a secondary role, affecting the streamflow response of catchments only during exceptionally intense precipitation events and occurring only in some areas of catchments (Betson, 1964; Dunne and Black, 1970). Soils saturation which vary in space and time during precipitation events can cause overland flow, called saturation excess overland flow (Dunne and Black, 1970): the water table (depth of the saturated zone in the soils) rises during a precipitation event and can eventually reach the ground surface – particularly in valleys, close to the river network – leading to overland flow through water exfiltration from soils and the inability of saturated soils to infiltrate the incoming rainfall.

During precipitation events, it has also been demonstrated that infiltrated water could significantly contribute to streamflow by lateral movement in the soil due the existence of preferential flow pathways such as macropores within the soil matrix (e.g. Mosley, 1979; Flury et al., 1994; Feyen et al., 1999). This is particularly the case in the top layers of soils where more

porosity is often observed. The variability of the connectivity of the preferential flow pathways is also recognized to play a significant role in the relative importance of subsurface contributions to streamflow: during a precipitation event, the increase of the water table gradually leads to the connections of preferential flow paths that eventually bring large contribution of water as subsurface flow. The variability of the connectivity of the preferential flow paths can explain the threshold in the streamflow response often observed at the hillslope scale or in small headwater catchments (Tromp-van Meerveld and McDonnell, 2006; Tromp-van Meerveld and McDonnell, 2006; Lehmann et al., 2007; Detty and McGuire, 2010; McMillan et al., 2011). The use of natural tracers such as stable isotopes of oxygen and hydrogen have led to the *"old water paradox"* (Kirchner, 2003): fast catchment reaction times to precipitation events are associated with dominant contributions of "old" water. Various mechanisms have been proposed along the years to account for this contribution of "old water" during precipitation events such as groundwater ridging (Sklash and Farvolden, 1979) or transmissivity feedback (Kendall et al., 1999). There are many mechanisms involved in the generation of fast subsurface flow in response to precipitation. For a given catchment, all these processes may be involved, in different parts of the catchment, at different times or for different precipitation events (Beven, 1989b). The mechanisms involved may vary depending on antecedent wetness conditions, rainfall intensities and duration, topographic and physical characteristics of soils.

Catchment streamflow response also exhibits specific behaviors outside of precipitation events. It is recognized that shallow and deep water storage in soil and bedrock contributes to streamflow outside of precipitation events (Freeze, 1974; Brutsaert and Nieber, 1977; Wittenberg and Sivapalan, 1999; Iwagami et al., 2010). These behaviors correspond to storage-discharge relationships of the groundwater reservoirs located in the catchment – in the soils and bedrock – and is therefore closely related to their *"geological nature"* (Brutsaert and Nieber, 1977). In addition, as shown in Figure 1.1, other hydrological processes, driven by energy inputs (solar radiation), affect the catchment behavior. They are related to plants and snow/ice storage/melt occurring both at daily (due to variations of energy inputs within a day) and yearly (due to seasonal variation of energy inputs throughout a year) time scales (Blöschl and Sivapalan, 1995). Catchments dominated by snow or ice have a strong yearly (resp. daily) cycle resulting in low streamflow during the snow accumulation period in Fall and Winter (resp. during night where there are no energy inputs) and high streamflow during Spring and Summer as a consequence of snow melt due to the increase of energy inputs during these seasons (resp. during daylight). Plants can have a similar effect as the root uptake of water varies both during the day and seasonally as a consequence of variations in energy inputs.

1.1.2 Catchment modeling

A way to capitalize our current knowledge of hydrological processes and/or test hypothesis of catchment functioning is to use hydrological models (Clark et al., 2011a, 2016; Hrachowitz and Clark, 2017). Hydrological models are mathematical and numerical tools that aim at predicting streamflow at the outlet of a catchment and/or other hydrological variables (e.g. soil water content, actual evapotranspiration). These models take as input precipitation and other meteorological data to account for energy inputs (e.g. potential evapotranspiration, air temperature or solar radiation) to simulate the catchment behavior and streamflow at its outlet.

Humans heavily rely on water for their livelihood (e.g. drinkable water, irrigation, hydro-power production, etc.) and are exposed to many water related risks (e.g. floods, droughts). Therefore, models that provide predictions for managing water resources and mitigating water related risks are particularly important (Montanari et al., 2013).

1.1.2.1 Modeling approaches

There is a large diversity of hydrological models, developed following different modeling strategies and for various aims (Clark et al., 2017). To clarify this large diversity, Hrachowitz and Clark (2017) proposed a synthetic overview of the different modeling approaches according to their process complexity and spatial resolution (Figure 1.2). Figure 1.2 clearly establishes two very contrasting approaches (two endpoints): fully distributed and physically based models (top right corner, continuum-based models) and lumped conceptual models (bottom left corner, bucket-based models).

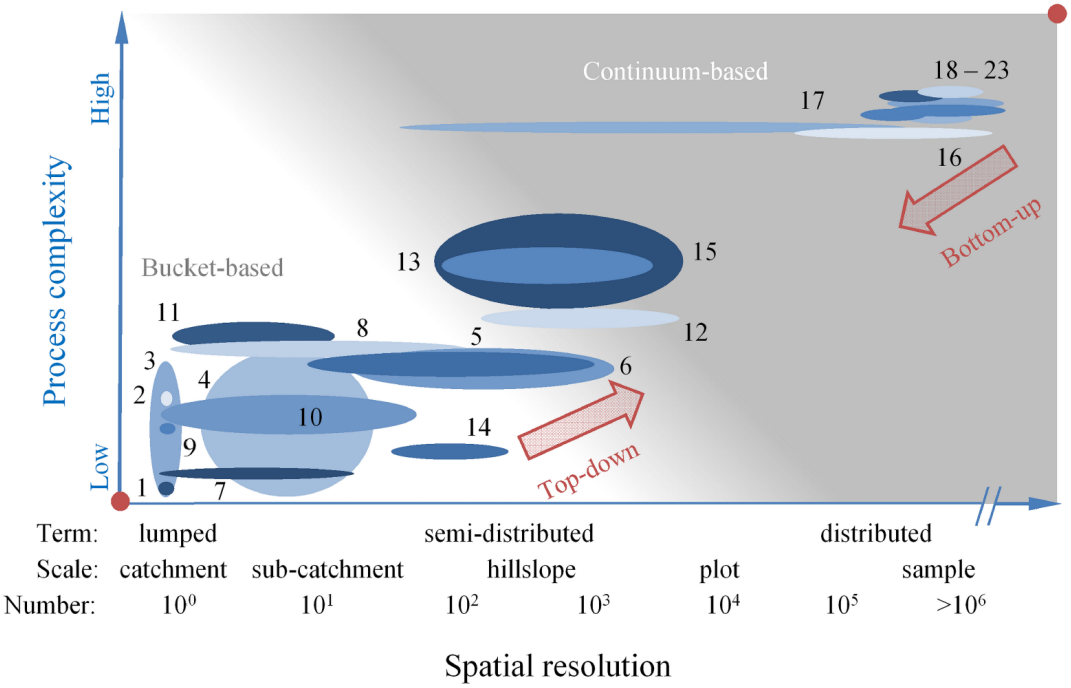

Figure 1.2: Schematic representation of the approximate position of a selection of 23 models (indicated by the numbers, see details in Hrachowitz and Clark (2017)) within the space of (x axis) spatial resolution and (y axis) process complexity. On the spatial resolution axis, the typical scale and number of spatial units are indicated. Process complexity axis refer to the number of processes explicitly accounted for in the models. From the two endpoints (red dots) of the spatial resolution and process complexity spectrum, the transition from white to grey background illustrate the transition from bucket-based to continuum-based models. (from Hrachowitz and Clark (2017))

Physically based models are developed following a bottom-up or upward approach. In this approach, the catchment behavior is the result of a very detailed representation of hydrological processes at small scale in the whole space domain of the catchment (Sivapalan et al., 2003). These types of models rely on small scale physics equations such as Richard's equation to represent the movement of water in the soil (e.g. CATHY model, Camporese et al., 2010). This physical representation of processes is based on partial differential equations that are numerically integrated to represent water flux in the whole catchment and simulate streamflow. If these models have been used for decades, they also have received many criticisms (Beven,

1989a; Grayson et al., 1992; Sivapalan et al., 2003; Sivapalan, 2006). The main drawbacks mentioned are that the equations used, relevant at very small scales (e.g. below 1 m), are applied at much larger scales (e.g. 50 m^2 in Camporese et al. (2010) and often more) where their underlying assumptions (e.g. uniformity) are no longer true. These models are also seen as largely over-parameterized models (i.e. they rely on many "free" parameters), demanding enormous amounts of data to properly constrain them. In addition, in spite of very detailed representation of hydrological processes, they are recognized to often fail at representing key features of the overall catchment response.

Following an opposite direction from the bottom up approach, many authors have advocated (e.g. Klemeš, 1983; Beven, 1989a; Sivapalan et al., 2003) and used (e.g. Jothityangkoon et al., 2001; Eder et al., 2003; Farmer et al., 2003; Adamovic et al., 2016) top-down (or downward) approaches for model development. These approaches are based on the understanding of catchment behavior, i.e. a perceptual model of how the system works, that results from the analysis of available data. This perceptual knowledge is then used to build a mathematical conceptual model representing the main hydrological processes (Sivapalan et al., 2003; Clark et al., 2016). Such models typically rely on a bucket or reservoir representation of water storage in the catchment with different reservoirs to account for different storages (e.g. soil, groundwater). The flux (input and output of these reservoirs) are represented by various mathematical equations. Some of these models are lumped i.e., representing the catchment as a whole (e.g. GR4J model, Perrin et al., 2003) or spatially distributed in space (e.g. SWAT model, Arnold et al. (1998) or TOPMODEL model, Beven and Kirkby (1979)). Lumped models ignore the heterogeneity of physical characteristics (e.g. soils, vegetation, geology) or rather they attempt to capture and *"describe large-scale manifestation of small-scale natural heterogeneity"* (Hrachowitz and Clark, 2017) in a parsimonious way. On the other hand, conceptual distributed models explicitly account for some of the spatial heterogeneity either by translating landscapes heterogeneity into varying model parameter values or by accounting for spatially heterogeneous precipitation (or temperature), or both (Hrachowitz and Clark, 2017). They are the result of an assemblage of multiple spatial units – which can be seen as individual lumped models – interconnected to represent the various fluxes in the catchment and simulate streamflow. In the literature, distributed models can refer either to physically-based or conceptual models. Physically based models, although involving actual physical equations are, to various degrees, the result of some conceptualization and simplification of nature (Hrachowitz and Clark, 2017). As such, they can sometimes be seen as particular kind of spatially distributed conceptual models (Beven, 1989a).

1.1.2.2 Accounting for hydrological processes in hydrological models

There are many discussions in the modeling community regarding the best ways to implement various hydrological processes and how spatial heterogeneity should be accounted for. In their commentary, Clark et al. (2016) advocated the need for a process representation in conceptual models that *"should be as deeply rooted as feasible in the available hydrologic theory"* that they defined as *"our explanations of individual processes, process interactions, patterns and scaling behavior"*. This process based approach to model development aims at gathering the large complexity of hydrological processes, as illustrated in the previous Section, within hydrological models. In particular, models should be able to explain and predict emergent catchment be-

haviors resulting from the combination – typically non linear and non additive – of hydrological processes identified at small-scales (Reggiani et al., 1998; Kirchner, 2006; McDonnell et al., 2007).

Hrachowitz and Clark (2017) listed the following hydrological processes with respect to *"major partitioning points"* of water storage and release at the catchment scale that are (1) near the ground surface – evaporation and sublimation, overland flow, infiltration – and (2) in the top part of the soils (root zone) – soil evaporation, plant transpiration, lateral flow (high permeability soil layers, preferential flows, etc.), percolation to the groundwater. They argue that all these processes affect any catchment – although in varying degrees depending on the climatic regions, catchment physical characteristics, current catchment state and meteorological conditions – and should therefore be represented in model. Various mathematical formalisms can be chosen to represent hydrological processes. For example, to represent water fluxes in the soils, partial differential equations (physically based models), reservoir-based approaches or even simple regression-based approaches may be chosen (Hrachowitz and Clark, 2017). Conceptual models have various degrees of complexity, as illustrated in Figure 1.2, which depend on the number of hydrological processes explicitly accounted for.

As an illustration, Figure 1.3 shows the diagrams describing the functioning – how the hydrological processes are represented – of two well-known models: the GR4J lumped model (Figure 1.3a, Perrin et al. (2003)) and the TOPMODEL distributed model (Figure 1.3b, Beven and Kirkby (1979)). In the GR4J model (Figure 1.3a, Perrin et al. (2003)), the storage in the soil and groundwater is represented by a unique *"production store"* which admits only a proportion of incoming net precipitation as a function of its water content. Transpiration may occur from this storage unit or water may be released through *"percolation"*, both mechanisms being functions of the production store water content. Streamflow at the catchment outlet is then computed following a *"unit hydrograph"* approach. In the TOPMODEL model (Figure 1.3b, Beven and Kirkby (1979)), several storage units are considered for each sub-catchment (or unit of space): (1) an *"interception and depression store"*, (2) a *"near surface infiltration store"* and (3) a *"subsurface saturated soil water store"*. Overland flow due to precipitation rates exceeding maximum soil infiltration rate or due to saturated soils is explicitly represented. In addition, for each sub-catchment, the model accounts for *"variable contributing area"* as a function of water storage in the subsurface saturated soil water store and topography, i.e. the variability of overland flow due to the variability in space of soil saturation is accounted for in the model. A subsurface flow contribution from the saturated soil water store is also represented as well as channel streamflow routing following a kinematic wave approach. In addition to being distributed, TOPMODEL includes much more complexity, i.e. more hydrological processes explicitly accounted for, in each of its spatial units than the GR4J model (see ellipses 9 for GR4J and 12 for TOPMODEL in Figure 1.2). Models such as TOPMODEL are often qualified as process-based models.

The unit of space used by distributed models can be of various sizes (e.g. from cm to km) and forms. Space can typically be divided according to (1) a regular grid of a given resolution (which is typically the case of physically based models, (e.g. Yilmaz et al., 2008; Pokhrel et al., 2012; Gharari et al., 2014), see Figure 1.4a), (2) sub-catchments (e.g. Reggiani et al., 1998) or (3) irregular shapes of space that account for the heterogeneity in the topography as well

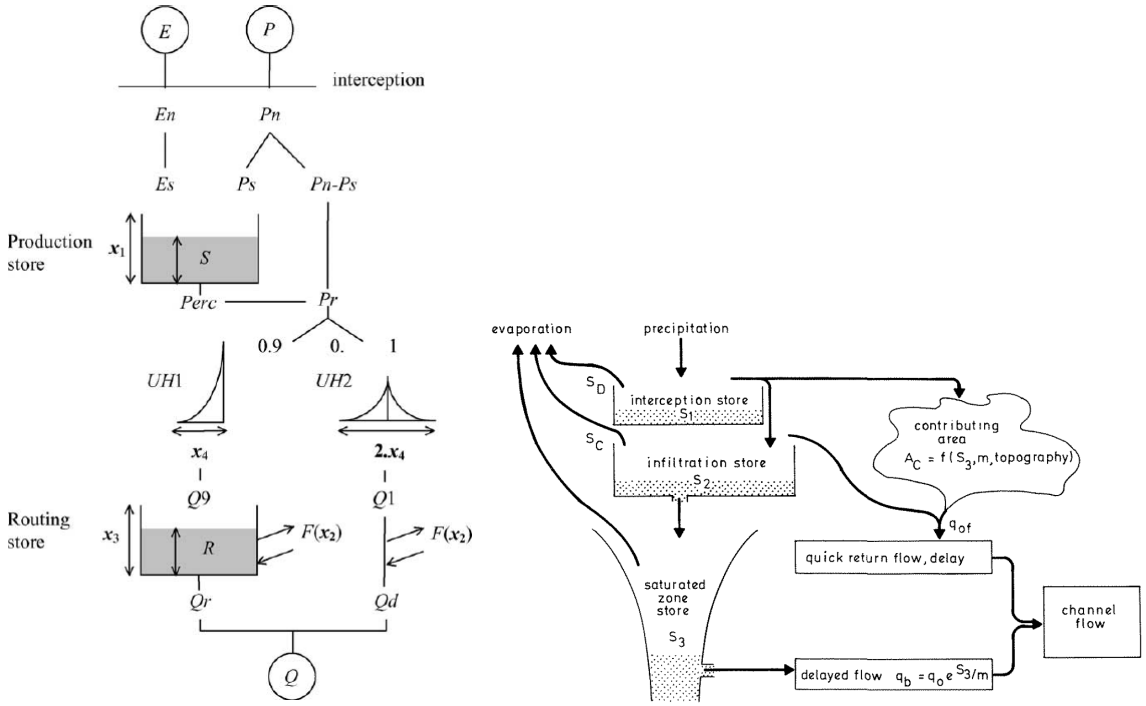

(a) Representation of hydrological processes in the GR4J lumped model (from Perrin et al. (2003))

(b) Representation of hydrological processes for sub-catchment in the TOPMODEL distributed model (from Beven and Kirkby (1979))

Figure 1.3: Diagrams representing the functioning of two hydrological models: GR4J and TOPMODEL

as other hydrologically relevant catchment physical characteristics such as land use, soils and geology (e.g. Hydrological Response Units (HRU) (Flügel, 1995; Krause, 2002; Krause et al., 2006; Kumar et al., 2013), see Figure 1.4b). Figure 1.4 illustrates two of these typical spatial distribution approaches.

One of the main advantage of distributed models with respect to lumped models is their ability to simulate the spatial distribution of hydrological processes and catchment states (over the lanscape) as well as to provide streamflow estimates, not only at the catchment outlet, but also along the entire length of the river network (Yilmaz et al., 2008). Another advantage, already mentioned above, is their ability to account for the spatial heterogeneity of landscape characteristics including the topography (including shade and aspect), the type of land-use and land cover, soils, geology and rivers physical characteristics (channel width, slope, etc.). Water management practices as well as other human induced effects can also be explicitly accounted for (e.g. irrigation, water uptake for industries and drinking water, dams, ditch, road, or even sewer networks, (e.g. Branger et al., 2010; Fuamba et al., 2019)). In the context of The Panta Rhei initiative of IHAS which has made the links between societies and hydrology as one of the key challenges for hydrological sciences in the scientific decade 2013-2022 (Montanari et al., 2013), the potential of distributed models is therefore particularly relevant. These models are recognized as valuable tools for studying the impact of climate or land use change on the hydrological functioning of catchments (Krause, 2002; Vandana et al., 2018), for water resources management and planning (including diffusive pollutant mitigation), mitigation of water related hazards such as floods and drought (Kampf and Burges, 2007; Yilmaz et al., 2008; Branger et al., 2010). In addition, it is worth noting that they can take advantage of the increasing availability of spatial data (snow cover, soil moisture, land surface temperature data, radar rainfall) both

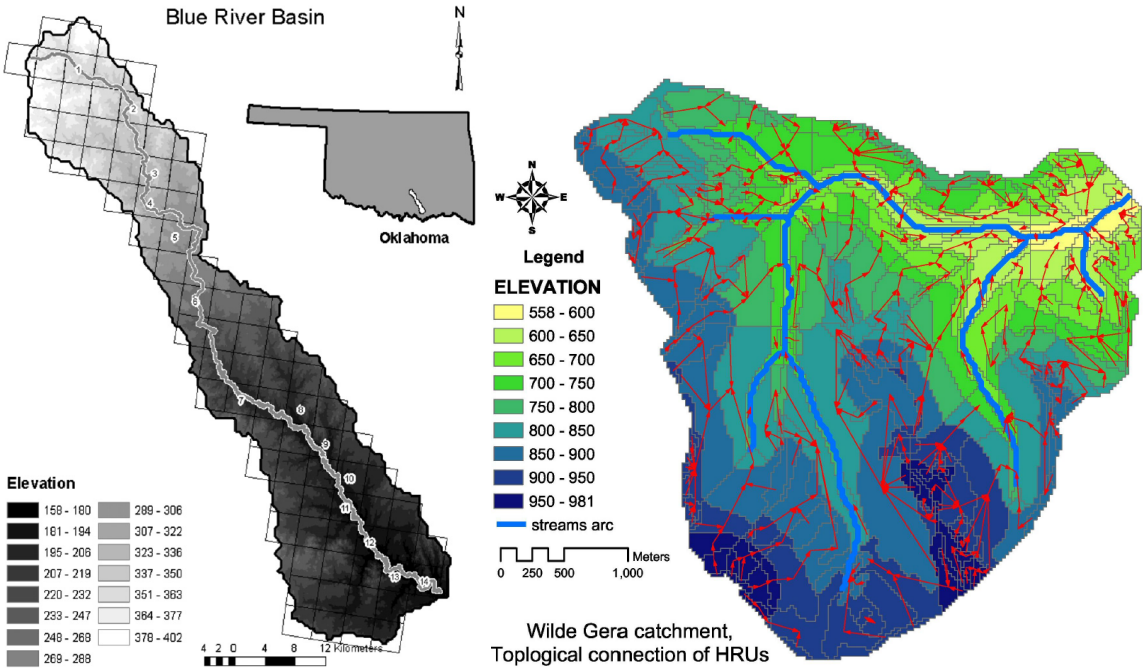

(a) Using a regular grid (from Pokhrel et al. (2012))

(b) Using Hydrological Response Units (HRU), irregular polygons resulting from a cross over between different spatial data (topography, land-use, soil type and geology) to have homogeneous units of space in terms of physical characteristics (from Krause et al. (2006))

Figure 1.4: Two examples of spatial distributions in hydrological distributed models

for their calibration or evaluation (Kampf and Burges, 2007) thus tackling one of their main shortcomings related to their over-parameterization as mentioned earlier.

1.1.3 Summary

There are many hydrological processes affecting catchment behaviors, and they occur at a large spectrum of spatial and temporal scales. Their role and importance vary greatly depending on climatic regions, catchment physical characteristics and current catchment state and meteorological conditions. Due to this complexity, the development of hydrological models to predict catchment response is a difficult task. Two main approaches in the development of models are often distinguished: the bottom-up and top-down approaches. There are many different ways of representing hydrological processes in hydrological models and the resulting models vary greatly in complexity. Regardless of the approach followed, many authors emphasize on the need of models that are as closely rooted in hydrological theory as possible.

One of the main distinctions among the existing models lies in their spatial distribution. Distributed models rely inevitably on a larger number of parameters than lumped models. However, they have the capacity to explicitly account for (1) spatial heterogeneity of landscapes and precipitation, (2) various human influences and (3) to simulate not only streamflow at the catchment outlet but also water availability and variability in space. This makes them well suited for many studies related the water resources management and water related risks. As pointed out by Kirchner (2006), a well balanced approach between lumped and distributed models is probably needed.

1.2 Process consistency in hydrological modeling

Process consistency in a hydrological model relates to its behavior and how consistent it is with respect to the actual catchment functioning or at least our expectations of how it is actually functioning. It relates to the degree of "realism" of the model. The process consistency of a model depends on its structure and specified value for its parameters. In this section we present the typical approaches of parameter identification for lumped and distributed models, how model consistency can be evaluated focusing either on its structure or parameters. The diagnostic approach to model evaluation, which rely on the use of hydrological signatures, is presented.

1.2.1 Parameter identification

1.2.1.1 Common calibration approaches

All hydrological models rely on a given number of parameters. There may be only a few parameters for lumped conceptual models (e.g. 4 parameters for the GR4J model, Perrin et al. (2003)) to several hundreds of parameters in the case of distributed models. Hydrological models are often calibrated against observed data – typically streamflow at the catchment outlet – to find the best optimal parameter set that lead to the best model performance. Performance is typically evaluated by comparing observed and simulated streamflow at the outlet of a catchment using a residual-based metrics (e.g. Nash Sutcliffe efficiency Nash and Sutcliffe (1970) or Kling-Gupta efficiency (Gupta et al., 2009)). A large variety of techniques has been developed by modelers to perform such calibration (e.g. global and local search algorithms to explore the parameter space) (Duan et al., 2003). Typically, the historical observed streamflow time series is divided into a calibration and a "validation" or evaluation period (Sivapalan et al., 2003; Gupta et al., 2008). The calibration period is used to find the optimal parameter set. The evaluation period is then used to evaluate whether or not the model is able to predict streamflow in an "unknown" period, i.e. that hasn't been used in the calibration (Figure 1.5a).

Different calibration approaches have been proposed in the last decades to achieve more realism in how models behave. Among these approaches, Monte Carlo procedures explore the parameter space and select only the sets of parameters for which some regression-based metrics measuring the distance between observation and simulation are minimized. For example, the Generalized Likelihood Uncertainty Estimation (GLUE) approach (Beven and Binley, 1992) and more generally, the Limit-of-Acceptability framework for which only parameter sets where the resulting simulation is within a certain range of acceptable values (according to some objective function or calibration criterion) are selected. These approaches enable the quantification of the uncertainty of model predictions due to model parameters uncertainty as they provide an ensemble of simulations instead of a single one. In addition, as one calibration criterion such as the Nash-Sutcliff efficiency cannot capture the whole spectrum of differences between observed and simulated data, multiple criteria (e.g. Nash-Sutcliffe efficiency applied on the log-transformed value of streamflow to focus on low streamflow values, a bias measure, a coefficient of determination, etc.) are often used in mutli-objective calibration procedures (e.g. Gupta et al., 1998).

1.2.1.2 Calibration in the case of distributed models

The application of automatic calibration procedures to models that rely on a large number of parameters such as either conceptual or physically-based distributed hydrological models is a difficult and cumbersome task. In addition, calibration of such models is heavily subject to equifinality issues (Beven and Binley, 1992), i.e. many different parameter sets can lead to similar simulated streamflow and similar performance. Note that lumped models are also confronted with equifinality issues, though, to a lesser extent. In the case of distributed models, different approaches are used to reduce the number of parameters that need to be calibrated. For example, some distributed parameters may be (1) fixed as they can be inferred from available data (e.g. soil characteristics or vegetation type), or (2) grouped in classes according to vegetation types, soil type, geology type, topographic similarities. In addition, sensitivity analyses are often used to reduce the parameter space prior to calibration (Herman et al., 2013) by identifying key model parameters or parameters that can be ignored (e.g. van Werkhoven et al., 2009).

Before automatic calibration was possible due to computer limitation, modelers relied on manual trial-and-error approaches to improve model performance (Koren et al., 2003). For complex models (e.g. distributed models with many parameters) "manual" approaches are still a common practice today (e.g. Yilmaz et al., 2008; Braud et al., 2010; Rozalis et al., 2010; Fuamba et al., 2019) as automatic calibration procedures, in addition to being difficult to undertake, often do not yield satisfactory results (Beven and Binley, 1992). Such approaches are facilitated for distributed models as they can take advantage of spatial data in the inference of its parameter values thought either *"physical or conceptual"* relationships that may be established with catchment physical characteristics (Koren et al., 2003; Yilmaz et al., 2008). Automatic procedures can also be deployed to transform distributed parameters into lumped parameters considering either multiplicative factors (e.g. Krause et al., 2006) or regionalization methods with various degrees of sophistication (e.g. Pokhrel et al., 2012; Kumar et al., 2013)

Calibration of (distributed or not) models for ungauged catchments (i.e. catchments where no streamflow data are available) often rely on regionalization strategies from other gauged catchments (e.g. based on catchment proximity, and/or similarity in physical characteristics (topography, vegetation, soil, geology) (Wagener et al., 2007)). Another solution to tackle the issue of prediction in these catchments is the use of distributed models that can be set up over large areas that include gauged and ungauged catchments. For example, McMillan et al. (2016) developed a national distributed hydrological model for the whole New Zealand territory that included many ungauged catchments. They chose not to rely on any calibration, even for catchments where data was available. Instead, they used available data sets describing relevant landscape features of New Zealand and accounted for different climatic regions. The use of an uncalibrated model, although it often yields poorer performance, has important advantages. As stated by McMillan et al. (2016) (and other authors, e.g. Fuamba et al., 2019) the links between the parameters and physical characteristics of catchment are not lost during the calibration: the specified parameters are not affected by the choice of calibration metrics, biases in model inputs, or compensation for model structure errors or between parameters.

1.2.2 Diagnostic approach to model evaluation

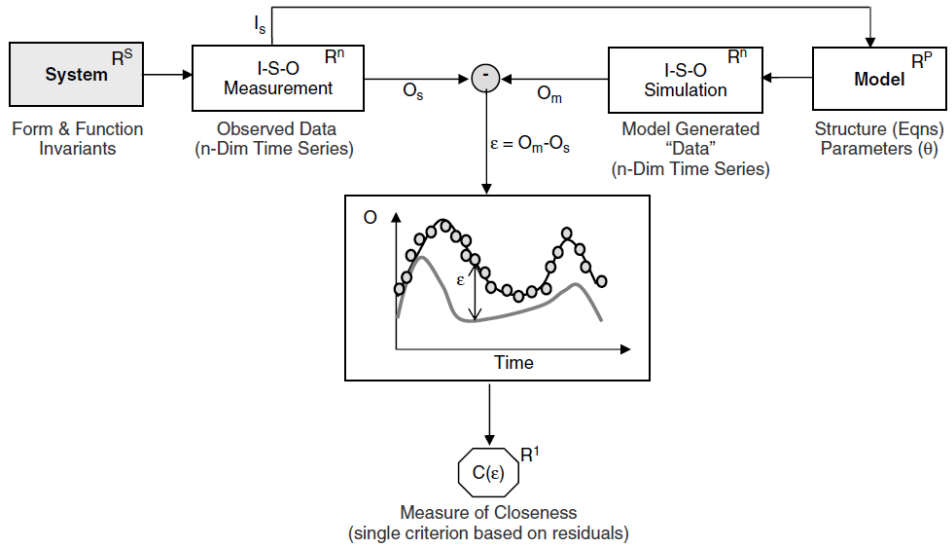

(a) Classical approach to model evaluation using regression based metrics to compare simulation with observation

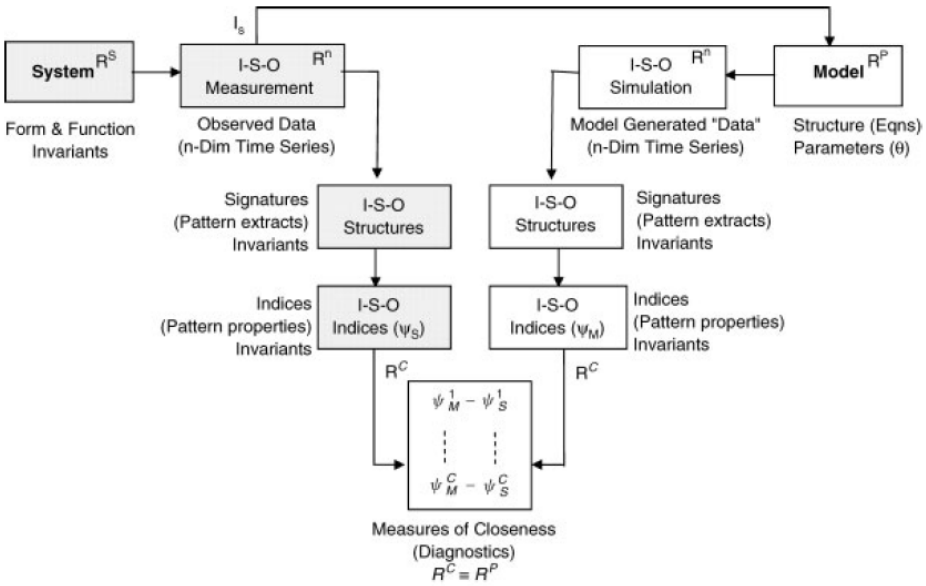

(b) Diagnostic approach to model evaluation using hydrological signatures to compare simulation with observation

Figure 1.5: Classical (a) and diagnostic (b) approach to model evaluation (from Gupta et al. (2008))

Regardless of the modeling approach (lumped, distributed, degree of complexity) and how model parameters were calibrated or specified, hydrological models need to be evaluated thoroughly. The model performance and its ability to represent the catchment in a realist and consistent way must be evaluated by confrontation with observation of the system behavior (catchment behavior) (Gupta et al., 2008). The common approach for the evaluation of a hydrological model is to compare streamflow simulations generated over a period in the past and to compare the results with observed streamflow data (Figure 1.5a). The comparison is typically based on a measure that summarizes the residual time series among which, the Nash-Sutcliffe efficiency (NSE) criterion (Nash and Sutcliffe, 1970) is the most widely used. As discussed by Schaefli and Gupta (2007), the NSE is difficult to interpret. Although multiple metrics can

be used, such as the percent bias, the NSE applied on log transformed streamflow value, or the Kling-Gupta efficiency (KGE), the evaluation remains limited given how poorly they can be related to specific behavior of the system (Gupta et al., 2008). The evaluation of a model should not only assess performance of the model, it should also evaluate how consistent/realistic model behavior is (Wagener, 2003), i.e. answers the question of whether the model has good performance for the right reasons (Klemeš, 1983; Grayson et al., 1992; Kirchner, 2006).

Model evaluation based on regression-based metrics typically yield poor diagnostics on the model, i.e. they – the regression-based metrics – are unable to identify what might be right or wrong in the model (Gupta et al., 2008). The evaluation of a hydrological model should not only aim at confronting the model with observations, it should address the question of *"how to link what we 'see' in the data to what is 'right' and 'wrong' with the model"* (Gupta et al., 2008). In other words, any evaluation methodology should be diagnostically meaningful as to be able to identify which part of the model is responsible for discrepancies found between simulations and observations. To this aim, Gupta et al. (2008) recommended that any evaluation methodology, to be diagnostically meaningful, should be rooted in hydrological theory, i.e. relate to our understanding (perceptual model) of the catchment functioning in terms of hydrological processes.

The large diversity of hydrological processes as depicted in Section 1.1.1 is the result of many experiments in catchments and hillslopes all around the world involving numerous measurements, detailed analyses and interpretations of their meaning in terms of hydrological processes. Collected data were typically analyzed in the context of some theories regarding the system functioning to test (validate/unvalidate) these theories or propose new ones. This process-based approach to consider data can overcome the limitation of model evaluation based on regression-based metrics. Instead of comparing observed and simulated data using these metrics, other "metrics" that characterize the data in a hydrological meaningful way could be used. These "process-based metrics" is what Gupta et al. (2008) call *"signature behaviors"*. These signature behaviors or hydrological signatures are the results of various analyses that can be done on data to extract their information content (Gupta et al., 2008). As illustrated in Figure 1.5b, an evaluation methodology that yields diagnostics on the model could be based on comparing observed and simulated hydrological signatures as their link to hydrological processes or at least our theories regarding the catchment functioning can help pinpoint which are the model components that need improvement (Gupta et al., 2008).

1.2.3 Hydrological signatures for the diagnostic and evaluation of models

Hydrological signatures can be defined as the results of any analysis of the data which, given our understanding of the system behavior (our theory), provides information on the hydrological functioning of a catchment. As pointed out by Gupta et al. (2008), this general definition of hydrological signatures makes the body of literature where they may be found very large and spanning multiple aspects of hydrological sciences. For example, Clausen and Biggs (2000) or Olden and Poff (2003) used flow variables or indices to describe different ecologically relevant aspects of the streamflow regime and related them to ecological processes for understanding and/or river management purposes. Ley et al. (2011) compared the results of catchment classification based on catchment physical characteristics or based on catchment response behavior

as described by *"key signature indices"*. Similarly, Sawicz et al. (2011) or Toth (2013) used hydrological signatures to classify hydrological catchments according to their similarity in terms of hydrological behavior. There are also examples where hydrological signatures are used to predict the hydrological functioning of ungauged catchments (e.g. Sauquet and Catalogne, 2011; Zhang et al., 2014). Finally, there are many examples of their use in the development (e.g. Farmer et al., 2003; Eder et al., 2003; McMillan et al., 2011; Clark et al., 2011b; Euser et al., 2013; Coxon et al., 2014), calibration (e.g. Shamir et al., 2005a; Westerberg et al., 2011; Pokhrel et al., 2012; He et al., 2015; Shafii et al., 2017) and evaluation of hydrological models (e.g. Yilmaz et al., 2008; McMillan et al., 2014; Fovet et al., 2015; Fuamba et al., 2019). In Section 1.3, hydrological signatures are presented in more detail.

Nowadays, the use of hydrological signatures instead of traditional regression-based metrics as calibration criteria in the calibration of models is common (e.g. Shamir et al., 2005b,a; Westerberg et al., 2011; Coxon et al., 2014; Pokhrel et al., 2012; Schaefli, 2016; Kundu et al., 2016; Mackay et al., 2018). As hydrological signatures may capture several contrasting aspects/features of streamflow that need to be reproduced by the model, calibration is expected to yield parameter sets that are more consistent. Such calibrations approaches typically rely on more or less complex sampling of the parameters space to generate multiple simulations. Afterwards, only "behavioral" parameter sets are selected, i.e. only the parameters sets that lead to simulations that are able to reproduce the hydrological signatures, are selected. In practice, they are often combined with traditional performance metrics. These studies, although they take advantage of hydrological signatures to extract more information from data than what are possible using classical performance metrics, are not related to the diagnostic approach to model evaluation as proposed by Gupta et al. (2008). These calibration approaches limit equifinality issues and likely yield more realistic and consistent models. However, they do not seek to evaluate the models in search of hydrological processes representations that could be improved.

1.2.3.1 Model development and model structure

Many studies investigate the use of hydrological signatures to evaluate multiple model structures as possible candidates to adequately represent the behavior of a catchment. For example, Euser et al. (2013) combined the capabilities of a Principal Component Analysis (PCA) with hydrological signatures to evaluate the performance and consistency of competing model structures (calibrated lumped models) for two small headwater catchments. A similar approach was followed by Hrachowitz et al. (2014). Coxon et al. (2014) investigated 78 model structures for 24 catchments using hydrological signatures to evaluate the different competing hypotheses. There are also examples of studies where authors study the effect of model distribution (e.g. Gharari et al., 2014; Euser et al., 2015; Fenicia et al., 2016) by differentiating for example wetlands, hill-slopes and plateaus (e.g. Gharari et al., 2014). Most of these studies rely on lumped models (or with very limited spatial distribution) with mostly simple structures. In addition, as in calibration approaches mentioned in the previous paragraph, hydrological signatures are often only considered as additional metrics rather than actual tools to derive information regarding the catchment behavior or scrutinize model functioning. There is no doubt that hydrological signatures used in these studies offer good capabilities to evaluate the performance and con-

sistency of the investigated models. However, the interpretation of hydrological signatures in terms of hydrological functioning and how detailed diagnostics on the evaluated model could be derived are not fully exploited.

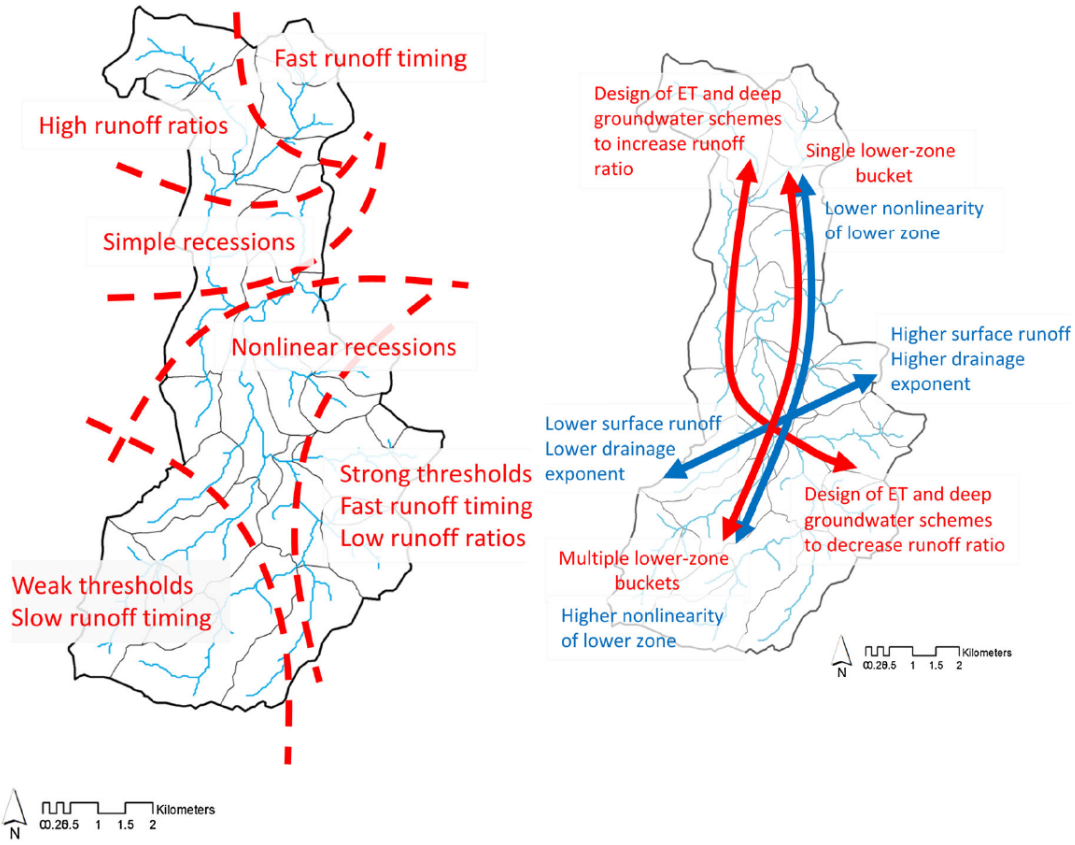

Figure 1.6: On the left, synthetic overview of the heterogeneity of hydrological processes found for the Mahurangi catchment in the study of McMillan et al. (2014) using hydrological signatures and, on the right, the derived recommendations regarding model structure (red arrows) or model parameters (blue arrows) variations across the catchment (from McMillan et al. (2014))

A contrasting example might be the two-part study of McMillan et al. (2011) and Clark et al. (2011b). They used hydrological signatures to first (1) identify important features in the hydrological response of two small experimental catchments (McMillan et al., 2011) in order to (2) select and evaluate different lumped conceptual models (Clark et al., 2011b). They based their evaluations and diagnostic on a detailed description and implication of the different hypotheses (model components) for representing different hydrological processes (overland flow and infiltration, soil storage and drainage, evapotranspiration, baseflow). Clark et al. (2011b) evaluated the model structure based on the knowledge acquired by *prior* analysis of the data (using hydrological signatures) of McMillan et al. (2011) along with visual comparisons between observed and simulated hydrological signatures. Interestingly, one of their results was that only the most complex model structure was able to reproduce some of the hydrological signatures suggesting the need for more complex, process based models (Clark et al., 2011b). Their approach was deeply rooted in hydrological theory with, as primary focus, the models abilities to realistically represent identified important aspects of catchment behavior.

There are other similar examples such as the study of Wrede et al. (2015) who used hydrological signatures and chemical tracer data to build a perceptual model of the functioning of 3 catchments before testing different model structures. McMillan et al. (2014) also did an

in-depth analysis of data using hydrological signatures to derive recommendations for the development of a model. They derived a synthetic overview describing the spatial heterogeneity of the dominant hydrological processes in the catchment (see Figure 1.6) highlighting the need for different processes representations in the model depending on location. They suggested that different model structures should be used for different sub-catchments or that a distributed and more complex model – flexible enough to account for this heterogeneity – should be set up. Figure 1.6(right) illustrates their recommendations regarding how model structure or model parameterization should vary in space.

1.2.3.2 Distributed models and the use of sensitivity analysis

Distributed models involve more complex structures (see Subsection 1.1.2). Due to their complex structure and the number of parameters they rely on, the evaluation of such models is often more difficult to undertake. Similarly to lumped models, they are most of the time only evaluated using regression-based metrics considering observed and simulated streamflow at the catchment outlet (e.g. Krause, 2002; Krause et al., 2006; Anquetin et al., 2010; Rozalis et al., 2010; Pokhrel et al., 2012; Kumar et al., 2013; Vandana et al., 2018). However, there are examples of more in-depth model evaluation aiming at providing diagnostic on the models using additional spatial data (e.g. Mendiguren et al., 2017; Fuamba et al., 2019), investigating internal model components (e.g. Pfannerstill et al., 2015; Guse et al., 2016a,b) or using hydrological signatures (e.g. Yilmaz et al., 2008; McMillan et al., 2016; Höllering et al., 2018). In such studies, the focus is on the model parameters and overall realism of hydrological processes representation.

There are a few examples where the diagnostic and evaluation of a distributed models rely on a sensitivity analysis. From the results of various previous studies about the catchment Pfannerstill et al. (2015) studied, they derived a number of hypotheses regarding how the catchment is supposed to behave in different periods of the year. Using a temporal sensitivity analysis (TEmporal Dynamic PAramater Sensitivity, TEDPAS) with the simulated streamflow at each day as target, they verified whether the processes dominance – inferred from the time series of sensitivity indices of each parameters – in different periods of the year corresponded to their *prior* hypotheses. Such a temporal analysis of sensitivity were also conducted by Guse et al. (2016a,b) focusing on different modeled components i.e. internal state variables or fluxes. Although they did not use hydrological signatures, these approaches provided relevant diagnostics information on models. Most commonly, sensitivity analysis of distributed models is done using regression-based metrics as targets. More recently, other variables have been used as targets (e.g. Pfannerstill et al., 2015; Guse et al., 2016a,b), but, as noted by Höllering et al. (2018), only a few studies use hydrological signatures (e.g. Yilmaz et al., 2008; Höllering et al., 2018).

In the context of an uncalibrated distributed model – *a priori* parameter estimates derived from soils and vegetation data – Yilmaz et al. (2008) undertook a diagnostic-evaluation based on hydrological signatures. They first performed a sensitivity analysis to check the consistency between hydrological signatures and the model parameters i.e. hydrological signatures targeting specific hydrological processes were checked to be affected by the parameters controlling these hydrological processes. This enabled them to successfully identify key parameters and derive

qualitative recommendations to improve the model. They then followed an automatic step-wise approach to constrain the parameters having the strongest effects. They were able to improve the match between some of the used hydrological signatures and to identify the main weaknesses in the model structure.

Similarly, in their study, Höllering et al. (2018) aimed at identifying sensitive parameters of a conceptual distributed model with respect to different hydrological signatures, for a set of 14 headwater catchments. They did not focus much on the discrepancies between observation and simulation. They focused more on establishing the links between hydrological signatures and model parameters. Although only little attention was given to the interpretation of the hydrological signatures themselves in terms of hydrological processes, their results provided an in-depth diagnostic of the model that they argued could be used for its improvement.

1.2.4 Conclusion

Although many sophisticated calibration methods are now used (e.g. multi-variate, multi-objective, limit of acceptability approaches), they are still too often simply based on streamflow time series and regression-based metrics (Gupta et al., 2008). It is today increasingly recognized that a shift from pure performance (as measure with regression-based metrics) towards process consistency is needed. In particular, models should not only have good predictive performance, they should behave and simulate the *"right"* catchment responses for the *"right"* reasons (Kirchner, 2006). Illustrating and contributing to this shift of paradigm, Gupta et al. (2008) outlined the diagnostic approach to model evaluation using hydrological signatures.

Hydrological signatures have been increasingly used since then to go towards more process based approaches to develop, calibrate/constraint, and evaluate hydrological models. However, when used in *posterior* evaluation of models they are most of the time used merely as additional metrics along classical regression-based metrics. There are however notable examples of studies where hydrological signatures are thoroughly used to evaluate models and help in the model development process. Only a few studies exploit the full potential of hydrological signatures in terms of interpretation regarding hydrological processes and/or model functioning, to derive useful diagnostics on models. In the case of distributed models, most of the existing studies take advantage of both hydrological signatures and the capabilities of sensitivity analysis to help in the diagnostic of models.

1.3 Hydrological signatures

As argued by Gupta et al. (2008), regression based metrics, such as the Nash-Sutcliffe efficiency, because they are poorly related to hydrological processes, are limited in terms of diagnostic power when evaluating a hydrological model. Instead of regression based metrics, they proposed to use process-based metrics, the so-called hydrological signatures, which can be more closely related to hydrological processes. As illustrated in the previous section, hydrological signatures have gained popularity in the modeling community for the development, calibration, and evaluation of hydrological models. Depending on authors, hydrological signatures can either be statistics to summarize the data in a few relevant *"indices"* or *"variables"* (e.g. Clausen and Biggs, 2000; Olden and Poff, 2003), plots or values that highlight relevant *"signals"* (e.g. Shamir et al., 2005b; Kundu et al., 2016), *"patterns"* (e.g. Eder et al., 2003; Yilmaz et al., 2008) or *"characteristics"* (e.g. Shamir et al., 2005a; Yadav et al., 2007; Yilmaz et al., 2008) in the data, or indicators resulting from more complex data analyses (e.g. McMillan et al., 2011, 2014). In this section we review the hydrological signatures used in the modeling community highlighting the main current limitations. We discuss the building of a hydrological signature set and how the relevance of individual hydrological signature should be evaluated.

1.3.1 An overview of hydrological signatures

Different hydrological signatures have been used in the modeling community following different data analysis approaches as summarized in Table 1.1. The different types of approaches described in Table 1.1 can roughly be categorized as follow: (1) flow magnitudes with no consideration of timing using the flow duration curve, (2) long term water partitioning in terms of volumes – between evapotranspiration and streamflow (the runoff coefficient) or between fast and slow flow volumes (the baseflow index) –, (3) catchment reactivity or timing characteristics – auto-correlation analysis, cross-correlation analysis, event timing analysis, rising and declining limb density, flashiness index –, (5) event scale water partitioning – event runoff coefficients – and (5) catchment storage-discharge relationship – analysis of the recessions.

As indicated by the number of references associated with the analysis of the flow duration curve (FDC) in Table 1.1, the FDC is the most commonly used approach to derive hydrological signatures (e.g. Yilmaz et al., 2008; Westerberg et al., 2011; Pokhrel et al., 2012; Casper et al., 2012; Euser et al., 2013; Vrugt and Sadegh, 2013; Hrachowitz et al., 2014; Coxon et al., 2014; Pfannerstill et al., 2014; Zhang et al., 2014; Gharari et al., 2014; Wrede et al., 2015; Fovet et al., 2015; Guse et al., 2016a; Kundu et al., 2016; Ley et al., 2016; McMillan et al., 2016; Fenicia et al., 2018; Höllering et al., 2018; Mackay et al., 2018, 2019; Todorović et al., 2019). The FDC is the empirical cumulative distribution of streamflow typically derived from hourly, daily or monthly streamflow time series (Vogel and Fennessey, 1994). For a given streamflow value, the FDC indicates the percentage of time the value was equaled or exceeded. As the FDC is a curve, several approaches have been used to derive single values to characterize it (see Figure 1.7). Typically, specific streamflow values corresponding to specific exceedance probability can be extracted (e.g. Westerberg et al., 2011; Casper et al., 2012; Pokhrel et al., 2012; Coxon et al., 2014; Höllering et al., 2018; Mackay et al., 2019; Todorović et al., 2019). The FDC can also be subdivided into several segments (e.g. Yilmaz et al., 2008; Casper et al.,

Table 1.1: Data analysis approaches commonly used to derive hydrological signatures.

Name	Description	References
Flow Duration Curve (FDC)	Empirical cumulative distribution of streamflow: for a given streamflow value, the FDC indicates the percentage of time the value was equaled or exceeded. The hydrological signatures derived from the FDC include specific percentile and slopes of high or medium segment of the FDC.	Yilmaz et al. (2008); Westerberg et al. (2011); Pokhrel et al. (2012); Casper et al. (2012); Euser et al. (2013); Vrugt and Sadegh (2013); Hrachowitz et al. (2014); Coxon et al. (2014); Pfannerstill et al. (2014); Zhang et al. (2014); Gharari et al. (2014); Wrede et al. (2015); Fovet et al. (2015); Guse et al. (2016b); Kundu et al. (2016); Ley et al. (2016); McMillan et al. (2016); Fenicia et al. (2018); Höllering et al. (2018); Mackay et al. (2018, 2019); Todorović et al. (2019)
Runoff coefficient	Ratio between the volume of streamflow and the volume of precipitation.	Yilmaz et al. (2008); Pokhrel et al. (2012); Vrugt and Sadegh (2013); Pfannerstill et al. (2014); Hrachowitz et al. (2014); McMillan et al. (2014); Zhang et al. (2014); Fovet et al. (2015); Westerberg and McMillan (2015); Teutschbein et al. (2015, 2018); Höllering et al. (2018)
Baseflow index	Ratio between the volume of baseflow and the volume of total streamflow; the baseflow component of streamflow is typically derived using a digital filter.	Vrugt and Sadegh (2013); McMillan et al. (2016); Fenicia et al. (2016); Pool et al. (2017); Fenicia et al. (2018); Höllering et al. (2018)
Autocorrelation	Streamflow autocorrelation; typically the 1-day lag autocorrelation of streamflow is considered.	Euser et al. (2013); Hrachowitz et al. (2014); Fovet et al. (2015); Kundu et al. (2016); Höllering et al. (2018); Mackay et al. (2018, 2019); Todorović et al. (2019)
Rising (declining) limb density	Ratio between the number of streamflow peaks and the total duration of rising (or declining) parts of streamflow.	Shamir et al. (2005b); Euser et al. (2013); Hrachowitz et al. (2014); Fovet et al. (2015); McMillan et al. (2016); Mackay et al. (2018)
Streamflow recessions	Analysis of the characteristics of the streamflow recessions; hydrological signatures that can be derived often include the recession time.	McMillan et al. (2011, 2014); Clark et al. (2011b); Pool et al. (2017); Höllering et al. (2018)
Cross-correlation	Correlation between streamflow and precipitation; the hydrological signatures used is the time taken for the correlation coefficient to drop below some threshold value.	Yilmaz et al. (2008); Wrede et al. (2015)
Flashiness Index	Sum of absolute values of streamflow differences (from one day to the next) divided by the sum of streamflow values.	Fenicia et al. (2016, 2018)
Event runoff coefficient	Ratio between event streamflow (or quickflow) volume and event precipitation volume.	McMillan et al. (2011); Clark et al. (2011b); Casper et al. (2012); McMillan et al. (2014); Ley et al. (2016)
Event timing	Time lag between the center of mass of event precipitation volume and event streamflow volume.	McMillan et al. (2011); Clark et al. (2011b); McMillan et al. (2014)

2012; Pokhrel et al., 2012; Pfannerstill et al., 2014; Guse et al., 2016a; Kundu et al., 2016; Ley et al., 2016; Mackay et al., 2018) or considered as whole (e.g. Euser et al., 2013) using some measure of distance between observed and simulated FDC (e.g. Nash-Sutcliffe efficiency (Euser et al., 2013), Root Mean Square Error (Pfannerstill et al., 2014), percent bias (Yilmaz et al., 2008; Pokhrel et al., 2012)). These approaches allow studying the catchment response in various conditions (Yilmaz et al., 2008; Euser et al., 2013): response to major event mainly driven by quickflow (high segment), response to intermediate event combining quickflow and baseflow (mid-segment) and response in low flow condition mainly controlled by groundwater discharge and evapotranspiration (low segment). The slope of the mid-segment of the FDC is also often used (e.g. Yilmaz et al., 2008; Casper et al., 2012; Pokhrel et al., 2012; Pfannerstill et al., 2014; Ley et al., 2016; Höllering et al., 2018; Mackay et al., 2018). A steep slope is an indication of a variable flow regime (Sawicz et al., 2011; Wrede et al., 2015) or small storage capacity (Yilmaz et al., 2008). On the other hand, a flat slope is an indication of low seasonality (Sawicz et al., 2011; Wrede et al., 2015) and/or large groundwater contribution due to large storage capacity (Yilmaz et al., 2008; Sawicz et al., 2011). More complex approaches can also be adopted, such as fitting a model to the FDC whose parameters can then be used as hydrological signatures (e.g. Vrugt and Sadegh, 2013; Zhang et al., 2014; Sadegh et al., 2016).

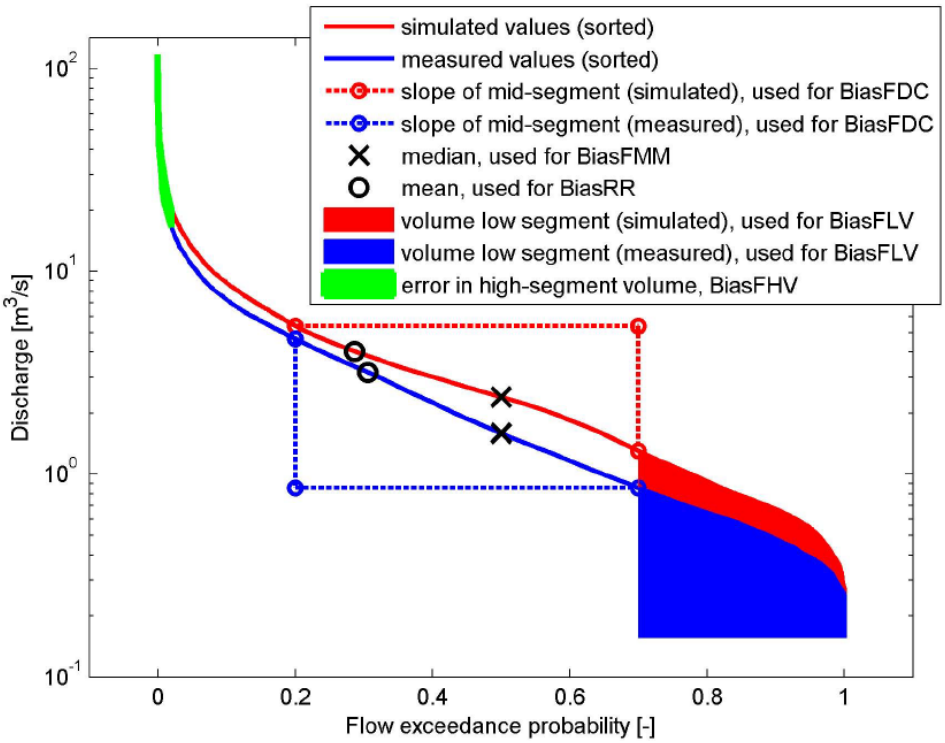

Figure 1.7: Example of flow duration curve and typical hydrological signatures that are used: high segment, low segment, median, mean, mid-segment slope (from Casper et al., 2012); in this example, observed and simulated hydrological signatures are directly compared using the percent bias.

Another commonly used hydrological signature is the runoff coefficient (Table 1.1). It is the ratio between the total volume of streamflow over the total volume of precipitation. It is used as a measure of the partitioning of input precipitation between streamflow and evapotranspiration (e.g. Yilmaz et al., 2008; Pokhrel et al., 2012; Vrugt and Sadegh, 2013; Pfannerstill et al., 2014; McMillan et al., 2014; Hrachowitz et al., 2014; Zhang et al., 2014; Fovet et al., 2015; Westerberg and McMillan, 2015; Teutschbein et al., 2015, 2018; Höllering et al., 2018). It is based on the

conservation of mass applied at the catchment scale (Equation 1.1): input water (precipitation, P) is released from the catchment either as evapotranspiration E or as streamflow Q.

$$\mathrm{d}S/\mathrm{d}t = P - E - Q \tag{1.1}$$

where $\mathrm{d}S/\mathrm{d}t$ is the variation of stored water in the catchment. For long enough periods (e.g. more than 10 years), storage variations can be neglected. Consequently, precipitation can be considered equaled to the sum of evapotranspiration and streamflow and the ratio Q/P gives the long term partitioning of water between evapotranspiration and streamflow.

Table 1.1 present other hydrological signatures that are commonly used although less often than the FDC based hydrological signatures or the runoff coefficient. Among these hydrological signatures, the baseflow index is relatively popular to study the long term partitioning between fast and slow flow. It is based on the separation of streamflow into a quick and fast flow component using a streamflow separation algorithms. Authors also often consider hydrological signatures that focus on the catchment reactivity. This is the case of the cross correlation between streamflow and precipitation (e.g. Yilmaz et al., 2008): the time lag at which the cross-correlation coefficient is maximized can be seen as a characteristic reaction time of the catchment. Others consider the auto-correlation structure of streamflow (e.g. Euser et al., 2013), the rising/declining limb density (e.g. Sawicz et al., 2011; Euser et al., 2013) or flashiness index (e.g. Fenicia et al., 2016) which they use as measures of hydrograph smoothness. They are often more difficult to relate to a particular aspect of the catchment functioning. Statistics derived from streamflow such as the annual streamflow average, monthly streamflow average or the coefficient of variation of streamflow are also often used as hydrological signatures (e.g. Coxon et al., 2014; Höllering et al., 2018; Mackay et al., 2018, 2019; Todorović et al., 2019; Pool et al., 2017; Zhang et al., 2014). These statistics also quantify streamflow characteristics that are often difficult to relate to particular hydrological processes. There is a large list of possible statistics (see for example, the long list proposed by Olden and Poff (2003)) and they were not reported in Table 1.1.

Other hydrological signatures which are seldom used investigate catchment behavior at the catchment scale focusing on event timing or event volume partitioning. For example, the average duration between the center of mass of event precipitation and event streamflow can be used to derive a characteristic catchment reaction time (e.g. McMillan et al., 2011). Another seldom used analysis approach is the analysis of streamflow recessions, i.e. declining parts of streamflow time series. The analysis of recession as a long history in hydrology to study the storage-discharge relationship of a catchment (e.g. Brutsaert and Nieber, 1977; Wittenberg and Sivapalan, 1999; Kirchner, 2009; Stoelzle et al., 2013). However, there are only a few examples of hydrological signatures derived from this type of analysis. For example, (McMillan et al., 2014) used a recession analysis to derive (1) an average catchment storage-discharge time characteristics and (2) a measure of catchment complexity or heterogeneity in terms of storage-discharge characteristics.

Most of the hydrological signatures presented here are based on streamflow time series. Other data may be used to derive hydrological signatures such as groundwater levels (e.g. Hrachowitz et al., 2014; Fovet et al., 2015; Heudorfer et al., 2019), soil moisture measurements (e.g. McMillan et al., 2011, 2014; Fuamba et al., 2019; Branger and McMillan, 2020), snow

cover extent derived from satellite data (e.g. Mackay et al., 2018). However, they rely on data that have coarse time resolution (e.g. satellite data) or that are far less available than streamflow which makes them usable only in a limited number of experimental catchments. On the other hand, streamflow is nowadays monitored in most countries via national or international monitoring networks (Mishra and Coulibaly, 2009). Similarly, meteorological data (e.g. precipitation, temperature, wind, radiation, etc.) are also widely available, in particular because of the increasing availability of climatic reanalysis products (e.g. Vidal et al., 2010; Caillouet et al., 2016). Only few studies take advantage of other data than streamflow that may however be widely available such as temperature data or solar radiations, wind, etc. A rare example is the study of Schaefli (2016) who used air temperature data to design hydrological signatures targeting snow processes.

1.3.2 Building a set of hydrological signatures

Hydrological signatures are typically used to focus on different aspects of catchment behavior as overviewed in the previous subsection. Therefore, authors often rely on multiple hydrological signatures. In a commentary, McMillan et al. (2017) briefly discussed the selection of hydrological signatures and noted that, in most of the studies they reviewed, little or no reason to justify the chosen set of hydrological signatures were reported. Many authors only mention that they selected multiple hydrological signatures to target different aspect of the streamflow and/or build their selection on previous work (e.g. Euser et al., 2013; Vrugt and Sadegh, 2013; Hrachowitz et al., 2014; Fenicia et al., 2018). In the next paragraphs, the way different authors chose to build their hydrological signatures set is briefly reviewed.

In the context of prediction of hydrological behavior in ungauged catchment Yadav et al. (2007) used a long list of possible hydrological signatures they mostly borrowed from hydro-ecological studies (Clausen and Biggs, 2000; Olden and Poff, 2003), that they divided into the following seven categories: *"magnitude of high flows, magnitude of low flows, magnitude of average flows, duration of flows, frequency, rate of change in flows, and timing of flow events"* (Yadav et al., 2007). Although many of the hydrological signatures they used were statistics (monthly max, mean, etc.) they aimed at characterizing the overall catchment behavior from widely available data (streamflow, precipitation and evapotranspiration) in a non-redundant way. Similarly, to assess the effect of climate change on catchment behavior Teutschbein et al. (2015) used hydrological signatures following the classification of Olden and Poff (2003) to characterize *"seasonal patterns, frequency/timing/duration of extreme flows as well as seasonal and annual flow variability"*. Another similar example of hydrological signatures selection is the study of Pool et al. (2017) who characterize different aspects of streamflow according to *"magnitude, ratio, frequency, variability, and date"*.

The choice of hydrological signatures may also be guided by the available data and objectives. McMillan et al. (2011) chose signatures according to the data types used (streamflow, precipitation, soil moisture) and their choices of model structure. In practice they attempted to characterize (1) the storage-discharge relationship of the catchment, (2) the behavior of water in the saturated and unsaturated zone associated with the balance between overland flow, subsurface flow, drainage, and threshold behaviors in the streamflow response. Mackay et al. (2018) also considered hydrological signatures from different types of data (ice melt data, snow

coverage data and streamflow). They subdivided the 33 selected hydrological signatures according to different aspects: average monthly streamflow, fast and slow streamflow generation (using the FDC), the timing and variance of streamflow and streamflow flashiness.

Following McMillan et al. (2011) who argue on the need to base the choice of hydrological signatures on available data and Sawicz et al. (2011) who insisted on the need to have interpretable link with catchment function, McMillan et al. (2014) chose signatures according to four *"themes"* related to characteristics of the (1) water balance, (2) hydrograph (event timing), (3) recessions, and (4) hydrological thresholds. This interpretable link with catchment function is also the basis of the hydrological signature selection in the study of Yilmaz et al. (2008). They selected hydrological signatures that they could relate to catchment function that they defined as (1) the overall water balance, (2) the vertical distribution of water between the fast and slow streamflow generation processes, (3 and 4) the redistribution of water in time and space. This approach follows the suggestion of Wagener et al. (2007) who proposed a perceptual model of catchment functioning that could be summarized in three main functions: partition, storage and release. Following such an approach can help selecting only hydrological signatures that can be related to hydrological processes and that collectively address all or most of the processes represented in a model.

1.3.3 Selecting/designing hydrological signatures

As highlighted in the previous subsection, hydrological signatures are often selected with little justifications. In addition, little attention is often given to the design of the hydrological signatures themselves. In particular, the relevance of the hydrological signatures are seldom assessed or even discussed. McMillan et al. (2017) provided a set of guidelines when selecting hydrological signatures to promote a more rigorous approach in the selection or design process. These guidelines are: (1) identifiability (the uncertainty associated with the hydrological signature should be small compared to the range of possible values it is likely to take), (2) robustness (the data collection design should not affect the hydrological signature), (3) consistency (the hydrological signatures should *"be comparable across catchment and insensitive to irrelevant factors"*), (4) representativeness (the hydrological signature should represent *"emergent, catchment-scale behavior"*) and (5) discriminatory power (differences in hydrological signature should reflect differences in hydrological functions of catchments and similar hydrological signature should reflect similar hydrological functioning). Although not stated explicitly, authors are most of the time concerned by the ability of the hydrological signatures to capture emergent catchment scale processes, i.e. the representativeness of the hydrological signatures (point 4 in McMillan et al. (2017)'s guidelines).

An important point raised in the guidelines of McMillan et al. (2017) is the sensitivity of hydrological signatures to uncertainty in the data (identifiability). Uncertainties in hydrological signatures may affect conclusions in studies where they are compared (Westerberg and McMillan, 2015) either between observation and simulation or between catchments. Measurements are affected by uncertainties that stem from many sources as reviewed by McMillan et al. (2012) for different types of hydrological data. As summarized by Westerberg and McMillan (2015), the main uncertainties in data that may affect hydrological signatures are due to: (1) measurement uncertainty (due to the instruments), (2) measurement representativeness (e.g. point

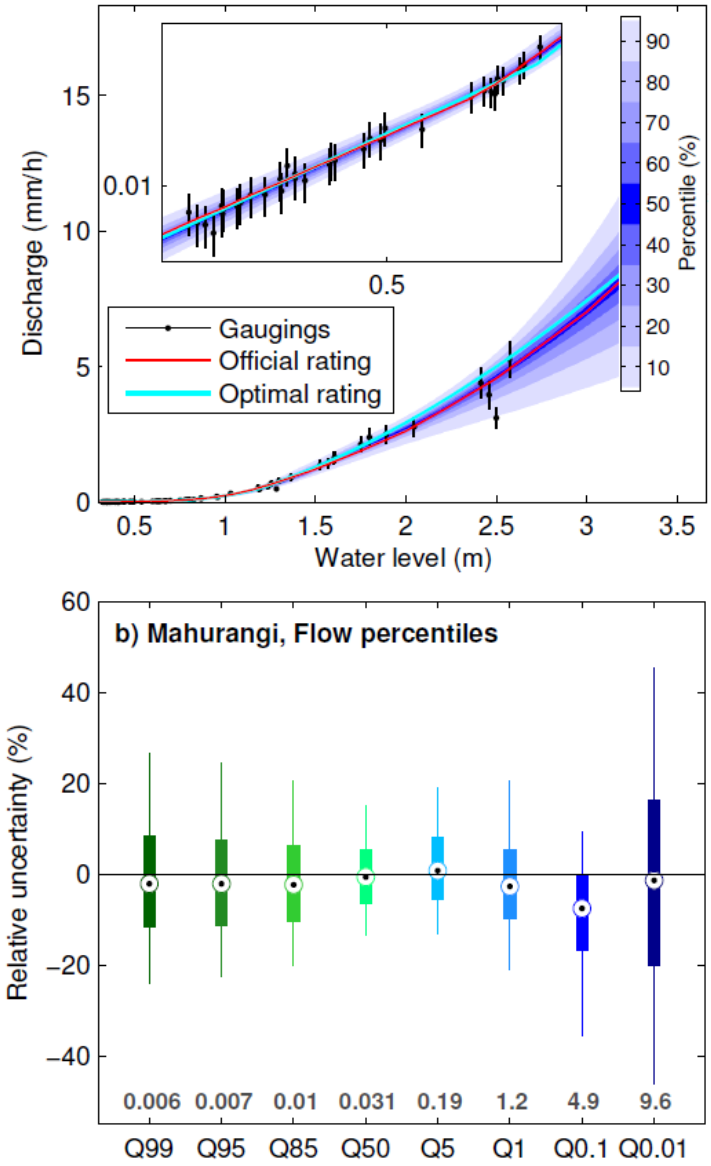

Figure 1.8: Example of uncertain in the rating curve and gaugings (top) and how different flow percentile (bottom) are affected by rating curve uncertainty (from Westerberg and McMillan 2015)

measurement *versus* catchment scale value) and (3) data management uncertainty (e.g. filling of missing values). Not many authors account for uncertainty when computing hydrological signatures. There are example, particularly in the calibration of hydrological models where uncertainties are used as bounds in Limit-Of-Acceptability frameworks (e.g. Westerberg et al., 2011; Coxon et al., 2014; Mackay et al., 2018). In these studies, the uncertainty due to the rating curve (i.e. relationship between water stage in the river and streamflow) is considered to compute the uncertainty associated with streamflow time series and hydrological signatures. In their study, Westerberg and McMillan (2015) considered the uncertainty associated with precipitation data (due to point measurement errors, instrument malfunction and interpolation errors) and streamflow data (due to the gaugings, i.e. individual measurements of both stage and streamflow at different flow magnitude which are used to calibrate the rating curve, and the approximation of the true relation between stage and streamflow, see Figure 1.8). They investigated the effects of uncertain data on different hydrological signatures. They found that the rating curve uncertainty could significantly affect the FDC. As shown in the bottom panel

of Figure 1.8, the uncertainty in the percentiles of the FDC mirror the uncertainty in the rating curve. The midsegment slope of the FDC was also found heavily influenced by rating curve uncertainty. The total runoff coefficient, that depends on both precipitation and streamflow, was found to be dominated by streamflow uncertainty. They also investigated the effect of subjective choices in the computation of hydrological signatures. For example, they found that using daily streamflow data instead of hourly streamflow data in the analysis of streamflow recessions led to significant differences, since within a single day, the shape of recessions could change dramatically in the catchment they studied.

Taking the FDC as an example, McMillan et al. (2017) argue that the robustness of the low section of the FDC could be significantly affected by the period of record used (see Vogel and Fennessey (1994)) as a consequence of rare prolonged drought that may have occured during a particular period. In addition, McMillan et al. (2017) demonstrated (using synthetic data) that the use of the mid-segment slope of the FDC could mask the importance of large and flashy contributions from one tributary. They demonstrated that this signature can represent *"accumulated flow behavior rather than average upstream behavior"* highlighting a possible issue in the representativeness of this hydrological signature. They argue that the mid-segment of the FDC should be used in combination with hydrological signatures characterizing its high flow segment to avoid possible misinterpretation.

For a hydrological signature to have discriminatory power, it must mirror difference in hydrological processes – that are targeted by the hydrological signature in question – between catchments (McMillan et al., 2017). When used in a modeling context, the discriminatory power can refer to how well it is able to constrain the model calibration such as in the Limit-of-Acceptability approach of Schaefli (2016). It can also be assessed in terms of how well it relates to specific components of a model (those representing the hydrological processes targeted by the hydrological signature) or even specific model parameters. Typically, sensitivity analyses using the hydrological signatures as targets can be used for that purpose (e.g. Yilmaz et al., 2008; Höllering et al., 2018). In the context of diagnostic-evaluation of hydrological model, the discriminatory power of a given hydrological signature can correspond to its diagnostic power, i.e. how well it is able to pinpoint precisely the model component or model parameter.

1.3.4 Conclusion

Hydrological signatures may be defined as the results, in the form of scalars (indices), of any analysis of hydrological data. Such a definition may include a large variety of data analysis and hydrological signatures. However, most of the studies rely on the same hydrological signatures. The most used hydrological signatures are derived from the FDC (e.g. percentiles, slopes of the mid-segment).

When building a set of hydrological signatures, there are many examples where authors give only little justification (McMillan et al., 2017). They often aim at capturing different aspect of the catchment behavior, typically focusing on different flow magnitudes with the FDC. Others justify the selection to capture the main functions of a catchment that typically include the partitioning of water (1) between streamflow and evapotranspiration (water balance), (2) between fast and slow streamflow generation processes. This approach can help in selecting hydrological

signatures that address all or most hydrological processes. Most of the hydrological signatures used are only based on streamflow time series, sometimes in combination with precipitation data (e.g. runoff coefficient). Although other relevant meteorological data are arguably also widely available (e.g. air temperature), they are almost never used.

The hydrological signatures themselves should be assessed in terms of their identifiability, robustness, consistency, representativness and discriminatory power (McMillan et al., 2017). The uncertainty of observed data (streamflow time series, precipitation) inevitably affect hydrological signatures (Westerberg and McMillan, 2015). They are most of the time not accounted for even though they may change conclusion when comparing catchments or observations with simulations. Moreover, assessing their discriminatory power or diagnostic power is particularly important when they are used in the context of diagnostic-evaluation of hydrological models.

1.4 Synthesis and research objectives

The review of the literature reveals the increasing popularity of hydrological signatures, in particular in the modeling community. Many directions to further explore hydrological signatures and their use are possible and, as highlighted in this review, several research gaps can be identified. The work presented in this PhD thesis addresses these gaps, summarized in the paragraphs below.

1.4.1 Identified research gaps

Under-evaluation of distributed models

Over the years, it has been gradually recognized that hydrological models should not only yield accurate prediction, they should be more rooted in hydrological theory and behave in a realistic and consistent way (Clark et al., 2016). Process-based distributed hydrological models can account for the diversity and spatial heterogeneity of hydrological processes. However, they rely on many parameters difficult to identify and are often under-evaluated (e.g. using only regression based metrics). The diagnostic approach to model evaluation based on hydrological signatures, as proposed by Gupta et al. (2008), is a promising way forward. However, it has only seldom been undertaken in the case of distributed models (e.g. Yilmaz et al., 2008; McMillan et al., 2016; Höllering et al., 2018).

Low diversity of hydrological signatures

Hydrological signatures are increasingly used for the calibration and the diagnostic-evaluation of hydrological models. However, the review of the literature shows that many studies overly rely on the flow duration curve to extract different indices describing its shape or to focus on specific streamflow magnitudes. The flow duration curve is often used in combination with other hydrological signatures such as the runoff coefficient, the streamflow auto-correlation or the rising limb density but the diversity of hydrological signatures used remain low. In addition, although there are other hydrological data that are both widely available and meaningful to characterize and quantify hydrological processes, mostly streamflow and precipitation data are used to derive hydrological signatures. In particular, data related to the energy input (e.g. solar radiation, air temperature) have rarely been used (Schaefli, 2016).

Weak use of the diagnostic power of hydrological signatures

Hydrological signatures used in the diagnostic and evaluation of hydrological models are often used simply as additional metrics to check the overall consistency of models (e.g. Pokhrel et al., 2012; Euser et al., 2013; Fenicia et al., 2016). Their interpretation in terms of catchment functioning or model functioning is often overlooked or weakly exploited. This is also the case when hydrological signatures are used in combination with a sensitivity analysis (e.g. Yilmaz et al., 2008; Höllering et al., 2018) although such an approach appear to be a promising way forward. Hydrological signatures should be as closely related to the underlying hydrological processes as possible to ensure stronger diagnostic power, i.e. how well they might be able

to identify what is wrong or right in a given model. In addition, the information content of hydrological data that is extracted using hydrological signatures, is inevitably reduced by the uncertainty associated with data which, in turns, reduce the diagnostic power of the hydrological signatures. Only few studies consider uncertainty when using hydrological signatures although it has been demonstrated that uncertainty could change interpretations (Westerberg and McMillan, 2015).

1.4.2 Research objectives and general methodology of the PhD

The main gaps listed above are addressed in this PhD thesis by focusing on two specific scientific questions:

How and how much information can be extracted from common hydrological data using hydrological signatures? Using only widely available data, but including more data than only streamflow and precipitation, the research presented in this manuscript focuses on the building of a set of hydrological signatures, going beyond the ones that are currently massively used in the modeling community. They should collectively address most of the hydrological processes relevant for a particular hydro-climatic context. As the set of hydrological signatures represents the information extracted from data, they should be linked as strongly as possible to particular hydrological processes to ensure reliable interpretations and diagnostic power. In addition, uncertainty is accounted for to avoid misinterpretations when used in the diagnostic and evaluation of a hydrological model.

How and how far can hydrological signatures be used to evaluate and derive diagnostics on a process-based distributed model? The research presented here also focuses on the evaluation and diagnostic of a distributed process-based model. Focusing on a reduced set of catchments, hydrological signatures are used to (1) evaluate the model by comparing observed and simulated hydrological signatures, (2) derive diagnostics by clearly identifying the model components and model parameters at fault for any processes that were found to be badly simulated and (3) provide and test recommendations for improving the accuracy, realism and process consistency of the model.

Research methodology

The research is based on two different datasets: (1) 10 small headwater mountainous catchments located in the Southern Sierra Nevada of California (USA) which are snow dominated catchment located under a Mediterranean climate and (2) 4 headwater catchments of the Ardèche catchment (France) characterized by a Mediterranean climate. The development of the methodology for the evaluation and diagnostic of a model relies on the J2000 process-based and distributed model, set up on the Ardèche catchment.

The selection of hydrological signatures from the literature along with the adaptation or development of new hydrological signatures that address different hydrological processes and aspects of the catchment behavior is detailed in two chapters: (1) in Chapter 3, snow dedicated hydrological signatures – using air temperature data in addition to precipitation and

streamflow data – are tested and evaluated in the context of the Southern Sierra catchments; (2) in Chapter 4, hydrological signatures – based only on precipitation and streamflow data – are presented in the context of the Ardèche catchment and the J2000 Ardèche model with a particular attention to their interpretations and potential diagnostic powers.

The careful selection and design of hydrological signatures is the basis for the evaluation and diagnostic the J2000 Ardèche model following the approach proposed by Gupta et al. (2008). In Chapter 5, using the hydrological signatures as targets, a sensitivity analysis of 4 sub-catchments of the J2000 Ardèche model is detailed: (1) links between hydrological signatures and model parameters / components are established, (2) the interpretations of the hydrological signatures are verified to be consistent with our expectation and (3) their diagnostic power is assessed. In Chapter 6, the differences between observed and simulated hydrological signatures and the results of the sensitivity analysis are used for an in-depth diagnostic of the J2000 Ardèche model. The diagnostic of the model yields improvements recommendations that are proposed and tested.

Finally, a concluding chapter synthesizes the research undertaken in the PhD thesis, highlighting its main contributions with respect to its objectives, and proposes perspectives for future researches.

Chapter 2

Material and methods

Contents

Introduction

The research presented in this manuscript is based on two datasets: 10 catchments of the Southern Sierra Nevada mountains (California, United States of America) and the Ardèche catchment (Southeast of France). These datasets were used for the development and selection of the hydrological signatures. In addition, the J2000 model was set up on the Ardèche catchment and used as our case study for the development of the diagnostic-evaluation methodology.

The Ardèche catchment was selected as it is well monitored and has been subject to many studies (e.g. Naulet et al., 2005; Braud et al., 2016c,a; Adamovic, 2014; Adamovic et al., 2015; Braud et al., 2017). In addition, detailed data was provided by the hydrometric station managers of several sub-catchments enabling detailed analysis of the uncertainty associated with stream-flow time series. In section 2.1, the Ardèche catchment and the available data are presented. Four sub-catchments, Meyras, Pont-de-Labeaume, Goulette and Claduègne, are presented in details as they were selected (as explained in Subsection 2.1.1.2) for a more focused and detailed analysis.

For the development and evaluation of snow dedicated hydrological signatures, data from 10 Critical Zone Observatory catchments located in the Southern Sierra Nevada mountains were used. They were chosen because they are strongly influenced by snow processes and collected data includes snow depth and snow water equivalent measurements. They are presented in Section 2.2.

The J2000 model was chosen as our case study for the development of the diagnostic and evaluation methodology. It was chosen as it is a typical process-based and distributed model whose parameterization and evaluation is challenging. The J2000 model is presented in detail in Section 2.3. Although our work is mainly focused on 4 sub-catchments (Section 2.1), the J2000 model was set up for the whole Ardèche catchment as detailed in Section 2.4. As the model will eventually include the effects of dams, irrigation and drinking water uptake, it made sense to have a running model for the whole catchment. The choice of the J2000 model was also due to the existing J2000-Rhône model (Branger et al., 2016), which includes the Ardèche catchment. The J2000-Rhône model is of interest for long term studies on water resources on the Rhône catchment. Hence, choosing the J2000 model will allow to eventually transfer the results obtained for the J2000-Ardèche model to the J2000-Rhône model.

2.1 The Ardèche catchment

2.1.1 Catchment and subcatchment description

2.1.1.1 Setting and hydro-climatic context

The Ardèche catchment is located in the South-East of France, West to the Rhône river (Figure 2.1). The catchment has an area of approximately 2388 km^2. The topography of the catchment ranges from about 1680 m in its West part, in Massif Central mountains, to about 42 m where the Ardèche river joins the Rhône river. The topography is characterized by steep slopes in its Western part, and deep canyons in which the Ardèche river flows downstream. The Ardèche river has a length of about 125 km and has two main tributaries: the Baume and Chassezac rivers.

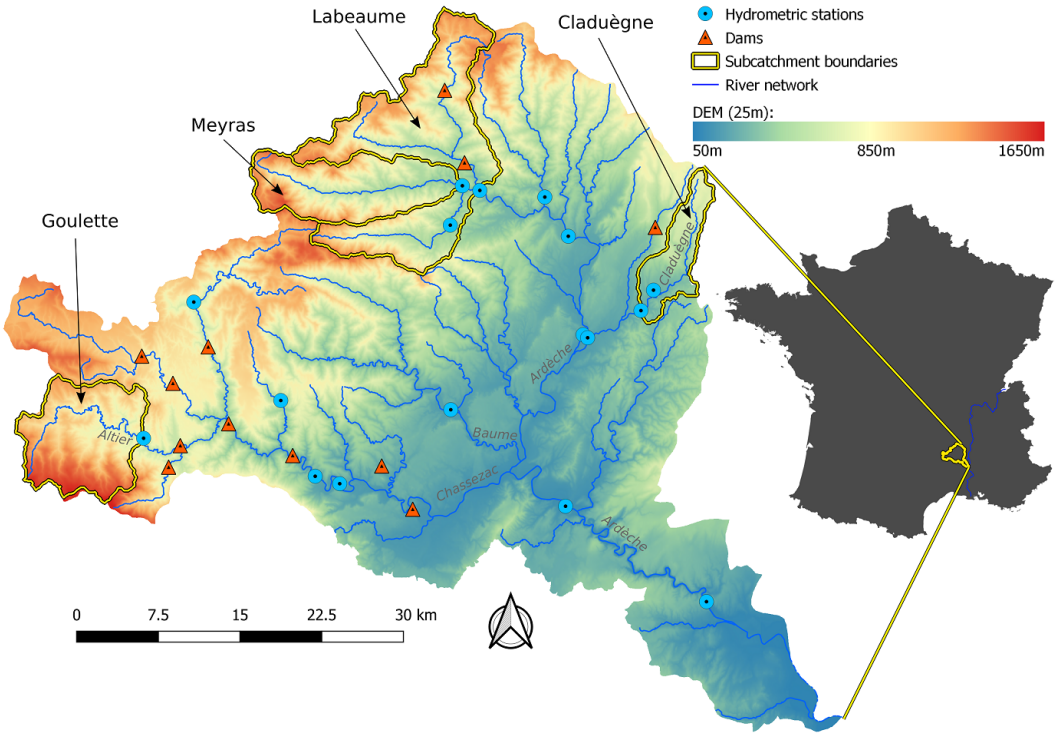

Figure 2.1: Localization of the Ardèche catchment and its topography, river network, hydrometric stations and dams. The four study subcatchments are highlighted. The topography is based on a 25 m DEM provided by IGN (http://www.ign.fr)

The Ardèche catchment experiences a Mediterranean climate characterized by heavy rainfall during Fall, a rainy season from September to February and a long dry season from March to August. The catchment has a quick response to precipitation events leading to flash floods in part due to the steepness of the catchment in its upper part (East), thin soils and impermeable bedrocks. Numerous dams are located in the catchment for hydro-power production (Figure 2.1). They heavily influence streamflow apart from floods conditions. In particular, water from the neighboring Loire river is routed within the Ardèche catchment for the Monpezat Hydro-power plant, located in the North-West, significantly affecting the water balance of the catchments located downstream.

2.1.1.2 Selection of 4 subcatchments

Table 2.1: Main physical characteristics of the Meyras, Pont-de-Labeaume, Goulette and Cladugne catchments

	Meyras	Pont-de-Labeaume	Goulette	Cladugne
Topography:				
- Area [km^2]	97	288	123	43
- Elevation†‡ [m]	894 (315/1548)	883 (294 / 1548)	1149 (628 / 1678)	481 (205 / 830)
- Mean slope† [%]	45	41	32	18
Geology	Metamorphic rocks (95%)	Metamorphic (66%), magmatic (21%) and volcanic rocks (11%)	Schists (66%) and magmatic rocks (25%)	Carbonates series (61%) and volcanic rocks (39%)
Soils	Shallow soils (40 cm), sandy-loam	Shallow soils (48 cm), sandy-loam	Very shallow soils (25 cm), loam (and sandy-loam, clay-loam)	Medium depth soils (78 cm), silt-loam (and silt-clay-loam)
Land-use	Forests (64%) and garrigues (21%)	Forests (64%), garrigues (19%) and grassland (16%)	Forests (50%), garrigues (25%) and grassland (22%)	Garrigues (31%), grassland (31%) and including grapevines and villages downstream

† Values derived from 25 m resolution DEM

‡ Mean (min/max)

To focus the analysis, only a few sub-catchments of the Ardèche catchment were selected (Figure 2.1): Meyras, Pont-de-Labeaume, Goulette and Cladugne. The selection criteria were (1) little human influence on streamflow data (or availability of data to correct the measured streamflow data in the case of Pont-de-Labeaume catchment), (2) homogeneity of each sub-catchment and (3) inter-catchment diversity, in terms of physical characteristics. Another criterion was the availability of additional data and various information on the hydrometric stations in order to be able to quantify the uncertainty associated with streamflow time series.

The catchments drainage areas vary between 43 km^2 (Cladugne) and 288 km^2 (Pont-de-Labeaume). The Meyras catchment (area of 97 km^2), is nested within the Pont-de-Labeaume catchment. The topography of the Ardèche catchment shown in Figure 2.1 is based on a 25 m DEM provided by IGN (`http://www.ign.fr`). Goulette has the highest mean elevation (above 1100 m) and Cladugne the lowest (below 500 m). Both Meyras and Pont-de-Labeaume have the steepest slopes (above 40% on average) whearas the Cladugne catchment has the less steep slopes (below 18% on average).

In the following Subsections, the geology, soils and land-use of the Ardèche catchment and of the 4 selected subcatchments (Meyras, Pont-de-Labeaume, Goulette and Cladugne) are detailed. Table 2.1 summarizes the main characteristics of each catchment.

2.1.1.3 Geology

The geology of the Ardèche catchment, presented in Figure 2.2, is the result of a simplification of a 1/50000 geology map provided by the BRGM[1] which was done during the MDR project (Branger et al., 2016). The very detailed distinctions done between types of geology was simplified into a small sub-set of geology types.

The geological patterns of the Ardèche catchment are quite complex as illustrated in Figure 2.2. The main geological entities are: (1) massive limestone, mostly downstream in the Eastern part of the catchment, (2) carbonates series and other sedimentary rocks in the middle part of the catchment, (3) metamorphic rocks in the Northern part of the catchment and (4) schists in the South-West part of the catchment. Other geological formations are worth noting: magmatic rock in the West part of the catchments and patches of volcanic rocks in the North part of the catchment.

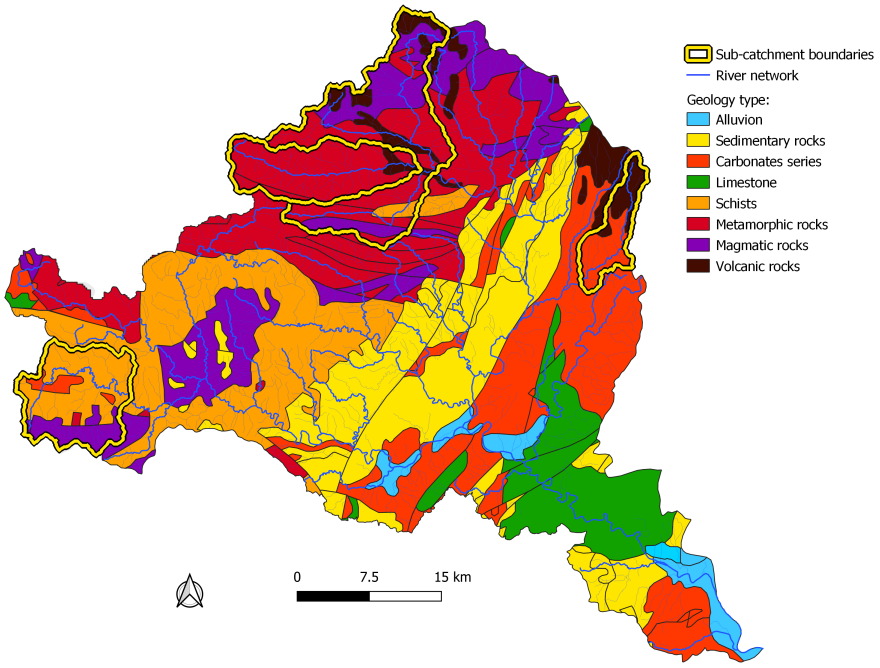

Figure 2.2: Main features of the geology of the Ardèche catchment (simplified by Branger et al. (2016) from a 1/50000 geological map provided by BRGM)

The Meyras catchment geology is dominated by metamorphic rocks (95%) with only 5% of volcanic rocks located downstream. Pont-de-Labeaume also rests mostly on metamorphic rocks (66%) but it also rests on a significant proportion of magmatic rocks (21%) and volcanic rocks (11%). The Goulette catchment rests mainly on schists (66%) and magmatic rocks (25%) with some minor patches of carbonates series. Cladužgne rests mainly on Carbonates series (61%) and volcanic rocks (39%). The main geology features of the four study catchments are reported in Table 2.1.

[1]Bureau de Recherches Géologiques et Minières (BRGM): https://www.brgm.fr/

2.1.1.4 Soils

Information on soils in the Ardèche catchment can be found in regional soil databases. They are the product of a national program for the inventory, management and conservation of soils (IGCS) that involves the French ministry of Agriculture and the National Institute of Agronomy Research (INRA) as well as several other entities (including ADEME, IRD, IGN and AFB). They provide information on soils such as depth, textures of the different horizons and organic matter content.

Bahl (2016) processed all the data (several MS-Access datatbases), to produce GIS layers which cover the Ardèche catchment. Results are spatially represented according to "cartographic units of soils" (UCS) provided in the original departemental databases. Figure 2.3 shows the soil depth, one of the field in the GIS layer produced by Bahl (2016). In the Ardèche catchment, soils are shallow (below 60 cm) except in the North-West and South-West (downstream part of the catchment) where deeper soils (80 - 120 cm) can be found (Figure 2.3). As soils drilling/digging is often blocked before reaching the actual bedrock, these soil depth should be seen as minimal soil depth. Information on soils textures indicate the Ardèche catchment is dominated by sandy loam soils and suggest – using a pedotransfer function (Bonnet, 2012) – low available water capacity (rarely exceeding 100 mm, see Appendix A, Figure A.2).

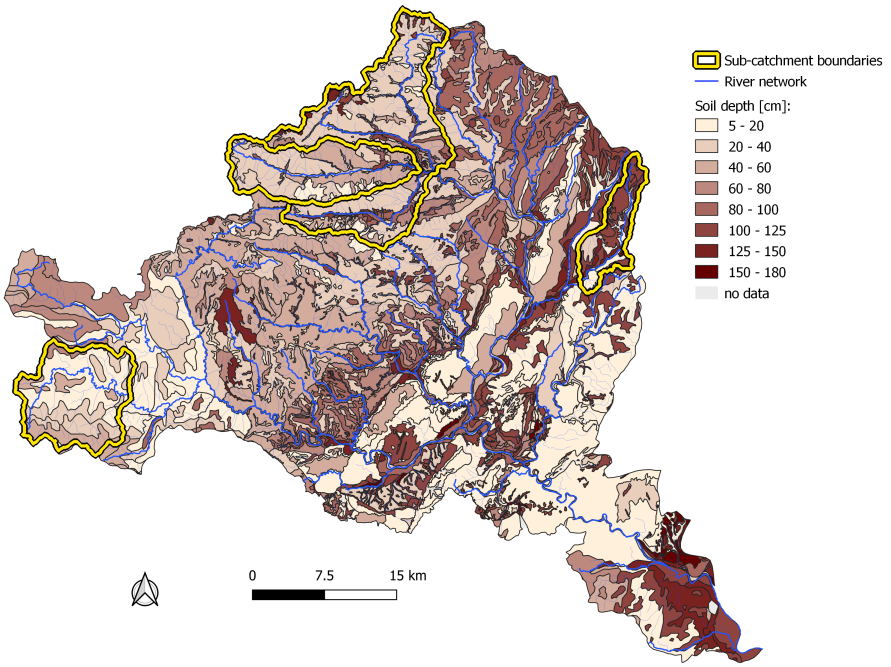

Figure 2.3: Soil depth in the Ardèche catchment (data from IGCS program processed by Bahl (2016))

The Meyras, Pont-de-Labeaume and Goulette catchments have very shallow soils (average depth of 40 cm, 48 cm and 25 cm respectively), in particular Goulette catchment. Soils are significantly deeper for the Cladueègne catchment (average depth of 78 cm). For Meyras and Pont-de-Labeaume, there are mostly sandy loam soils with proportion of silt and clay rarely exceeding 30% and 10% respectively. The proportions of silt and clay are higher for Goulette and Cladueègne. Goulette is dominated by loam soils and Cladueègne by silt-loam soils. Compared to the other 3 catchments, Cladueègne has a larger available water capacity (as estimated using pedotransfer function). These main soils characteristics of the four study catchments are

reported in Table 2.1.

It is important to stress that the soil depth data presented here are to be used cautiously given weathered bedrock is not accounted for: weathered bedrocks is likely deep in some cases, particularly for granite (metamorphic rocks, magmatic rocks), significantly affecting soil/groundwater water storage capacity (Vannier et al., 2013). In addition, the study of Braud et al. (2017) – which focuses on top soil permeability measurements in the Cévenne-Vivarais region (which include the Ardèche catchment) – showed an impact of land-use and geology that was not captured if only considering pedotransfer functions. Therefore, the average soil texture data considered here are also to be considered cautiously given how it may vary greatly within the soil profile and be a relatively weak predictor of soil properties such as the actual available water capacity.

2.1.1.5 Land-use

The Ardèche catchment is mostly forested. The land-use map in Figure 2.4 is the result of the analysis of 4 spectral bands of the remote sensed data from Landsat8 satellites at two specific dates (Andrieu, 2015a)[2]. It has a 30 m resolution. Land use was classified in several categories which include different forest types (coniferous, broadleave, mixed, garrigues) and different types of agricultural use (late and early crops, grapevines, permanent grassland). Figure 2.4 shows that the Ardèche catchment is mostly forested with a mix of conifer and broadleaf trees, with a large proportion of garrigues. Garrigues are bushes typical of the Mediterranean area and Mediterranean trees such as evergreen oak (*Quercus Ilex*), Cade (*Juniperus Oxycedrus*) or Olive tree (*Olea Europaea*). The Ardèche catchment also includes permanent grassland, mostly located in the upper parts of the catchment. Crops (late and early) and vineyards are mostly located in the middle and bottom parts of the catchment. Similarly to urban areas (small villages), agriculture represents only a moderate proportion of the Ardèche catchment area.

Meyras, Pont-de-Labeaume and Goulette are largely covered by forests (coniferous, broadleave and mixed forests) that represent respectively 64%, 64% and 50% of the total area of the catchments. They also include significant proportions of garrigues (21%, 19% and 25% respectively) and permanent grassland (5%, 16% and 22% respectively). The Claduègne catchment is different in terms of land-use. It is dominated by garrigues (31%) and permanent grassland (31%) and includes agricultural land (mostly grapevines, 5%) and some villages (6%), mostly downstream. The dominant land-use types of each study catchments are reported in Table 2.1.

From our field knowledge of the Claduègne catchment, the proportion of agricultural land found here seems quite underestimated. A more precise land-use map (5 m resolution) of the Claduègne catchment (Andrieu, 2015b), also based on remote sensed data, shows significant differences and suggest a much larger proportion of agricultural land and less garrigue areas (see Figure A.3). Although these differences might be the consequence of the higher resolutions and differences in the land-use classification methodology, they suggest that the information provided by these maps should be considered cautiously, in particular for Claduègne.

[2] http://data.datacite.org/10.14768/MISTRALS-HYMEX.1377

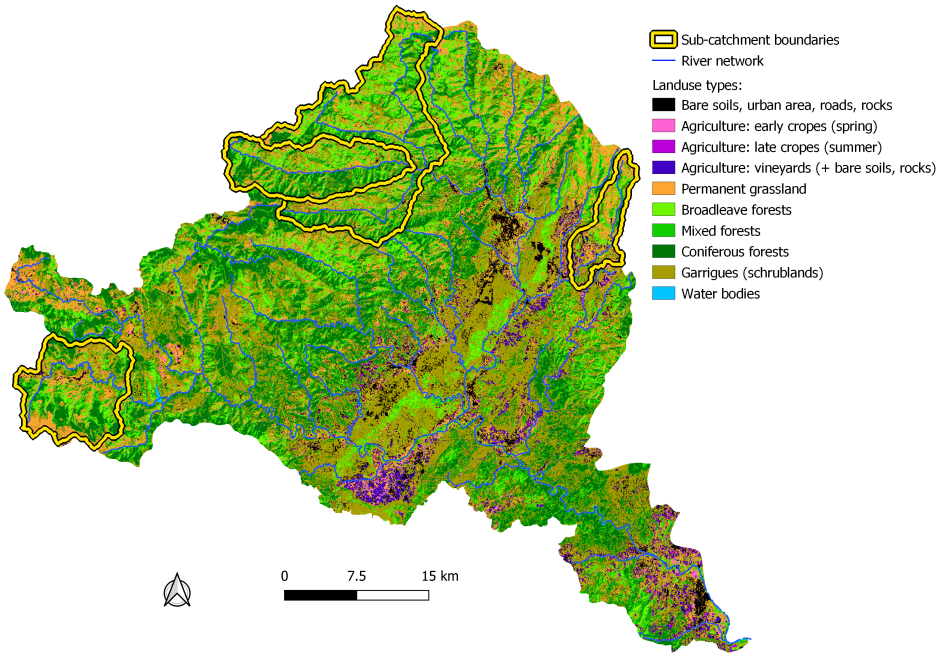

Figure 2.4: Land-use in the Ardèche catchment (Source: Andrieu (2015a))

2.1.2 Meteorological data

SAFRAN is the result of the reanalysis and downscaling of mesoscale atmospheric variables of Météo-France (Vidal et al., 2010). The SAFRAN data set includes 7 meteorological variables (rainfall, snowfall, temperature, specific air humidity, wind speed, long and short wave solar radiation) from 1958 to 2019 at a hourly resolution, over the whole French territory on a 8x8 km^2 grid.

Here, 3 meteorological variables were considered: precipitation P, reference evapotranspiration E_{REF} and temperature T. They were needed at a daily time resolution for the whole Ardèche catchment and in particular for the four study subcatchments Meyras, Pont-de-Labeaume, Goulette and Claduègne. Although the Ardèche catchment, as part of the OHM-CV observatory, includes a dense network of meteorological stations monitoring precipitation and temperature (Nord et al., 2017), climate reanalysis SAFRAN (Vidal et al., 2010) was used to be consistent with other studies done at larger scale (e.g. the whole Rhône catchment, Branger et al. (2016)), the lack of meteorological stations in the most elevated parts of the catchment (see Nord et al. 2017) and because it includes all the necessary variables in a homogeneous way, over a long period of time with no gaps.

The standard method for the computation of the reference evapotranspiration is the Penman-Monteith equation (Monteith, 1965; Allen et al., 1998). The Penman-Monteith equation yields the evapotranspiration that would occur on grassland in the absence of water stress. Its value is then typically modulated using coefficients that depend on the type of vegetation and stage of development (Allen et al., 1998): the crop coefficients. The Penman-Monteith equation requires as inputs the temperature, specific air humidity, wind speed and solar radiations which are all available in the SAFRAN dataset. The reference evapotranspiration was computed using SAFRAN data at a hourly time steps for all SAFRAN grid cells and all time steps. In the study daily aggregated data are used.

The precipitation data used in this study are the sum of rainfall and snowfall provided by the SAFRAN dataset. They were aggregated from hourly to daily time resolution.

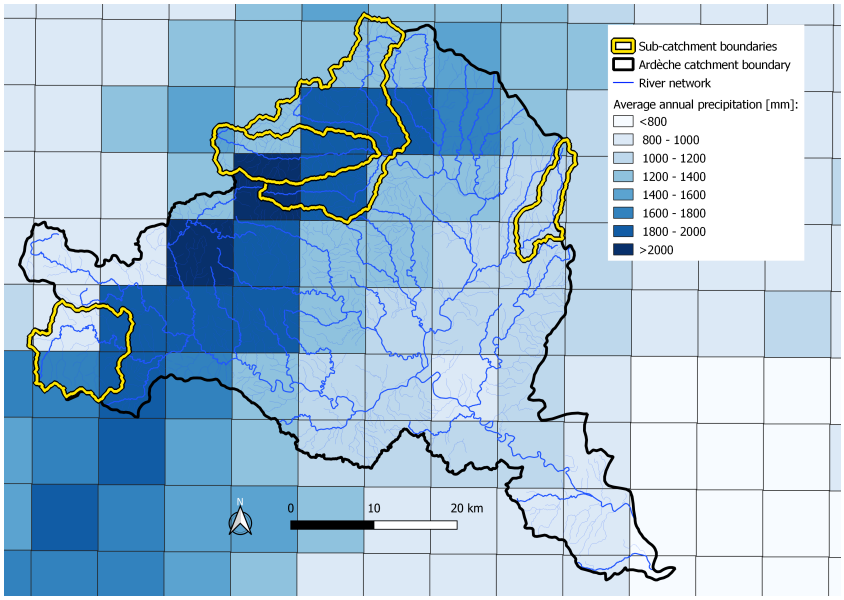

(a) Average annual precipitation

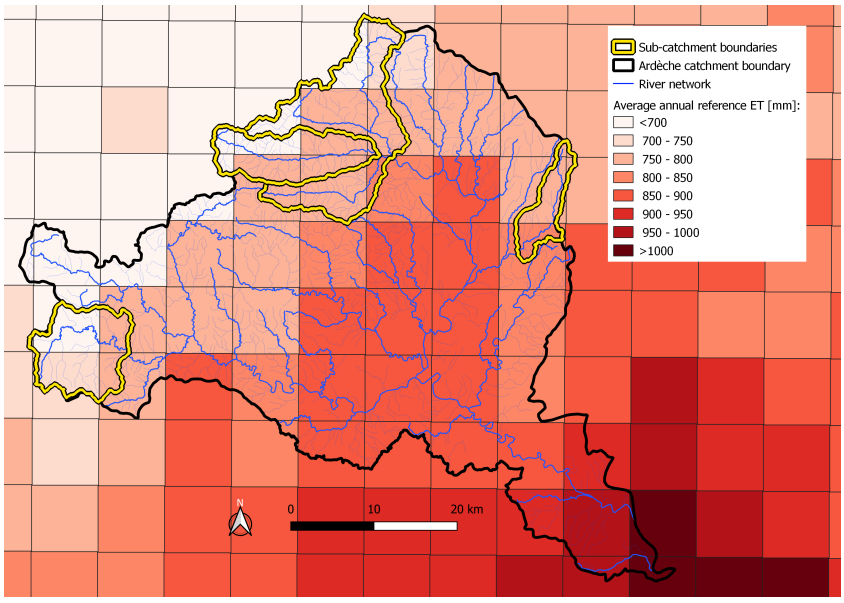

(b) Average annual reference evapotranspiration

Figure 2.5: Average annual precipitation and reference evapotranspiration computed over all available hydrological year (from September, 1st 1958 to August, 31st 2018) for each SAFRAN grid cell.

Figure 2.5a shows the average annual precipitation of each SAFRAN grid cell. It shows large differences depending on the SAFRAN cell, from less than 800 mm/year to more than 2000 mm/year. A gradient is visible from the lowest to the highest part of the Ardèche catchment with larger annual precipitation affecting the upper part. Figure 2.5b shows the average annual reference evapotranspiration of each SAFRAN grid cell. It shows a similar gradient with elevation, with larger average annual reference evapotranspiration in the lowest part of the catchment (about 1000 mm/year) and smaller in the highest part (about 700 mm/year).

Table 2.2 gathers catchment scale statistics on precipitation, reference evapotranspiration and temperature. They were obtained by aggregating data at the scale of the Ardèche, Meyras,

Table 2.2: Statistics on catchment scale precipitation, reference evapotranspiration and temperature computed over all the available hydrological years (from September, 1st 1958 to August, 31st 2018) for the Ardèche catchment and the 4 study catchments

	Ardèche	Meyras	Pont-de-Labeaume	Goulette	Claduègne
Precipitation					
Average annual [mm]	1376	1821	1756	1507	1138
Daily average [mm]	3.77	4.99	4.81	4.13	3.12
Daily maximum [mm]	186	301	283	216	172
$T_{P=100\text{mm/day}}$ † [years]	1.46	0.462	0.522	1.07	1.77
Reference evapotranspiration					
Average annual [mm]	819	755	759	730	809
Daily average [mm]	2.24	2.07	2.08	2.00	2.22
Daily maximum [mm]	8.25	7.90	7.92	8.03	8.24
Daily minimum [mm]	0.125	0.111	0.109	0.127	0.0559
Temperature					
Daily average [°C]	10.6	7.93	8.41	6.9	11.2
Daily maximum [°C]	28.9	27	27.4	25.4	30.4
Daily minimum [°C]	-13.4	-17.2	-16.6	-18.2	-13

† return period corresponding to a daily precipitation of 100 mm/day

Pont-de-Labeaume, Goulette and Claduègne catchments considering the mean of SAFRAN cells weighted by the proportion of overlapping area between catchment boundaries and SAFRAN cells. Table 2.2 shows larger average annual precipitation for Meyras and Pont-de-Labeaume and lower for Claduègne. It also shows that the chance of occurrence of a daily precipitation of 100 mm is about twice a year for Meyras and Pont-de-Labeaume, once a year for Goulette and less than once every one and half year for Claduègne. This indicates much more intense precipitation for Meyras and Pont-de-Labeaume compared to Claduègne.

Table 2.2 also shows that the average annual reference evapotranspiration is similar across our study catchments with only slightly higher values for Claduègne. Claduègne also experiences, on average, higher temperatures compared to the other catchments whereas Goulette experiences the lowest temperatures, reflecting the differences in elevation between these catchments.

2.1.3 Streamflow data of the selected Ardèche subcatchments

The four study catchments, Meyras, Pont-de-Labeaume, Goulette and Claduègne, have hydrometric stations continuously monitoring river stage at their outlet. The hydrometric stations of Meyras and Pont-de-Labeaume catchments are both managed by the Service de Prévision des Crues (SPC) Grand-Delta. The hydrometric stations of Goulette and Claduègne are managed by EDF and IGE respectively. Measurements started in June 1984, January 1980, January 1983 and October 2011 for Meyras, Pont-de-Labeaume, Goulette and Claduègne respectively. Part of data were provided by the SPC Grand-Delta, EDF and IGE during the FloodScale project (Braud et al., 2016b).

The water stage measurements are converted by the station managers into streamflow using a rating curve, a relation linking stage and streamflow. Rating curves are mathematical equations calibrated against gaugings which are individual "simultaneous" measurements of both streamflow and river stage. It is well recognized that the conversion of stage time series to streamflow time series using rating curves is a major source of uncertainty (McMillan et al.,

2012) which can be found dominant with respect to precipitation uncertainties (Westerberg and McMillan, 2015) (see Subsection 1.3.3 in Chapter 1). We chose to recompute the streamflow time series in order to account for the associated uncertainties. It also ensures a more homogeneous dataset given that the 4 hydrometric stations have different station managers with different practices.

The uncertainty associated with rating curves can be estimated using various methods (Kiang et al., 2018). We chose to use the state-of-the-art BaRatin method proposed by Le Coz et al. (2014), a Bayesian approach that enables the quantification and propagation of uncertainty associated with the rating curve to streamflow time series. This method provides more physically based estimation of streamflow in the extrapolated part of the rating curve, i.e. where no gaugings are available, which is typically the case at high and low flows. In addition, this method provides rating curve ensembles which can be used easily to propagate the uncertainty to subsequent analysis. As shown by Horner et al. (2018b), the errors affecting the continuous stage measurements, particularly if of a systematic nature, can have significant impact of the streamflow time series. Therefore, the propagation of stage measurement errors was also accounted for following the approach they proposed.

2.1.3.1 The uncertain streamflow time series of the four study catchments

Streamflow time series were recomputed using the stage time series, the gaugings and information on the hydraulic configuration of the sites following the methodology described in detail by Le Coz et al. (2014) and Horner et al. (2018b). The method of Le Coz et al. (2014) – BaRatin method – follows a Bayesian approach which is based on (1) the definition of rating curve models and the specification of *a priori* parameter distributions from a hydraulic analysis of the site, (2) uncertain calibration data — the gaugings which are pairs of measurements of both streamflow and river stage — and (3) a Markov Chain Monte Carlo (MCMC) sampling procedure used to infer the *posterior* distributions of the rating curve parameters. The methodology of Horner et al. (2018b) accounts for two types of errors that are supposed to affect stage time series: (1) non-systematic errors due to waves and instrumental noise and (2) systematic errors due to stage sensor calibration drifts. An overview of the methodology followed is proposed in Appendix B.1.

The uncertain streamflow time series were computed as detailed in the Appendices B.2, B.3, B.4 and B.5 for Meyras, Pont-de-Labeaume, Goulette and Claduègne catchments respectively. All the time series were aggregated at a daily time step. The general characteristics of the corresponding 4 hydrometric stations and the main information regarding the application of the methodology are reported in Table 2.3. Goulette hydrometric station has a large concrete weir controlling the stage-streamflow relationship whereas, for the 3 other catchments, the river bed morphology is the main control. As a consequence, many rating curve shifts, that were accounted for, occurred for Meyras, Pont-de-Labeaume and Claduègne.

Table 2.3 also presents the time range of the time series, the proportion of missing values and the number of complete hydrological years, i.e. years starting from September 1st with less than 5% of missing days. More than 22 valid hydrological years are available for Meyras, Pont-de-Labeaume and Goulette whereas only 6 valid hydrological years are available for Claduègne.

Table 2.3 also presents the average and maximum daily streamflow and a low flow indices – minimum value of the average of 10 consecutive days – of the four study catchments with their associated uncertainties. In the remaining of this subsection, more details on the resulting daily uncertain streamflow time series of the 4 study catchments are provided.

Table 2.3: Main characteristics of the hydrometric station, BaRatin application and resulting daily uncertain streamflow time series for Meyras, Pont-de-Labeaume, Goulette and Cladugne.

	Meyras	Pont-de-Labeaume	Goulette	Cladugne
General characteristics of the hydrometric stations				
Catchment area [km^2]	97	288	123	43
Longitude [°]	4.269783	4.290402	3.888046	4.478971
Latitude [°]	44.670387	44.66619	44.460512	44.56217
River name	Ardèche	Ardèche	Altier	Cladugne
Influenced	No	Yes	No	No
Manager	SPC GD	SPC GD	EDF	IGE
Information on the application of BaRatin				
Type of low flow control	Natural	Natural	Weir	Natural
Number of controls	3	3	3	3
Number of gaugings	247	253	122	39
Number of stable periods	18	13	2	3
Characteristics of the available time series				
Start of stage records	1984-06-27	1980-01-01	1983-01-01	2011-10-01
End of stage records	2017-10-02	2013-01-01	2014-03-31	2018-12-31
Length [days]	12151	12055	11413	1918
Missing values [%]	3.0	21	0.23	2.7
Valid hydrological years†	27	22	29	6
Computed uncertain streamflow statistics				
Mean [m^3.s^{-1}]	3.7 [3.5, 3.8]	9.5 [9.3, 10.0]	2.9 [2.8, 3.0]	0.76 [0.68, 0.83]
Daily maximum [m^3.s^{-1}]	230 [200, 290]	510 [370, 640]	150 [140, 170]	59 [48, 64]
AM_{10}‡	0.0049 [0, 1.7]	0 [0, 26]	1.3 [0.98, 2.00]	0.26 [0.034, 1.7]

† a valid hydrological year starts on September 1st and contains more than 95% of valid time steps (non-missing).
‡ minimum value of the average of 10 consecutive days (using a rolling mean)

2.1.3.2 Meyras

The stage time series of Meyras was downloaded from the Banque Hydro database[1], from the June 1984 to October 2017. The station managers provided the gaugings as well as information on the rating shifts and hydraulic configuration of the site. Due to many bed morphological modifications, mainly occuring during the largest flood events, the relation between stage and streamflow was found to have changed 17 times (Figure B.2) during the period considered (Appendix B.2).

Figure 2.6 shows the daily uncertain streamflow time series for a high and low flow period. It shows that stage time series errors affect the uncertainty of the streamflow time series mainly at low flow. At high flow, the uncertainty due to the rating curves largely dominates. Figure 2.7 shows the monthly streamflow time series over the two decades. It shows that there are large inter-periods differences in the impact of uncertainty from the rating curve reflecting the differences in the amount of information provided by the gaugings for the different periods.

[1] http://www.hydro.eaufrance.fr/

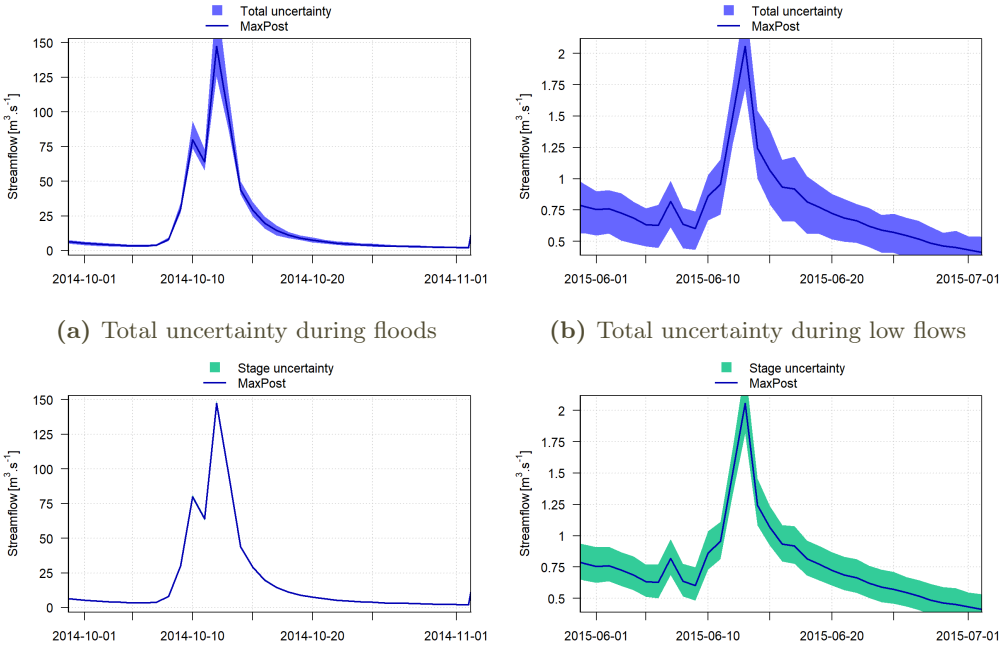

(a) Total uncertainty during floods

(b) Total uncertainty during low flows

(c) Stage uncertainty during floods

(d) Stage uncertainty during low flows

Figure 2.6: Daily streamflow time series and associated total (a and b) and stage (c and d) uncertainty for a flood event of late 2014 (left) and low flow month of 2015 (right) in the Meyras catchments.

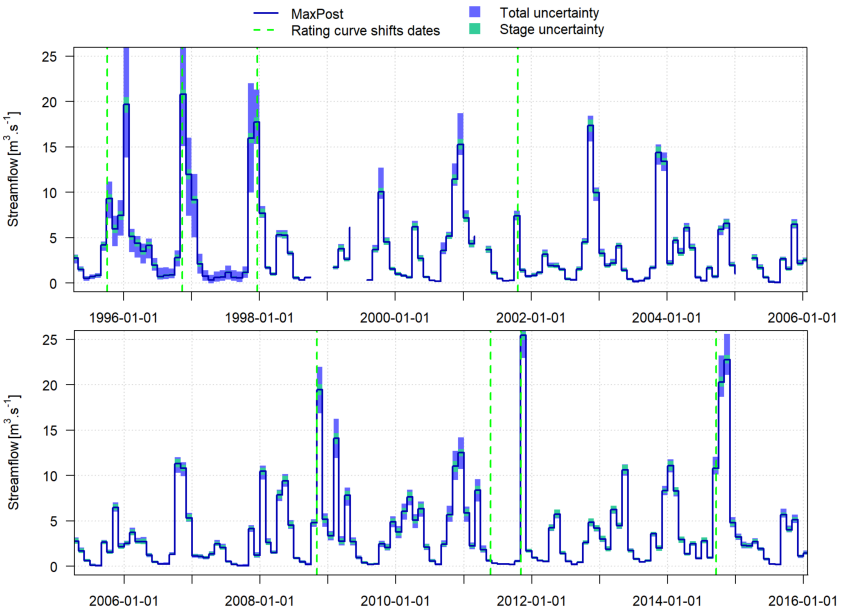

Figure 2.7: Monthly average of streamflow for two decades (from 1995 to 2015) of the Meyras catchment.

2.1.3.3 Pont-de-Labeaume

The hydrometric station at the outlet of the Pont-de-Labeaume catchment is also managed by the SPC Grand-Delta who provided the gaugings and historical information on the rating curve shifts. The stage time series was downloaded from the Banque Hydro database[3] and ranges between January 1980 and January 2013. Large gaps in the time series, particularly from 1995 to 2000, resulted in only 22 valid hydrological years (starting September 1st and containing more than 95% of days with no gaps)

The resulting daily uncertain streamflow time series was corrected to account for the influence of the Montpezat hydropower dam located upstream. Water from the nearby upstream Loire catchment are redirected into the Pont-de-Labeaume catchment through this dam inducing significant bias in the water balance of the catchment. Using the discharge data of the penstocks of the Montpezat dams, provided by EDF from January 1980 and January 2013, the methodology proposed by Noël (2014) to de-influence the data was applied. Details on the computation of the de-influenced daily uncertain time series are provided in Appendix B.3.

High and low flow examples of daily streamflow time series, with and without the applied correction are proposed in Figure 2.8. The correction significantly reduced the total volume of streamflow as is illustrated in the monthly values shown in Figure 2.9.

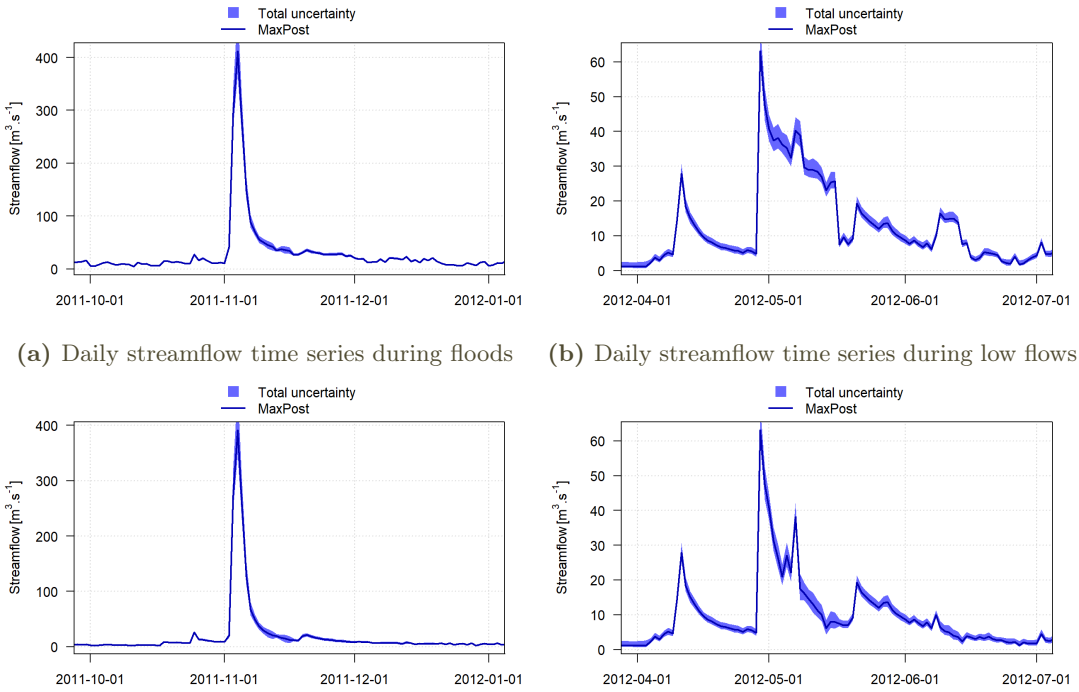

(a) Daily streamflow time series during floods

(b) Daily streamflow time series during low flows

(c) Daily de-influenced streamflow time series during floods

(d) Daily de-influenced streamflow time series during low flows

Figure 2.8: Daily streamflow time series and associated total uncertainty for the flood event of late 2011 (left) and low flow period of 2012 (right) in the Pont-de-Labeaume catchments. (a) and (b): influenced daily time series; (c) and (d): de-influenced daily time series.

[3] http://www.hydro.eaufrance.fr/

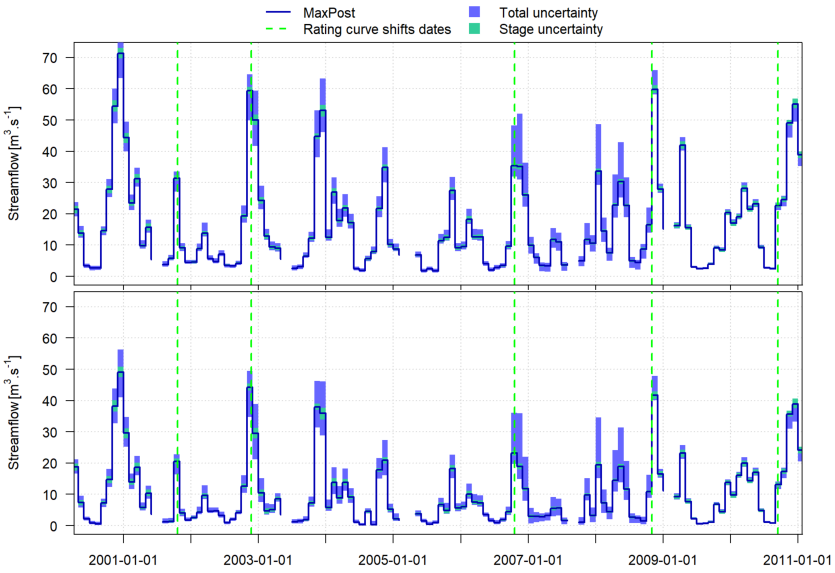

Figure 2.9: Monthly average of streamflow of one decade – from 2000 to 2010 – in the Pont-de-Labeaume catchment. Top: Observed monthly average of streamflow; Bottom: De-influenced monthly average of streamflow.

2.1.3.4 Goulette

The hydrometric station at the outlet of the Goulette catchment is managed by EDF who provided the gaugings and the stage time series from January 1983 to March 2013. The stage time series had very few missing value resulting in 29 valid hydrological years. Only one small rating curve shift was identified. This is mainly due to the stability of a large artificial weir located downstream of the stage sensor that controls the stage-streamflow relationship for a large range of stage values. Details on the computation of the daily uncertain streamflow time series are provided in Appendix B.4. Figure 2.10 presents examples of the daily uncertain streamflow time series of a high and low flow period.

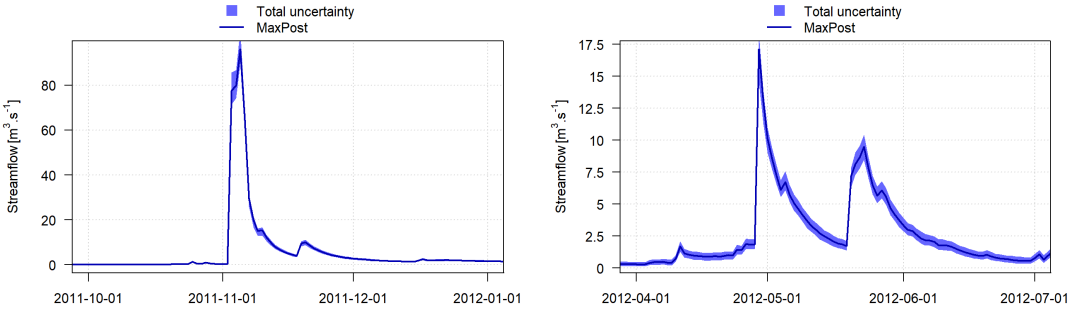

(a) Daily streamflow time series during floods **(b)** Daily streamflow time series during low flows

Figure 2.10: Daily streamflow time series and associated total uncertainty for the flood event of late 2011 (left) and low flow period of 2012 (right) in the Goulette catchments.

2.1.3.5 Claduègne

The hydrometric station at the outlet of the Claduègne catchment is managed by IGE who provided the gaugings and the stage time series from October 2011 to December 2018. Therefore, only 6 valid hydrological years are available for this catchment. For this station, only one

rating shift was identified by the station manager. However, the analysis of the stage time series revealed another very likely shift that was also accounted for (Figure B.18). Detail on the computation of the daily uncertain streamflow time series are provided in Appendix B.5.

Detailed data on the stage time series were provided by the station managers. It enabled a detailed quantification of the stage errors which were found small. Hence, the daily uncertainty streamflow time series is mainly affected by uncertainty originating from the rating curve uncertainty particularly at low flow. Figure 2.11 shows examples of the daily uncertain streamflow time series for a high and low flow period.

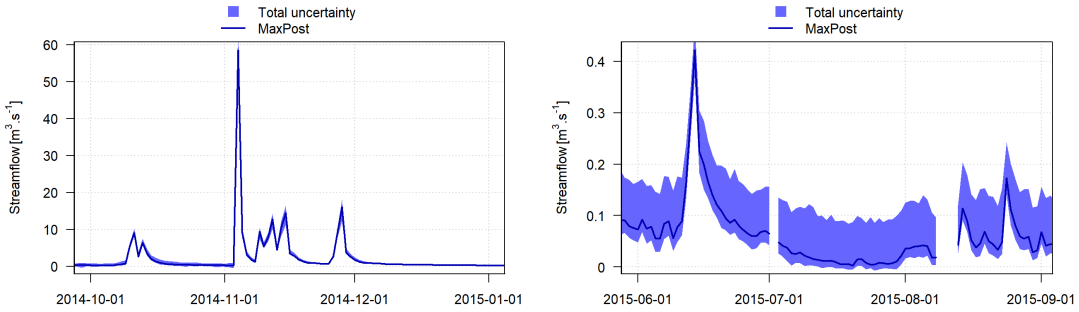

(a) Daily streamflow time series during floods **(b)** Daily streamflow time series during low flows

Figure 2.11: Daily streamflow time series and associated total uncertainty for the flood event of late 2014 (left) and low flow period of 2015 (right) in the Claduègne catchments.

2.2 The Southern Sierra CZO catchments

2.2.1 Catchments characteristics and climate

The study catchments are the Providence Creek and Bull Creek catchments of the Southern Sierra Critical Zone Observatory (CZO) located in California, United States. These catchments are part of the Kings River Experimental Watersheds (KREW) operated by the U.S. Forest Service (Hunsaker and Safeeq, 2017, 2018). A detailed description of the catchments and a synthesis of the measurements can be found in O'Geen et al. (2018).

The Providence Creek catchments are the P300, P301, P303, P304 and D102 catchments (see Figure 2.12). The P301, P303 and P304 catchments are nested within the larger P300 catchment. The Bull Creek catchments are the B200, B201, B203, B204 and T003 catchments (see Figure 2.12) with the B201, B203 and B204 catchments nested within the B200 catchment. The Providence and Bull catchments have elevations ranging from 1500 m to 2000 m and from 2000 m to 2500 m, respectively. They are located close enough to each other to assume they have similar climate. Details on the catchments characteristics (area, average elevation, elevation variation, aspect and slope) are given in Table 2.4.

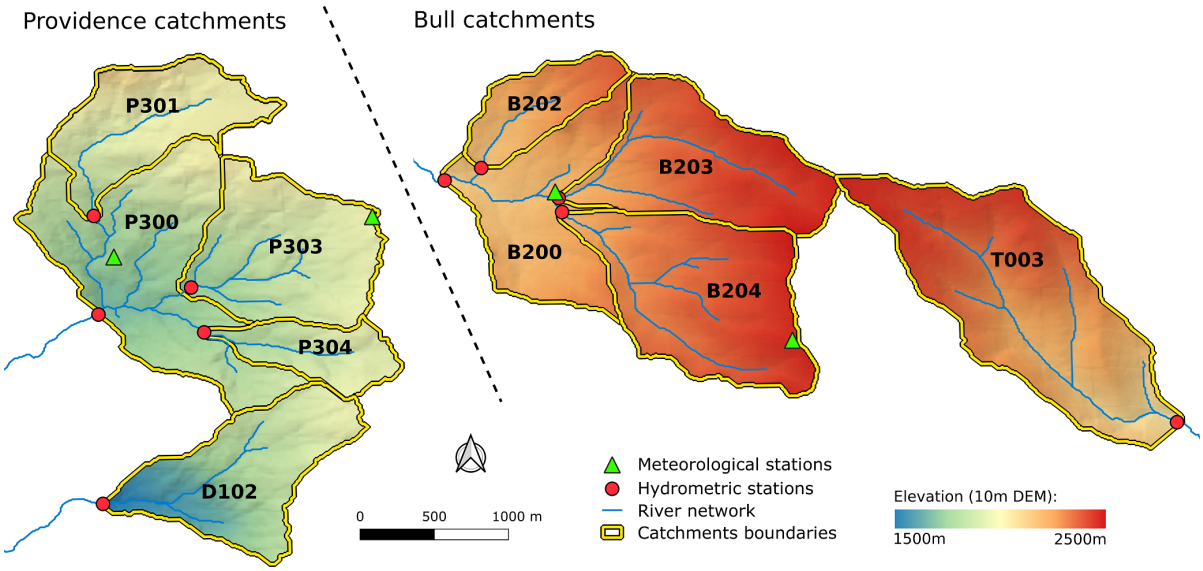

Figure 2.12: Boundaries of the Providence creek catchments (left) and Bull Creek catchments (top right) and localization of the hydrometric and meteorological stations.

Details on the geology, soil types and vegetation can be found in Johnson et al. (2011); Hunsaker et al. (2012); Safeeq and Hunsaker (2016). Only the main characteristics are reported here. All catchments rest on granite substratum. Providence catchments, except P301, are dominated by Shaver soils with rooting depth from 1 m to 2 m. P301 catchment is dominated by Gerle-Cagwin soils which have shallower rooting depth (from 0.76 m to 1.03 m). Bull catchments are dominated by Cagwin soils which have rooting depth between 0.5m and 1m. Overall, soils have moderate (Shaver and Gerle-Cagwin) to high permeability (Cagwin) with various water holding capacities (Shaver > Gerle-Cagwin > Cagwin).

Catchments are largely covered (96 % to 100 %) by the Southern Sierra mixed-conifer forest which is mainly a mix of red fir (*Abies magnifica*), white fir (*Abies concolor*), ponderosa pine

Table 2.4: Main topographic characteristics of the Southern Sierra CZO catchments.

Site	Catchment	Drainage area (ha)	Average elevation† (m)	Elevation variation (m)	Average aspect (degrees)	Average slope (%)
Bull	B203	138	2373	303	235	18
Bull	B204	167	2365	289	235	17
Bull	T003	228	2289	414	142	24
Bull	B201	53	2257	225	228	18
Bull	B200	474	2122	367	231	18
Providence	P301	99	1979	318	208	19
Providence	P303	132	1905	292	233	20
Providence	P304	49	1899	213	249	22
Providence	P300	461	1883	424	223	21
Providence	D102	121	1782	491	246	27

† above see level

(*Pinus ponderosa*), Jeffrey pine (*Pinus jeffreyi*), sugar pine (*Pinus lambertiana*), incense cedar (*Calocedrus decurrens*). Also, around 1-4 % of the area consist of rock outcrops in the Bull catchments (Safeeq and Hunsaker, 2016).

The study catchments are located under the Californian Mediterranean climate characterized by long Summer droughts and wet Winters (Goulden et al., 2012; Hunsaker et al., 2012; Safeeq and Hunsaker, 2016). Over the years from 2004 to 2014, the average yearly precipitation ranged from 1234 mm/year to 1392 mm/year with more than 95 % of precipitation falling during Fall, Winter and Spring (Safeeq and Hunsaker, 2016). Precipitation mostly occurs "during large frontal storms that move off the Pacific Ocean from West to East" (Goulden et al., 2012). A large part of the precipitation is lost to the atmosphere through evapotranspiration (Bales et al., 2018; O'Geen et al., 2018) as illustrated by the runoff coefficient ranging from 17.7 % (P303) to 42.9 % (B203) calculated by Safeeq and Hunsaker (2016).

The Providence and Bull catchments are snow-dominated catchments with large influence of snow accumulation and snow melt on the streamflow response. They are located in the transition zone between rainfall and snowfall (Bales et al., 2011). There is large inter-year variability of snow accumulation with dry years having very little snow accumulation and wet years having very large snow accumulation. Extreme dry years are characterized by higher air temperatures, little precipitation and intermittent snow cover.

2.2.2 Data

Streamflow is monitored at the outlet of each catchment (Hunsaker and Safeeq, 2017). For all catchments, stage is continuously measured and converted to streamflow. Conversion is done using the established discharge relationships between stage and streamflow as water goes through Parshall-Montana flumes (P301, P303, P304, D102, B201, B203, B204) or V-notch weirs (T003, P300). Each site equipped with Parshall-Montana flumes has one flume with a 30-122cm throat width to measure high flows and another one with a 8-15cm throat width to measure moderate and low flows. In the case of B200, a stage-discharge relationship was built from individual stage and streamflow measurements (gaugings) of different flow magnitudes.

Both sets of catchments include an upper and lower meteorological stations (Hunsaker and Safeeq, 2018). They are positioned in open clearings with diameters at least as wide as the height

of the surrounding trees and are therefore not subject to shading from trees or terrain (Safeeq and Hunsaker, 2016). The four meteorological stations continuously measure precipitation, air temperature, relative humidity, solar radiation, wind speed and direction and snow depth. In addition, the two upper meteorological stations measure snow water equivalent. Details on the equipment used are provided by Hunsaker et al. (2012).

For the precipitation measurements, gauges are located 3 m above the ground and equipped with windshield. Nontoxic propylene-glycol antifreeze is used to properly measure snow fall and a mineral-based oil is used to limit underestimation due to evaporation. Snow depth is monitored at the upper and lower meteorological stations using acoustic snow-depth sensors positioned 5 m above the ground. The Providence and Bull upper meteorological stations include snow pillows to measure snow water equivalent. For each station, 4 snow pillows are grouped to form a 2.4 m by 3.0 m rectangular pillow that continuously measures snow weight.

Daily streamflow data from October 1st, 2003 to September 30th, 2015 are available for catchments P301, P303, P304, D102, B201, B203, B204, T003. For the two larger catchments, P300 and B200, daily streamflow data are available only from December, 2005 and July 2006, respectively. Precipitation data are available from October 2003 (resp. 2004) to September 2017 for the Providence (resp. Bull) catchments. Air temperature data are available from October 2002 to September 2017. Snow depth data are available from October 2002 (resp. 2003) to September 2017 for the Providence (resp. Bull) catchments. SWE data are available from October 2003 to September 2017.

2.3 The J2000 model

2.3.1 General presentation of J2000

The J2000 model is a distributed and process-based model developed at the Friedrich Schiller University of Jena (Germany) (Krause et al., 2006). It has been previously used in many studies. For example, the model was used to investigate groundwater recharge (Schaefli et al., 2013; Watson et al., 2018), the impact of land use change (Krause, 2002; Branger et al., 2013) or the impact of climate change (Gao et al., 2012; Nepal et al., 2014; Nepal, 2016) on catchment behavior and water resources. A modified version of J2000 was set up on the whole Rhône catchment (Branger et al., 2016) to account for irrigation, water uptake for drinking water, and the effects of dams. The model was used to investigate human influence on the natural hydrological regime of the Rhône catchment and study the effect of climate change (Branger et al., 2016). The J2000 is, in most cases, used for long term studies.

The J2000 model is distributed according to the Hydrological Response Unit approach (Flügel, 1995). The HRU is the elementary unit at which the processes are represented. They are irregular units of space supposed to be homogeneous in terms of hydrological processes (Flügel, 1995). They are the results of an overlay of a digital elevation model (DEM), a land-use map, a soil map and geology map. The HRU-Delin tool, used to create the HRUs for J2000 is presented in Subsection 2.3.3.

The J2000 model is coded in Java. It runs within the JAMS (Jena Adaptable Modeling Software) modeling platform (Kralisch, 2006). The different hydrological processes are implemented in individual modules that are interconnected to each others. The hydrological processes represented in the model are detailed in Subsection 2.3.2. As presented in Appendix C.2, JAMS also includes many modules that deal with reading/storing/converting/writing inputs/states/outputs variables of the model. In addition, a set of R tools – the J2K-RUI – was developed to facilitate the edition of a J2000 model as detailed in Appendix C.3.

2.3.2 Hydrological processes representation in J2000

The J2000 model is a process-based or process-oriented model: many hydrological processes are explicitly accounted for although not using micro-physics equations such as Richard's equations. Like many process-based conceptual models, it follows a reservoir approach. The reservoirs represent different types of storage (vegetation canopy, soil, groundwater) that are interconnected using various mathematical formulations. The hydrological processes are represented in the J2000 model at a daily time scale. The representation of the hydrological processes is summarized in Figure 2.13. The processes represented in J2000 are:

- the partitioning of the input precipitation into rainfall or snowfall as a function of air temperature;
- the vegetation interception (by plant canopy) depending on the type of plant, period of the year and the type of precipitation (rain or snow);
- the snow accumulation and snow melt following an enhanced degree-day approach;

- the overland flow due to (1) the sealing of surface, (2) excess of soil maximum infiltration rate (infiltration excess overland flow), (2) saturated soils (saturation excess overland flow) and (3) water exfiltration from soils;
- the soil storage including water fixed to soils particles (stored in small pores), available for plant transpiration, and water in large pores, that can be drained;
- the lateral and vertical (percolation) subsurface flow as a function of soil saturation, drainage capacity of soils and topographic average slope;
- the groundwater storage and water release from groundwater as a function of its water content;
- the water evaporation from the canopy and surface water, and the plant transpiration from the soils, using the reference evapotranspiration and its modulation by the type of land-use and period of the year.
- the streamflow routing in the river network, following a kinematic wave approach and depending on reach width, rugosity, slope and length.

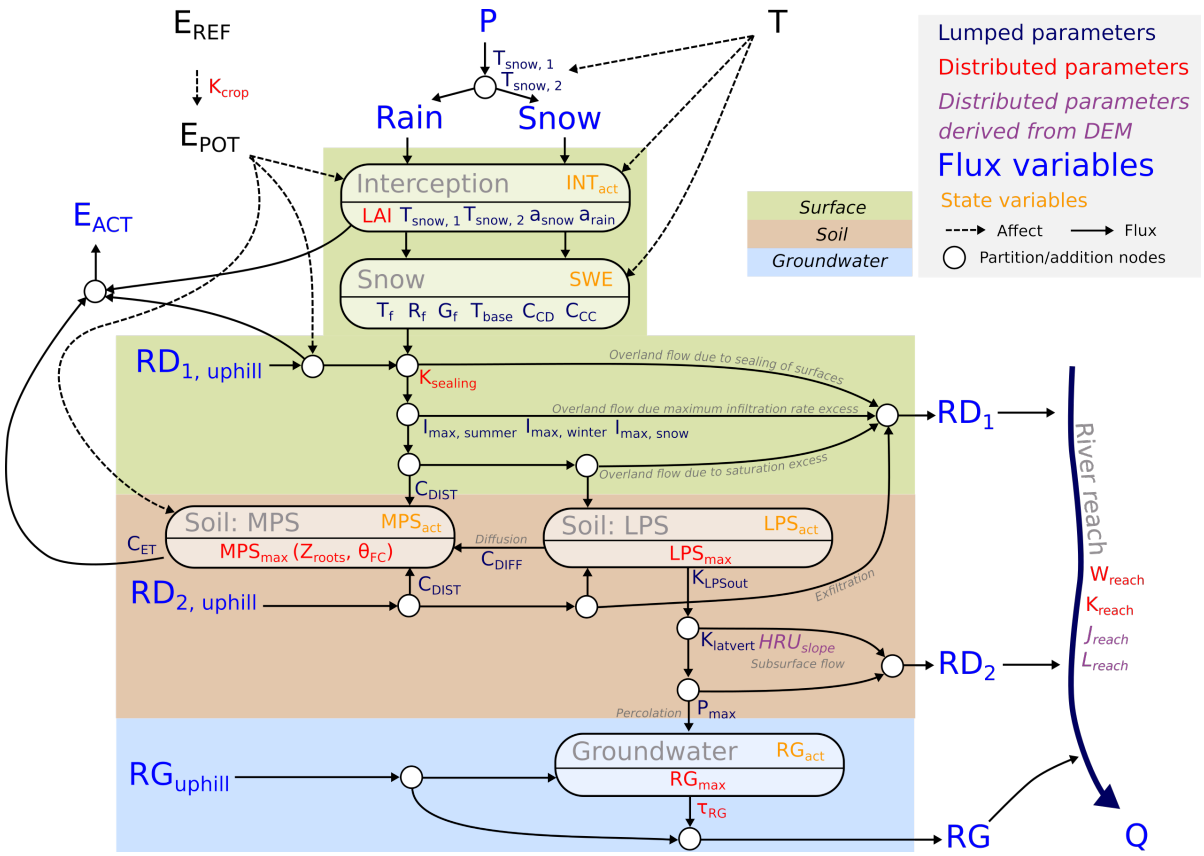

Figure 2.13: Diagram describing the hydrological processes representation in the J2000 model.

These hydrological processes are detailed in the following subsections. They depend on many parameters, lumped or distributed, that are presented in Table 2.5. The J2000 model used in our work differ slightly from the one used by Branger et al. (2013) or Branger et al. (2016): (1) some minor bugs were corrected, (2) some processes were slightly modified/simplified (see Appendix C.1 for details on the bug fix and modifications) Details on the processes represented in the model, listed above and summarized in Figure 2.13, are provided in the following Subsections.

Table 2.5: Parameters of the J2000 model

Name	Type	Description
Parameters related to vegetation		
K_{crop}	Distributed	Crop coefficient used to compute the potential evapotranspiration from the reference evapotranspiration. For each type of land-use, there 12 values, one for each month.
LAI	Distributed	Leaf Area Index corresponding to the proportion of surface covered by leaves. It is used to compute the maximum interception capacity. For each type of land-use, there are 12 values, one for each month.
a_{snow}	Lumped	Maximum interception storage capacity per unit of LAI in case of snowfall.
a_{rain}	Lumped	Maximum interception storage capacity per unit of LAI in case of rainfall.
Z_{roots}	Distributed	Roots depth. It is distributed according to the type of land-use.
Parameters related to snow		
$T_{\text{snow},1}$	Lumped	Temperature where there are 50% of rain and 50% of snow.
$T_{\text{snow},2}$	Lumped	Temperature difference from $T_{\text{snow},1}$ above (resp. below) which there is only rainfall (resp. only snowfall).
T_{base}	Lumped	Minimum temperature at which snow melt occur
T_{f}	Lumped	Temperature factor of the degree-day snow melt model.
R_{f}	Lumped	Rainfall factor of the degree-day snow melt model which modulates the effect of the heat from input from rainfall on snow melt.
G_{f}	Lumped	Ground or soil factor of the degree-day snow melt model which modulates the effect of soil heat on snow melt.
C_{CD}	Lumped	Critical density of snow. When snow pack density exceeds its value, it releases water.
C_{CC}	Lumped	Cold content coefficient that modulates the effect of temperature in the increase of temperature of the snow pack.
Parameters related to the ground surface		
K_{sealing}	Distributed	Sealing coefficient giving the proportion of sealed surface (impervious surface). It is distributed according to the type of land-use.
$I_{\text{max,summer}}$	Lumped	Maximum soil infiltration rate during the Summer months (from May to October).
$I_{\text{max,winter}}$	Lumped	Maximum soil infiltration rate during the Winter months (from November to April).
$I_{\text{max,snow}}$	Lumped	Maximum soil infiltration rate when the ground is snow covered.
Parameters related to soils		
C_{DIST}	Lumped	Coefficient modulating the inflow into the MPS reservoir in the infiltration process.
C_{DIFF}	Lumped	Coefficient modulating the inflow into the MPS reservoir in the diffusion process, i.e. when water is diffused from large pores (LPS reservoir) to smaller pores (MPS reservoir).

Table continues next page ...

... table continued

Name	Type	Description
θ_{FC}	Distributed	Field capacities of the soil horizons (10cm thick soil layers). It is distributed according to the soil types. For each soil type, there are as many values as the number of soil layers thus representing the soil depth.
LPS_{max}	Distributed	Maximum storage capacity of the LPS reservoir, corresponding to the air capacity or porosity of the soil. It is distributed according to the type of soil.
K_{LPSout}	Lumped	Coefficient controlling how easy/fast the LPS reservoir is able to drain.
$K_{latvert}$	Lumped	Coefficient controlling the weight given to the slope of the HRU in the partition of water between lateral subsurface flow and percolation to the groundwater reservoir.
C_{ET}	Lumped	Coefficient modulating the capacity of plants to widthraw water from the MPS reservoir when the MPS saturation is below its value.
Parameters related to groundwater		
P_{max}	Lumped	Maximum rate of inflow into the groundwater reservoir (maximum percolation rate).
RG_{max}	Distributed	Maximum storage capacity of the groundwater RG reservoir. It is distributed according to the type of geology.
τ_{RG}	Distributed	Groundwater reservoir depletion time characteristic. It is distributed according to the type of geology.
Parameters related to river reaches		
W_{reach}	Distributed	Width of the reach. Every reach can have a different width.
K_{reach}	Distributed	Strickler coefficient (roughness) of the reach. Every reach can have a different Strickler coefficient.

2.3.2.1 Regionalization of meteorological forcings

The three meteorological variables required by the J2000 model are the precipitation, the reference evapotranspiration and the air temperature. The J2000 model includes a regionalization module that computes a meteorological variable V at the scale of a HRU as a function of the n nearby meteorological stations following the inverse distance method. In our cases, the SAFRAN data are used (see Section 2.1.2). As SAFRAN data are provided on 8x8 km^2 grid, hence a much larger scale than the average size of the HRUs, only the data from the closest SAFRAN cell was taken. This approach provides the three needed meteorological variables of J2000 for each HRU and for each time step t: precipitation $P(t)$, reference evapotranspiration $E_{REF}(t)$ and air temperature $T(t)$.

The temperature unit expected by the model is degree Celsius. For precipitation and reference evapotranspiration, the model expects millimeters per day. Most of the modules of J2000 expect water volumes in Liters. Therefore, within J2000, inputs P and E_{REF} are first converted in Liters for each HRU. In the following Subsections, if not stated otherwise, all water volumes are expressed in Liters and flux in Liters per day .

2.3.2.2 Potential evapotranspiration

The reference evapotranspiration $E_{\mathrm{REF}}(t)$ corresponds to the evapotranspiration that would occur for a uniform and well irrigated grassland. It is therefore modulated using a parameter specific to the type of land-use and the period of the year to account for different stages in the plants physiological functioning throughout the year. This parameter is the crop coefficient K_{crop}. It is distributed according to the type of land-use and for each land-use class, it can take 12 different values depending on the period of the year, i.e. one value for each month. A potential evapotranspiration $E_{\mathrm{POT}}(t)$ – corresponding to the maximum actual evapotranspiration that can occur if there is enough water available – is computed using the equation:

$$E_{\mathrm{POT}}(t) = K_{\mathrm{crop}} \times E_{\mathrm{REF}}(t) \tag{2.1}$$

$E_{\mathrm{POT}}(t)$ is used to compute the actual evapotranspiration $E_{\mathrm{ACT}}(t)$ occuring as direct evaporation in the intercepted water by the vegetation canopy ($E_{\mathrm{interception}}(t)$) or at the ground surface ($E_{\mathrm{ground}}(t)$), or as plant transpiration ($E_{\mathrm{transpiration}}(t)$):

$$E_{\mathrm{ACT}}(t) = E_{\mathrm{interception}}(t) + E_{\mathrm{ground}}(t) + E_{\mathrm{transpiration}}(t) \tag{2.2}$$

The actual evapotranspiration cannot exceed the potential evapotranspiration and is limited by the water available for evaporation or plant transpiration. These different evapotranspiration mechanisms are further described in the following subsections.

2.3.2.3 Rain/snow partitioning

The precipitation falling on a given HRU is partitioned between liquid precipitation (rainfall) and solid precipitation (snowfall) as a function of air temperature T. This partitioning is controlled by two parameters $T_{\mathrm{snow},1}$ and $T_{\mathrm{snow},2}$. $T_{\mathrm{snow},1}$ is the temperature at which there is 50% of rainfall and snowfall whereas $T_{\mathrm{snow},2}$ is the required variation of temperature to go from this 50% mix to only rainfall or only snowfall. This is illustrated in Figure 2.14. The proportion of rainfall p_{R}, for each time step t is computed as follows:

$$p_{\mathrm{R}}(t) = \begin{cases} 0 & \text{if} \quad T(t) \leq (T_{\mathrm{snow},1} - T_{\mathrm{snow},2}) \\ \dfrac{(T_{\mathrm{snow},1} + T_{\mathrm{snow},2} - T(t))}{2 \times T_{\mathrm{snow},2}} & \text{if} \quad (T_{\mathrm{snow},1} - T_{\mathrm{snow},2}) < T(t) < (T_{\mathrm{snow},1} + T_{\mathrm{snow},2}) \\ 1 & \text{if} \quad T(t) \geq (T_{\mathrm{snow},1} + T_{\mathrm{snow},2}) \end{cases} \tag{2.3}$$

where $T(t)$ is the air temperature at time t. Snowfall, P_{snow}, and rainfall, P_{rain}, are then computed as follows:

$$P_{\mathrm{snow}}(t) = P(t) \times (1 - p_{\mathrm{R}}(t)) \tag{2.4}$$

$$P_{\mathrm{rain}}(t) = P(t) \times p_{\mathrm{R}}(t) \tag{2.5}$$

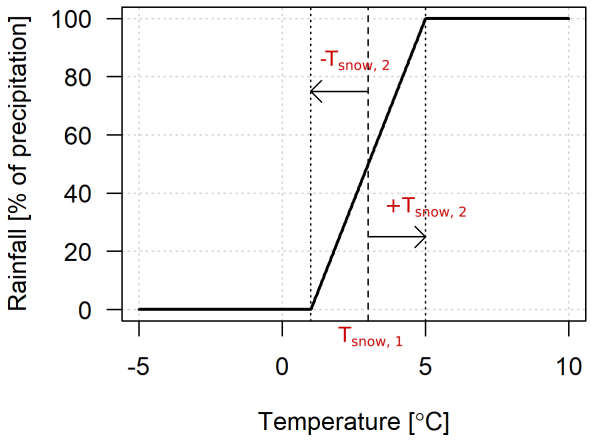

Figure 2.14: Partitioning of input precipitation into rainfall or snowfall in J2000. In this example, $T_{\text{snow},1} = 3°\text{C}$ and $T_{\text{snow},2} = 2°\text{C}$.

2.3.2.4 Vegetation interception

Incoming precipitation (rainfall and snowfall) on a HRU is intercepted by the vegetation as long as the interception maximum capacity is not exceeded. The maximum interception capacity is based on the Leaf Area Index (LAI): the total surface represented by leaves per unit of space. It depends on the type of vegetation and the period of the year. The parameter LAI is distributed according to the type of land-use. For each type of land-use, LAI takes 12 different values depending on the period of the year: one value for each month.

The maximum interception capacity also depends on the type of precipitation: liquid or solid. In case of solid precipitation, more water may be intercepted. This is modulated by the parameters a_{snow} and a_{rain} which represent the volume of water that may be intercepted by unit of Leaf Area Index (which is unit-less). The maximum interception capacity, INT_{max}, is computed as follows:

$$INT_{\text{max}}(t) = \begin{cases} LAI(t) \times a_{\text{snow}} \times HRU_{\text{area}} & \text{if} \quad T(t) \leq (T_{\text{snow},1} - T_{\text{snow},2}) \\ LAI(t) \times a_{\text{rain}} \times HRU_{\text{area}} & \text{if} \quad T(t) > (T_{\text{snow},1} - T_{\text{snow},2}) \end{cases} \tag{2.6}$$

where HRU_{area} is the area of the HRU. All the incoming water is intercepted by vegetation until INT_{max} is exceeded. Any excess reaches the ground surface as throughfall: $P_{\text{net, snow}}(t)$ and $P_{\text{net, rain}}(t)$. Note that, according to Equation 2.6, an increase of temperature above $T_{\text{snow},1} - T_{\text{snow},2}$ leads to a change of state of the water stored and hence to an excess of water that is released as liquid throughfall ($P_{\text{net, snow}}(t)$). This means than when a mix of solid and liquid water is stored by the vegetation, the model considers that it is only liquid water.

The water stored by the vegetation at a given time t, $INT_{\text{act}}(t)$, may only be depleted through direct evaporation depending on the potential evapotranspiration:

$$E_{\text{interception}}(t) = \begin{cases} INT_{\text{act}}(t) & \text{if} \quad INT_{\text{act}}(t) \leq E_{\text{POT}}(t) \\ E_{\text{POT}}(t) & \text{if} \quad INT_{\text{act}}(t) > E_{\text{POT}}(t) \end{cases} \tag{2.7}$$

with $E_{\text{interception}}(t)$ the water being evaporated from the vegetation interception reservoir. The water content in the interception reservoir is then updated: $INT_{\text{act}}(t) = INT_{\text{act}}(t) - E_{\text{interception}}(t)$.

2.3.2.5 Snow accumulation and snow melt

Solid precipitation that reaches the ground surface, $P_{\text{net, snow}}(t)$, is first handled by the snow module of J2000. At each time step t, solid precipitation is added to the Snow Water Equivalent state variable of the model, $SWE(t)$:

$$SWE(t) = SWE(t) + P_{\text{net, snow}}(t) \tag{2.8}$$

Snow storage may only be depleted through melting processes. Sublimation and snow transport (erosion, accumulation) are not considered. Snow melt is based on the computation of a "melt energy potential" M_{POT} following the degree-day approach of Hock (2003) enhanced by considering the increase of the snow pack temperature due to the energy input of liquid precipitation and potential energy input from the ground:

$$M_{\text{POT}}(t) = T_{\text{f}} \times (T(t) - T_{\text{base}}) + R_{\text{f}} \times T(t) \times P_{\text{net, rain}}(t) + G_{\text{f}} \tag{2.9}$$

where T_{f}, T_{base}, R_{f} and G_{f} are the temperature factor, the base temperature (temperature at which snow melt is triggered), the rain factor and the ground factor, respectively.

The variable CC, the "cold content" of the snow pack, represents the energy needed to increase the temperature of the snow pack at 0°C where snow melt occurs. Snow melt occurs only if CC, which is a negative variable, reaches 0. It is updated from one time step to the next, as a function of the air temperature $T(t)$ and a coefficient C_{CC}:

$$CC(t) = \begin{cases} CC(t-1) + C_{\text{CC}} \times 24 \times T(t) & \text{if} \quad T < 0 \\ CC(t-1) & \text{if} \quad T \geq 0 \end{cases} \tag{2.10}$$

The snow that melts at a given time step t, $M(t)$, depends on the variable CC and M_{POT} and is computed as follows:

$$M(t) = \begin{cases} M_{\text{POT}}(t) + CC(t) & \text{if} \quad M_{\text{POT}}(t) + CC(t) > 0 \\ 0 & \text{if} \quad M_{\text{POT}}(t) + CC(t) \leq 0 \end{cases} \tag{2.11}$$

The cold content, CC, is also updated as function of the potential snow melt:

$$CC(t) = \begin{cases} M_{\text{POT}}(t) + CC(t) & \text{if} \quad M_{\text{POT}}(t) + CC(t) < 0 \\ 0 & \text{if} \quad M_{\text{POT}}(t) + CC(t) \geq 0 \end{cases} \tag{2.12}$$

Snow melt $M(t)$ and incoming liquid precipitation $P_{\text{net, rain}}(t)$ increase the liquid water content S_{liquid} of the snow pack. It increases the global density of the snow pack, S_{density}. The water actually released from the snow pack, the actual snow melt $M_{\text{ACT}}(t)$, depends on this density and on the snow critical density C_{CD}:

$$M_{\text{ACT}}(t) = \left[1 - \text{e}^{-\left(\frac{C_{\text{CD}}}{S_{\text{density}}}\right)^4} \right] \times S_{\text{liquid}}(t) \tag{2.13}$$

To summarize the effect of the J2000 snow module, $P_{\text{net rain}}(t)$ and $M_{\text{ACT}}(t)$ are the two variables that eventually contain the water that reaches the ground surface. If there is no snow on the ground ($SWE(t) = 0$) and there is no solid precipitation ($P_{\text{net, snow}}(t) = 0$), $P_{\text{net rain}}(t)$ is unchanged and $M_{\text{ACT}}(t) = 0$. Otherwise, $P_{\text{net rain}}(t) = 0$ and only the variable $M_{\text{ACT}}(t)$ contains the water that reaches the ground.

2.3.2.6 Soils: infiltration, overland flow, transpiration and drainage

For a given HRU, the water that reaches the ground, $P_{\text{net}}(t)$, is the sum of snow melt, $M_{\text{ACT}}(t)$, vegetation throughfall, $P_{\text{net rain}}(t)$, and the overland flow from uphill HRUs, $RD_{1,\text{ uphill}}$:

$$P_{\text{net}}(t) = P_{\text{net rain}}(t) + M_{\text{ACT}}(t) + RD_{1,\text{ uphill}} \tag{2.14}$$

This water may infiltrate into the soil or generate an overland flow, RD_1, that is routed to a downhill HRU or to a reach, according to the topology of the model.

Infiltration excess overland flow Overland flow can be generated due to sealed ground surfaces. The distributed parameter K_{sealing} represents the proportion of sealed surface of the HRU. It is distributed according to the type of land-use. The overland flow due to the sealing of surfaces, $RD_{1,\text{ sealing}}(t)$, for a given time step t, is:

$$RD_{1,\text{ sealing}}(t) = P_{\text{net}}(t) \times K_{\text{sealing}} \tag{2.15}$$

Overland flow can also be generated because of an excess of the maximum infiltration rate of the soils (infiltration excess overland flow). The maximum infiltration rate of soils is represented by 3 lumped parameters: $I_{\text{max,summer}}$, $I_{\text{max,winter}}$ and $I_{\text{max,snow}}$. Note that they are specified in mm.day^{-1} and are first converted in L.day^{-1}. They account for the variability of this maximum depending on the season i.e. lower infiltration rate capacity is expected in Summer – defined in J2000 as the months from May to October – and depending on whether there is a snow cover i.e. lower maximum infiltration rate capacity is expected if there is snow. For each time step t, the overland flow $RD_{1,\text{ rate excess}}$ is computed as follows if $(P_{\text{net}}(t) - RD_{1,\text{ sealing}}(t)) > I_{\text{max}}$:

$$RD_{1,\text{ rate excess}}(t) = P_{\text{net}}(t) - RD_{1,\text{ sealing}}(t) - I_{\text{max}} \tag{2.16}$$

Otherwise, $RD_{1,\text{ rate excess}}(t) = 0$.

The two overland flow components ($RD_{1,\text{ sealing}}(t)$ and $RD_{1,\text{ rate excess}}(t)$) can be evaporated if $E_{\text{POT}}(t) > 0$, generating the evapotranspiration flux $E_{\text{ground}}(t)$. The remaining water, $I_{\text{POT}}(t)$, corresponds to the potential amount of water that may infiltrate into the soil:

$$I_{\text{POT}}(t) = P_{\text{net}}(t) - RD_{1,\text{ sealing}}(t) - RD_{1,\text{ rate excess}}(t) - E_{\text{ground}}(t) \tag{2.17}$$

Soil infiltration and saturation excess overland flow The soil is represented by two different reservoirs, the MPS (Middle Pore Storage) and LPS (Large Pore Storage) reservoirs. The MPS reservoir represents small pores in which water is held against gravity but can still be withdrawn by plants for transpiration. The LPS reservoir represents larger pores in the soil

where water is not held against gravity and hence can move vertically (percolation) or laterally (subsurface flow).

The maximum storage capacity of the MPS reservoir $MPS_{\max}$ depends on the root depth of vegetation Z_{root}, distributed according to the type of land-use, and the field capacities of the different soil horizons/layers ($i = 1, ..., n$) $\theta_{\text{FC},\,i}$, distributed according to the type of soil. The field capacity parameters $\theta_{\text{FC},\,i}$ (in mm.dm^{-1}) of all the layers (10 cm thick layers) that are within the root zone depth are summed to yield $MPS_{\max}$. The maximum storage capacity of the LPS reservoir, $LPS_{\max}$, corresponds to the air capacity, that is, the total porosity of the soil. It is distributed according to the type of soil. Two state variables represent the current water content of both reservoirs: MPS_{act} and LPS_{act}.

The water that can potentially infiltrate into the soil is stored in the variable $I_{\text{POT}}(t)$. The inflow into the MPS reservoir is controlled by the following equation (see Figure 2.15):

$$MPS_{\text{inflow}} = I_{\text{POT}}(t) \times \left[1 - \text{e}^{-\frac{C_{\text{DIST}}}{\theta_{\text{MPS}}(t)}}\right] \tag{2.18}$$

where C_{DIST} is a coefficient and θ_{MPS} is the saturation of the MPS reservoir ($\theta_{\text{MPS}} = MPS_{\text{act}}(t)/MPS_{\max}$). The actual inflow into the MPS reservoir depends on its current water content and maximum storage capacity: if $MPS_{\text{inflow}} > (MPS_{\max} - MPS_{\text{act}}(t))$, then the inflow is $MPS_{\text{inflow}} = MPS_{\max} - MPS_{\text{act}}(t)$.

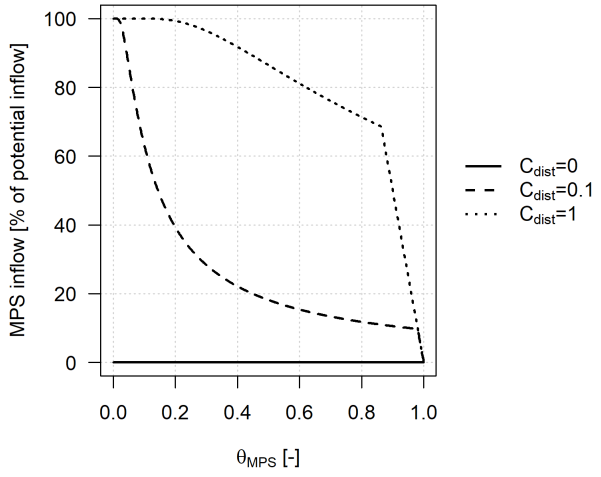

Figure 2.15: Effect of the coefficient C_{DIST} on the proportion of $I_{\text{POT}}(t)$ going into the MPS reservoir. In this example, the potential inflow $I_{\text{POT}}(t)$ represents 20% of $MPS_{\max}$.

The water inflow in the LPS reservoir corresponds to the remaining water;

$$LPS_{\text{inflow}} = I_{\text{POT}}(t) - MPS_{\text{inflow}} \tag{2.19}$$

Similarly to the MPS reservoir, the actual inflow cannot exceed the LPS reservoir maximum capacity: if $LPS_{\text{inflow}} > (LPS_{\max} - LPS_{\text{act}}(t))$ then, the inflow into the LPS reservoir is $LPS_{\text{inflow}} = LPS_{\max} - LPS_{\text{act}}(t)$. If any, the remaining water produces an overland flow, representing the saturation excess overland flow:

$$RD_{1,\,\text{saturation excess}}(t) = I_{\text{POT}}(t) - MPS_{\text{inflow}} - LPS_{\text{inflow}} \tag{2.20}$$

In addition, water from uphill HRUs that arrives as subsurface flow, $RD_{2,\,\text{uphill}}$, follows the same chain of processes: (1) inflow in MPS following Equation 2.18, (2) inflow in LPS following Equation 2.19. Any excess can then generate an overland flow, $RD_{1,\,\text{exfiltration}}(t)$, which in this case, can be seen as exfiltration.

The sum of the three types of overland flow gives the total overland flow $RD_1(t)$:

$$RD_1(t) = RD_{1,\,\text{sealing}}(t) + RD_{1,\,\text{rate excess}}(t) + RD_{1,\,\text{saturation excess}}(t) + RD_{1,\,\text{exfiltration}}(t) \quad (2.21)$$

Diffusion A diffusion mechanism is also considered in the soil module of J2000 to represent water from large pores going into the smaller pores, i.e. from the LPS reservoir to the MPS reservoir. This diffusion of water, $LPS_{\text{diffusion}}$, depends on the water content of the LPS reservoir, $LPS_{\text{act}}(t)$, the saturation of MPS, θ_{MPS}, and a coefficient, C_{DIFF} (see Figure 2.16). It is implemented as follows:

$$LPS_{\text{diffusion}} = \begin{cases} LPS_{\text{act}}(t) \times \left[1 - \text{e}^{-\frac{C_{\text{DIFF}}}{\theta_{\text{MPS}}}}\right] & \text{if} \quad MPS_{\text{act}}(t) > 0 \\ 0 & \text{if} \quad MPS_{\text{act}}(t) = 0 \end{cases} \quad (2.22)$$

The calculated diffusion cannot exceed the water content of LPS ...

$$LPS_{\text{diffusion}} = LPS_{\text{act}}(t) \quad \text{if} \quad LPS_{\text{diffusion}} > LPS_{\text{act}}(t)$$

... or the remaining available storage of MPS

$$LPS_{\text{diffusion}} = MPS_{\text{max}} - MPS_{\text{act}}(t) \quad \text{if} \quad LPS_{\text{diffusion}} > (MPS_{\text{max}} - MPS_{\text{act}}(t))$$

The MPS and LPS reservoir water content are then updated: $MPS\text{act}(t) = MPS_{\text{act}}(t) + LPS_{\text{diffusion}}$ and $LPS\text{act}(t) = LPS\text{act}(t) - LPS_{\text{diffusion}}$.

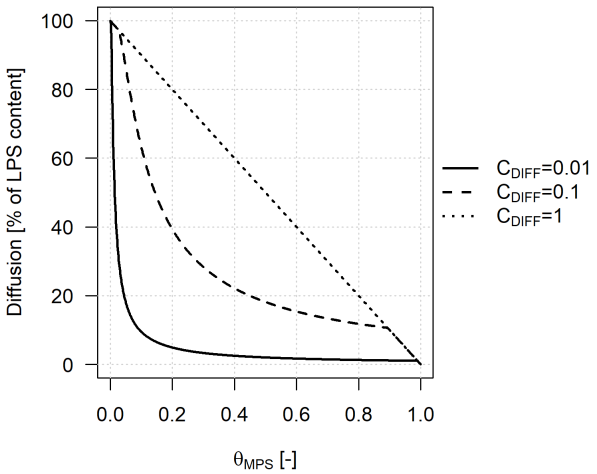

Figure 2.16: Effect of the coefficient C_{DIFF} on the proportion of the LPS reservoir content being diffused to the MPS reservoir. In this example, the LPS reservoir is fully saturated and has the same size than the MPS reservoir.

Plant transpiration The water in the MPS reservoir can only be released through plant transpiration. The plant transpiration is computed as a function of MPS saturation, θ_{MPS}, evapotranspiration demand, E_{POT}, and a coefficient C_{ET}:

$$E_{\mathrm{transpiration}}(t) = \begin{cases} \theta_{\mathrm{MPS}}/C_{\mathrm{ET}} \times E_{\mathrm{POT}} & \text{if} \quad \theta_{\mathrm{MPS}} < C_{\mathrm{ET}} \\ E_{\mathrm{POT}} & \text{if} \quad \theta_{\mathrm{MPS}} \geq C_{\mathrm{ET}} \end{cases} \tag{2.23}$$

If the computed plant transpiration exceeds the water content of the MPS reservoir ($E_{\mathrm{transpiration}}(t) > MPS_{\mathrm{act}}(t)$), then $E_{\mathrm{transpiration}}(t) = MPS_{\mathrm{act}}(t)$. The content of the MPS reservoir is then updated accordingly: $MPS\mathrm{act}(t) = MPS\mathrm{act}(t) - E_{\mathrm{transpiration}}(t)$.

Soil drainage: subsurface flow and percolation The water in the LPS reservoir can be released either through the diffusion to the MPS reservoir (see above) or through soil drainage. Soil drainage depends on the overall soil saturation, $\theta_{\mathrm{SOIL}}(t)$:

$$\theta_{\mathrm{SOIL}}(t) = \frac{MPS_{\mathrm{act}}(t) + LPS_{\mathrm{act}}(t)}{MPS_{\mathrm{max}} + LPS_{\mathrm{max}}} \tag{2.24}$$

The capacity of the soil to drain is controlled by the lumped parameter K_{LPSout}. The water released from the LPS reservoir, $LPS_{\mathrm{out}}(t)$, is computed as follows:

$$LPS_{\mathrm{out}}(t) = LPS_{\mathrm{act}}(t) \times \theta_{\mathrm{SOIL}}(t)^{K_{\mathrm{LPSout}}} \tag{2.25}$$

Figure 2.17 shows the effect of parameter K_{LPSout} on $LPS_{\mathrm{out}}(t)$: the larger it is the more saturated the soil needs to be to generate the same LPS outflow (in proportion of LPS water content).

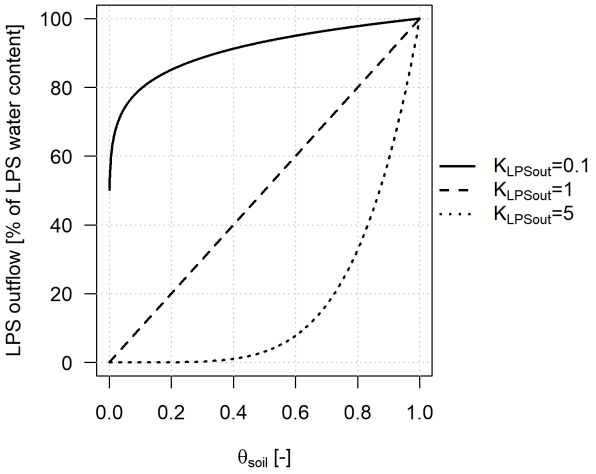

Figure 2.17: LPS outflow as a function of total soil saturation θ_{SOIL} for 3 values of K_{LPSout}. In this example, the MPS reservoir has a storage capacity of 0.

This water ($LPS_{\mathrm{out}}(t)$) may move laterally, generating a subsurface flow $RD_2(t)$ or percolate to the groundwater reservoir, $P_{\mathrm{perc}}(t)$. The partitioning between these two outcomes is controlled by the average slope of the HRU, HRU_{slope}, and a lumped parameter K_{latvert}. The proportion of subsurface flow p_{RD2} is computed as follows:

$$p_{RD2}(t) = \tan\left(HRU_{\mathrm{slope}}\right) \times K_{\mathrm{latvert}} \tag{2.26}$$

In addition, $p_{RD2}(t)$ is constrained between 0 and 1. The percolation can then be computed:

$$P_{\text{perc}}(t) = LPS_{\text{out}}(t) \times (1 - p_{RD2}(t)) \tag{2.27}$$

However, percolation cannot exceed a maximum percolation rate defined by the global parameter $P_{\max}$. Therefore, the subsurface flow is given by:

$$RD_2(t) = \begin{cases} RD_2(t) = LPS_{\text{out}}(t) \times p_{RD2}(t) + (P_{\text{perc}}(t) - P_{\max}) & \text{if} \quad P_{\text{perc}}(t) > P_{\max} \\ RD_2(t) = LPS_{\text{out}}(t) \times p_{RD2}(t) & \text{if} \quad P_{\text{perc}}(t) \leq P_{\max} \end{cases} \tag{2.28}$$

Figure 2.18 shows the effect parameter K_{latvert} and $P_{\max}$ have on the partitioning between subsurface flow and percolation. The larger K_{latvert}, the more subsurface flow is generated for a given HRU slope. Parameter $P_{\max}$ acts as a threshold for low slope values.

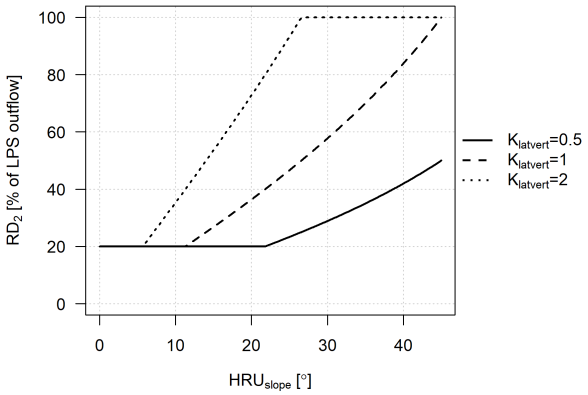

Figure 2.18: Subsurface flow RD_2 as a function of HRU slope for different values of parameter K_{latvert}. In this example, $P_{\max}$ is set at 20% of the LPS outflow.

2.3.2.7 Groundwater storage and release

In previous versions of J2000, two groundwater reservoirs were considered, one for relatively fast groundwater contributions and the other one for relatively slow flow contributions. The J2000 Rhône model was simplified by considering only a single groundwater reservoir. The same simplification was used here.

The size of the RG reservoir, $RG_{\max}$, is a distributed parameter that depends on the type of geology. The water that percolates, $P_{\text{perc}}(t)$ goes into the groundwater reservoir RG: $RG_{\text{act}}(t) = RG_{\text{act}}(t) + P_{\text{perc}}(t)$. $RG_{\text{act}}(t)$ is the water content of the RG reservoir at time t. If the water going in the RG reservoir exceeds its remaining storage capacity, the excess is added to the subsurface flow component $RD_2(t)$.

Water is released from the groundwater reservoir, generating a groundwater flow $RG(t)$ as a function of its water content, $RG_{\text{act}}(t)$, and a depletion time parameter, τ_{RG}, following a linear storage-outflow relationship:

$$RG(t) = \frac{1}{\tau_{\text{RG}}} \times RG_{\text{act}}(t) \tag{2.29}$$

Figure 2.19 shows the effect of different values for the depletion time parameter τ_{RG}: the larger it is, the slower is the depletion of the RG reservoir.

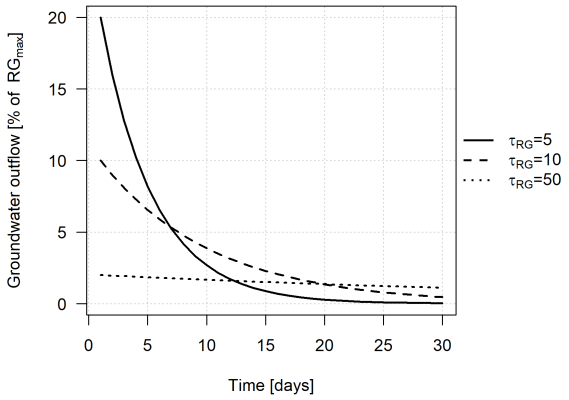

Figure 2.19: Groundwater outflow $RG(t)$ (in proportion of $RG_{\max}$) as a function of time for different depletion time parameter τ_{RG}. In this example, there is no inflow in the RG reservoir.

Groundwater flow from uphill HRUs, $RG_{2,\,\mathrm{uphill}}$, also fills the RG reservoir until it is full. Any excess is directly routed downhill to the next HRU or reach.

2.3.2.8 Streamflow routing in the river network

The three components of flow, overland flow $RD_1(t)$, subsurface flow $RD_2(t)$ and groundwater flow $RG(t)$ are routed downhill from HRU to HRU, following the model topology for a particular catchment. These flow components eventually reach a river reach and are added to the volume of water in this reach. In the model river network (the reaches), the sum of these components is the total streamflow $Q(t)$. The flow routing between reaches is done following a kinematic wave approach.

First, the volume of water within the reach, $Q(t)$, is updated according to the incoming water from upstream reaches or HRUs, $Q_{\mathrm{in}}(t)$:

$$Q(t) = Q(t) + Q_{\mathrm{in}}(t) \tag{2.30}$$

In the reach routing module of J2000, computation is done using streamflow Q in m^3/s. A Manning's equation is used to compute the flow velocity V considering a rectangular channel with a width W_{reach}, a slope J_{reach} and a Strickler coefficient (roughness) K_{reach}. The computation is done in an iterative way until the difference between velocities computed at iteration i and $i-1$ is below a threshold value ϵ ($\epsilon = 0.001$): $V_i - V_{i-1} \leq \epsilon$. For an iteration i ($i > 1$), the Manning's equation used is:

$$V_i = K \times \sqrt{J} \times \left(\frac{Q/V_{i-1}}{W + 2 \times (Q/V_{i-1} \times W)} \right)^{2/3} \tag{2.31}$$

The volume of streamflow of a given reach that is routed to the next (downstream) reach, $Q_{\mathrm{out}}(t)$, is then computed as a function of the current volume of water in the reach $Q(t)$, the computed flow velocity V and the length L_{reach} of the current reach:

$$Q_{\mathrm{out}}(t) = Q(t) \times \mathrm{e}^{-\frac{1}{V \times 3600/L_{\mathrm{reach}}}} \tag{2.32}$$

The routing of streamflow in reaches depends on reach characteristics that are most of the time directly derived from the DEM (J_{reach}, L_{reach}). Other reach characteristics are parameters that need to be specified by the user: K_{reach} and W_{reach}. Also note that the routing modules keeps track of the relative contributions of the different flow components generated in the HRUs: $RD_1(t)$, $RD_2(t)$ and $RG(t)$.

2.3.3 Tools associated to J2000

2.3.3.1 JAMS

The Jena Adaptable Modeling Software (JAMS) is a modular modeling framework (Kralisch, 2006). It includes many modules that represent different processes or that perform different tasks such as the management of inputs and outputs. It contains many models including the water balance model J2000g (Krause and Hanisch, 2009), the nutrient transport model J2000s (Fink et al., 2007), the SIMPLEFLOOD model (Adamovic et al., 2016) and the J2000 model (Krause et al., 2006).

The J2000 model includes many modules (also called components) that do different tasks or represent different hydrological processes. They are stored in contexts which can store variables accessible by all the modules that it contains. Different types of contexts that do different tasks also exists including a temporal context and a spatial context that allow iterating over time steps and HRUs/reaches. The modules communicate between each other through variables and HRU and reach objects that are attached to each context.

In Appendix C.2, further details on JAMS and the structure of the J2000 within JAMS, i.e. how the different components and contexts are organized. Appendix C.2, also details how the structure of the J2000 model was re-created, based on the J2000 Rhône model, to allow for more flexibility and clarity when set up on a new catchment.

2.3.3.2 HRU-Delin

At Irstea, during the MDR (Modélisation Distribuée du Rhône) project (Branger et al., 2016), the HRU-Delin tool was developed from a previously existing tool (GRASS-HRU, developed at the University of Jena, Germany) in order to create HRUs for the J2000 model. HRU-Delin uses various spatial data to create the HRUs: a Digital Elevation Model (DEM), a geological map, a soil/pedology map, and a land-use map. Moreover, HRU-Delin creates the topology of the J2000 model, i.e. the drainage network of the model which corresponds to the links between HRUs, the links between HRUs and river reaches as well as the links between the river reaches. It takes into account the location of hydrometric stations and dams to cut the hydrographic network at the right locations and to properly delineate the corresponding sub-catchments. The 4 steps for HRU-Delin, given in the work-flow diagram in Figure 2.20, can be summarized as follows:

1. Using a drainage algorithm, various maps are derived from the DEM including the river network, catchment slopes and aspects; the DEM and derived maps are reclassified according to a specified resolution to be used in the GIS cross-over and HRU delineation

process; hydrometric station (or dams) within the area of interest are selected;

2. The hydrometric stations are relocated to be positioned on the calculated river network computed in step 1; the river network is cut at the hydrometric stations locations and the corresponding sub-catchments are computed;

3. A cross-over of reclassified DEM, pedology, geology and land-use maps is performed. It is constrained by the sub-catchments and a size threshold. It identifies homogeneous areas and computes the final HRUs;

4. The topology between HRUs and the river reaches is computed according to elevation information derived from the DEM. The J2000 topology files are created: hrus.par and reach.par.

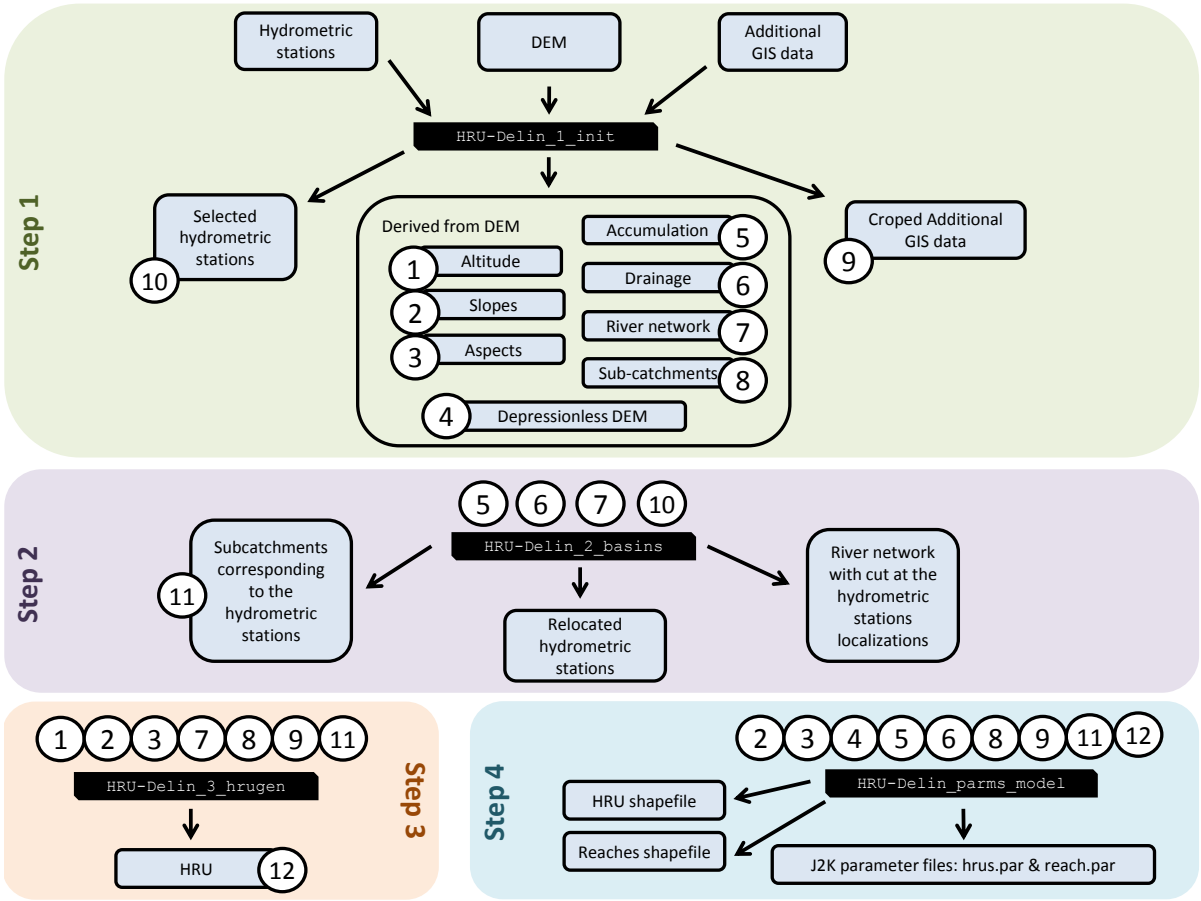

Figure 2.20: Work-flow and general functioning of HRU-Delin. Numbers identify intermediate outputs/inputs of HRU-Delin used in the 4 steps.

Note that a major bug of HRU-Delin was identified and led to significant modification of the associated code (see Appendix C.4.2).

The HRU-Delin tool relies on several parameters that affect its behavior and the results. The main parameters are (1) the reclassification resolution of the DEM elevation, slope and aspect, (2) the minimum size of the subcatchments computed with the draining algorithm (which affects the resolution of the river network) and (3) the minimum size of a HRU. In addition, the resolution of the input raster data directly affects the results. The type of land-use, soil and geology is pre-processed to yield, as input to HRU-Delin, raster maps, where pixels

can take only a finite number of values corresponding to the type of land-use, soil or geology. These values are the classes of land-use, soil and geology, used to parameterize the J2000 model.

HRU-Delin produces two main parameter files of the J2000 model: the HRU and reach parameter files. They contain physical characteristics of the HRU and reaches derived from the DEM and the topology of the model, i.e. how flow is to be routed between HRUs, between HRUs and reaches and between reaches. Further details are provided in Appendix C.4.1.

2.4 The J2000 Ardèche model

2.4.1 J2000 setup on the Ardèche catchment

2.4.1.1 HRUs of the Ardèche catchment

The HRU-Delin tool was used to create the HRUs of the model and topology of the J2000 Ardèche model. The deployment of HRU-Delin requires several spatial data (see Section 2.3.3) which are: (1) the hydrometric station (and dams) locations, (2) the DEM and (3) the land-use, soil and geology raster layers. Most of the hydrometric station and dams of the Ardèche catchment were considered (see Figure 2.1) to enable future use of the model for other subcatchments than the 4 selected subcatchments and the consideration of the influence of dams.

The DEM provided by IGN and used in Figure 2.3.3 has a 25 m X and Y resolution. This high resolution was unnecessary for our application. Therefore it's resolution was first decreased to 50 m. The data presented in Section 2.1.1 were used to create the input land-use, soil and geology raster layers.

The land-use data (Andrieu, 2015a) are in a raster format and are classified in 10 different categories (see Figure 2.4). The soil data presented in Figure 2.3 need to be classified and rasterized. For the soil data, the classification proposed by Bahl (2016) was used: the soil is classified according to 4 soil depths. The classification of the geology used by Branger et al. (2016) in the J2000-Rhône mode was used here: it is based on the type of geology and permeability characteristics. The reclassification of the data leads to 10 land-use classes, 4 soil classes and 7 geology classes.

HRU-Delin was run and resulted in 1474 HRUs with a average area of about 1.5 km^2 (95% of the HRUs have area between 1 km^2 and 2.24 km^2). Figure 2.21 shows the HRUs land-use classes, soil classes and geology classes. Note that part of the information was lost in the HRU delineation process. For example, the Cladugne catchment includes some portion of grapevines and other agricultural land but no HRU represents these types of land-use.

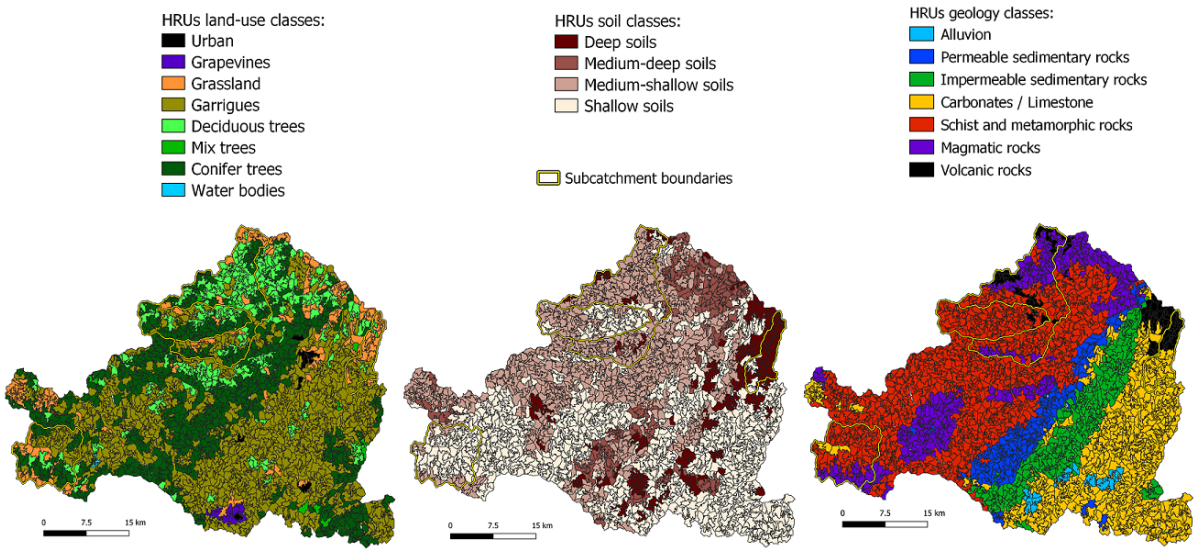

Figure 2.21: The 1474 HRUs computed by HRU-Delin for the J2000 Ardèche model. HRUs are colored according to their attributed class of land-use, soil and geology.

2.4.1.2 Parameters of J2000 for the Ardèche catchments

The specification of the lumped and distributed parameters of the J2000 Ardèche model is presented here. The model parameters (Table 2.5) of the J2000 Ardèche model were largely specified based on the parameters used for the J2000 Rhône model (Branger et al., 2016). Table 2.6 presents the values specified for the lumped parameters. Tables 2.7, 2.8 and 2.9 present the values specified for the distributed parameters of the J2000 Ardèche model.

Lumped parameters

Table 2.6: Values specified for the lumped parameters of the J2000 Ardèche model

Name	Value	Unit
a_{snow}	1.5	km
a_{rain}	1	km
$T_{\text{snow},1}$	2	°C
$T_{\text{snow},2}$	3	°C
T_{base}	0	°C
T_{f}	1.84	mm.°C
R_{f}	0.0125	$°C^{-1}$
G_{f}	0	mm
C_{CD}	0.7	$g.cm^{-3}$
C_{CC}	0.0012	-
$I_{\text{max,summer}}$	40	$mm.day^{-1}$
$I_{\text{max,winter}}$	50	$mm.day^{-1}$
$I_{\text{max,snow}}$	20	$mm.day^{-1}$
C_{DIST}	0	-
C_{DIFF}	5	-
K_{LPSout}	5	-
K_{latvert}	1	-
C_{ET}	0.9	-
P_{max}	20	$mm.day^{-1}$

The two parameters that modulate the interception maximum storage capacity depending on the type of precipitation (liquid/solid) a_{snow} and a_{rain} were specified as in Branger et al. (2016) in order to have more interception in case of snowfall. Given Equation 2.6, the value of 1.5 km (resp. 1.0 km) for a_{snow} (resp. a_{rain}) means the interception maximum storage capacity for a LAI of 1 is 1.5 mm in case of snowfall (resp. 1.0 mm in case of rainfall). The unit of a_{snow} and a_{rain} comes from Equation 2.6.

The snow parameters were based on the detailed study of Gouttevin et al. (2017). They noted very low sensitivity of the result of the J2000 model to the rain factor R_{f}, ground factor G_{f} and T_{base} of the snow melt model and therefore specified their value to 0.0125, 0 and 0 respectively. The value specified for the rain factor corresponds to its physical value. They also noted a low sensitivity to the cold content factor C_{CC}, the default value of the J2000 model, 0.0012, was therefore used. Finally, following the recommendation of Gouttevin et al. (2017) the snow critical density was fixed to 700 kg/m^3. Gouttevin et al. (2017) optimized the temperature factor for the whole Rhône catchment and found a an optimal value of 1.84 mm/°C which is used here.

In the J2000 Rhône model, the maximum rates of infiltration in the soil ($I_{\text{max,summer}}$, $I_{\text{max,winter}}$, $I_{\text{max,snow}}$) were distributed according to the type of land-use to account for observed differences between forests and other type of land-use (Branger et al., 2016). However, using their parameterization in the case of the Ardèche catchment resulted in very little differences between the type of land-use: 50 mm.day^{-1} (resp. 60 mm.day^{-1}) for forests and 40 mm.day^{-1} (resp. 50 mm.day^{-1}) for all other types of land-use for $I_{\text{max,summer}}$ (resp. $I_{\text{max,winter}}$), and no differences for $I_{\text{max,snow}}$. Therefore, it was simplified here to consider a unique set of values for these three parameters, making them lumped parameters: 40 mm.day^{-1}, 50 mm.day^{-1} and 20 mm.day^{-1} for $I_{\text{max,summer}}$, $I_{\text{max,winter}}$ and $I_{\text{max,snow}}$ respectively.

The parameters controlling the distribution (C_{DIST}) and diffusion (C_{DIFF}) mechanisms were set in order to (1) make all the water go first in LPS (no infiltration into MPS, see Figure 2.15) and then (2) as long as there is water in LPS and room for more water in MPS, make all the water go into the MPS reservoir (maximum diffusion, see Figure 2.16): a value of 0 for C_{DIST} and a value of 5 for C_{DIFF}. This is the same parameterization as the J2000 Rhône model.

The parameter controlling the drainage of the LPS reservoir, K_{LPSout}, was set at 5, which make soil drainage possible only when the soil saturation is above approximately 50%, (Figure 2.17). The parameter K_{latvert} which controls the weight of the HRU slope on the partitioning of water between lateral subsurface flow and percolation was set to 1. This specification leads to approximately 50% of lateral subsurface flow for slope values of about 30° (see Figure 2.18). The maximum percolation rate to the groundwater reservoir, P_{max}, and the parameter affecting the capacity of plants to widthraw water from the MPS reservoir (when not close to saturation), C_{ET}, were set at 20mm.day^{-1} and 0.9, respectively. All these parameters were kept unchanged from the J2000 Rhône model.

Distributed parameters

Similarly to most of the lumped parameters, the specification of the distributed parameters was based on the J2000 Rhône model. However, the parameterization was simplified and as the classes of land-use differ largely some adaptations were required.

Table 2.7 shows the monthly values of K_{crop} and LAI specified for each class of land-use. All forests were specified to have the same values. Although the LAI value of conifer trees should not vary as much throughout the year, it was seen as a reasonable first approximation. Note that in the J2000 Rhône model, no distinction was done between these different types of forests. Garrigue and grassland also share the same value of monthly K_{crop} and LAI. Although larger K_{crop} value should be considered during the Summer months for garrigues as they include Mediterranean trees in addition to the low vegetation of bushes. Very low K_{crop} and LAI values were specified for grapevines as there are mostly bare soils surrounding the actual grapevines. For urban areas and water bodies the values used in the J2000 Rhône model were simplified and used here.

Table 2.7 also shows the value specified for the sealing coefficients K_{sealing} and the depth of roots, Z_{roots}. K_{sealing} was set at 20% for forests, 10% for grassland and garrigues and 50% for urban areas and grapevines. The root depth is used in combination with the field capacity parameters θ_{FC} – distributed according to the type of soil (Table 2.8) – to compute the maximum

storage capacity of the MPS reservoir. The way the parameters are currently specified disable the effect of the root depth: root depth is always larger than the soil depth. The soil depth corresponds to the number of layers of 10 cm of soil specified for the field capacity parameter (see Table 2.8 where each row containing a θ_{FC} value corresponds to a 10 cm soil layer). Therefore, the size of the MPS reservoir, MPS_{max}, only depends on the depth of the soils. The value of MPS_{max} is the sum of the 11 values of θ_{FC} shown in Table 2.8: 125 mm for deep soil, 86 mm for medium-deep soils, 54 mm for medium-shallow soils and 25 mm for shallow soils.

Table 2.7: Specified values for the parameter distributed according to the type of land-use

		Urban	Grapevines	Grassland	Deciduous trees	Mix trees	Conifer trees	Garrigues	Water bodies
Z_{root} [dm]		7.5	10	15	15	15	15	15	30
$K_{sealing}$ [-]		0.5	0.5	0.1	0.2	0.2	0.2	0.1	0
K_{crop} [-]	January	1	0.5	1	1	1	1	1	0.5
	February	1	0.5	1	1	1	1	1	0.5
	Marsh	1	0.5	1	1.1	1.1	1.1	1	0.5
	April	1	0.5	1	1.1	1.1	1.1	1	0.75
	May	1	0.5	1	1.2	1.2	1.2	1	1
	June	1	0.5	1	1.2	1.2	1.2	1	1
	July	1	0.5	1	1.2	1.2	1.2	1	1
	August	1	0.5	1	1.2	1.2	1.2	1	1
	September	1	0.5	1	1.1	1.1	1.1	1	1
	October	1	0.5	1	1.1	1.1	1.1	1	0.75
	November	1	0.5	1	1	1	1	1	0.5
	December	1	0.5	1	1	1	1	1	0.5
LAI [-]	January	1.5	0	1	2	2	2	1	1
	February	1.5	0	1	2.5	2.5	2.5	1	1.5
	Marsh	1.5	0	1.5	3	3	3	1.5	2
	April	1.5	0	2	3.5	3.5	3.5	2	2.5
	May	1.5	0	2.5	4	4	4	2.5	3
	June	1.5	0	3	4	4	4	3	4
	July	1.5	0	3	4	4	4	3	4
	August	1.5	0	2.5	4	4	4	2.5	3
	September	1.5	0	2	3.5	3.5	3.5	2	2.5
	October	1.5	0	1.5	3	3	3	1.5	2
	November	1.5	0	1	2.5	2.5	2.5	1	1.5
	December	1.5	0	1	2	2	2	1	1

The size of the LPS reservoir, LPS_{max}, represents the amount of porosity (large pores) of the soil. Currently, the value of LPS_{max} that were specified are mostly based on soil depth (see Table 2.8). Note that the size of the LPS reservoir is larger than the size of the MPS reservoir for all classes of soils.

Table 2.9 presents the two parameters distributed according to the type of geology: the size of the groundwater reservoir RG_{max} and the groundwater reservoir depletion time characteristics τ_{RG}. The values used here were mostly based on those used in the J2000 Rhône model. The largest groundwater storage capacity, RG_{max}, is specified for alluvium (1000 mm) and permeable sedimentary rocks (700mm). The smallest values are specified for impermeable sedimentary rocks (100 mm) and volcanic rocks (200 mm). The groundwater reservoir depletion time characteristics τ_{RG} range from 20 days (Alluvium, volcanic rocks and carbon-

Table 2.8: Specified values for the parameter distributed according to the type of soil.

		Deep	Medium-deep	Medium-shallow	Shallow
$LPS_{\max}$ [mm]		250	180	140	130
θ_{FC} [mm.dm^{-1}] †	Layer 1	11.33	10.77	10.83	12.25
	Layer 2	11.33	10.77	10.83	12.25
	Layer 3	11.33	10.77	10.83	0
	Layer 4	11.33	10.77	10.83	0
	Layer 5	11.33	10.77	10.83	0
	Layer 6	11.33	10.77	0	0
	Layer 7	11.33	10.77	0	0
	Layer 8	11.33	10.77	0	0
	Layer 9	11.33	0	0	0
	Layer 10	11.33	0	0	0
	Layer 11	11.33	0	0	0

† One value every 10cm of soils (Layers); 11 Layers of soils are shown here.
θ_{FC} is specified for 30 layers, but with zeros for all the layers not shown here.

ates/limestone) to 70 days for permeable sedimentary rocks and are set to 30 days for the other geology classes.

Table 2.9: Specified values for the parameter distributed according to the type of geology.

	Alluvion	Schists and metamorphic rocks	Magmatic rocks	Volcanic rocks rocks	Permeable sedimentary rocks	Carbonates series and limestone	Impermeable sedimentary rocks
$RG_{\max}$ [mm]	1000	400	500	200	700	500	100
τ_{RG} [days]	20	30	30	20	70	20	30

The Strickler coefficients (roughness), K_{reach}, were set to 30 m$^{1/3}$.s^{-1} for all reaches. This is the value that is recommended from previous hydraulic modeling work done on the Ardèche river (Adamovic, 2014). The widths of the river reaches, W_{reach}, were specified according to their Strahler order. Manual measurements done on orthophotos of typical river reaches belonging to the different Strahler orders were used to derive a typical width value for each Strahler order: 50 m for order 4, 30 m for order 3, 20 m for order 2 and 10 m for order 1.

All the distributed parameters that are directly derived from the DEM were not modified. For the reaches, these distributed parameters are the slope, J_{reach} and length L_{reach}. For the HRUs, these distributed parameters are the size HRU_{area} and average slope HRU_{slope}.

Table 2.10 shows the aggregated value of the distributed parameters at the scale of each of study catchment. It provides an overview of how the parameters are affecting the different study catchments given the spatial heterogeneity in land-use, soil and geology (and reach characteristics) specified in the HRU delineation process. Table 2.10 shows that the Claduègne catchments differ largely from the other catchments with more soil storage, faster groundwater depletion and slightly less interception and evapotranspiration demand.

Table 2.10: Aggregated value of the distributed parameters at the scale of each of study catchment. Parameters were aggregated using a weighted mean (according to the area of HRUs); parameters expressed in millimeters were aggregated according to weighted sum.

	$LAI^{\dagger}$ [−]	$K_{\text{crop}}{}^{\dagger}$ [−]	K_{sealing} [−]	$MPS_{\max}$ [mm]	$LPS_{\max}$ [mm]	$RG_{\max}$ [mm]	τ_{RG} [day]	HRU_{slope} [°]	W_{reach} [m]	J_{reach} [°]
Meyras	2.89	1.08	0.179	38.4	135	392	29.6	22.4	10	2.73
Pont-de-Labeaume	2.83	1.08	0.175	51.5	144	401	29	20.8	11.4	3.06
Goulette	2.45	1.05	0.146	30.3	132	430	29.3	16.4	17.4	2.33
Cladugne	1.92	1.01	0.106	105	227	388	20	9.26	10	2.55

† The average value computed over the 12 months is considered here.

2.4.2 Default simulation

From these parameters, a default simulation was run. The model was run from January 1st, 1970 to August 31st, 2019. Given the available observed streamflow time series (Table 2.3), this ensures at least 10 years of warm up. In the comparison of observed and simulated streamflow data, the modeling time range leads to 27, 22, 29 and 6 hydrological year (i.e. starting September 1st) for Meyras, Pont-de-Labeaume, Goulette and Cladugne catchments.

We used 5 performance metrics to evaluate the performance of the model for the four study catchments (see Section 1.2.1.1): the Nash-Sutcliff Efficiency applied on streamflow values, P_{NSE}, and log-transformed streamflow values, $P_{\text{NSE.log}}$, as well as, the Kling-Gupta Efficiency, P_{KGE}, the correlation coefficient, P_{R^2} and the relative bias, P_{BIAS} ($\sum(Q_{\text{sim}} - Q_{\text{obs}}) / \sum Q_{\text{obs}}$). The computed performance metrics are reported in Figure 2.22. Figure 2.22 shows overall

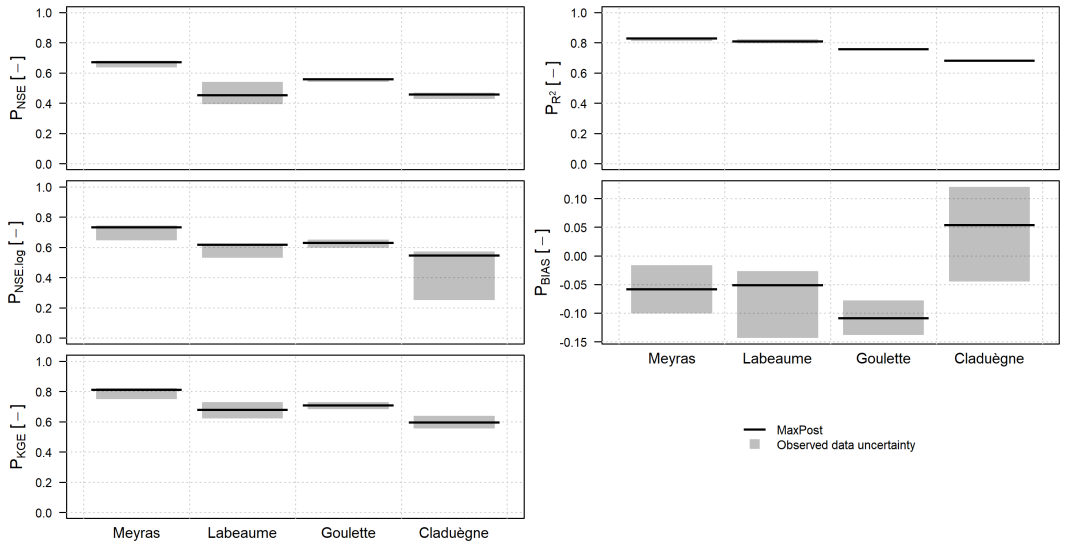

Figure 2.22: Performance metrics computed from the default simulation of the J2000 Ardèche model for the four study catchments, Meyras, Pont-de-Labeaume, Goulette and Cladugne.

average to good performance, in particular for an uncalibrated hydrological model. P_{NSE} is above 0.4 for all catchments with the best performance for Meyras (about 0.7). $P_{\text{NSE.log}}$ gives slightly better performance (above about 0.5, except for Cladugne catchment) suggesting that the model is better at simulating low flows. Slightly better performances are also found using P_{KGE} (above 0.6). The coefficients of correlation, P_{R^2}, are overall good (above 0.7) with the best performance for Meyras and the worst one for Cladugne. Finally, P_{BIAS} indicates that streamflow is, on average, underestimated for Meyras, Pont-de-Labeaume and Goulette and

overestimated for Cladueègne.

Figure 2.23 shows the observed (with uncertainty) and simulated streamflow time series of the four study catchments over a whole hydrological year chosen arbitrarily. It illustrates the results of the default simulation and shows how it differs from observation.

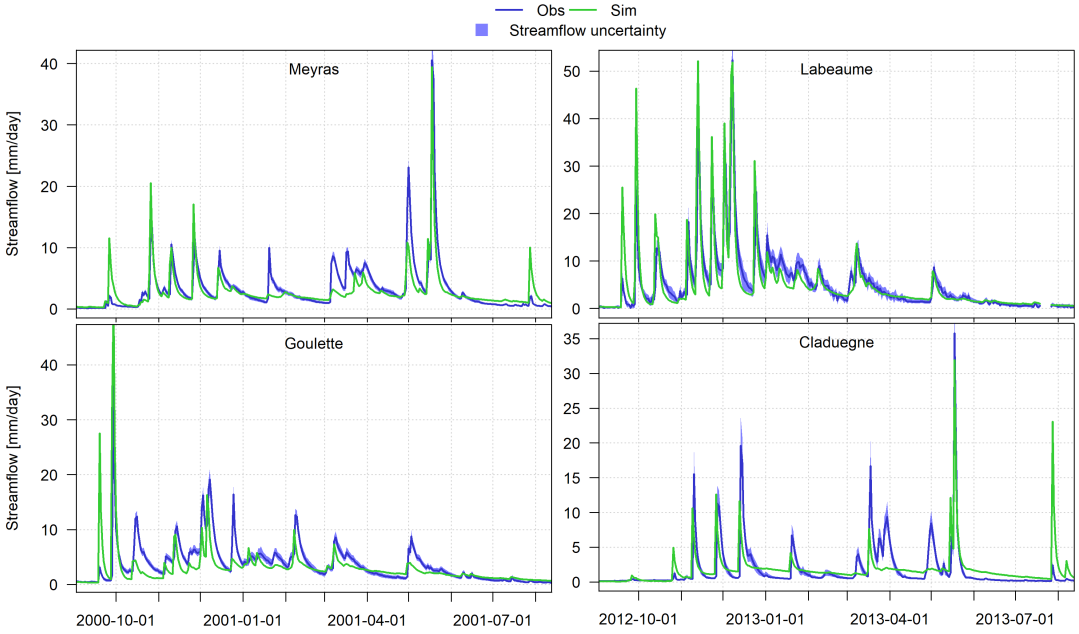

Figure 2.23: Streamflow time series from the default simulation of the J2000 Ardèche model and the corresponding observed (with uncertainty) streamflow time series, over a whole hydrological year, for the four study catchments

Chapter 3

Snow related hydrological signatures

Contents

The relevance of the hydrological signatures depends on the hydro-climatic context. For example, if only considering the Rhône catchment (South East of France), a large heterogeneity of hydro-climatic contexts can be found with, for example, Mediterranean catchments, low land continental catchments, and Alpine catchments. Different hydrological signatures need to be considered depending on these contexts. In particular, snow-dominated catchments such as the Alpine catchments, which have a very distinct streamflow response, require hydrological signatures that focus specifically on the snow processes.

In this chapter, 5 hydrological signatures that focus on snow processes are investigated. We aim at evaluating these hydrological signatures taking advantage of additional snow measurements data available in a set of 10 catchments of the Southern Sierra (California, USA, see Chapter 2, Section 2.2). We focus on the design, relevance, limitations and hydrological process interpretation of the hydrological signatures. We also demonstrate the usefulness of additional data, rarely available, for the evaluation of hydrological signatures based only on widely available data. In addition, some of the hydrological signatures presented in this chapter are based on air temperature data which is also widely available. Therefore, this chapter also stresses the importance of using all the widely available data to derive meaningful hydrological signatures to gain further insights into the hydrological functioning of catchments. The hydrological signatures presented in this chapter, combined with streamflow and precipitation hydrological signatures presented in Chapter 4, form a set of hydrological signature that is able to characterize catchment functioning in a broad range of hydro-climatic contexts.

The methodology and results are presented as a paper that was published in *Hydrological Processes* (Horner et al., 2020).

Introduction

The hydrological function of catchments where a large part of the precipitation falls as snow exhibits a strong seasonal cycle in the streamflow response. The seasonal variation of streamflow is due to the accumulation of snow resulting in no or low streamflow during winter and snow melt resulting in an extended streamflow peak during Spring and Summer. Understanding the main factors that drive accumulation and melting of snow in snow-dominated catchments is necessary to understand the hydrological behaviors of these catchments and to be able to predict their streamflow response.

Hydrological signatures are metrics resulting from analysis of hydrological data that can be used to gain more insights into the dominant streamflow generation processes. They are valuable for many purposes as they summarize the data into a reduced set of values that are relevant to characterize important aspects of the catchment functioning. For example, they are useful for catchment classification (e.g. Sawicz et al. 2011; Toth 2013) and hydrological model development (e.g. Farmer et al. 2003; Eder et al. 2003; McMillan et al. 2011; Clark et al. 2011b), evaluation (e.g. Euser et al. 2013; Yilmaz et al. 2008) and calibration (e.g. Shamir et al. 2005b; Westerberg et al. 2011; Pokhrel et al. 2012). Although they are increasingly applied to additional data types (e.g. Branger and McMillan 2020; Heudorfer et al. 2019), they are typically computed from widely available data such as precipitation and streamflow time series.

Some widely used hydrological signatures such as the baseflow index, quantiles or slopes derived from the flow duration curve, recession constants, monthly streamflow average, etc. were used in catchments where snow processes played an important role (e.g. Hingray et al. 2010; Sawicz et al. 2011; Kelleher et al. 2015; Safeeq and Hunsaker 2016; Mackay et al. 2018; Todorović et al. 2019). To some extent, these signatures successfully identify dominant driving mechanisms in streamflow generation involving snow accumulation and melt processes. However, they are often not very specific to snow processes, addressing, for example, the effect of storage and release of water stored as snow as well as subsurface storage and depletion characteristics. To our knowledge, hydrological signatures that (1) take advantage of precipitation and air temperature data as additional widely available data and (2) focus more specifically on snow processes have received little attention. For example, Schaefli (2016) proposed original hydrological signatures using only precipitation, streamflow and air temperature data to focus on snow related processes. They were used in the development and calibration of a hydrological snow model for the 43 km^2 Dischmabach Alpine catchment located in Switzerland. However, they were applied only to a single catchment with a specific hydro-climatic context: Mountainous climate typical of the European Alps, with grassland, bare soils and rock outcrops land-use. Moreover, the scarcity of data, particularly snow measurements, in this catchment did not enable any checks regarding the relevance and interpretation of the hydrological signatures.

In this paper, we propose to address the above shortcomings by testing in details the hydrological signatures proposed by Schaefli (2016) and adapting them to a larger variety of hydro-climatic contexts. We also propose a new hydrological signature to quantify snow storage. These signatures are derived only from streamflow, precipitation and air temperature data. They are tested in the Mediterranean mountainous context of the Southern Sierra in California

(United States) where 10 Critical Zone Observatory (CZO) catchments are used as our case study. Our investigation takes advantage of additional snow measurements available in these catchments as well as inter-catchment differences in elevation. It addresses two main questions related to the data used and the amount of information that can be extracted using the tested hydrological signatures: (1) can average snow melt and accumulation dynamics be captured using only streamflow and air temperature data? (2) can total snow storage be estimated using only streamflow and precipitation data?

We first describe the ten catchments of our case study (Section 3.1.1) and then present the five investigated hydrological signatures (Section 3.1.2). Our method of investigation is then detailed in Section 3.1.3. Results are presented in Section 3.2 and discussed in Section 3.3 before a concluding section.

3.1 Methodology, study sites and data

3.1.1 Case study: the Southern Sierra CZO catchments

3.1.1.1 Catchments characteristics and climate

The study catchments are the Providence Creek and Bull Creek catchments of the Southern Sierra Critical Zone Observatory (CZO) located in California, United States. These catchments are part of the Kings River Experimental Watersheds (KREW) operated by the U.S. Forest Service (Hunsaker and Safeeq, 2017, 2018). A detailed description of the catchments and a synthesis of the measurements can be found in O'Geen et al. (2018).

The Providence Creek catchments are the P300, P301, P303, P304 and D102 catchments (see Figure 3.1). The P301, P303 and P304 catchments are nested within the larger P300 catchment. The Bull Creek catchments are the B200, B201, B203, B204 and T003 catchments (see Figure 3.1) with the B201, B203 and B204 catchments nested within the B200 catchment. The Providence and Bull catchments have elevations ranging from 1500 m to 2000 m and from 2000 m to 2500 m, respectively. They are located close enough to each other to assume they have similar climate. Details on the catchments characteristics (area, average elevation, elevation variation, aspect and slope) are given in Table 3.1.

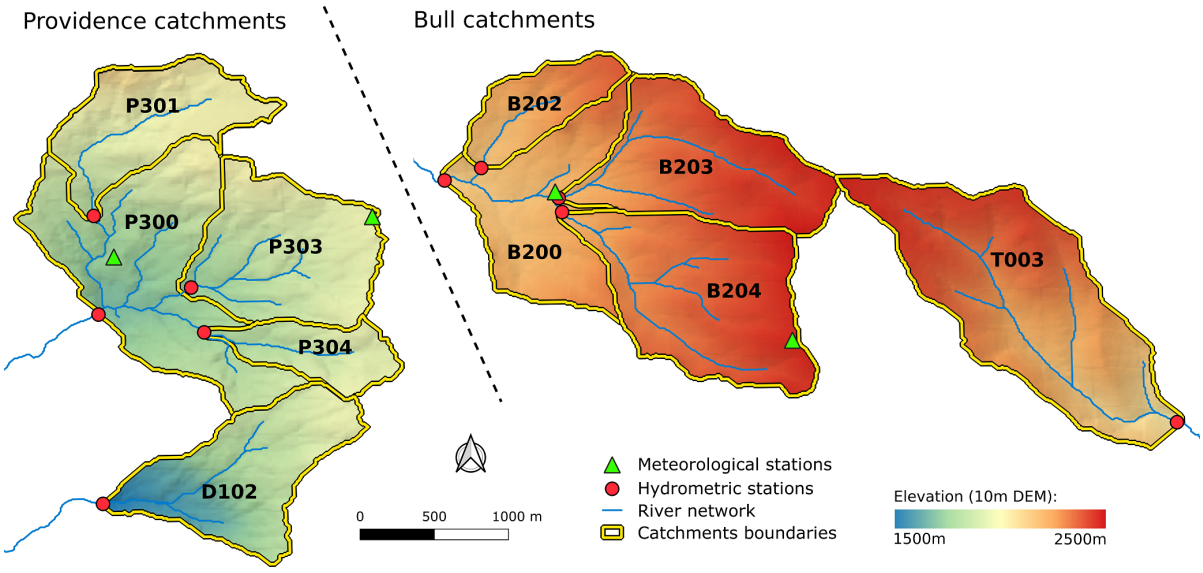

Figure 3.1: Boundaries of the Providence creek catchments (left) and Bull Creek catchments (top right) and localization of the hydrometric and meteorological stations.

Details on the geology, soil types and vegetation can be found in Johnson et al. (2011); Hunsaker et al. (2012); Safeeq and Hunsaker (2016). Only the main characteristics are reported here. All catchments rest on granite substratum. Providence catchments, except P301, are dominated by Shaver soils with rooting depth from 1 m to 2 m. P301 catchment is dominated by Gerle-Cagwin soils which have shallower rooting depth (from 0.76 m to 1.03 m). Bull catchments are dominated by Cagwin soils which have rooting depth between 0.5m and 1m. Overall, soils have moderate (Shaver and Gerle-Cagwin) to high permeability (Cagwin) with various water holding capacities (Shaver > Gerle-Cagwin > Cagwin).

Table 3.1: Main topographic characteristics of the Southern Sierra CZO catchments.

Site	Catchment	Drainage area (ha)	Average elevation† (m)	Elevation variation (m)	Average aspect (degrees)	Average slope (%)
Bull	B203	138	2373	303	235	18
Bull	B204	167	2365	289	235	17
Bull	T003	228	2289	414	142	24
Bull	B201	53	2257	225	228	18
Bull	B200	474	2122	367	231	18
Providence	P301	99	1979	318	208	19
Providence	P303	132	1905	292	233	20
Providence	P304	49	1899	213	249	22
Providence	P300	461	1883	424	223	21
Providence	D102	121	1782	491	246	27

† above see level

Catchments are largely covered (96 % to 100 %) by the Southern Sierra mixed-conifer forest which is mainly a mix of red fir (*Abies magnifica*), white fir (*Abies concolor*), ponderosa pine (*Pinus ponderosa*), Jeffrey pine (*Pinus jeffreyi*), sugar pine (*Pinus lambertiana*), incense cedar (*Calocedrus decurrens*). Also, around 1-4 % of the area consist of rock outcrops in the Bull catchments (Safeeq and Hunsaker, 2016).

The study catchments are located under the Californian Mediterranean climate characterized by long Summer droughts and wet Winters (Goulden et al., 2012; Hunsaker et al., 2012; Safeeq and Hunsaker, 2016). Over the years from 2004 to 2014, the average yearly precipitation ranged from 1234 mm/year to 1392 mm/year with more than 95 % of precipitation falling during Fall, Winter and Spring (Safeeq and Hunsaker, 2016). Precipitation mostly occurs "during large frontal storms that move off the Pacific Ocean from West to East" (Goulden et al., 2012). A large part of the precipitation is lost to the atmosphere through evapotranspiration (Bales et al., 2018; O'Geen et al., 2018) as illustrated by the runoff coefficient ranging from 17.7 % (P303) to 42.9 % (B203) calculated by Safeeq and Hunsaker (2016).

The Providence and Bull catchments are snow-dominated catchments with large influence of snow accumulation and snow melt on the streamflow response. They are located in the transition zone between rainfall and snowfall (Bales et al., 2011). There is large inter-year variability of snow accumulation with dry years having very little snow accumulation and wet years having very large snow accumulation. Extreme dry years are characterized by higher air temperatures, little precipitation and intermittent snow cover.

3.1.1.2 Data

Streamflow is monitored at the outlet of each catchment (Hunsaker and Safeeq, 2017). For all catchments, stage is continuously measured and converted to streamflow. Conversion is done using the established discharge relationships between stage and streamflow as water goes through Parshall-Montana flumes (P301, P303, P304, D102, B201, B203, B204) or V-notch weirs (T003, P300). Each site equipped with Parshall-Montana flumes has one flume with a 30-122cm throat width to measure high flows and another one with a 8-15cm throat width to measure moderate and low flows. In the case of B200, a stage-discharge relationship was built from individual stage and streamflow measurements (gaugings) of different flow magnitudes.

Both sets of catchments include an upper and lower meteorological stations (Hunsaker and Safeeq, 2018). They are positioned in open clearings with diameters at least as wide as the height of the surrounding trees and are therefore not subject to shading from trees or terrain (Safeeq and Hunsaker, 2016). The four meteorological stations continuously measure precipitation, air temperature, relative humidity, solar radiation, wind speed and direction and snow depth. In addition, the two upper meteorological stations measure snow water equivalent. Details on the equipment used are provided by Hunsaker et al. (2012).

For the precipitation measurements, gauges are located 3 m above the ground and equipped with windshield. Nontoxic propylene-glycol antifreeze is used to properly measure snow fall and a mineral-based oil is used to limit underestimation due to evaporation. Snow depth is monitored at the upper and lower meteorological stations using acoustic snow-depth sensors positioned 5 m above the ground. The Providence and Bull upper meteorological stations include snow pillows to measure snow water equivalent. For each station, 4 snow pillows are grouped to form a 2.4 m by 3.0 m rectangular pillow that continuously measures snow weight.

Daily streamflow data from October 1st, 2003 to September 30th, 2015 are available for catchments P301, P303, P304, D102, B201, B203, B204, T003. For the two larger catchments, P300 and B200, daily streamflow data are available only from December, 2005 and July 2006, respectively. Precipitation data are available from October 2003 (resp. 2004) to September 2017 for the Providence (resp. Bull) catchments. Air temperature data are available from October 2002 to September 2017. Snow depth data are available from October 2002 (resp. 2003) to September 2017 for the Providence (resp. Bull) catchments. SWE data are available from October 2003 to September 2017.

3.1.2 Set of signatures

We propose a set of 5 hydrological signatures that are summarized in Table 3.2 and detailed below. All of the signatures are based on Schaefli (2016) except the estimation of snow storage following the P-Q approach (Section 3.1.2.3). The set of signatures includes 2 slopes derived from two different periods in the relation between streamflow and air temperature regimes (Section 3.1.2.1), the dates of streamflow regime maxima (Section 3.1.2.2) and 2 snow storage estimates (Section 3.1.2.3).

While we aim at generalizing the hydrological signatures of Schaefli (2016) so they might be applicable in a larger variety of hydro-climatic contexts, some hydrological signatures, although succinctly presented here, were discarded from our analysis. In particular, in the Southern Sierra, unlike most typical Alpine catchments (e.g. such as the Dischmabach catchment, Schaefli 2016), (1) low flow occurs during Summer and is therefore not related to snow accumulation and (2) precipitation has a strong seasonal cycle and cannot be considered approximately constant throughout the year (see precipitation and streamflow for a typical hydrological year in Appendix D, Figure D.1). As a consequence, snow accumulation could not be characterized from streamflow regime magnitude or streamflow and air temperature regimes relationship. In addition, the Mass Curve Technique (MCT) approach of Schaefli (2016) was modified so it can be applied in contexts where precipitation cannot be considered approximately constant during a whole hydrological year which resulted in only one snow estimate, instead of two. We also

consider a new snow storage estimation method.

Table 3.2: Hydrological signatures used in this paper. The periods T_+Q_+ and T_+Q_- refer to specific parts of the temperature-streamflow regimes cycle. T_+ or Q_+ (resp. Q_-) stand for periods where the air temperature or streamflow regimes increase (resp. decrease).

Notation	Unit	Name/Description
$\delta_{T_+Q_+}$	°C/(mm/day)	temperature-streamflow slope of period T_+Q_+
$\delta_{T_+Q_-}$	°C/(mm/day)	temperature-streamflow slope of period T_+Q_-
$t_{Q\max}$	day	Timing of maximum streamflow regime
S_{MCT}, $S_{\mathrm{MCT},y}$	mm	MCT† estimation of snow storage from snow accumulation period
S_{PQ}, $S_{\mathrm{PQ},y}$	mm	P-Q‡ estimation of snow storage

† Approach based on the Mass Curve Technique

‡ Approach based on the difference between cumulative precipitation and cumulative streamflow

In the following sections, precipitation P, air temperature T and streamflow Q time series are used in different ways. From the time series of a variable X, we define the inter-annual daily mean of each calendar day of a hydrological year, $\overline{X}$, and the corresponding "regime" curve, X_{regime}, and cumulative curve X_{cum}. The regime curve X_{regime} is computed from $\overline{X}$ by applying a 30-days window rolling mean. The cumulative curve, X_{cum}, is computed for each day d of a hydrological year:

$$X_{\mathrm{cum}}(d) = \sum_{t \leq d} \overline{X}(t) \tag{3.1}$$

3.1.2.1 Temperature-streamflow slopes

To quantify and characterize snow melt and accumulation dynamics, slopes can be derived from the relations between streamflow and air temperatures regimes. The streamflow (resp. air temperature) regime, Q_{regime} (resp. T_{regime}), is defined as the 30-day smoothed (rolling mean) inter-annual mean of streamflow on each calendar day of a hydrological year (Schaefli, 2016) (see Figure 3.2(a)). The temperature-streamflow slopes are defined considering the relation between the air temperature regime and streamflow regime (Figure 3.2(b)). Slopes for different periods of the year are derived by linear regression ($T_{\mathrm{regime}} = \delta_{\mathrm{period}} \times Q_{\mathrm{regime}} + b$). In order to adapt the periods to a larger variety of climatic contexts, we consider a set of rules for the definition of the periods and the calculation of slopes. These rules are based on specific features of the temperature-streamflow cycle (maxima, minima) and, when no specific feature can be used, fixed dates. We created periods defined as particular segments in the temperature-streamflow cycle (see Figure 3.2):

- **air temperature and streamflow rising (T_+Q_+ period):** starting at the start of spring (April 1$^{\mathrm{st}}$ in our case study) to the date of maximum streamflow; streamflow increases with air temperature reflecting the increase in snow melt rate and responsive area (Schaefli et al., 2013) i.e. more area affected by snow melt and rainfall;
- **air temperature rising and streamflow declining (T_+Q_- period):** from the date of maximum streamflow to the date of maximum air temperature; streamflow decreases while air temperature continues to increase indicating a turning point where the snow stored in the catchment is no longer large enough to support the high streamflow rate of the previous period; this period reflects the decrease of snow melt affected area;

- **1st period with air temperature and streamflow declining (T_-Q_{-1} period):** from the date of maximum air temperature regime to the start of the third month of Summer (September 1st in our case study) ; streamflow continues to decrease and air temperature starts to decrease characterizing a period where mostly soil/groundwater depletion contributes to streamflow with large impact of evapotranspiration and only minor contributions from snow remaining at the highest elevations;
- **2nd period with air temperature and streamflow declining (T_-Q_{-2} period):** from the start of the third month of Summer (September 1st in our case study) to the start of the third month of Fall (December 1st in our case study); streamflow decreases with air temperature reflecting the decrease in responsive area (Schaefli et al., 2013) in the catchment, i.e. decrease of area affected by rainfall to the profit of snowfall.

Given that in the Southern Sierra catchment, streamflow minima occur in Summer (see typical hydrological year in Figure D.1), outside of the snow accumulation period, only the first two periods listed above, the T_+Q_+ and T_+Q_- periods, are kept to derive hydrological signatures characterizing snow melt dynamics.

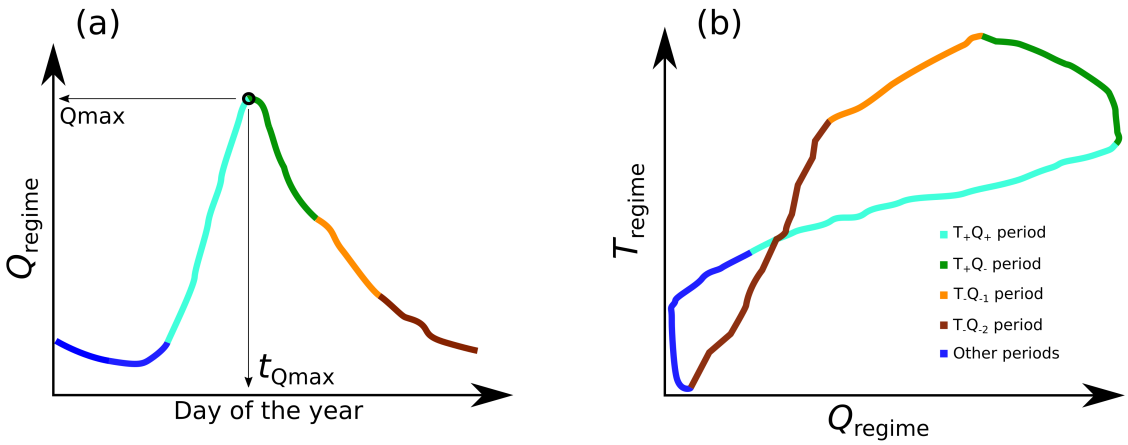

Figure 3.2: Illustration of (a) the streamflow regime used to derive the date of maximum streamflow $t_{Q\max}$ and (b) the temperature-streamflow regimes cycle used to derived slopes for different periods of the year. The different considered periods are highlighted with colors (defined in details in Section 3.1.2.1). (Adapted from Schaefli (2016))

3.1.2.2 Timing of streamflow regime maxima

As Schaefli (2016), we use the date of maximum streamflow, $t_{Q\max}$ (see Figure 3.2(a)) as a signature that captures the average temporal dynamics of the seasonal pattern of streamflow due to snow melt. The date $t_{Q\max}$ characterizes an important aspect of snow melt dynamics where a certain proportion of the snow-pack has melted away. Note that this date is used to define the end (resp. start) of the T_+Q_+ (resp. T_+Q_-) (Section 3.1.2.1).

3.1.2.3 Snow storage estimation

The Mass Curve Technique approach The Mass Curve Technique (MCT) approach was originally proposed by Gao et al. (2014) to estimate the root zone depth and used by Schaefli

(2016) to derive two snow storage estimates per year (see Schaefli (2016) and Appendix D.2). Due to the approximately constant precipitation rates in her case study, Schaefli (2016) was able to derive two snow estimates, one from the accumulation period and one from the melting period. In the original MCT approach, the slope of cumulative precipitation is used to find the tangents (parallel to precipitation) at the two inflection points of the cumulative streamflow sigmoid curve (visible in the top panel of Figure 3.3). In the case of the Southern Sierra catchments, precipitation can be considered approximately constant only during Fall, Winter and half of Spring (top panel of Figure 3.3). As a consequence, the use of tangents to derive snow storage estimates by computing the difference in intercepts of the two cumulative streamflow tangents (as done in the original MCT approach) is not possible. Therefore, in order to make the MCT approach usable in our case (and other hydro-climatic context where the "approximately constant precipitation" condition is only partly true) only the first inflection point of streamflow was used to compute a single snow storage estimate.

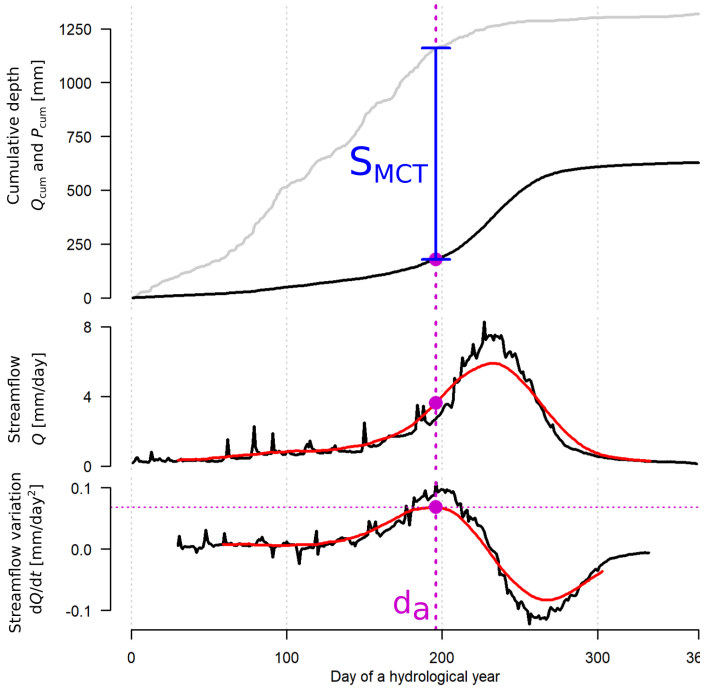

Figure 3.3: Schematic explanation of the estimation of water stored as snow in the catchment using the Mass Curve Technique approach. Top panel: inter-annual average of cumulative precipitation P_{cum} (gray line) and streamflow Q_{cum} (black line) on each hydrological year calendar day; the vertical blue lines shows the snow estimates S_{MCT}. Middle panel: streamflow Q (black line) and its 30-days smoothed version (red line) used to compute streamflow derivative. Bottom panel: streamflow derivative $\mathrm{d}Q/\mathrm{d}t$ (black line) and its 30-days smoothed version (red line); the dates of its maxima d_a (purple dot) define the date of the first inflection point of Q_{cum} used to derive S_{MCT}.

We used the cumulative curves P_{cum}, and streamflow, Q_{cum}, considering only the period where precipitation is approximately constant (from October 1$^{\text{st}}$ to May 15$^{\text{th}}$ in our case study). From the cumulative streamflow curve Q_{cum} and its sigmoid shape, a low and high streamflow period are identified. The low flow period corresponds to the snow accumulation period whereas the high streamflow periods correspond to the melt period. The transition date, d_a, between the low and high streamflow period corresponds approximately to the first inflection point in the sigmoid shape of Q_{cum}. It can be found using the maximum of the second derivative of Q_{cum} as illustrated in Figure 3.3. Assuming that, during the snow accumulation period, i.e. before d_a,

the actual cumulative evapotranspiration and the cumulative change in subsurface storage are small compared with the cumulative change of snow storage, a snow storage estimate, S_{MCT}, is given by the difference between cumulative precipitation and cumulative streamflow at day d_a:

$$S_{\mathrm{MCT}} = P_{\mathrm{cum}}(d_a) - Q_{\mathrm{cum}}(d_a) \tag{3.2}$$

The MCT approach can also be applied on a yearly basis to derive a snow estimate $S_{\mathrm{MCT},y}$ using the cumulative curves of precipitation and streamflow of each hydrological year y.

The MCT approach is based on the assumption that the differences between incoming precipitation and catchment streamflow release holds information on snow storage. It assumes that subsurface water storage and evapotranspiration (and sublimation) are small compared to snow storage. These assumptions are not true in the case of the Southern Sierra catchments as there is large evapotranspiration and possible significant subsurface storage (see Section 3.1.1 and Bales et al. 2018; O'Geen et al. 2018). However, in spite of these limitations (discussed further in Section 3.3), we argue (and test if) it can still be used to derive relevant information on snow storage.

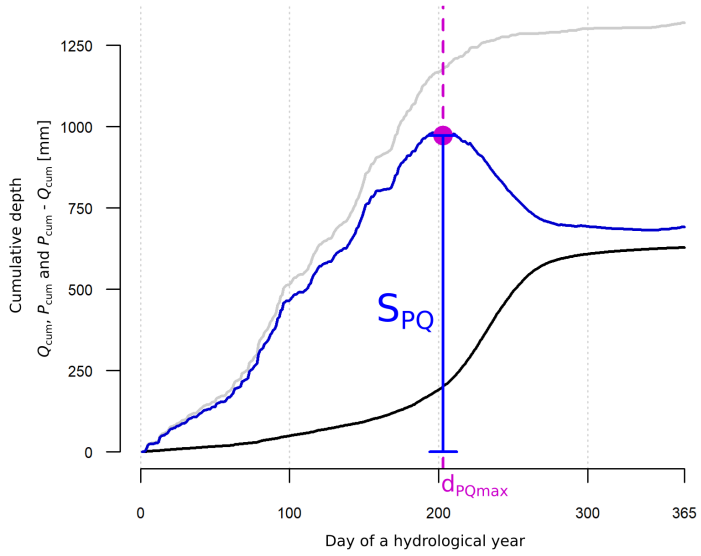

Figure 3.4: Schematic explanation of the P-Q approach to derive a snow storage estimate. The difference $P_{\mathrm{cum}} - Q_{\mathrm{cum}}$ (blue line) is computed from the inter-annual average of cumulative precipitation P_{cum} (gray line) and streamflow Q_{cum} (black line) on each hydrological year calendar day. The maximum of $P_{\mathrm{cum}} - Q_{\mathrm{cum}}$ curve at day $d_{PQ\mathrm{max}}$ (purple dot) is used as a snow storage estimate S_{PQ}.

The P-Q approach An alternative approach is also proposed to estimate snow storage. The P-Q approach considers the difference between precipitation and streamflow cumulative curves, $P_{\mathrm{cum}} - Q_{\mathrm{cum}}$. The P-Q curve rises during the snow accumulation period due to small streamflow values. It reaches a maximum and starts decreasing at day $d_{PQ\mathrm{max}}$ when the streamflow rate starts to be larger than the precipitation rate as a consequence of snow melt contributions. This is illustrated in Figure 3.4. Assuming evapotranspiration and subsurface storage small in front

of snow storage, another value of snow storage S_{PQ} is given by:

$$S_{\mathrm{PQ}} = P_{\mathrm{cum}}(d_{PQ\mathrm{max}}) - Q_{\mathrm{cum}}(d_{PQ\mathrm{max}}) \tag{3.3}$$

The P-Q approach can also be applied on a yearly basis. For each hydrological year y, the cumulative precipitation and streamflow curves can be used to derive a snow storage estimate, $S_{\mathrm{PQ},y}$.

3.1.2.4 Computation of the hydrological signatures for the Southern Sierra catchments

Only complete hydrological years are used, i.e. years starting on October 1$^{\mathrm{st}}$ and ending on September 30$^{\mathrm{th}}$, and common to all time series. For catchments B200 and P300 years from 2006 to 2014 (9 years) are used. For the remaining 8 catchments, years from 2003 to 2014 (12 years) are used.

In the definition of the different periods of the temperature-streamflow regimes cycle, some specific dates relative to the hydrological year are used (see Section 3.1.2.1). In our case, the following dates are used: (1) April 1$^{\mathrm{st}}$ (start of spring, day 183), (2) September 1$^{\mathrm{st}}$ (start of the third month of Summer, day 336) and (3) December 1$^{\mathrm{st}}$ (start of the third month of Fall, day 62). The dates of the streamflow regime maxima, t_{Qmax}, defining the start (resp. end) of the $\mathrm{T_+Q_-}$ period (resp. $\mathrm{T_+Q_+}$ period) are reported in Table 3.2. The dates of the air temperature regime maxima, defining the end of the $\mathrm{T_+Q_-}$ period are June 17$^{\mathrm{th}}$ (day 290) and June 14$^{\mathrm{th}}$ (day 287) for the Providence and Bull catchments respectively.

For each of the 10 study catchments, the slopes derived from the temperature-streamflow regimes cycle δ_{period} and the streamflow regimes maxima t_{Qmax}, are computed on average using all available hydrological years. Snow estimates are computed both considering the inter-annual average of each hydrological year calendar day (S_{MCT} and S_{PQ}) and for each hydrological year y ($S_{MCT,y}$ and $S_{PQ,y}$).

3.1.3 Analysis methodology

3.1.3.1 Information extracted from snow measurements

The additional snow measurements available for the Southern Sierra CZO catchments, snow depth and snow water equivalent (SWE) measurements, are used to assess the relevance of the 5 investigated hydrological signatures and verify our hypotheses regarding their interpretations. As mentioned in Section 3.1.1.2, snow measurements are acquired only in specific locations within each set of catchments (see Figure 3.1): for each set of catchments (1) one SWE time series measured in one of the most elevated areas and (2) two snow depth time series, one measured in a low elevation area (SDL) and the other one measured in high elevation area (SDU).

Snow measurements are used to extract information regarding snow storage and snow melt

dynamics. Key reference values are extracted from snow measurements as described in the paragraph below. The same approach as the one used to compute the air temperature and streamflow regimes (Section 3.1.2.1) is used to compute the snow depth regimes and SWE regimes ($S_{\mathrm{SWEregime}}$).

Snow seasons Dates are extracted as detailed in Figure 3.5: start and end of (1) the snow season, $t_{SWE\mathrm{start}}$ and $t_{SWE\mathrm{end}}$, (2) snow accumulation season, $t_{SWE\mathrm{start}}$ and $t_{SWE\mathrm{max}}$ and (3) snow melt season, $t_{SWE\mathrm{max}}$ and $t_{SWE\mathrm{end}}$.

Snow melt affected area Following the same approach, the snow depth regimes are used to derive the dates of the end of the snow season in the lower (resp. upper) parts of the catchments: $t_{SDL\mathrm{end}}$ (resp. $t_{SDU\mathrm{end}}$). These two dates are used to infer how spread in time the end of the snow season is between the upper and lower parts of each set of catchments. As no spatial information regarding snow melt affected area is available, these two dates are used to infer the rate of change in snow melt affected area: the more spread in time the end of the snow season is between the upper and lower parts of each set of catchments, the slower the variation in snow melt affected area is.

Snow melt rates For both sets of catchments, the derivatives of the SWE regimes, $\mathrm{d}S_{\mathrm{SWEregime}}/\mathrm{d}t$, give a reference of the average snow accumulation/melt rates over the snow season. These derivatives are used to infer the overall/average snow melt rate and how fast/slow the change in snow melt rates are in the two sets of catchments throughout the snow melt season.

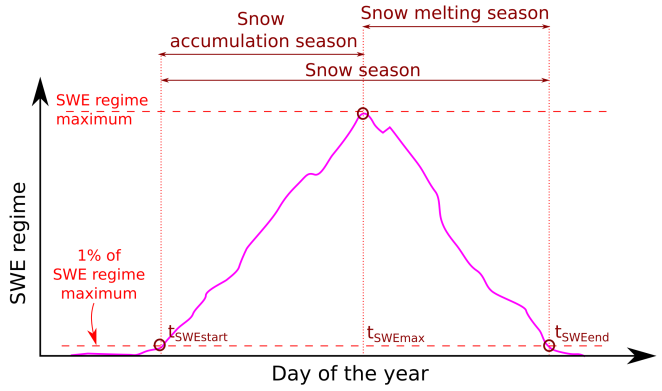

Figure 3.5: Illustration of the method used to extract the key dates from SWE regime (purple line). The three extracted dates define the whole snow season, the snow accumulation season and the snow melt period. The first and last dates, $t_{SWE\mathrm{start}}$ and $t_{SWE\mathrm{end}}$, are defined respectively as the first and last day of a hydrological year where the SWE regime is above 1% of its maximum.

Snow volumes The maximum of the inter-annual average of each calendar day of the SWE time series is computed for both the upper Providence and Bull meteorological station: S_{SWEmax}. The two obtained values, one for each set of catchments, are used as reference of the average volume of snow storage. As SWE data are measured in the highest elevations parts of each set of catchments, S_{SWEmax} represents a maximum snow storage reference. Using yearly SWE time series, yearly snow storage references, $S_{\mathrm{SWEmax},y}$, are also extracted for both sets of catchments.

Catchment scale snow storage and and melt dynamics The pieces of information extracted from the snow measurements are used as references, not as actual values representative of catchment scale snow processes. We acknowledge that the point measurements used here cannot capture spatial heterogeneity and inter-catchment differences. Large spatial variations in snow cover (total volume and melt dynamics) are expected in our study catchments given the spatial heterogeneity of incoming snowfall and the inter-catchment differences in elevation, aspect and other physical characteristics. Although the values we extracted from snow data are not representative of catchment scale snow accumulation and melt in an absolute way, we consider that the relative differences between years and between the Providence (low elevation) and Bull (high elevation) sets of catchments hold nevertheless relevant information. In particular, we argue they can be used as reference values to compare the Providence catchments with the Bull catchments or compare years.

3.1.3.2 Evaluation of hydrological signatures

In this section we describe the relevance tests of the 5 investigated hydrological signatures. The information derived from snow data (Section 3.1.3.1) and differences in catchment average elevations are used to evaluate the relevance and process interpretation of the hydrological signatures. The different tests are identified by letters for easy referencing in the result Section 3.2.

Test A: are the hydrological signature derived from air temperature and streamflow regimes relevant? The relevance of the hydrological signatures is first assessed by verifying that basic requirements are met: (A1) is the relation between air temperature and streamflow regimes linear during the period used to derive slopes $\delta_{\mathrm{T_+Q_+}}$, $\delta_{\mathrm{T_+Q_-}}$? (A2) are slopes $\delta_{\mathrm{T_+Q_+}}$ and $\delta_{\mathrm{T_+Q_-}}$ and the date of streamflow regime maxima $t_{Q\mathrm{max}}$, related to snow processes? To check if these signatures are related to snow processes, we verify that the periods used to define $\delta_{\mathrm{T_+Q_+}}$, $\delta_{\mathrm{T_+Q_-}}$ (and $t_{Q\mathrm{max}}$) include the hypothesized processes, i.e. snow melt processes. To this end, we verify that the period considered are within the snow melt season by using the starting and ending dates of the snow seasons derived from SWE data, $t_{SWE\mathrm{max}}$ and $t_{SWE\mathrm{end}}$ (see Section 3.1.3.1 and Figure 3.5). We also use the end of the snow melt season inferred from snow depth data, $t_{SDL\mathrm{end}}$ and $t_{SDU\mathrm{end}}$, as we expect an earlier end of snow melt season for catchment located at lower elevations.

Test B: can snow melt rates be quantified? The $\delta_{\mathrm{T_+Q_+}}$ is supposed to reflect the increase of snow melt rates as air temperature increases. We hypothesize that larger snow melt rates and a faster increase of snow melt rates result in a faster increase of streamflow and hence a larger streamflow maximum. According to the definition of $\delta_{\mathrm{T_+Q_+}}$, a larger streamflow regime maximum implies a smaller $\delta_{\mathrm{T_+Q_+}}$, i.e. a less steep slope during the $\mathrm{T_+Q_+}$ period. This hypothesis is verified by comparing the Providence catchments with the Bull catchments. The variation of $\mathrm{d}S_{\mathrm{SWEregime}}/\mathrm{d}t$ is used as a snow melt rate reference during the snow melt season. By comparing the Providence and Bull catchments, we verify that larger snow melt rate and/or a faster increase of snow melt rate i.e. faster variations of $\mathrm{d}S_{\mathrm{SWEregime}}/\mathrm{d}t$, is linked to smaller $\delta_{\mathrm{T_+Q_+}}$.

Test C: can variations in snow melt affected area be quantified? The temperature-streamflow regime slopes, $\delta_{\mathrm{T_+Q_+}}$ and $\delta_{\mathrm{T_+Q_-}}$, are supposed to reflect the increase and decrease of snow melt affected area respectively. We hypothesize that faster increase and decrease of snow melt affected area, which implies faster change in streamflow rates, is linked to a larger streamflow regime peak and hence smaller $\delta_{\mathrm{T_+Q_+}}$ and smaller $\delta_{\mathrm{T_+Q_-}}$, i.e. less steep slopes. This hypothesis is verified by comparing the Providence catchments with the Bull catchments using the dates of the end of snow season as computed from snow depth data at the upper ($t_{SDU\mathrm{end}}$) and lower ($t_{SDL\mathrm{end}}$) meteorological stations. Comparing these two sets of catchments, we verify if a larger difference $t_{SDU\mathrm{end}}$ - $t_{SDL\mathrm{end}}$ is linked to larger $\delta_{\mathrm{T_+Q_+}}$ and larger $\delta_{\mathrm{T_+Q_-}}$.

Test D: are the signatures derived from streamflow and temperatures regimes sensitive to snow storage? It is possible that the temperature-streamflow slopes, $\delta_{\mathrm{T_+Q_+}}$ and $\delta_{\mathrm{T_+Q_-}}$, and the date of the streamflow regime maxima, $t_{Q\mathrm{max}}$, are sensitive to the average total snow storage: larger volumes of snow storage should induce larger volumes of snow melt, larger catchment scale snow melt rates and a slower change of snow melt affected area. As a consequence, we expect larger streamflow regime peaks, and hence smaller $\delta_{\mathrm{T_+Q_+}}$ and $\delta_{\mathrm{T_+Q_-}}$, as well as later streamflow peak dates, i.e. larger $t_{Q\mathrm{max}}$. As the volumes of snow storage are expected to be strongly correlated with elevations (e.g. Blöschl et al. 1991; Tennant et al. 2017; Mackay et al. 2018), we verify if these signatures are correlated with catchment average elevation.

Test E: can inter-annual average snow storage be quantified? To test the relevance of the two inter-annual average snow storage estimates, S_{MCT} and S_{PQ}, we first compare the Providence catchments with the Bull catchments. We use the SWE regime maxima S_{SWEmax} corresponding to both sets of catchment and verify (E1) that S_{MCT} and S_{PQ} are below S_{SWEmax} (as it is a maximum snow storage reference, see Section 3.1.3.1) and (E2) that the differences in snow estimates (S_{MCT} or S_{PQ}) between both sets of catchments are similar (or at least consistent) with the differences found in S_{SWEmax} . To further test the relevance of S_{MCT} and S_{PQ}, we verify that they are correlated with the average catchment elevations (test E3) as the volumes of accumulated snow are expected to be strongly correlated with elevation (see previous paragraph, test D).

Test F: can yearly snow storage be quantified? To test the relevance of the yearly snow storage estimates, $S_{\mathrm{MCT},y}$ and $S_{\mathrm{PQ},y}$, we compare them with yearly SWE maxima, $S_{\mathrm{SWEmax},y}$. We verify that difference between snow rich (large $S_{\mathrm{SWEmax},y}$) and snow poor (small $S_{\mathrm{SWEmax},y}$) years is reproduced by the yearly snow storage estimates.

3.2 Results

3.2.1 Air temperature and streamflow regimes

Table 3.3: Hydrological signatures (see Table 3.2) values obtained for the 10 investigated catchments (Table 3.1). The two last columns presents the mean (standard deviation) computed over the Bull and Providence catchments.

Name	B203	B204	T003	B201	B200	P301	P303	P304	P300	D102	Bull†	Providence†
δ_{T+Q+}	1.23	1.23	2	2.23	2.32	3.33	5.95	6.01	6.23	10.8	1.8 (0.534)	6.47 (2.71)
δ_{T+Q-}	-1.46	-1.72	-2.76	-2.91	-3.91	-3.23	-4.72	-6.68	-5.44	-7.48	-2.55 (0.99)	-5.51 (1.66)
$t_{Q\max}$	233	235	232	226	219	218	212	223	211	197	229 (6.52)	212 (9.78)
S_{MCT}	974.3	1058	1004	1011	976	913.2	930.8	957.7	885.3	825.2	1005 (33.93)	902.4 (50.59)
S_{PQ}	972	1049	1005	1012	974	961.1	1007	966	947.6	986.5	1002 (31.62)	973.7 (23.41)

† Mean (standard deviation) computed over all Bull or Providence catchments

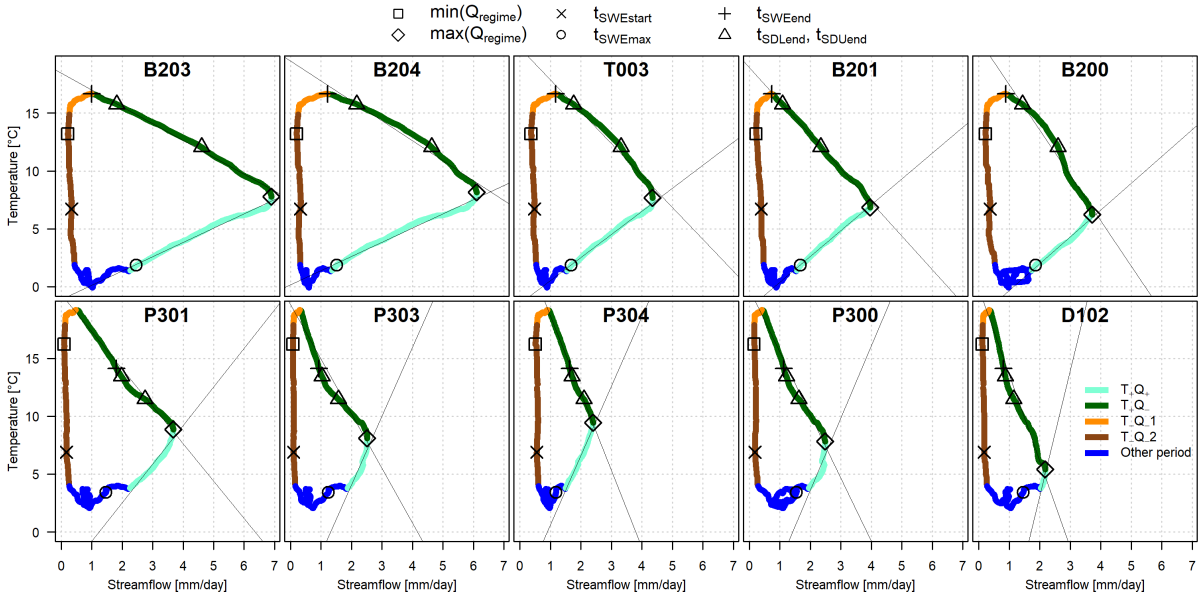

Figure 3.6: Relation between streamflow and air temperature regimes of the Bull catchments (top row) and Providence catchments (bottom row). Catchments are ordered by decreasing mean elevations (see Table 3.1) from left to right and top to bottom. Colors identify the different periods. Time follows a counter-clockwise direction and the start of the hydrological year is during the T_-Q_{-2} period (brown). The black straight lines illustrate the obtained slopes for the periods T_+Q_+ and T_+Q_- (see values in Table 3.3). Squares: streamflow regime minima and maxima ($\min(Q_{\mathrm{regime}})$ and $\max(Q_{\mathrm{regime}})$). Circles: SWE regime maxima (S_{SWEmax}). Crosses: snow season start and end dates (t_{SWEstart} t_{SWEend}). Triangles: snow-melt season end dates according to snow depth measurements at the lower and upper meteorological stations (t_{SDLend}, t_{SDUend}).

3.2.1.1 Relevance of the hydrological signatures focusing on snow melt dynamics

Hydrological signatures values computed for all catchments as well as the mean and standard deviation of the signatures for the Bull and Providence sets of catchments are presented in Table 3.3. Figure 3.6 presents the temperature-streamflow regime cycles for all catchments using colors to identify the different derived periods. It shows that the proposed definition of the periods T_+Q_+, T_+Q_-, T_-Q_{-1} and T_-Q_{-2}, successfully identifies the different parts in the temperature-streamflow regime cycle. It also shows that during the two periods used to derive hydrological signatures, the periods T_+Q_+ and T_+Q_-, the relation between air temperature

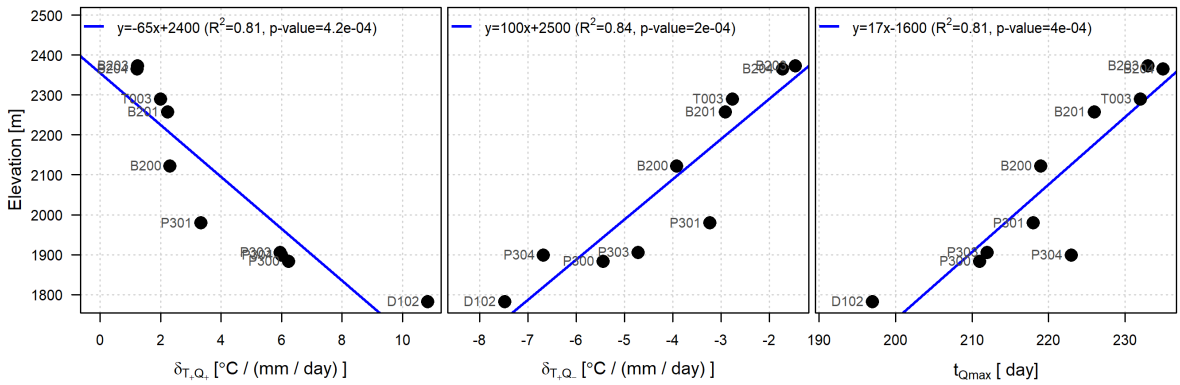

Figure 3.7: Relations between catchment average elevations and hydrological signatures $\delta_{T_+Q_+}$, $\delta_{T_+Q_-}$, and $t_{Q\max}$. Each dot is a catchment and the blue lines are the results of the linear regressions (see equations at the top of each plots with associated coefficient of determination and p-value).

and streamflow regimes can be considered approximately linear (Test A1). However, for the catchment with lowest average elevation (D102), the T_+Q_+ period is too short to have a well defined period.

Figure 3.6 shows that the T_+Q_+ and T_+Q_- periods (and the date of streamflow regime maxima $t_{Q\max}$) are within the snow melt seasons (Test A2). However, only half the T_+Q_- periods are within the snow melt season for the Providence catchments. These results show that hydrological signatures $\delta_{T_+Q_+}$ and $t_{Q\max}$ are relevant to quantify snow melt processes. For $\delta_{T_+Q_-}$, the results show that it is linked only partly to snow melt processes for the Providence catchments: during the T_+Q_- period, a small change of slope occur approximately at the end of the snow melt season suggesting that $\delta_{T_+Q_-}$ should be smaller (less steep) if only the snow melt period was considered for its computation.

As expected the two other periods, T_Q_1 and T_Q_2, are irrelevant. T_Q_1 spans only a small part of the temperature-streamflow regime cycle and is not related to snow processes. T_Q_2 period has an almost vertical slope: streamflow regime stays very low and air temperature regime decreases almost from its maximum to its minimum. The end of this period corresponds to the start of the snow accumulation season. However, as expected, the shift from rainfall to snowfall is not captured given that the streamflow regime has reached its minimal value before, in late Summer. During the accumulation period (between t_{SWEstart} and t_{SWEmax} in Figure 3.6), no clear relation can be established between air temperature and streamflow.

3.2.1.2 Quantifying snow melt rates and snow melt affected area

Figure 3.6 and Table 3.3 show that the slopes of both the T_+Q_+ and T_+Q_- periods are steeper for the Providence catchments (absolute values between 3.23 and 6.68, omitting the D102 catchment) than for the Bull catchments (absolute values between 1.23 and 3.91). During the T_+Q_+ period, SWE data indicates overall smaller snow melt rates (at least considering the whole snow melt season) and a slower increase of snow melt rate (Figure D.2) for the Providence catchments compared with the Bull catchments (Test B). This confirms our hypothesis: steeper slopes (larger $\delta_{T_+Q_+}$) are related to smaller snow melt rates and slower increase in snow melt rate. Figure 3.6 also shows that the end of the snow melt period is less spread in time between the upper and lower parts of the catchments for the Providence catchments compared with the

Bull catchments (Test C): confirming our hypothesis, these results suggest that steeper slopes ($\delta_{T_+Q_+}$ and $\delta_{T_+Q_-}$) are related to faster increase/decreases of snow melt affected area.

In Figure 3.7, the correlation of slopes, $\delta_{T_+Q_+}$ and $\delta_{T_+Q_-}$, and streamflow regime maxima dates, $t_{Q\max}$, with the catchments average elevations are shown (Tests D). Significant (p-value < 0.05) and large ($R^2 > 0.8$) correlations are found for all three hydrological signatures. These results suggest that these three hydrological signatures are sensitive to the average volume of snow storage. They confirm our hypotheses (test D) that these signatures are linked to the volume of snow melt, snow melt rate and snow melt affected area.

Figure 3.7 also shows that dates $t_{Q\max}$ for the P304 catchment is approximately 10 days late compared to what is expected considering the linear regression (Figure 3.7). The P304 catchment also stands out by the higher streamflow values during the dry season (Figure 3.6).

3.2.2 Snow storage estimations

3.2.2.1 Estimating average snow storage

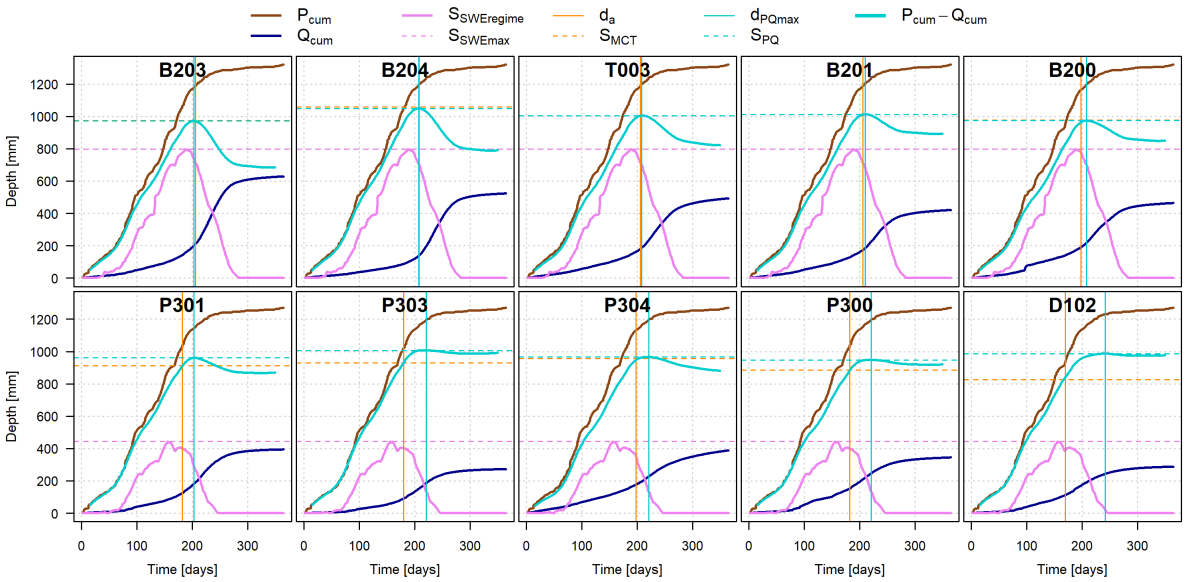

Figure 3.8: Estimation of snow storage using the Mass Curve Technique (MCT) approach and the P-Q approach on inter-annual daily average of cumulative precipitation P_{cum} (brown line) and streamflow Q_{cum} (blue lines). The SWE regimes $S_{\text{SWEregime}}$ (pink line) and their maxima (dashed pink line) are shown. The vertical (resp. horizontal) solid (resp. dashed) orange lines show the date of first inflection point of Q_{cum}, d_a (resp. the snow storage estimate S_{MCT}). The vertical (resp. horizontal) solid (resp. dashed) cyan lines show the date of the maximum of the $P_{\text{cum}} - Q_{\text{cum}}$ curve, d_{PQmax} (resp. the snow storage estimate S_{PQ}).

Figure 3.8 and Table 3.3 show that snow storage estimates S_{MCT} range between 974 mm and 1058 mm (resp. between 825 mm and 957 mm) for the Bull (resp. Providence) catchments. These values are above the maximum snow storage reference derived from SWE data, S_{SWEmax}, which is 797 mm and 443 mm for Bull and Providence catchments respectively. Therefore, test E1 fails: the snow storage estimates S_{MCT} are largely overestimated. The difference in S_{MCT} between Bull and Providence catchment is approximately 100 mm with more snow estimated for the Bull catchments (Table 3.3). The difference between maximum snow storage reference, S_{SWEmax}, between the Bull and Providence catchment is 354 mm with more snow for the Bull

catchments. Therefore, test E2 is only partly sucessfull: while more snow is estimated for the Bull catchments, the difference between the Bull and Providence catchment isn't as large as it should be.

Figure 3.8 also shows the snow storage estimates obtained using the P-Q approach, S_{PQ}. The P-Q approach yields snow storage estimates for all catchments ranging from 948mm to 1050mm (Table 3.3). Figure 3.8 shows that snow storage estimates are overall smaller for the Providence catchments (from 948mm to 1010mm) than for the Bull catchments (from 972 to 1050mm). Similarly to the MCT snow storage estimates, S_{MCT}, the P-Q approach snow storage estimates S_{PQ} are largely overestimated (test E1 fails). The differences in S_{PQ} between the Bull and Providence catchments (about 75 mm) are smaller than in the case of MCT approach. Test E2 partly fails but the smaller differences between the Providence and Bull catchment suggest the P-Q approach is less able to capture inter-catchment differences in snow storage.

As shown in Figure 3.8, similar snow storage estimates are obtained using both approaches in the case of the Bull catchments. However, notable differences are obtained for the Providence catchments. This is a consequence of the dates of the maxima of $P_{\mathrm{cum}} - Q_{\mathrm{cum}}$, d_{PQmax}, which are found later than the dates of the first inflection point of Q_{cum}, d_a in the case of the Providence catchments. For both sets of catchments, Figure 3.8 shows that dates d_a successfully captures the maxima of the SWE regime suggesting that they well capture the end (start) of the snow accumulation (snow melt) period.

The shapes of the cumulative precipitation curves (brown curves in Figure 3.8) show, as expected, that the assumption of inter-annual average precipitation being approximately constant is true only for about the 200-230 first days of a hydrological year but not true if considering the whole hydrological year. This confirms that the original MCT approach proposed by Schaefli (2016) to derive an additional snow estimate from the melting period cannot be done in the case of the Southern Sierra catchments. The MCT and P-Q approaches suppose that evapotranspiration and subsurface storage are small compared to snow storage. However, as expected, this is not true for the Southern Sierra catchments as shown by the large differences between the sum of inter-annual average of precipitation and streamflow (last day of the cumulative curve presented in Figure 3.8), consequence of large proportions of input precipitation being evapotranspirated.

3.2.2.2 Inter-catchment differences in snow storage

In Figure 3.9, snow estimates S_{MCT} and S_{PQ} are compared with the catchments average elevations. The correlation is significant (p-value < 0.05) for both approaches (test E3): more snow storage are estimated for catchments with higher average elevations. The correlation is stronger (R^2 of 0.75) for S_{MCT} estimates. These results suggest that the snow storage estimates, particularly S_{MCT} estimates, can partly capture inter-catchment differences in snow storage.

Significant scattering is observed in the case of S_{PQ}. In particular, estimates for catchments D102 and P303 (resp. B203) are largely overestimated (resp. underestimated) when compared to what would be expected given the slope of the regression line. Figure 3.8 shows that catchments D102 and P303 (resp. B203) are those with the larger (resp. smaller) evapotranspiration (see difference between P_{cum} and Q_{cum} at the last day of the hydrological year in Figure 3.8).

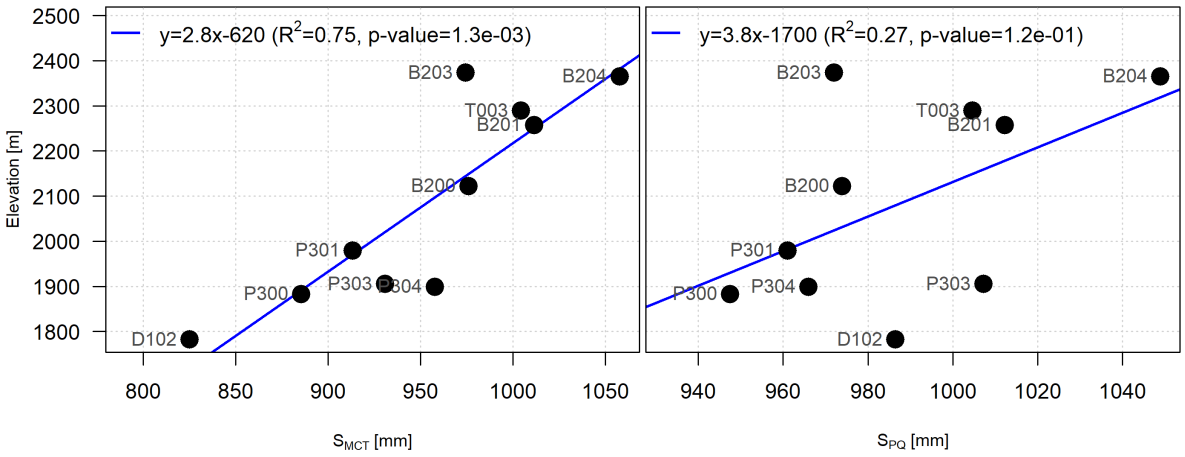

Figure 3.9: Relations between catchments average elevations and snow estimates S_{MCT} and S_{PQ}. Each dot is a catchment and the blue lines are the results of the linear regressions (see the equation at the top of each plot with associated coefficient of determination and p-value).

The P-Q approach is therefore more sensitive to evapotranspiration. It is partly due to the later date used to derive S_{PQ}, which includes a period where evapotranspiration affects streamflow more significantly.

3.2.2.3 Inter-years differences in snow storage

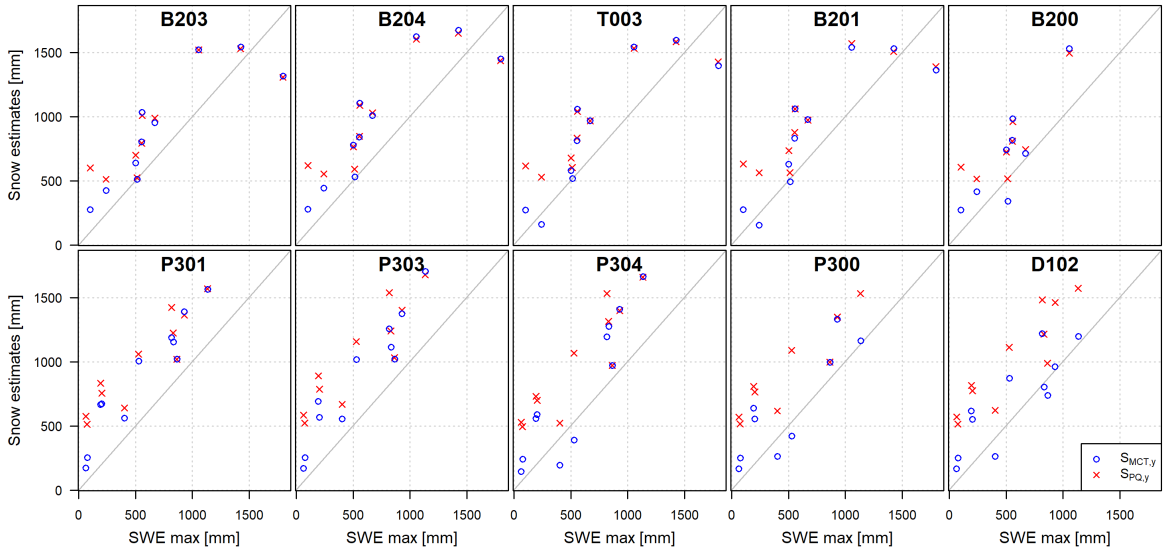

Figure 3.10: Comparison of yearly estimates of snow storage using the MCT approach (circles $S_{\mathrm{MCT,y}}$) and the P-Q approach (crosses, $S_{\mathrm{PQ,y}}$) with yearly SWE maxima, $S_{\mathrm{SWEmax},y}$, for all available years and all catchments.

Both the MCT and P-Q approaches were applied on a yearly basis to get yearly snow storage estimates. Figure 3.10 presents the comparisons of the yearly snow storage estimates, $S_{\mathrm{MCT,y}}$ and $S_{\mathrm{PQ,y}}$, with the yearly SWE maxima, $S_{\mathrm{SWEmax},y}$, for each available hydrological year and each catchment. It shows that the differences between snow poor and snow rich years is captured by both approaches (test F): small $S_{\mathrm{MCT,y}}$ and $S_{\mathrm{PQ,y}}$ are obtained for years with small $S_{\mathrm{SWEmax},y}$. These results suggest that inter-years differences in snow storage can be captured

by both approaches.

3.3 Discussion

3.3.1 Capturing snow melt dynamics

The definitions of the different periods of the temperature-streamflow regime cycle enable us to identify successfully the snow melt period. In the case of the Providence catchment, located at lower elevations than the Bull catchments, snow has completely melted away before the end of T_+Q_- period. This suggests that the period definition proposed here is more relevant for catchments with a higher degree of snow influence. The snow accumulation period could not be used as a signature in the case of the Southern Sierra catchment as the low flow occurs in Summer and is not related to snow accumulation.

The T_+Q_+ and T_+Q_- slopes are found to be related to streamflow regimes maxima (as air temperature regime magnitudes are similar across all meteorological stations, Figure 3.6) with steeper slopes for catchments at lower elevations where streamflow regimes maxima are smaller. Following the assumption that catchment average elevation can be used as a proxy to infer differences in snow storage, these relations are likely the consequence of less snow stored at lower elevations due to a combination of lower total precipitation and a shorter snowfall season. It was hypothesized that less snow implied (1) faster change in snow melt area and (2) smaller catchment scale snow melt rates. The time spread of the end of the snow melt season between high and low elevations parts of the catchments inferred from snow depth data supports the former hypothesis: steeper slopes ($\delta_{T_+Q_+}$ and $\delta_{T_+Q_-}$) are related to slower change in snow melt affected area. The smaller snow melt rate and slower change in snow melt rates found for the Providence catchments – inferred from snow water equivalent (SWE) data – supports the later hypothesis: steeper slopes ($\delta_{T_+Q_+}$ and $\delta_{T_+Q_-}$) are related to faster snow melt rates and faster change in snow melt rates.

Overall, these results suggest that the T_+Q_+ and T_+Q_- slopes can reflect changes in snow melt affected areas and snow melt rates. However, these results could also be caused by higher yields at higher elevations which induce larger streamflow peaks and hence less steep T_+Q_+ and T_+Q_- slopes. Higher yields are indeed found in the Bull catchments due to less evapotranspiration and less sublimation (Hunsaker et al., 2012) and shallower, more drainable soils (Goulden et al., 2012).

Dates of streamflow regime maxima, $t_{Q\max}$, are found to be linked to snow melt as they are located well within the snow melt season. For the Southern Sierra catchments, an observed difference of approximately 20 days in this timing is found between the Providence and Bull catchments. This difference could be the consequence of large differences in total snow storage as a clear linear link exists between $t_{Q\max}$ and catchment average elevation. Dates $t_{Q\max}$ are also found in periods where snow melt rates, according to SWE data, are the highest (Figure D.2), in particular for the two catchments that include the SWE data measurements (P303 and B204, Figure 3.1). This suggests that this signature is able to capture the high snow melt rate period which is a key period characterizing snow melt dynamics. However, differences in air temperatures in late Winter (before the start of the T_+Q_+ period) may also affect the dates of the streamflow regimes maxima: before the start of the T_+Q_+ period, the higher air temperatures in the Providence catchments cause more liquid precipitation and more snow melt

leading to an earlier rise of streamflow and earlier streamflow regimes maxima. The later $t_{Q\max}$ for the P304 catchment, compared to what was expected given the elevation regression line, could be caused by the probable larger subsurface storage in this catchment (as suggested by the larger Summer flows and by Safeeq and Hunsaker 2016): more subsurface storage imply a more dampened streamflow response, i.e. streamflow rises slower and with a longer delay after a precipitation or snow melt event.

3.3.2 Estimating snow storage

Both the MCT and P-Q approaches yielded snow storage estimates, S_{MCT} and S_{PQ}, that are largely overestimated. They were expected to be smaller than the SWE maxima used as a reference of maximum snow storage. In addition, differences in S_{MCT} and S_{PQ} between the Providence and Bull catchments were found too small compared to what was expected given the differences in SWE maxima references. These results are the consequences of the underlying assumptions of both methods – evapotranspiration and subsurface storage should be small compared with snow storage – which are not true in our study catchments (Bales et al., 2018; O'Geen et al., 2018). Larger differences between the two sets of catchments were obtained with S_{MCT} estimates compared with S_{PQ} estimates suggesting the MCT approach is less sensitive to these assumptions violations. This is due to the later dates, $d_{\mathrm{PQ}\max}$, used to infer S_{PQ}, which causes more evapotranspiration affecting the snow storage estimation, in particular at low elevation (e.g. in the case of Providence catchments). Further investigations could be undertaken in the Providence catchment using actual evapotranspiration estimates derived from flux tower data in the P301 catchment (Bales et al., 2018; O'Geen et al., 2018) to investigate in details how and to what degree evapotranspiration affects the snow storage estimates S_{MCT} and S_{PQ}.

Since that subsurface storage is ignored, the snow storage estimates obtained with both approaches should be higher than the actual snow storage. Similarly, as the water loss to the atmosphere (evapotranspiration) is neglected in both approaches, both snow storage estimates are expected to consider this loss as being water stored as snow. As a consequence, the estimation approaches should both give higher snow storage estimates in comparison to the actual snow storage. Our results show that this is clearly the case. This overestimation is larger in the case of the Providence catchment where there are larger proportions of water being evapotranspirated.

The effects of the assumptions underlying the snow storage estimations approaches could possibly be reduced considering an adaptation of the methodology. For example, air temperature data could be used to estimate evapotranspiration over each day of a hydrological year: considering that the difference between precipitation and streamflow volumes over a hydrological year corresponds to the total water loss to the atmosphere L_Y, daily evapotranspiration (and other loss) could be inferred by weighting L_Y with daily air temperature while keeping the overall annual loss the same. A similar approach was followed by de Boer-Euser et al. (2016) to estimate evapotranspiration from long term average water balance and daily potential evapotranspiration estimates. Similarly, air temperature could be used to approximately infer the start of the snow accumulation season (e.g. using an air temperature threshold) in order to discard precipitation data that only contributed to the increase in subsurface storage, streamflow

and evapotranspiration before the start of the snow accumulation season. These modifications might reduce the effect of the assumptions violation taking advantage of air temperature as an additional widely available data to retrieve more information on catchment functioning.

Regardless of the limitations due to the assumptions violations, results show that the dates of the first inflection point of streamflow, d_a, was possibly relevant to capture SWE maxima and hence the start of the snow melt season. This date itself could be used as a hydrological signature as it might be able to capture a key date in the snow accumulation and melt dynamics. The MCT and P-Q approach differ mostly in how the dates (d_a and d_{PQmax}), used to derive S_{MCT} and S_{PQ}, are computed. Results show that the MCT approach was more relevant as dates d_{PQmax} were found later in the year for the Providence catchments, towards the end of the snow melt season, not at the end of the snow accumulation season. As a consequence a period without snow accumulation and with larger evapotranspiration is considered in the computation of S_{PQ} making it less relevant than S_{MCT}.

Results also suggest that the snow storage estimates are relevant to infer inter-catchment differences in snow storage, in particular with S_{MCT} estimates. Results also suggest that inter-years differences in snow storage could be successfully captures. The actual (inter-catchment or inter-years) differences might need to be considered cautiously as it might only be possible to infer whether there is more or less snow storage. In addition, when comparing catchments, one should make sure that differences in evapotranspiration and subsurface storage between the compared catchments are small in order for the differences in snow storage estimates to be caused by actual differences in snow accumulation, not subsurface storage.

3.3.3 Representativeness of meteorological and snow data

The evaluation of the hydrological signatures was based on the assumptions that (1) elevation could be used as a proxy to infer inter-catchment differences in snow storage and (2) snow depth and snow water equivalent data could be used to extract relevant reference values to define the snow season, changes in snow melt affected areas, change in snow melt rates and maximum snow storage. The snow data used here are point data and are not necessarily representative of catchment scale snow processes. Therefore, our results are inevitably subject to limitations due to the effect of heterogeneity in solid precipitation, and catchment physical characteristics (elevation, aspect, land-use).

However, the available SWE and snow depth data, which are rarely available, provide valuable information on the hydrological functioning of a catchment regarding snow processes. The way they were used in our study limits the risk of any misinterpretations: the pieces of information derived from snow data were used (1) as reference values, not actual catchment scale values, (2) to compare two sets of catchments, not individual catchments, (3) and, to the exception of the yearly reference snow storage maxima, $S_{\mathrm{SWEmax},y}$, they were derived from inter-annual average of each calendar day.

Similarly, the precipitation and air temperature data used in this study are derived, for each set of catchments, from two meterological stations. These data might also not be representative of catchment scale precipitation or air temperature. However, given the small size of the study catchments, between 49 ha and 474 ha, the four meteorological stations used are likely sufficient.

Gridded precipitation products such as the 1 km grid Daymet daily data (Thornton et al., 2017) could also have been used. However such products are the results of meteorological models which are not likely to include the data provided by the four meteorological stations of our study catchments and that are also prone to uncertainties and representatives errors as well as biases in mountainous regions (e.g. Gottardi et al. 2012).

3.3.4 Hydro-climatic contexts and relevance of the snow hydrological signatures

From the four slopes that could possibly be derived from the temperature-streamflow regime cycle, only those where air temperature regime increases, T_+Q_+ and T_+Q_- slopes, were found to be related to snow processes in our study catchments. Unlike typical Alpine catchments such as the Dischmabach catchment investigated by Schaefli (2016), the shift between rainfall and snowfall, as air temperature decreases, which should induce a decrease of streamflow could not be captured in our case. This is one major difference between our study catchments and the one of Schaefli (2016). Another notable difference is the strong seasonality of precipitation with almost no precipitation during the Summer months, which prevented us from using the full potential of the original MCT approach i.e. the melting period could not be used to derive an additional snow storage estimate. The large evapotranspiration and the significant subsurface water storage also affected greatly the snow storage estimates with only inter-catchment and inter-years relative differences being relevant in our case. In hydro-climatic contexts where the underlying assumptions of the snow storage estimation methods are true, they might provide accurate absolute snow storage estimates.

Our results confirm the interpretations of Schaefli (2016) regarding the T_+Q_+ and T_+Q_- slopes: they are likely related to snow melt rates and snow melt affected area. These signatures are also found more relevant for the higher elevation Bull catchments than for the lower elevation Providence catchments as the duration and linearity of the T_+Q_+ periods can be questioned for some of the Providence catchments and only half of the T_+Q_- periods are found to be during a snow melt affected period for all the Providence catchments. Similarly the overestimation of snow storage estimates was found larger for the low elevation Providence catchments suggesting that they were less relevant than for the, more snow-influenced, Bull catchments. Overall, our results suggest that the relevance of the snow hydrological signatures is linked to the degree of snow influence of the investigated catchment, the more snow influenced, the more relevant.

3.3.5 Implications and usefulness of the snow signatures

The five hydrological signatures we investigated have the potential to provide relevant insights into catchment functioning in terms of (1) snow melt dynamics (snow melt rate and snow melt affected area) and (2) snow storage. The insights the snow signatures provide are useful mostly relatively, i.e. comparing catchments or hydrological years. In more typical Alpine-like catchments, insights into snow accumulation dynamics (e.g. decrease of responsive area) could potentially also be provided using the temperature-streamflow regimes relations. Finally, as the hydrological signatures are computed only from widely available data, precipitation, streamflow and air temperature, they can be applied in many catchments.

The snow hydrological signatures could be particularly relevant in studies where catchments are compared or where the year-to-year variability is explored. They can provide information to better understand differences in snow processes and/or verify/support hypotheses regarding differences in snow processes. To give a few examples, they can help answer questions such as (1) is snow melt faster (faster changes in snow melt rates and/or snow melt affected areas) in this catchment? (2) is there more snow accumulation, on average, in this catchment? (3) is there more snow storage during these years?

They also have the potential to be useful in catchment classification scheme based on catchment behaviors (e.g. Wagener et al. 2007; Sawicz et al. 2011; Toth 2013) or in the development, calibration and evaluation of hydrological models (e.g. Hingray et al. 2010; Kelleher et al. 2015; Schaefli 2016). They would mostly be useful when snow processes are represented using a temperature-index approach (e.g. Hock 2003; Valéry et al. 2014) rather than an energy balance approach (e.g. Lafaysse et al. 2011; Lehning et al. 2006; Herrero et al. 2009) since only average snow melt dynamics and snow storage can be investigated. The temperature-streamflow regime analysis can help identify problems in the parameters that control snow melt (e.g. temperature factor in a degree-day approach) and the snow storage estimates could be used to focus more specifically on the parameters controlling the accumulation of snow in the catchments, typically the parameters controlling the partitioning of input precipitation into rain and snow.

Conclusion

We investigated five hydrological signatures to characterize and quantify snow processes. These hydrological signatures are derived only from widely available data: streamflow, precipitation and air temperature. Our study aimed at testing whether information could be derived regarding (1) average snow melt dynamics and (2) snow storage. These signatures were applied to ten catchments in the Southern Sierra (California, USA), located under a mountainous Mediterranean climate and evaluated using snow measurements and differences in catchment elevation. Two hydrological signatures, derived from the relation between streamflow and air temperature during the snow melt season, were found to be linked to snow melt rates, changes in snow melt rates and/or change in snow melt affected areas thus characterizing important aspects of the average catchment snow melt dynamics. In addition, the dates of streamflow maxima were found to capture the highest snow melt rate periods. These three signatures were also found to be linked to snow storage which implied differences in snow melt rates, snow melt affected areas, and overall snow melt volumes. Finally, two approaches, the MCT and P-Q approaches, were used to compute inter-annual average and yearly snow storage estimates. The snow storage estimates were found largely overestimated due to the violation of the assumptions underlying the methodologies, i.e. negligible subsurface storage and evapotranspiration. However, inter-catchments and inter-years differences were successfully captured by the MCT approach snow estimates.

The research presented in the article addresses a more general question regarding the information content of data (Gupta et al., 2008). In our case, the data is the widely available streamflow, precipitation and air temperature time series and information is extracted by means of five hydrological signatures. The information we expected to extract from data was on snow melt dynamics and snow storage. Therefore, the additional available snow data were relevant to guide our interpretations. We verified our expected interpretations of the hydrological signatures, i.e. the content of information of the hydrological signatures, by verifying the consistency with the additional snow data and across the ten investigated catchments. This study illustrates the importance of highly instrumented sites to design, test, evaluate and interpret hydrological signatures that are based on widely available data, before applying them in other catchments.

Using only widely available data – precipitation, streamflow and air temperature – the five hydrological signatures investigated here are valuable to characterize and quantify inter-catchment (and inter-years) differences in catchment scale snow melt rates, snow melt affected areas and snow storage. Key aspects of the catchment functioning of snow-dominated catchments are therefore addressed by the investigated hydrological signatures. When studying several catchments, they can be valuable to gain more insights into differences in snow processes between catchments, for the classification of catchments based on catchment behavior or, by comparing observed with simulated hydrological signatures, for the development, calibration and evaluation of hydrological models.

Chapter 4

Streamflow and precipitation based hydrological signatures

Contents

Introduction

Any type of hydrological data might be used to derive hydrological signatures. Most authors use streamflow and precipitation data that are largely available. As detailed in Chapter 3, temperature data, also widely available, can be used to derive relevant hydrological signatures for snow dominated catchments. In this chapter, we detail a set of hydrological signatures only derived from streamflow and precipitation data for catchments without significant snow influence.

The approach followed to build the set of hydrological signatures was primarily based on a comprehensive review presented in Chapter 1 (Section 1.3). However, the analysis of the discrepancies between observed and simulated data on the Ardèche study subcatchments and a particular focus on the processes interpretation of the hydrological signatures also guided the building of the set. This led to the selection of already existing hydrological signatures, including some based on the widely used flow duration curve (see Section 1.3), as well as the emergence of new hydrological signatures, in order to address particular aspects of the observation/simulation discrepancies. The new hydrological signatures presented here were developed in order to capture a broader range of hydrological processes or at least gain more insights into the hydrological functioning of a catchment using only streamflow and precipitation data.

The particularities of the J2000 model and Ardèche catchment hydro-climatic context necessarily imply some hydrological processes are not addressed. The main objective of the J2000 model, which runs at a daily time step, is the long term assessment of water resources. Therefore, the set hydrological signatures does not address hydrological processes typically related to floods. This is particularly true in the case of the Ardèche catchment where the typical reaction time is within a couple of hours (Naulet et al., 2005). In addition, hydrological signatures targeting snow processes, as detailed in Chapter 3 are irrelevant in the case of the Ardèche catchment.

The set of hydrological signatures is to be used for the diagnostic and evaluation of a hydrological model. This requires that the hydrological signatures are able to capture relevant differences between observed and simulated data to identify differences between the actual catchment functioning and modeled catchment functioning. Therefore, we emphasize the importance of their interpretations in terms of hydrological processes which, although probably not sufficient, ensure their diagnostic power when interpreting differences between observed and simulated data.

The hydrological signatures detailed in this chapter are presented in Table 4.1. The set includes 12 hydrological signatures that aim at characterizing different aspects of the catchment response. In particular, different temporal scales are considered: (1) the long term water partitioning (fast versus slow flow generation processes, evapotranspiration versus streamflow), (2) average seasonal variations in catchment behavior, (3) average event-scale recession behaviors.

In Table 4.1, the hydrological signatures are organized according to the type of data analysis approach used. They are presented in the following sections accordingly. In Section 4.1, the runoff coefficient is presented followed by the presentation of the hydrological signatures derived

from the flow duration curve in Section 4.2. The hydrological signatures derived from the the analysis of baseflow, including the baseflow index and a new hydrological signature based on the baseflow regime, are presented in Section 4.3. We introduce an original approach – the P-Q approach – based on the analysis of the inter-annual average cumulative curve of streamflow and precipitation to derive hydrological signatures (Section 4.4). Finally, in Section 4.5, original hydrological signatures based on the analysis streamflow recessions are presented. Section 4.6 synthesizes the set of hydrological signatures focusing on their interpretation in terms of hydrological processes and discusses their limits and relevance.

Table 4.1: The set of hydrological signatures and the associated temporal scale and analysis approaches.

Symbol	Name	Temporal scale
Runoff coefficient		
S_{RC}	Runoff coefficient	Long term (volumes)
Flow duration curve (FDC)		
$S_{\text{FDC.slope}}$	FDC mid-segment slope	Long term (flow magnitude)
$S_{\text{FDC.Q90}}$	FDC 90% quantile	
$S_{\text{FDC.Q10}}$	FDC 10% quantile	
Baseflow analysis		
S_{BFI}	Baseflow index	Long term (volumes)
$S_{\text{BFR.mag}}$	Baseflow regime magnitude	Seasonal variation (dry/wet season)
Streamflow regime analysis, the P-Q approach		
$S_{\text{PQ.dry}}$	P-Q curve† dry period slope	Seasonal variation (dry/wet season)
$S_{\text{PQ.wet}}$	P-Q curve† wet period slope	
$S_{\text{PQ.strength}}$	P-Q curve† threshold strength	
$S_{\text{PQ.date}}$	P-Q curve† breackpoint date	
Streamflow recessions analysis		
$S_{\text{REC.}\tau\text{early}}$	Early recession time	Event (streamflow recessions)
$S_{\text{REC.}\tau\text{late}}$	Late recession time	

† the P-Q curve is the difference between cumulative precipitation and cumulative streamflow regimes‡

‡ the regime of variable V is defined as the inter-annual calendar day average of V over a hydrological year

4.1 Runoff coefficient

The runoff coefficient or runoff ratio is often reported in hydrological studies as a value giving a general idea of the catchment response (Blume et al., 2007). It is also widely used as a hydrological signature (e.g. Yilmaz et al. (2008); Pokhrel et al. (2012); Vrugt and Sadegh (2013); Pfannerstill et al. (2014); McMillan et al. (2014); Hrachowitz et al. (2014); McMillan et al. (2014); Zhang et al. (2014); Fovet et al. (2015); Westerberg and McMillan (2015); Teutschbein et al. (2015, 2018); Höllering et al. (2018)). It is based on the conservation of mass of water applied at the catchment scale (Equation 4.1): input water (precipitation) is released from the catchment either as evapotranspiration or as streamflow.

$$\Delta S/\Delta t = P - E - Q \tag{4.1}$$

where $\Delta S/\Delta t$ is the variation of stored water in the catchment, and P, E and Q are the precipitation, evapotranspiration and streamflow volumes respectively, computed over the period Δt. For a long enough period, the variation of storage in the catchment can be neglected, i.e. $\Delta S \ll P$, Q, and E. Consequently, precipitation can be considered equal to the sum of evapotranspiration and streamflow: $P = Q + E$. The runoff coefficient is then defined as the long term ratio between the total volume of streamflow and the total volume of precipitation. Given the streamflow and precipitation time series $Q(t)$ and $P(t)$ (with a regular time step), the runoff coefficient, S_{RC}, is:

$$S_{\mathrm{RC}} = \frac{\sum_{t=t_1}^{t_2} Q(t)}{\sum_{t=t_1}^{t_2} P(t)} \tag{4.2}$$

where t_1 and t_2 are the start and end of the period considered. For examples, Sawicz et al. (2011) used 10 hydrological years in their calculation and McMillan et al. (2014) used 4 hydrological years.

The runoff coefficient represents the proportion of input water – precipitation – being released from the catchment as streamflow (Sawicz et al., 2011). A high runoff coefficient indicates a catchment where a large amount of water is, on average, released as streamflow whereas a low runoff ratio indicates a catchment where a large amount of water is released as evapotranspiration (Sawicz et al., 2011), if other release fluxes such as groundwater fluxes are considered negligible. In other words, this is a signature that measures the long term partitioning of input water between streamflow and evapotranspiration.

Figure 4.1 shows the observed and simulated runoff coefficients for the four study catchments. Observed runoff coefficients are similar for Meyras, Pont-de-Labeaume and Goulette (about 0.65-0.7) but much smaller for Claduègne (about 0.45). This shows the ability of the runoff coefficient to capture differences in the hydrological functioning of the catchments. Figure 4.1 also shows differences between observed and simulated S_{RC}, suggesting that the long term partitioning of water between streamflow and evapotranspiration in the model is different from the real catchments.

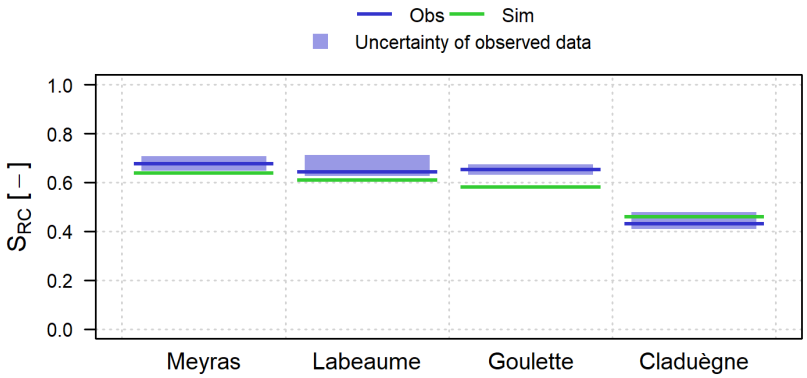

Figure 4.1: Observed and simulated runoff coefficient, S_{RC}, of the four study catchments.

4.2 Flow duration curve

4.2.1 Definition and interpretation

The flow duration curve (FDC) is the empirical cumulative distribution of streamflow typically derived from hourly or daily streamflow time series (Vogel and Fennessey, 1994). For a given streamflow value, the FDC indicates the proportion of time the value was equaled or exceeded. A FDC is an empirical cumulative probability density function indicating the streamflow value Q_p corresponding to its probability to be equaled or exceeded p:

$$p = F_{\mathbf{Q}}(Q_p) = \mathrm{P}(\mathbf{Q} \geq Q_p) \tag{4.3}$$

$$Q_p = F_{\mathbf{Q}}^{-1}(p) \tag{4.4}$$

where $\mathbf{Q}$ is the vector of all the values of streamflow within the time series considered.

The FDC characterizes the catchment response in terms of magnitude without consideration of timing. As already mentioned in Chapter 1 (Section 1.3.1), the different parts of the FDC (high flow, medium flow and low flow) can be related to different hydrological processes: overland flow, sub-surface flow and groundwater flow. The overall steepness of the FDC is often seen as a measure of the dampening effect of the catchment related to the partitioning and release of water from different catchment storages (Yilmaz et al., 2008).

4.2.2 Observed and simulated flow duration curve

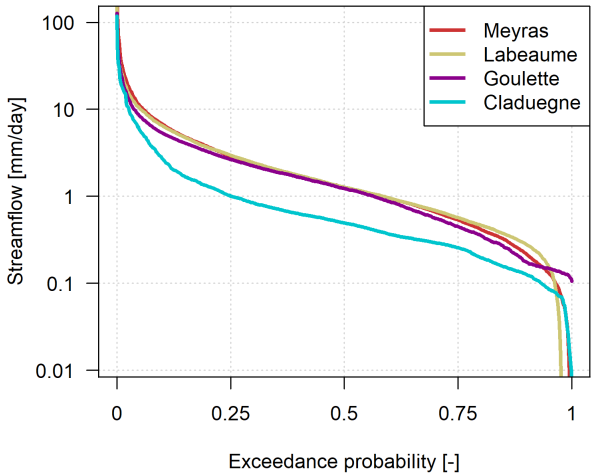

Figure 4.2: Flow duration curves computed on observed streamflow time series for the four study catchments.

Figure 4.2 shows the FDCs of the four study catchments. There are only little differences between catchments except for Claduègne which has a similarly shaped FDC but with lower streamflow values overall.

Figure 4.3 compares observed and simulated FDC of the four study catchments. Clear differences are visible here showing that the FDC captures differences between observed and simulated catchment streamflow response. The main differences visible in Figure 4.3 are at

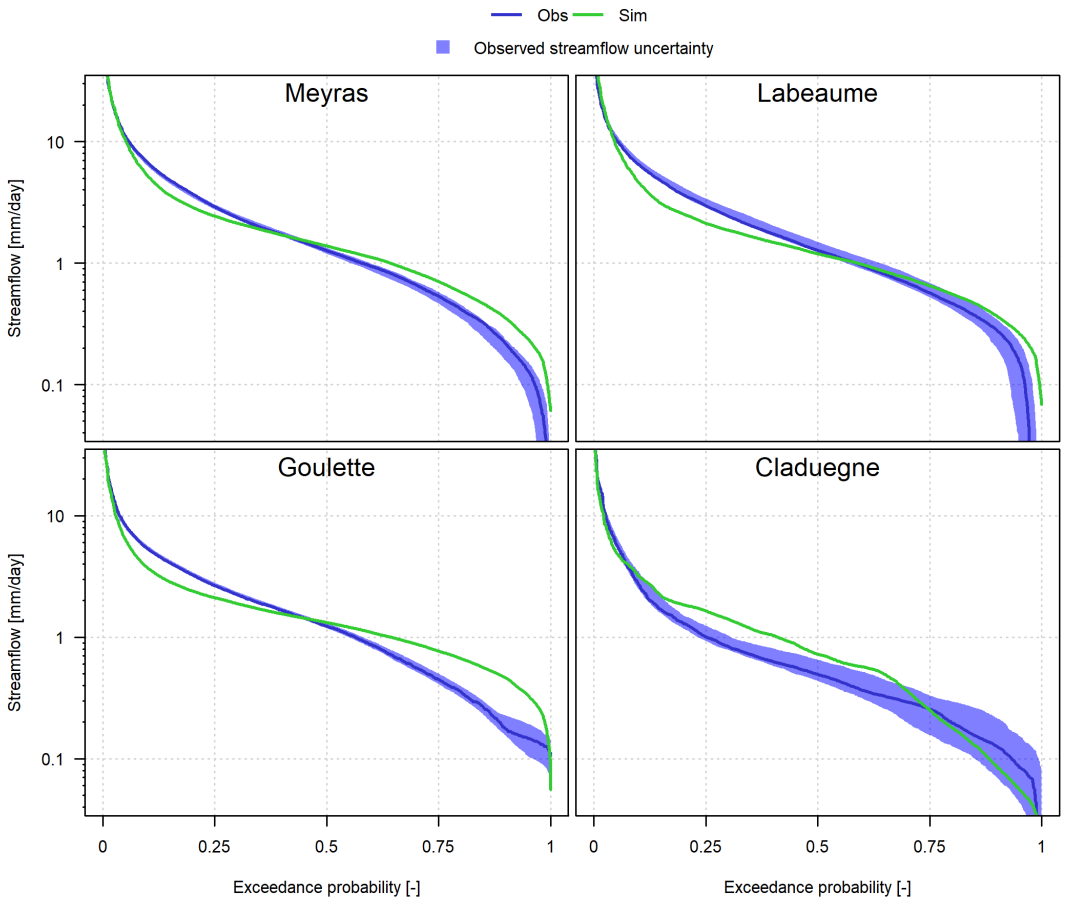

Figure 4.3: Observed and simulated flow duration curves of the four study catchments.

low and high flows and in the general steepness of the FDC: for catchments Meyras, Pont-de-Labeaume and Goulette, observed high flows are larger, observed low flows are smaller and the observed FDCs are steeper.

4.2.3 Deriving hydrological signatures from the flow duration curve

As detailed in Chapter 1, the FDC is widely used and many hydrological signatures describing its shape have been proposed. Among the proposed hydrological signatures, the slope of the mid-segment slope of the FDC (Yilmaz et al., 2008; Casper et al., 2012; Pokhrel et al., 2012; Pfannerstill et al., 2014; Ley et al., 2016; Höllering et al., 2018; Mackay et al., 2018) is selected here because of its ability to describe the FDC shape and the strength of the link with the catchment functioning highlighted by many authors (Yilmaz et al., 2008; Sawicz et al., 2011; Wrede et al., 2015). The slope of the mid-segment of the FDC, $S_{\text{FDC.slope}}$, can be defined as follows:

$$S_{\text{FDC.slope}} = \frac{\log(Q_{p_{\text{low}}}) - \log(Q_{p_{\text{high}}})}{p_{\text{high}} - p_{\text{low}}} \tag{4.5}$$

where p_{low} and p_{high} are two exceedance probabilities. Following Yadav et al. (2007); Sawicz et al. (2011); McMillan et al. (2017), p_{low} and p_{high} were set at 0.33 and 0.66 respectively. As demonstrated by McMillan et al. (2017), this hydrological signature alone can lead to misinterpretation (see Chapter 1, Section 1.3.1). Following their recommendation, two hydrological signatures – $S_{\text{FDC.Q10}}$ and $S_{\text{FDC.Q90}}$ – were added to characterize the low and high parts of the

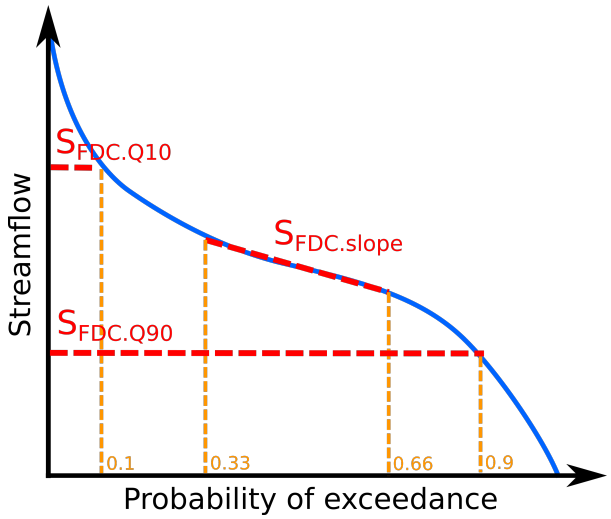

Figure 4.4: Diagram illustrating the typical shape of a flow duration curve (in blue) and the three hydrological signatures used to describe its shape: the high and low flow streamflow values, $S_{\text{FDC.Q10}}$ and $S_{\text{FDC.Q90}}$, and the slope of the mid-segment, $S_{\text{FDC.slope}}$.

FCD: the values of streamflow corresponding to a low and high exceedance probabilities (set at 0.1 and 0.9 respectively) characterizing the high and low streamflows respectively. Using Equation 4.4, these hydrological signatures are defined as:

$$S_{\text{FDC.Q10}} = Q_{0.1} = F_{\mathbf{Q}}^{-1}(0.1) \tag{4.6}$$

$$S_{\text{FDC.Q90}} = Q_{0.9} = F_{\mathbf{Q}}^{-1}(0.9) \tag{4.7}$$

A diagram illustrating the 3 hydrological signatures is proposed in Figure 4.4 .

As shows in Figure 4.5, these three hydrological signatures are well able to capture the main differences between observed and simulated FDC visible in Figure 4.3: larger high values, smaller low values and steeper slopes of the observed FDC for Meyras, Pont-de-Labeaume and Goulette.

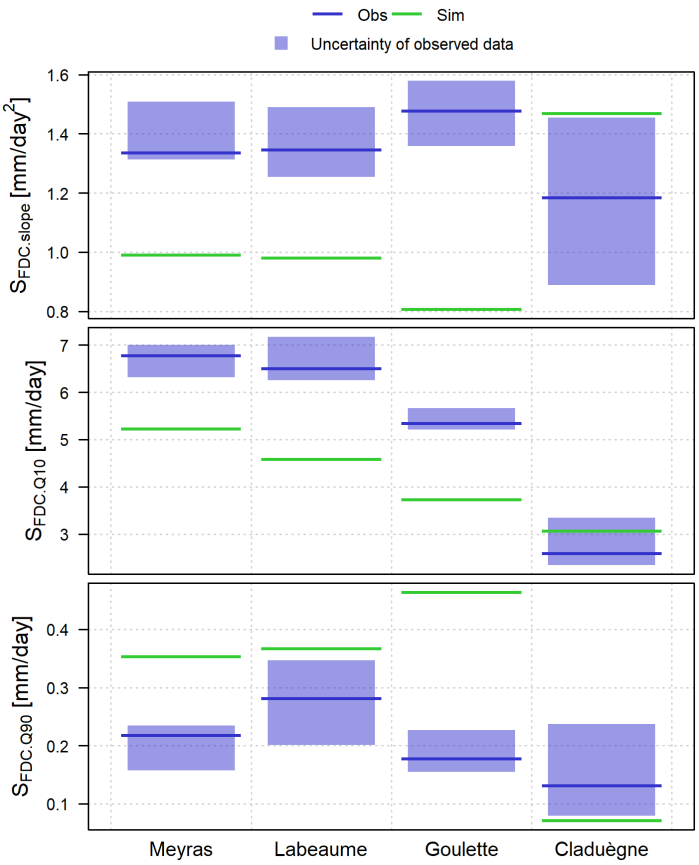

Figure 4.5: Observed and simulated hydrological signatures $S_{\text{FDC.Q10}}$, $S_{\text{FDC.Q90}}$ and $S_{\text{FDC.slope}}$ derived from the observed and simulated FDC.

4.3 Baseflow analysis

4.3.1 Baseflow time series and baseflow regime

4.3.1.1 Baseflow extraction

Separation of streamflow into two components - commonly termed quickflow and baseflow - is often done to distinguish water originating from slow processes (*"groundwater discharging into the stream"* resulting in the baseflow component) from water originating from fast processes (*"overland or near-surface flow"* resulting in the quickflow component) (Chapman, 1999; Stewart, 2015):

$$Q(t) = Q_{BF}(t) + Q_{QF}(t) \tag{4.8}$$

where Q_{BF} and Q_{QF} are the baseflow and quickflow components of total streamflow $Q(t)$, respectively.

Various baseflow separation techniques can be used (Furey and Gupta, 2001; Stewart, 2015; Mei and Anagnostou, 2015): analytical methods, graphical methods, filtering methods, recession analysis methods and tracer based methods. Analytical methods are based on groundwater and overland flow theories (Stewart, 2015) and are seldom used. Tracer based methods are based on tracer data, e.g. stable water isotope data, to infer proportions of water from the groundwater aquifer or from rainfall (e.g. (Singh and Stenger, 2018)). These methods require data rarely available and is mostly dedicated to experimental catchments. Graphical, filter based and recession based methods have been the most used techniques because of their ease of use and the common availability of streamflow data (Stewart, 2015), the only required data for these methods.

As slow response is related to smooth streamflow time series, high frequency patterns in streamflow time series can be associated with direct runoff and, low frequency pattern, with baseflow (Eckhardt, 2005, 2008). This idea leads to identify baseflow by applying low pass filters on streamflow time series (Eckhardt, 2008). Many filtering algorithms have been developed over the years. One of the most commonly used filtering algorithm is the one proposed by Lyne and Hollick (1979):

$$Q_{QF}(t) = kQ_{QF}(t-1) + \frac{1+k}{2}\left(Q(t) - (Q(t-1)\right) \tag{4.9}$$

where k is a filter parameter. Since the work of Lyne and Hollick (1979), other digital filtering algorithms have been proposed: the Chapman & Maxwell filter (Chapman and Maxwell, 1996; Chapman, 1999), the Boughton algorithm (Chapman, 1999) and the generalization of the Chapman & Maxwell algorithm of Eckhardt (Eckhardt, 2005, 2008). All these algorithms were implemented and compared. Results (not shown) showed that they all behave similarly. Only the Lyne & Hollick algorithm is presented here to represent the family of filter-based algorithms as it is the most used filter (e.g. Sawicz et al. (2011); Sivapalan et al. (2011); Vrugt and Sadegh (2013); Shafii et al. (2017); Fenicia et al. (2018)).

In the family of graphical methods to extract baseflow, the one of Gustard et al. (1992) is often employed (e.g. Beck et al. (2017); Pool et al. (2017)). It relies on two parameters: a time window d and a parameter k. This algorithm can be described in 3 steps as follows:

1. Given a streamflow time series $Q(t)$, the minimum of each d-day non-overlapping window of $Q(t)$ is identified.
2. Pivot points – identified minima (multiplied by k) that are below both the previous and next identified minima – are then selected.
3. A baseflow time series $Q_{BF}(t)$ is then computed by interpolating values between the selected minima with the constraint that $Q_{BF}(t) \leq Q(t)$.

All these algorithms rely on one or more parameters which are often set arbitrarily. For example, Sawicz et al. (2011), among others (e.g. Sivapalan et al. (2011); Shafii et al. (2017)), chose to use a value of 0.925 for the Lyne & Hollick algorithm according to what Eckhardt (2008) used in his study. Similarly, Beck et al. (2017) and Pool et al. (2017) used the Gustard algorithm using a time window d of 5 days (and $k = 0.9$) following the recommendation of Gustard et al. (1992). Figure 4.6 compares the observed baseflow time series computed from the Lyne & Hollick and Gustard algorithms over the same period (using the default parameter values). The main difference between these two algorithms is their sensitivity to streamflow events: the former being more strongly affected than the latter. Note that a lower k value in the Gustard algorithm would also lead to more sensitivity to the streamflow events. The Gustard algorithm captures well the general dynamics of slow flow and is closer to what we expect the slow contributions from catchment storage look like. As noted by Sawicz et al. (2011), when using this algorithm only for comparison purposes, the attention given to the algorithm itself or its parameters isn't of primary importance as only relative differences are of interest. Therefore, we chose here to use the Gustard algorithm with its default parameters values ($d = 5$ and $k = 0.9$).

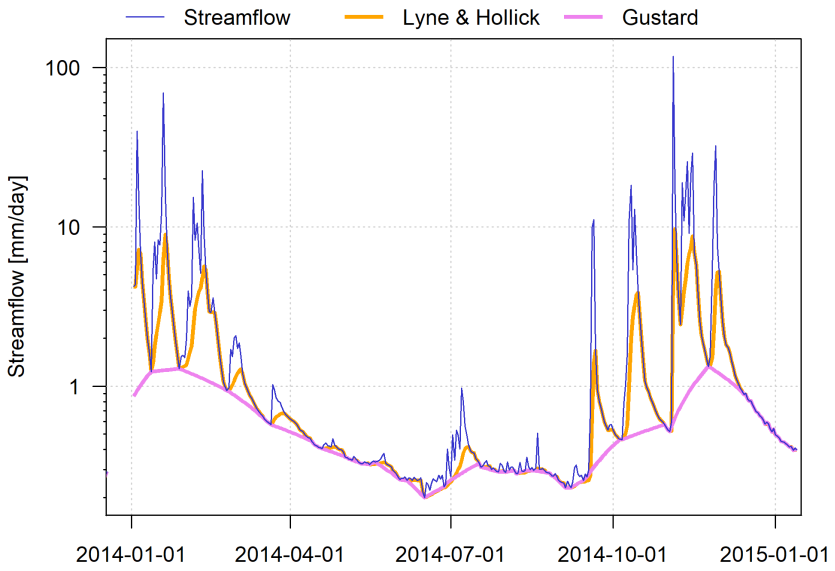

Figure 4.6: Observed baseflow of the Claduègne catchment over the year 2014 computed using the Lyne & Hollick method ($k = 0.925$) and the Gustard algorithm ($d = 5$ and $k = 0.9$).

4.3.1.2 Baseflow regime

To scrutinize the baseflow time series further, we here compute the baseflow regime. We define the baseflow regime as the inter-annual average of baseflow for each calendar day d of a hydro-

logical year: $\overline{Q}_{BF}(d)$ with d the day of a hydrological year ($d = 1, 2, ..., 365$ – we omit the 366th day). Figure 4.7 shows the resulting observed and simulated baseflow regime of the four study catchments. The baseflow regime captures the long term average of slow flow throughout a hydrological year. As the extracted baseflow is mostly related to slow generation processes such as groundwater outflow and slow sub-surface flow, the baseflow regime shows the variations of these contributions throughout a hydrological year. These variations can be attributed to catchment storage and release rate: soil/groundwater storage, soil drainage, lateral / vertical drainage, groundwater depletion rates.

Figure 4.7 shows that simulated baseflow of Claduègne is much larger than observed baseflow. It also shows that this difference is, on average, due mostly to the Winter months. Globally, for all study catchments, Figure 4.7 shows differences between observed and simulated data in the baseflow regime range of variations. For Claduègne, the simulated range of variation is much larger than the observed range of variation whereas the opposite is visible for the other 3 catchments. Compared with the observed baseflow regime, the maximum of simulated baseflow regime of Meyras, Pont-de-Labeaume and Goulette, which occur during Winter or Spring is smaller; the opposite is found considering the minimum of simulated baseflow regime of Meyras, Pont-de-Labeaume and Goulette. The larger minimum of simulated baseflow regime is particularly obvious for Goulette.

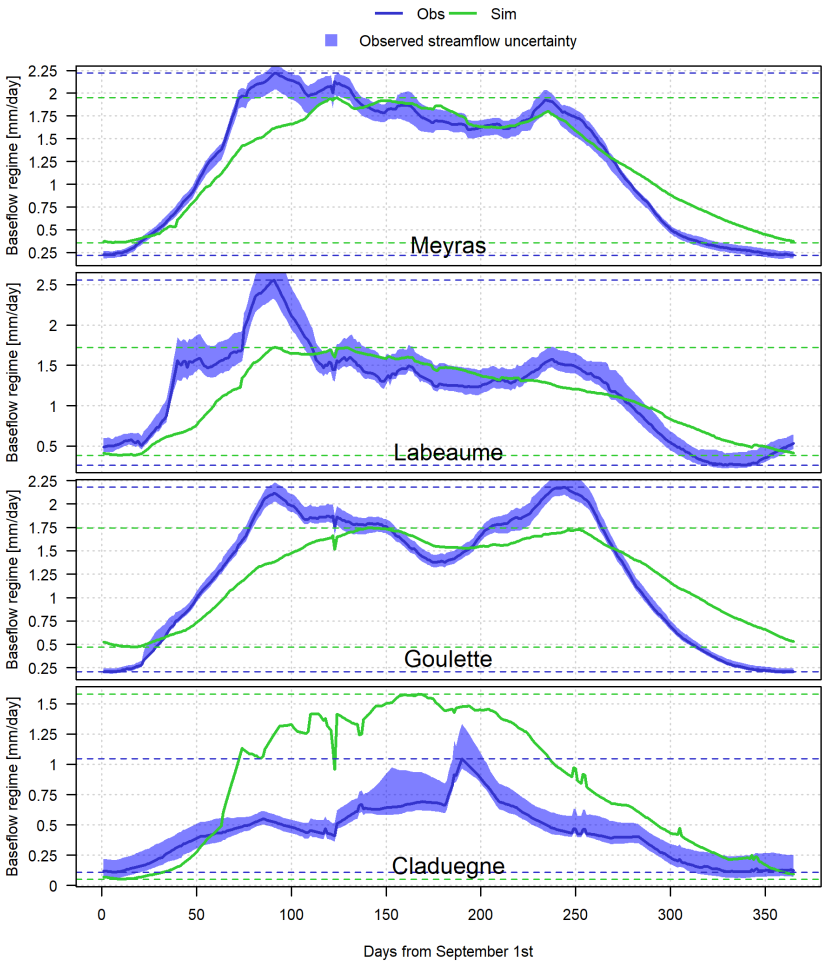

Figure 4.7: Observed and simulated baseflow regime, $\overline{Q}_{BF}$, of the four study catchments. The dashed horizontal lines show the minimum and maximum of the baseflow regime.

4.3.2 Hydrological signatures derived from the analysis of baseflow

4.3.2.1 Baseflow index

The separated baseflow and quickflow components of streamflow are commonly used to compute the baseflow index, S_{BFI}. It is the ratio between baseflow volume and total streamflow volume (e.g. Chapman, 1999; Eckhardt, 2008; Sawicz et al., 2011; Vrugt and Sadegh, 2013; Fenicia et al., 2016; Shafii et al., 2017) computed over a long period of time:

$$S_{\text{BFI}} = \frac{\sum_t Q_{QF}(t)}{\sum_t Q(t)} \tag{4.10}$$

The baseflow index, S_{BFI}, is used here as a hydrological signature to study the relative importance of slow flow components – as computed using the Gustard algorithm – with respect to total streamflow. This hydrological signature quantifies the long term partitioning between fast and slow flow.

Figure 4.8 shows the observed and simulated baseflow index, S_{BFI}, computed for the 4 study catchments. Observed and simulated S_{BFI} are similar for Meyras, Pont-de-Labeaume and Goulette but very different for Cladužgne. This shows that the large difference between observed and simulated data visible in Figure 4.7 for Cladužgne is captured by the baseflow index.

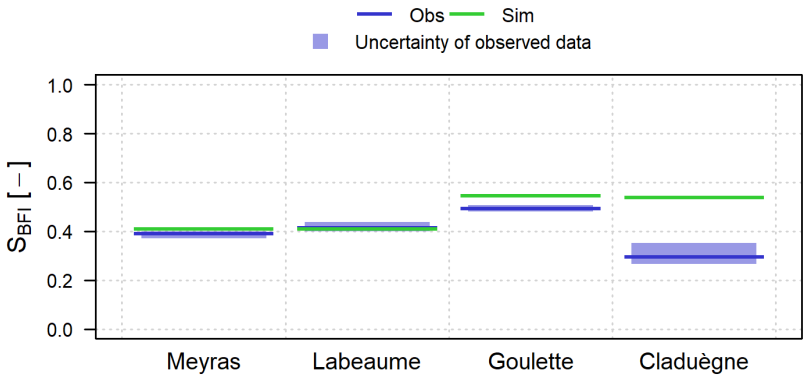

Figure 4.8: Observed and simulated baseflow index, S_{BFI}, of the four study catchments using the baseflow time series extracted using the Gustard algorithm.

4.3.2.2 Baseflow magnitude

Figure 4.7 clearly shows differences between observed and simulated baseflow regime between the dry and wet periods. The maximum, $Q_{\text{BFR.max}}$, and minimum, $Q_{\text{BFR.min}}$, of the baseflow regime, $\overline{Q}_{BF}$, can be extracted to characterize its magnitude of variation. The relative difference between these two values, $S_{\text{BFR.mag}}$, which measures the magnitude of variation of the baseflow regime relative to its maximum is computed:

$$S_{\text{BFR.mag}} = \frac{Q_{\text{BFR.max}} - Q_{\text{BFR.min}}}{Q_{\text{BFR.max}}} \tag{4.11}$$

$S_{\text{BFR.mag}}$ is used as a hydrological signature to characterize the seasonal magnitude of baseflow. $Q_{\text{BFR.min}}$ quantifies the importance of slow flow contribution in dry conditions – mostly due to groundwater release – and $Q_{\text{BFR.max}}$ characterize the slow flow contribution in wet conditions. If $Q_{\text{BFR.min}}$ is mostly linked to groundwater contributions, $Q_{\text{BFR.max}}$ is likely linked to a mix of groundwater contributions and soil contributions through lateral drainage. $S_{\text{BFR.mag}}$ varies between 0 and 1 and characterize the magnitude of slow flow contributions between the dry and wet period; the closer it is to 1 the larger the seasonal variation. Variation of slow flow contribution between dry and wet conditions, as measured by $S_{\text{BFR.mag}}$, is likely related to the overall catchment storage capacity and release rates. Only the baseflow regime magnitude, $S_{\text{BFR.mag}}$, is used as a hydrological signature.

Figure 4.9 shows the observed and simulated baseflow regime magnitude, $S_{\text{BFR.mag}}$ computed for the four study catchments. It shows that the larger simulated baseflow regime magnitude found for Claduègne (Figure 4.7) as well as the smaller simulated baseflow regime magnitudes found for Meyras, Pont-de-Labeaume and Goulette (Figure 4.7) are captured.

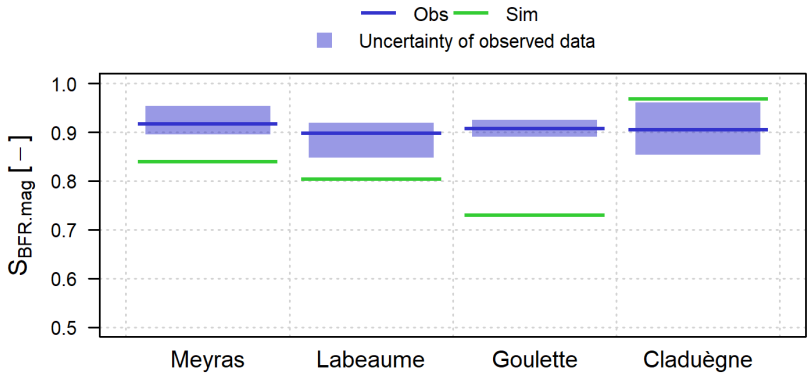

Figure 4.9: Observed and simulated baseflow regime magnitude, $S_{\text{BFR.mag}}$, of the four study catchments.

The baseflow regime curves shown in Figure 4.7 show interesting features other than magnitudes. Particularly, the rate of $\overline{Q}_{BF}$ increase, in Fall, and decrease, in Summer are very different between observed and simulated data. These features could be linked to the dynamics of catchment recharge and discharge. Quantifying these aspects of the baseflow regime could potentially lead to meaningful hydrological signatures. These aspects were not considered here as they are partly addressed by the hydrological signatures based on the analysis of streamflow/precipitation regimes (the P-Q approach presented in Section 4.4) and recessions (Section 4.5).

4.4 Streamflow response in dry and wet conditions: the P-Q approach

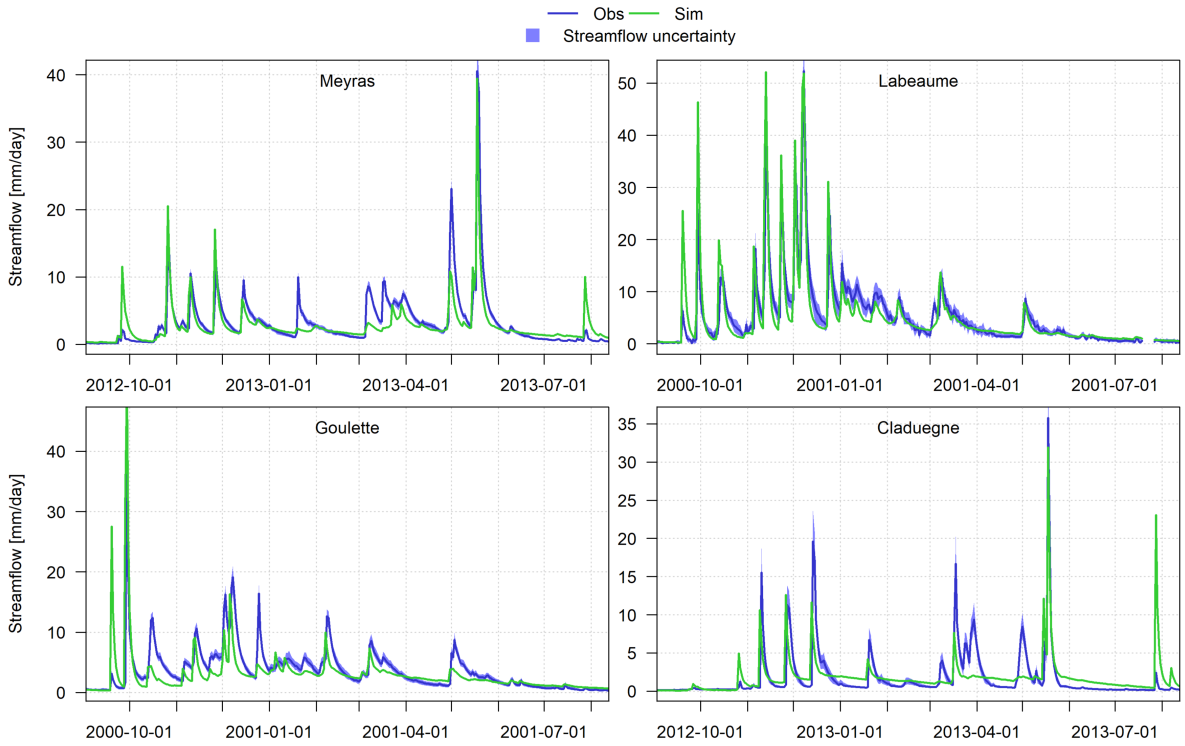

Figure 4.10: Observed and simulated streamflow time series of the four study catchment for a whole hydrological year.

Figure 4.10 shows the observed and simulated streamflow time series of the four study catchments for a whole hydrological year. It shows a clear difference between observed and simulated streamflow events during Fall (September, October and November): simulated streamflow peaks are systematically overestimated. Later in the year (Winter and Spring), the opposite observation can be made: simulated streamflow peaks are globally underestimated. This indicates differences in the catchment reactivity between Fall and Winter/Spring that is not reproduced by the model.

The differences in catchment streamflow response highlighted here can be attributed to differences in catchment wetness state between Fall and Winter. At the start of a hydrological year, the catchment is relatively dry following the Summer months. Precipitations during Fall contribute to the catchment re-wetting and therefore generate less streamflow than when the catchment is wet, in Winter. This can be a consequence of less overland flow (as there is no saturated soil) or catchment storage depletion contributions. In addition, evapotranspiration can be expected to still be large during Fall, contributing to the drying out of the soils.

The change in streamflow response between the dry and wet periods highlighted with Figure 4.10 can also be seen considering the inter-annual calendar day average of streamflow over a hydrological year. Focusing only on the first half of the year (Fall and Winter), Figure 4.11a shows that the same differences between observed and simulated data are found: overestimated (resp. underestimated) simulated streamflow during the dry (resp.wet) period. Figure 4.11b

shows the corresponding cumulative curves. As cumulative curves are less noisy, the differences between observed and simulated data appeared clearer: an overestimation of the simulated streamflow cumulative curve for the first 90 days (approximately) and then an underestimation.

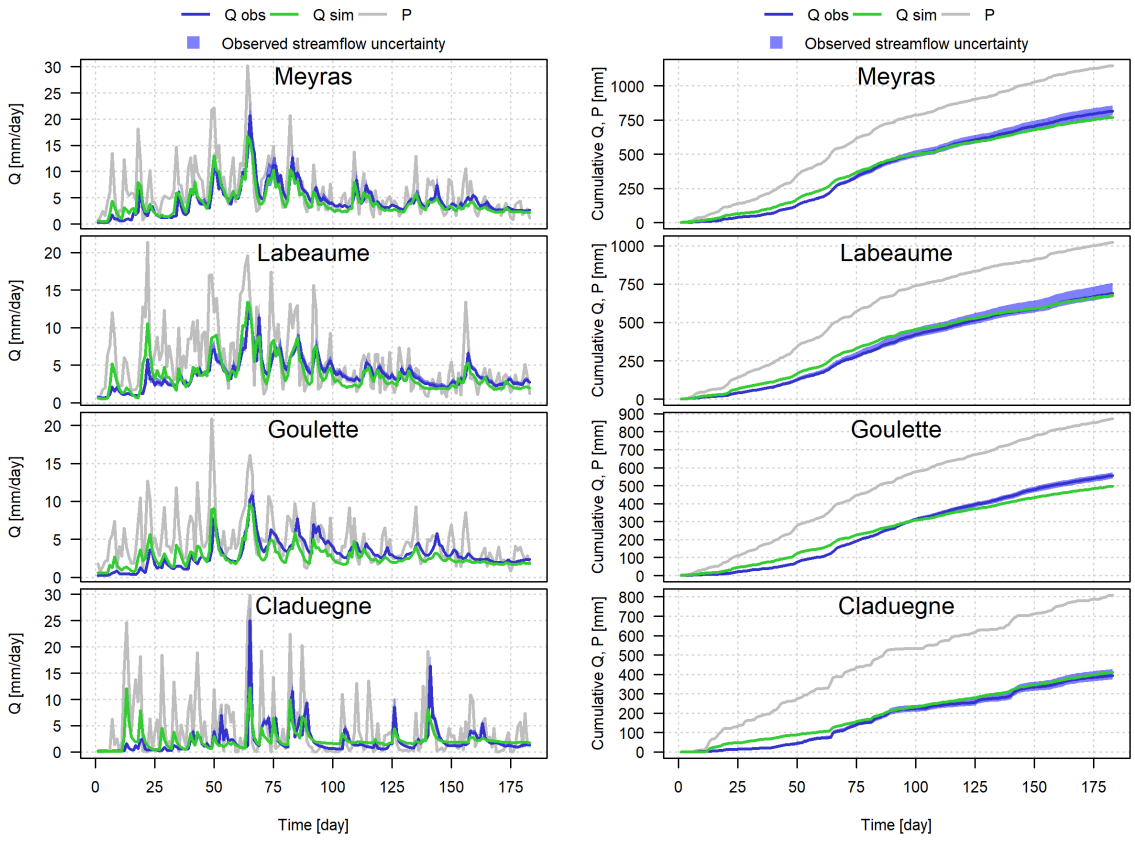

(a) Streamflow and precipitation rates **(b)** Cumulative streamflow and precipitation

Figure 4.11: Inter-annual calendar day mean over a hydrological year of observed and simulated streamflow (Q) and precipitation (P) rates (a) and cumulative curves (b) of the four study catchments.

These results show that observed catchment streamflow response changes in the first half of a hydrological year with less streamflow being generated during the first months and *vice-versa* after about 90 days. They also show clear differences between observed and simulated data: the change in catchment streamflow response is less visible if at all visible in simulated data. In the following subsection, the P-Q approach followed to derive hydrological signatures targeting this aspect of catchment behavior is described.

4.4.1 The P-Q approach

The inter-annual calendar day average of streamflow $\overline{Q}(d)$ and precipitation $\overline{P}(d)$ (Figure 4.11a) have 365 values, one for each calendar day d of a hydrological year (the 366$^{\text{th}}$ day is omitted). The difference of the corresponding cumulative curves for each calendar day d, $R_{\text{C}}(d)$, is:

$$R_{\text{C}}(d) = \sum_{k=1}^{d} \overline{P}(k) - \sum_{k=1}^{d} \overline{Q}(k) \tag{4.12}$$

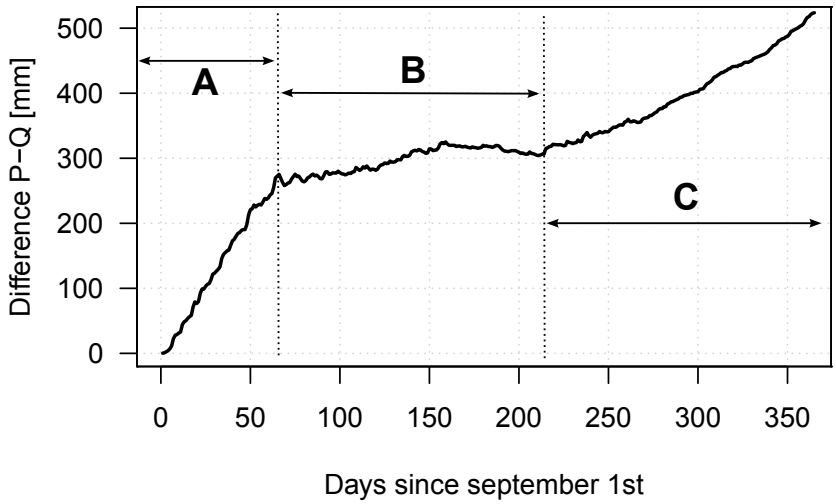

Figure 4.12: Example of P-Q curve $R_C(d)$ over a whole hydrological year. Its different periods are identified by letters and transitions with vertical dotted lines.

The P-Q curve $R_C(d)$ represents the cumulative amount of input precipitation that has not (yet) generated any streamflow. This water is stored in the catchment to be released as evapotranspiration or as streamflow. The different parts of the P-Q curve $R_C(d)$ are illustrated in Figure 4.12. They can be interpreted as follows:

- **Part A:** the steep slope of the dry period (Fall) is due to little streamflow as a consequence of (1) little overland flow (no saturation excess overland flow) and (2) little or no sub-surface or groundwater flow as the catchment is dry. In addition, evapotranspiration might limit catchment storage recharge during this period. Also note that, the more precipitation during this period, the steeper the slope will be; however more precipitation also increases the chance of more overland flow due to infiltration rate excess which, in this case, would lead to a less steep slope.

- **Part B:** The relatively flat slope of the wet period (Winter) is due to large streamflow as a consequence of (1) saturation excess overland flow, (2) large catchment storage water release from soil (sub-surface flow) and groundwater; a flat slope indicates that the amount of input precipitation that does infiltrate into the soil is completely compensated by catchment storage water release and overland flow.

- **Transition A/B:** The time required to have this shift between the dry and wet catchment streamflow response behaviors is influenced by (1) precipitation (and soil infiltration) and evapotranspiration rates during the dry period and (2) catchment storage capacity and dryness state at the start of a hydrological year. The larger the catchment storage capacity is (and the drier the catchment is), the more time it will need to be re-filled, which should lead to a later shift in $R_C(d)$. Similarly the smaller the precipitation rates and soil infiltration (resp. the larger the evapotranspiration rates) are during the dry period, the more time it will take to re-fill catchment storage; this should also lead to a later shift in $R_C(d)$. Also note that faster overall catchment storage release rate could delay the change of state of catchment (as refilling takes more time due to a faster release) and cause a later shift; alternatively it could also induce an earlier change in the catchment behavior (earlier shift) as less water needs to enter the system before it starts to behave

differently.

- **Part C:** Although we do not investigate the late part of the $R_C(d)$, its visible increase in Figure 4.13 is likely due to the increase of evapotranspiration throughout Spring and Summer which leads to less streamflow generation and the drying out of the catchment.

Figure 4.13 shows the resulting P-Q curves for the four study catchments. A clear threshold is visible, especially in observed data (towards day 90): fast increase of $R_C(d)$ followed by a slow increase of $R_C(d)$ after the threshold. This change of trend is less visible in simulated data and seems to occur later in the hydrological year.

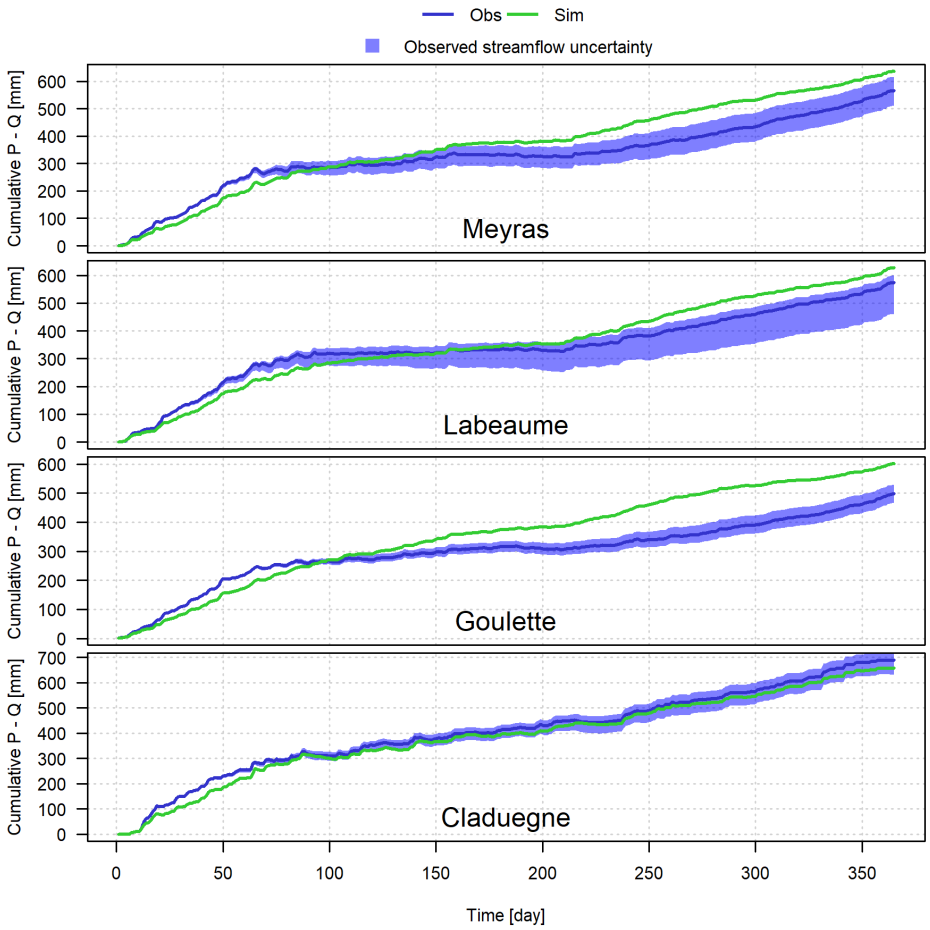

Figure 4.13: Observed and simulated $R_C(d)$ of the four study catchments over a whole hydrological year.

4.4.2 Hydrological signatures derived from the P-Q curve

The P-Q curve, $R_C(d)$, is used to extract 4 hydrological signatures that characterize its shape in the first half of a hydrological year (Fall and Winter): the slope of the curve during the dry and wet period $S_{PQ.dry}$ and $S_{PQ.wet}$, the strength of the threshold, $S_{PQ.strength}$, computed from the dry and wet slopes (Equation 4.13), and the date of the threshold, $S_{PQ.date}$. A segmented regression (Muggeo, 2003, 2008) is used to estimate $S_{PQ.dry}$, $S_{PQ.wet}$ and $S_{PQ.date}$. The 15 first days are omitted as they show more variability and prevent the segmented regression to converge toward a break-point within the expected range of values (approximately between

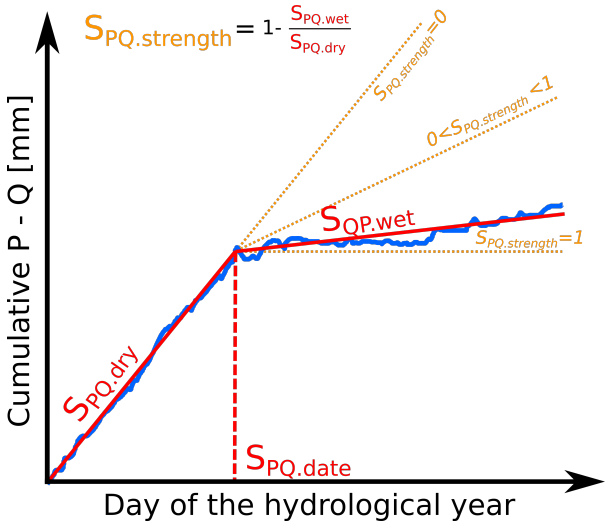

Figure 4.14: Diagram illustrating the four hydrological signatures derived following the P-Q approach: the slopes of the dry and wet period, $S_{\text{PQ.dry}}$ and $S_{\text{PQ.wet}}$, and the threshold strength and date, $S_{\text{PQ.strength}}$ and $S_{\text{PQ.date}}$.

day 30 and day 150). Only the first half of a hydrological year is considered in the segmented regression, i.e. from day 15 to day 183. The intercept of the first segment was forced to zero as $R_{\text{C}}(0) = 0$ and the initial guess of the break-point (required by the method, see Muggeo (2003, 2008)) was set at day 90. The segmented regression estimates the threshold date $S_{\text{PQ.date}}$, the slope of the first segment, $S_{\text{PQ.dry}}$, and the slope of the second segment, $S_{\text{PQ.wet}}$. The strength of the threshold, $S_{\text{PQ.strength}}$, is then computed using the estimated slopes:

$$S_{\text{PQ.strength}} = 1 - \frac{S_{\text{PQ.wet}}}{S_{\text{PQ.dry}}} \tag{4.13}$$

The definition of $S_{\text{PQ.strength}}$ is so that if there is no break-point ($S_{\text{PQ.dry}} = S_{\text{PQ.wet}}$), it yields 0, and if the second slope is horizontal ($S_{\text{PQ.wet}} = 0$), it yields 1. Figure 4.14 is a diagram illustrating the four extracted hydrological signatures using the $R_{\text{C}}(d)$ curve and the segmented linear regression.

Figure 4.15 shows the derived hydrological signatures. The segmented regression successfully captures the shift in R_{C} for all study catchments considering either observed or simulated data. Even when the shift isn't well visible (e.g. Goulette catchment), it is detected. The derived hydrological signatures reflect the visible differences between catchments. For example the weakest (resp. strongest) threshold identified for Claduègne (resp. Pont-de-Labeaume) is well captured by $S_{\text{PQ.strength}}$. Figure 4.15 also shows that differences between observed and simulated data are successfully captured by the derived hydrological signatures. The observed steeper (resp. less steep) slopes of the dry period (resp. wet period) are captured by $S_{\text{PQ.dry}}$ (resp. $S_{\text{PQ.wet}}$). The weaker threshold as well as the later change of trend in simulated data are also captured by $S_{\text{PQ.strength}}$ and $S_{\text{PQ.date}}$ respectively.

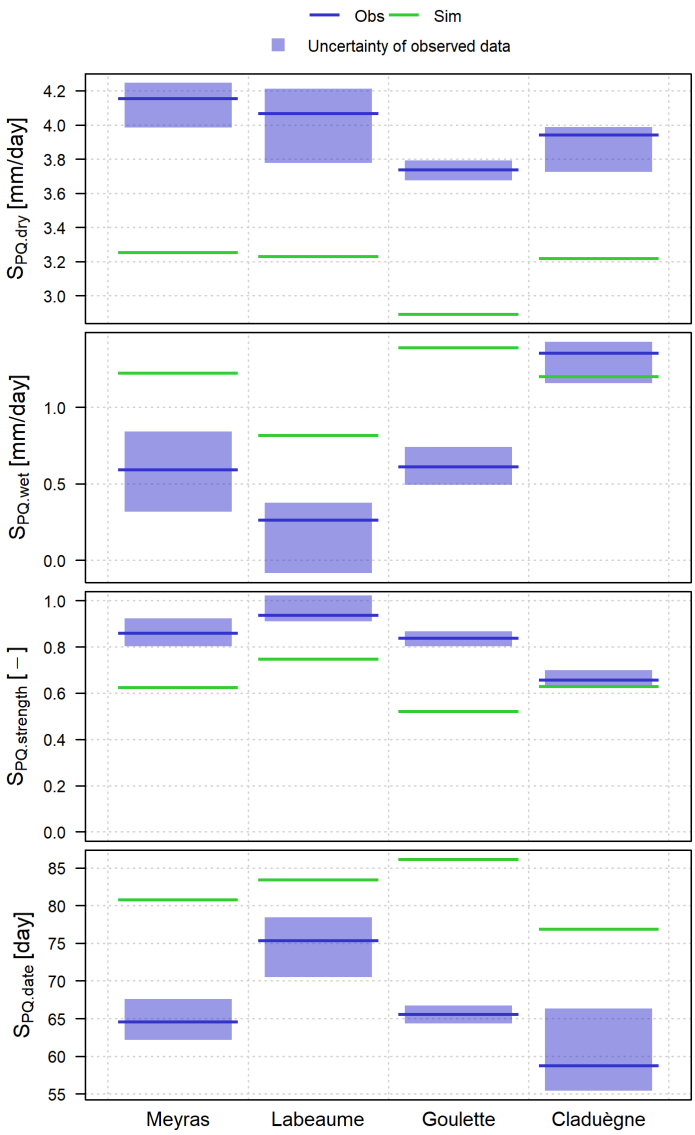

Figure 4.15: Observed and simulated hydrological signatures resulting from the P-Q approach: $S_{\mathrm{PQ.dry}}$, $S_{\mathrm{PQ.wet}}$, $S_{\mathrm{PQ.strength}}$ and $S_{\mathrm{PQ.date}}$.

4.5 Characteristics of streamflow recessions

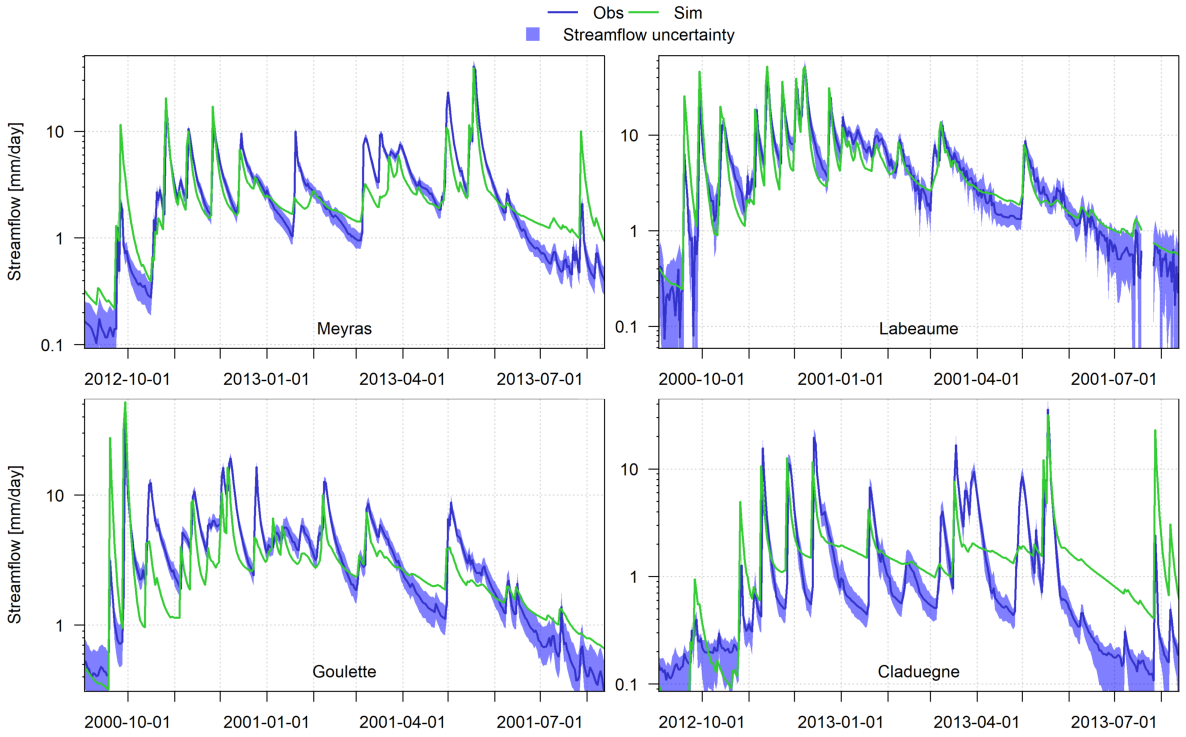

Figure 4.16: Observed and simulated streamflow time series of the four study catchment for a whole hydrological year (arbitrarily chosen: 2012-2013 for Meyras and Cladugne and 2000-2001 for Pont-de-Labeaume and Goulette). Note that a log scale is used for the y axis.

Figure 4.16 shows the observed and simulated streamflow time series of the four study catchments for a whole hydrological year arbitrarily chosen. The log scale axis for streamflow makes the recessions well visible and allows identifying their main features that might be worth capturing in the analysis of recessions. For all catchments, a change of trend between the early part and the late part of recessions can be identified, in particular for Meyras and Cladugne. These breakpoints are less visible in the case of Pont-de-Labeaume and Goulette where a smoother transition occurs between early and late parts of recessions. Figure 4.16 also shows important differences between observed and simulated streamflow recessions: simulated recessions are (1) globally slower, (2) faster at first and then slower and (3) transitions between the early and late parts of the recessions are more abrupt.

4.5.1 Recession analysis methods

4.5.1.1 Theoretical basis

Recession analysis is the analysis of the declining parts of streamflow, i.e. when $\mathrm{d}Q(t)/\mathrm{d}t < 0$ where $Q(t)$ is streamflow at time t. It is used to study the storage-discharge relationship of catchments (e.g. Brutsaert and Nieber (1977); Wittenberg and Sivapalan (1999); Kirchner (2009); Stoelzle et al. (2013)). At any given time t, the water mass balance equation at the catchment scale is:

$$\frac{\mathrm{d}S(t)}{\mathrm{d}t} = P(t) - E(t) - Q(t) \tag{4.14}$$

where $\mathrm{d}S(t)/\mathrm{d}t$ is the variation of catchment water storage between two consecutive time steps. In the case where precipitation $P(t)$ and evapotranspiration $E(t)$ are small compared to streamflow $Q(t)$, i.e. $P(t) << Q(t)$ and $E(t) << Q(t)$, Equation 4.14 becomes:

$$\frac{\mathrm{d}S(t)}{\mathrm{d}t} = -Q(t) \tag{4.15}$$

The storage-streamflow relationship of the catchment (Equation 4.15) is often investigated considering that the relation between catchment storage $S(t)$ and streamflow $Q(t)$ can be modeled using a power-law model (Brutsaert and Nieber, 1977; Wittenberg and Sivapalan, 1999; Kirchner, 2009; Stoelzle et al., 2013; McMillan et al., 2017; Bart and Tague, 2017):

$$S(t) = cQ(t)^d \tag{4.16}$$

If d is set to 1, Equation 4.16 becomes a linear model. Combining Equations 4.15 and 4.16 (and a parameter transformation, see Appendix E.2) leads to the widely used following differential equation:

$$-\frac{\mathrm{d}Q(t)}{\mathrm{d}t} = aQ(t)^b \tag{4.17}$$

Equation 4.17 has the following solution (see Wittenberg and Sivapalan (1999) and Appendix E.2):

$$Q(t) = \begin{cases} Q(0)\left(1 + a(b-1)Q(0)^{b-1}t\right)^{1/(b-1)} & \text{if} \quad b \neq 1 \\ \\ Q(0)\mathrm{e}^{-at} & \text{if} \quad b = 1 \end{cases} \tag{4.18}$$

4.5.1.2 Extracting recessions

The analysis of recession supposes to first isolate the recession periods, i.e. the periods where $\mathrm{d}Q(t)/\mathrm{d}t < 0$ and precipitation and evapotranspiration are small compared to streamflow. A large variety of methods can be adopted for this purpose (e.g. Kirchner, 2009; Stoelzle et al., 2013; Vannier et al., 2013) either extracting all the recessions together or by identifying individual recession events. Stoelzle et al. (2013) summarized the typical requirements for recession period extraction based on criterion on streamflow only:

- it must focus only on declining parts of hydrographs i.e. $\mathrm{d}Q/\mathrm{d}t < 0$;
- it must exclude early parts of recession to avoid direct runoff;
- it must be long enough to ensure that the studied recession is *"connected to pure storage depletion"* (Stoelzle et al., 2013) and/or to ensure *"a certain consistency in the observations"* (Vannier et al., 2013).

The recession extraction method can be based on other data such as rainfall and temperature. For example, Kirchner (2009) used two alternative methods to select recession periods: (1) using rainfall data and temperature data he selected periods where both potential evapotranspiration and rainfall were 10 times smaller than streamflow; (2) he selected night periods (using solar flux data) with no rainfall (note that sub-daily data are required in that case).

Table 4.2: Statistics on the extracted recessions for the four study catchments for both observed and simulated streamflow time series

	Meyras	Pont-de-Labeaume	Goulette	Claduègne
Observed streamflow time series†				
Number of recessions	305 [303, 315]	310 [297.975, 317]	332 [327.975, 341.025]	53 [52, 59]
Long recessions‡ [%]	29.5 [28.1, 30.2]	2.9 [2.23, 4.35]	21.7 [20, 22]	32.1 [26.7, 33.9]
Average recession length [day]	15.2 [15, 15.3]	9.61 [9.33, 9.99]	14 [13.6, 14]	15.2 [14.1, 15.4]
Simulated streamflow time series				
Number of recessions	316	263	339	58
Long recessions‡ [%]	31	31	29	31
Average recession length [day]	15.8	15.8	15.2	15.5

† brackets indicate the 95% uncertainty interval due to streamflow uncertainty in the computation of the recession statistics
‡ long recession are defined here as recession longer than 20 days

Several recession extraction algorithms were tested and compared. The approach we decided to follow is graphically based and relies only on streamflow data. The early parts of the recessions are not discarded because we wish to characterize both the early and late part of recessions.

Based on the local minima and maxima of the streamflow time series, the extraction procedure approach enables the identification of individual recession events. It requires to specify 3 parameters, Q_{th}, L_{min} and L_{max} and can be decomposed in the following steps:

- **smoothing**: to reduce noise in the streamflow time series, they are smoothed using a mean applied on a 3-days sliding window;
- **local maxima and minima**: local maxima and minima are then extracted; only maxima above a streamflow Q_{th}, are kept to ensure that only significant streamflow peaks are selected; each selected maximum is then associated with the following minimum thus defining a recession period.
- **length criteria**: only recession period longer than L_{min} are kept; if recession period are longer than L_{max}, they are truncated.
- **streamflow recessions**: recession segments are extracted according to the obtained recession periods from the original (un-smoothed) streamflow time series.

The 3 parameters were set following a trial-and-error approach, according to visual inspections of the resulting extracted recession periods: $Q_{\text{th}} = Q_{0.5}$ where $Q_{0.5}$ is the median streamflow value, $L_{\text{min}} = 5$ and $L_{\text{max}} = 30$.

Table 4.2 gives an overview of the extracted recessions for all study catchments: the number of recessions, their average length and the proportion of long recession (> 20 days). For all catchments except Claduègne, more than 300 recession events were extracted from observed streamflow time series. For Claduègne, Only 53 recession events were extracted due to the shorter time series. For all catchments except Pont-de-Labeaume, the average length of the recessions was about 15 days. Shorter recessions were extracted for Pont-de-Labeaume due to much larger noise in the observed streamflow time series. The proportion of long recessions is thus very small (about 3%) for Pont-de-Labeaume compared with the other catchments (between about 20% and 30%).

4.5.2 Early and late recession times

Figure 4.16 clearly shows that, in the case of our study catchments, the recession rates of the early and late parts of the recessions are different. An original approach was considered to capture both the early and late recession time characteristics.

In this approach, the early and late parts of each recession are considered separately. From visual inspections of streamflow recessions we identified two segments of the recessions which were approximately linear for most recessions: the 5 first days of the recessions and the tail of the recessions, starting 15 days after the start of the recessions. Equation 4.18, with b set to 1, is fitted against each recession, considering separately the early and late part of the recessions. Figure 4.17 provides two examples of recession events with the fitted early and late part of the recessions. The inverse of the parameter a of Equation 4.18 is used to define two new hydrological signatures: (1) the early recession time $S_{\mathrm{REC}.\tau\mathrm{early}}$ and (2) the late recession time $S_{\mathrm{REC}.\tau\mathrm{late}}$. The medians taken over all the obtained recession times define the early recession time $S_{\mathrm{REC}.\tau\mathrm{early}}$ and the late recession time $S_{\mathrm{REC}.\tau\mathrm{late}}$ used as hydrological signatures. The early part of recessions is set between day $d_{\mathrm{early,\,start}}$ (set to 1, i.e. the start of the recession) and date $d_{\mathrm{early,\,end}}$ (set to 5 in our case). Similarly, the late part of the recession is set between day $d_{\mathrm{late,\,start}}$ (set to 15 in our case) and date $d_{\mathrm{late,\,end}}$ (set to 30 in our case). Not all recessions yielded results as at least 5 time steps are required when fitting the recession to ensure a robust fit. In particular only a portion of the extracted recession were longer than 20 days (see Table 4.2) which is the minimum length a recession must have to be able to estimate a late recession time.

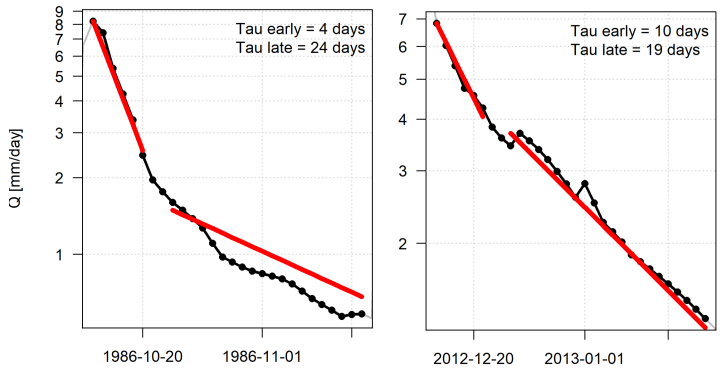

Figure 4.17: Example of two recession fitted using Equation 4.18, with b set to 1 to extract the early and late recession times, τ_{early} and τ_{late}. The red lines are the obtained fit.

The early recession time, $S_{\mathrm{REC}.\tau\mathrm{early}}$, focuses only on the first days of recessions and characterizes the average catchment water release characteristics just after a precipitation event. Therefore, it should focus on quickly depleting water storage in the catchment e.g. fast soil lateral drainage as well as, to a smaller extent, the decrease rate of overland flow contributions, immediately after a precipitation event. The late recession time, $S_{\mathrm{REC}.\tau\mathrm{late}}$, should characterize slowly depleting catchment storage e.g. the slow groundwater storage-release characteristics.

Figure 4.18 shows the observed and simulated early and late recession times, $S_{\mathrm{REC}.\tau\mathrm{early}}$ and $S_{\mathrm{REC}.\tau\mathrm{late}}$, of the four study catchments. For all catchments, $S_{\mathrm{REC}.\tau\mathrm{early}}$ (ranging between 4 and 12 days) are smaller than $S_{\mathrm{REC}.\tau\mathrm{late}}$ (ranging between 10 and 70 days) indicating that the rate of change in streamflow between the early and late part of recession is captured: faster at first and

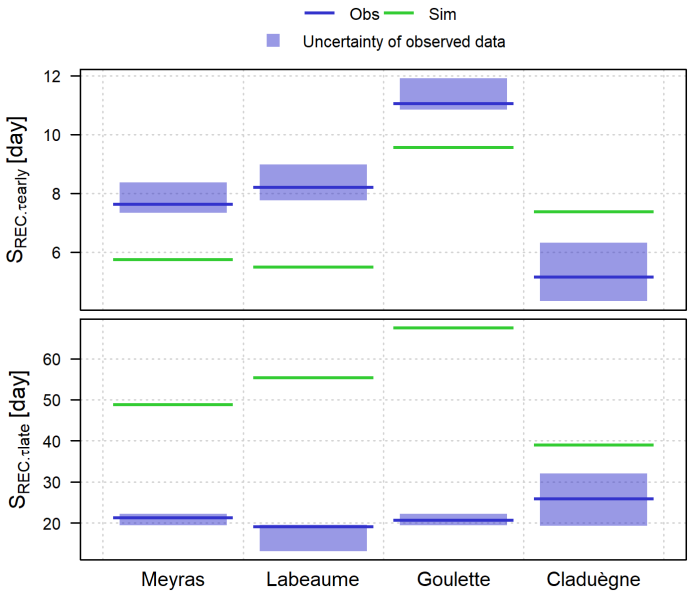

Figure 4.18: Observed and simulated hydrological signatures $S_{\mathrm{REC}.\tau\mathrm{early}}$ and $S_{\mathrm{REC}.\tau\mathrm{late}}$ derived from the analysis of recessions. The results are shown for the four study catchments.

then slower. Simulated $S_{\mathrm{REC}.\tau\mathrm{early}}$ are smaller than the observed $S_{\mathrm{REC}.\tau\mathrm{early}}$ for all catchments except Cladugne indicating steeper early recessions in simulated streamflow time series. A closer look at the Cladugne streamflow time series in Figure 4.16 shows that early parts of recessions might indeed be steeper in observed streamflow time series. The differences between observed and simulated $S_{\mathrm{REC}.\tau\mathrm{late}}$ are larger than in the case of $S_{\mathrm{REC}.\tau\mathrm{early}}$: simulated $S_{\mathrm{REC}.\tau\mathrm{late}}$ (ranging between 40 and 70 days) are larger than observed $S_{\mathrm{REC}.\tau\mathrm{late}}$ (ranging between 10 and 30 days). These results show that the slower simulated late recessions visible in Figure 4.16 for all catchments are captured by this hydrological signature.

The extraction of the early and late recession times, $S_{\mathrm{REC}.\tau\mathrm{early}}$ and $S_{\mathrm{REC}.\tau\mathrm{late}}$, relies on all the recession events. Statistics on the resulting individual values, $\tau_{\mathrm{early},\,i}$ and $\tau_{\mathrm{late},\,i}$ (with $i = 1, 2, ..., n$, where n is the number of recession events) shows reasonable inter-event variations. For example, 90% of observed early (resp. late) recession times computed for all recession events of the Meyras catchment range between 2.1 and 20 days (resp. between 18 and 41 days). Other more traditional recession analysis approaches were tested including fitting the power law model of Equation 4.17 (see Appendix E.1.3.3) to estimate parameter a and b. However, this alternative approach was not retained due to too large inter-event variation in the resulting signatures.

4.6 Synthesis and discussion

4.6.1 Synthesis

Table 4.3: Selected hydrological signatures

Signature	Unit	Description
Flow duration curve		
$S_{\text{FDC.slope}}$	mm/day	Slope of the mid-segment of the flow duration curve
$S_{\text{FDC.Q90}}$	mm/day	Streamflow equaled or exceeded 90% of the time
$S_{\text{FDC.Q10}}$	mm/day	Streamflow equaled or exceeded 10% of the time
Runoff coefficient		
S_{RC}	-	Long term ratio between streamflow volume and precipitation volume
Baseflow analysis		
S_{BFI}	-	Long term ratio between baseflow volume and streamflow volume
$S_{\text{BFR.mag}}$	-	Baseflow regime(1) magnitude: $(S_{\text{BFR.max}} - S_{\text{BFR.min}})/S_{\text{BFR.max}}$
Streamflow regime(2) analysis, the P-Q approach		
$S_{\text{PQ.dry}}$	mm/day	Slope of the P-Q curve(3) during the dry period, i.e. before the threshold, $S_{\text{PQ.strength}}$.
$S_{\text{PQ.wet}}$	mm/day	Slope of the P-Q curve(3) during the wet period, i.e. after the threshold, $S_{\text{PQ.strength}}$.
$S_{\text{PQ.strength}}$	-	Strength of the threshold between the dry and wet period in the P-Q curve(3): $1 - (S_{\text{PQ.wet}}/S_{\text{PQ.dry}})$
$S_{\text{PQ.date}}$	day	Number of days, from september 1st, before the threshold in the P-Q curve(3).
Streamflow recessions analysis		
$S_{\text{REC.}\tau\text{early}}$	day	Early recession time: median values of the parameter τ obtained by fitting(4) to the early part of each recession event ($\leq$ 5 days)
$S_{\text{REC.}\tau\text{late}}$	day	Late recession time: median values of the parameter τ obtained by fitting(4) to the late part of each recession event ($\geq$ 15 days)

(1) the inter-annual average of baseflow on each calendar day of a hydrological year

(2) the streamflow regime (and precipitation regime) is defined as the inter-annual average of streamflow on each calendar day of a hydrological year

(3) the P-Q curve is the difference between the cumulative precipitation regime(2) and the cumulative streamflow regimes(2)

(4) by linear regression, using equation $Q(t) = Q(0)\text{e}^{-t/\tau}$ in log space, where Q(t) is streamflow at time t relative to the start of the recession ($t = 0$)

In this chapter, a set of 12 hydrological signatures was detailed. The set of hydrological signatures is presented in Table 4.3. The building of this set of hydrological signatures was based on a broad review of the literature on hydrological signatures and the visual analysis of observed and simulated data of four catchments. Some of the approaches and hydrological signatures presented here are new: the analysis of the baseflow regime, the analysis of early and late recessions and the analysis of the streamflow regime.

The hydrological signatures are to be used for the diagnostic and evaluation of a hydrological model. Their interpretation in terms of hydrological processes is therefore important to understand differences between catchments and between simulated and observed data. This link between hydrological processes and hydrological signature is called discriminatory power by McMillan et al. (2017) which, in the case of models, can be termed diagnostic power. As a consequence the main criterion used in the selection and design of the hydrological signatures presented in this chapter was the interpretation in terms of hydrological processes as well as their ability to capture differences between observed and simulated data.

Other hydrological signatures than those presented here, found in the literature, were also

tested (see Appendix E.1) but not kept as they were found irrelevant for our study catchments. Event-based approaches, the auto-correlation of streamflow and the cross-correlation between streamflow and precipitation, the rising and declining limb density were not kept because of (1) the too coarse daily time resolution, or (2) the lack of meaningful differences between observed and simulated data or between catchments (as tested with our four study catchments) or (3) weak or unclear link with hydrological processes.

The selected hydrological signatures were designed to be applicable and relevant in a broader range of context than the Ardèche catchment. The four study catchments, Meyras, Pont-de-Labeaume, Goulette and Claduègne, were mostly used to illustrate and test them i.e. verify that the differences (between catchment and between observation and simulation) visible in the data could be captured. This is illustrated by the work of Abdillahi Robleh (2019) who used most of the hydrological signatures presented in this chapter on a larger set of sub-catchments of the Rhône catchment of various sizes and physical characteristics, and located in various hydro-climatic contexts.

4.6.2 A set of hydrological signatures to characterize long term emergent hydrological processes

Table 4.4: Selected and designed hydrological signatures and their interpretation in terms of hydrological processes

Signature	Interpretation	A larger value indicates ...
S_{RC}	Long term proportion of input precipitation that is released as streamflow. It measures the partitioning between evapotranspiration and streamflow.	less evapotranspiration to the profit of streamflow due to (1) smaller evapotranspiration demand (smaller plant transpiration need) and/or (2) less water available for plant transpiration (in the soils) or evaporation (surface ponding, canopy interception)
$S_{\mathrm{FDC.slope}}$	Distribution of medium flow between fast and slow streamflow generation processes measuring the dampening effect of the catchment.	a weaker catchment dampening effect with more variable streamflow due to smaller catchment storage, less vertical drainage, and/or faster catchment release rates (from soils or groundwater)
$S_{\mathrm{FDC.Q90}}$	Catchment streamflow response in low flow conditions mostly affected by groundwater contributions.	more groundwater contribution due to more vertical drainage, larger groundwater storage and/or slower groundwater release rates.
$S_{\mathrm{FDC.Q10}}$	Catchment streamflow response in high flow conditions, during precipitation events mostly driven by overland flow and fast soil drainage.	larger overland flow contributions due to smaller maximum soil infiltration rates and/or more frequently saturated soils (smaller soil storage capacity or more slowly draining soils) and/or faster soil drainage.

Table continues next page ...

... table continued

Signature	Interpretation	A larger value indicates ...
S_{BFI}	Long term proportion of slow flow contributions with respect to total streamflow. It measures the partitioning between fast flow generation processes (overland flow and fast sub-surface flow) and slow flow contributions (slow soil lateral flow and groundwater flow).	more groundwater and slow sub-surface flow contributions (resp. less overland flow and fast sub-surface flow contributions) due to more soil infiltration and/or more soil vertical drainage.
$S_{\text{BFR.mag}}$	Difference in slow flow contributions between dry and wet conditions.	lower dry low flow contributions relatively to the wet period due to smaller catchment storage and/or faster catchment release rates (from soils/groundwater).
$S_{\text{PQ.dry}}$	Catchment streamflow generation deficit with respect to precipitation inputs due to soil recharge and evapotranspiration in dry conditions, during the re-wetting period (Fall).	less overland flow (more infiltration) and/less catchment storage depletion due to drier catchment state, slower soil drainage, more vertical drainage and/or more evapotranspiration, in dry conditions, during the re-wetting period.
$S_{\text{PQ.wet}}$	Catchment streamflow generation deficit with respect to precipitation inputs due infiltration and overall catchment storage and release rate.	less overland flow (more infiltration) and less/slower catchment storage depletion due to larger catchment storage, slower soil drainage, more vertical drainage, smaller/slower groundwater release rate, in wet conditions, after the re-wetting period.
$S_{\text{PQ.strength}}$	Differences in streamflow response between the dry period and wet period. It measures how much streamflow response to precipitation varies between the dry and wet periods of the first half of a hydrological year.	stronger/larger differences in infiltration rates between dry and wet conditions due to differences in soils wetness states and/or stronger/larger differences in catchment storage depletion between dry and wet conditions due to larger differences in overall catchment wetness state.
$S_{\text{PQ.date}}$	Time required for a catchment to change of behavior in terms of streamflow response due to the change in its wetness state, i.e. it measures the length of the dry period that occurs during Fall.	that more time are required to refill catchment storage due to a drier catchment, larger catchment storage capacity, slower refilling (less infiltration more evapotranspiration), slower or faster (both possible) overall catchment storage release rates.
$S_{\text{REC.}\tau\text{early}}$	Catchment release rate immediately after a precipitation event. It focuses on quickly catchment depleting reservoirs or overland flow contributions.	slower catchment storage discharge rates from quickly depleting water storage in the catchment (less/slower fast lateral drainage from soils) and/or less overland flow.
$S_{\text{REC.}\tau\text{late}}$	Catchment storage release rate due to slowly catchment depleting reservoirs.	slower catchment storage release rates from slowly depleting catchment storage due to slower soil drainage, more vertical soil drainage and/or slower groundwater release.

The different data analysis approaches used to derived hydrological signatures investigate hydrological processes in terms of (1) volumes (S_{RC} and S_{BFI}), magnitude and frequency (hydrological signatures based on the flow duration curve), (2) seasonal change / dynamics (hydrological sig-

natures based on the baseflow regime and P-Q curve) and (3) event scale behaviors (hydrological signatures based on the analysis of recessions). Only long term – pluri-annual – average/median catchment behaviors are characterized and quantified. However, the target hydrological processes are investigated considering their effect at different temporal scales: annual, seasonal and event scales.

Table 4.4 summarizes how each hydrological signature might be interpreted in terms of catchment functioning. Following Wagener et al. (2007), the main functions of a catchment can be viewed as the partitioning, storage and release of water. These three main aspects of catchment functioning are addressed by the selected hydrological signatures. From Table 4.4 it is possible to derive hypothesized links between the main aspects of catchment functioning in terms of partitioning, storage and release. Figure 4.19 shows a diagram illustrating these main aspects of catchment functioning and how each hydrological signature might be related to them.

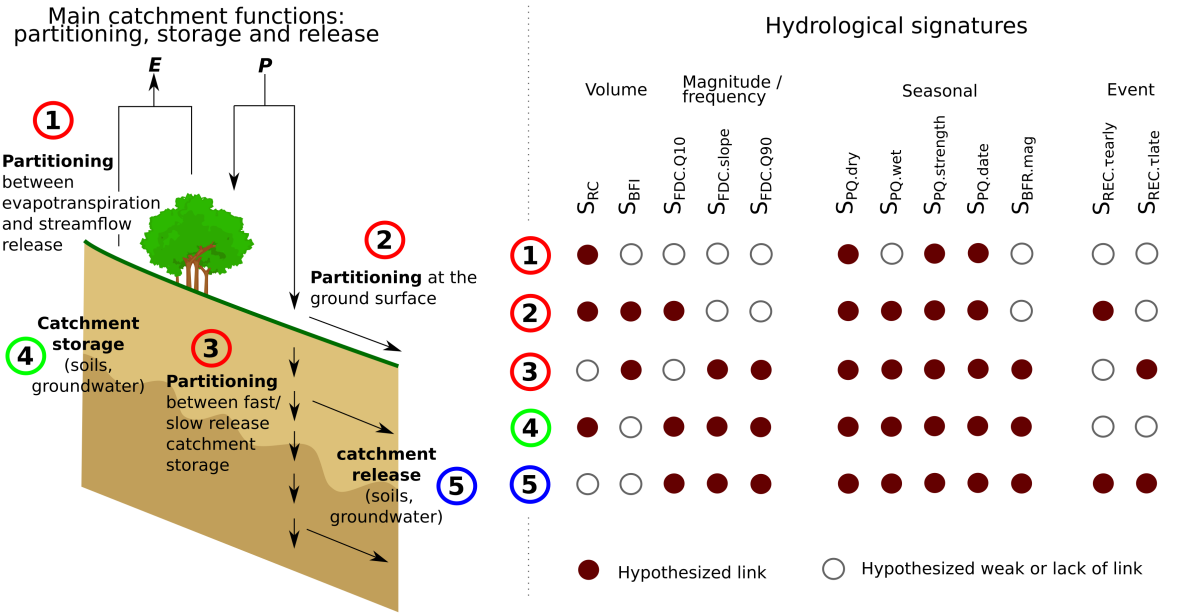

Figure 4.19: Relation between the main catchment functions (illustrated by the diagram on the left and corresponding colors) and the hydrological signatures classified according to the temporal scale of investigation.

Although, in the ideal case, each hydrological process should be linked to one hydrological signature, this is in practice difficult if possible at all. Figure 4.19 clearly shows that, for all hydrological signatures, no unique links can be established, i.e. none of the hydrological signature is specific to a particular hydrological process or catchment function. For example, the long term runoff coefficient, S_{RC} (see Section 4.1), informs on the partition of the input precipitation between the two possible outputs, evapotranspiration and streamflow However, the evapotranspiration is the results of both a demand for evapotranspiration (i.e. energy inputs and the plants need for water) and the available water for evaporation (e.g. at the ground surface) and transpiration (the water available in the soil for the plant to use). Therefore, the runoff coefficient targets the evaporation and transpiration processes as well as other hydrological processes such as water ponding at the ground surface, infiltration into the soil, soil water storage and drainage, etc. This complexity highlights the need to combine multiple approaches

to derive hydrological signatures in order to disentangle the impact of different hydrological processes and build a sound understanding of the catchment functioning.

Figure 4.19 also shows that the hydrological signatures are redundant, i.e. the same catchment functions are targeted by multiple signatures. This is however necessary given the absence of "unique" link between hydrological signatures and catchment function. Because each signature has multiple interpretation, using multiple signatures can help identify more precisely the particular hydrological processes at play. In other words, the combination of different temporal scales as well as the combination of different data analysis approaches, enable a finer investigation of catchment behavior and internal catchment functioning.

For example, let's consider the vertical partitioning of water in the catchment in fast or slow drainage catchment storage. Figure 4.19 (and the details in Table 4.4) shows that multiple hydrological signatures can address this catchment function. More vertical drainage can imply more slow flow (resp. less fast flow due to fast soil drainage). As a consequence, the baseflow index, S_{BFI}, is expected to be larger. However, a larger S_{BFI} can also be due the ground surface partitioning function of the catchment with more infiltration at the expanse of overland flow. The slope of the flow duration curve, $S_{\text{FDC.slope}}$, which is expected to be flatter with more vertical drainage (larger catchment dampening effect), can be used to confirm (or not) this hypothesis of catchment functioning. Furthermore, investigating the seasonal aspect of slow flow contribution using the $S_{\text{BFR.mag}}$ can also help as more vertical drainage should cause larger baseflow during the dry period (as flow is more delayed) and hence a smaller baseflow magnitude, $S_{\text{BFR.mag}}$. At the event scale, $S_{\text{REC.}\tau\text{late}}$ should also be larger with more vertical drainage as the overall catchment storage depletion is expected to be slower. In this example, the additional hydrological signatures used, $S_{\text{FDC.slope}}$, $S_{\text{BFR.mag}}$ and $S_{\text{REC.}\tau\text{late}}$ are also not specific to vertical drainage. For example, a larger dampening effect as measured by $S_{\text{FDC.slope}}$ can be caused by larger catchment storage or slower soil drainage. Again, other hydrological signatures can be used to discriminate between different hypotheses.

This example illustrates how using multiple hydrological signatures is necessary to characterize the hydrological functioning of a catchment. The redundancy of signatures is necessary to overcome their lack of specificity. This example also illustrates how challenging it can be. We argue that the use of multiple hydrological signatures, scrutinizing the data following different approaches – related to different perceptual models of how the catchment is functioning (Gupta et al., 2008) – is essential to understand and investigate the internal dynamics of the catchment. We also argue that different temporal scales (e.g. annual, seasonal, event) are essential for that purpose.

4.6.3 Evaluating the set of hydrological signatures

The hydrological signatures should be evaluated in terms of their identifiability, robustness, consistency, representativeness and discriminatory/diagnostic power, following the guidelines of McMillan et al. (2017) (see Section 1.3.2 in Chapter 1).

Identifiability

The uncertainty associated with observed streamflow data was accounted for here for the

computation of observed hydrological signatures. The uncertainty sources accounted for are the uncertainty in the rating curve model parameters, the structural errors of the rating curve model and the non-systematic and systematic errors affecting stage time series. The resulting uncertainty associated with the hydrological signatures are smaller than the inter-catchment differences or observed versus simulated hydrological signatures. This suggests that all the selected hydrological signatures can be well identified.

Some of the hydrological signatures (S_{RC}, $S_{\mathrm{PQ.dry}}$, $S_{\mathrm{PQ.wet}}$, $S_{\mathrm{PQ.strength}}$ and $S_{\mathrm{PQ.date}}$) also rely on precipitation data which can also be a major source of uncertainty (McMillan et al., 2012). The impact of precipitation uncertainty was not accounted for here, implying that the uncertainty associated with the signatures computed from precipitation data is underestimated. Precipitation uncertainty was not considered given that streamflow uncertainty was found as the dominant source of uncertainty by Westerberg and McMillan (2015) for the runoff coefficient. However, further work should be undertaken to verify if precipitation uncertainty can always be considered small in front of streamflow uncertainty. This could be done following the methodology of Westerberg and McMillan (2015), a space-time precipitation simulator (Leblois and Creutin, 2013) or using climate reanalysis products that provide ensembles to account for the uncertainty (e.g. Caillouet et al. (2016); Devers (2019)).

Figure 4.20 shows details of the different streamflow uncertainty sources and their impacts on the hydrological signatures. It shows that considering non-systematic errors i.e. stage non-systematic errors and structural errors of the rating curve can lead to significant bias in the uncertainty associated with some of the hydrological signatures (see red stars in Figure 4.20). As the "most likely" streamflow time series is computed using the $MaxPost$ rating curve without any stage errors or rating curve errors, the corresponding uncertainty bounds can be biased due to the "noisy" aspect of time series – that constitute the ensemble of possible streamflow time series – affected by non-systematic errors and the way some of the hydrological signatures are computed (particularly signatures targeting low streamflow values). To overcome this issue, the uncertainty associated with observed hydrological signatures presented in this chapter and in the remaining of the manuscript was computed using only systematic uncertainty sources: rating curve parameters and systematic stage errors. This choice was followed for all signatures to have a consistent approach and analysis. As shown in Figure 4.20, considering only these two sources of uncertainty resulted in very similar range of uncertainty for most of the hydrological signatures. However, some of the hydrological signatures were more affected by non-systematic errors: the baseflow regime based hydrological signatures and the early recession times. This larger sensitivity is due to the large structural errors of the rating curve at low and high flows (in the extrapolated parts or the rating curves). As a consequence, the uncertainty associated to these observed hydrological signatures are underestimated. Future work should investigate how the uncertainty originating from non-systematic errors can be propagated to hydrological signatures without inducing such bias in the resulting uncertainty bounds.

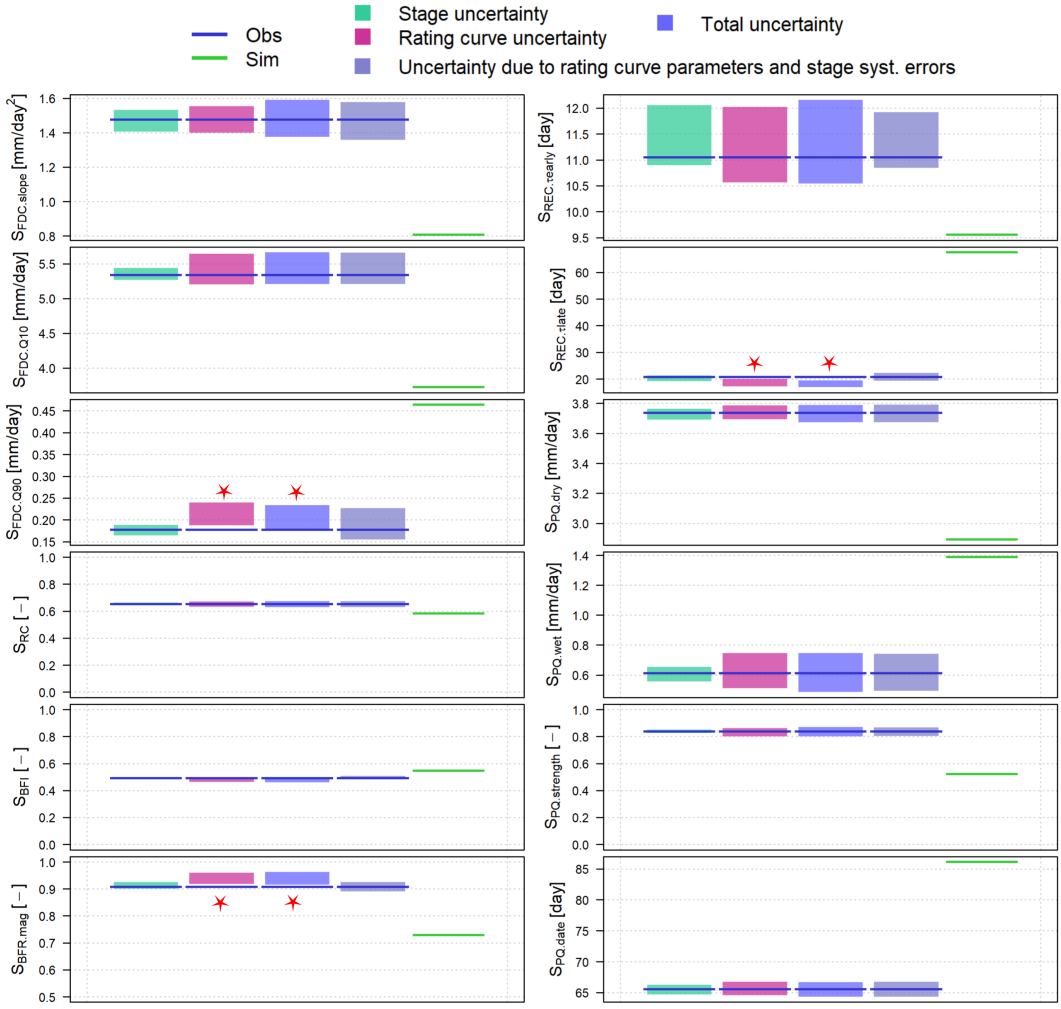

Figure 4.20: Observed and simulated selected hydrological signatures of the Goulette catchment. The uncertainty associated with streamflow time series originating from different sources is detailed. Red starts highlight the uncertainty sources and signatures where the *MaxPost* is found outside the 95% uncertainty boundaries.

Robustness

The hydrological signatures should also be tested in terms of robustness i.e. are they insensitive to the length of the time series, aspects of the data collections or data pre-processing? All observed data were processed in a similar way (see Section 2.1.3 in Chapter 2) but the stage time series originate from different hydrometric station managers with potentially different practices. Simulated data are also very different in nature which may affect the result of the hydrological signatures. However, consistent results were obtained across the investigated catchments and the differences between observed and simulated data did not suggest any robustness issue.

Robustness issues due the length of the time series can potentially be important in our case as for the Claduègne catchment only 6 complete hydrological years were available. Most importantly, the differences between observed and simulated hydrological signatures should not be affected by the length of the time series. Figure 4.21 shows, for the Goulette catchment, the hydrological signatures computed using increasingly long time series (from 1 to 29 years). This preliminary investigation of the sensitivity of the hydrological signatures to the time series length indicates different robustness depending on the hydrological signatures. If differences

between observed and simulated hydrological signatures are relatively stable considering only two years for some of them, others require 5-years-long time series or even 10-15-years-long time series. These preliminary results call for further investigation into the robustness of the selected hydrological signatures regarding the length of the time series.

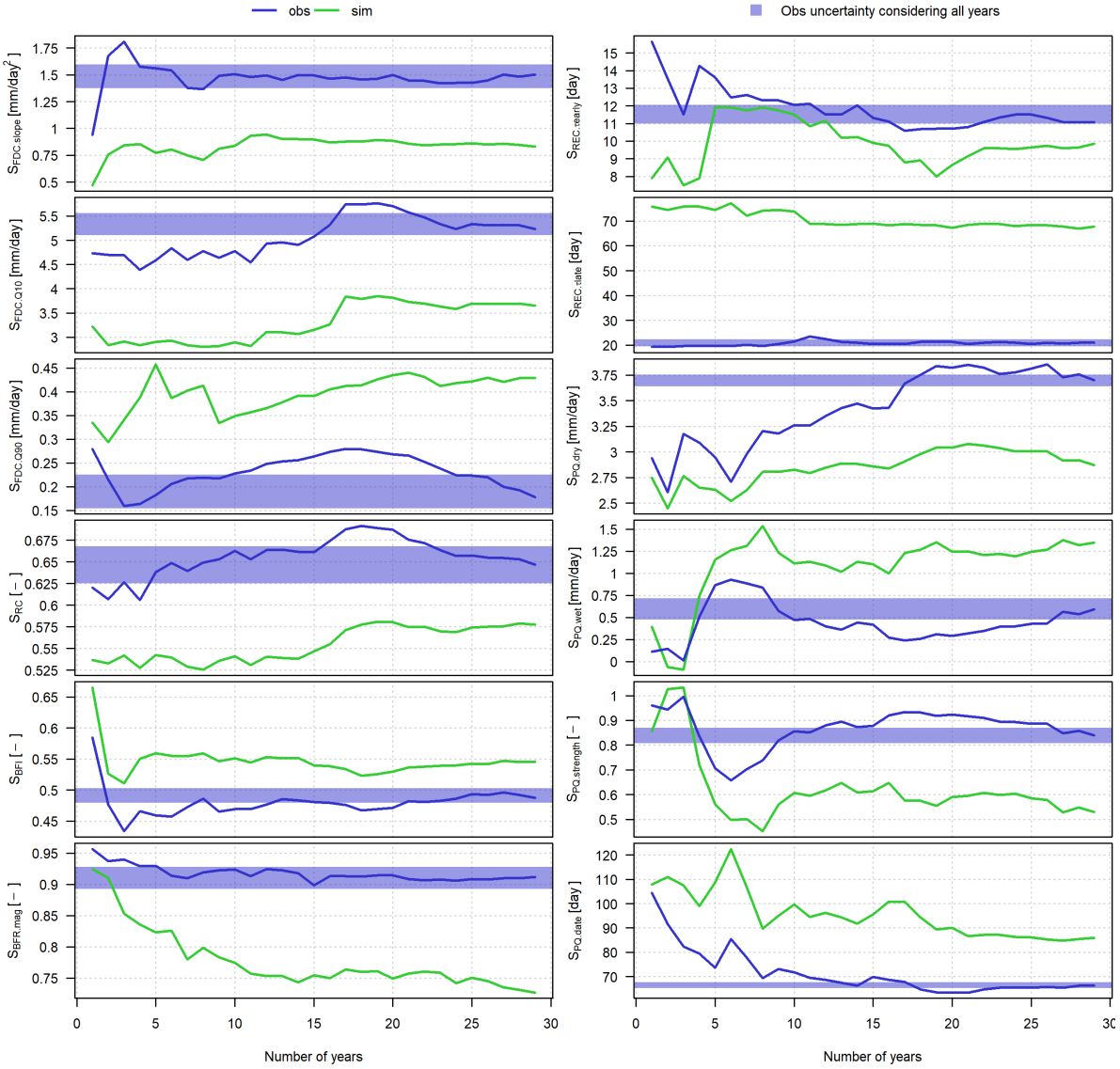

Figure 4.21: Observed and simulated selected hydrological signatures of the Goulette catchment computed using different number of years starting backward from the latest available data.

Consistency

The hydrological signatures should not be sensitive to irrelevant factors such as catchment area (McMillan et al., 2017). The streamflow time series we used are normalized by catchment area limiting potential consistency issues.

Some of the hydrological signatures rely on subjective choices or parameters that must be defined by the user. This is the case of the baseflow analysis (baseflow extraction algorithm parameters) and the recession analysis (recession extraction algorithm, definition of early and late recession periods). This can result in inconsistent hydrological signatures, i.e. hydrological signatures sensitive to irrelevant factors. However, the hydrological signatures are to be

used in relative way – inter-catchment differences and more importantly differences between observed and simulated hydrological signatures – rather than in an absolute way. Therefore, these subjective choices and parameters should have only little effect on the results of our analysis which is mostly based on comparing observed and simulated hydrological signatures (Chapter 6). Nonetheless, the impact of subjective choices should be investigated: they should be verified not to affect the results of the analysis based on the comparison between observed and simulated hydrological signatures.

Representativeness

The selected hydrological signatures are mostly based on streamflow data which inevitably aggregate the hydrological behavior at the catchment scale thus limiting potential issues in their representativeness (as could be the case when using point measurements such as groundwater levels). However, as argued by McMillan et al. (2017), representativeness issues can still arise for hydrological signatures based on streamflow. They should capture the average behavior of all upstream tributaries. Although this should be investigated further, no representativeness issue could be identified when comparing Pont-de-Labeaume with Meyras which is nested with the Pont-de-Labeaume catchment.

The representativeness of the hydrological signatures can also be evaluated in terms of how well they can actually represent the hydrological processes occurring in the catchment. Similarly to what as been detailed in Chapter 3, additional data could be useful to evaluate the selected hydrological signatures.

Diagnostic power

The selection and design of the hydrological signatures was based on their potential diagnostic/discriminatory power and their link to hydrological processes. The inter-catchment and observed versus simulated comparisons of the hydrological signatures done in this chapter showed that they potentially held discriminatory/diagnostic power.

Conclusion

In this chapter, we built a set of 12 hydrological signatures (see Table 4.3). They were selected or designed according to their ability to describe/capture hydrological-processes-interpretable differences between the four study catchments, Meyras, Pont-de-Labeaume, Goulette and Claduègne, and between observed and simulated data. Only streamflow and precipitation data – widely available – were used to derive hydrological signatures. The temporal resolution of the model – daily time step – and the modeling objectives were also accounted for. Studying the catchment functioning only by its two ends – input precipitation and output streamflow – and using daily time series challenged our ability to find or design informative hydrological signatures.

Among the 12 selected hydrological signatures (Table 4.3), 6 hydrological signatures are from the literature. In particular, the widely used flow duration curve was considered here (Section 4.2) to derive $S_{\text{FDC.slope}}$, $S_{\text{FDC.Q10}}$ and $S_{\text{FDC.Q90}}$. The runoff coefficient, S_{RC} (Section 4.1), and the baseflow index, S_{BFI} (Section 4.3.2.1), were also considered in our set of hydrological signatures. Two original hydrological signatures were derived from the analysis of recessions (Section 4.5.2): the early and late recession times, $S_{\text{REC.}\tau\text{early}}$ and $S_{\text{REC.}\tau\text{late}}$. Finally, the P-Q approach (Section 4.4) was used to derive 4 original hydrological signatures, $S_{\text{PQ.dry}}$, $S_{\text{PQ.wet}}$, $S_{\text{PQ.strength}}$ and $S_{\text{PQ.date}}$.

We demonstrated that additional data analysis approaches can be used to further characterize catchment functioning and differences between observed and simulated data. We went beyond the widely used hydrological signatures – mostly based on the flow duration curve – to propose new hydrological signatures and new analysis approaches to derive hydrological signatures that are meaningful/useful in the quantification and characterization of average and emergent catchment-scale hydrological processes. Together, the hydrological signatures target the main functions of a catchment in terms of water partitioning, storage and release according to different temporal scales of investigation (pluri-annual, seasonal and event scales).

The selected hydrological signatures are to be used for the diagnostic and evaluation of the J2000 Ardèche model. The J2000 model is mostly dedicated to long term studies focusing on water volumes and their spatial and temporal variability such as climate change studies or land-use change studies. Therefore, the current set of hydrological signatures addresses most of the average and long-term emergent catchment behaviors relevant for these types of studies. In addition, it is important to stress that the hydrological signatures are not to be used simply as additional metrics in the evaluation of the model. Their interpretation in terms of hydrological processes (see Section 4.6.2 and Table 4.4) is important to derive informative diagnostics on the model functioning.

In this chapter, for some of the hydrological signatures, large differences between observed and simulated data were obtained but not discussed. They are investigated further in Chapter 5 and Chapter 6.

Chapter 5

Linking hydrological signatures and modeled hydrological processes

Contents

Introduction

The J2000 model was set up on the Ardèche catchment. Four sub-catchments were selected in order to focus the analysis of the results: Meyras, Pont-de-Labeaume, Goulette and Claduègne (see Chapter 2, Sections 2.3 and 2.1). The default simulations of the J2000 Ardèche model, presented in Section 2.4.2, showed acceptable results in terms of performance metrics, in particular given that the model wasn't calibrated. In this chapter we introduce the diagnostic-evaluation of the J2000 Ardèche model, focusing on the four study catchments and using 12 hydrological signatures. Together, the 12 hydrological signatures presented in Chapter 4 aim at capturing the average, emergent, catchment-scale hydrological processes. Focusing on the four study catchments, these hydrological signatures can be used to quantify differences between observed and simulated catchment behavior. The main question addressed in this chapter is: how useful this set of hydrological signatures can be for the diagnostic-evaluation of the J2000 Ardèche model?

We first undertake a preliminary evaluation and diagnostic on the model (Section 5.1) by comparing observed and simulated hydrological signatures of the four study catchments. The hydrological signatures that are considered are the runoff coefficient (S_{RC}), the mid-segment slopes and percentiles of the flow duration curve ($S_{\mathrm{FDC.slope}}$, $S_{\mathrm{FDC.Q10}}$ and $S_{\mathrm{FDC.Q90}}$), the baseflow index and baseflow magnitude (S_{BFI} and $S_{\mathrm{BFR.mag}}$), the 4 signatures derived from the P-Q approach ($S_{\mathrm{PQ.dry}}$, $S_{\mathrm{PQ.wet}}$, $S_{\mathrm{PQ.strength}}$ and $S_{\mathrm{PQ.date}}$) and the early and late recession times ($S_{\mathrm{REC.}\tau\mathrm{early}}$ and $S_{\mathrm{REC.}\tau\mathrm{late}}$). This analysis aims at identifying which are the modeled hydrological processes that are well or badly represented in the model. As highlighted in Section 5.1, the links between the hydrological signatures and modeled processes is difficult to establish, limiting our ability to derive clear diagnostics on the model. As a consequence, in Section 5.2 we detail a global sensitivity analysis on the hydrological signatures as model outputs, deployed on four sub-J2000 models corresponding to the four study catchments.

The sensitivity analysis aims at establishing clear links between hydrological signatures and model parameters and thus modeled hydrological processes. The results of the sensitivity analysis are detailed in Section 5.3. The links between hydrological signatures and model parameters are used to evaluate the relevance and diagnostic power of the hydrological signatures by (1) interpreting these links in terms of model functioning to verify the consistency between our hypothesized hydrological signatures interpretations and (2) evaluating the strength – how strong are the links – and specificity – is the signature linked to one or more model parameters – of the links.

5.1 Preliminary model evaluation and diagnostic

In this section we visually analyze the differences between observed and simulated hydrological signatures to evaluate and derive diagnostic on the J2000 Ardèche model focusing on the four study catchments: Meyras, Pont-de-Labeaume, Goulette and Claduègne. We base our interpretation on the expected interpretation of each hydrological signature (see Table 4.4 in Chapter 4). We focus on each of the 12 hydrological signatures in Section 5.1.1 and then propose a synthesis of the results (Section 5.1.2), and highlight the difficulty to derive clear diagnostics on the model (Section 5.1.3).

Observed and simulated hydrological signatures were computed over the same time period for each catchment. We only used "valid" hydrological year – i.e. with less than 5% of missing values – and propagated missing values to simulated data in order to compare exactly the same periods. For Meyras, Pont-de-Labeaume, Goulette and Claduègne, 27, 22, 29 and 6 hydrological years were hence used to compute the hydrological signatures (see details on available streamflow data in Section 2.1.3.1 and Table 2.3).

5.1.1 Comparing observed and simulated hydrological signatures

5.1.1.1 Runoff coefficient

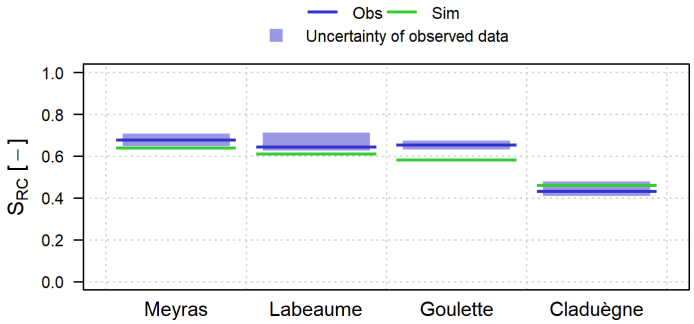

Figure 5.1: Observed and simulated runoff coefficient, S_{RC}, of the four study catchments Meyras, Pont-de-Labeaume, Goulette and Claduègne.

Figure 5.1 shows the observed and simulated runoff coefficient, S_{RC}, of the four study catchments. It shows that for Meyras, Pont-de-Labeaume and Goulette, simulated S_{RC} are slightly underestimated whereas there is a good match in the case of Claduègne. For all catchments except Claduègne, these results indicate that the evapotranspiration is overestimated (by the model) at the expense of streamflow, suggesting (1) too much evapotranspiration demand and/or (2) too much water available for plant transpiration (in the soil) or direct evaporation (at the ground surface or in the vegetation canopy).

Too much evapotranspiration could be linked to too large crop coefficient, K_{crop}, in these catchments. Too much water available in the soil could be related to too much infiltration (parameters K_{sealing}, $I_{\mathrm{max,summer}}$ and $I_{\mathrm{max,winter}}$), too large soil storage (parameters MPS_{max} and LPS_{max}) or not enough soil drainage (parameter K_{LPSout}). Too much water at the ground surface or in the vegetation canopy could be related to not enough infiltration (unlikely given that there is no surface storage represented in the model) or too much water interception by

the vegetation (LAI).

5.1.1.2 Flow duration curve

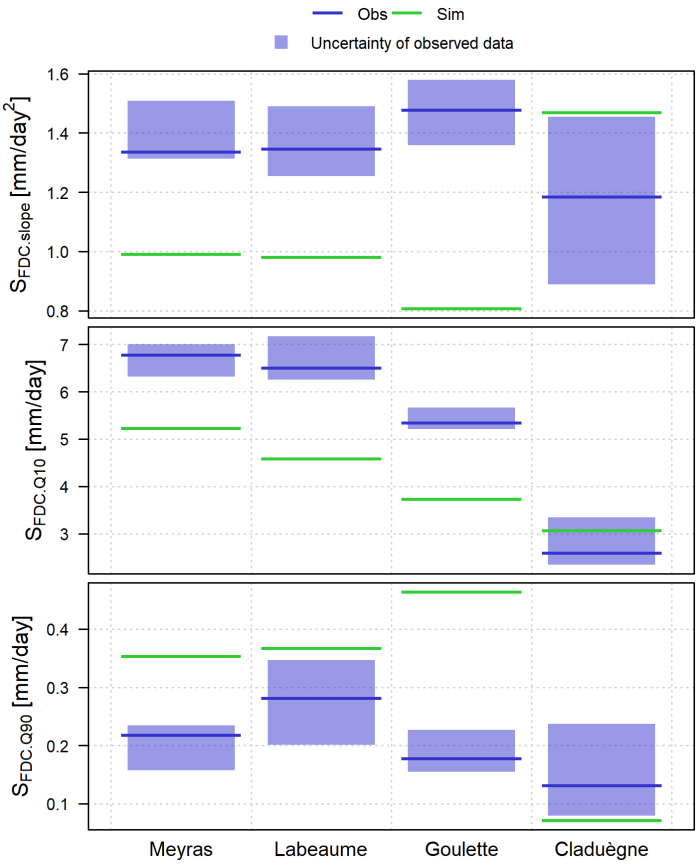

Figure 5.2: Observed and simulated hydrological signatures derived from the flow duration curve, $S_{\text{FDC.slope}}$, $S_{\text{FDC.Q10}}$ and $S_{\text{FDC.Q90}}$, of the four study catchments Meyras, Pont-de-Labeaume, Goulette and Cladugne.

Figure 5.2 shows the 3 hydrological signatures derived from the flow duration curve: the slope of the mid-segment $S_{\text{FDC.slope}}$ and high $S_{\text{FDC.Q10}}$ and low $S_{\text{FDC.Q90}}$ flow percentiles. Large differences between observed and simulated hydrological signatures are obtained for Meyras, Pont-de-Labeaume and Goulette whereas only small differences are obtained for Cladugne.

The slope of the mid-segment of the flow duration curve, $S_{\text{FDC.slope}}$, are underestimated for Meyras, Pont-de-Labeaume and Goulette (particularly for Goulette) and slightly overestimated for Cladugne. For Meyras, Pont-de-Labeaume and Goulette, these results indicate an overestimated dampening effect with less variable streamflow due to too large catchment storage (in the soil or groundwater, i.e. related to parameters $MPS_{\max}$, $LPS_{\max}$ and $RG_{\max}$) and/or too slow catchment water release rates (parameters K_{LPSout}, K_{latvert}, $P_{\max}$, τ_{RG}).

The high flow percentile, $S_{\text{FDC.Q10}}$ is underestimated for Meyras, Pont-de-Labeaume and Goulette and a good match is found in the case of Cladugne. For Meyras, Pont-de-Labeaume and Goulette, these results suggest not enough fast flow contributions due too much soil infiltration (parameters K_{sealing}, $I_{\max,\text{summer}}$ and $I_{\max,\text{winter}}$) and/or not fast enough soil drainage (parameter K_{LPSout}) and/or not enough lateral soil drainage (parameter K_{latvert} and $P_{\max}$).

The low flow percentile, $S_{\text{FDC.Q90}}$ is overestimated for Meyras, Pont-de-Labeaume and

Goulette (particularly for Meyras and Goulette) and slightly underestimated for Cladugne. For Meyras, Pont-de-Labeaume and Goulette, these results indicate too much slow flow contribution related to too much vertical drainage (parameter K_{latvert} and P_{max}) and/or too slow groundwater release (parameter τ_{RG}).

5.1.1.3 Baseflow index and baseflow regime magnitude

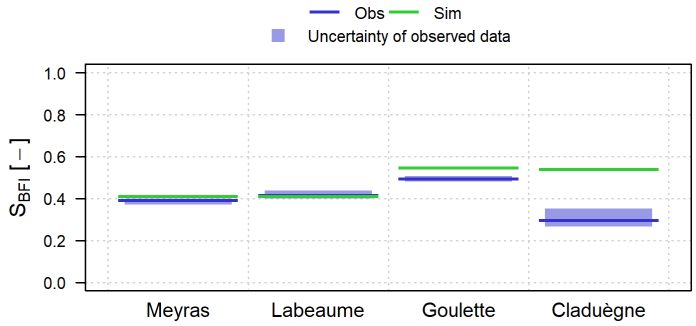

Figure 5.3: Observed and simulated baseflow index, S_{BFI}, of the four study catchments Meyras, Pont-de-Labeaume, Goulette and Cladugne.

Figure 5.3 shows the observed and simulated baseflow index, S_{BFI}, of the four study catchments. It shows that observed and simulated S_{BFI} match for Pont-de-Labeaume whereas a simulated S_{BFI} is slightly (resp. largely) overestimated in the case of Meyras and Goulette (resp. Cladugne). In the case of Cladugne, the large overestimation suggests too much slow flow contributions due to too much soil infiltration (parameters K_{sealing}, $I_{\text{max,summer}}$, $I_{\text{max,winter}}$ and $I_{\text{max,snow}}$) and/or too much vertical drainage (parameters K_{latvert} and P_{max}).

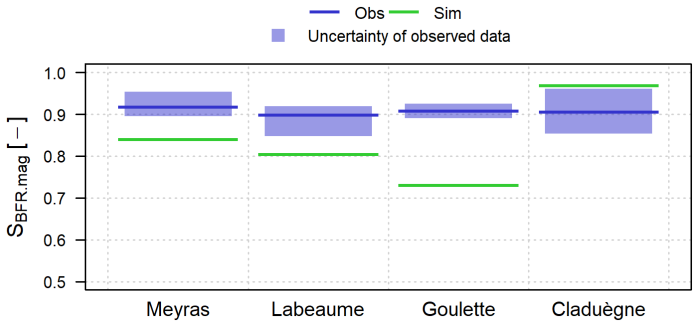

Figure 5.4: Observed and simulated baseflow regime magnitude, $S_{\text{BFR.mag}}$, of the four study catchments Meyras, Pont-de-Labeaume, Goulette and Cladugne.

Figure 5.4 shows the observed and simulated baseflow regime magnitude, $S_{\text{BFR.mag}}$, of the four study catchments. It shows that simulated $S_{\text{BFR.mag}}$ is underestimated for all catchments (particularly for Goulette) except Cladugne where a slight overestimation is obtained. The underestimation of simulated $S_{\text{BFR.mag}}$ suggests too much slow flow contributions during the dry period and not enough slow flow contribution during the wet period. This could be the consequence of too large catchment storage (parameters MPS_{max}, LPS_{max} and RG_{max}) and/or too slow catchment release rate (parameters K_{LPSout}, K_{latvert}, P_{max} and τ_{RG}).

5.1.1.4 Streamflow response during and after the re-wetting period

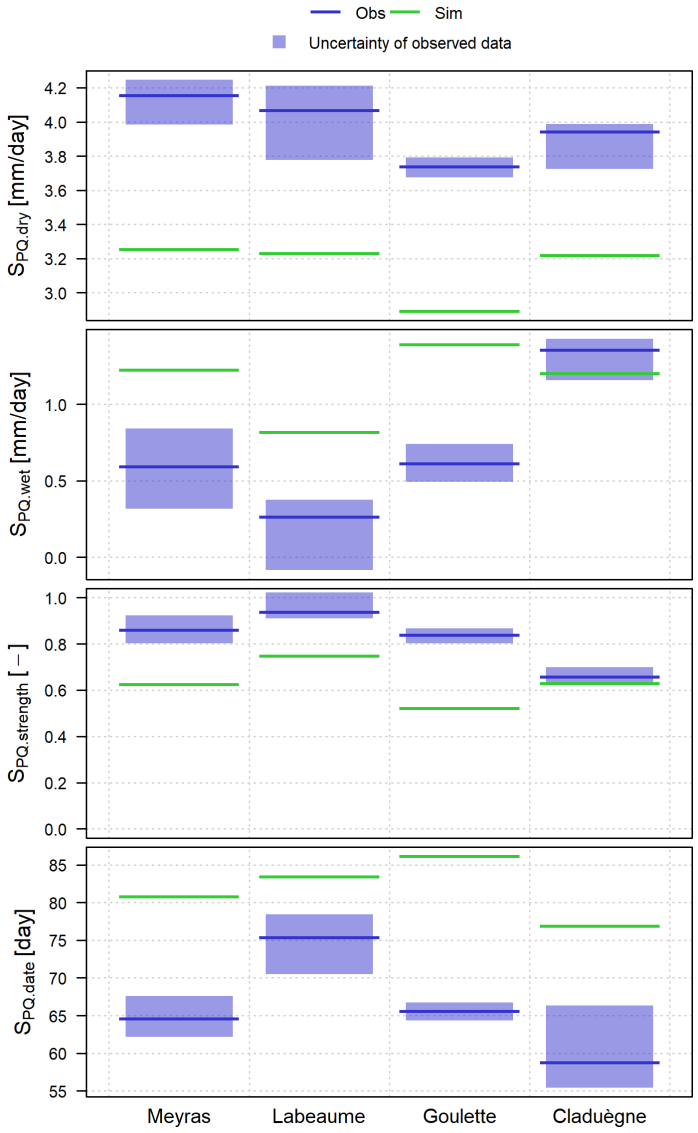

Figure 5.5: Observed and simulated hydrological signatures derived from the P-Q approach of the four study catchments Meyras, Pont-de-Labeaume, Goulette and Cladugne: the slope of the P-Q curve during the dry ($S_{\mathrm{PQ.dry}}$) and wet ($S_{\mathrm{PQ.wet}}$), the strength ($S_{\mathrm{PQ.strength}}$) and date ($S_{\mathrm{PQ.date}}$) of the shift in the P-Q curve between the dry and wet period.

Figure 5.5 shows the observed and simulated hydrological signatures derived from the P-Q approach: $S_{\mathrm{PQ.dry}}$, $S_{\mathrm{PQ.wet}}$, $S_{\mathrm{PQ.strength}}$ and $S_{\mathrm{PQ.date}}$. They characterize the change in catchment streamflow response during and after the re-wetting period, between the dry and wet periods.

Figure 5.5 shows that the simulated slope of the P-Q curve during the dry period, $S_{\mathrm{PQ.dry}}$, is underestimated for all catchments. After the shift in streamflow response, the simulated slope of the P-Q curve during the wet period, $S_{\mathrm{PQ.wet}}$, is overestimated for all catchment except Cladugne where it matches. As a consequence, Figure 5.5 shows that the simulated shift strength, $S_{\mathrm{PQ.strength}}$, is underestimated for all catchments except Cladugne. These results indicate that there is too much simulated streamflow during the dry period for all catchments and not enough during the wet period for all catchments except for Cladugne.

These results suggest there is too much (resp. not enough) overland flow and/or too fast (resp. too slow) catchment water release during the dry (resp. wet period). This could possibly be caused by issues in the seasonal variation of soil maximum infiltration rates controlled by parameters $I_{\text{max,summer}}$ and $I_{\text{max,winter}}$: too small $I_{\text{max,summer}}$ and too large $I_{\text{max,winter}}$.

For the dry period, these results might also be the consequence of too fast soil drainage related to too small soil storage capacity (parameters MPS_{max} and LPS_{max}), too easily drainable soil (parameter K_{LPSout}) or not enough vertical drainage (parameters K_{latvert} and P_{max}), leading to too much catchment storage depletion during this period. On the other hand, the underestimation of streamflow response during the wet period might be due to too much catchment storage and too slow storage depletion. These results are contradictory except if we incriminate, in this case, groundwater storage (RG_{max}) and groundwater storage depletion rate (parameter τ_{RG}) which could be expected to have large effect on model behavior in wet conditions.

In the simulation, the date of the shift between the dry and wet period, $S_{\text{PQ.date}}$, is overestimated for all catchments, in particular Goulette. These results suggest too large catchment storage (parameters MPS_{max}, LPS_{max} and RG_{max}), not enough soil infiltration during the dry period (parameters K_{sealing} and $I_{\text{max,summer}}$) and/or too much evapotranspiration demand (too large K_{crop}). It could also suggest issues in the speed (too fast or too slow, both being possible interpretation, see Table 4.4) of overall catchment water release rates (parameters K_{LPSout}, K_{latvert}, P_{max} and τ_{RG}).

5.1.1.5 Streamflow recession characteristics

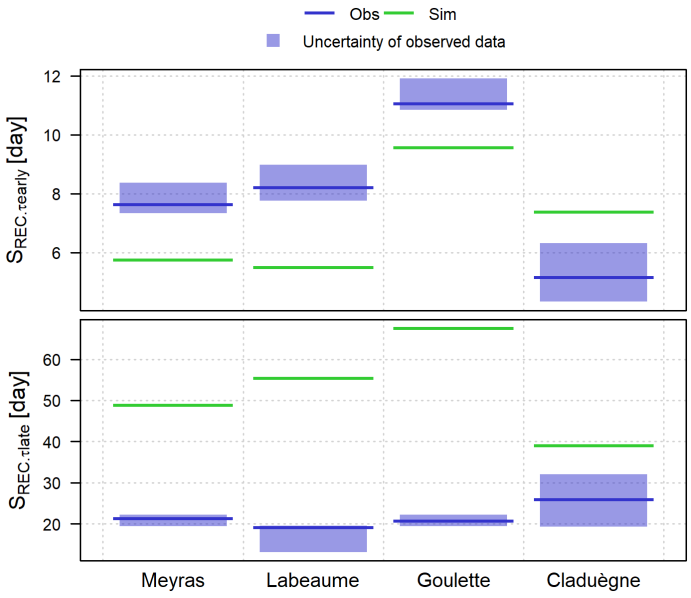

Figure 5.6: Observed and simulated early ($S_{\text{REC.}\tau\text{early}}$) and late ($S_{\text{REC.}\tau\text{late}}$) recession time of the four study catchments Meyras, Pont-de-Labeaume, Goulette and Cladugne.

Figure 5.6 shows the early and late recessions times, $S_{\text{REC.}\tau\text{early}}$ and $S_{\text{REC.}\tau\text{late}}$, of the four study catchments. It shows that simulated $S_{\text{REC.}\tau\text{early}}$ is underestimated for all catchments except Cladugne where it is found overestimated. This suggests too fast catchment storage release from quickly depleting reservoirs (parameters K_{LPSout}, K_{latvert} and P_{max}) and/or too much overland flow (parameters K_{sealing}, $I_{\text{max,summer}}$ and $I_{\text{max,winter}}$) resulting in too large

streamflow peaks and hence too fast early recessions.

Figure 5.6 also shows that simulated $S_{\text{REC.}\tau\text{late}}$ is largely (resp. slightly) overestimated for Meyras, Pont-de-Labeaume and Goulette (resp. Claduègne). This suggests too much vertical drainage (parameters K_{latvert} and P_{max}) and/or too slow groundwater depletion (parameter τ_{RG}).

5.1.2 Synthesis of the identified model issues

5.1.2.1 Evapotranspiration demand and vegetation interception

The evapotranspiration demand (parameters K_{crop}) and vegetation interception (parameters LAI) are possibly responsible for the underestimated runoff coefficient, S_{RC}, found for Meyras, Pont-de-Labeaume, and Goulette. For these 3 catchments, results suggest too large K_{crop} and/or too large LAI. Since these catchments are mostly covered by forests, these parameters, distributed according to the type of land-use, might need to be modified for the forests land-use classes. However, the underestimated S_{RC} could also be caused by too much water available in the soils for plant transpiration as discussed later.

5.1.2.2 Soil infiltration and overland flow

Soil infiltration is controlled by the proportion of sealed surface (parameter K_{sealing}, distributed according to the type of land-use), the maximum infiltration rates in Summer, $I_{\text{max,summer}}$, and Winter, $I_{\text{max,winter}}$, and also, how likely/often the soils might be saturated (which is controlled by soil storage and depletion parameters, i.e. parameters MPS_{max}, LPS_{max} and K_{LPSout}).

The underestimated S_{RC} found for Meyras, Pont-de-Labeaume and Goulette might suggest K_{sealing} is too small and $I_{\text{max,summer}}$ and/or $I_{\text{max,winter}}$ too large for these catchments resulting in too much water infiltration and hence too much water available in the soil for plant transpiration. However, the underestimated $S_{\text{FDC.Q10}}$ and $S_{\text{REC.}\tau\text{early}}$ found for these catchment suggest the opposite: too large K_{sealing} and too small $I_{\text{max,summer}}/I_{\text{max,winter}}$. Given that the underestimation is larger in the case of $S_{\text{FDC.Q10}}$ and $S_{\text{REC.}\tau\text{early}}$ and that these two hydrological signatures are expected to be more exclusively related to the partitioning of water at the ground surface, the second hypothesis seems more likely. Also note that the overestimated S_{BFI} for Claduègne could also indicate too small K_{sealing} and too large $I_{\text{max,summer}}/I_{\text{max,winter}}$ for this catchment.

The large underestimation of $S_{\text{PQ.dry}}$ found for all catchments might suggest that the maximum infiltration rate in Summer, $I_{\text{max,summer}}$, is too small for all catchments. This is also supported by the too late date in the shift in catchment streamflow response, $S_{\text{PQ.date}}$, found for all catchments. The strength of the shift between the dry and wet period, $S_{\text{PQ.strength}}$, found underestimated for all catchment but Claduègne, could also suggest that the maximum infiltration rate in Winter, $I_{\text{max,winter}}$, is too large for Meyras, Pont-de-Labeaume and Goulette. However, this contradicts the results from $S_{\text{FDC.Q10}}$ and $S_{\text{REC.}\tau\text{early}}$, which are arguably more likely.

Overall, these results suggest too much overland flow for Meyras, Pont-de-Labeaume and

Goulette (and possibly not enough for Cladugne) due too large K_{sealing} or too small $I_{\text{max,summer}}$ and $I_{\text{max,winter}}$ for Meyras, Pont-de-Labeaume and Goulette and to a lesser extent, Cladugne. Parameters $I_{\text{max,summer}}$ and $I_{\text{max,winter}}$, which are lumped parameters, could be increased for all catchment to allow for more infiltration during large precipitation events. To address inter-catchment differences, given that only K_{sealing} is currently distributed according to the type of land-use, these results might also suggest that the sealing of surface for forests should be specified smaller (currently set at 0.2, see Table 2.7).

5.1.2.3 Soil storage

Soil storage is controlled by parameters LPS_{max} and MPS_{max} which are currently only distributed according to the type of soil. The large (resp. small) underestimation of $S_{\text{FDC.slope}}$ and $S_{\text{BFR.mag}}$ (resp. S_{RC}) suggest that soil storage is overestimated, i.e. that LPS_{max} or MPS_{max} are too large, only in the case of Meyras, Pont-de-Labeaume and Goulette. These results are also partly supported by the overestimated $S_{\text{PQ.date}}$ found for all catchments. However, these results are contradicted by the underestimated $S_{\text{PQ.dry}}$ found for all catchments which might suggest too small soil storage. While it is difficult to discriminate between these contradicting hypotheses, there seems to be more evidence pointing towards overestimated soil storage in the case of Meyras, Pont-de-Labeaume and Goulette.

5.1.2.4 Soil drainage and the partitioning between lateral and vertical drainage

Soil drainage is controlled by the lumped parameter K_{LPSout} (the larger, the more saturated the soil needs to be to drain water) and two lumped parameters controlling the split between vertical and later drainage: parameter K_{latvert} which gives more or less weight to the average slope of the HRU in the partitioning (the larger, the more lateral drainage for a given slope value) and parameter P_{max}, the maximum percolation rate to the groundwater (the smaller the less vertical drainage). Most of the hydrological signatures pointed towards possible mis-specification of these three parameters.

The slight underestimation of S_{RC} found for Meyras, Pont-de-Labeaume and Goulette could point towards not enough soil drainage, i.e. too large K_{LPSout}. For these three catchments, this result is also supported by the underestimated (resp. overestimated) $S_{\text{FDC.slope}}$, $S_{\text{FDC.Q10}}$ and $S_{\text{BFR.mag}}$ (resp. $S_{\text{PQ.date}}$). The large underestimation of $S_{\text{FDC.slope}}$ for these catchments could also be a consequence of too much vertical drainage at the expanse of lateral drainage caused by too small K_{latvert} and/or too large P_{max}. These hypotheses are also supported by the underestimated (resp. overestimated) $S_{\text{FDC.Q10}}$ and $S_{\text{BFR.mag}}$ (resp. $S_{\text{FDC.Q90}}$, $S_{\text{PQ.date}}$ and $S_{\text{REC.}\tau\text{late}}$).

These hypotheses of model dis-functioning imply that the 3 lumped parameters K_{LPSout}, K_{latvert} and P_{max} should be distributed as modifying them would also affect the Cladugne catchment where for some of these hydrological signatures opposite results where obtained (see results of S_{RC}, $S_{\text{FDC.slope}}$, $S_{\text{FDC.Q10}}$, $S_{\text{FDC.Q90}}$).

5.1.2.5 Groundwater storage and release

The large underestimation of $S_{\text{FDC.slope}}$ found for Meyras, Pont-de-Labeaume and Goulette could also suggest too much groundwater storage – too large $RG_{\max}$– and/or too slow groundwater depletion – too large τ_{RG}. The underestimated strength in the shift between the dry and wet period, $S_{\text{PQ.strength}}$, found for these 3 catchments also suggests too much groundwater storage and/or too slow groundwater depletion. These results are also supported by the too late shift date, $S_{\text{PQ.date}}$, found for all catchments. The underestimated (resp. overestimated) $S_{\text{BFR.mag}}$ (resp. $S_{\text{FDC.Q90}}$ and $S_{\text{REC.}\tau\text{late}}$) found for Meyras, Pont-de-Labeaume and Goulette (and Claduègne in the case of $S_{\text{REC.}\tau\text{late}}$) also suggests too slow groundwater depletion.

In the case of groundwater storage and groundwater release rate, results are consistent for all hydrological signatures: groundwater storage might be overestimated (too large $RG_{\max}$) and groundwater release rate too slow (too large τ_{RG}). Although two hydrological signatures point towards this issue for all catchments ($S_{\text{PQ.date}}$ and $S_{\text{REC.}\tau\text{late}}$), these model issues seem to be mostly affecting Meyras, Pont-de-Labeaume and Goulette.

5.1.3 Conclusion: diagnostic power of the hydrological signatures based on visual analysis

The evaluation and diagnostic of the model based on the hydrological signatures that was synthesized in the previous subsections highlighted many possible issues in the model. Several hypotheses of model dis-functioning were proposed. However, in most cases, no clear cut diagnostics could be derived due to some methodological limitations as detailed in the next paragraphs: (1) the multiplicity of hypotheses for one single hydrological signature, (2) inter-signatures discrepancies in derived diagnostics and (3) inter-catchment discrepancies in derived diagnostics.

Considering one hydrological signature, there might be multiple causes, in the model functioning, that explain the differences between observation and simulation. For example, the underestimated baseflow regime magnitude, $S_{\text{BFR.mag}}$, found for Meyras, Pont-de-Labeaume and Goulette was hypothesized to be caused by too much soil storage, not enough soil drainage, too much vertical drainage and/or too slow groundwater depletion. Combining these results with the results of other hydrological signatures might help discriminate between these hypotheses. However, the previous subsection highlights that it might be a challenging task if possible at all.

Deriving clear diagnostics on the model functioning is further complexified by discrepancies in the results of the evaluation/diagnostic analysis either between hydrological signatures or between catchments. For example, for Meyras, Pont-de-Labeaume and Goulette, both the underestimated $S_{\text{BFR.mag}}$ and $S_{\text{FDC.slope}}$ suggested too much vertical drainage in the model. However, the underestimated $S_{\text{PQ.dry}}$ found for all catchments suggested too much lateral drainage. This illustrates inter-signatures discrepancies in the derived diagnostics. Inter-catchment discrepancies can also prevent clear diagnostics. For example, the underestimation of $S_{\text{BFR.mag}}$ and $S_{\text{FDC.slope}}$ also suggests too fast (resp. too slow) groundwater depletion for Claduègne (resp. for Meyras, Pont-de-Labeaume and Goulette). However, this is then contradicted considering $S_{\text{REC.}\tau\text{late}}$ which is overestimated for all catchments, suggesting groundwater depletion was too

slow for all catchments, including Claduègne.

These limitations call for a methodology that would enable identifying and discriminating between the multiple possible issues in the model functioning. In particular, these limitations point towards the limited diagnostic power of the hydrological signatures considered in the analysis presented here. By diagnostic power, we mean the ability of a given hydrological signature to pinpoint precisely a particular modeled process. This ability is related to both the design of the signatures and how we can relate the signatures to model functioning. Focusing on the second aspect, two characteristics of the hydrological signatures should be assessed: how specific it is to modeled hydrological processes i.e. how many processes is it linked to and how strong or clear are the links with the modeled processes.

To tackle these limitations we propose to use a sensitivity analysis using the hydrological signatures as targets. The sensitivity analysis, detailed in the next sections, has the following aims: (1) identify the parameters each hydrological signature is related to, (2) evaluate the diagnostic power of each hydrological signature considering the specificity and strength of signature-parameter links and (3), along the way, verify our hypothesized interpretations – detailed in Chapter 4 and used here for the preliminary diagnostic of the model – of each hydrological signature. The sensitivity analysis follows the methodology described in Section 5.2 and the results are detailed in Section 5.3.

5.2 Sensitivity analysis

"Sensitivity Analysis (SA) investigates how the variation in the output of a numerical model can be attributed to variations of its input factors" (Pianosi et al., 2016). Many different approaches of sensitivity analysis have been used in the realm of environmental modeling as reviewed by Pianosi et al. (2016). One of the common distinctions made among the existing methods is the use of One-At-a-Time SA (OAT) versus Global Sensitivity Analysis (GSA). In OAT approaches the sensitivity of the model output is assessed by varying one input factor at a time while keeping the other factors fixed (e.g. Yilmaz et al., 2008). In GSA approaches, the sensitivity is assessed by varying all the input factors simultaneously (e.g. Haghnegahdar et al., 2017; Höllering et al., 2018). The latter approach allows a more relevant assessment of the sensitivity of the model output to model input factors as it enables the characterization and quantification of the input factors interactions (Pianosi et al., 2016).

Following the studies of Yilmaz et al. (2008) or Höllering et al. (2018), we here use a sensitivity analysis to help in the diagnostic and evaluation of the J2000 model using the hydrological signatures as model outputs. Focusing on the four study catchments, Meyras, Pont-de-Labeaume, Goulette and Claduègne, we propose to use the state-of-the-art variance-based global sensitivity analysis approach of Sobol-Jansen (Jansen, 1999; Saltelli et al., 2010) to compute, for each catchment and each selected model output (hydrological signatures), the first and the total order sensitivity indices.

5.2.1 A variance-based sensitivity analysis method

5.2.1.1 Variance decomposition and sensitivity indices

The theoretical basis of variance-based approach to sensitivity analysis is given below. It is mainly taken from Saltelli et al. (2010).

Let f be a model with k input factors X_i ($i = 1,\ 2,\ ...,\ k$). Let Y be the scalar output of f: $Y = f(X_1, X_2, ..., X_k)$. Following the notation of Saltelli et al. (2010), (1) $E_{X_i}(\cdot)$ (resp. $V_{X_i}(\cdot)$) is the mean (resp. variance) of the argument $(\cdot)$ considering all factors fixed except X_i and (2) $E_{\boldsymbol{X}_{\sim \boldsymbol{i}}}(\cdot)$ (resp. $V_{\boldsymbol{X}_{\sim \boldsymbol{i}}}(\cdot)$) is the mean (resp. variance) of the argument $(\cdot)$ considering only X_i fixed.

Variance based approaches to sensitivity analysis are based on a decomposition of the variance of the model output Y according to the relative effects of the different input factors. They aim at quantifying how the different input factors contribute to the output variance $V(Y)$. The variance of the model output can be decomposed by the sum of the variances due to the main effect of each parameter and the sum of the variances due to the parameter interactions:

$$\begin{aligned} V(Y) &= V_1 + ... + V_k + V_{1,2} + ... + V_{k-1,k} + V_{1,2,3} + ... + V_{1,...,k} \\ &= \sum_{i=1}^{k} V_i + \sum_{i=1}^{k} \sum_{j>i} V_{i,j} + ... + V_{1,...,k} \end{aligned} \tag{5.1}$$

where

$$V_i = V_{X_i}(E_{\boldsymbol{X}_{\sim \boldsymbol{i}}}(Y|X_i))$$

is the part of the variance attributed to the main effect of input factor X_i,

$$V_{i,j} = V_{X_i X_j}(E_{\boldsymbol{X}_{\sim \boldsymbol{ij}}}(Y|X_i, X_j)) - V_{X_i}(E_{\boldsymbol{X}_{\sim \boldsymbol{i}}}(Y|X_i)) - V_{X_j}(E_{\boldsymbol{X}_{\sim \boldsymbol{j}}}(Y|X_j))$$

is the part of the variance due to the interaction between input factors X_i and X_j, and so on for higher order terms.

Two sensitivity indices are typically used: the first order and the total order sensitivity indices. For an input factor X_i, the first (or main) order sensitivity index is defined as:

$$S_i = \frac{V_{X_i}(E_{\boldsymbol{X}_{\sim \boldsymbol{i}}}(Y|X_i))}{V(Y)} \tag{5.2}$$

The first order sensitivity index corresponds to the proportion of variation of the model output Y due only to the variations of the input factor X_i. It does not consider any interaction that may exist between parameters.

The total order sensitivity index is defined as:

$$\begin{aligned} S_{Ti} &= \textstyle\sum_{i=1}^{k} S_i + \sum_{i=1}^{k} \sum_{j>i} S_{i,j} + ... + S_{1,...,k} \\ &= \frac{E_{\boldsymbol{X}_{\sim i}}(V_{X_i}(Y|\boldsymbol{X}_{\sim i}))}{V(Y)} \end{aligned} \tag{5.3}$$

It corresponds to the proportion of variation of the model output due to the variation of the input factor X_i and all the interactions this factor may have with all the other input factors.

5.2.1.2 Estimating the sensitivity indices

In practice, the first and total sensitivity indices cannot be computed analytically and need to be estimated using many model simulations exploring as well as possible the entire input factor space. In this section, the approach of Jansen (1999) and Saltelli et al. (2010) used for that purpose is described.

Let $\boldsymbol{A}$ and $\boldsymbol{B}$ be two matrices containing samples of the model input factors. These two matrices have k columns (the number of factors) and N rows (the number of sets of input factors, to define usually between 500 and 1000 according to Saltelli (2004)). The first order and total order sensitivity indices can be estimated using these two matrices and an additional matrix $\boldsymbol{A}^{(i)}$ where all columns are taken from $\boldsymbol{A}$ except column i which is taken from $\boldsymbol{B}$. Jansen (1999) and Saltelli et al. (2010) proposed the following equation to compute the first and total order sensitivity indices:

$$S_i = \frac{V_{X_i}(E_{\boldsymbol{X}_{\sim i}}(Y|X_i))}{V(Y)} = \frac{V(Y) - \frac{1}{2N}\sum_{j=1}^{N}\left(f(\boldsymbol{B}_{j.}) - f(\boldsymbol{A}_{j.}^{(i)})\right)^2}{V(Y)} \tag{5.4}$$

$$S_{Ti} = \frac{E_{\boldsymbol{X}_{\sim i}}(V_{X_i}(Y|\boldsymbol{X}_{\sim i}))}{V(Y)} = \frac{\frac{1}{2N}\sum_{j=1}^{N}\left(f(\boldsymbol{A}_{j.}) - f(\boldsymbol{A}_{j.}^{(i)})\right)^2}{V(Y)} \tag{5.5}$$

where $\boldsymbol{Z}_{j.}$ indicates the row j of a matrix $\boldsymbol{Z}$. For example, $f(\boldsymbol{A}_{j.})$ is the model output consid-

ering the sets of parameters in row j of $\boldsymbol{A}$.

From Equations 5.4 and 5.5, given the number of parameters k and the number of rows N in $\boldsymbol{A}$, $\boldsymbol{B}$ and $\boldsymbol{A}^{(i)}$, the number of required simulations N_{SIM} (i.e. runs of the model f) to compute both the total and first order indices is: $N_{\text{SIM}} = 2 \times N + N \times k = N \times (k+2)$. If only one of the indices is needed, the number of model runs required is $N \times (k+1)$.

Matrices $\boldsymbol{A}$ and $\boldsymbol{B}$ can be generated using Latin Hypercube or Quasi-Random sampling to explore as efficiently as possible the input factor space. However, in the present work, $\boldsymbol{A}$ and $\boldsymbol{B}$ were generated using uniform random sampling considering the uniform distribution $\mathcal{U}(0,1)$. The creation of the SA experimental design, i.e. the matrix of all the input factors sets to feed the model f with, and the computation of the first and total order sensitivity analysis indices were done using the *sensitivity* *R* package (Iooss et al. (2018)[1]). The *sensitivity* package also includes a bootstrap procedure that was used to estimate the uncertainty associated with the first order and total order sensitivity indices. The number of bootstrap replicates was set to 200.

5.2.2 Set up of the sensitivity analysis and analysis of the results

5.2.2.1 J2000 sub models and simulation time range

As the J2000 model running time is highly dependent on the number of HRUs, 4 sub-models were created from the J2000 Ardèche model by extracting the required topology from the J2000 parameter files using the J2K-RUI toolbox (Section C.3 and Appendix C). The sensitivity analysis were done on each of these sub-models. The model was run, for each sub-catchment, according to the time range of available observed data (Table 2.3) with at least 10 years of warm up. However, in the case of Claduègne catchment, the latest forcing data were not readily available at the time the sensitivity analysis was done. Therefore, the time range of the simulation considered for this catchment only includes the 4 (out of 6) first whole hydrological years (2012-2016).

5.2.2.2 Model outputs

The model outputs used in the sensitivity analysis are the 12 investigated hydrological signatures presented in Chapter 4: $S_{\text{FDC.slope}}$, $S_{\text{FDC.Q10}}$, $S_{\text{FDC.Q90}}$, S_{BFI}, $S_{\text{BFR.mag}}$, $S_{\text{PQ.dry}}$, $S_{\text{PQ.wet}}$, $S_{\text{PQ.strength}}$, $S_{\text{PQ.date}}$, $S_{\text{REC.}\tau\text{early}}$ and $S_{\text{REC.}\tau\text{late}}$. The first order indices, S_i, and total order indices, S_{Ti}, are computed independently (on the same sampling of the parameter space) for each hydrological signature.

5.2.2.3 Sub-selection of investigated parameters

The deployment of the sensitivity analysis requires to first select the input factors to investigate. Although input factors could include, in the case of the J2000 model, meteorological forcing or the chosen spatial discretization (HRUs), we here focus on the J2000 model parameters. As listed in Table 2.5, J2000 relies on 29 model parameters. 10 of these parameters are distributed

[1] https://CRAN.R-project.org/package=sensitivity

in space according to HRUs and their corresponding land-use, soil and geology classes. In the case of the J2000 Ardèche model, considering the number of land-use (8), soil (4) and geology classes (7), the total number of parameters is in fact 54 ($4 \times 8 + 2 \times 4 + 2 \times 7 = 54$; considering K_{crop}, LAI and θ_{FC} as single parameters). Following the SA methodology described in the previous section, considering 1000 rows in the two input matrices ($N = 1000$), 56000 model runs would be required. Although this number of model runs might be manageable given the computation time of the J2000 model (although very long with huge result file difficult and long to process), a subset of parameters was first selected.

Guided by the results of previous studies on the J2000 model (e.g. Branger et al. (2016); Gouttevin et al. (2017)) and many trial-and-error SA experiments (see Appendix F.1 for a preliminary detailed sensitivity analysis of the four sub-catchments), some of the J2000 model parameters listed in Table 2.5 were not considered in the SA:

- The two parameters modulating the maximum interception storage capacity (INT_{max}), a_{rain} and a_{snow} were not considered. In addition, the preliminary sensitivity analysis (Appendix F.1) showed that the parameter LAI had no effect on the model behavior and was therefore not retained in the SA.

- Snow is expected to have only little influence on the Ardèche catchment. Following the result of the sensitivity analysis done by Gouttevin et al. (2017) on the snow module of the J2000 model, most parameters related to snow processes were discarded. In addition, our preliminary sensitivity analyses (Appendix F.1) showed that the 3 main snow related parameters, $T_{\text{snow},1}$, $T_{\text{snow},2}$ and T_{f}, as well as the maximum infiltration rate in Winter, $I_{\text{max,snow}}$, had very little effect on the model behavior. As a consequence, no snow related parameter was considered in the SA.

- As detailed in Section 2.4.1.2, only the field capacity parameters θ_{FC} actually affects MPS_{max} given the specified soil depth (z_{roots}). Here, only the resulting value, MPS_{max}, was considered as an input factor for the SA.

- The two parameters controlling the distribution and diffusion of water between the MPS and LPS reservoir, C_{DIST} and C_{DIFF}, were not considered as the way they are currently specified is part of how we want the model to behave (see explanation in Section 2.4.1.2). For the same reason, the parameter C_{ET} that modulates how plants are able to withdraw water from the MPS reservoir for transpiration was also not considered.

- All reach parameters (controlling flow routing) are derived from the DEM except the width, W_{reach}, and rugosity, K_{reach}. Our preliminary sensitivity analysis (Appendix F.1) demonstrated these two parameters had no effect on the model behavior and were therefore not considered here. Note that in the preliminary analysis their ranges of variation were kept narrow since the default values used were supported by past hydraulic studies (Adamovic, 2014).

As a result, 11 parameters were kept for the deployment of the SA including 6 distributed parameters (see Figure 5.7) and implying a total number of simulations, N =13 0000.

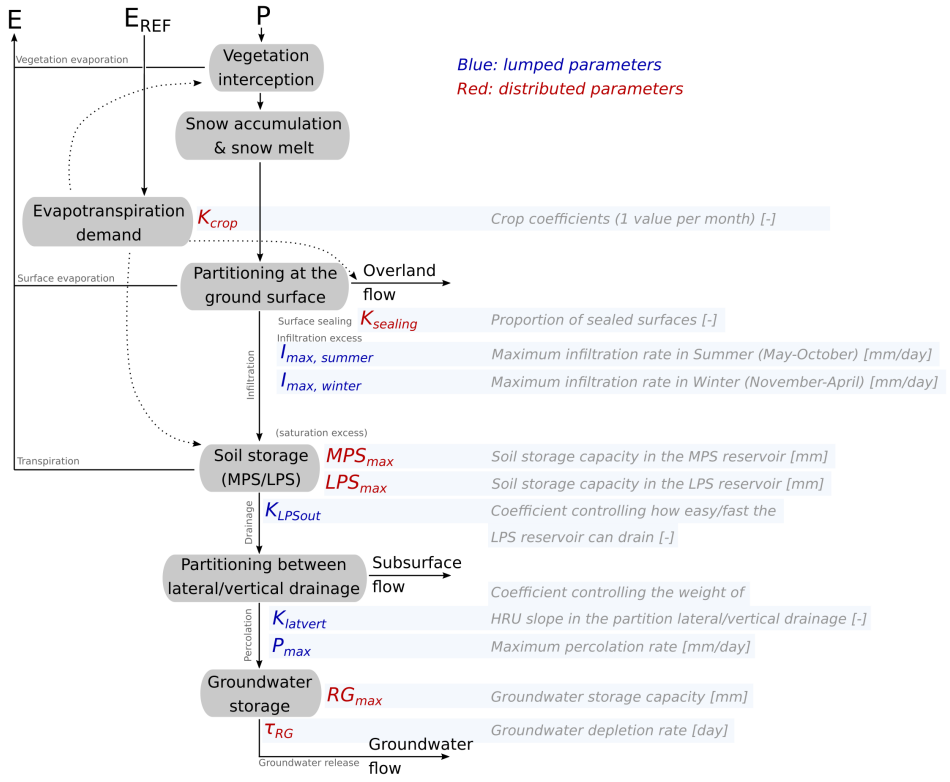

Figure 5.7: Simplified diagram of the J2000 model and associated model parameters selected for the sensitivity analysis.

5.2.2.4 Handling distributed parameters

In addition a specific strategy was set for distributed parameters to limit the number of actual parameters to investigate in the SA. Distributed parameters can be handled by considering only the dominant HRU types as in the study of Haghnegahdar et al. (2017). Another strategy is to keep the spatial pattern of the distributed parameter and use a multiplier to perturb the parameters (e.g. Yilmaz et al. 2008). The preliminary sensitivity analysis described in Appendix F.1 followed a similar strategy: instead of multiplicative factors (as in Yilmaz et al. 2008), additive factors were used to perturb the distributed parameters. However this approach yielded results difficult to interpret given how the distributed parameters may vary depending on the initial/default values of the distributed parameter and the range of variations of the additive (or multiplicative) factor (Appendix F.1.3).

As a consequence, the strategy we decided to finally use was to make all distributed parameters lumped parameters. In other words, all soil, geology and land-use classes were attributed the same parameter values for each simulation as if the distributed parameters were lumped. Therefore, in the sensitivity analysis of the four study catchments, the only differences that remain and might explain inter-catchment differences in the results are: (1) the forcings (precipitation, reference evapotranspiration, air temperature), (2) the number, the sizes and the slopes slopes of the HRUs and (3) the period considered to compute the hydrological signatures (see Table 2.3, minus hydrological years 2017 and 2018 for Cladueègne).

The 12 values of the crop coefficient, K_{crop}, required a special treatment in order to have only parameter (not 12) to investigate in the sensitivity analysis. For the 12 monthly values of K_{crop}, the relative magnitude of the seasonal variation defined in the default simulation (see

Table 2.7) was kept. Only the change in the absolute magnitude was investigated by adding a fixed value (via an additive factor F_{Kcrop}) in order to investigate the effect the 12 values of K_{crop} together have on the model outputs. To be consistent with the other parameters (i.e. no differences between land-use classes), all HRUs were considered to have forest land-use, i.e. the relative magnitude of K_{crop} set for the sensitivity analysis is the one of the forests (± 0.1 depending on the month, see Table 2.7).

As the sensitivity analysis only aims at establishing and characterizing the links between hydrological signatures and model parameters, considering distributed parameters as lumped parameters is expected to have no effect on our conclusions. We only aim at establishing clear links between hydrological signatures and model parameters by identifying, for each hydrological signatures, which are the influential parameters. Therefore, this simplification, while not affecting our conclusions, makes it possible to specify clear parameter variation ranges (see Section 5.2.2.5 and Table 5.1) which should yield results easier to interpret compared to the preliminary SA described in Appendix F.1. Also note that this choice implies that distributed parameters will likely be found to have a larger effect that they would normally have if distributed.

5.2.2.5 Explored parameter space

The explored range of values for each parameter was chosen to stay within realistic model behaviors. Following the recommendations of Saltelli (2004), all parameters were sampled in a uniform distribution $\mathcal{U}(a, b)$ as no information could support any more precise distributions. The lower (a) and upper (b) bounds specified for each parameter is reported in Table 5.1.

Table 5.1: Selected lumped and distributed parameters for the sensitivity analysis. Default values (in the default simulation) and ranges of variations (a and b) used for the specifications of the uniform distributions $\mathcal{U}(a, b)$ where the parameters were sampled.

Name	Unit	Default†	Range $\mathcal{U}(a, b)$	
			a	b
Lumped parameters				
$I_{\text{max,summer}}$	mm·day^{-1}	40	20	100
$I_{\text{max,winter}}$	mm·day^{-1}	50	20	100
K_{LPSout}	–	5	1	10
K_{latvert}	–	1	0.5	2
P_{max}	mm·day^{-1}	20	0	30
Distributed parameters				
K_{crop}‡	–	1.06	(-2)	(+0.3)
K_{sealing}	–	0.15	0	0.6
τ_{RG}	day	27	10	60
MPS_{max}	mm	56	10	100
LPS_{max}	mm	160	20	200
RG_{max}	mm	403	30	300

† The default values reported here are the one used in default simulation presented in Section 2.4 For distributed parameters, the mean taken over the 4 study catchments (see Table 2.10) is reported.
‡ The range indicated for K_{crop} (in parentheses) is the range of the applied additive modifications to K_{crop} 12 default values, set as forests for all land-use classes (i.e. between 1 and 1.2, see Table 2.7).

5.2.2.6 Interpretation methodology

The GSA method used here gives the first and total order sensitivity indices for all parameters. The total order indices, S_{Ti}, are used to quantify the effect of each parameter on each hydrological signature. For each parameter, comparisons with the first order indices, S_i, are used to quantify the part of the effect due to the model parameter interactions with all the other model parameters.

Finally, the trend linking a parameter F with the model output Y (a hydrological signature), the slope a of the linear regression $Y = a \times F + b$, is used to have the general trend of the relationship between the parameter and the model output. This slope only gives a general trend as complex relationship such as threshold or bell-like curves cannot be captured. For more complex relationships between model outputs and parameters, more insights can be provided by a careful exploration of the scatter plots.

5.3 Detailed results of the sensitivity analysis used to link hydrological signatures and model parameters

The sensitivity analysis of the J2000 model focused on the the 4 sub-models of the J2000 Ardèche model corresponding to the four study catchments Meyras, Pont-de-Labeaume, Goulette and Claduègne. The model outputs considered for the computation of first order and total order sensitivity indices, S_i and S_{Ti}, are each of the 12 hydrological signatures. In this section the results of the sensitivity analysis are presented. Detailed and additional results of the sensitivity analysis are reported in Appendix F.2. The results of the sensitivity analysis are used to (1) identify, for each hydrological signature, which model parameters it is linked to, (2) verify our interpretation of the hydrological signatures in terms of hydrological processes (as represented in the J2000 model) and (3) evaluate the diagnostic power of the hydrological signatures – how well-defined the links are and how consistent interpretations are.

5.3.1 Sensitivity of the hydrological signatures to the model parameters

Figure 5.8 shows the first and total order sensitivity indices, S_i and S_{Ti}, of the 12 hydrological signatures, for the 4 study catchments. Given that large uncertainties are associated with the first order indices (as expected for small first order indices, see Iooss and Lemaître, 2015), for readability, only the lower boundary of the uncertainty of the indices are reported in Figure 5.8. More details are provided in Appendix F.2 where detailed results are reported (including Figure F.2 which shows both the first and total order sensitivity indices). Note that this choice does not affect the analysis and has for consequence that the different between S_i and S_{Ti} is an estimate of the maximum interaction.

Overall, Figure 5.8 shows that the results are consistent across the 4 investigated catchments. Only a few notable differences between catchments can be seen for some parameters and some hydrological signatures. Mostly the Claduègne catchment is found to differ from the other 3 catchments: K_{sealing} is found very influential for signatures $S_{\text{FDC.Q10}}$ and $S_{\text{REC.}\tau\text{early}}$ in the case of Claduègne while only small effects are found for the other 3 catchments; similarly, τ_{RG} is found to have large influence for Claduègne compared with the other 3 catchments for signatures $S_{\text{FDC.slope}}$ and $S_{\text{REC.}\tau\text{late}}$; $RG_{\max}$ is found to have only little influence for Claduègne compared with the other 3 catchments. Another well visible inter-catchment difference in the sensitivity indices corresponds to parameter K_{latvert} (e.g. for signatures $S_{\text{FDC.slope}}$ and $S_{\text{REC.}\tau\text{late}}$): large sensitivity indices for Meyras, medium for Pont-de-Labeaume, small for Goulette and very small or null for Claduègne.

The only differences between catchments that might explain the differences of the sensitivity indices between the 4 catchments are (1) the forcings, (2) the number, sizes and slopes of the HRUs and (3) the period considered to compute the hydrological signatures. As parameter K_{latvert} controls the partitioning of water between lateral and vertical water drainage (i.e. subsurface flow or percolation) by giving more or less weight to the average slope of the HRU, the inter-catchment differences reflect the differences in steepness of the catchments: Meyras is the steepest catchment whereas Claduègne is the less steep catchment (see Table 2.1). Similarly, the larger influence of τ_{RG} found for Claduègne could also be attributed to the lower HRUs

slopes of this catchment. The large influence of K_{sealing} might be the consequence of differences in meteorological forcings with more frequent low rate precipitation events for Claduègne. The small influence of $RG_{\max}$ in the case of Claduègne might be a consequence of the shorter period considered for the computation of the hydrological signatures: the effect of long term catchment storage might be visible only if long periods are considered for the computation of the hydrological signatures.

As only the lower boundary of the first order indices is reported in Figure 5.8, the differences between the total and first order indices indicate the maximum part of the parameters interactions on the total effect. Figure 5.8 shows that, for most parameters and most hydrological signatures, the sensitivities of the hydrological signatures to the model parameters are mostly caused by direct influence of the parameter with only little interaction. Noteworthy exceptions are the hydrological signature S_{BFI}, $S_{\text{PQ.strength}}$, $S_{\text{PQ.date}}$ and $S_{\text{REC.}\tau\text{early}}$. To a lesser extent, the sensitivity indices of hydrological signatures $S_{\text{FDC.slope}}$, $S_{\text{PQ.wet}}$ and $S_{\text{REC.}\tau\text{late}}$ also show significant interactions between model parameters. Large parameter interaction inevitably lead to difficulties in identifying how the model parameters affect the hydrological signatures. Therefore, the more parameter interaction there is, the weaker the diagnostic power of the hydrological signatures is likely to be. In addition, we can note that more interaction leads to more uncertainty in the estimated total sensitivity indices.

Figure 5.8 shows that 2 of the J2000 model parameters are particularly influential: the size of the soil "large-pore" reservoir, $LPS_{\max}$, and the groundwater depletion rate τ_{RG}. Other model parameters can also be identified as influential: the crop coefficient, K_{crop}, the maximum infiltration rate in Summer, $I_{\text{max,summer}}$, the maximum percolation rate, $P_{\max}$, the size of the groundwater reservoir, $RG_{\max}$, the parameter controlling the partitioning of water between lateral (sub-surface flow) and vertical (percolation) drainage, K_{latvert}, and the parameter controlling how fast/easy soils can drain, K_{LPSout}. On the other hand, other parameters are found to have only small effect for all catchments and all hydrological signatures. This is the case of the size of the MPS reservoir, $MPS_{\max}$, where the water available for plant transpiration is stored, as well as the maximum infiltration rate in Winter, $I_{\text{max,winter}}$.

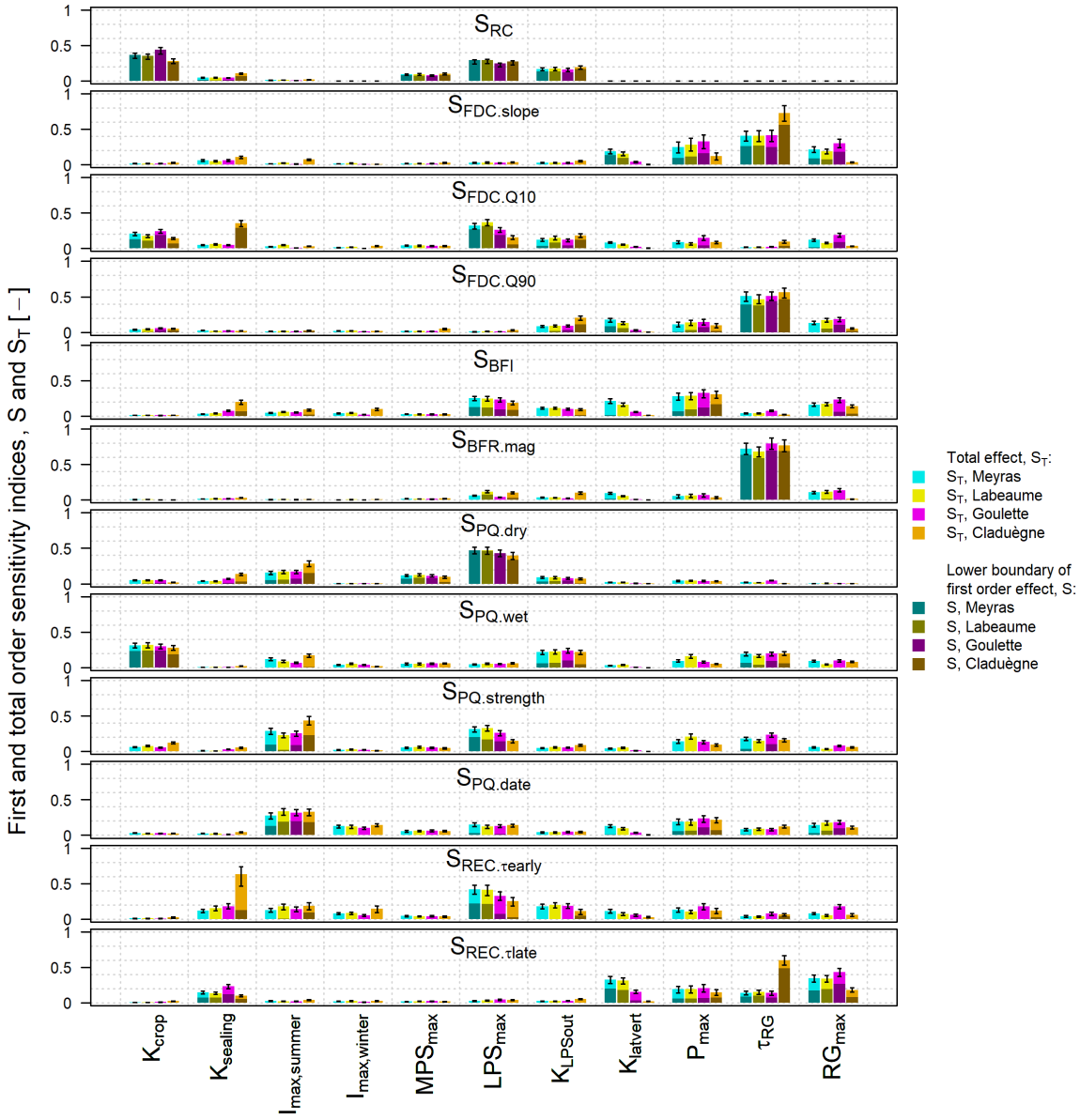

Figure 5.8: First and total order sensitivity indices of the J2000 model parameters for the four study catchments and each hydrological signature (rows). The effect of parameters are significant when above a threshold of 0.05. For readability and given the large uncertainty associated with the estimated first order effects, S, only the lower boundary of the uncertainty of first order indices are reported here. See Figure F.2 for detailed results.

5.3.2 Interpreting the links between hydrological signatures and model parameters

The sensitivity led to 13 000 model runs, corresponding to 13 000 model parameter sets. It is therefore possible to investigate the relationship between each hydrological signature and each model parameter using scatter plots. In Appendix F.2, these scatter plots are proposed for all the study catchments (Figures F.3, F.4, F.5 and F.6). For each couple hydrological signature / model parameter, where the total sensitivity index, S_T, is above 0.05 (threshold of significance), the sign of the slope resulting from a linear regression can be used to have a general idea of the trend linking the hydrological signature and the model parameter. This trend gives a general idea of how the hydrological signature will be affected if the parameter is increased or decreased. These trends are reported in Figure 5.9, for all study catchments.

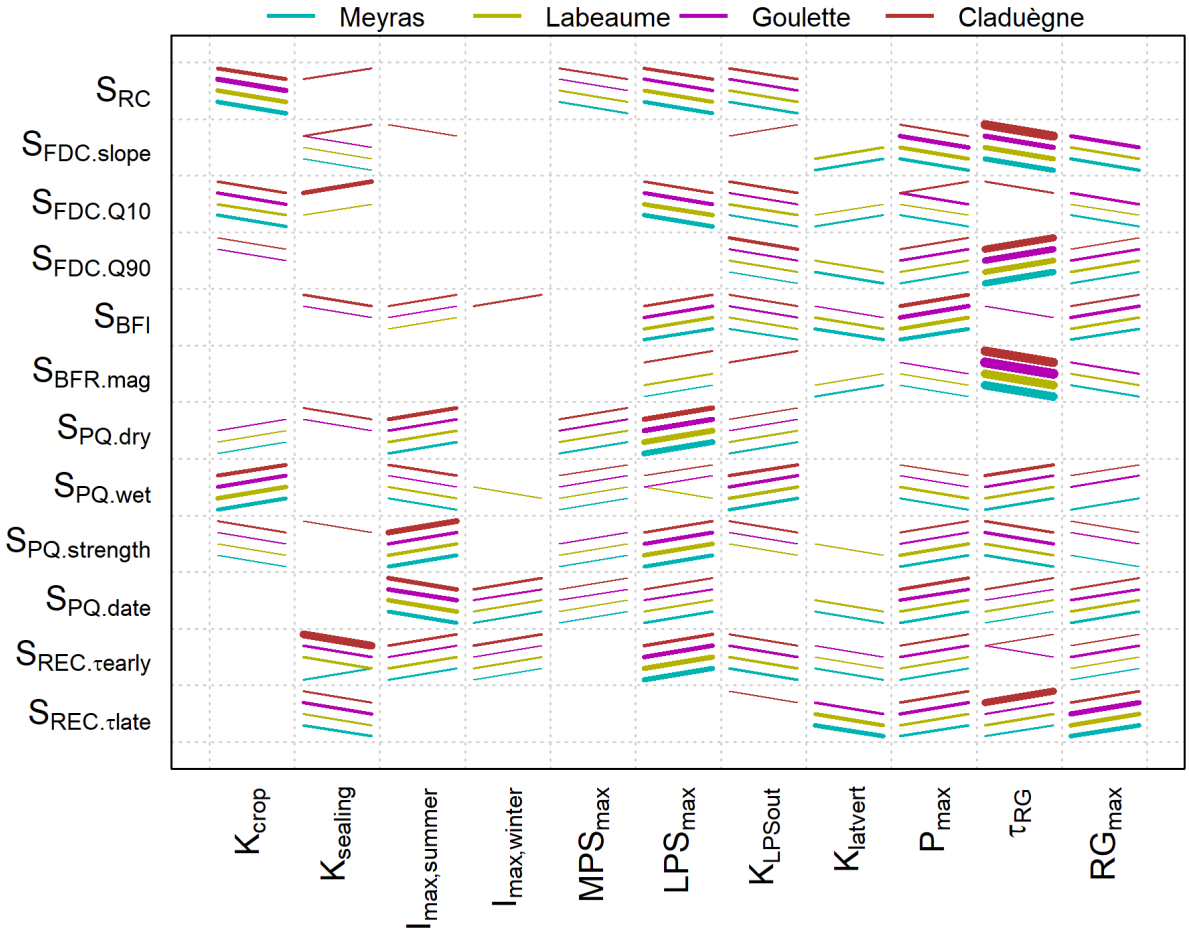

Figure 5.9: General trend linking hydrological signatures and model parameters for the four study catchments. The signs of the slopes of the regression lines linking model parameters and hydrological signatures are used to characterize how they are related. The general trend is shown only when the total order sensitivity index, S_T, is greater than 0.05: the thicker the line is, the larger S_T is.

Figure 5.9 shows consistent results between catchments: the same sign of the slope of the linear regression is obtained across the 4 catchments. Some exceptions can be noticed for $S_{\text{REC.}\tau\text{early}}$, $S_{\text{PQ.wet}}$, $S_{\text{FDC.Q10}}$ and $S_{\text{FDC.slope}}$. These exceptions are due to small total order indices and/or large interactions between model parameters (see Figure 5.8). This indicates that the general trend is mostly relevant when the total order effect is mainly due to first order effects of the parameter.

In the subsections that follow, the links between hydrological signatures and model parameters are detailed in terms of model functioning using the results of the sensitivity analyses presented in Figure 5.8 and the general trends presented in Figure 5.9. For each hydrological signature, we verify the consistency between the sensitivity analysis results and our hypothesized interpretations and assess the overall diagnostic power it has on the J2000 model.

5.3.2.1 Runoff coefficient, S_{RC}

The runoff coefficient, S_{RC}, is supposed to target the partitioning of input precipitation between evapotranspiration and streamflow. It should measure the long term split of water (in terms of volume) between these two possible outcomes. As hypothesized in Chapter 4 (Table 4.4), a larger S_{RC} should indicate that there is less evapotranspiration to the profit of streamflow as a consequence of less evapotranspiration demand and/or less available water for direct evaporation (from surface water ponding or canopy intercepted water) or plant transpiration (from the soils).

Figure 5.8 and Figure 5.9 show that a larger S_{RC} is linked to (1) less evapotranspiration demand (smaller K_{crop}) and (2) smaller soil storage (smaller LPS_{max} and smaller MPS_{max}) and more easily drainable soils (smaller K_{LPSout}). These results show that, in the J2000 model, a larger S_{RC} is due to less evapotranspiration demand and less water available in the soils for plant transpiration due to less infiltration and shallower soils draining more easily. These results confirm our hypotheses.

Interestingly, the size of the MPS reservoir, MPS_{max}, affects only weakly evapotranspiration although plant transpiration only withdraws water from this reservoir. The amount of available water for plant transpiration seems to be mostly linked to the LPS reservoir and its drainage characteristics. This might be a consequence of the order, in a given time step, of the hydrological processes occurring in a HRU: (1) the water infiltrating in the soils is routed to the LPS reservoir; (2) LPS_{max} then releases water according to the overall soil saturation (i.e. including water content of both the LPS and MPS reservoirs) and parameter K_{LPSout}; (3) the water in the LPS reservoir is transferred to fill the MPS reservoir. Therefore, smaller LPS reservoir (smaller LPS_{max}) and more easily drainable soils (smaller K_{LPSout}), lead to more water short-cutting the MPS reservoir where plant transpiration occurs.

The signature-parameter links are strong with no or very little interaction. Confirming our hypothesized interpretation, S_{RC} targets two main aspects of model functioning both related to the partitioning of water between evapotranspiration and streamflow. Overall, these results indicate that S_{RC} has a strong diagnostic power.

5.3.2.2 Hydrological signatures based on the flow duration curve

Slope of the flow duration curve, $S_{\mathrm{FDC.slope}}$

The slope of the mid-segment of the flow duration curve, $S_{\mathrm{FDC.slope}}$, should measure the dampening effect of the catchment due the partitioning of water between fast and slow streamflow generation processes. A larger $S_{\mathrm{FDC.slope}}$ should be related to a weaker dampening effect (or flashier catchment response) which was hypothesized (see Table 4.4 in Chapter 4) to be due to smaller catchment storage and/or faster release of water from catchment storage (from soils

or groundwater).

Figure 5.8 shows that $S_{\text{FDC.slope}}$ is linked to the groundwater storage depletion rate τ_{RG}, the parameters controlling the partitioning between lateral (subsurface flow) and vertical (percolation to the groundwater) soil drainage, K_{latvert} and P_{max}, and groundwater storage, RG_{max} (except for Claduègne). Figure 5.9 shows that a larger $S_{\text{FDC.slope}}$ is due to faster groundwater depletion rates (smaller τ_{RG}), more subsurface flow at the expense of percolation (smaller K_{latvert}, smaller P_{max}) and smaller groundwater storage (smaller RG_{max}). These results show that, in the J2000 model, the dampening effect is due to groundwater inflow (percolation), groundwater storage capacity and release rate. Although storage in the soils is found to have no effect these results confirm our hypotheses regarding the interpretation of $S_{\text{FDC.slope}}$.

These results indicate that $S_{\text{FDC.slope}}$ is strongly related to specific aspects of model functioning, vertical/lateral soil drainage partitioning and groundwater storage and release. Although there are significant interactions between model parameters, these results suggest that $S_{\text{FDC.slope}}$ has a moderately good diagnostic power.

High flow, $S_{\text{FDC.Q10}}$

$S_{\text{FDC.Q10}}$ was hypothesized to focus on fast streamflow generation processes, i.e. overland flow related processes: a larger $S_{\text{FDC.Q10}}$ should indicate more overland flow (due to surface sealing, infiltration excess and saturation excess).

Figure 5.8 shows that it is only weakly linked to overland flow processes; only in the case of Claduègne is this signature sensitive to the proportion of sealed surface (K_{sealing}). $S_{\text{FDC.Q10}}$ is found sensitive mainly to soil storage (LPS_{max}) and drainage (K_{LPSout}), and evapotranspiration demand (K_{crop}). Figure 5.9 shows that a larger $S_{\text{FDC.Q10}}$ is linked to smaller soil storage (smaller LPS_{max}), more easily drainable soils (smaller K_{LPSout}) and less evapotranspiration demand (smaller K_{crop}). These results are similar to those obtained for the runoff coefficient S_{RC} and suggest that $S_{\text{FDC.Q10}}$ is sensitive to the partitioning of water between evapotranspiration and streamflow.

These unexpected results show that $S_{\text{FDC.Q10}}$ is irrelevant to characterize fast streamflow generation processes related to the partitioning of water at the ground surface. Therefore, our hypotheses are not confirmed. In addition, $S_{\text{FDC.Q10}}$ is also found weakly related, mainly through parameters interactions, to other parameters (e.g. K_{latvert}, P_{max}, RG_{max}). Overall, this hydrological signature does not bring new information on the model functioning and has poorer diagnostic power than the runoff coefficient.

Low flows, $S_{\text{FDC.Q90}}$

Hydrological signatures $S_{\text{FDC.Q90}}$ was hypothesized to be mostly linked to slow flow generation processes (Table 4.4): a larger $S_{\text{FDC.Q90}}$ should indicate more groundwater contributions due to more vertical drainage, more groundwater storage and/or slower groundwater release.

Figure 5.8 shows that $S_{\text{FDC.Q90}}$ is mostly linked to the depletion rate of groundwater storage, τ_{RG}. To a lesser extent, it is also found linked to the partitioning between lateral and vertical soil drainage (K_{latvert} and P_{max}), groundwater storage (RG_{max}) and soil drainage (K_{LPSout}).

Figure 5.9 shows that a larger $S_{\text{FDC.Q90}}$ is linked to slower groundwater depletion rate (larger τ_{RG}), more percolation at the expanse of subsurface flow (larger K_{latvert}), larger groundwater storage (large RG_{max}) and more soil drainage (smaller K_{LPSout}). These results confirm our interpretation hypotheses and indicate that the groundwater depletion rate, τ_{RG}, has the greatest influence.

Overall, the large and strong effects of τ_{RG}, the moderate parameter interactions and the consistency with our hypothesized interpretations suggest $S_{\text{FDC.Q90}}$ has a moderately good diagnostic power.

5.3.2.3 Hydrological signatures based on the analysis of baseflow

Baseflow index, S_{BFI}

S_{BFI} is expected to measure the long term split of water between fast and slow streamflow generation processes. A larger S_{BFI} was hypothesized to indicate less overland flow and/or more vertical drainage. The results of the sensitivity analysis (Figure 5.8 and Figure 5.9) partly confirm these hypotheses: a larger S_{BFI} is linked to more percolation at the expanse of subsurface flow (smaller K_{latvert} and larger P_{max}). On the other hand, it is found only weakly linked to the partitioning of water at the ground surface.

Unexpectedly, results indicate that a larger S_{BFI} is also linked to larger soil storage capacity (larger LPS_{max}), more soil drainage (smaller K_{LPSout}) and larger groundwater storage (larger RG_{max}). The sensitivity to soil storage might be explained by the decrease of the probability of saturation excess overland flow with larger soil storage capacity. However, given that in the default simulation of the model (Section 2.4.2) investigations of internal model state variables show that LPS_{max} is never saturated – e.g. for Meyras catchment, the average LPS reservoir saturation is, 95% of the time, below 49% – this explanation appears unlikely. Larger S_{BFI} being linked to larger LPS_{max} can also be explained as follows: larger soil storage can induce more "delayed" soil drainage as soils need more water to refill and generate significant drainage.

Results show that S_{BFI} cannot be linked clearly to a particular modeled hydrological process and that most of the links are due to large interactions between model parameters. In addition, our hypothesized interpretation are only partly confirmed. Overall, these results suggest this signature has poor diagnostic power.

Baseflow regime magnitude, $S_{\text{BFR.mag}}$

$S_{\text{BFR.mag}}$ is supposed to be a measure of the magnitude of the variation of slow generation processes throughout a hydrological year, between wet and dry conditions. A larger $S_{\text{BFR.mag}}$ was hypothesized to indicate smaller catchment storage and/or faster catchment storage depletion. Only the latter hypothesis is confirmed by the results of the sensitivity analysis (Figure 5.8 and Figure 5.9): a larger $S_{\text{BFR.mag}}$ is almost exclusively linked to faster groundwater depletion (smaller τ_{RG}).

The specificity of $S_{\text{BFR.mag}}$ to one single parameter (τ_{RG}), the very small parameter interactions and the consistency of the results with our hypothesized interpretation suggest $S_{\text{BFR.mag}}$ as a strong diagnostic power.

5.3.2.4 Hydrological signatures based on the P-Q approach

P-Q curve dry period slope, $S_{\text{PQ.dry}}$

The slope of the P-Q curve during the dry period, $S_{\text{PQ.dry}}$, was hypothesized to reflect soil replenishment, the lack of catchment storage contributions and evapotranspiration losses during the re-wetting period: a larger $S_{\text{PQ.dry}}$ should indicate (1) more soil infiltration, (2) less catchment storage contributions and/or (3) larger evapotranspiration during this period.

Figure 5.8 and Figure 5.9 show that $S_{\text{PQ.dry}}$ is strongly linked to soil storage, moderately linked to ground surface partitioning, and weakly linked to soil drainage and evapotranspiration demand: a larger $S_{\text{PQ.dry}}$ is linked to larger soil storage capacity (mainly larger LPS_{max} but also larger MPS_{max}), more infiltration / less overland flow (larger $I_{\text{max,summer}}$ and smaller K_{sealing}), less soil drainage (larger K_{LPSout}) and less evapotranspiration demand (smaller K_{crop}). As soil drainage is conditioned by the saturation of the soils, larger soil storage leads to less drainage which affects the amount of water available for plant transpiration. As a consequence, $S_{\text{PQ.dry}}$ is strongly linked to evapotranspiration. For the most part, these results confirm our hypothesized interpretations.

$S_{\text{PQ.dry}}$ is found linked to many model parameters but the effect of soil storage (LPS_{max}) is found largely dominant with only very little parameter interactions. Therefore, this hydrological signature is likely relevant and powerful for the diagnostic of the J2000 model to focus on soil storage and its interplay with the amount of water available for plant transpiration.

P-Q curve wet period slope, $S_{\text{PQ.wet}}$

The slope of the P-Q curve during the wet period, $S_{\text{PQ.wet}}$, was hypothesized to reflect the large contributions from catchment storage depletion and more overland flow (partly due to more saturation excess overland flow) occurring during the wet period, just after the re-wetting period: a larger $S_{\text{PQ.wet}}$ should indicate (1) more soil infiltration during the wet period due to larger maximum infiltration rate or larger soil storage (i.e. less saturation excess overland flow) and/or (2) less water being released from the catchment due to slower soil drainage (or more vertical drainage) and slower groundwater release (less catchment storage depletion contributions during the wet period as released later, i.e. in the second half of the hydrological year, not considered in the computation of $S_{\text{PQ.wet}}$).

Figure 5.8 and Figure 5.9 show that a larger $S_{\text{PQ.wet}}$ is mainly linked to more evapotranspiration demand (larger K_{crop}), less soil drainage (larger K_{LPSout}) and slower groundwater depletion storage (larger τ_{RG}). Therefore, our hypotheses are only partly confirmed: larger $S_{\text{PQ.wet}}$ is linked to slower overall catchment release rate (from soils or groundwater). However, the effect of evapotranspiration demand (and maximum soil infiltration rate in Summer) was unexpected.

Unexpectedly, a larger $S_{\text{PQ.wet}}$ is found linked to more evapotranspiration demand (larger K_{crop}) and smaller maximum soil infiltration during the Summer months (smaller $I_{\text{max,summer}}$) both affecting model behavior mostly during the dry months. A possible explanation is that more overland flow during Summer (hence, outside of the wet period) and more evapotranspiration demand (which affect mostly Summer) lead to less water having refilled soil and

groundwater storages which, in turns, lead to less catchment storage contributions during the wet period (i.e. steeper P-Q curve).

Interpretations of $S_{\text{PQ.wet}}$ are only weakly confirmed since evapotranspiration demand has unexpectedly the strongest effect and large interactions are found between model parameters for the other influential parameters (Figure 5.8). Overall, these results suggest that this hydrological signature has poor diagnostic power. However, the link of $S_{\text{PQ.wet}}$ to soil drainage (K_{LPSout}) combined with the absence of link to soil storage (LPS_{max} or MPS_{max}) might be useful for the diagnostic of this particular aspect of model functioning.

P-Q curve change of trend strength, $S_{\text{PQ.strength}}$

The strength of the change of trend between the dry and wet period in the P-Q curve, $S_{\text{PQ.strength}}$, computed from $S_{\text{PQ.dry}}$ and $S_{\text{PQ.wet}}$, is a relative and unitless hydrological signature that aggregates both $S_{\text{PQ.dry}}$ and $S_{\text{PQ.wet}}$. Accordingly, $S_{\text{PQ.strength}}$ is expected to mirror the results obtained for $S_{\text{PQ.dry}}$ and $S_{\text{PQ.wet}}$.

Figure 5.8 shows $S_{\text{PQ.strength}}$ is sensitive to $I_{\text{max,summer}}$ and LPS_{max} (like $S_{\text{PQ.dry}}$) as well as, P_{max} and τ_{RG} (like $S_{\text{PQ.wet}}$). Figure 5.8 also shows it is not sensitive to K_{crop} and K_{LPSout} (unlike $S_{\text{PQ.wet}}$). Therefore, these results only partly mirror the results obtained for $S_{\text{PQ.dry}}$ and $S_{\text{PQ.wet}}$ and similar interpretations can be derived here using Figure 5.9 (see previous paragraphs). Figure 5.8 also shows that there are larger interactions between parameters compare to both $S_{\text{PQ.dry}}$ and $S_{\text{PQ.wet}}$. As a consequence, $S_{\text{PQ.strength}}$ has likely a poorer diagnostic power than the two hydrological signature it is computed from.

P-Q curve shift date, $S_{\text{PQ.date}}$

The date in the change of trend, $S_{\text{PQ.date}}$, was hypothesized to reflect the time needed for the catchment to change of state: a larger $S_{\text{PQ.date}}$ should indicate that more time is required to refill catchment storage as a consequence of a drier catchment (at the start of a hydrological year) or smaller catchment storage capacity and/or less infiltration or more evapotranspiration during Fall. Note that a larger $S_{\text{PQ.date}}$ was also hypothesized to reflect faster or slower overall release rate from catchment storage.

Figure 5.8 shows that $S_{\text{PQ.date}}$ is linked to ground surface partitioning (parameters $I_{\text{max,summer}}$ and $I_{\text{max,winter}}$), soil storage (MPS_{max} and LPS_{max}), vertical/lateral soil drainage partitioning (parametres K_{latvert} and P_{max}), groundwater storage (RG_{max}) and release (τ_{RG}). These results indicate that $S_{\text{PQ.date}}$ is not specific to a particular modeled hydrological process. In addition mostly weak links can be identified. Overall, these results suggest this hydrological signature has poor diagnostic power.

In terms of the interpretation, Figure 5.9 shows that a larger $S_{\text{PQ.date}}$ is linked to (1) less (resp. more) infiltration during the Summer (resp. Winter) i.e. smaller $I_{\text{max,summer}}$ (resp. larger $I_{\text{max,winter}}$), (2) more soil storage (larger MPS_{max} and LPS_{max}), (3) more vertical drainage (smaller K_{latvert} and larger P_{max}), (4) more groundwater storage (larger RG_{max}) and (5) slower groundwater release (larger τ_{RG}). Our hypothesized interpretations regarding soil infiltration during the dry months and soil storage are confirmed. In addition, the results of the sensi-

tivity analysis clarify our hypothesized interpretation regarding the speed of overall catchment storage release rate: a larger $S_{\text{PQ.date}}$ is related to slower overall catchment release rates. This result indicates that the change of catchment behavior, as measured by $S_{\text{PQ.date}}$, is related to catchment storage and release characteristics: the faster it starts to release water after the dry months, the smaller (the earlier) $S_{\text{PQ.date}}$ is.

$S_{\text{PQ.date}}$ targets many model parameters through weak links and many parameter interactions suggesting poor diagnostic power. However, our hypothesized interpretation are all confirmed and also clarified. In addition, Figure 5.8 shows that $S_{\text{PQ.date}}$ is the signature with the strongest link to $I_{\text{max,summer}}$ indicating it can be potentially useful to investigate the partitioning of water at the ground surface.

5.3.2.5 Hydrological signatures based on the analysis of streamflow recessions

Early recession time, $S_{\text{REC.}\tau\text{early}}$

The early recession time, $S_{\text{REC.}\tau\text{early}}$, is supposed to characterize quickly depleting catchment storage and/or possibly overland flow. A larger $S_{\text{REC.}\tau\text{early}}$ was hypothesized to indicate slower water release from quickly draining soils and/or possible less overland flow.

Figure 5.8 shows that $S_{\text{REC.}\tau\text{early}}$ is linked to many parameters including ground surface partitioning parameters (K_{sealing}, $I_{\text{max,summer}}$ and $I_{\text{max,winter}}$), soil storage (LPS_{max}) and drainage (K_{LPSout}). Figure 5.9 shows that a larger $S_{\text{REC.}\tau\text{early}}$ is linked to less overland flow due to less sealed surface (smaller K_{sealing}, mostly for Claduègne) and larger maximum infiltration rate in both Summer and Winter (larger $I_{\text{max,summer}}$ and $I_{\text{max,winter}}$) confirming our hypothesis. Figure 5.9 also shows inconsistent results: a larger $S_{\text{REC.}\tau\text{early}}$ is linked to less soil drainage due to larger catchment storage (larger LPS_{max}) or more soil drainage due to more easily drainable soils (smaller K_{LPSout}).

The inconsistency between LPS_{max} and K_{LPSout} might be due to the large interactions between parameters. Given the stronger effect found for LPS_{max} and the larger interactions in the total effect of K_{LPSout}, it is more likely that a larger $S_{\text{REC.}\tau\text{early}}$ is linked to less soil drainage due to more soil storage (larger LPS_{max}), thus confirming our hypothesis.

Overall, these results confirm our hypothesized interpretations. However, $S_{\text{REC.}\tau\text{early}}$ is found related to many parameters and there are large inter-parameters interactions indicating it is not very specific and that the links with model parameters are difficult to interpret. These results suggest that $S_{\text{REC.}\tau\text{early}}$ has a relatively poor diagnostic power.

Late recession time, $S_{\text{REC.}\tau\text{late}}$

The late recession time, $S_{\text{REC.}\tau\text{late}}$, is supposed to characterize slowly depleting catchment storage. A larger $S_{\text{REC.}\tau\text{late}}$ was hypothesized to indicate slower release from soils, more vertical drainage and/or slower groundwater depletion. As shown by Figure 5.8 and Figure 5.9, these hypotheses are, for the most part, confirmed by the results of the sensitivity analysis: a larger $S_{\text{REC.}\tau\text{late}}$ is linked to more percolation at the expense of subsurface flow (smaller K_{latvert} and larger P_{max}) and slower groundwater depletion rates (larger τ_{RG}).

Unexpectedly, groundwater storage capacity, $RG_{\max}$, is found to have the greatest effect and soils drainage (K_{LPSout}) has no influence. Results indicate that more groundwater storage in the J2000 model results, in average, in less steep recessions.

The large influence of $RG_{\max}$ is only true for Meyras, Pont-de-Labeaume and Goulette which have the longest periods available for the computation of $S_{\text{REC}.\tau\text{late}}$. The larger effect of τ_{RG} found for Claduègne might indicate that if a shorter period is considered, the depletion rate is more influential than groundwater storage capacity. However, it might also be caused by the small slopes of Claduègne and the resulting small subsurface flow contributions: the lack of influence of K_{latvert} might cause τ_{RG} to have a stronger effect on the streamflow recession rate.

Overall, our hypotheses regarding the interpretation of $S_{\text{REC}.\tau\text{late}}$ are confirmed and the unexpected influence of $RG_{\max}$ can be explained. It is found quite specific to groundwater processes with only moderate interactions between parameters suggesting that this signature has a moderately good diagnostic power. In addition, the strong effect of $RG_{\max}$ might be useful for the diagnostic of this particular aspect of the model functioning as the influence of $RG_{\max}$ is found relatively limited for all the other hydrological signatures.

Although the effect is small (Figure 5.8), Figure 5.9 shows that a larger $S_{\text{REC}.\tau\text{late}}$ can be caused by a smaller proportion of sealed surface (smaller K_{sealing}). A possible explanation of this unexpected result is that more infiltration during small precipitation events can lead to no streamflow rise (hence, no new recession event detected) but to a slower decrease of streamflow due to more subsurface flow contributions, and hence, a larger late recession time.

5.3.3 Synthesis

The results of the sensitivity analysis gave insights into the relationships between hydrological signatures and model parameters. It enabled the verification of the signatures interpretation hypotheses (detailed in Chapter 4) and the signature evaluation in terms of diagnostic power.

Most of our hypothesized interpretations of the hydrological signatures were found consistent with the sensitivity analysis results, in particular for S_{RC}, $S_{\text{FDC.slope}}$, $S_{\text{FDC.Q90}}$, $S_{\text{BFR.mag}}$, $S_{\text{PQ.dry}}$ and $S_{\text{REC}.\tau\text{late}}$. To a lesser extent, hypothesized interpretation of $S_{\text{PQ.date}}$ and $S_{\text{REC}.\tau\text{early}}$ were also found consistent with the sensitivity analysis results. On the other hand, for $S_{\text{FDC.Q10}}$, S_{BFI} and $S_{\text{PQ.wet}}$ results did not confirm our hypotheses.

The diagnostic power of the hydrological signatures was evaluated considering the strength and specificity of the links between signatures and model parameters using the total sensitivity indices and the relative importance of parameter interactions assessed from the first order sensitivity indices. Apart from $S_{\text{BFR.mag}}$, none of the hydrological signatures could be exclusively related to one model parameter. However, the diagnostic power of the hydrological signatures was judged good when little parameter interactions affect the total sensitivity indices and that the influential parameters was clearly related to one or two aspects of model functioning. In addition, the consistency of the results with our hypothesized interpretation also weighted in this assessment.

Little parameter interactions were found for S_{RC}, $S_{\text{FDC.Q90}}$, $S_{\text{BFR.mag}}$ and $S_{\text{PQ.dry}}$. These hydrological signatures were found clearly linked to a small number of parameters which are

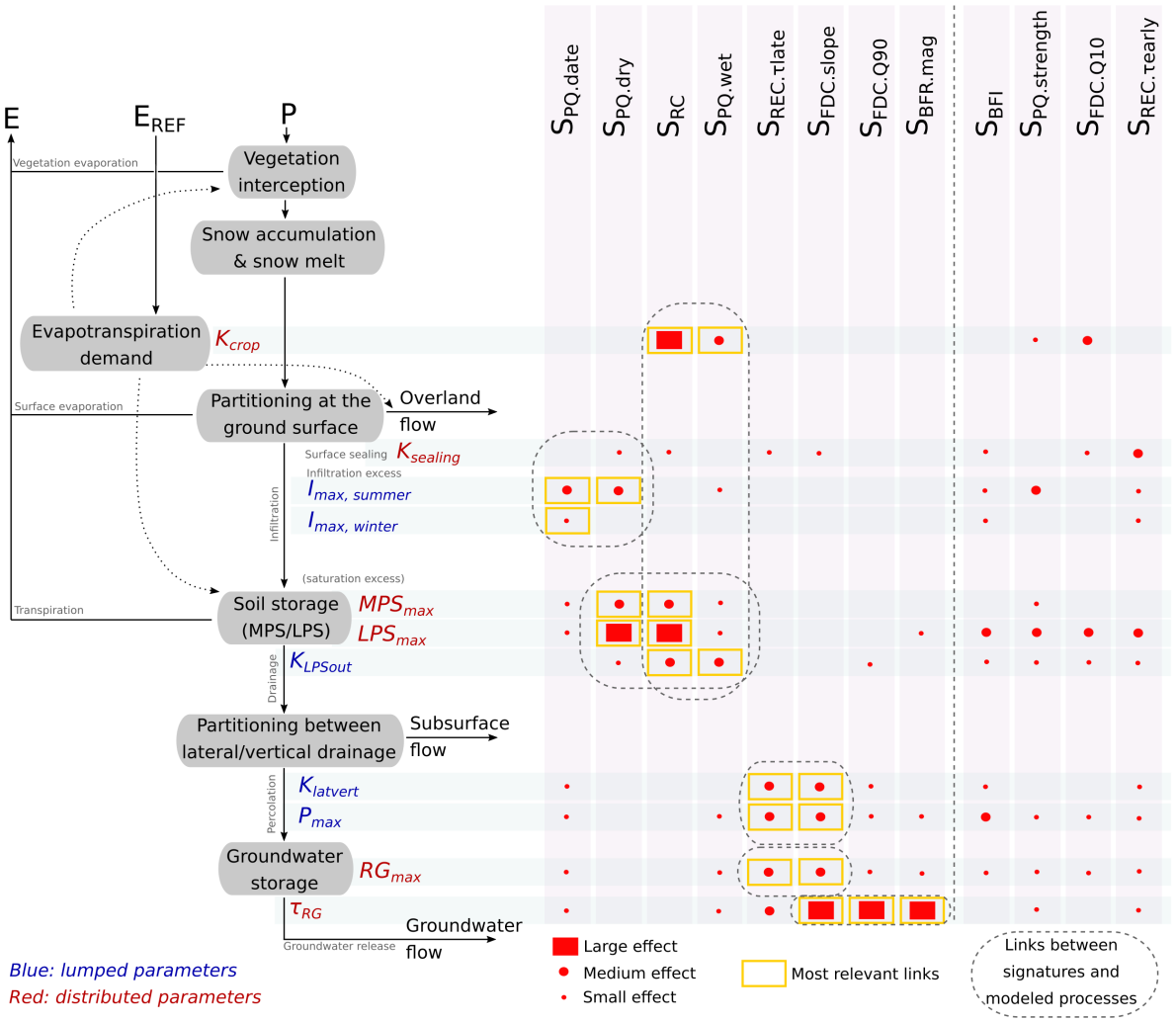

Figure 5.10: Synthetic overview of the links between hydrological signatures and model parameters. On the left: simplified diagram of the J2000 model and associated model parameters, investigated in the sensitivity analysis. On the right: mapping between model parameters (rows) and hydrological signatures (columns) derived from the sensitivity analysis results.

related to particular aspect of model functioning: (1) S_{RC} is clearly linked to evapotranspiration demand and available water for plant transpiration, (2) $S_{\mathrm{PQ.dry}}$ is clearly linked to ground surface partitioning and available water for plant transpiration, (3) $S_{\mathrm{FDC.Q90}}$ and $S_{\mathrm{BFR.mag}}$ are clearly linked to slow streamflow generation processes. Although more interactions affect the sensitivity indices of $S_{\mathrm{FDC.slope}}$ and $S_{\mathrm{REC.}\tau\mathrm{late}}$, both signatures were found clearly related to slow flow generation processes. In particular, they are the two signatures with the strongest links to parameters K_{latvert} (partitioning between vertical/lateral soil drainage) and RG_{max} (groundwater storage) and have likely good potential diagnostic power regarding these aspects of model functioning.

Finally, despite the large interactions and lack of specificity, $S_{\mathrm{PQ.wet}}$ and $S_{\mathrm{PQ.date}}$ were found to be potentially useful for the diagnostic of the model. $S_{\mathrm{PQ.wet}}$ was found linked to evapotranspiration demand and soil drainage without being influenced by soil storage making it potentially useful if combination with S_{RC} and $S_{\mathrm{PQ.dry}}$ to have a finer diagnostic on the partitioning of water between evapotranspiration and streamflow in the model. $S_{\mathrm{PQ.date}}$ was found to have the strongest link to ground surface partitioning in Summer (maximum infiltration

rate $I_{\text{max,summer}}$) and can therefore be potentially useful for the diagnostic of this aspect of the model functioning.

From the detailed analysis proposed in the previous section it is possible to identify which are the hydrological signatures that are the most relevant to investigate particular aspects of the model functioning. Figure 5.10 summarizes the main links between hydrological signature and model parameters and highlights which are the groups of links that are the most relevant to focus on different aspects of the J2000 model:

- partitioning between evapotranspiration and streamflow related to evapotranspiration demand and available water for plant transpiration (parameters K_{crop}, MPS_{max}, LPS_{max} and K_{LPSout}): S_{RC}, $S_{\text{PQ.dry}}$, and $S_{\text{PQ.wet}}$.
- partitioning at the ground surface (K_{sealing}, $I_{\text{max,summer}}$ and $I_{\text{max,winter}}$): $S_{\text{PQ.dry}}$ and $S_{\text{PQ.date}}$ (and also possibly $S_{\text{REC.}\tau\text{early}}$).
- partitioning between vertical and lateral drainage (K_{latvert} and P_{max}): $S_{\text{REC.}\tau\text{late}}$ and $S_{\text{FDC.slope}}$.
- groundwater storage (RG_{max}): $S_{\text{REC.}\tau\text{late}}$ and $S_{\text{FDC.slope}}$.
- groundwater release rate (τ_{RG}): $S_{\text{BFR.mag}}$, $S_{\text{FDC.Q90}}$ and $S_{\text{FDC.slope}}$.

It is important to stress that all these results are only valid within the context of the J2000 Ardèche model and only for the four study catchments (and their specificity in terms of size, number of HRUs, slope, etc.). The results may also differ if the sensitivity analyses were to be done on another periods with different meteorological data. Other sensitivity analysis of the J2000 model should be undertaken in other catchments to verify what is consistent (or not) across catchments and how it can be related to specific aspects of the catchments (e.g. climate, slope, etc.).

Conclusion

In Section 5.1, discrepancies between observed and simulated hydrological signatures were analyzed to derive a preliminary diagnostic of the J2000 model. The results highlighted issues in (1) the partitioning of water between evapotranspiration and streamflow (too much evapotranspiration demand, too much soil storage, not enough soil drainage for forests), (2) too much overland flow, particularly in Summer, (3) too much vertical drainage at the expense of lateral drainage (sub-surface flow) and (4) too large groundwater storage and/or too slow groundwater depletion. Due to the difficulty to discriminate between multiple model dis-functioning hypotheses and to pinpoint clearly the model parameters at fault, a sensitivity analysis (Section 5.2 and Section 5.3) was undertaken.

In Section 5.3, the results of the sensitivity analysis were analyzed in order to clearly establish the links between model parameters and hydrological signatures, verify our hypothesized interpretation regarding the hydrological signatures and evaluate the diagnostic power of the hydrological signatures. Overall, results showed that our hypothesized interpretation were consistent with the results of the sensitivity analysis. However, the results also highlighted that in some cases these hypothesized interpretations could be wrong (e.g. $S_{\text{FDC.Q10}}$), or very weakly confirmed by the results of the sensitivity analysis due to parameter interactions and the lack of specificity of the hydrological signature (e.g. $S_{\text{REC.}\tau\text{early}}$, S_{BFI}). The results of the sensitivity analysis were used to identify which are the hydrological signatures (and links with model parameters) that are the most relevant for the diagnostic of the model (Figure 5.10.). Results suggest the diagnostic evaluation of the model should be mostly based on S_{RC}, $S_{\text{FDC.slope}}$, $S_{\text{FDC.Q90}}$, $S_{\text{BFR.mag}}$, $S_{\text{PQ.dry}}$, $S_{\text{REC.}\tau\text{late}}$, $S_{\text{PQ.date}}$ and $S_{\text{PQ.wet}}$.

This chapter has presented an original approach to evaluate the relevance of the hydrological signatures for the diagnostic-evaluation of a particular model. The sensitivity analysis combined with the J2000 model as hypothesis testing tool provided new insights into how the hydrological signatures could be interpreted. The results presented in this chapter are only valid for our specific case study and other sensitivity analyses should be done on a larger set of catchments to identify consistent results and how other factors such as the climatic context affect the results. However, applied to a specific context, this approach stands as an alternative approach to the one detailed in Chapter 3 where additional snow data were used in the assessment of the relevance and interpretation of snow related hydrological signatures. It could be repeated with any model, any catchment and any hydrological signature.

The results of the sensitivity analysis support the diagnostic-evaluation of the J2000 Ardèche model based on the discrepancies between observed and simulated hydrological signatures. The better understanding of the links between hydrological signatures and model functioning and the new insights into the relevance and interpretation of the hydrological signatures themselves should lead to a more in-depth diagnostic of the model. In Chapter 6, the most relevant signatures-parameters links identified in this chapter are combined with the differences between observed and simulated hydrological signatures to derive a clear diagnostic of the model in order to propose and test improvement recommendations.

Chapter 6

Improving processes realism of the J2000 process-based distributed hydrological model

Contents

Introduction

In this chapter, the diagnostic and improvement of the J2000 Ardèche model is detailed. It combines the approach based on the interpretation of the differences between observed and simulated hydrological signatures (Section 5.1) with the results of the sensitivity analysis (Section 5.3) that were detailed in Chapter 5. In particular, the diagnostic and improvement of the model presented in this chapter uses the clear understanding of the relationships between hydrological signatures and model parameters provided by the results of the sensitivity analysis.

The results of the sensitivity analysis suggested that the diagnostic of the J2000 Ardèche model should be based on a sub-set of hydrological signatures. The most relevant links between hydrological signatures and model parameters were clearly identified (see Figure 5.10 in Chapter 5). In particular, two main groups of hydrological signatures can be identified, focused on (1) soil processes including infiltration, storage and drainage as well as evapotranspiration and (2) groundwater processes including percolation to the groundwater reservoir, groundwater storage and release. Therefore, in Section 6.1, we propose an in-depth diagnostic of the J2000 Ardèche model based on two subsets of hydrological signatures: (1) S_{RC}, $S_{\mathrm{PQ.dry}}$, $S_{\mathrm{PQ.wet}}$ and $S_{\mathrm{PQ.date}}$ to investigate soil processes and (2) $S_{\mathrm{FDC.slope}}$, $S_{\mathrm{FDC.Q90}}$, $S_{\mathrm{BFR.mag}}$ and $S_{\mathrm{REC.}\tau\mathrm{late}}$ to focus on groundwater processes.

The results of the model diagnostic are used to establish a list of model modification recommendations that are tested and evaluated in Section 6.2. The J2000 Ardèche model improvement is evaluated in terms of processes, realism using the hydrological signatures and streamflow time series, and performance, using performance metrics. Finally, in Section 6.3, the main results are summarized highlighting the main methodological limitations and perspectives for future research.

6.1 Combining hydrological signatures mismatch and sensitivity analysis results for the diagnostic of the J2000 Ardèche model

In Chapter 5, the main model issues identified were: (1) too large groundwater storage and/or too slow groundwater depletion, (2) too much vertical drainage at the expanse of lateral drainage, (3) too large soil storage, not enough soil drainage affecting streamflow response dynamics and the partitioning of water between evapotranspiration and streamflow and finally, (4) too much overland flow, particularly in Summer. The results of the sensitivity analysis enabled a clearer understanding of the links between hydrological signatures and model parameters and highlighted the limited diagnostic power of some signatures used in the preliminary model diagnostic. In particular, some of the conclusions that were drawn from this preliminary analysis might be no longer relevant given the new insights provided by the sensitivity analysis. As a consequence, in this section, a new and in-depth diagnosic of the J2000 model is proposed based on two subsets of hydrological signatures focusing on soil processes (Section 6.1.1) and groundwater processes (Section 6.1.2). The overall results of this diagnostic are summarized in Section 6.1.3.

6.1.1 Soil infiltration, storage and release

To investigate soil processes in the model we use signatures S_{RC} (runoff coefficient), $S_{\mathrm{PQ.dry}}$ (slope of the P-Q curve during the re-wetting period), $S_{\mathrm{PQ.wet}}$ (slope of the P-Q curve after the re-wetting period) and $S_{\mathrm{PQ.date}}$ (date of the shift of the P-Q curve). Observed and simulated hydrological signatures for the four study catchments are presented in Figure 6.1. These hydrological signatures are used to investigate the long term partitioning between streamflow and evapotranspiration, soil storage and release and soil infiltration. We focus mainly on the following parameters: the crop coefficients, K_{crop}, the soil storage maximum capacities, MPS_{max} and LPS_{max}, the soil "drainability" parameter, K_{LPSout}, and the three main parameters controlling soil infiltration, the sealing of surface K_{sealing} as well as the maximum infiltration rate in Summer, $I_{\mathrm{max,summer}}$, and Winter, $I_{\mathrm{max,winter}}$.

6.1.1.1 Long term partitioning between evapotranspiration and streamflow

Figure 6.1 shows that there is an overall good match between observed and simulated S_{RC}. According to the results of the sensitivity analysis, the slight underestimation of simulated S_{RC} for Meyras, Pont-de-Labeaume and Goulette might be caused by either too much evapotranspiration demand or too much water available in the soils for plant transpiration.

Currently, evapotranspiration demand, i.e. the monthly values of parameter K_{crop}, for Meyras, Pont-de-Labeaume and Goulette are similar and correspond to the forest land-use classes (deciduous, coniferous and mixed forests). They are larger (average value of K_{crop}– for all months and all HRUs – of about 1.05-1.08, see Table 2.10) than in the case of Claduègne (average value of K_{crop} of about 1.01, see Table 2.10)) which is dominated by garrigues and grasslands land-use classes. While results suggest K_{crop} for forests should be decreased, such a modification

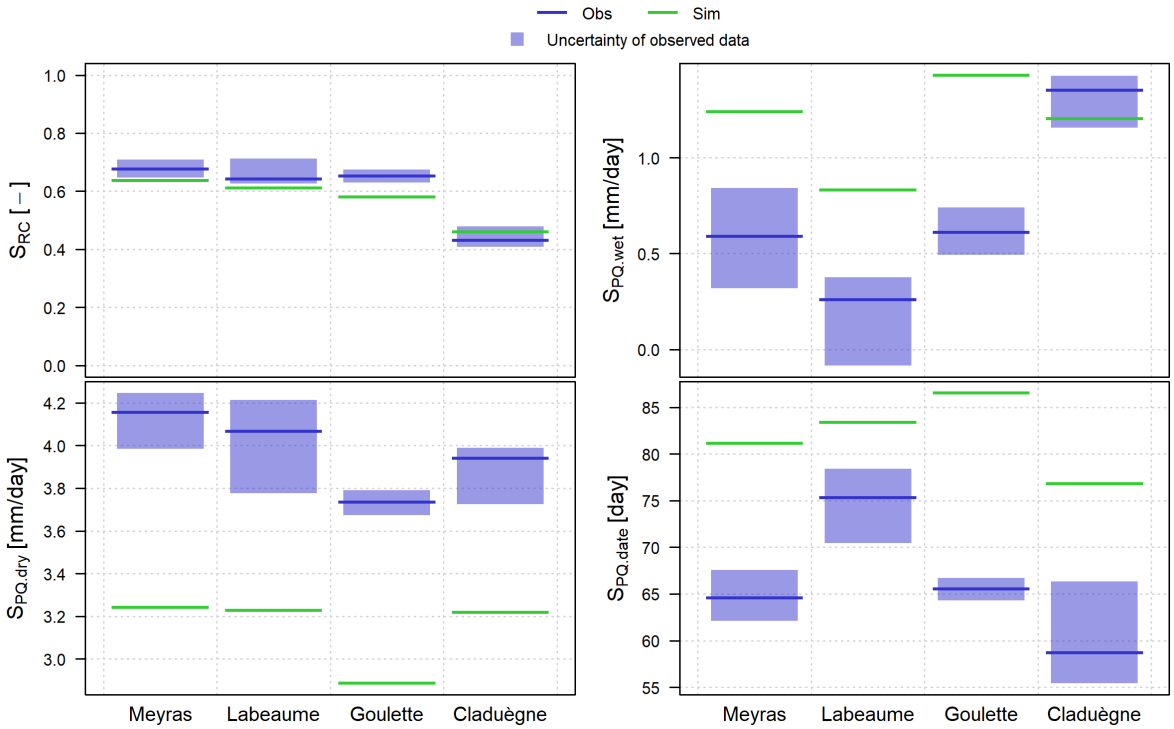

Figure 6.1: Observed and simulated hydrological signatures targeting surface and soil processes. Results are shown for the four study catchments.

would imply smaller differences between forests and grassland/garrigues that would no longer be large enough to be realistic. Therefore, the slight overestimation of evapotranspiration of Meyras, Pont-de-Labeaume and Goulette is more likely related to too much water available in the soils for plant transpiration.

Results of the sensitivity analysis suggest that soil storage (mainly the large-pore soil storage reservoir, $LPS_{\max}$) should be decreased for Meyras, Pont-de-Labeaume and Goulette. For these catchments only two soil classes are represented: the medium-to-shallow soil class and the shallow soil class. They correspond to $LPS_{\max}$ values of 140 mm and 130 mm respectively. These values are already relatively small and decreasing them might lead to unrealistically small soil storage for these catchments.

The underestimated S_{RC} found for Meyras, Pont-de-Labeaume and Goulette could also indicate issues in soil drainage characteristics. In particular, the lumped parameter K_{LPSout} could be decreased to allow for more soil drainage for these catchments. Since such a modification would also affect Cladugne, these results might suggest this parameter should be distributed. Distributing K_{LPSout} could make sense given that the ability of soils to drain is likely to vary depending on the types of soils. In particular, Meyras, Pont-de-Labeaume and Goulette have soils with much larger proportion of sand than Cladugne where soils have larger proportion of silt and clay (see Table 2.1). A larger proportion of sand arguably implies soils more able to drain than soils with a larger proportions of silt or clay. This supports the idea of distributing K_{LPSout} according to the type of soils which would enable us to specify a larger "drainability" for Meyras, Pont-de-Labeaume and Goulette.

These hypotheses of model dis-functioning and the associated modifications suggested here should be considered cautiously given that the differences between observed and simulated S_{RC}

are small. In particular it is possible that they simply reflect biases in the meteorological forcings since such biases were already identified by Adamovic (2014) for the Ardèche catchment, and more generally, are known to affect climate reanalysis products such as the one we use here (see, for example, Gottardi et al. (2012)). Although the same precipitation was used in the computation of observed and simulated S_{RC}, simulated streamflow can be affected by a significant negative bias in precipitation resulting in an underestimated simulated S_{RC}. These results suggest uncertainty associated with precipitation should be accounted for (Renard et al., 2011; Leblois and Creutin, 2013; Caillouet et al., 2016; Devers, 2019), in particular if the uncertainty estimation takes into account systematic errors.

6.1.1.2 Catchment streamflow response during and after the re-wetting period

The results of the sensitivity analysis showed that $S_{\mathrm{PQ.dry}}$ is linked to soil storage (mainly LPS_{max}). They also showed that $S_{\mathrm{PQ.wet}}$ was linked to the evapotranspiration demand (K_{crop}) and soil "drainability" (K_{LPSout}) with no or very weak link to soil storage. For these two hydrological signatures, which reflect catchment streamflow response during the re-wetting period ($S_{\mathrm{PQ.dry}}$) and after ($S_{\mathrm{PQ.wet}}$), there are large differences between observation and simulation (see Figure 6.1).

Figure 6.1 shows that simulated $S_{\mathrm{PQ.dry}}$ are underestimated for all catchments suggesting, unlike the results obtained with S_{RC}, not enough soil storage i.e. too small LPS_{max}. These results suggest LPS_{max} is too small for all catchments resulting in too much soil drainage, and hence too much streamflow during the re-wetting period. Results of the sensitivity analysis showed that $S_{\mathrm{PQ.dry}}$ is almost exclusively related to LPS_{max}. Only issues in the maximum infiltration rate in Summer, $I_{\mathrm{max,summer}}$, could also explain the underestimated simulated $S_{\mathrm{PQ.dry}}$.

Currently, soil storage parameters (LPS_{max} and MPS_{max}) are distributed according to soil depth derived from a soil database whose relevance was briefly questioned in Section 2.1.1.4. Four soil classes were distinguished to account for four soil depths and parameters MPS_{max} and LPS_{max} were specified accordingly (see Table 2.8). Using such soil data, primarily designed for agronomic studies, inevitably implies that weathered bedrock is not accounted for. However, as suggested by Vannier et al. (2013) water storage in weathered bedrock can be large in the Cévenne-Vivarais region – which includes the Ardèche catchment – in particular for schists, metamorphic rocks and magmatic rocks which are the dominant geology types found for Meyras, Pont-de-Labeaume and Goulette (see Figure 2.2). More generally, there is evidence that using such a soil database leads to underestimated soil storage values for all the Cévenne-Vivarais region regardless of the geology (Braud et al., 2016b). Although it is unclear whether weathered bedrock should be accounted for with the groundwater storage of the J2000 model or with soil storage, the increase of LPS_{max}, suggested here, appears reasonable. In addition, we can assume weathered bedrock to have a large hydraulic conductivity and many preferential flow paths that could justify its representation as "soil" in the J2000 model.

The modifications suggested here imply that the spatial representation of soil parameters is currently not appropriate since only soil depth data were used. It suggests other factors should also be accounted as the type of geology and, ideally, information on the depth of weathered bedrock. However the maximum infiltration rate in Summer, $I_{\mathrm{max,summer}}$, could also

be responsible for the mismatch between observed and simulated $S_{\text{PQ.dry}}$.

Figure 6.1 shows that simulated $S_{\text{PQ.wet}}$ are overestimated for all catchments but Claduègne. According to the results of the sensitivity analysis, these results might indicate too much evapotranspiration demand, i.e. too large K_{crop}, for these catchments. However, as discussed above for S_{RC} such a modification is probably not relevant given the small differences in K_{crop} between land-use classes. Another possible issue might be related to the seasonal variation of K_{crop}. Given that $S_{\text{PQ.wet}}$ focuses on the wet months, hence outside of Spring and Summer where large evapotranspiration is expected, these results might indicate that a stronger seasonal variation might be needed for forests (currently varying between 1, in Winter, and 1.2, in Summer, see Table 2.7). For example, it could be reasonable to specify lower K_{crop} for forests during Fall and Winter (e.g. around 0.8 or even 0.5), in particular for deciduous trees. Such a modification could also explain the overestimation of evapotranspiration indicated by the underestimated S_{RC}.

The overestimated simulated $S_{\text{PQ.wet}}$ found for Meyras, Pont-de-Labeaume and Goulette might also suggest not enough or not fast enough soil drainage (too large K_{LPSout}) after the re-wetting period resulting in not enough streamflow during this period. These results are consistent with what was suggested above in the case of S_{RC}: K_{LPSout} should be distributed according to the type of soils and allow for more drainage in the case of Meyras, Pont-de-Labeaume and Goulette. However, results of the sensitivity analysis indicated that $S_{\text{PQ.dry}}$ was also weakly related to K_{LPSout} (see Figure 5.8). Therefore, it is likely that modifying K_{LPSout} will also affect $S_{\text{PQ.dry}}$ and according to the sensitivity analysis results, not in the desired way (see Figure 5.9).

Finally, $S_{\text{PQ.wet}}$ was also found linked, although only weakly, to groundwater storage depletion, τ_{RG}, indicating that the overestimated simulated $S_{\text{PQ.wet}}$ found for Meyras, Pont-de-Labeaume and Goulette could be explained by other model issues related to groundwater processes (see Section 6.1.2).

6.1.1.3 Soil infiltration

To investigate the partitioning of water at the ground surface, the results of the sensitivity analysis suggested that $S_{\text{PQ.dry}}$ and $S_{\text{PQ.date}}$ were relevant hydrological signatures. The underestimation of simulated $S_{\text{PQ.dry}}$ found for all catchments (Figure 6.1) suggests that the maximum infiltration rate in Summer, $I_{\text{max,summer}}$, is too small resulting in too much overland flow during the dry months of the re-wetting period. Similarly, according to the results of the sensitivity analysis (Figure 5.9), the overestimation of simulated $S_{\text{PQ.date}}$ found for all catchments (Figure 6.1) suggests that the maximum infiltration rate in Summer, $I_{\text{max,summer}}$, and in Winter, $I_{\text{max,winter}}$, are too small and too large respectively.

Parameters $I_{\text{max,summer}}$ and $I_{\text{max,winter}}$ are currently lumped and set at 40 mm/day and 50 mm/day respectively. Results suggest that $I_{\text{max,summer}}$ should be larger than $I_{\text{max,winter}}$. Typically, if neglecting the repealing effect of dry soils, soils are expected to have a larger maximum infiltrate rate in dry conditions than in wet conditions. Since the difference between $I_{\text{max,summer}}$ and $I_{\text{max,winter}}$ should not be too large to remain within a realistic parameterization, these results suggest $I_{\text{max,summer}}$ should be increased by at least 10 mm/day but not more than

20 mm/day or 30 mm/day.

6.1.2 Percolation and groundwater storage and release

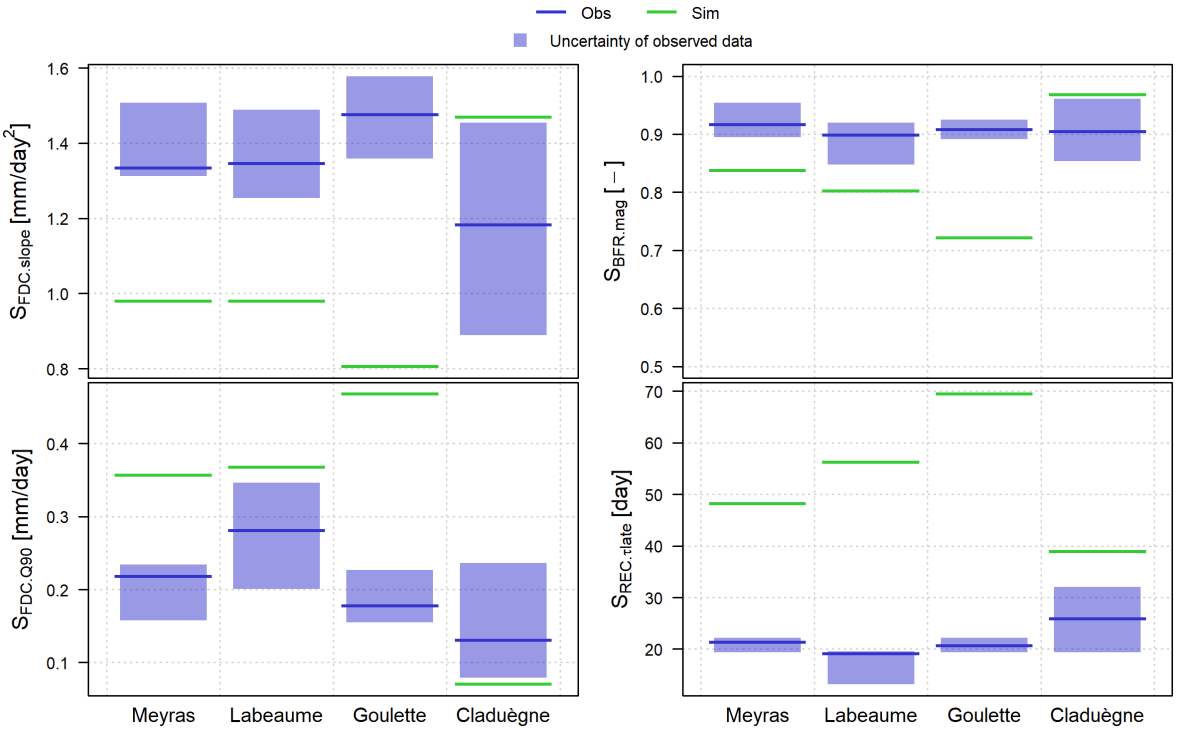

Figure 6.2: Observed and simulated hydrological signatures focusing on groundwater processes. Results are shown for the four study catchments.

6.1.2.1 Partitioning between vertical and lateral drainage

The results of the preliminary diagnostic of the J2000 Ardèche model (Section 5.1) suggested, in the case of Meyras, Pont-de-Labeaume and Goulette, not enough soil drainage and too much vertical drainage at the expanse of lateral drainage. The results of the sensitivity analysis (Section 5.3) showed that $S_{\text{FDC.slope}}$ (slope of the mid-segment of the flow duration curve) and $S_{\text{REC.}\tau\text{late}}$ (late recession time) were the most relevant hydrological signatures to focus more specifically on the partitioning between vertical and lateral soil drainage, i.e. on the two lumped parameters K_{latvert} and P_{max}. The effect of parameter K_{latvert} was found correlated with the average catchment slope; it affects mostly Meyras and Pont-de-Labeaume and only slightly Goulette. On the other hand, parameter P_{max} affect the vertical/lateral drainage partitioning regardless of catchment slope.

Figure 6.2 shows that simulated $S_{\text{FDC.slope}}$ is underestimated for all catchments except Cladugne where it is slightly overestimated. It also shows that simulated $S_{\text{REC.}\tau\text{late}}$ is overestimated for all catchments, in particular, Meyras, Pont-de-Labeaume and Goulette. These results suggest too much percolation, i.e. that parameter K_{latvert} is too small and P_{max} too large. Modifying K_{latvert} will mostly affect Meyras and Pont-de-Labeaume and only slightly Goulette where the worse mismatches between observed and simulated $S_{\text{FDC.slope}}$ and $S_{\text{REC.}\tau\text{late}}$ are found (Figure 6.2). Therefore, it is more likely that the lateral/vertical drainage partition-

ing issue might be caused by a too large maximum percolation rate $P_{\max}$. Because K_{latvert} does not have any effect on Claduègne, parameter τ_{RG} is found more influential for $S_{\text{FDC.slope}}$ and $S_{\text{REC.}\tau\text{late}}$. It could be possible that K_{latvert} needs to be increased to affect Meyras, Pont-de-Labeaume and possibly Goulette while issues in the groundwater depletion rate, τ_{RG}, explains the hydrological signature mismatch in the case of Claduègne.

Detailed results of the sensitivity analysis (see Appendix F.2, e.g. Figure F.3) show that the effect of $P_{\max}$ is a consequence of its large effect when specified below approximately 5 mm/day; for larger values of $P_{\max}$, the parameter has no effect on the model behavior. Statistics on percolation rate internal model variable, P_{perc}, in the default simulation, shows that P_{perc} is on average much lower than the default $P_{\max}$ value, set at 20 mm/day: for example, over the period 1990-2010, catchment average P_{perc} never exceeds 16 mm/day for all catchments. Therefore, the results of the sensitivity analysis reflect that, regardless of soil drainage (i.e. the amount of water released from soil that is partitioned between later and vertical flux), only very low $P_{\max}$ values can affect the actual percolation rate. It is difficult to predict how decreasing $P_{\max}$ would affect the different catchments, in particular if soil storage is to be increased as suggested in Section 6.1.1; soil storage increase implies smaller soil drainage rates and hence smaller percolation rates. While decreasing $P_{\max}$ can be a possible option to increase lateral drainage, the small range of possible values (e.g. between 1 mm/day and 5 mm/day) implies that small changes will have large effect on model behavior making modifications difficult.

We focused here on how modifying parameters K_{latvert} and $P_{\max}$ could help in increasing lateral drainage. However, the amount of lateral drainage and percolation can also be controlled by groundwater storage capacity, $RG_{\max}$, a parameter which was also found to have a significant influence on $S_{\text{FDC.slope}}$ and $S_{\text{REC.}\tau\text{late}}$. Much lower $RG_{\max}$ value would imply that lateral soil drainage is generated because of a "saturated" RG reservoir. Such a model behavior is meaningful: it can represent the rise of the deep water table above the bedrock where, for example, the combination of preferential flow path ways connections and high hydraulic pressure induce a rise in lateral soil drainage. Such a model behavior does not affect the default model simulation due to the large $RG_{\max}$ values. Currently, given the default parameter values for $RG_{\max}$ (between 388 mm and 430 mm when aggregated at the catchments scales, see Table 2.10), the groundwater reservoir is never filled : considering the period 1990-2010, 95% of the time, the RG reservoir is filled at about 38% in the case of Meyras, Pont-de-Labeaume, and Goulette and 23% in the case of Claduègne.

6.1.2.2 Groundwater storage and release rate

The underestimated $S_{\text{FDC.slope}}$ for Meyras, Pont-de-Labeaume and Goulette could suggest a too large $RG_{\max}$ for these three catchments, in particular for Goulette. In addition, the overestimation of $S_{\text{REC.}\tau\text{late}}$ found for all catchments suggest that $RG_{\max}$ is too large for all catchments including Claduègne. Given that the differences are larger in the case of Meyras, Pont-de-Labeaume and Goulette and that in the case of Claduègne, $S_{\text{FDC.slope}}$ is not sensitive to $RG_{\max}$, these results suggest that $RG_{\max}$ should be decreased for all catchments, in particular Goulette (and possibly Pont-de-Labeaume).

The underestimated (resp. overestimated) $S_{\text{FDC.slope}}$ for Meyras, Pont-de-Labeaume and

Goulette (resp. Cladugne) could also suggest a too slow (resp. fast) groundwater depletion i.e. too large (resp. small) τ_{RG}. This is confirmed by the results of $S_{FDC.Q90}$ (the low flow percentile) and $S_{BFR.mag}$ (the baseflow regime magnitude), the latter being almost exclusively related to groundwater depletion rate.

In the case of Cladugne, τ_{RG} was found to have a strong effect on $S_{REC.\tau late}$ suggesting it should be decreased rather than increased as suggested considering $S_{FDC.slope}$, $S_{FDC.Q90}$ and $S_{BFR.mag}$. Only the overestimation of simulated $S_{REC.\tau late}$ suggests it should be decreased. Since the mismatch found for $S_{REC.\tau late}$ might also be due to too much groundwater storage, these results suggest that RG_{max} should be decreased for this catchment, in particular if τ_{RG} is to be increased. Therefore, the decrease of RG_{max} suggested for all catchments might need to be even larger in the case of Cladugne.

Given the larger overestimation (resp. underestimation) of $S_{FDC.Q90}$ (resp. $S_{BFR.mag}$) found for Goulette compared with Pont-de-Labeaume, we can suspect that τ_{RG} should be decreased more in the case of Goulette. Similarly, results might suggest τ_{RG} should be decrease slightly less in the case of Pont-de-Labeaume given the slightly smaller overestimation (resp. underestimation) of $S_{FDC.Q90}$ (resp. $S_{BFR.mag}$) found for this catchment.

Both τ_{RG} and RG_{max} are distributed according to the type of geology. Meyras, Pont-de-Labeaume and Goulette have similar geology, dominated by schists, metamorphic rocks and magmatic rocks, while Cladugne is dominated by carbonates and volcanic rocks (see Figure 2.21 and Table 2.1 in Chapter 2). Results suggest that RG_{max} should be decreased for all these geology classes. The inter-catchment differences suggest τ_{RG} should be decreased for schists and metamorphic rocks and magmatic rocks geology classes and possibly, slightly increased for carbonates and volcanic rocks geology classes.

The larger decreased of τ_{RG} suggested for Goulette compared with Pont-de-Labeaume cannot be solved given that these two catchments currently have very similar geologies in the model (see Figure 2.21). The current spatial representation of the geology in the model is not appropriate to account for differences between Goulette and Pont-de-Labeaume. Therefore, results suggest that distinguishing schists from other metamorphic rocks and in particular granite (currently considered as similar in the J2000 Ardèche model) is necessary given that Goulette is covered by 66% of schists geology, a type of geology mostly absent from the other 3 catchments (see Table 2.1 and Figure 2.2). Note that such a modification implies that the HRU delineation must be changed completely.

6.1.3 Overall model diagnostic

Overall, the diagnostic of the model highlighted several issues in the representation of hydrological processes in the J2000 model regarding its parameterization and structure. General recommendations to improve the model behavior were suggested. The main issues that were identified, and the general recommendations are summarized below.

Soil processes

Results suggested not enough soil storage for all catchments indicating that LPS_{max} should

be increased for all catchments. Using only soil depth data to distribute in space the soil storage capacity, particularly for the LPS reservoir, might be inappropriate. Results suggest that geological characteristics should be accounted for since weathered bedrock might need to be considered when specifying the overall soil storage capacity.

Results also suggested a possible need to distribute K_{LPSout} according to the types of soils to allow for different "drainability" characteristics depending on the soil texture or other soil (or weathered bedrock) characteristics (e.g. preferential flow paths). Finally, a possible issues in the specification of the maximum infiltration rates was identified suggesting that it should be larger during Summer, i.e. $I_{\mathrm{max,summer}}$ should be increased.

Groundwater processes

While possible issues in the specifications of lumped parameters P_{max} and K_{latvert} were suggested, results globally pointed toward issues in the groundwater storage and release characterisitics, i.e. the distributed parameters RG_{max} and τ_{RG}. Results suggested groundwater storage should be decreased for all catchments, in particular Cladu\`egne and Goulette. They also suggested $\tau_{\mathrm{RG}}$ should be decreased for Meyras, Pont-de-Labeaume and Goulette and increased for Cladu\`egne. Finally, possible issues in the spatial representation of geology related to the distinction of schists from metamorphic rocks in order to represent the difference in behavior of Goulette in comparison to Pont-de-Labeaume were also highlighted.

6.2 Improvement of the J2000 Ardèche model processes realism

The model modification recommendations resulting from the in-depth diagnostic detailed in Section 6.1.1 and 6.1.2 and summarized in Section 6.1.3, need to be tested and evaluated. The modifications we propose to undertake are presented in detail in Section 6.2.1. The results of these modifications are then evaluated in Section 6.2.2 using hydrological signatures, performance metrics and visual comparison of streamflow time series.

6.2.1 Model modifications

6.2.1.1 Considered modification recommendations

Some of the modification recommendations point toward structural deficiencies of the J2000 Ardèche model related to the spatial representations of soils and geology. As a consequence, addressing these issues would require modifying the HRU delineation by considering other input spatial data to distribute soil and geology parameters. While such modifications should be tested in future research, they are not considered here. However, as detailed below, it is possible to test some of these suggested modifications within the current spatial representation of soils and geology.

In addition, a "conservative" approach was considered for the selection of model modifications. That is, when competing modifications are suggested, we chose in priority the one that implies the less or smallest change (from the default parameterization) unless strong evidence suggests otherwise.

Soil infiltration, storage and release

Among the modification recommendations, the increase of soil storage, mainly related to parameter $LPS_{\max}$, suggested issues in the current spatial representation of soils. Results suggested that geological information should also be accounted for as weathered bedrock might have a significant effect on the actual soil storage. Modifying the J2000 Ardèche model accordingly would require to compute new HRUs with new spatial data, a modification that was not considered here. Given the current spatial representation of soils (Figure 2.21), we applied the change to the current soil classes, i.e. the "shallow", "medium-to-shallow", "deep-to-shallow" and "deep" soil classes (although these names might no longer be relevant).

Results also suggested that lumped parameter K_{LPSout} should be modified and distributed in space. However, this change was not considered here since it might affect other hydrological signatures in undesired ways and other changes are possible to solve the identified issues. Modification of the crop coefficients was also not considered, at least at first, because it might only compensate for biases in forcing data.

Regarding soil infiltration, results suggested the maximum infiltration rate in Summer, $I_{\text{max,summer}}$, should be increased and be larger than $I_{\text{max,winter}}$, to allow for more infiltration during large precipitation events. Decreasing $I_{\text{max,winter}}$ was also suggested by the results. However, to keep the difference between $I_{\text{max,winter}}$ and $I_{\text{max,summer}}$ small, only the increase of $I_{\text{max,summer}}$ was considered.

Percolation and groundwater storage and release

Results suggested the lumped parameters K_{latvert} and $P_{\max}$ might need to be modified to allow for more lateral drainage at the expanse of percolation. However, inter-catchment differences in hydrological signatures did not enable a clear recommendation as to how they should be modified to appropriatly solve the hydrological signature mismatch for all catchments. Moreover, the distributed parameters $RG_{\max}$ and τ_{RG} could also explain the differences between observed and simulated hydrological signatures, including the increase of lateral drainage. Therefore, following our conservative approach, we only considered the modification of $RG_{\max}$ and τ_{RG}.

Results suggested schists and metamorphic rocks should be distingished in the distribution of $RG_{\max}$ and τ_{RG} to solve inter-catchment differences, particularly between Goulette and Pont-de-Labeaume. However, since such a modification would require re-computing HRUs accordingly, this modification was not considered. Modifications of $RG_{\max}$ and τ_{RG} for the different geology classes was only considered within the current geology spatial distribution.

6.2.1.2 Methodology and resulting modifications

Methodology

The results of the sensitivity analysis can only suggest how parameters can be modified, i.e. they provide information only on whether parameters should be increased or decreased. Therefore, no clear cut recommendations regarding the actual parameter values that should be specified were provided in the diagnostic of the model. To overcome this limitation, a trial-and-error approach was followed to modify the model in order to resolve the mismatch between observed and simulated hydrological signatures.

Starting from different modification recommendations (e.g. the mismatch between observed and simulated $S_{\text{BFR.mag}}$ which was found almost exclusively related to τ_{RG}), parameters were modified, staying within realistic range, and results were analyzed considering the following questions: (1) did the change improve the match of the considered hydrological signature? (2) was the magnitude of the change too large or too small? (3) were other hydrological signatures impacted in an undesired way? and if so, are there other (meaningful) modifications that can compensate? This iterative process allowed us to identify gradually which were the most relevant changes, in terms of magnitude, for all parameters. It was repeated several times considering different hydrological signatures as starting point in order to verify whether no other modifications could achieve similar or better results (in terms of hydrological signature match). The new parameter values were specified so they could be still considered realistic or at least reasonable given the J2000 model structure and our knowledge regarding the actual hydrological processes occurring in the study catchments.

Intermediate results of the trial-and-error process are not presented. Only the end result is presented and the associated modifications are described in the next paragraphs.

Modifications

Table 6.1 summaries the changes that were considered for the parameters distributed ac-

Table 6.1: Parameters distributed according to soil and geology, before (default simulation) and after (new simulation) modification. Only the geology classes that are relevant for the study catchments are shown here.

		deep	medium-deep	medium-shallow	shallow
Soils	*Parameter* $LPS_{\max}$ [mm]				
	Default	250	180	140	130
	New	325	300	275	250
	Parameter $MPS_{\max}$ [mm]				
	Default	123	86	54	25
	New	150	130	110	90
		Schists / Metamorphic	Magmatic	Carbonates	Volcanic
Geology	*Parameter* $RG_{\max}$ [mm]				
	Default	400	500	500	200
	New	70	70	50	50
	Parameter τ_{RG} [day]				
	Default	30	30	20	20
	New	20	20	30	30

cording to soil and geology. Only one lumped parameter, the maximum infiltration rate in Summer $I_{\max,\mathrm{summer}}$ was changed. It was set at 70 mm/day (default value of 40 mm/day, see Table 2.6), that is, 20 mm/day above the maximum infiltration rate in Winter, $I_{\max,\mathrm{winter}}$ (set at 50 mm/day, see Table 2.6).

Table 6.1 shows that the $LPS_{\max}$ was largely increased for all soil classes, in particular the "medium-shallow" and "shallow" soil classes that affect Meyras, Pont-de-Labeaume and Goulette. The inter-classes differences were also kept to reflect that deeper soils are still expected for Claduègne compared to the other catchments. None of the recommendation suggested $MPS_{\max}$ to be increased. However, for consistency with $LPS_{\max}$, $MPS_{\max}$ was also increased for all soil classes, in particular those affecting Meyras, Pont-de-Labeaume and Goulette.

Table 6.1 shows that groundwater storage, $RG_{\max}$, was dramatically decreased for all the geology classes that are relevant for out study catchments. This large change was necessary to generate significant lateral flow for all catchments and was judged realistic given our lack of knowledge on actual groundwater storage. $RG_{\max}$ was decreased from values around 200-500 mm to values around 50-70 mm. $RG_{\max}$ is now set at 70 mm for schist/metamorphic rocks and magmatic rocks, the two geology classes affecting Meyras, Pont-de-Labeaume and Goulette, and at 50 mm, for carbonates and volcanic rocks, the two geology classes affecting mostly Claduègne.

Table 6.1 shows that groundwater depletion rate, τ_{RG}, wasn't modified much. Faster groundwater depletion rates were specified for schist/metamorphic rocks and magmatic rocks (from 30 days to 20 days) whereas slower groundwater depletion were specified for carbonates and volcanic rocks (from 20 days to 30 days).

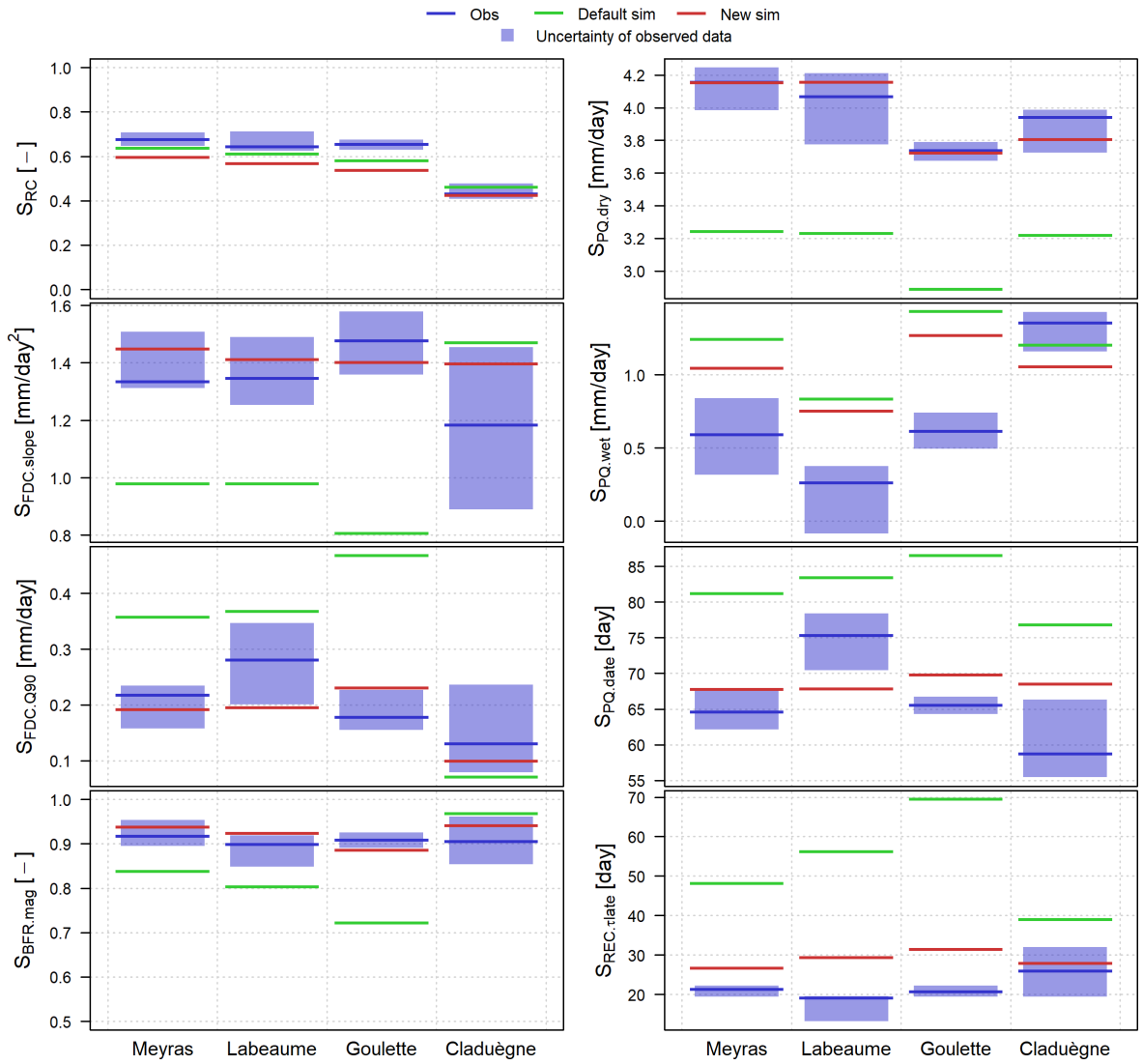

Figure 6.3: Observed and simulated hydrological signatures of the four study catchments. Two simulations are shown: the default simulation (green) and the new simulation (red), after the modifications of parameters $I_{\max,\text{summer}}$, $LPS_{\max}$, $MPS_{\max}$, $RG_{\max}$ and τ_{RG} were applied.

6.2.2 Evaluating the improvement of the J2000 Ardèche model

6.2.2.1 Improved match between observed and simulated hydrological signatures

Figure 6.3 shows the observed and simulated hydrological signatures, for the four study catchments, before and after the modifications detailed in the previous section were applied. Overall, it shows that the match between observed and simulated hydrological signatures has greatly improved for all catchments and all hydrological signatures, in particular for $S_{\text{FDC.slope}}$, $S_{\text{BFR.mag}}$ and $S_{\text{PQ.dry}}$. There are however a few exceptions: the larger underestimation of S_{RC} for Meyras, Pont-de-Labeaume and Goulette and the larger underestimation of $S_{\text{PQ.wet}}$ in the case of Cladugne. In addition, considering the uncertainties associated with the observed hydrological signatures, some differences are still too large to be acceptable: simulated $S_{\text{PQ.wet}}$ and $S_{\text{REC.}\tau\text{late}}$ are still overestimated for Meyras, Pont-de-Labeaume and Goulette and simulated $S_{\text{PQ.date}}$ is now underestimated for Pont-de-Labeaume and still overestimated for Goulette and Cladugne.

Figure 6.3 shows that simulated $S_{\text{REC.}\tau\text{late}}$ is still overestimated for Meyras, Pont-de-Labeaume and Goulette indicating that recessions are, on average, too slow in the model. None of the tested modifications was able to achieve a match for $S_{\text{REC.}\tau\text{late}}$ and these catchments without degrading the match of other hydrological signatures e.g. leading to an underestimated simulated $S_{\text{PQ.dry}}$ indicating too much streamflow during Fall or an overestimated $S_{\text{FDC.slope}}$ indicating a too flashy catchment. This results point toward possible issues in the structure of the J2000 model.

The larger underestimation of S_{RC} obtained for Meyras, Pont-de-Labeaume and Goulette shows that the long term overestimation of evapotranspiration was worsened by the increase of soil storage and hence the increase of the amount of water available for plant transpiration. Decreasing K_{crop} for forests as if they were only grassland (i.e. K_{crop} set at 1 throughout the year) was not enough to resolve the mismatch (results not shown). However, including large seasonal variations in K_{crop} for the forest land-use classes (K_{crop} varying between 0.2 in Winter and 1.2 in Summer) was able to improve the mismatch for both S_{RC} and $S_{\text{PQ.wet}}$ (see Figure 6.4). The improvement of $S_{\text{PQ.wet}}$ indicates that more streamflow is thus generated after the re-wetting period period. The other hydrological signatures were only marginally affected (results not shown). These additional results suggest that adding more seasonal variation in the evapotranspiration demand, in particular for forests, can improve the model behavior.

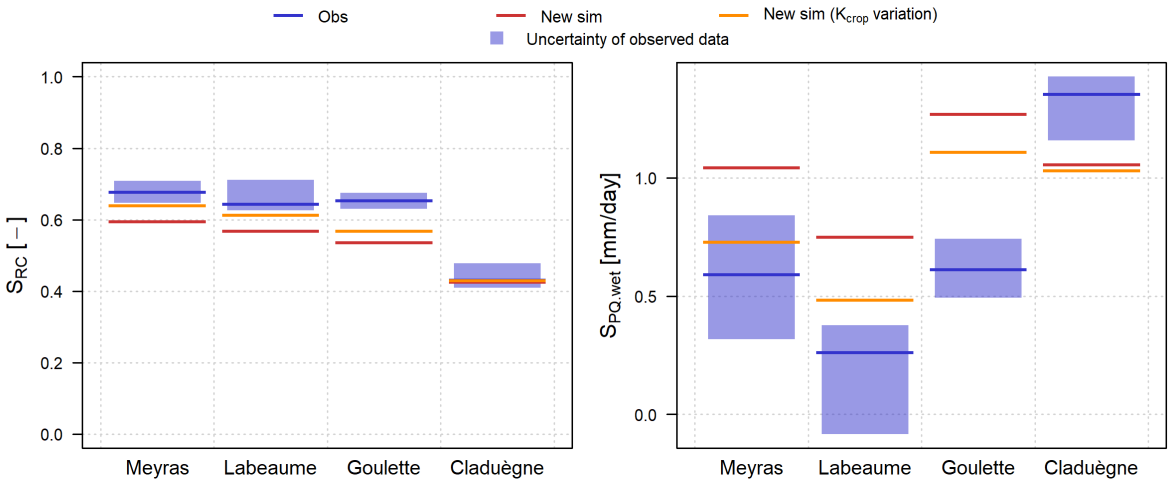

Figure 6.4: Observed and simulated S_{RC} and $S_{\text{PQ.wet}}$ of the four study catchments. Two simulations are shown: the new simulation with default values of K_{crop} for forest – between 1 and 1.2 – (red) and with a strong seasonal variation of K_{crop} for forests – between 0.2 and 1.2 – (orange).

It is also possible that an unknown structural deficiency of the model related to how plants are able to withdraw water from soils explains the overestimation of evapotranspiration. Because the land-use data were identified as possibly erroneous in the case of Cladugne (see Section 2.1.1.5), these results might also possibly indicate that the proportion of forests for these catchments are overestimated. For example, in the case of Goulette, the large proportion of garrigues (see Figure 2.21 and Table 2.1) seems unlikely given the average high elevation of the catchment (1149 m, see Table 2.1). As already mentioned, significant biases in the forcing data could also cause these results and a combination of all these causes is also possible.

Regarding signature $S_{\text{PQ.wet}}$, we were unable to find a combination of parameters that led to satisfactory results while not affecting negatively the other hydrological signatures. Only

including more seasonal variation in K_{crop} for forest was able to significantly decrease the mismatch without affecting the other hydrological signatures (see Figure 6.4). However, Figure 6.4 shows that the modification of K_{crop} is still not enough for Pont-de-Labeaume and Goulette and has worsened the results for Cladugne. This points toward a possible issue in the model structure that might be unable to account for different drainage characteristics depending on the catchment wetness state. This aspect of catchment functioning is currently controlled by parameter K_{LPSout} which modulates soil drainage according to the overall soil saturation. While it could be possible to distribute K_{LPSout} according to soil properties to account for the different behavior visible for Cladugne, these results might also suggest that a more complex mechanism might be needed to account for the observed larger streamflow contribution in wet conditions for Pont-de-Labeaume and Goulette. For example, the observed larger streamflow contributions observed in wet conditions might be due to a threshold behavior caused, for example, by the connections of preferential flow paths, currently not represented in the model.

6.2.2.2 Performance metrics

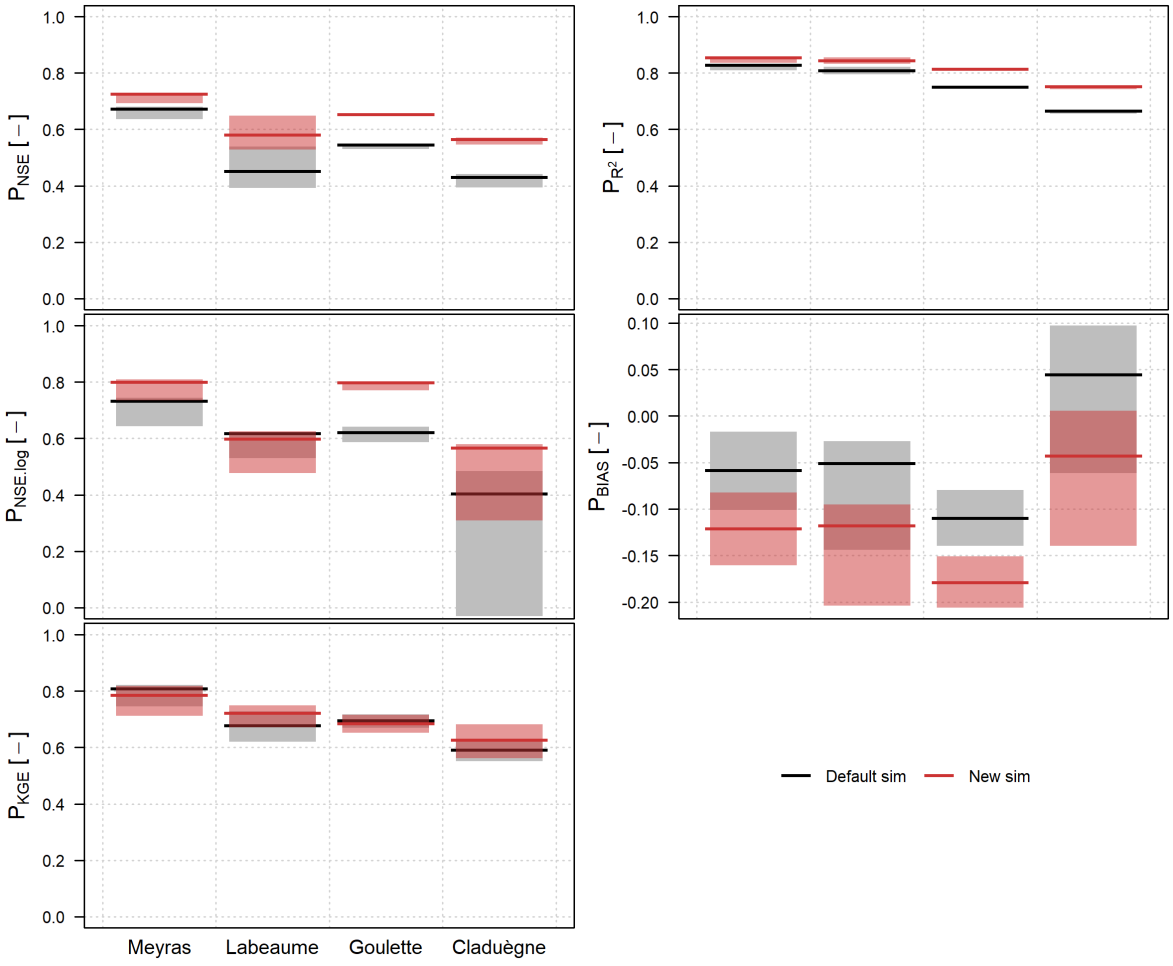

Figure 6.5: Performance metrics computed for the four study catchments before (Default simulation) and after (New simulation) the modifications of parameters $I_{\text{max,summer}}$, LPS_{max}, MPS_{max}, RG_{max} and τ_{RG} were applied.

Figure 6.5 shows the performance metrics computed for all catchments, before and after the modification of the model parameterization. Overall, it shows that performance metrics only

moderately improved. Better $P_{\text{NSE.log}}$ (except for Pont-de-Labeaume) and P_{R^2} are obtained. The performance, as measured by P_{KGE}, did however not increase much or even, for Meyras and Goulette, slightly decreased. Overall, these results illustrate that such performance metrics are unable to capture the large improvement we obtained in terms of hydrological processes realism – as measured by the hydrological signatures (Figure 6.3) –. Figure 6.5 also shows that the percent bias, P_{BIAS}, did worse. This reflects the larger overestimation of evapotranspiration reflected by the larger underestimation of S_{RC} (Figure 6.3).

6.2.2.3 Streamflow time series

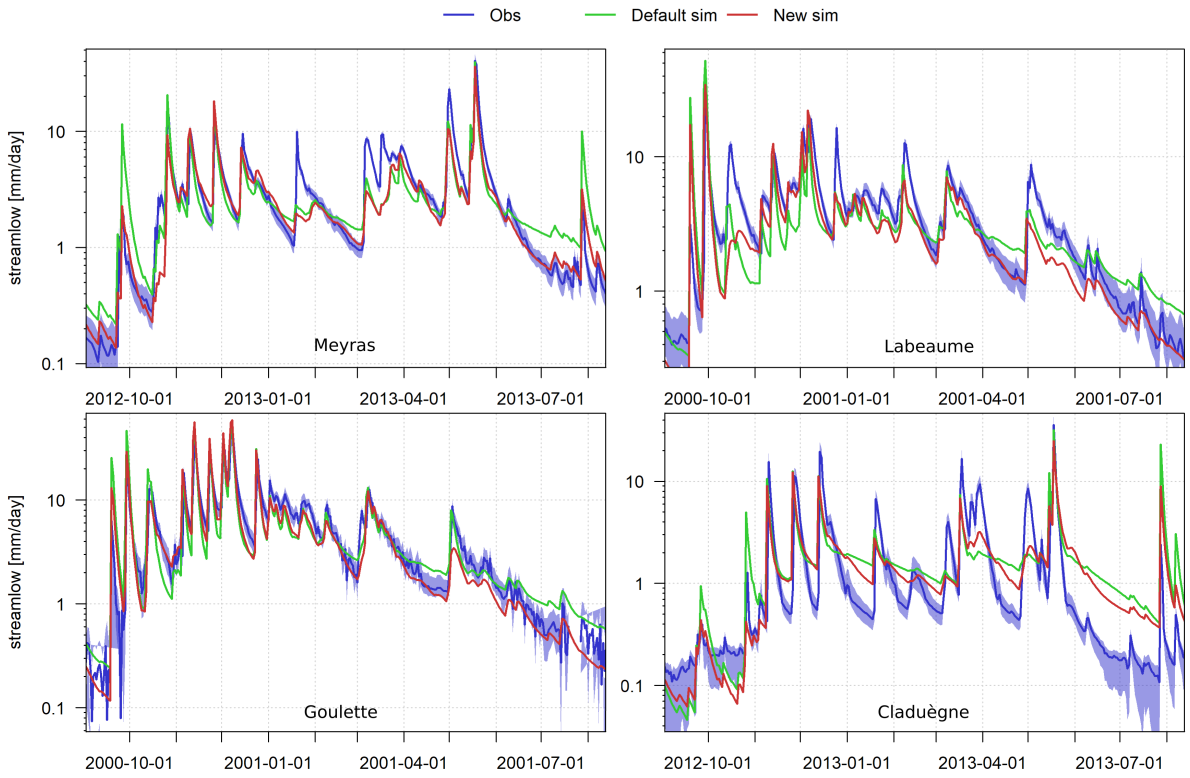

Figure 6.6: Observed and simulated streamflow time series of the four study catchments for a whole hydrological year (arbitrarily chosen: 2012-2013 for Meyras and Cladugne and 2000-2001 for Pont-de-Labeaume and Goulette). Two simulated streamflow time series are shown: before (Default simulation) and after (New simulation) the modifications of parameters $I_{\text{max,summer}}$, LPS_{max}, MPS_{max}, RG_{max} and τ_{RG} were applied.

Figure 6.6 shows the observed and simulated (before and after model modification) streamflow time series of the four study catchments for a whole hydrological year. It shows that, for all catchments, simulated catchment streamflow response dynamics has largely improved compared to the default simulation. However, we note that for Cladugne we obtained only a moderate improvement compared to the other three catchments; in particular low flows are still significantly overestimated. The main improvements that are visible in Figure 6.6 are the recession behaviors and low flow values for all catchments as well as the decrease of catchment responsiveness in the first months of the year (during the re-wetting period), particularly visible for Meyras. Figure 6.6 also shows that catchment streamflow during the wet months, following the re-wetting period, is still slightly underestimated (see for example Goulette) reflecting the remaining overestimation of $S_{\text{PQ.wet}}$ (Figure 6.3).

The moderate improvement visible for Claduègne in Figure 6.6 suggests important remaining issues for this catchment. However, this is not reflected by the hydrological signatures (Figure 6.3): for Claduègne, only $S_{\text{PQ.wet}}$ and $S_{\text{PQ.date}}$ remain underestimated and overestimated respectively with the larger underestimation of $S_{\text{PQ.wet}}$ reflecting the overestimated low streamflow during the wet months visible in Figure 6.6. As a consequence, during the step-by-step improvement of the model, we were unable to identify and correct these issues.

In the case of Claduègne, the differences between the observed and the new simulated streamflow time series (Figure 6.6) might suggest too much catchment storage (particularly groundwater storage) and/or not fast enough overall catchment release. However, by modifying parameters $MPS_{\max}$, $LPS_{\max}$, $RG_{\max}$ and τ_{RG}, we were unable to achieve better results while staying within realistic parameters ranges. For example, one of our "best" solution in terms of visual match between observed and simulated streamflow time series was to greatly decrease soil and groundwater storage to values around 50 mm and 20 mm for $LPS_{\max}$ and $MPS_{\max}$ respectively (results not shown). These values were considered too small to be realistic: it implied too large differences with the other catchments and very little soil storage for the catchment which should have the deepest soils (even if we could hypothesize no weathered bedrock in the case of Claduègne).

Further modifications were tested to improve simulated streamflow for Claduègne. Among the tested solutions, we found out that decreasing parameter K_{LPSout} (from 5 to 1, see Figure 2.17) improved the results, in terms of streamflow time series, even more than decreasing soil and groundwater storage (see results for Claduègne between January 2013 and May 2013, in Figure 6.7). However, it greatly impacted (negatively) other hydrological signatures (results not shown), in particular $S_{\text{PQ.dry}}$, reflecting that such a modification also implies much more streamflow during the re-wetting period (visible from September to November 2012 in Figure 6.7). This result supports the hypothesis of a structural issue in the way soils drain.

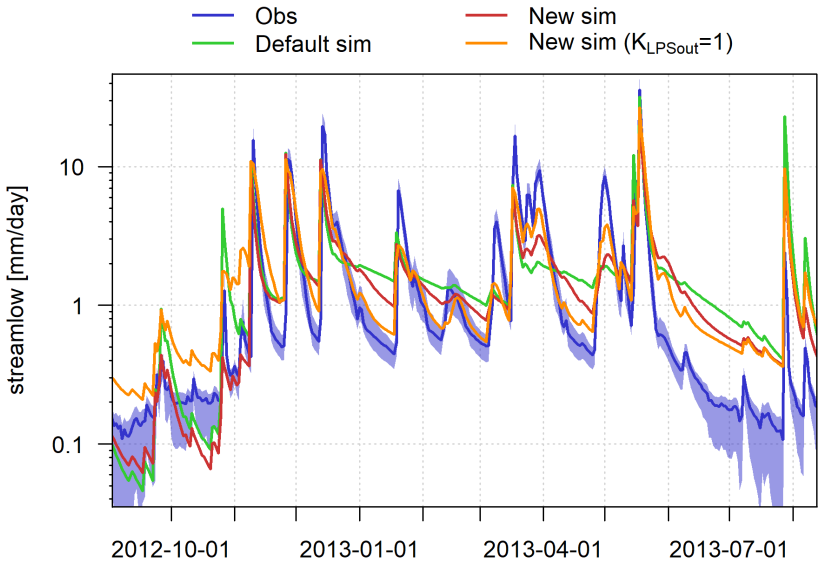

Figure 6.7: Observed and simulated streamflow time series of Claduègne for a whole hydrological year (arbitrarily chosen: 2012-2013). Three simulated streamflow time series are shown: before (Default simulation), after the modifications of parameters $I_{\max,\text{summer}}$, $LPS_{\max}$, $MPS_{\max}$, $RG_{\max}$ and τ_{RG} (New simulation) were applied and after modifying K_{LPSout} from 5 to 1.

As already mentioned, the implementation of soil drainage process, controlled by param-

eter K_{LPSout} and soil storage saturation, might not be sophisticated enough (see current implemetation in Section 2.3.2.6). In particular, it fails to account for a threshold behavior due to catchment wetness state, or at least a strong difference in catchment release characteristics between dry and wet conditions. These new results might indicate that very little soil drainage should occur when soils are dry and that drainage should increase quickly when a given soil saturation is reached. Also note that when soils are close to saturation, in the current implementation of soil drainage (Section 2.3.2.6), the LPS reservoir empties almost completely which appears unrealistic and could explain the overestimated streamflow during the wet months for Claduègne.

Since parameter K_{LPSout} is lumped, its modification implies that all catchments are affected. The differences between catchments might suggest K_{LPSout} should be distributed as already suggested earlier. However, this will introduce another degree of freedom in the model that might be unnecessary if the current implementation of soil drainage is modified. Overall, these results call for future investigation regarding the implementation of soil drainage and/or the potential value and implication of distributing K_{LPSout}. They also call for further investigation on the functioning of the Claduègne catchment.

6.3 Model improvement: limitations, implication and perspectives

6.3.1 Identified issues and new insights on the J2000 model

The methodology deployed in this chapter aimed at improving the representation of hydrological processes in the J2000 Ardèche model using hydrological signatures and their links with model parameters provided by the sensitivity analysis (Section 6.1). The improvement of the model, detailed in Section 6.2, reveled that mainly four parameters needed to be adjusted to improve the overall match between observed and simulated hydrological signatures: the large-pore soil storage reservoir size, $LPS_{\max}$, the groundwater storage size, $RG_{\max}$, the groundwater depletion rate, τ_{RG}, and the maximum soil infiltration rate in Summer, $I_{\max,\mathrm{summer}}$. This provides new insights into which are the primary parameters that are to be well specified to improve the overall model behavior.

To improve hydrological signatures match, the main modifications were the large increase (resp. decrease) of soil storage (resp. groundwater storage). The increase of soil storage was found consistent with the conclusions of other studies (e.g. Vannier et al., 2013; Braud et al., 2016b) that highlighted the significant role of weathered bedrock in the overall soil storage capacity that should be accounted for in hydrological models. Another modification was the increase of the maximum infiltration rate in Summer, $I_{\max,\mathrm{summer}}$, to decrease the amount of overland flow generated during large precipitation events during Summer and Fall.

The improvement of the model also provided new insights regarding the spatial distribution of soil and geological characteristics for the J2000 Ardèche model. As mentioned above, the importance of geological properties, i.e. the amount of possible storage in weathered bedrock, should be accounted in the spatial distribution of soils properties, i.e. parameters $MPS_{\max}$, $LPS_{\max}$. It was highlighted that the use of a soil database, primarily dedicated for agronomic studies, was irrelevant to specify soil properties, particularly if only considering a soil depth variable. Regarding the spatial distribution of geological properties, results also suggested that schists and other metamorphic rocks should be distinguished. In particular, schists were found to likely have faster release rates than other metamorphic rocks. In particular, compared to granite, schists have a physical structure organized in large flat "sheets" with a preferred orientation. This specific structure could arguably be responsible for higher hydraulic conductivity and therefore supports our modification recommendation.

Another issue that was identified was related to plant transpiration. Results suggested that much stronger seasonal variation in K_{crop} should be considered for forests. However, the issue identified might also be due, at least partly, to biases in the meteorological data used.

However, another possible issue related to soil drainage pointed toward a general structural deficiency of the J2000 model. It was suggested that the current soil drainage component of the J2000 model was inappropriate to represent a strong change in catchment streamflow release characteristics between dry and wet conditions. Although the identified issue might be only relevant for the J2000 Ardèche model, and more specifically, the Claduègne catchment, it could also be an issue affecting the models for any (or most) catchments. Since this missing behavior

can be related to the role of preferential flow paths or change in hydrodynamics properties according to soil saturation, it is likely a missing behavior for many catchments. Along with recent works on the Claduègne catchment (Huza et al., 2014; Uber et al., 2018, 2019), a new project is currently under construction. It could shed some lights into the Claduègne catchment functioning as well as soil drainage implementation in the J2000 model.

6.3.2 Limits and generalization of the methodology

The general methodology followed for the diagnostic and improvement of the J2000 Ardèche model can be summarized in the following steps:

1. select and/or design a set of hydrological signatures relevant for the investigated catchment;
2. understand the links between hydrological signatures and model parameters using a sensitivity analysis;
3. resolve the mismatch between observed and simulated hydrological signatures by modifying, in a meaningful and justifiable way, the model parameters;
4. evaluate the results by comparing hydrological signatures and streamflow time series to highlight remaining issues and identify possible structural model issues;

As discussed below, this methodology can (1) be applied to any catchment and any model, (2) be improved and (3) combined with other approaches

Application to other catchments and other hydrological models

The diagnostic and improvement of the J2000 Ardèche model was based on four study catchments. Although some general issues in the J2000 Ardèche model were identified, results are likely only relevant for these four catchments, not for the whole Ardèche catchment. In particular, considering distributed catchment characteristics according to soil, geology and land-use classes, only the classes represented in these four catchments were investigated.

To investigate properly the parameters distributed according to the different soil, geology and land-use classes, more catchments should be investigated. Both the diversity and similarity in terms of physical characteristics is important for that purpose. It is necessary to have catchments with all the different soil, geology and land-use classes to investigate the parameters of all the classes considered in the model. In addition, it is necessary to have catchments sharing the same classes to verify that consistent results (e.g. similar mismatch between observed and simulated hydrological signatures) are obtained for these catchments.

Given the large human influence on the Ardèche catchment, due mainly to the presence of dams, investigating other Ardèche sub-catchments is not straightforward. For most sub-catchments, it would require to "naturalize" streamflow time series using data provided by the dams managers as done for Pont-de-Labeaume. Another possibility would be to deploy the J2000 model on additional catchments. Following the preliminary investigation of Abdillahi Robleh (2019), the J2000 Rhône model (Branger et al., 2016), is currently subject to such a

diagnostic-evaluation approach with a set of 45 catchments with different types of geology (see Figure 6.8).

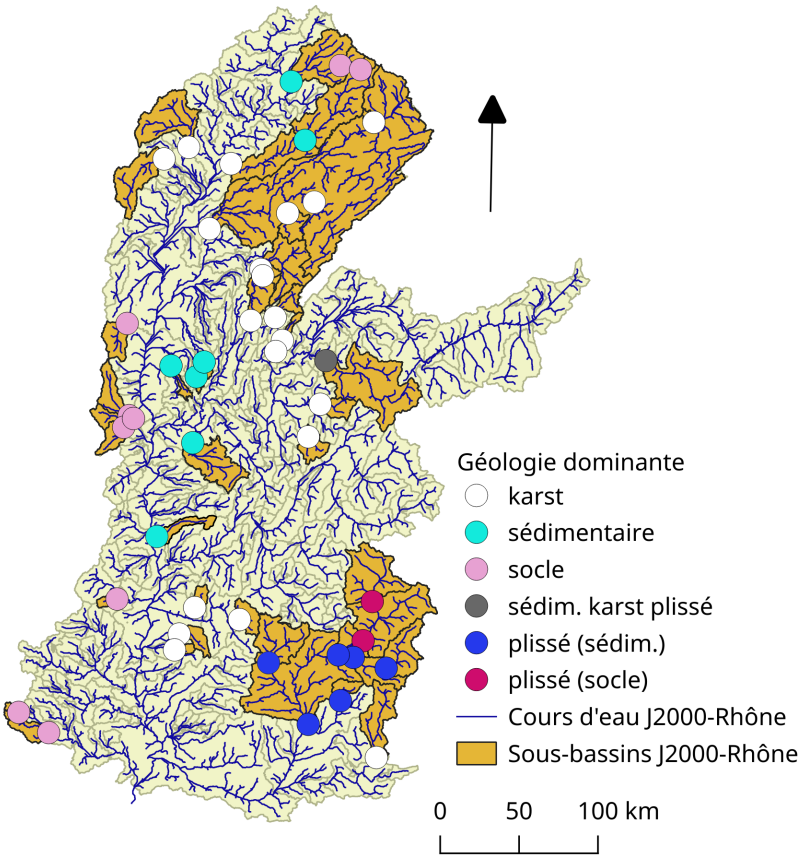

Figure 6.8: Rhône catchment and the 45 sub-catchments considered for a diagnostic-evaluation based on hydrological signatures

Finally, the diagnostic-evaluation methodology proposed in this chapter is not only applicable to the J2000 model. Other process-based and distributed models could also be investigated in a similar way. Such work could highlight what is only true for the J2000 model and what is consistent across different models. For example, given the structural differences of models, different hydrological processes implementations could be tested. To give another example, in the case of the Ardèche catchment, it could be verified whether similar magnitudes of soil and groundwater storage are recommended.

A manual calibration

The improvement of the model detailed in Section 6.2 was based on an iterative trial-and-error approach. Changes were iteratively made considering different hypotheses and reasoning on model functioning and actual catchment functioning. We always kept a particular attention to the change made by judging whether the new values were realistic. However, this approach remains a manual multi-objective calibration of the model and it necessarily implies some limitations inherent to any calibration. In particular, there are risks of modifying a parameters to compensate inappropriately for another mis-specified parameter leading to an improvement in the hydrological signatures not for the right reasons. However, we argue that such risks are

reduced due to (1) the manual calibration which allows reasoning at each step of the model improvement, (2) the use of hydrological signatures rather than performance metrics which allow process-based reasoning and (3) the fact that multiple hydrological signatures, characterizing catchment behavior in different ways, are used.

A possible future research could be focused on how the diagnostic and improvement of the model detailed in this chapter could be automated. Combining constraints on parameters (range of realistic values), process constraint (Hrachowitz et al., 2014) (e.g. $I_{\text{max,summer}}$ should be larger than $I_{\text{max,winter}}$, LPS_{max} should be larger than MPS_{max}, more evapotranspiration demand (larger K_{crop}) is expected for forests), multiple hydrological signatures and multiple catchments within an automatic or semi-automatic algorithm to search the parameter space for one or several optimal solutions could be possible. In addition, the uncertainty associated with observed data could be used to prevent over-fitting. Such an automatic calibration approach, although computationally intensive, would be more reproducible than the manual approach we followed here.

Split sample approach applied to the methodology

Hydrological signatures are used for both the diagnostic of the model and the evaluation of the "improved" model. More importantly, the same period of simulation was used for both. Our conclusions could be strengthened considering different simulation periods following the traditional split sample calibration-evaluation approach. Such an approach would be difficult to undertake in our case given that long time series are required for the computation of the hydrological signatures. However, while only 6 years of data were available for Claduègne, we were still able to have a relevant diagnostic of the model for this catchment suggesting that even 6 years of data might be sufficient. This relates to the robustness of the hydrological signatures with respect to irrelevant factor such as the length of the time series discussed in Chapter 4. Therefore, an important perspective of this work could be to apply the diagnostic-evaluation approach proposed in this chapter considering different periods for the diagnostic and evaluation of the "improved" model.

Strength and weaknesses of the hydrological signatures

The sensitivity analysis results enable the selection of a subset of 8 out of 12 hydrological signatures for the in-depth diagnostic of the model detailed in this chapter. They successfully provided relevant diagnostics and guidance when manually improving the model parameterization. Among the new hydrological signatures, original to this research, the baseflow regime magnitude, $S_{\text{BFR.mag}}$, provided valuable insights, in particular because it could be very clearly related to one particular model parameter, τ_{RG}. We also found that the slope of the P-Q curve during the re-wetting period and after, i.e. $S_{\text{PQ.dry}}$ and $S_{\text{PQ.wet}}$, were very valuable to properly constraint the model behavior during our manual model parameterization. These two hydrological signatures also allowed identifying the issue related to the change in soil drainage characteristics between dry and wet condition mentioned above.

The 8 hydrological signatures were all necessary to guide us in the improvement of the model. There are no evidence however that they were sufficient to diagnose and improve all

components of the model. The large differences between observed and simulated streamflow time series that were remaining for Claduègne after improving the model (Figure 6.6) where associated to only little mismatch between observed and simulated hydrological signatures. This result suggests that the 8 hydrological signatures used here might not be sufficient to fully characterize catchment behavior. Other hydrological signatures are likely required to be able to identify these remaining differences in catchment behavior.

Improved model realism?

This chapter was dedicated to the improvement of the J2000 Ardèche model focusing on how hydrological processes are represented within. An important question is: did we actually improve the realism of the model? This question relates to the main assumption underlying the use of hydrological signatures, that is, hydrological signatures are able to quantify and characterize differences in hydrological processes. By design, hydrological signatures are expected to be more relevant to assess model processes realism that regression based metrics. Following this assumption, we argue that by improving the match between observed and simulated hydrological signatures, we improved the process realism of the model.

Hydrological signatures are designed to capture what we can visually see in streamflow time series. By visually comparing observed and simulated streamflow time series to further evaluate the improvement of the model, we therefore took a step back and verified that the overall catchment streamflow was better reproduced. These comparisons confirmed that the overall model behavior improved. Finally, to further support the model realism was indeed improved, it is important to stress that most of the recommendations were not only guided by the hydrological signatures mismatches. Reasoning based on our knowledge of catchment functioning, taken from other studies, also guided, or at least justified, some of the changes made.

More generally, different approaches might be combined to further strengthen our conclusions. The use of hydrological signatures based on widely available data – the main purpose of this PhD thesis – could be combined to other approaches such as the detailed investigation of internal model behavior (e.g. Pfannerstill et al., 2015) or the use of other types of data (e.g. soil humidity (Branger and McMillan, 2020), groundwater level (Gottardi et al., 2012), remote sensing data (Mendiguren et al., 2017)) which provide an independent source of information. The diagnostic and improvement of the model could be deployed independently following these different approaches to strengthen, refine and validate the conclusions that may be drawn.

Conclusion

In this chapter an in-depth diagnostic of the model based on hydrological signatures focusing on soil processes and groundwater processes (Section 6.1) supported the improvement of the J2000 Ardèche model (Section 6.2). The improvement of the model involved two major modifications: (1) the increase of soil storage and (2) the decrease of groundwater storage. These parameters, related to the overall catchment storage and release characteristics are two of the main model issues that were corrected. The results also highlighted possible structural issues in the J2000 Ardèche model related to the spatial distribution of soil and geology parameters, and the implementation of soil drainage and plant transpiration. In Section 6.3, results were summarized and the methodology was discussed with respect to its current limitations and possible future research that could be undertaken.

We were able to obtain much better simulations considering the large decrease of the differences between observed and simulated hydrological signatures and streamflow time series. The diagnostic and improvement methodology followed in this chapter improved the overall model consistency in terms of behavior and its overall realism in terms of hydrological processes representation. These results highlight the usefulness of hydrological signatures for the diagnostic and process realism improvement of process-based distributed model such as the J2000 model.

General conclusion and perspectives

Synthesis

The research presented in this PhD thesis addressed two main scientific questions related to the information content of hydrological signatures and their use for the diagnostic, improvement and evaluation of a process-based distributed model: (1) *"How and how much information can be extracted from common hydrological data using hydrological signatures?"* and (2) *"How and how far can hydrological signatures be used to evaluate and derive diagnostics on a process-based distributed model?"*. To address the first question, we proposed a set of hydrological signatures, using commonly available data, including air temperature, and proposed a methodology to evaluate their information content using additional data that we illustrated on a set of snow dedicated signatures. To address the second question, we combined a sensitivity analysis with hydrological signatures to guide or interpretation of the signatures, evaluate their diagnostic power and undertake a diagnostic and improvement of a process-based distributed model. The main aspects of our approaches and our main results are synthesized in the paragraphs below.

Building a set of hydrological signature

Using only widely available data – streamflow, precipitation and air temperature – a set of hydrological signatures was built including already existing signatures as well as new ones. They were selected or designed in two distinct contexts: (1) the Mediterranean context of the Ardèche catchment (South East of France) focusing on four sub-catchments and using precipitation data and both observed and simulated (using the J2000 Ardèche model) streamflow time series (Chapter 4) and (2) the snow dominated mountainous context of the Southern Sierra (California, USA) where 10 catchments were investigated and air temperature was used in addition to precipitation and streamflow (Chapter 3).

Some hydrological signatures were directly taken from the literature: high/low flow percentiles and slope of the flow duration curve, runoff coefficient and baseflow index. Focusing on snow processes, hydrological signatures proposed by Schaefli (2016) were also investigated: timing of streamflow regime maxima, two signatures derived from the temperature-streamflow regime cycle, and a snow storage estimate derived from the Mass Curve Technique (MCT) approach. To complement this set of existing signatures, new signatures were also designed: baseflow regime magnitude, four signatures characterizing the seasonal change in streamflow response during and after the re-wetting period (the so-called P-Q approach) and early and late recession times characterizing streamflow recessions. The P-Q approach was also used to derive a snow storage estimate.

These hydrological signatures were selected or designed with a particular focus on their interpretation in terms of catchment functioning. Together, they can characterize long term emergent catchment behaviors at an annual, seasonal and event temporal scale in wide variety of hydro-climatic contexts.

Evaluating the information content of hydrological signatures

Chapter 3 presented a research, submitted and under review in *Hydrological Processes*, that focused on snow dedicated hydrological signatures and their information content. In this re-

search, using snow measurements (snow depth and snow water equivalent data), we verified whether our hypothesized interpretations were true, i.e. do the investigated snow hydrological signatures target the intended hydrological processes? We found that (1) the three signatures focusing on snow melt dynamics were relevant, (2) among the two investigated snow storage estimates (MCT and P-Q approaches) only the MCT approach yielded meaningful results despite the main method assumption being not true and (3) that no absolute quantification of snow processes was possible, i.e. only inter-catchments (and inter-years) differences were found relevant. Although these snow signatures were not investigated in a modeling context nor in the European Alps, we believe they can provide valuable insights in a modeling context, particularly for the J2000 Rhône model which includes many snow dominated catchments .

This research proposed an original approach that takes advantage of additional and rarely available data to verify the hypothesized interpretations of hydrological signatures in terms of hydrological processes. It highlighted the value of highly instrumented sites to evaluate the relevance of signatures and provide guidance for their interpretations when used in other catchments where additional data are not available.

Relevance and diagnostic power of hydrological signatures

In Chapter 5, we investigated the relevance and diagnostic power of the hydrological signatures presented in Chapter 4 using a sensitivity analysis of the J2000 Ardèche model with the signatures as outputs. This sensitivity analysis aimed at (1) identifying which parameters the hydrological signatures were sensitive to and (2) verifying, in the context of the J2000 Ardèche model, our hypotheses regarding the interpretations of the hydrological signatures. The results enabled the assessment of the diagnostic power of the hydrological signatures for the J2000 Ardèche model considering the specificity and strength of the links parameter-signature for each signature. Among the 12 investigated signatures 8 were found to have satisfactory diagnostic power. They were found related to two main aspects of the model functioning.: surface/soil processes and groundwater processes. The runoff coefficient, the slopes of the P-Q curve during and after the re-wetting period and date in the P-Q curve shift were identified as valuable hydrological signatures to focus on surface and soil processes, particularly on soil storage. The baseflow regime magnitude, the slope of the flow duration curve, the low flow percentile and the late recession time were found valuable to focus more specifically on groundwater processes including the partitioning between vertical and lateral soil drainage as well as groundwater storage and release.

We demonstrated the value of combining a sensitivity analysis with hydrological signatures to gain insights into how the hydrological signatures are to be interpreted in the context of the J2000 Ardèche model, a necessary step to guide us in its diagnostic and improvement. Furthermore, similarly to the evaluation of the relevance of hydrological signatures based on the use of additional data, this model-based approach was also found valuable to evaluate their information content.

Diagnostic and improvement of a distributed hydrological model

In Chapter 6, we presented an in-depth diagnostic of the J2000 Ardèche model. This work

combined the results of the sensitivity analysis (Chapter 5) and the visual comparisons of observed and simulated hydrological signatures to identify the main deficiencies of the J2000 Ardèche model.

The model diagnostic led to the formulation of improvement recommendations : the increase of soil storage and the decrease of groundwater storage for all types of soils and geologies, the increase or decrease of groundwater depletion rate depending on geology types and the increase of the maximum infiltration rates. These recommendations were the basis for the modification of the model which was done following a trial-and-error approach to gradually decrease the mismatch between observed and simulated hydrological signatures. We were able to significantly reduce these mismatches for most hydrological signatures reflecting an overall improvement of the model behavior.

The approach we followed also provided interesting insights into possible additional parameterization deficiencies of the J2000 Ardèche model related to the spatial distribution of soils and geological characteristics as well as on the representation of soil drainage and plant transpiration. We also found that the overall improved model behavior was only weakly reflected by performance metrics illustrating their weakness in assessing model behavior. However, visual comparisons of observed and simulated streamflow time series revealed that some issues remained, in particular for one of our study catchments. This suggested that our set of hydrological signatures was not sufficient to fully characterize the behavior of this catchment.

Genericity of the results and approaches

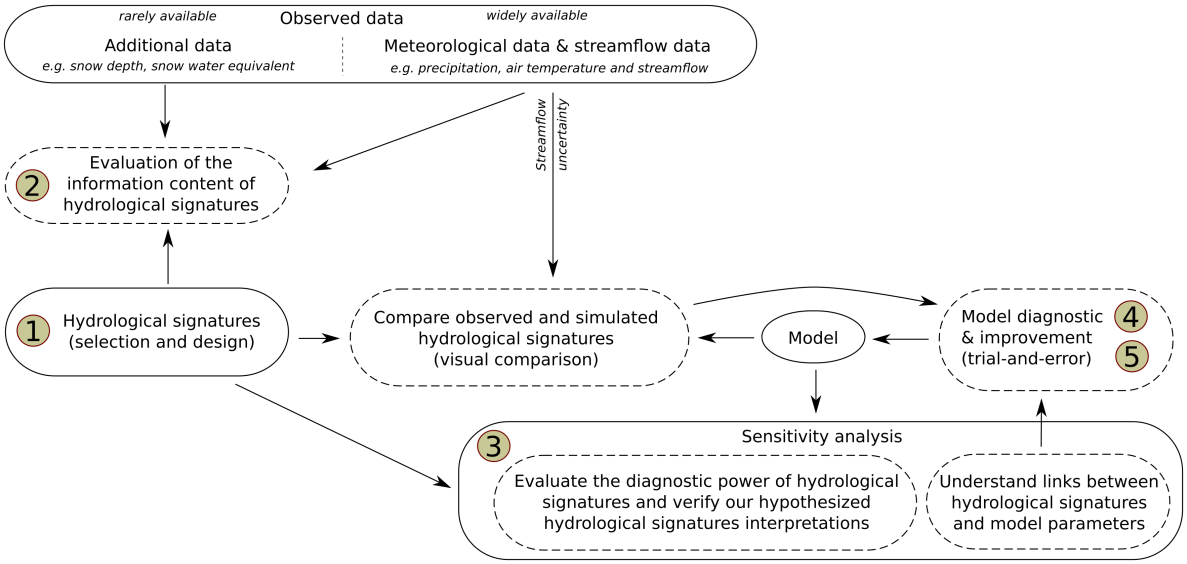

Figure B: General approach followed in the PhD thesis

The general approach followed in this PhD thesis can be summarized as follows (see Figure B):

1. selection and design of hydrological signatures;
2. evaluation of their information content using additional data to understand how they are related to particular hydrological processes;
3. evaluation of the diagnostic power of hydrological signatures by evaluating the specificity of the hydrological signatures to particular modeled processes and the strength of the links parameter-signature through a sensitivity analysis;
4. in-depth diagnostic of the model combining the results of a sensitivity analysis and visual comparisons of observed and simulated hydrological signatures;
5. model improvement following a trial-and-error approach;

As detailed in the next paragraphs, the different aspects of our methodology and some of our results are not specific to our study cases. They are relevant to many other catchments and other hydrological models.

Although the hydrological signatures were selected or designed in two specific contexts (Ardèche and Southern Sierra), they target different hydrological processes that are relevant for a wide variety of catchments beyond Mediterranean and snow dominated catchments. The emphasis on their interpretations in terms of hydrological processes and to collectively characterize long term emergent catchment behaviors at different temporal scale (annual, seasonal and event) supports their transposition to many other catchments around the world. However, they might not be suited for studies related to flood generation processes or in very different hydro-climatic contexts such as in arid or semi-arid regions where other dominant hydrological processes are at play. In addition, at large (e.g. larger than 1000 km^2) or very small (e.g.

smaller than 0.5 km^2) spatial scales, different emergent behaviors might need to be characterized requiring other or at least additional signatures. Nonetheless, within reasonably similar contexts as those of our study sites, the proposed set of hydrological signatures is relevant.

We proposed an original approach to evaluate the information content of hydrological signatures using additional data. This approach is not limited to our particular case study and could be transpose to any hydrological signatures – not only snow dedicated signatures – and make use of any type of additional data that might be available in other catchments. If the general idea of the approach is transferable, the specificity of the additional data and of the catchment can lead to challenging questions that are probably too specific to be part of a generic methodology. One particular challenge that likely applies in most cases, is the comparison of pieces of information that are derived from data representative of very different spatial and/or temporal scales. This was illustrated in our case with the comparison of catchment scale hydrological signatures with snow measurements at specific locations within the catchments, requiring particular attention in the interpretations and discussions of the results. Similar questions will inevitably arise when using soil moisture data or remote sensing data. Therefore, while the approach is not generic *per se*, we provided an example of application and demonstrated the potential of the approach that we hope can lead to future similar studies.

The sensitivity analysis we undertook enabled the evaluation of the diagnostic power of the hydrological signatures and the clarification of their interpretations (at least in the J2000 Ardèche context). To some extent, some of these results can be extrapolated to other catchments and models. However, two key points need to be considered carefully beforehand: the topographic characteristics and hydro-climatic context of the catchment as well as the structure (implementation of hydrological processes) of the model. Slightly different results were obtained depending on the study catchment caused by differences in topography (average catchment slope in our case) and meteorological characteristics (more intense and larger volume of precipitations at higher elevation in our case). These differences were related to different model parameters being found influential for some of the hydrological signatures, slightly affecting the way they could be interpreted. However, no significant inter-catchment differences in the overall diagnostic power of the signatures nor in the overall interpretation regarding the family of processes they are related to (soil/surface processes, groundwater processes) were found. Therefore, we argue that the diagnostic power and interpretation of the hydrological signatures can be extrapolated to catchments with similar topographic characteristics and climate.

Extrapolation to other models is possible providing that they clearly represent the two main families of processes we found our signatures targeted, i.e. soil/surface processes and groundwater processes, which is the case of most hydrological models. Such an extrapolation is however of limited interest for the diagnostic and improvement of a model as the clear link between signatures and parameters cannot be transferred. However, the general methodology we propose to evaluate the diagnostic power of hydrological signatures and understand their links with the model functioning is not limited to our case study. Such an approach could be applied to any catchments and any model, including lumped and distributed model. The approach is therefore generic and our research provided an example of how it could be deployed in the case of a distributed model.

Two particular aspects of the sensitivity analysis are worth pointing out as they likely apply

to any future application of the proposed approach. First, we want to highlight that removing most of the distribution in the sensitivity analysis, not only reduces computation time but makes the interpretation of the results easier. In our work, we suggested a specific method to limit the size of the parameter space to explore in the sensitivity analysis by considering distributed parameters as lumped. While we demonstrated it is a relevant method, alternatives are possible including the one employed by Höllering et al. (2018) who considered the dominant classes of geology/soil/land-use. Second, we argue that the use of a Global Sensitivity Analysis (GSA) rather than a One-At-a-Time (OAT) sensitivity analysis is necessary to fully evaluate the diagnostic power of hydrological signatures. A global sensitivity analysis accounts for interactions that can be used to evaluate the strength of the signature-parameter links, a key characteristics when evaluating the diagnostic power of a particular hydrological signature.

The combination of hydrological signatures and a sensitivity analysis, which has rarely been done for distributed models (e.g. Yilmaz et al. 2008; Höllering et al. 2018), is applicable to any catchment and any model (lumped or distributed). The originality of the approach we proposed is that this combination serves the building of an in-depth understanding of both the model behavior and the real catchment behavior. It focuses on this detailed understanding to guide the improvement of the model in term of hydrological processes realism. While in the case of lumped models (or models with limited distribution) this approach could (relatively easily) be automated – e.g. in a limits of acceptability framework and/or with processes/parameters constraint – in the case of distributed models it can be the basis of the expert-based manual model improvement approach they often require (e.g. Yilmaz et al. 2008; Braud et al. 2010; Rozalis et al. 2010; Branger et al. 2016; Fuamba et al. 2019).

Although the proposed set of hydrological signatures, the approaches developed during this PhD thesis and some of our results are, to some extent, generic, there are important limitations and many perspectives to further explore the use and usefulness of hydrological signatures. In the next paragraphs we summarize some of the main challenges that remain and perspectives for future research.

Perspectives

Selection, design and interpretation of hydrological signatures

The selection and design of hydrological signatures is determined by the objectives of a particular study and the context they are to be applied to. It can also be constrained by several aspects such as the available data or temporal resolution of time series (e.g. daily). In this PhD thesis, our study sites (the Ardèche sub-catchments and Southern Sierra catchments) and our model (J2000) mostly dedicated toward long-term studies guided and constrained the selection and design of the hydrological signatures (see for example Appendix E.1 which briefly presents hydrological signatures that were finally not retained in our work). An important perspective is therefore how other hydrological signatures might be used and be useful in other contexts, with different objectives and constraints. This is for example the case of hydrological signatures focusing on processes emergent at shorter time scales such as event based signatures to investigate fast flow generation processes and catchment threshold behaviors.

In our research we only briefly investigated the sensitivity of hydrological signatures to streamflow uncertainty and neglected the effect of other sources of uncertainty such as precipitation uncertainty. Precipitation uncertainties could be accounted for in various ways (e.g. Renard et al. 2011; Leblois and Creutin 2013; Caillouet et al. 2016; Devers 2019). They could have significant impact on some signatures including the runoff coefficient, particularly if accounting for possible biases (systematic errors). However, when comparing hydrological signatures between catchments or between observation and simulation, we made only a limited use of the streamflow uncertainty estimates. Therefore, a perspective would be to more clearly define how uncertainties are to be used in the diagnostic and improvement methodology. In particular, specific metrics could be used or developed to indicate whether differences between catchments or observation and simulation are significant. As mentioned by Horner et al. (2018b), comparing uncertain data affected by systematic errors remains an unsolved methodological challenge.

The uncertainty associated with hydrological signatures refers to their *identifiability* in the five guidelines proposed by McMillan et al. (2017) for the design of hydrological signatures. We only briefly investigated the hydrological signatures with respect to these guidelines. Therefore, another perspectives would be to investigate more thoroughly the set of signatures with respect to these guidelines. The relevance of the hydrological signatures in terms of *robustness* (with respect to time series length for example) and *consistency* (with respect to subjective choices necessary in the definition of some hydrological signatures) could be further investigated. Their *representativeness* (their ability to represent catchment scale behaviors) could also be further explored by focusing on nested catchments and how different spatial scales and degrees of spatial aggregation affect them. In particular, situations where two catchments nested within a larger one have very contrasting behaviors could be highly valuable to understand how hydrological signatures aggregate these two different behaviors similarly to the synthetic example proposed by McMillan et al. (2017). Finally, although not included in the guidelines of McMillan et al. (2017), their sensitivity to various human influences (e.g. uptakes, dams) could be evaluated to understand to what extent they might be relevant when applied to human-influenced catchments, i.e. the majority of catchments in the world.

There are also important perspectives regarding the role of other hydrological data types (e.g. soil moisture, groundwater levels, remote sensing) to derive more information on the functioning of catchments using hydrological signatures. First, the approach proposed in Chapter 3 where additional data are used to evaluate the information content of hydrological signatures deserves to be repeated in other catchments, using the same or other signatures, and using other types of additional data. Second, these other data types could also be used to derive meaningful hydrological signatures as already demonstrated by several authors (e.g. McMillan et al. 2011, 2014; Hrachowitz et al. 2014; Mackay et al. 2018; Heudorfer et al. 2019; Branger and McMillan 2020). In particular, hydrological signatures derived from remote sensing data, which are increasingly available at finer temporal and spatial scales, could provide meaningful insights into the functioning of catchments.

Model diagnostic and improvement of the methodology

The sensitivity analysis of the J2000 model using hydrological signatures as model outputs was found highly relevant to identify how they are related to model functioning. As discussed earlier, while some results could be extrapolated to other catchments and other model, it remains unclear as to what extent our results are model/catchment specific. Therefore, an interesting perspective would be to do sensitivity analyses in other hydro-climatic contexts and/or using other hydrological models. Such studies could clarify what is consistent or not across different catchments and different models, highlighting key catchment characteristics (e.g. topography, climate) and key model components, and possibly providing valuable insights into how hydrological signatures are to be interpreted in various hydro-climatic contexts, even outside of a modeling context.

The diagnostic and improvement of the J2000 Ardèche model was based only on 4 subcatchments. As a consequence, we were able to investigate only a relatively small proportion of the actual spatial heterogeneity of catchment physical characteristics represented in the model. There are therefore significant perspectives regarding how the spatial distribution of physical characteristic in a given model could be investigated. In particular, a much broader set of catchments is necessary to (1) investigate all the different types of land-use, soil and geology and (2) investigate the consistency for catchments that share similar characteristics. This can be related to the value of integrating in the methodology a "spatial cross evaluation" where a set of catchments (with as much diversity as possible) is used for the diagnostic and improvement of the model while another set of catchments is used to evaluate the resulting improved model. Such an improvement of the methodology, specific to distributed model, would greatly strengthen the confidence we have in the improved model regarding its overall spatial consistency.

While a "spatial cross evaluation" could bring significant improvement to the methodology, there are also methodological improvement perspectives into the integration of a "temporal cross evaluation". Hydrological signatures could be computed on two distinct periods for the diagnostic and improvement of the model and the evaluation of the improved model. This could also strengthen the confidence we have in the improved model in terms of hydrological processes realism and on the results of prospective studies.

The use of hydrological signatures in the diagnostic and improvement of the model can be seen as a way to translate a part of the expertise of the modelers, necessary in manual model improvement approaches, into process-based metrics. Therefore, it introduces more reproducibility in manual approaches which is often seen as one of their main drawback. However, the trial-and-error approach we followed in our work, for the improvement of the J2000 Ardèche model, is currently lacking a clear methodology that could be reproduced easily. We suggested to start the trial-and-error process focusing on one hydrological signatures – which we suggested could be the one the most specific to one parameter – and gradually improve the mismatch between observed and simulated hydrological signatures; we proposed a set of questions the modeler had to consider at each step and suggested the whole process should be repeated with different starting point (hydrological signature). However, this remains a relatively poor set of guidelines that call for future research into the definition of a clear and reproducible general methodology that could be applied to a distributed model.

J2000 application

Many technical adjustment and developments were made during this PhD that go beyond the development of *R* codes for the computation of hydrological signatures: some bugs were corrected for J2000 and HRU-Delin (tool used for the HRU delineation), a *R* user interface was developed to facilitate the set up of a J2000 model from *R* for any catchment and a detailed workflow for the application of a sensitivity analysis for any J2000 model was built. Therefore, new J2000 models can easily be deployed in other catchments, with the possibility to undertake new sensitivity analyses. These technical aspects are particularly helpful for future research using the J2000 model and to address some of the perspective that were listed above.

Among the possible future research involving the J2000 model, there are numerous possibilities related to the J2000 Rhône model that mirror some of the perspectives mentioned above. In particular, we would like to emphasize on the importance of extending the approach followed in the case of the Ardèche catchment to the whole Rhône catchment and include a much larger set of catchments as already initiated in the work of Abdillahi Robleh (2019). This would enable to investigate a larger diversity of catchments in terms of physical characteristics and a larger variety of hydro-climatic contexts that, among other things, could confirm some of our results obtained in the Ardèche catchment.

Bibliography

Abdillahi Robleh, K.
2019. Diagnostic du modèle hydrologique distribué J2000-Rhône à l'aide de signatures hydrologiques. Master's thesis, Sorbonne Université.

Adamovic, M.
2014. *Development of a data-driven distributed hydrological model for regional scale catchments prone to Mediterranean flash floods. Application to the Ardèche catchment, France.* PhD thesis, École Doctorale Terre Univers Environnement.

Adamovic, M., F. Branger, I. Braud, and S. Kralisch
2016. Development of a data-driven semi-distributed hydrological model for regional scale catchments prone to Mediterranean flash floods. *Journal of Hydrology*, 541:173 – 189.

Adamovic, M., I. Braud, F. Branger, and J. W. Kirchner
2015. Assessing the simple dynamical systems approach in a Mediterranean context: application to the Ardèche catchment (France). *Hydrology and Earth System Sciences*, 19(5):2427–2449.

Allen, R. G., L. S. Pereira, D. Raes, and M. Smith
1998. Crop evapotranspiration - Guidelines for computing crop water requirements - FAO Irrigation and drainage paper 56. *FAO - Food and Agriculture Organization of the United Nations, Rome, 1998.*

Andrieu, J.
2015a. Landcover map Ardèche, Cèze and Gardon basins. Technical report, ESPRI/IPSL.

Andrieu, J.
2015b. Landcover map Cladu̇ègne catchment. Technical report, ESPRI/IPSL.

Anquetin, S., I. Braud, O. Vannier, P. Viallet, B. Boudevillain, J.-D. Creutin, and C. Manus
2010. Sensitivity of the hydrological response to the variability of rainfall fields and soils for the gard 2002 flash-flood event. *Journal of Hydrology*, 394(1):134 – 147.

Arnold, J. G., R. Srinivasan, R. S. Muttiah, and J. R. Williams
1998. Large area hydrologic modeling and assessment Part I: model development. *JAWRA Journal of the American Water Resources Association*, 34(1):73–89.

Bahl, N.
2016. Dérivation de paramètres caractéristiques du sol pour la modélisation hydrologique sur la région rhône-alpes. mathesis, ENGEES.

Bales, R., M. Goulden, C. Hunsaker, M. Conklin, P. Hartsough, A. O'Geen, J. Hopmans, and M. Safeeq
2018. Mechanisms controlling the impact of multi-year drought on mountain hydrology. *Scientific Reports*, 8(1).

Bales, R. C., J. W. Hopmans, A. T. O'Geen, M. Meadows, P. C. Hartsough, P. Kirchner, C. T. Hunsaker, and D. Beaudette
2011. Soil moisture response to snowmelt and rainfall in a sierra nevada mixed-conifer forest. *Vadose Zone Journal*, 10(3):786–799.

Bart, R. R. and C. L. Tague
2017. The impact of wildfire on baseflow recession rates in california. *Hydrological Processes*, 31(8):1662–1673.

Beck, H. E., A. I. J. M. van Dijk, A. de Roo, E. Dutra, G. Fink, R. Orth, and J. Schellekens
2017. Global evaluation of runoff from 10 state-of-the-art hydrological models. *Hydrology and Earth System Sciences*, 21(6):2881–2903.

Betson, R. P.
1964. What is watershed runoff? *Journal of Geophysical Research (1896-1977)*, 69(8):1541–1552.

Beven, K.
1989a. Changing ideas in hydrology — the case of physically-based models. *Journal of Hydrology*, 105(1):157 – 172.

Beven, K.
1989b. *Interflow*, Pp. 191–219. Dordrecht: Springer Netherlands.

Beven, K. and A. Binley
1992. The future of distributed models: Model calibration and uncertainty prediction. *Hydrological Processes*, 6(3):279–298.

Beven, K. J.
2000. Uniqueness of place and process representations in hydrological modelling. *Hydrology and Earth System Sciences*, 4(2):203–213.

Beven, K. J. and M. J. Kirkby
1979. A physically based, variable contributing area model of basin hydrology / un modèle à base physique de zone d'appel variable de l'hydrologie du bassin versant. *Hydrological Sciences Bulletin*, 24(1):43–69.

Blöschl, G., R. Kirnbauer, and D. Gutknecht
1991. Distributed snowmelt simulations in an alpine catchment: 1. model evaluation on the basis of snow cover patterns. *Water Resources Research*, 27(12):3171–3179.

Blöschl, G. and M. Sivapalan
1995. Scale issues in hydrological modelling: A review. *Hydrological Processes*, 9(3-4):251–290.

Blume, T., E. Zehe, and A. Bronstert
2007. Rainfall-runoff response, event-based runoff coefficients and hydrograph separation. *Hydrological Sciences Journal*.

Bonnet, S.
2012. Cartographie des zones potentielles de production ou d'accumulation du ruissellement de surface en région Cévenole. mathesis, Université Montpellier 2 – Faculté des Sciences.

Branger, F., I. Braud, S. Debionne, P. Viallet, J. Dehotin, H. Henine, Y. Nedelec, and S. Anquetin
2010. Towards multi-scale integrated hydrological models using the liquid® framework. overview of the concepts and first application examples. *Environmental Modelling & Software*, 25(12):1672 – 1681.

Branger, F., I. Gouttevin, F. Tilmant, T. Cipriani, C. Barachet, M. Montginoul, C. Le Gros, E. Sauquet, I. Braud, and E. Leblois
2016. Modélisation hydrologique distribuée du Rhône, Rapport Final. techreport, Irstea.

Branger, F., S. Kermadi, C. Jacqueminet, K. Michel, M. Labbas, P. Krause, S. Kralisch, and I. Braud
2013. Assessment of the influence of land use data on the water balance components of a peri-urban catchment using a distributed modelling approach. *Journal of Hydrology*, 505:312 – 325.

Branger, F. and H. K. McMillan
2020. Deriving hydrological signatures from soil moisture data. *Hydrological Processes*, 34(6):1410–1427.

Braud, I., J. Andrieu, P. Ayral, C. Bouvier, F. Branger, J. Carreau, G. Delrieu, J. Douvinet, R. Freydier, E. Leblois, J. Le Coz, P. Martin, G. Nord, N. Patris, S. Perez, B. Renard, J. L. Seidel, and J. Vandervaere
2016a. Floodscale : Observation et modélisation hydro-météorologique multi-échelles pour la compréhension et la simulation des crues éclairs, rapport scientifique final du projet, anr-2011 bs56 027 01.

Braud, I., J. Andrieu, P.-A. Ayral, C. Bouvier, F. Branger, J. Carreau, G. Delrieu, R. J. Douvinet, Freydier, E. Leblois, J. L. Coz, P. Martin, G. Nord, N. Patris, S. Perez, B. Renard, J.-L. Seidel, and J.-P. Vandervaere
2016b. Floodscale : Observation et modélisation hydro-météorologique multi-échelles pour la compréhension et la simulation des crues éclairs. Technical report, Rapport scientifique final du projet ANR-2011 BS56 027 01.

Braud, I., P.-A. Ayral, C. Bouvier, F. Branger, G. Delrieu, G. Dramais, J. Le Coz, E. Leblois, G. Nord, and J.-P. Vandervaere
2016c. Advances in flash floods understanding and modelling derived from the floodscale project in south-east france. *E3S Web Conf.*, 7:04005.

Braud, I., J.-F. Desprats, P.-A. Ayral, C. Bouvier, and J.-P. Vandervaere
2017. Mapping topsoil field-saturated hydraulic conductivity from point measurements using different methods. *Journal of Hydrology and Hydromechanics*, 65.

Braud, I., H. Roux, S. Anquetin, M.-M. Maubourguet, C. Manus, P. Viallet, and D. Dartus
2010. The use of distributed hydrological models for the Gard 2002 flash flood event: Analysis of associated hydrological processes. *Journal of Hydrology*, 394(1):162 – 181.

Brutsaert, W. and J. L. Nieber
1977. Regionalized drought flow hydrographs from a mature glaciated plateau. *Water Resources Research*, 13(3):637–643.

Caillouet, L., J.-P. Vidal, E. Sauquet, and B. Graff
2016. Probabilistic precipitation and temperature downscaling of the twentieth century reanalysis over france. *Climate of the Past*, 12(3):635–662.

Camporese, M., C. Paniconi, M. Putti, and S. Orlandini
2010. Surface-subsurface flow modeling with path-based runoff routing, boundary condition-based coupling, and assimilation of multisource observation data. *Water Resources Research*, 46(2).

Casper, M. C., G. Grigoryan, O. Gronz, O. Gutjahr, G. Heinemann, R. Ley, and A. Rock
2012. Analysis of projected hydrological behavior of catchments based on signature indices. *Hydrology and Earth System Sciences*, 16(2):409–421.

Chapman, T.
1999. A comparison of algorithms for streamflow recession and basefow separation. *Hydrological Processes*, 13:701–714.

Chapman, T. G. and A. I. Maxwell
1996. Baseflow separation - comparison of numerical methods with tracer experiments. In *Hydrology and Water Resources Symposium*, Hobart, Tasmania. Institute of Engeneering of Australia, Hydrology and Water Resources Symposium.

Clark, M., D. Kavetski, and F. Fenicia
2011a. Pursuing the method of multiple working hypotheses for hydrological modeling. *Water Resources Research*, 47(9).

Clark, M. P., M. F. P. Bierkens, L. Samaniego, R. A. Woods, R. Uijlenhoet, K. E. Bennett, V. R. N. Pauwels, X. Cai, A. W. Wood, and C. D. Peters-Lidard
2017. The evolution of process-based hydrologic models: historical challenges and the collective quest for physical realism. *Hydrology and Earth System Sciences*, 21(7):3427–3440.

Clark, M. P., H. K. McMillan, D. B. G. Collins, D. Kavetski, and R. A. Woods
2011b. Hydrological field data from a modeller's perspective: Part 2: process-based evaluation of model hypotheses. *Hydrological Processes*, 25(4):523–543.

Clark, M. P., D. E. Rupp, R. A. Woods, H. J. Tromp-van Meerveld, N. E. Peters, and J. E. Freer
2009. Consistency between hydrological models and field observations: linking processes at the hillslope scale to hydrological responses at the watershed scale. *Hydrological Processes*, 23(2):311–319.

Clark, M. P., B. Schaefli, S. J. Schymanski, L. Samaniego, C. H. Luce, B. M. Jackson, J. E. Freer, J. R. Arnold, R. D. Moore, E. Istanbulluoglu, and S. Ceola
2016. Improving the theoretical underpinnings of process-based hydrologic models. *Water Resources Research*, 52(3):2350–2365.

Clausen, B. and B. J. F. Biggs
2000. Flow variables for ecological studies in temperate streams: groupings based on covariance. *Journal of Hydrology*, 237(3):184 – 197.

Coxon, G., J. Freer, T. Wagener, N. A. Odoni, and M. Clark
2014. Diagnostic evaluation of multiple hypotheses of hydrological behaviour in a limits-of-acceptability framework for 24 UK catchments. *Hydrological Processes*, 28(25):6135–6150.

Dai, A.
2010. Drought under global warming: a review. *WIREs Climate Change*.

de Boer-Euser, T., H. K. McMillan, M. Hrachowitz, H. C. Winsemius, and H. H. G. Savenije
2016. Influence of soil and climate on root zone storage capacity. *Water Resources Research*, 52(3):2009–2024.

Detty, J. M. and K. J. McGuire
2010. Topographic controls on shallow groundwater dynamics: implications of hydrologic connectivity between hillslopes and riparian zones in a till mantled catchment. *Hydrological Processes*, 24(16):2222–2236.

Devers, A.
2019. *Vers une réanalyse hydrométéorologique à l'échelle de la France sur les 150 dernières années par assimilation de données dans des reconstructions ensemblistes*. PhD thesis, Université Grenoble Alpes.

Duan, Q., H. V. Gupta, S. Sorooshian, A. N. Rousseau, and R. Turcotte
2003. *Calibration of Watershed Models*, volume 6. American Geophysical Union, Whashington D.C.

Dunne, T. and R. D. Black
1970. Partial area contributions to storm runoff in a small new england watershed. *Water Resources Research*, 6(5):1296–1311.

Eckhardt, K.
2005. How to construct recursive digital filters for baseflow separation. *Hydrological Processes*, 19:507–515.

Eckhardt, K.
2008. A comparison of baseflow indices, which were calculated with seven different baseflow separation methods. *Journal of Hydrology*, 352:168–173.

Eder, G., M. Sivapalan, and H. P. Nachtnebel
2003. Modelling water balances in an alpine catchment through exploitation of emergent properties over changing time scales. *Hydrological Processes*, 17(11):2125–2149.

Euser, T., M. Hrachowitz, H. C. Winsemius, and H. H. Savenije
2015. The effect of forcing and landscape distribution on performance and consistency of model structures. *Hydrological Processes*, 29(17):3727–3743.

Euser, T., H. C. Winsemius, M. Hrachowitz, F. Fenicia, S. Uhlenbrook, and H. H. G. Savenije
2013. A framework to assess the realism of model structures using hydrological signatures. *Hydrology and Earth System Sciences*, 17(5):1893–1912.

Farmer, D., M. Sivapalan, and C. Jothityangkoon
2003. Climate, soil, and vegetation controls upon the variability of water balance in temperate and semiarid landscapes: Downward approach to water balance analysis. *Water Resources Research*, 39(2).

Fenicia, F., D. Kavetski, P. Reichert, and C. Albert
2018. Signature-domain calibration of hydrological models using approximate bayesian computation: Empirical analysis of fundamental properties. *Water Resources Research*, 54(6):3958–3987.

Fenicia, F., D. Kavetski, H. H. G. Savenije, and L. Pfister
2016. From spatially variable streamflow to distributed hydrological models: Analysis of key modeling decisions. *Water Resources Research*, 52(2):954–989.

Feyen, H., H. Wunderli, H. Wydler, and A. Papritz
1999. A tracer experiment to study flow paths of water in a forest soil. *Journal of Hydrology*, 225(3):155 – 167.

Fink, M., P. Krause, S. Kralisch, U. Bende-Michl, and W.-A. Flügel
2007. Development and application of the modelling system j2000-s for the eu-water framework directive. *Advances in Geosciences*, 11:123–130.

Flury, M., H. Flühler, W. A. Jury, and J. Leuenberger
1994. Susceptibility of soils to preferential flow of water: A field study. *Water Resources Research*, 30(7):1945–1954.

Flügel, W.-A.
1995. Delineating hydrological response units by geographical information system analyses for regional hydrological modelling using prms/mms in the drainage basin of the river bröl, germany. *Hydrological Processes*, 9(3-4):423–436.

Fovet, O., L. Ruiz, M. Hrachowitz, M. Faucheux, and C. Gascuel-Odoux
2015. Hydrological hysteresis and its value for assessing process consistency in catchment conceptual models. *Hydrology and Earth System Sciences*, 19(1):105–123.

Freeze, R. A.
1974. Streamflow generation. *Reviews of Geophysics*, 12(4):627–647.

Fuamba, M., F. Branger, I. Braud, E. Batchabani, P. Sanzana, B. Sarrazin, and S. Jankowfsky
2019. Value of distributed water level and soil moisture data in the evaluation of a distributed

hydrological model: Application to the PUMMA model in the Mercier catchment (6.6 km^2) in France. *Journal of Hydrology*, 569:753 – 770.

Furey, P. R. and V. K. Gupta
2001. A physically based filter for separating base flow from streamflow time series. *Water Resources Research*, 37(11):2709–2722.

Gao, H., M. Hrachowitz, S. J. Schymanski, F. Fenicia, N. Sriwongsitanon, and H. H. G. Savenije
2014. Climate controls how ecosystems size the root zone storage capacity at catchment scale. *Geophysical Research Letters*, 41(22):7916–7923.

Gao, T., S. Kang, P. Krause, L. Cuo, and S. Nepal
2012. A test of j2000 model in a glacierized catchment in the central tibetan plateau. *Environmental Earth Sciences*, 65(6):1651–1659.

Gharari, S., M. Hrachowitz, F. Fenicia, H. Gao, and H. H. G. Savenije
2014. Using expert knowledge to increase realism in environmental system models can dramatically reduce the need for calibration. *Hydrology and Earth System Sciences*, 18(12):4839–4859.

Gobiet, A., S. Kotlarski, M. Beniston, G. Heinrich, J. Rajczak, and M. Stoffel
2014. 21st century climate change in the european alps—a review. *Science of The Total Environment*, 493:1138 – 1151.

Gottardi, F., C. Obled, J. Gailhard, and E. Paquet
2012. Statistical reanalysis of precipitation fields based on ground network data and weather patterns: Application over french mountains. *Journal of Hydrology*, 432-433:154–167.

Goulden, M. L., R. G. Anderson, R. C. Bales, A. E. Kelly, M. Meadows, and G. C. Winston
2012. Evapotranspiration along an elevation gradient in california's sierra nevada. *Journal of Geophysical Research: Biogeosciences*, 117(G3).

Gouttevin, I., M. Turko, F. Branger, E. Leblois, and J.-E. Sicart
2017. Amélioration de la modélisation hydrologique distribuée en conditions naturelles dans les Alpes. Technical report, Irstea.

Grayson, R. B., I. D. Moore, and T. A. McMahon
1992. Physically based hydrologic modeling: 2. is the concept realistic? *Water Resources Research*, 28(10):2659–2666.

Gupta, H. V., H. Kling, K. K. Yilmaz, and G. F. Martinez
2009. Decomposition of the mean squared error and NSE performance criteria: Implications for improving hydrological modelling. *Journal of Hydrology*, 377(1):80 – 91.

Gupta, H. V., S. Sorooshian, and P. O. Yapo
1998. Toward improved calibration of hydrologic models: Multiple and noncommensurable measures of information. *Water Resources Research*, 34(4):751–763.

Gupta, H. V., T. Wagener, and Y. Liu
2008. Reconciling theory with observations: elements of a diagnostic approach to model evaluation. *Hydrological Processes*, 22(18):3802–3813.

Guse, B., M. Pfannerstill, A. Gafurov, N. Fohrer, and H. Gupta
2016a. Demasking the integrated information of discharge: Advancing sensitivity analysis to consider different hydrological components and their rates of change. *Water Resources Research*, 52(11):8724–8743.

Guse, B., M. Pfannerstill, M. Strauch, D. E. Reusser, S. Lüdtke, M. Volk, H. Gupta, and N. Fohrer
2016b. On characterizing the temporal dominance patterns of model parameters and processes. *Hydrological Processes*, 30(13):2255–2270.

Gustard, A., A. Bullock, and J. M. Dixon
1992. Low flow estimation in the United Kingdom. Technical report, Tech. Rep. 108, Institute of Hydrology, Wallingford, UK.

Haghnegahdar, A., S. Razavi, F. Yassin, and H. Wheater
2017. Multicriteria sensitivity analysis as a diagnostic tool for understanding model behaviour and characterizing model uncertainty. *Hydrological Processes*, 31(25):4462–4476.

Harman, C. J., M. Sivapalan, and P. Kumar
2009. Power law catchment-scale recessions arising from heterogeneous linear small-scale dynamics. *Water Resources Research*, 45(W9404).

He, Z. H., F. Q. Tian, H. V. Gupta, H. C. Hu, and H. P. Hu
2015. Diagnostic calibration of a hydrological model in a mountain area by hydrograph partitioning. *Hydrology and Earth System Sciences*, 19(4):1807–1826.

Herman, J. D., J. B. Kollat, P. M. Reed, and T. Wagener
2013. Technical note: Method of morris effectively reduces the computational demands of global sensitivity analysis for distributed watershed models. *Hydrology and Earth System Sciences*, 17(7):2893–2903.

Herrero, J., M. Polo, A. Moñino, and M. Losada
2009. An energy balance snowmelt model in a mediterranean site. *Journal of Hydrology*, 371(1):98 – 107.

Heudorfer, B., E. Haaf, K. Stahl, and R. Barthel
2019. Index-based characterization and quantification of groundwater dynamics. *Water Resources Research*, 55(7):5575–5592.

Hingray, B., B. Schaefli, A. Mezghani, and Y. Hamdi
2010. Signature-based model calibration for hydrological prediction in mesoscale alpine catchments. *Hydrological Sciences Journal*, 55(6):1002–1016.

Hock, R.
2003. Temperature index melt modelling in mountain areas. *Journal of Hydrology*, 282(1):104 – 115.

Höllering, S., J. Wienhöfer, J. Ihringer, L. Samaniego, and E. Zehe
2018. Regional analysis of parameter sensitivity for simulation of streamflow and hydrological fingerprints. *Hydrology and Earth System Sciences*, 22(1):203–220.

Horner, I., F. Branger, H. McMillan, O. Vannier, and I. Braud
2020. Information content of snow hydrological signatures based on streamflow, precipitation and air temperature. *Hydrological Processes*, 34(12):2763–2779.

Horner, I., J. Le Coz, B. Renard, and F. Branger
2018a. Impact de la sensibilité des contrôles hydrauliques sur les incertitudes hydrométriques. *La Houille Blanche*, (1):27–35.

Horner, I., B. Renard, J. Le Coz, F. Branger, H. K. McMillan, and G. Pierrefeu
2018b. Impact of stage measurement errors on streamflow uncertainty. *Water Resources Research*, 54(3):1952–1976.

Horton, R. E.
1933. The role of infiltration in the hydrologic cycle. *Transactions of the American Geophysical Union*, 14:446–460.

Hrachowitz, M. and M. P. Clark
2017. Hess opinions: The complementary merits of competing modelling philosophies in hydrology. *Hydrology and Earth System Sciences*, 21(8):3953–3973.

Hrachowitz, M., O. Fovet, L. Ruiz, T. Euser, S. Gharari, R. Nijzink, J. Freer, H. H. G. Savenije, and C. Gascuel-Odoux
2014. Process consistency in models: The importance of system signatures, expert knowledge, and process complexity. *Water Resources Research*, 50(9):7445–7469.

Hunsaker, C. T. and M. Safeeq
2017. Kings river experimental watersheds stream discharge. *Fort Collins, CO: Forest Service Research Data Archive*.

Hunsaker, C. T. and M. Safeeq
2018. Kings river experimental watersheds meteorology data. *Fort Collins, CO: Forest Service Research Data Archive*.

Hunsaker, C. T., W. Thomas W., and B. Roger C.
2012. Snowmelt runoff and water yield along elevation and temperature gradients in california's southern sierra nevada. *Journal of the American Water Resources Association*, 48(4):667–678.

Huza, J., A. Teuling, I. Braud, J. Grazioli, L. Melsen, G. Nord, T. Raupach, and R. Uijlenhoet
2014. Precipitation, soil moisture and runoff variability in a small river catchment (arde'che, france) during hymex special observation period 1. *Journal of Hydrology*, 516:330–342.

Iooss, B., A. Janon, G. Pujol, K. Boumhaout, S. D. Veiga, T. Delage, J. Fruth, L. Gilquin, J. Guillaume, L. Le Gratiet, P. Lemaitre, B. L. Nelson, F. Monari, R. Oomen, O. Rakovec, B. Ramos, O. Roustant, E. Song, J. Staum, R. Sueur, T. Touati, and F. Weber
2018. *sensitivity: Global Sensitivity Analysis of Model Outputs*. R package version 1.15.2.

Iooss, B. and P. Lemaître
2015. A review on global sensitivity analysis methods. In *Uncertainty management in Simulation-Optimization of Complex Systems: Algorithms and Applications*, C. Meloni and G. Dellino, eds. Springer.

Iwagami, S., M. Tsujimura, Y. Onda, J. Shimada, and T. Tanaka
2010. Role of bedrock groundwater in the rainfall–runoff process in a small headwater catchment underlain by volcanic rock. *Hydrological Processes*, 24(19):2771–2783.

Jansen, M. J.
1999. Analysis of variance designs for model output. *Computer Physic Communications*, 117:35 – 43.

Johnson, D., C. Hunsaker, D. Glass, B. Rau, and B. Roath
2011. Carbon and nutrient contents in soils from the kings river experimental watersheds, sierra nevada mountains, california. *Geoderma*, 160(3):490 – 502.

Jothityangkoon, C., M. Sivapalan, and D. Farmer
2001. Process controls of water balance variability in a large semi-arid catchment: downward approach to hydrological model development. *Journal of Hydrology*, 254(1):174 – 198.

Kampf, S. K. and S. J. Burges
2007. A framework for classifying and comparing distributed hillslope and catchment hydrologic models. *Water Resources Research*, 43(5).

Kelleher, C., T. Wagener, and B. McGlynn
2015. Model-based analysis of the influence of catchment properties on hydrologic partitioning across five mountain headwater subcatchments. *Water Resources Research*, 51(6):4109–4136.

Kendall, K., J. Shanley, and J. McDonnell
1999. A hydrometric and geochemical approach to test the transmissivity feedback hypothesis during snowmelt. *Journal of Hydrology*, 219(3):188 – 205.

Kiang, J. E., C. Gazoorian, H. McMillan, G. Coxon, J. Le Coz, I. K. Westerberg, A. Belleville, D. Sevrez, A. E. Sikorska, A. Petersen-Øverleir, T. Reitan, J. Freer, B. Renard, V. Mansanarez, and R. Mason
2018. A comparison of methods for streamflow uncertainty estimation. *Water Resources Research*, 54(10):7149–7176.

Kirchner, J. W.
2003. A double paradox in catchment hydrology and geochemistry. *Hydrological Processes*, 17(4):871–874.

Kirchner, J. W.
2006. Getting the right answers for the right reasons: Linking measurements, analyses, and models to advance the science of hydrology. *Water Resources Research*, 42(3).

Kirchner, J. W.
2009. Catchment as simple dynamical system: Catchment characterization, rainfall-runoff model, and doing hydrology backward. *Water Resources Research*, 45:W02429.

Klemeš, V.
1983. Conceptualization and scale in hydrology. *Journal of Hydrology*, 65(1):1 – 23.

Koren, V., M. Smith, and Q. Duan
2003. *Use of a Priori Parameter Estimates in the Derivation of Spatially Consistent Parameter Sets of Rainfall-Runoff Models*, Pp. 239–254. American Geophysical Union (AGU).

Kralisch, S.
2006. Jams - a framework for natural resource model development and application. In *The International Environmental Modelling & Software Society*.

Krause, P.
2002. Quantifying the impact of land use changes on the water balance of large catchments using the j2000 model. *Physics and Chemistry of the Earth, Parts A/B/C*, 27(9):663 – 673.

Krause, P., F. Bäse, U. Bende-Michl, M. Fink, W. Flügel, and B. Pfennig
2006. Multiscale investigations in a mesoscale catchment: hydrological modelling in the Gera catchment. *Advances in Geosciences*, 9:53–61.

Krause, P. and S. Hanisch
2009. Simulation and analysis of the impact of projected climate change on the spatially distributed waterbalance in thuringia, germany. *Advances in Geosciences*, 21:33–48.

Kumar, R., L. Samaniego, and S. Attinger
2013. Implications of distributed hydrologic model parameterization on water fluxes at multiple scales and locations. *Water Resources Research*, 49(1):360–379.

Kundu, D., F. F. van Ogtrop, and R. W. Vervoort
2016. Identifying model consistency through stepwise calibration to capture streamflow variability. *Environmental Modelling & Software*, 84:1 – 17.

Lafaysse, M., B. Hingray, P. Etchevers, E. Martin, and C. Obled
2011. Influence of spatial discretization, underground water storage and glacier melt on a physically-based hydrological model of the upper durance river basin. *Journal of Hydrology*, 403(1):116 – 129.

Lang, D. T. and The CRAN Team
2019. *XML: Tools for Parsing and Generating XML Within R and S-Plus*. R package version 3.98-1.20.

Le Coz, J., B. Camenen, G. Dramais, M. Ferry, J. L. Rosique, and J. Ribot-Bruno
2011. *Contrôle des débits réglementaires. Application de l'article L. 214-18 du Code de l'environnement*. Onema/Irstea.

Le Coz, J., B. Renard, L. Bonnifait, F. Branger, and R. Le Boursicaud
2014. Combining hydraulic knowledge and uncertain gaugings in the estimation of hydrometric rating curves: A bayesian approach. *Journal of Hydrology*, 509:573 – 587.

Leblois, E. and J.-D. Creutin
2013. Space-time simulation of intermittent rainfall with prescribed advection field: Adaptation of the turning band method. *Water Resources Research*, 49(6):3375–3387.

Lehmann, P., C. Hinz, G. McGrath, H. J. Tromp-van Meerveld, and J. J. McDonnell
2007. Rainfall threshold for hillslope outflow: an emergent property of flow pathway connectivity. *Hydrology and Earth System Sciences*, 11(2):1047–1063.

Lehning, M., I. Völksch, D. Gustafsson, T. A. Nguyen, M. Stähli, and M. Zappa
2006. ALPINE3D: a detailed model of mountain surface processes and its application to snow hydrology. *Hydrological Processes*, 20(10):2111–2128.

Ley, R., M. C. Casper, H. Hellebrand, and R. Merz
2011. Catchment classification by runoff behaviour with self-organizing maps (SOM). *Hydrology and Earth System Sciences*, 15(9):2947–2962.

Ley, R., H. Hellebrand, M. C. Casper, and F. Fenicia
2016. Comparing classical performance measures with signature indices derived from flow duration curves to assess model structures as tools for catchment classification. *Hydrology Research*, 47(1):1–14.

Lyne, V. and M. Hollick
1979. Stochastic time-variable rainfall-runoff modelling. In *Hydrology and Water Ressources Symposium*, Pp. 89–92, Perth, Australia. Institution of Engineers.

Mackay, J. D., N. E. Barrand, D. M. Hannah, S. Krause, C. R. Jackson, J. Everest, and G. Aðalgeirsdóttir
2018. Glacio-hydrological melt and run-off modelling: application of a limits of acceptability framework for model comparison and selection. *The Cryosphere*, 12(7):2175–2210.

Mackay, J. D., N. E. Barrand, D. M. Hannah, S. Krause, C. R. Jackson, J. Everest, G. Aðalgeirsdóttir, and A. R. Black
2019. Future evolution and uncertainty of river flow regime change in a deglaciating river basin. *Hydrology and Earth System Sciences*, 23(4):1833–1865.

Mangin, A.
1984. Pour une meilleure connaissance des systemes hydrologiques à partir des analyses corrélatoire et spectrale. *Journal of Hydrology*, 67:25–43.

Mansanarez, V., B. Renard, J. L. Coz, M. Lang, and M. Darienzo
2019. Shift happens! Adjusting stage-discharge rating curves to morphological changes at known times. *Water Resources Research*, 55(4):2876–2899.

McDonnell, J. J., M. Sivapalan, K. Vaché, S. Dunn, G. Grant, R. Haggerty, C. Hinz, R. Hooper, J. Kirchner, M. L. Roderick, J. Selker, and M. Weiler
2007. Moving beyond heterogeneity and process complexity: A new vision for watershed hydrology. *Water Resources Research*, 43(7).

McMillan, M. Gueguen, E. Grimon, R. Woods, M. Clark, and D. E. Rupp
2014. Spatial variability of hydrological processes and model structure diagnostics in a 50 km^2 catchment. *Hydrological Processes*, 28(18):4896–4913.

McMillan, H., D. Booker, and C. Cattoën
2016. Validation of a national hydrological model. *Journal of Hydrology*, 541:800 – 815.

McMillan, H., J. Freer, F. Pappenberger, T. Krueger, and M. Clark
2010. Impacts of uncertain river flow data on rainfall-runoff model calibration and discharge predictions. *Hydrological Processes*, 24(10):1270–1284.

McMillan, H., T. Krueger, and J. Freer
2012. Benchmarking observational uncertainties for hydrology: rainfall, river discharge and water quality. *Hydrological Processes*, 26(26):4078–4111.

McMillan, H., I. Westerberg, and F. Branger
2017. Five guidelines for selecting hydrological signatures. *Hydrological Processes*, Pp. n/a–n/a.

McMillan, H. K., M. P. Clark, W. B. Bowden, M. Duncan, and R. A. Woods
2011. Hydrological field data from a modeller's perspective: Part 1. Diagnostic tests for model structure. *Hydrological Processes*, 25(4):511–522.

Mei, Y. and E. N. Anagnostou
2015. A hydrograph separation method based on information from rainfall and runoff records. *Journal of Hydrology*, 523:636 – 649.

Mendiguren, G., J. Koch, and S. Stisen
2017. Spatial pattern evaluation of a calibrated national hydrological model – a remote-sensing-based diagnostic approach. *Hydrology and Earth System Sciences*, 21(12):5987–6005.

Merz, R., G. Blöschl, and J. Parajka
2006. Spatio-temporal variability of event runoff coefficients. *Journal of Hydrology*, 331:591–604.

Mishra, A. and P. Coulibaly
2009. Developments in hydrometric network design: A review. *Reviews of Geophysics*, 47(2).

Molina-Sanchis, I., R. Lazaro, E. Arnau, and A. Calvo-Cases
2016. Rainfall timing and runoff: The influence of the criterion for rain event separation. *Journal of Hydrology and Hydromechanics*, 64(3):226–236.

Montanari, A., G. Young, H. Savenije, D. Hughes, T. Wagener, L. Ren, D. Koutsoyiannis, C. Cudennec, E. Toth, S. Grimaldi, G. Blöschl, M. Sivapalan, K. Beven, H. Gupta, M. Hipsey, B. Schaefli, B. Arheimer, E. Boegh, S. Schymanski, G. D. Baldassarre, B. Yu, P. Hubert, Y. Huang, A. Schumann,

D. Post, V. Srinivasan, C. Harman, S. Thompson, M. Rogger, A. Viglione, H. McMillan, G. Characklis, Z. Pang, and V. Belyaev
2013. "Panta Rhei—Everything Flows": Change in hydrology and society — The IAHS Scientific Decade 2013–2022. *Hydrological Sciences Journal*, 58(6):1256–1275.

Monteith, J.
1965. *The State and Movement of Water in Living Organism*, chapter Evaporation and Environment, Pp. 205 – 234. Fogg, B.D.

Mosley, M. P.
1979. Streamflow generation in a forested watershed, new zealand. *Water Resources Research*, 15(4):795–806.

Muggeo, V.
2008. Segmented: An r package to fit regression models with broken-line relationships. *R News*, 8:20–25.

Muggeo, V. M. R.
2003. Estimating regression models with unknown break-points. *Statistics in Medicine*, 22(19):3055–3071.

Nash, J. E. and J. V. Sutcliffe
1970. River flow forecasting through conceptual models part i — A discussion of principles. *Journal of Hydrology*, 10(3):282 – 290.

Naulet, R., M. Lang, T. B. Ouarda, D. Coeur, B. Bobée, A. Recking, and D. Moussay
2005. Flood frequency analysis on the ardèche river using french documentary sources from the last two centuries. *Journal of Hydrology*, 313(1):58 – 78.

Nepal, S.
2016. Impacts of climate change on the hydrological regime of the koshi river basin in the himalayan region. *Journal of Hydro-environment Research*, 10:76 – 89.

Nepal, S., P. Krause, W.-A. Flügel, M. Fink, and C. Fischer
2014. Understanding the hydrological system dynamics of a glaciated alpine catchment in the himalayan region using the j2000 hydrological model. *Hydrological Processes*, 28(3):1329–1344.

Noël, J. F.
2014. Naturalisation de débits observés sur le bassin versant de l'Ardèche. Impact sur les indicateurs hydrologiques. Master's thesis, ENTPE.

Nord, G., B. Boudevillain, A. Berne, F. Branger, I. Braud, G. Dramais, S. Gérard, J. Le Coz, C. Legoût, G. Molinié, J. Van Baelen, J.-P. Vandervaere, J. Andrieu, C. Aubert, M. Calianno, G. Delrieu, J. Grazioli, S. Hachani, I. Horner, J. Huza, R. Le Boursicaud, T. H. Raupach, A. J. Teuling, M. Uber, B. Vincendon, and A. Wijbrans
2017. A high space–time resolution dataset linking meteorological forcing and hydro-sedimentary response in a mesoscale Mediterranean catchment (Auzon) of the Ardèche region, France. *Earth System Science Data*, 9(1):221–249.

O'Geen, A., M. Safeeq, J. Wagenbrenner, E. Stacy, P. Hartsough, S. Devine, Z. Tian, R. Ferrell, M. Goulden, J. Hopmans, and R. Bales
2018. Southern sierra critical zone observatory and kings river experimental watersheds: A synthesis of measurements, new insights, and future directions. *Vadose Zone Journal*, 17(1).

Olden, J. D. and N. L. Poff
2003. Redundancy and the choice of hydrologic indices for characterizing streamflow regimes. *River Research and Applications*, 19(2):101–121.

Perrin, C., C. Michel, and V. Andréassian
2003. Improvement of a parsimonious model for streamflow simulation. *Journal of Hydrology*, 279(1):275 – 289.

Pfannerstill, M., B. Guse, and N. Fohrer
2014. Smart low flow signature metrics for an improved overall performance evaluation of hydrological models. *Journal of Hydrology*, 510:447 – 458.

Pfannerstill, M., B. Guse, D. Reusser, and N. Fohrer
2015. Process verification of a hydrological model using a temporal parameter sensitivity analysis. *Hydrology and Earth System Sciences*, 19(10):4365–4376.

Pfister, L., J.-F. Iffly, L. Hoffman, and J. Humbert
2002. Use of regionalized stormflow coefficients with a view to hydroclimatological hazard mapping. *Hydrological Sciences Journal*, 43(3).

Pianosi, F., K. Beven, J. Freer, J. W. Hall, J. Rougier, D. B. Stephenson, and T. Wagener
2016. Sensitivity analysis of environmental models: A systematic review with practical workflow. *Environmental Modelling & Software*, 79:214 – 232.

Pokhrel, P., K. K. Yilmaz, and H. V. Gupta
2012. Multiple-criteria calibration of a distributed watershed model using spatial regularization and response signatures. *Journal of Hydrology*, 418-419:49 – 60.

Pool, S., M. J. P. Vis, R. R. Knight, and J. Seibert
2017. Streamflow characteristics from modeled runoff time series – importance of calibration criteria selection. *Hydrology and Earth System Sciences*, 21(11):5443–5457.

Quintana-Seguí, P., F. Habets, and E. Martin
2011. Comparison of past and future mediterranean high and low extremes of precipitation and river flow projected using different statistical downscaling methods. *Natural Hazards and Earth System Sciences*, 11(5):1411–1432.

R Core Team
2018. *R: A Language and Environment for Statistical Computing*. R Foundation for Statistical Computing, Vienna, Austria.

Rawls, W. and D. Brakensiek
1985. *Watershed Management in the Eighties*, chapter Prediction of soil water properties for hydrologic modeling, Pp. 293 — 299. American Society of Civil Engineers, New York, NY.

Reggiani, P., M. Sivapalan, and S. M. Hassanizadeh
1998. A unifying framework for watershed thermodynamics: balance equations for mass, momentum, energy and entropy, and the second law of thermodynamics. *Advances in Water Resources*, 22(4):367 – 398.

Renard, B., V. Garreta, and M. Lang
2006. An application of bayesian analysis and markov chain monte carlo methods to the estimation of a regional trend in annual maxima. *Water Resources Research*, 42(12).

Renard, B., D. Kavetski, E. Leblois, M. Thyer, G. Kuczera, and S. Franks
2011. Toward a reliable decomposition of predictive uncertainty in hydrological modeling: Characterizing rainfall errors using conditional simulation. *Water Resources Research*, 47(11):W11516.

Rivera-Ramirez, H. D., G. S. Warner, and F. N. Scatena
2002. Prediction of master recesion curves and baseflow recessions in the Luquillo montains if Puerto Rico. *Journal of the American Water Resources Association*, 38(3):693–704.

Rozalis, S., E. Morin, Y. Yair, and C. Price
2010. Flash flood prediction using an uncalibrated hydrological model and radar rainfall data in a mediterranean watershed under changing hydrological conditions. *Journal of Hydrology*, 394(1):245 – 255.

Sadegh, M., J. A. Vrugt, H. V. Gupta, and C. Xu
2016. The soil water characteristic as new class of closed-form parametric expressions for the flow duration curve. *Journal of Hydrology*, 535:438 – 456.

Safeeq, M. and C. T. Hunsaker
2016. Characterizing runoff and water yield for headwater catchments in the southern sierra nevada. *Journal of the American Water Resources Association JAWRA*, 52(6):1327–1346.

Saltelli, A.
2004. *Sensitivity Analysis In Practice: a guide to assessing scientific models*. John Wiley & Sons Ltd.

Saltelli, A., P. Annoni, I. Azzini, F. Campolongo, M. Ratto, and S. Tarantola
2010. Variance based sensitivity analysis of model output. design and estimator for the total sensitivity index. *Computer Physics Communications*, 181(2):259 – 270.

Sauquet, E. and C. Catalogne
2011. Comparison of catchment grouping methods for flow duration curve estimation at ungauged sites in France. *Hydrology and Earth System Sciences*, 15(8):2421–2435.

Sawicz, K., T. Wagener, M. Sivapalan, P. A. Troch, and G. Carrillo
2011. Catchment classification: empirical analysis of hydrologic similarity based on catchment function in the eastern USA. *Hydrology and Earth System Sciences*, 15(9):2895–2911.

Schaefli, B.
2016. Snow hydrology signatures for model identification within a limits-of-acceptability approach. *Hydrological Processes*, 30(22):4019–4035.

Schaefli, B. and H. V. Gupta
2007. Do nash values have value? *Hydrological Processes*, 21(15):2075–2080.

Schaefli, B., A. Rinaldo, and G. Botter
2013. Analytic probability distributions for snow-dominated streamflow. *Water Resources Research*, 49(5):2701–2713.

Schmidt, G. and C. Benítez-Sanz
2012. Topic report on: Assessment of water scarcity and drought aspects in a selection of european union river basin management plans. Technical report, Study by Intecsa-Inarsa for the European Commission (under contract "Support to the implementation of the Water Framework Directive (2000/60/EC)"(070307/2011/600310/SER/D.2)).

Shafii, M., N. Basu, J. R. Craig, S. L. Schiff, and P. Van Cappellen
2017. A diagnostic approach to constraining flow partitioning in hydrologic models using a multiobjective optimization framework. *Water Resources Research*, 53(4):3279–3301.

Shamir, E., B. Imam, H. V. Gupta, and S. Sorooshian
2005a. Application of temporal streamflow descriptors in hydrologic model parameter estimation. *Water Resources Research*, 41(6).

Shamir, E., B. Imam, E. Morin, H. V. Gupta, and S. Sorooshian
2005b. The role of hydrograph indices in parameter estimation of rainfall-runoff models. *Hydrological Processes*, 19(11):2187–2207.

Singh, S. K. and R. Stenger
2018. Indirect methods to elucidate water flows and contaminant transfer pathways through mesoscale catchments – a review. *Environmental Processes*, 5(4):683–706.

Sivapalan, M.
2006. *Pattern, Process and Function: Elements of a Unified Theory of Hydrology at the Catchment Scale*, chapter 13. American Cancer Society.

Sivapalan, M., G. Blöschl, L. Zhang, and R. Vertessy
2003. Downward approach to hydrological prediction. *Hydrological Processes*, 17(11):2101–2111.

Sivapalan, M., M. A. Yaeger, C. J. Harman, X. Xu, and P. A. Troch
2011. Functional model of water balance variability at the catchment scale: 1. evidence of hydrologic similarity and space-time symmetry. *Water Resources Research*, 47(2):n/a–n/a.

Sklash, M. G. and R. N. Farvolden
1979. The role of groundwater in storm runoff. *Journal of Hydrology*, 43(1):45 – 65.

Stewart, M. K.
2015. Promising new baseflow separation and recession analysis methods applied to streamflow at Glendhu Catchment, New Zealand. *Hydrology and Earth System Sciences*, 19:2587–2603.

Stoelzle, M., K. Stahl, and M. Weiler
2013. Are streamflow recession characteristics really characteristic? *Hydrology and Earth System Sciences*, 17:817–828.

Tafasca, S.
2017. Utilisation de la mesure de vitesse pour l'estimation du débit dans un cours d'eau à forte pente avec transport solide. Master's thesis, Grenoble INP - ENSE3.

Talei, A. and L. H. C. Chua
2012. Influence of lag time on event-based rainfall–runoff modeling using the data driven approach. *Journal of Hydrology*, 438:223 – 233.

Tennant, C. J., A. A. Harpold, K. A. Lohse, S. E. Godsey, B. T. Crosby, L. G. Larsen, P. D. Brooks, R. W. V. Kirk, and N. F. Glenn
2017. Regional sensitivities of seasonal snowpack to elevation, aspect, and vegetation cover in western north america. *Water Resources Research*, 53(8):6908–6926.

Teutschbein, C., T. Grabs, R. H. Karlsen, H. Laudon, and K. Bishop
2015. Hydrological response to changing climate conditions: Spatial streamflow variability in the boreal region. *Water Resources Research*, 51(12):9425–9446.

Teutschbein, C., T. Grabs, H. Laudon, R. H. Karlsen, and K. Bishop
2018. Simulating streamflow in ungauged basins under a changing climate: The importance of landscape characteristics. *Journal of Hydrology*, 561:160 – 178.

Thornton, P., M. Thornton, B. Mayer, Y. Wei, R. Devarakonda, R. Vose, and R. Cook
2017. Daymet: Daily surface weather data on a 1-km grid for north america, version 3.

Todorović, A., M. Stanić, Željko Vasilić, and J. Plavšić
2019. The 3DNet-Catch hydrologic model: Development and evaluation. *Journal of Hydrology*, 568:26 – 45.

Toth, E.
2013. Catchment classification based on characterisation of streamflow and precipitation time series. *Hydrology and Earth System Sciences*, 17(3):1149–1159.

Troch, P. A., G. F. Martinez, V. R. N. Pauwels, M. Durcik, M. Sivapalan, C. Harman, P. D. Brooks, H. Gupta, and T. Huxman
2009. Climate and vegetation water use efficiency at catchment scales. *Hydrological Processes*, 23(16):2409–2414.

Tromp-van Meerveld, H. J. and J. J. McDonnell
2006. Threshold relations in subsurface stormflow: 1. a 147-storm analysis of the panola hillslope. *Water Resources Research*, 42(2).

Tromp-van Meerveld, H. J. and J. J. McDonnell
2006. Threshold relations in subsurface stormflow: 2. the fill and spill hypothesis. *Water Resources Research*, 42(2):n/a–n/a.

Uber, M., C. Legout, G. Nord, C. Crouzet, F. Demory, and J. Poulenard
2019. Comparing alternative tracing measurements and mixing models to fingerprint suspended sediment sources in a mesoscale mediterranean catchment. *Journal of Soils and Sediments*, 19(9):3255–3273.

Uber, M., J.-P. Vandervaere, I. Zin, I. Braud, M. Heistermann, C. Legoût, G. Molinié, and G. Nord
2018. How does initial soil moisture influence the hydrological response? a case study from southern france. *Hydrology and Earth System Sciences*, 22(12):6127–6146.

Valéry, A., V. Andréassian, and C. Perrin
2014. 'As simple as possible but not simpler': What is useful in a temperature-based snow-accounting routine? Part 1 – comparison of six snow accounting routines on 380 catchments. *Journal of Hydrology*, 517:1166 – 1175.

van Werkhoven, K., T. Wagener, P. Reed, and Y. Tang
2009. Sensitivity-guided reduction of parametric dimensionality for multi-objective calibration of watershed models. *Advances in Water Resources*, 32(8):1154 – 1169.

Vandana, K., A. Islam, P. P. Sarthi, A. K. Sikka, and H. Kapil
2018. Assessment of potential impact of climate change on streamflow: a case study of the Brahmani River basin, India. *Journal of Water and Climate Change*, 10(3):624–641.

Vannier, O., I. Braud, and S. Anquetin
2013. Regional estimation of catchment-scale soil properties by means of streamflow recession analysis for use in distributed hydrological models. *Hydrological Processes*, 28(26):6276–6291.

Vidal, J.-P., E. Martin, L. Franchistéguy, M. Baillon, and J.-M. Soubeyroux
2010. A 50-year high-resolution atmospheric reanalysis over France with the Safran system. *International Journal of Climatology*, 30(11):1627–1644.

Vogel, R. M. and N. M. Fennessey
1994. Flow-duration curves. i: New interpretation and confidence intervals. *Journal of Water Resources Planning and Management*, 120(4):485–504.

Vrugt, J. A. and M. Sadegh
2013. Toward diagnostic model calibration and evaluation: Approximate bayesian computation. *Water Resources Research*, 49(7):4335–4345.

Wagener, T.
2003. Evaluation of catchment models. *Hydrological Processes*, 17(16):3375–3378.

Wagener, T., M. Sivapalan, P. Troch, and R. Woods
2007. Catchment classification and hydrologic similarity. *Geography Compass*, 1/4:901–931.

Watson, A., J. Miller, M. Fleischer, and W. de Clercq
2018. Estimation of groundwater recharge via percolation outputs from a rainfall/runoff model for the verlorenvlei estuarine system, west coast, south africa. *Journal of Hydrology*, 558:238 – 254.

Westerberg, I. K., J.-L. Guerrero, P. M. Younger, K. J. Beven, J. Seibert, S. Halldin, J. E. Freer, and C.-Y. Xu
2011. Calibration of hydrological models using flow-duration curves. *Hydrology and Earth System Sciences*, 15(7):2205–2227.

Westerberg, I. K. and H. K. McMillan
2015. Uncertainty in hydrological signatures. *Hydrology and Earth System Sciences*, 19(9):3951–3968.

Wittenberg, H. and M. Sivapalan
1999. Watershed groundwater balance estimation using streamflow recession analysis and baseflow separation. *Journal of Hydrology*, 219:20–33.

Woods, R.
2006. *Hydrologic Concepts of Variability and Scale*, chapter 3. American Cancer Society.

Wrede, S., F. Fenicia, N. Martínez-Carreras, J. Juilleret, C. Hissler, A. Krein, H. H. G. Savenije, S. Uhlenbrook, D. Kavetski, and L. Pfister
2015. Towards more systematic perceptual model development: a case study using 3 Luxembourgish catchments. *Hydrological Processes*, 29(12):2731–2750.

Yadav, M., T. Wagener, and H. Gupta
2007. Regionalization of constraints on expected watershed response behavior for improved predictions in ungauged basins. *Advances in Water Resources*, 30:1756–1774.

Yilmaz, K. K., H. V. Gupta, and T. Wagener
2008. A process-based diagnostic approach to model evaluation: Application to the NWS distributed hydrologic model. *Water Resources Research*, 44(9).

Zabaleta, A. and I. Antigüedad
2013. Streamflow response of a small forested catchment on different timescales. *Hydrology and Earth System Sciences*, 17(1):211–223.

Zhang, Y., J. Vaze, F. H. S. Chiew, J. Teng, and M. Li
2014. Predicting hydrological signatures in ungauged catchments using spatial interpolation, index model, and rainfall–runoff modelling. *Journal of Hydrology*, 517:936 – 948.

Appendix A

Additional details on the physical characteristics of the Ardèche catchment

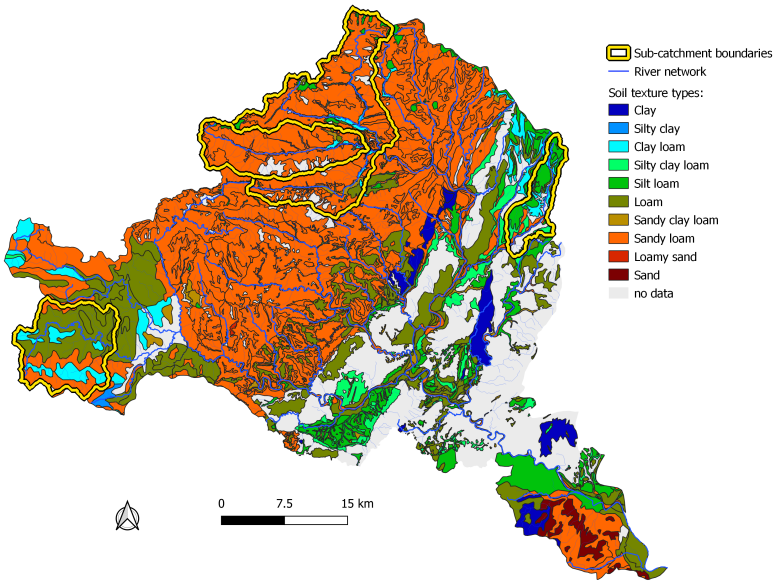

Figure A.1: Dominant texture type of the Ardèche catchment.

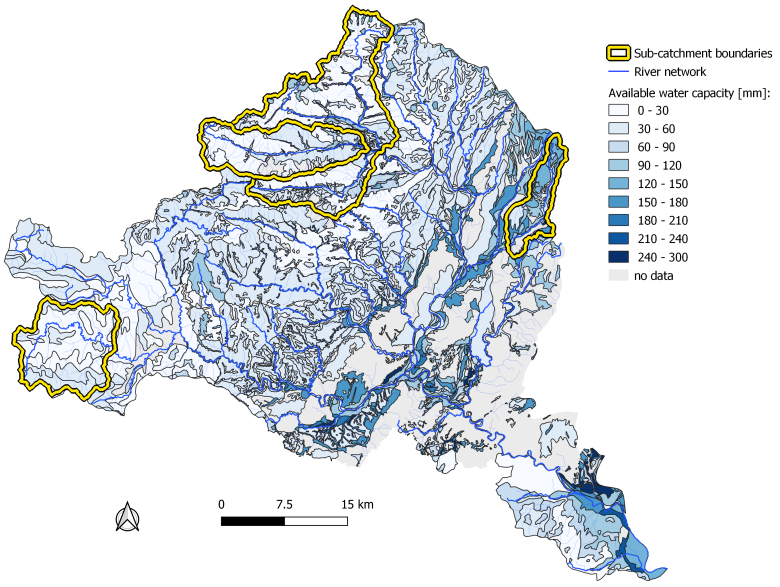

Figure A.2: Soil available water capacity in the Ardèche catchment derived from soil texture information using the pedotransfer function of Rawls and Brakensiek (1985) following the methodology of Bonnet (2012)

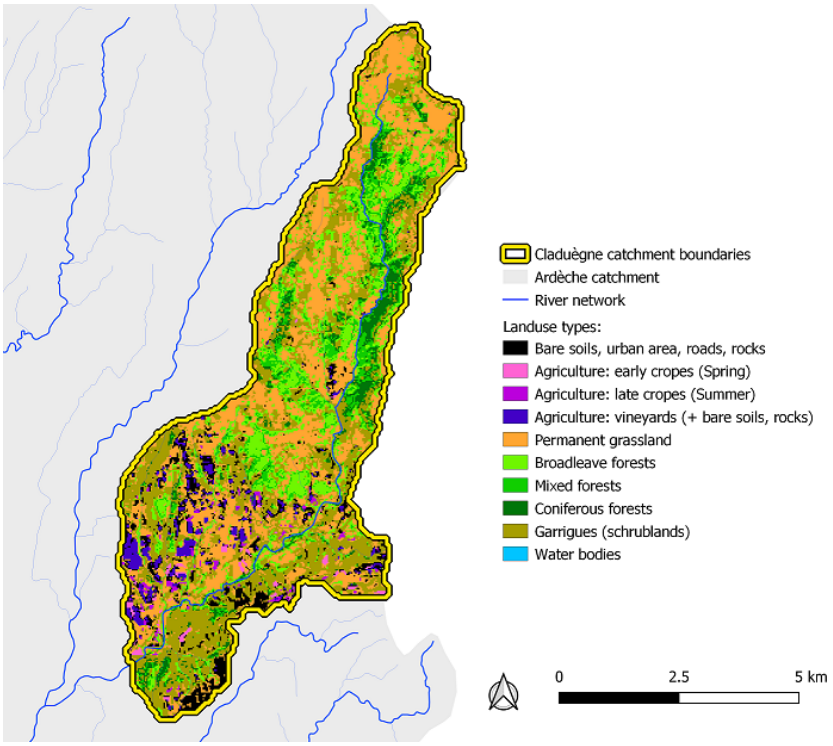

(a)

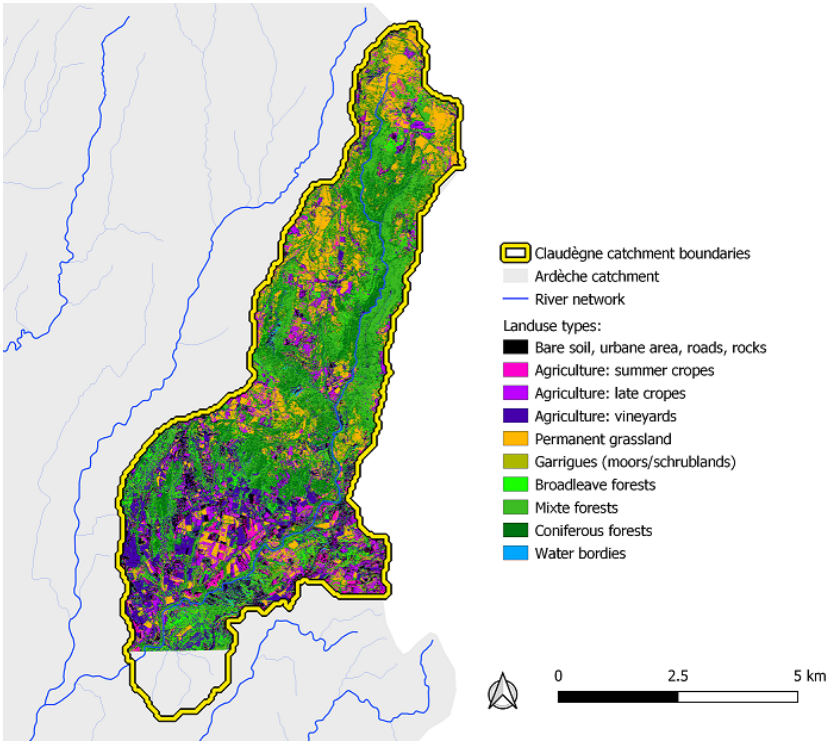

(b)

Figure A.3: Land-use of Cladugne according to Andrieu (2015a) (a) and Andrieu (2015b) (b).

Appendix B

Streamflow time series uncertainty estimation

B.1 Methodology for the computation of daily uncertain streamflow time series

Streamflow time series were recomputed using the stage time series, the gaugings and information on the hydraulic configuration of the sites following the methodology described in detail by Le Coz et al. (2014) and Horner et al. (2018b). The method of Le Coz et al. (2014) – BaRatin method – follows a Bayesian approach which is based on (1) the definition of rating curve models and the specification of *a priori* parameter distributions from a hydraulic analysis of the site, (2) uncertain calibration data — the gaugings which are pairs of measurements of both streamflow and river stage — and (3) a Markov Chain Monte Carlo (MCMC) sampling procedure used to infer the *posterior* distributions of the rating curve parameters. The methodology of Horner et al. (2018b) accounts for two types of errors that are supposed to affect stage time series: (1) non-systematic errors due to waves and instrumental noise and (2) systematic errors due to stage sensor calibration drifts.

The rating curve equation is a mathematical representation of the stage-streamflow relationship derived from a hydraulic analysis of the hydrometric station: hydraulic controls – physical elements/characteristics of the area surrounding the location of the stage sensor – are identified and used to specify the rating curve equation and *prior* distributions of its parameters using simplified hydraulic equations (e.g. simplified Manning-Strickler equation or typical weir equations).

The gaugings with known uncertainties are used to calibrate the *a priori* defined rating curve equation. The exact uncertainty associated with gaugings is often not known and typical uncertainty values, specified according to the gauging technique, are hence used (e.g. Le Coz et al., 2011, 2014; Horner et al., 2018b). A MCMC sampling approach (see details in Renard et al. (2006)) is used to infer the *posterior* distribution of the rating curve parameters $\boldsymbol{\theta}$. A resulting ensemble of n rating curve – corresponding to an ensemble of n parameter sets – account for the uncertainty associated with the rating curve. In addition, a *MaxPost* rating curve, corresponding to the set of parameter $\boldsymbol{\theta}_{MP}$ maximizing the *posterior* distribution, is kept to represent the most likely rating curve.

In the approach proposed by Horner et al. (2018b), stage time series are supposed to be affected by two types of errors: (1) non-systematic errors due to waves and instrumental noise and (2) systematic errors due to stage sensor calibration drifts. Typical magnitudes of the waves observed for a given hydrometric station or from the standard deviation of repeated measurements of the same "real" stage value can be used to estimate non-systematic errors. Systematic errors are typically based on the expert judgment of the station managers or from detailed information the periodicity of re-calibration, observed sensor drifts and applied corrections.

Using the measured stage time series and the stage error models of Horner et al. (2018b), an ensemble of n stage time series are computed. They are then used to compute n streamflow time series using the n rating curves estimated by the BaRatin method. The resulting ensemble of n streamflow time series accounts for all the uncertainty sources: (1) the non-systematic stage time series errors, (2) the systematic stage time series errors, (3) the parametric uncertainty of rating curve and (4) the structural errors of the rating curve model. Horner et al. (2018b) provide details on how different uncertainty sources affecting the resulting streamflow time series can be separated.

At a given time t in the streamflow time series, n values of streamflow are possible. Statistics – typically the 95% interval – on these values are used to quantify the uncertainty associated with streamflow. The *MaxPost* streamflow time series, computed from the actual measured stage time series and *MaxPost* rating curve, is used as a reference streamflow time series.

B.2 Meyras

B.2.1 Hydraulic controls and rating shifts

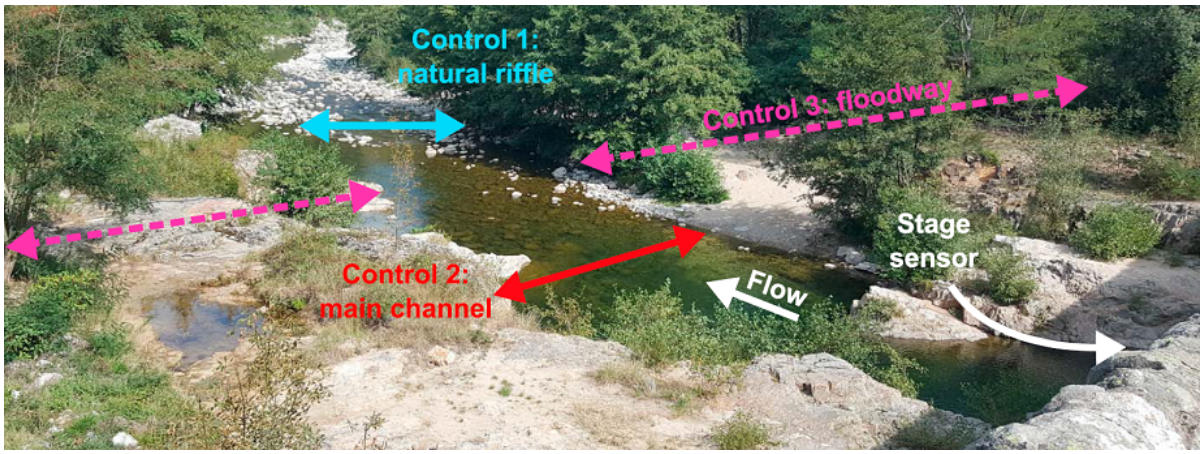

Figure B.1: Picture of the river directly downstream of the hydrometric station at the outlet of the Meyras catchment. The different hydraulic controls are identified (from Mansanarez et al. (2019), picture taken by Irstea in October 2016).

In their study, Mansanarez et al. (2019) used the hydrometric station located at the outlet of the Meyras catchment. Following their hydraulic analysis (see Figure B.1), three main hydraulic controls are identified: (1) for low stage, a natural riffle (modeled using a simplified rectangular weir equation), (2) for medium stage, the river channel (modeled using a simplified Manning-Strickler equation) and (3) for high stage, the addition of the flood plain (modeled using a simplified Manning-Strickler equation). The combination and activation of these three controls (the column in the matrix below) can be expressed as a "hydraulic control" matrix where a 1 (resp. 0) indicates an active hydraulic control:

$$\begin{array}{r} \text{low stage} \\ \text{medium stage} \\ \text{high stage} \end{array} \begin{pmatrix} 1 & 0 & 0 \\ 0 & 1 & 0 \\ 0 & 1 & 1 \end{pmatrix}$$

The corresponding mathematical equation of the rating curve that links river stage h with streamflow Q is:

$$Q(h) = \begin{cases} 0 & \text{for} \quad h \leq k_1 \\ a_1(h-k_1)^{c_1} & \text{for} \quad k_1 < h \leq k_2 \\ a_2(h-k_2)^{c_2} & \text{for} \quad k_2 < h \leq k_3 \\ a_2(h-k_2)^{c_2} + a_3(h-k_3)^{c_3} & \text{for} \quad h > k_3 \end{cases} \tag{B.1}$$

The parameters a_i, c_i and k_i are derived from each hydraulic control i from the type of control and information on the geometry of the controls. Here, the values used by Mansanarez et al. (2019) are used; the *prior* parameter values used are reported in Table B.1. Note that in Table B.1, *prior* values of k_1 – the minimum stage – and k_2 – the first transition stage – are not given as they will depend on the period considered. The last transition stage k_3 is kept wide (±40 cm) as its effective value isn't very well known due to the complexity of the topography.

The hydrometric station manager of Meyras, the Service de Prévision des Crues (SPC) Grand-Delta has provided us with gaugings and historical information that includes documented shifts. The stage time series, from July 1984 tà September 2017, was downloaded from the Banque Hydro[1] database at a variable time step. From the historical information, the visual inspection of the minimal value of the

[1] http://www.hydro.eaufrance.fr/

Table B.1: *Prior* parameter values used for the application of the BaRatin method on the Meyras hydrometric station. $\mathcal{N}(\mu,\ \sigma)$ stands for a Gaussian distribution with mean μ and standard-deviation σ.

Hydraulic control	Parameter	*Prior* values
	k_1	-
Natural riffle	a_1	$\mathcal{N}(14.2,\ 5)$
	c_1	$\mathcal{N}(1.5,\ 0.025)$
	k_2	-
River channel	a_2	$\mathcal{N}(26.5,\ 8.5)$
	c_2	$\mathcal{N}1.67,\ 0.025)$
	k_3	$\mathcal{N}(1.2,\ 0.2)$
Flood plain	a_3	$\mathcal{N}(32,\ 11)$
	c_3	$\mathcal{N}(1.67,\ 0.025)$

stage time series, and a detailed analysis of the gaugings, 17 rating curve shifts were identified and kept in our analysis (see Figure B.2). Most of rating shifts were due to river morphological changes due to floods. The minimum stage values k_1 were specified, for each stable period, using the minimum stage value of the period (Figure B.2) as an upper boundary of the 95% uncertainty interval of the effective "crest" level of the river riffle specified to be ±20cm. The first transition stage k_2 was specified according to k_1 by adding 40cm and using the same uncertainty (± 20 cm). The *prior* value used for k_1 and k_2 for each stable period are reported in Table B.2.

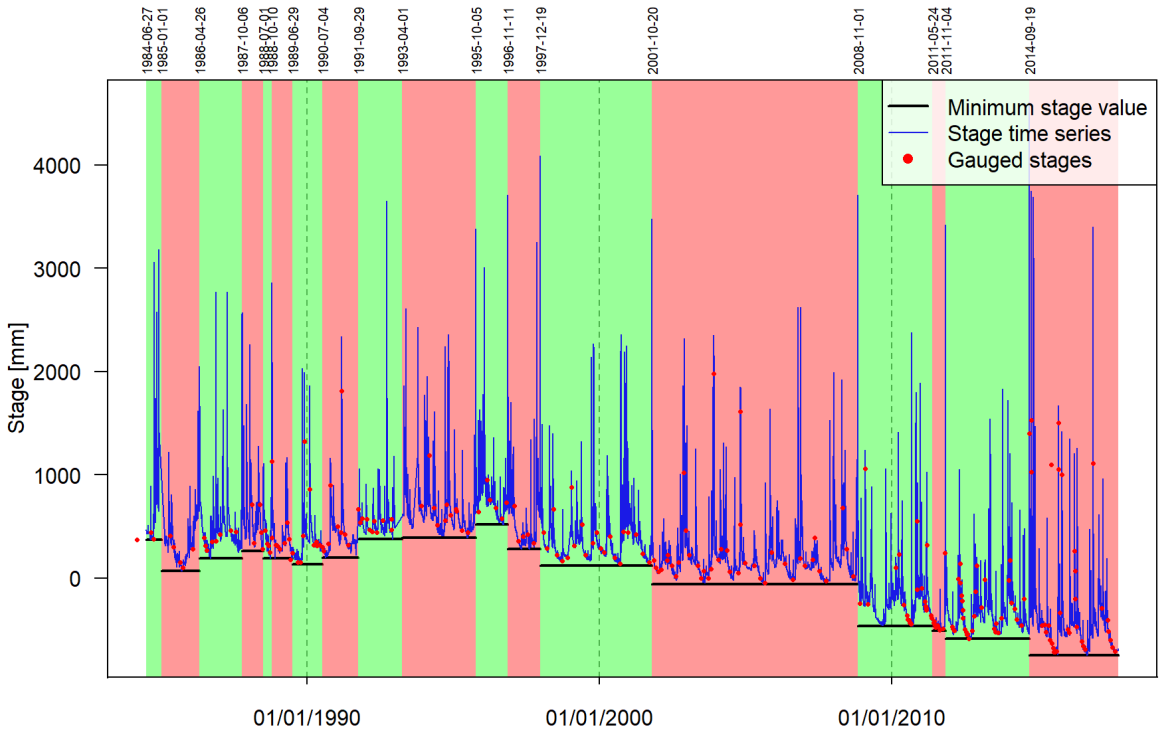

Figure B.2: Stage time series of the Meyras catchment. The identified stable period are shown with different background colors. The date of each shifts are indicated in the top of the plot.

B.2.2 Uncertain rating curve estimation

All gaugings that were flagged as suspicious by the station managers were removed from the analysis. There remained 247 gaugings for the analysis that were divided into the different stable periods (last

Table B.2: *Prior* parameter values of k_1 and k_2 used for the application BaRatin method for each stable period for the Meyras hydrometric station. $\mathcal{N}(\mu,\ \sigma)$ stands for a Gaussian distribution with mean μ and standard-deviation σ. The date of the start of each stable period are reported in the first column and the number of gaugings available for each period is reported in the last column.

Date (DD/MM/YYYY)	k_1	k_2	Number of gaugings
27/06/1984	$\mathcal{N}(0.17,\ 0.1)$	$\mathcal{N}(0.57,\ 0.1)$	3
01/01/1985	$\mathcal{N}(-0.13,\ 0.1)$	$\mathcal{N}(0.27,\ 0.1)$	5
26/04/1986	$\mathcal{N}(-0.01,\ 0.1)$	$\mathcal{N}(0.39,\ 0.1)$	8
06/10/1987	$\mathcal{N}(0.06,\ 0.1)$	$\mathcal{N}(0.46,\ 0.1)$	5
01/07/1988	$\mathcal{N}(-0.01,\ 0.1)$	$\mathcal{N}(0.39,\ 0.1)$	4
10/10/1988	$\mathcal{N}(-0.01,\ 0.1)$	$\mathcal{N}(0.39,\ 0.1)$	10
29/06/1989	$\mathcal{N}(-0.07,\ 0.1)$	$\mathcal{N}(0.33,\ 0.1)$	9
04/07/1990	$\mathcal{N}(0.00,\ 0.1)$	$\mathcal{N}(0.4,\ 0.1)$	9
29/09/1991	$\mathcal{N}(0.18,\ 0.1)$	$\mathcal{N}(0.58,\ 0.1)$	11
01/04/1993	$\mathcal{N}(0.19,\ 0.1)$	$\mathcal{N}(0.59,\ 0.1)$	11
05/10/1995	$\mathcal{N}(0.32,\ 0.1)$	$\mathcal{N}(0.72,\ 0.1)$	6
11/11/1996	$\mathcal{N}(0.08,\ 0.1)$	$\mathcal{N}(0.48,\ 0.1)$	5
19/12/1997	$\mathcal{N}(-0.079,\ 0.1)$	$\mathcal{N}(0.321,\ 0.1)$	23
20/10/2001	$\mathcal{N}(-0.263,\ 0.1)$	$\mathcal{N}(0.137,\ 0.1)$	41
01/11/2008	$\mathcal{N}(-0.662,\ 0.1)$	$\mathcal{N}(-0.262,\ 0.1)$	28
24/05/2011	$\mathcal{N}(-0.708,\ 0.1)$	$\mathcal{N}(-0.308,\ 0.1)$	10
04/11/2011	$\mathcal{N}(-0.787,\ 0.1)$	$\mathcal{N}(-0.387,\ 0.1)$	23
19/09/2014	$\mathcal{N}(-0.949,\ 0.1)$	$\mathcal{N}(-0.549,\ 0.1)$	36

column in Table B.2). Uncertainties associated with gaugings were specified according to the method used to measure streamflow: 5% for ADCP and dilution gaugings, 10% for the veolcity-area method when there are multiple point measurements for each vertical and 15% for all other methods or when the method is unknown.

The application of the BaRatin method for each period resulted in many parameter sets each representing a possible rating curve. The parameter set corresponding to the maximum of the posterior distribution, the $MaxPost$, was kept along 200 parameter sets used to account for the uncertainty of the rating curve. The resulting rating curve for the 18 stable periods are shown in Figure B.3. It shows that the rating curve uncertainties are very large – in particular the structural uncertainties – for periods where only a few gaugings are available or if the gauged stages range is small. This is realistic given the lack of information we have on these periods. In Figure B.3 the shaded grey area (total uncertainty including parametric and structural uncertainties) is noisy and goes below the plot area for some stage values: this is only due to the way the structural error is samples for each stage value and the log scale used for the streamflow axis.

B.2.3 Computing uncertain streamflow time series

The stage time series where then propagated through the computed rating curves. First, stage errors were specified using typical values of errors expected for this type of river: (1) non-systematic errors between ±0.5 cm ($\sigma^h_{NS} = 0.0025$) for the lowest stages and ±5 cm ($\sigma^h_{NS} = 0.025$)for the highest stages and (2) systematic errors of ±2 cm ($\sigma^h_{NS} = 0.01$) for all stage values with a re-sampling periodicity of 60 days. The standard-deviation of non-systematic errors were linearly interpolated according to stage values from the lowest to the highest stage values. Using the standard-deviation of systematic errors, the error was sampled once for each period between the re-calibration dates specified every 60 days. For each stable period, 200 stage time series were thus computed and propagated through the 200 rating curves and $MaxPost$ rating curve estimated using BaRatin. Resulting streamflow time series

were concatenated to have the full length of the streamflow time series. The streamflow time series were then aggregated at a daily time scale.

Figure B.4 shows portions of the resulting daily streamflow time series for a high and low flow period. For the selected periods, it shows that the uncertainty due to the rating curve dominates for high flows (Figures B.4a, B.4c and B.4e) whereas at low flows both stage errors and rating curve uncertainty have significant impact on the resulting streamflow time series (Figures B.4b, B.4d and B.4f). The impact of the rating curve uncertainty will vary greatly between stable periods due to how well the available gaugings were able to constrain the *posterior* uncertainty of the rating curve (Figure B.3). This is illustrated by the monthly average of streamflow for three decades shown in Figure B.5.

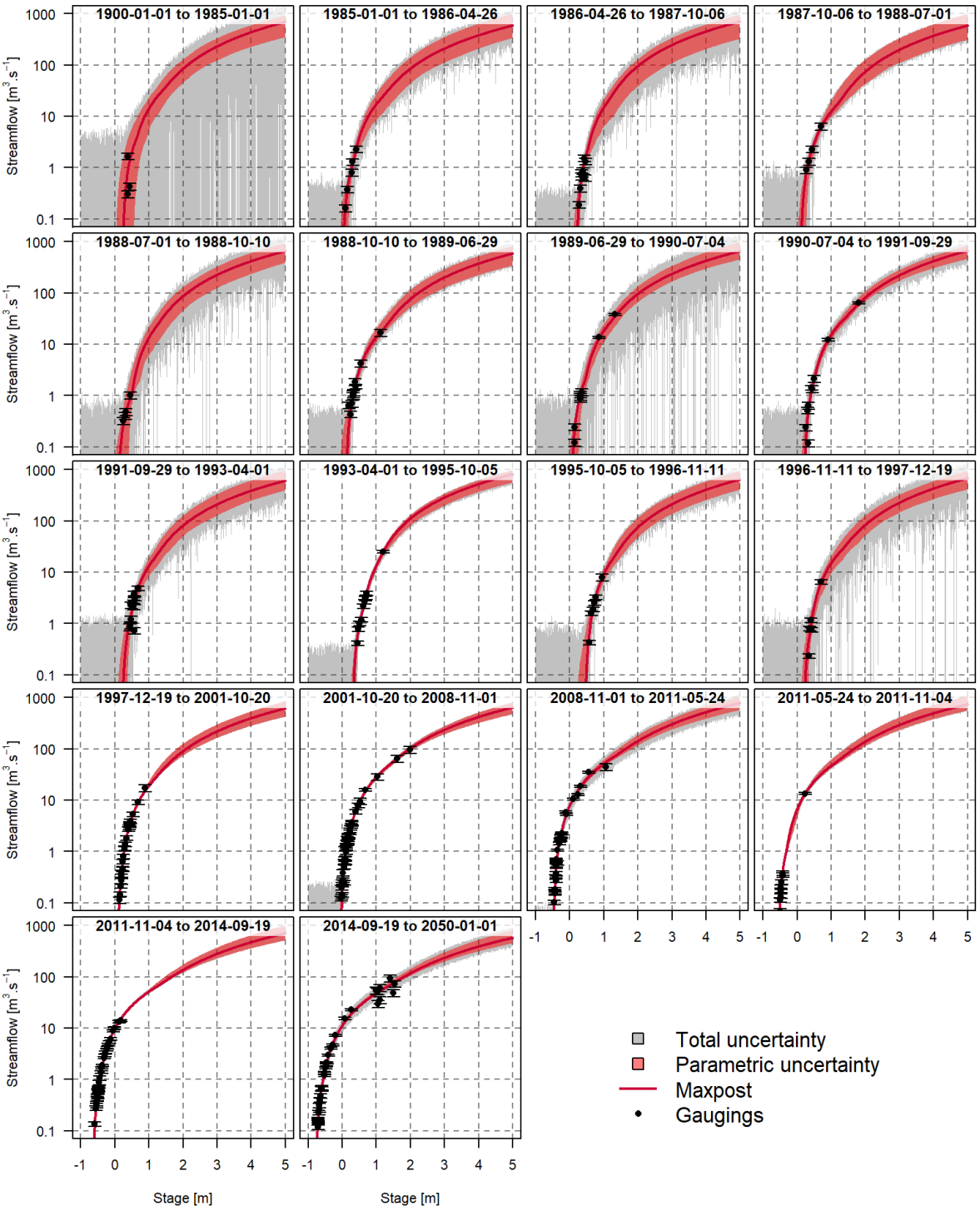

Figure B.3: Rating curve estimated using BaRatin for all the stable periods of Meyras.

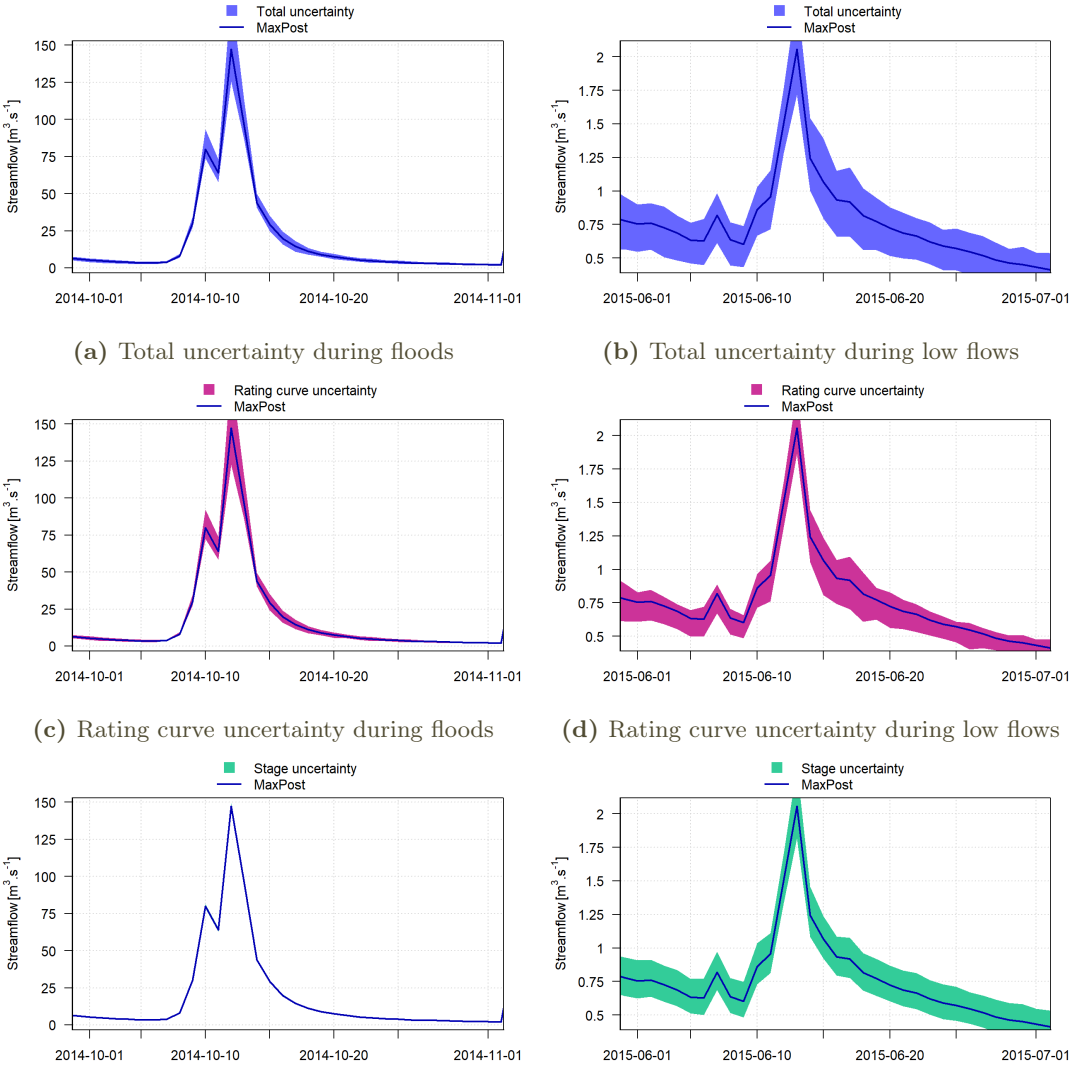

(a) Total uncertainty during floods

(b) Total uncertainty during low flows

(c) Rating curve uncertainty during floods

(d) Rating curve uncertainty during low flows

(e) Rating curve uncertainty during floods

(f) Rating curve uncertainty during low flows

Figure B.4: Streamflow time series and associated uncertainty for the flood events of late 2014 (left) and low flow period of 2015 (right) in the Meyras catchments. Results considering the impact of different uncertainty sources are shown: total uncertainty (top), only rating curve uncertainty (middle) and only stage uncertainty (bottom).

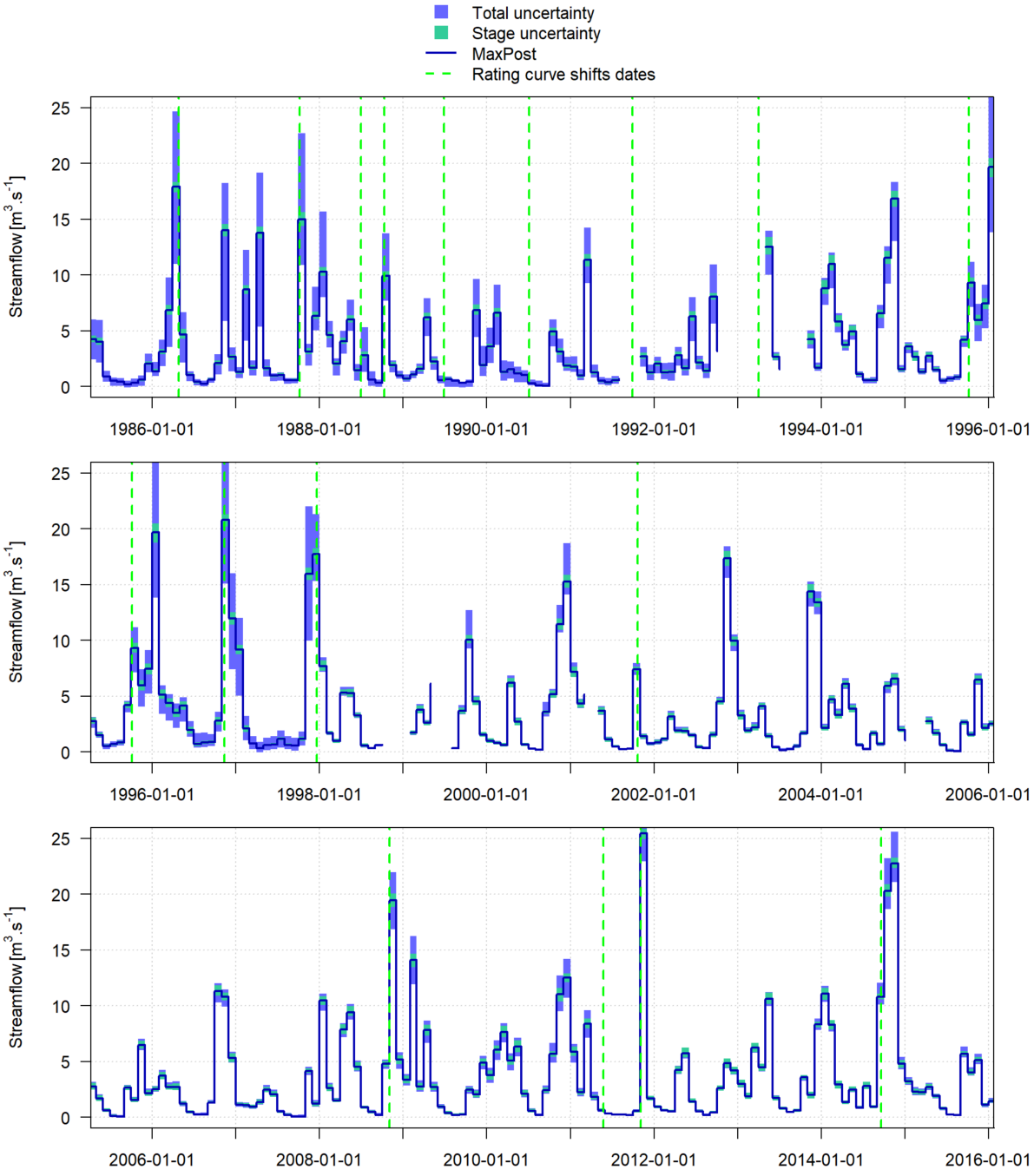

Figure B.5: Monthly average of streamflow for three decades – from 1985 to 2015 – for the Meyras catchment.

B.3 Pont-de-Labeaume

B.3.1 Hydraulic controls and rating shifts

Figure B.6: Pictures of the river directly downstream of the hydrometric station of Pont-de-Labeaume (left, taken from the bridge) and of the bridge were the water stage sensor is located (right, taken from the left bank). (pictures taken by Irstea in April 2013)

In 2013, Raphaël Le Boursicaud (Irstea, HHLY) applied the BaRatin method to the hydrometric station of Pont-de-Labeaume. Part of his work was used here in particular the mathematical equation used to model the rating curve and the *prior* parameter values. No details on the hydraulic analysis were found, hence, the application of BaRatin described here is slightly simplified and less confident in the *prior* parameter values used. In this previous BaRatin application two hydraulic controls were considered to account for overflow on the river banks. The last control which was supposed to occur for stage value exceeding 3.6 m was not considered here. Since the stage reference scale was moved in January 1989 (considered here as a rating curve shift), stage measurements almost never exceeded 3.6 m (see Figure B.7) and because no information could be found to support this choice, this simplification appeared reasonable. Therefore, in our application of BaRatin to the Pont-de-Labeaume hydrometric station, three different hydraulic controls are supposed to affect the relationship between stage and streamflow for different river stage: (1) a natural riffle for low stage (visible in Figure B.6, left), (2) a channel control of the river bed for medium to high stage, and (3) an additional channel control due to the overflow of water on the river banks for the highest stage values. This analysis results in the following rating curve equation:

$$Q(h) = \begin{cases} 0 & \text{for} \quad h \leq k_1 \\ a_1(h-k_1)^{c_1} & \text{for} \quad k_1 < h \leq k_2 \\ a_2(h-k_2)^{c_2} & \text{for} \quad k_2 < h \leq k_3 \\ a_2(h-k_2)^{c_2} + a_3(h-k_3)^{c_3} & \text{for} \quad h > k_3 \end{cases} \tag{B.2}$$

The prior parameter values used for a_i, c_i and k_i are reported in Table B.3. The minimum stage values as well as all the transition stage between the hydraulic controls (all k_i) were set to different *prior* values for the different stable period to account for rating shifts. Even the last transition stage was considered as the change of reference stage scale affected the stage time series dramatically (about 1m). Note that the change of reference stage scale was considered here as a rating curve shifts. All the transition stage (k_i) were specified relatively to the minimum stage value of the rating curve (k_1): +0.4 m for k_2 and +2.5 m for k_1.

The hydrometric station manager of Pont-de-Labeaume is the SPC Grand-Delta who has provided us with gaugings and historical information that includes documented shifts. The stage time series was downloaded from the Banque Hydro[2] database at a variable time step. The downloaded time series ranged from January 1980 to January 2013 but included large gaps. From the historical information, the visual inspection of the minimal value of the stage time series, and a detailed analysis of the gaugings for

[2] http://www.hydro.eaufrance.fr/

Table B.3: *Prior* parameter values used for the application of the BaRatin method on the Pont-de-Labeaume hydrometric station. $\mathcal{N}(\mu,\ \sigma)$ stands for a Gaussian distribution with mean μ and standard-deviation σ.

Hydraulic control	Parameter	*Prior* values
	k_1	-
Natural riffle	a_1	$\mathcal{N}(20,\ 5)$
	c_1	$\mathcal{N}(1.5,\ 0.025)$
	k_2	-
River channel	a_2	$\mathcal{N}(50,\ 15)$
	c_2	$\mathcal{N}1.67,\ 0.025)$
	k_3	-
Flood plain	a_3	$\mathcal{N}(90,\ 20)$
	c_3	$\mathcal{N}(1.67,\ 0.025)$

the different periods, 12 rating curve shifts were identified (see Figure B.7 and Table B.4). As mentioned above, the rating shift occurring in January 1989 is the modification of the stage reference scale. It affected the stage measurements greatly as can be seen in Figure B.7. The minimum stage values k_1 were specified for each stable period using the minimum stage value of the period (Figure B.7) as an upper boundary of the 95% uncertainty interval of the effective "crest" level of the river riffle specified to be ±20 cm. The first transition stage k_2 was specified according to k_1 by adding 40 cm and using the same uncertainty (± 20 cm). The second transition stage k_3 was specified according to k_1 by adding 250 cm and using a larger uncertainty (± 50 cm). The *prior* values used for k_1, k_2 and k_3 for each stable period are reported in Table B.4.

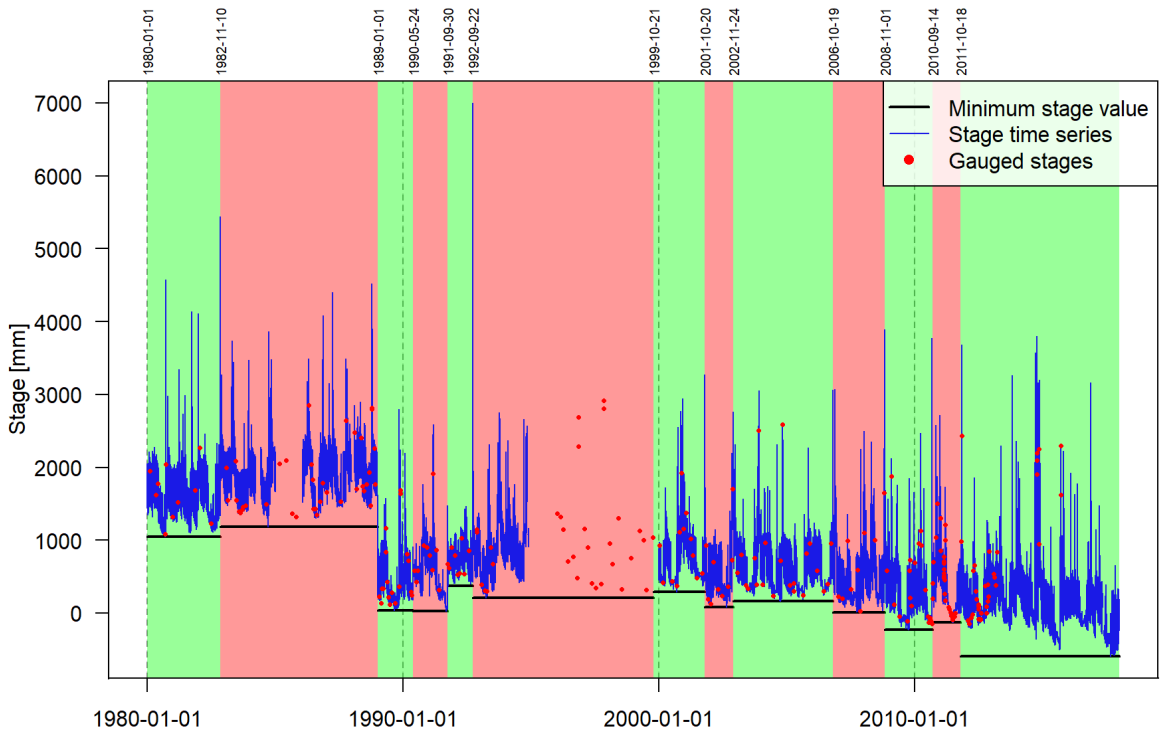

Figure B.7: Stage time series of the Pont-de-Labeaume catchment. The identified stable period are shown with different background colors. The date of each shifts are indicated in the top of the plot.

Table B.4: *Prior* parameter values of k_1, k_2 and k_3 used for the application BaRatin method for each stable period for the Pont-de-Labeaume hydrometric station. $\mathcal{N}(\mu,\ \sigma)$ stands for a Gaussian distribution with mean μ and standard-deviation σ. The date of the start of each stable period are reported in the first column and the number of gaugings available for each period is reported in the last column.

Date (DD/MM/YYYY)	k_1	k_2	k_3	Number of gaugings
01/01/1980	$\mathcal{N}(0.85,\ 0.1)$	$\mathcal{N}(1.25,\ 0.1)$	$\mathcal{N}(3.35,\ 0.25)$	10
10/11/1982	$\mathcal{N}(0.98,\ 0.1)$	$\mathcal{N}(1.38,\ 0.1)$	$\mathcal{N}(3.48,\ 0.25)$	37
01/01/1989	$\mathcal{N}(-0.16,\ 0.1)$	$\mathcal{N}(0.24,\ 0.1)$	$\mathcal{N}(2.34,\ 0.25)$	18
24/05/1990	$\mathcal{N}(-0.17,\ 0.1)$	$\mathcal{N}(0.23,\ 0.1)$	$\mathcal{N}(2.33,\ 0.25)$	10
30/09/1991	$\mathcal{N}(0.17,\ 0.1)$	$\mathcal{N}(0.57,\ 0.1)$	$\mathcal{N}(2.67,\ 0.25)$	9
22/09/1992	$\mathcal{N}(0.01,\ 0.1)$	$\mathcal{N}(0.41,\ 0.1)$	$\mathcal{N}(2.51,\ 0.25)$	31
21/10/1999	$\mathcal{N}(0.09,\ 0.1)$	$\mathcal{N}(0.49,\ 0.1)$	$\mathcal{N}(2.59,\ 0.25)$	12
20/10/2001	$\mathcal{N}(-0.12,\ 0.1)$	$\mathcal{N}(0.28,\ 0.1)$	$\mathcal{N}(2.38,\ 0.25)$	9
25/11/2002	$\mathcal{N}(-0.04,\ 0.1)$	$\mathcal{N}(0.36,\ 0.1)$	$\mathcal{N}(2.46,\ 0.25)$	22
20/10/2006	$\mathcal{N}(-0.19,\ 0.1)$	$\mathcal{N}(0.21,\ 0.1)$	$\mathcal{N}(2.31,\ 0.25)$	9
01/11/2008	$\mathcal{N}(-0.43,\ 0.1)$	$\mathcal{N}(-0.03,\ 0.1)$	$\mathcal{N}(2.07,\ 0.25)$	22
14/09/2010	$\mathcal{N}(-0.33,\ 0.1)$	$\mathcal{N}(0.07,\ 0.1)$	$\mathcal{N}(2.17,\ 0.25)$	29
18/10/2011	$\mathcal{N}(-0.79,\ 0.1)$	$\mathcal{N}(-0.39,\ 0.1)$	$\mathcal{N}(1.71,\ 0.25)$	35

B.3.2 Uncertain rating curve estimation

A total of 253 gaugings were available for the estimation of the Rating curves (Table B.4). The uncertainty associated with gaugings were specified according to the gauging technique, similarly to those of Meyras: 5% for ADCP and dilution gaugings, 10% for the veolcity-area method when there are multiple point measurements for each vertical and 15% for all other or unknown techniques.

The thirteen resulting rating curves are reported in Figure B.8. The large number of gaugings for all periods (last column in Table B.4) leads to relatively well defined rating curves. However, we can see large uncertainties for the period from May 1990 to September 1991 due to the small number of gaugings which appear to be more scattered than for the other periods. In addition, for some of the periods, the rating curves remain quite uncertainty for the high streamflow values (e.g. first period or period from September 1991 to September 1992).

B.3.3 Computing uncertain streamflow time series

To account for the uncertainty associated with stage time series, the same method and values than those used for the Meyras hydrometric station were used for Pont-de-Labeaume: (1) non-systematic errors between ±0.5 cm ($\sigma^h_{NS} = 0.0025$) for the lowest stages and ±5 cm ($\sigma^h_{NS} = 0.025$) for the highest stages and (2) systematic errors of ±2 cm ($\sigma^h_{NS} = 0.01$) for all stage values with a re-sampling periodicity of 60 days. The 200 stage time series were then computed using the stage error model of Horner et al. (2018b) and used to compute 200 streamflow time series using the 200 rating curves. The resulting instantaneous (variable time step) uncertain streamflow time series are illustrated for a high and low streamflow period in Figure 2.8.

B.3.4 De-influencing daily streamflow time series

The Pont-de-Labeaume hydrometric station is located downstream of the Montpezat hydropower dam which significantly influence the natural streamflow. This is particularly visible considering sub-daily data (Figures B.9a and B.9b) but it is also visible at a daily time scale (Figures B.9c and B.9d). In particular, a water derivation from the upper part of the Loire catchment, located North-West of the

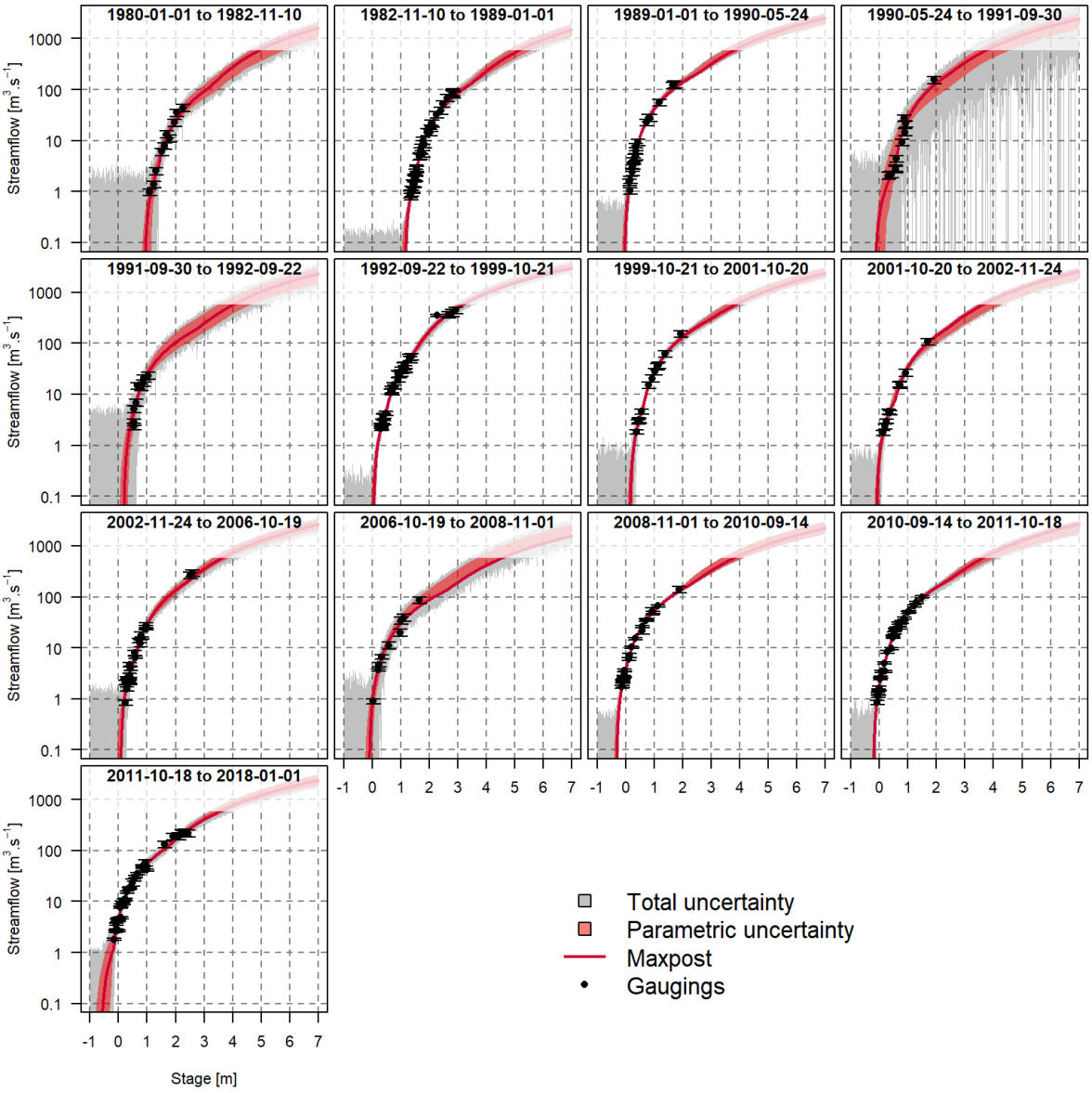

Figure B.8: Rating curve estimated using BaRatin for all the stable periods of Pont-de-Labeaume.

Ardèche catchment, significantly biases the water balance of the Pont-de-Labeaume catchment. The Montpezat dam manager, EDF, provided us with the daily water discharge going through the penstocks of Montpezat from 1958 to 2013 which enabled us to correct the data. During his Master Thesis, Noël (2014) proposed a methodology to de-influence the streamflow observations of several subcatchments of the Ardèche catchment including Pont-de-Labeaume. For Pont-de-Labeaume, he derived the following equation to calculate the "natural" streamflow Q_{NAT} as a function of observed streamflow Q_{OBS} and Montpezat dam discharge Q_{DAM} for each time step (day) t:

$$Q_{\mathrm{NAT}}(t) = Q_{\mathrm{OBS}}(t) - Q_{\mathrm{DAM}}(t) \tag{B.3}$$

This equation was used to compute the de-influence streamflow time series of Pont-de-Labeaume. Note that in rare cases this equation resulted in negative streamflow in which cases Q_{NAT} was set to 0. This data "correction" significantly modifies the streamflow time series at a daily resolution (Figures B.9e and B.9f) but also for longer time intervals (e.g. monthly, Figure B.10). In particular, it corrects the large bias in the Pont-de-Labeaume catchment water balance due to the excess water from the Loire catchment derivation.

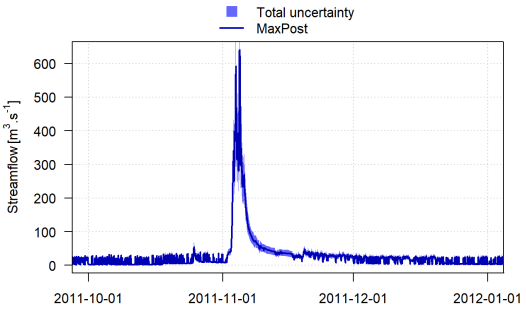

(a) Instantaneous streamflow time series during floods

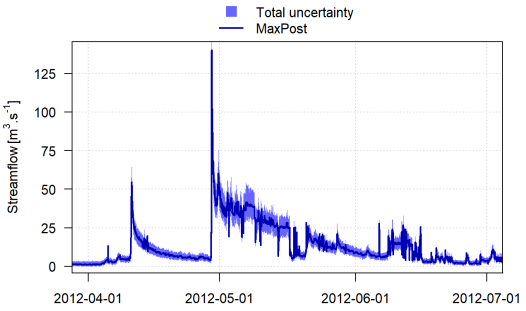

(b) Instantaneous streamflow time series during low flows

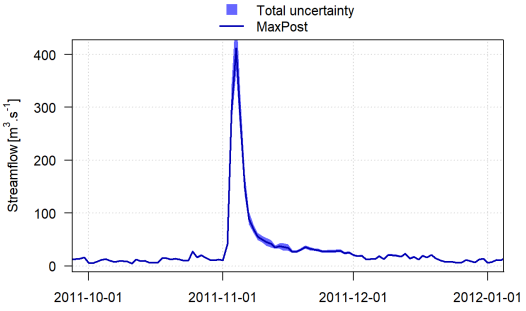

(c) Daily streamflow time series during floods

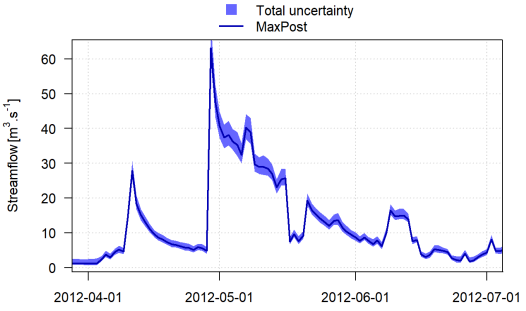

(d) Daily streamflow time series during low flows

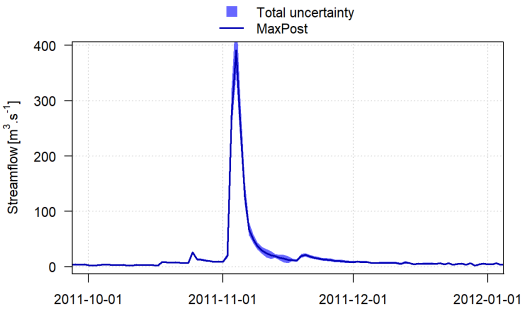

(e) Daily de-influenced streamflow time series during floods

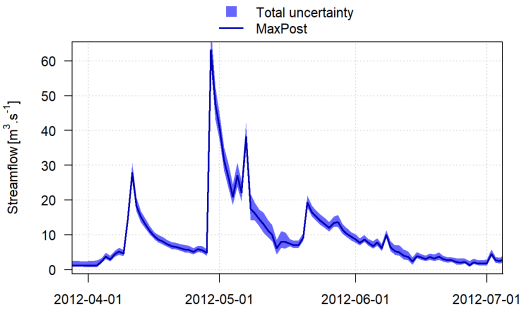

(f) Daily de-influenced streamflow time series during low flows

Figure B.9: Streamflow time series and associated total uncertainty for the flood event of late 2011 (left) and low flow period of 2012 (right) in the Pont-de-Labeaume catchments. (a) and (b): instantaneous time series; (c) and (d): daily time series; (e) and (f): de-influenced daily time series.

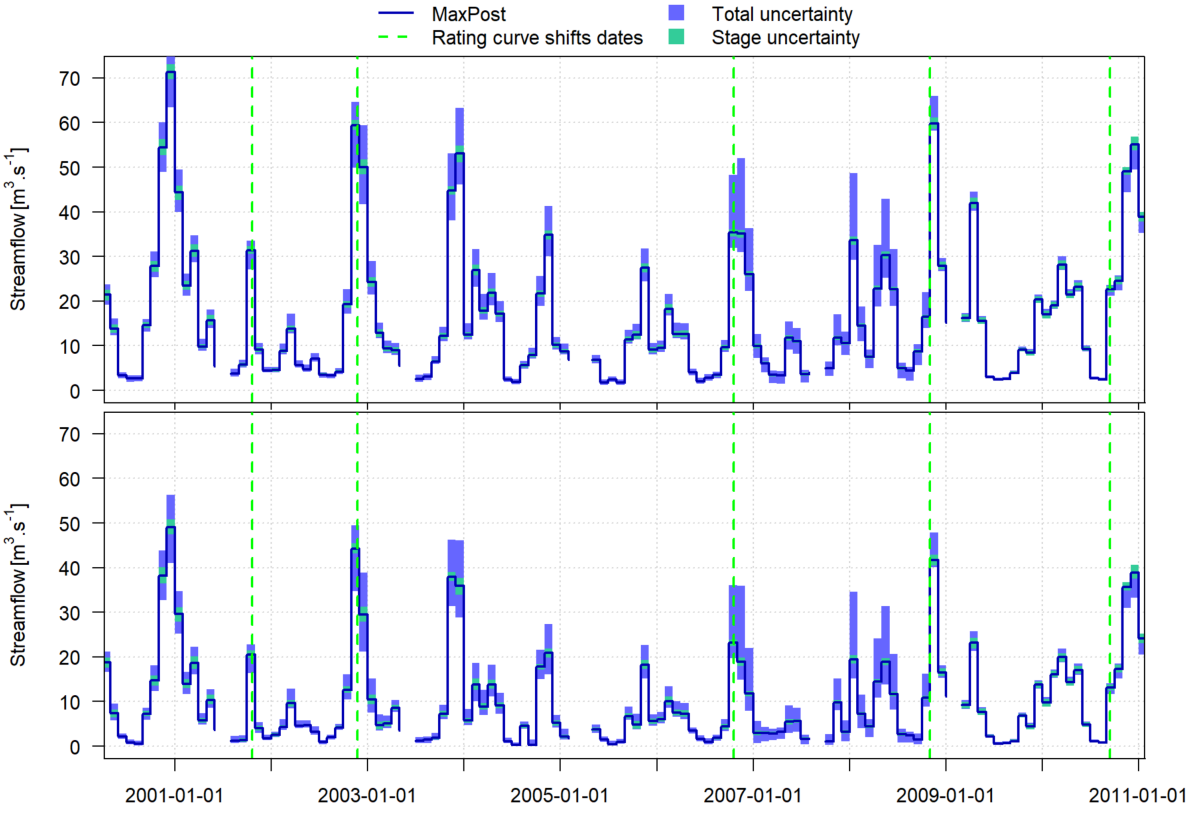

Figure B.10: Monthly average of streamflow of one decade – from 2000 to 2010 – in the Pont-de-Labeaume catchment. Top: Observed monthly average of streamflow; Bottom: De-influenced monthly average of streamflow.

B.4 Goulette

B.4.1 Hydraulic controls and rating shifts

Figure B.11: Picture of the weir located downstream of the water stage sensor (located of the left bank). (pictures taken by Irstea in April 2013)

In 2013, Raphaël Le Boursicaud (Irstea, HHLY) also applied the BaRatin method to the hydrometric station of Goulette. His work was re-used here for the definition of the rating curve mathematical equation and the specification of the *prior* parameter values. Figure B.11 shows a picture of the weir located downstream of the water stage sensor. This weir controls the relationship between stage and streamflow for a large range of stage values. According to the existing application of the BaRatin method to this hydrometric station, a hydraulic control by the river channel and banks takes over only for the highest stage values. Following the previous hydraulic analysis of the site, the following hydraulic controls are considered: (1) a small weir, a notch located within the main weir, for the smallest stage values, (2) the main weir, added to the small one, for the medium to high stage values and (3) for the highest stage values, a control by the channel and river banks. This analysis led to the following rating curve equation:

$$Q(h) = \begin{cases} 0 & \text{for} \quad h \leq k_1 \\ a_1(h-k_1)^{c_1} & \text{for} \quad k_1 < h \leq k_2 \\ a_1(h-k_1)^{c_1} + a_2(h-k_2)^{c_2} & \text{for} \quad k_2 < h \leq k_3 \\ a_3(h-k_3)^{c_3} & \text{for} \quad h > k_3 \end{cases} \tag{B.4}$$

The hydrometric station manager, EDF, provided the gaugings and the stage time series from January 1983 to March 2014. EDF identified a rating curve shift in September 1994 but the reason of this shift remains unknown. Analysis of the gaugings between the two stable periods (before and after the shift) confirms that a rating shift did occur (Figure B.12). It is likely that the shift is due to the modification of the banks on one the sides of the weir e.g. a rock being removed increasing the effective width of the main weir. This hypothesized explanation is consistent with the difference in the gaugings between the current period and the previous one (Figure B.12): for example, for a stage value of 0.5 m, the change of control induced an increase of the corresponding streamflow. In our application of BaRatin, two different periods are considered. However, the same *prior* values are used for both periods as the differences between both periods are small and the number of gaugings is sufficiently large to properly constrain the rating curves of both periods. The *prior* parameter values used are reported in Table B.5.

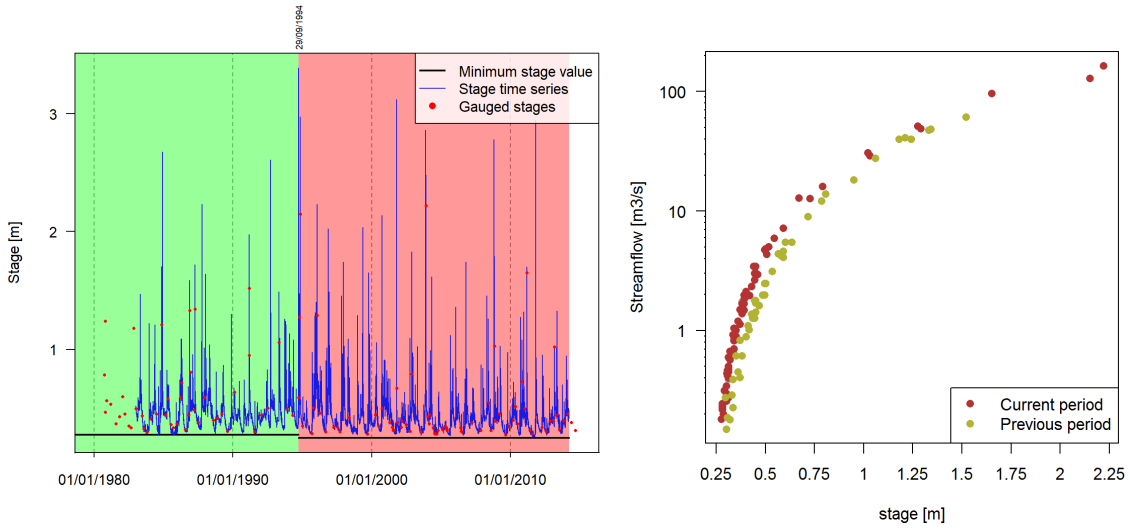

(a) Stage time series, September 1994 shift and gauged stage

(b) Gaugings of the current period (1994-09-29 to today) and previous period (before 1994-09-29).

Figure B.12: Stage time series, rating curve shift and gaugings of the Goulette hydrometric station

Table B.5: *Prior* parameter values used for the application of the BaRatin method on the Goulette hydrometric station. $\mathcal{N}(\mu,\ \sigma)$ stands for a Gaussian distribution with mean μ and standard-deviation σ.

Hydraulic control	Parameter	*Prior* values
	k_1	$\mathcal{N}(0.04,\ 0.005)$
Small weir	a_1	$\mathcal{N}(1,\ 0.25)$
	c_1	$\mathcal{N}(1.5,\ 0.025)$
	k_2	$\mathcal{N}(0.25,\ 0.05)$
Main weir	a_2	$\mathcal{N}(41,\ 5.5)$
	c_2	$\mathcal{N}1.5,\ 0.025)$
	k_3	$\mathcal{N}(0.7,\ 0.15)$
Flood plain	a_3	$\mathcal{N}(53,\ 11.5)$
	c_3	$\mathcal{N}(1.67,\ 0.025)$

B.4.2 Uncertain rating curve estimation

Figure B.12b shows the 122 gaugings available used in the application of BaRatin: 47 gaugings for the first period (before September 1994) and 75 gaugings for the second period (after September 1994). Following the work of Raphaël Le Boursicaud, a ±7% uncertainty was attributed to all gaugings. The resulting two rating curves are shown in Figure B.13. Due to the large number of gaugings for both periods, the uncertainty associated with both rating curves are rather small.

B.4.3 Computing uncertain streamflow time series

EDF provided the stage time series from January 1983 to April 2014 at an hourly time step. Although it is a fixed time step, they are actual instantaneous measurements: one instantaneous measurement kept every hour. The number of time steps is hence very large (273912 time steps) which leads to computer memory storage issues in the application of BaRatin. In addition, this is an unnecessary time resolution given that stage sometimes does not change much over multiple hours, in particular at low flow (see Figure B.14). Therefore, a sub-sampling of the stage time series was undertaken with the following rules: (a) remove time steps when there is no observed variation of stage (<0.005 m) and (b)

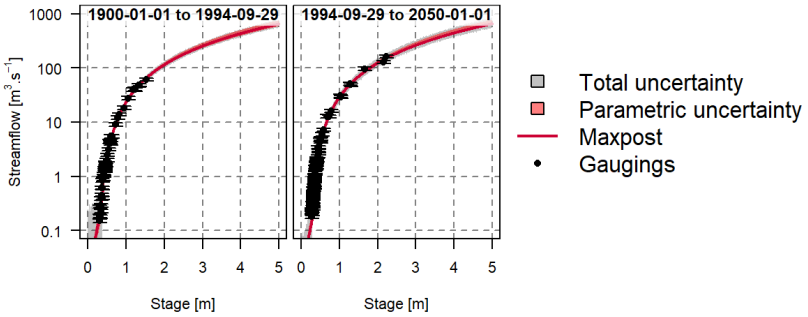

Figure B.13: Rating curve estimated using BaRatin for the two stable periods of Goulette.

keep at least one time step per day. This led to a significant reduction of the number of time step (from 273912 to 127502): only 47% of the original time series were kept. This sub-sampling is illustrated in Figure B.14.

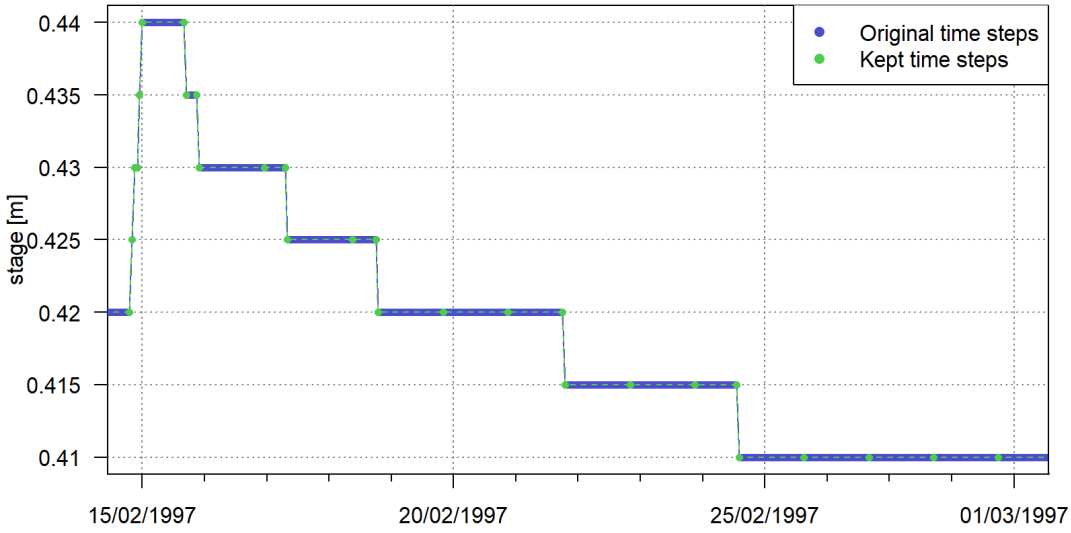

Figure B.14: Illustration of the sub-sampling of the stage time series of Goulette.

Figure B.14 shows that the stage measurements have a 5 mm height resolution. Accordingly, the stage non-systematic errors were set to range between ±5 mm ($\sigma^h_{NS} = 0.0025$) for the lowest stage value and ±5 cm ($\sigma^h_{NS} = 0.025$) for the highest stage values. Systematic errors were set at ±2 cm ($\sigma^h_{NS} = 0.01$) with a re-sampling periodicity 60 days.

Samples of the resulting uncertain instantaneous streamflow time series are shown in Figures B.15a and B.15b. The corresponding daily aggregated data are shown in Figures B.15c and B.15d. The monthly aggregated values from 1990 to 2000 are shown in Figure B.16. We note that the uncertainty due to stage measurement errors have large impacts on monthly streamflow values. As non-systematic errors affecting stage are averaged out in the time aggregation, this uncertainty arise mainly from stage systematic errors (Horner et al., 2018b). This large impact of stage errors on streamflow uncertainty might in part be due to the low sensitivity of the hydraulic controls, i.e. a small variation of stage inducing a large variation of streamflow (Horner et al., 2018a). This is also partly due to the low uncertainty affecting the rating curves.

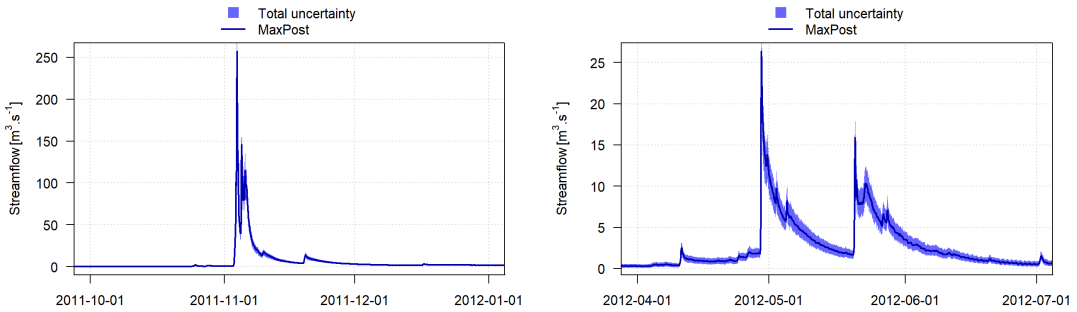

(a) Instantaneous streamflow time series during floods

(b) Instantaneous streamflow time series during low flows

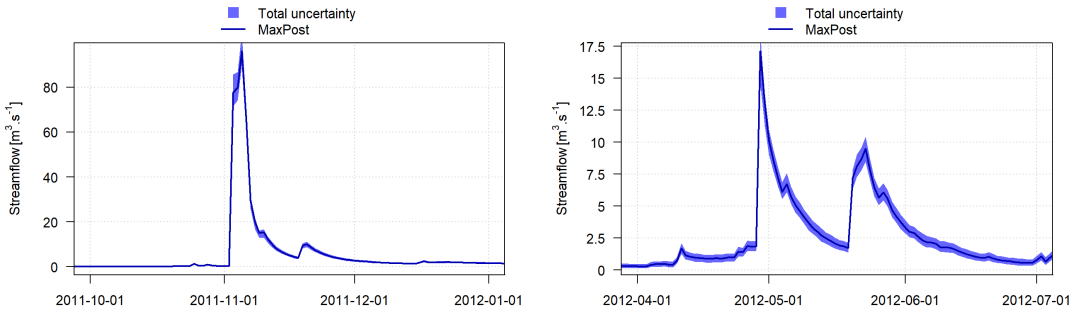

(c) Daily streamflow time series during floods

(d) Daily streamflow time series during low flows

Figure B.15: Streamflow time series and associated total uncertainty for the flood event of late 2011 (left) and low flow period of 2012 (right) in the Goulette catchments. (a) and (b): instantaneous time series; (c) and (d): daily time series.

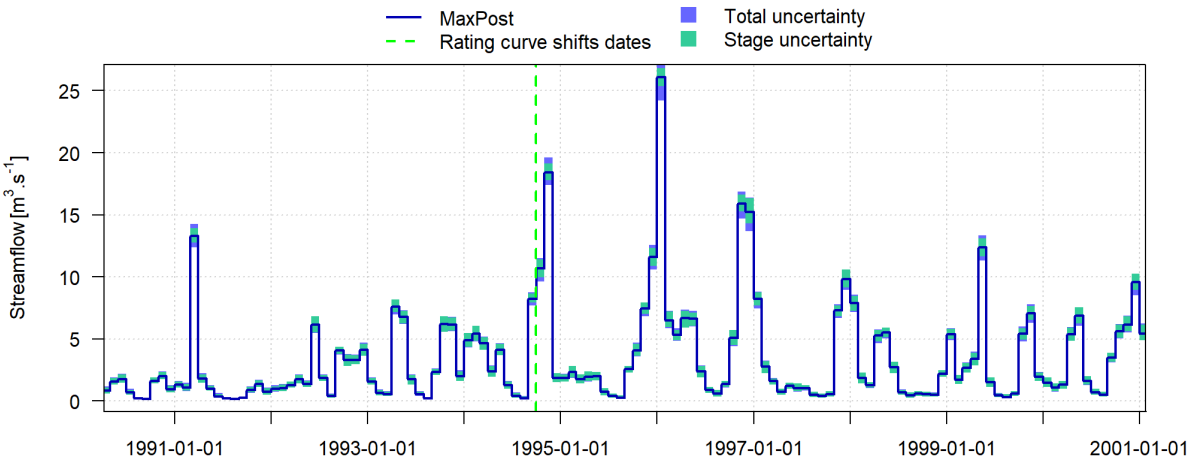

Figure B.16: Monthly average of streamflow of one decade – from 1990 to 2000 – in the Goulette catchment.

B.5 Cladužgne

Figure B.17: Picture of the hydrometric station of Cladužgne. The Red line locates the natural riffle controlling the stage-streamflow relationship at low flow. (picture taken from Tafasca (2017)).

B.5.1 Hydraulic controls and rating shifts

The Cladužgne catchment is part of the OHM-CV observatory Gazel-Clauègne experimental catchment (Nord et al., 2017). The hydrometric station is managed by IGE who provided us with the gaugings and stage time series from October 2011 to December 2018. During his internship, Tafasca (2017) applied the BaRatin method to the hydrometric station of Cladužgne. The hydraulic analysis and resulting rating curve equation as well as the *prior* parameter values used are well documented in his Master Thesis and are used here for the application of BaRatin with only minor modifications. Figure B.17 shows the Cladužgne hydrometric station and the low flow control (identified by a red line). In his application of BaRatin Tafasca (2017) considered (1) a first control by a natural riffle for the lowest stage values, (2) replaced for medium stage values by a control by the river channel and (3) an additional control by the river bank for the highest stage values. The rating curve equation derived from the analysis of Tafasca (2017) is:

$$Q(h) = \begin{cases} 0 & \text{for} \quad h \leq k_1 \\ a_1(h-k_1)^{c_1} & \text{for} \quad k_1 < h \leq k_2 \\ a_2(h-k_2)^{c_2} & \text{for} \quad k_2 < h \leq k_3 \\ a_2(h-k_2)^{c_2} + a_3(h-k_3)^{c_3} & \text{for} \quad h > k_3 \end{cases} \tag{B.5}$$

The *prior* parameter used are reported in Table B.6.

According to the station manager and Tafasca (2017), a major flood event in November 2014 caused significant morphological modification of the river bed inducing a shift in the relation between stage and streamflow. Therefore, Tafasca (2017) considered two periods in the application of BaRatin. However, the low stage values during the Summer of year 2014, before the shift, appear clearly higher than all other low stage values of previous Summers (see Figure B.18). This clearly indicates another shift occured during the flood of January 2014. The lack of low flow gaugings between January 2014 (first shift) and November 2014 (second shift, identified by Tafasca (2017)) cannot confirm this first rating curve shift. Nevertheless, three distinct periods were finally distinguished in our study (Table B.7). The *prior* parameter values for k_1 and k_2 (Table B.7) were specified using the uncertainty ranges used by Tafasca (2017) (± 0.1 m for both k_1 and k_2) and the minimum of stage time series for each stable periods.

Table B.6: *Prior* parameter values used for the application of the BaRatin method on the Cladugne hydrometric station. $\mathcal{N}(\mu,\ \sigma)$ stands for a Gaussian distribution with mean μ and standard-deviation σ.

Hydraulic control	Parameter	*Prior* values
	k_1	-
Natural riffle	a_1	$\mathcal{N}(4,\ 1.25)$
	c_1	$\mathcal{N}(1.5,\ 0.025)$
	k_2	-
River channel	a_2	$\mathcal{N}(27,\ 7.5)$
	c_2	$\mathcal{N}1.67,\ 0.025)$
	k_3	$\mathcal{N}(1.3,\ 0.2)$
River banks	a_3	$\mathcal{N}(17,\ 6)$
	c_3	$\mathcal{N}(1.67,\ 0.025)$

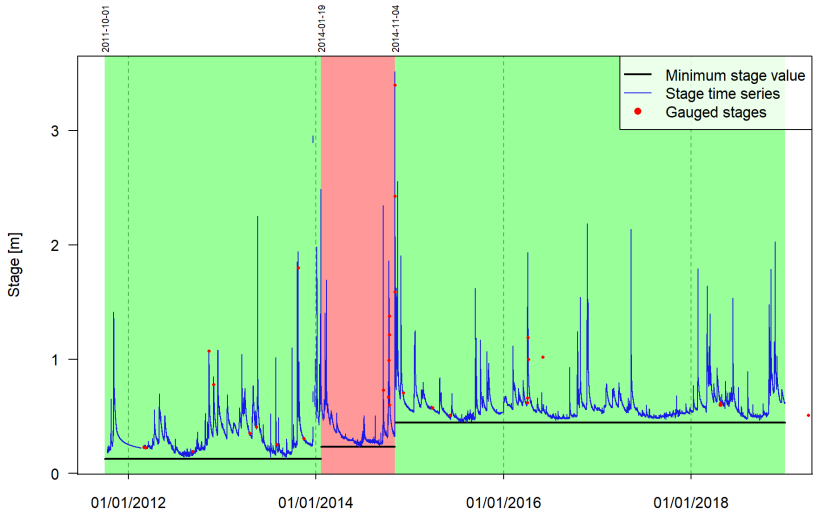

Figure B.18: Stage time series of the Cladugne catchment. The identified stable period are shown with different background colors. The date of each shifts are indicated in the top of the plot.

B.5.2 Uncertain rating curve estimation

For all periods, 39 gaugings were available (last column in Table B.7). Their uncertainty were specified according to the gauging methods (±10% for dilution gaugings and for the velocity area method and ±20% for surface velocity gaugings) or, when available, the recommendations of the field staff. The resulting rating curves for the three considered periods are presented in Figure B.19. Note that the lack of low streamflow gaugings in 2014 makes the uncertainty of the low flow section of the rating curve very large, reflecting the *prior* uncertainty specified for the low flow control.

B.5.3 Computing uncertain streamflow time series

In addition to the stage time series from October 2011 to December 2018, the station managers provided data regarding the validity of the stage measurements. In particular, the standard-deviation of the 30 measurements done at each time step to compute the stage value (mean) were available for years 2015 and 2016. Their analysis were used to specify the standard-deviation of the non-systematic errors affecting stage measurements. For each time step, the standard-deviation is linearly interpolated according to the stage value between the two extremes: $\sigma^h_{NS} = 0.001$ m for the lowest stage value and $\sigma^h_{NS} = 0.06$ m. In addition, differences between the reference stage scale and the stage sensors were available for each

Table B.7: *Prior* parameter values of k_1 and k_2 used for the application BaRatin method for each stable period for the Claduègne hydrometric station. $\mathcal{N}(\mu,\ \sigma)$ stands for a Gaussian distribution with mean μ and standard-deviation σ. The date of the start of each stable period are reported in the first column and the number of gaugings available for each period is reported in the last column.

Date (DD/MM/YYYY)	k_1	k_2	Number of gaugings
01/10/2011	$\mathcal{N}(0.02,\ 0.05)$	$\mathcal{N}(0.32,\ 0.05)$	14
19/01/2014	$\mathcal{N}(0.13,\ 0.05)$	$\mathcal{N}(0.43,\ 0.05)$	9
04/11/2014	$\mathcal{N}(0.34,\ 0.05)$	$\mathcal{N}(0.64,\ 0.05)$	16

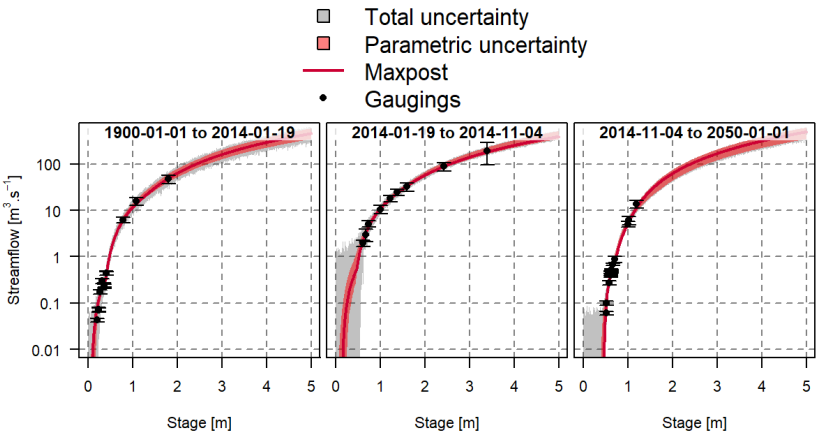

Figure B.19: Rating curves estimated using BaRatin for the three stable periods of Claduègne.

gaugings. The stage measurement correction applied by the station managers to account for stage sensors calibration drift were also available for the year 2015 and 2016. The analysis of these pieces of data led a small systematic error standard-deviation ($\sigma^h_{NS} = 0.005$ m) and a re-sampling periodicity of only 15 days.

Similarly to the Pont-de-Labeaume stage time series, a sub-sampling of the data was done with the same criterion; only 34% of the time steps were kept for the computation of the streamflow time series. The resulting instantaneous and daily aggregated streamflow time series and their associated uncertainty are shown for a high and low flow period in Figure B.20. Note that, as a consequence of the way the structural uncertainty of the rating curve is accounted for – errors sampled in a Gaussian distribution after the computation of streamflow through the 200 rating curves – Figure B.20 shows that the 95% uncertainty interval goes below zero during the low periods. Figure B.21 shows the monthly values over the whole available time series. It shows that uncertainty of globally larger, especially at low flow, for the year 2014 (second stable period). It also shows that the uncertainty of the rating curve largely dominates; the uncertainty due to the stage measurement errors is very small.

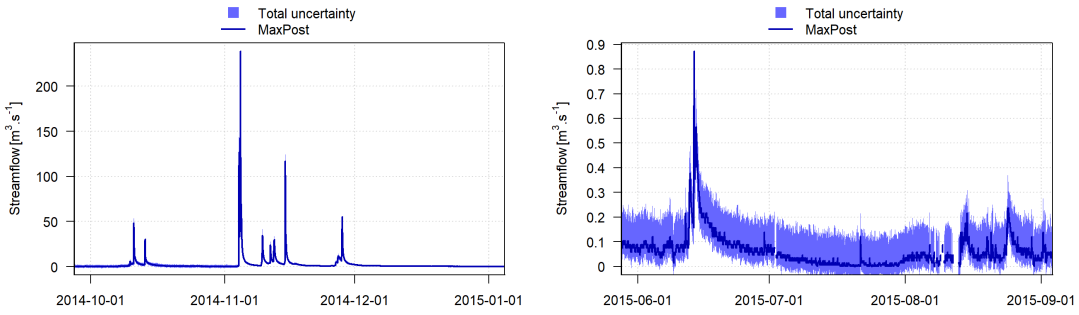

(a) Instantaneous streamflow time series during floods

(b) Instantaneous streamflow time series during low flows

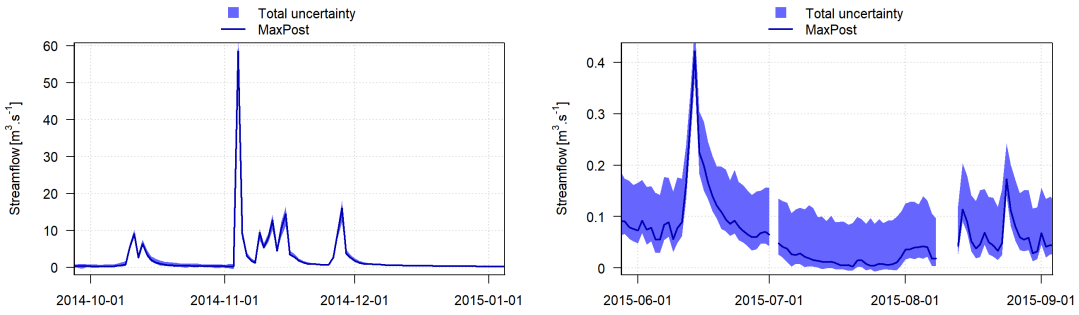

(c) Daily streamflow time series during floods

(d) Daily streamflow time series during low flows

Figure B.20: Streamflow time series and associated total uncertainty for the flood event of late 2014 (left) and low flow period of 2015 (right) in the Cladugne catchments. (a) and (b): instantaneous time series; (c) and (d): daily time series.

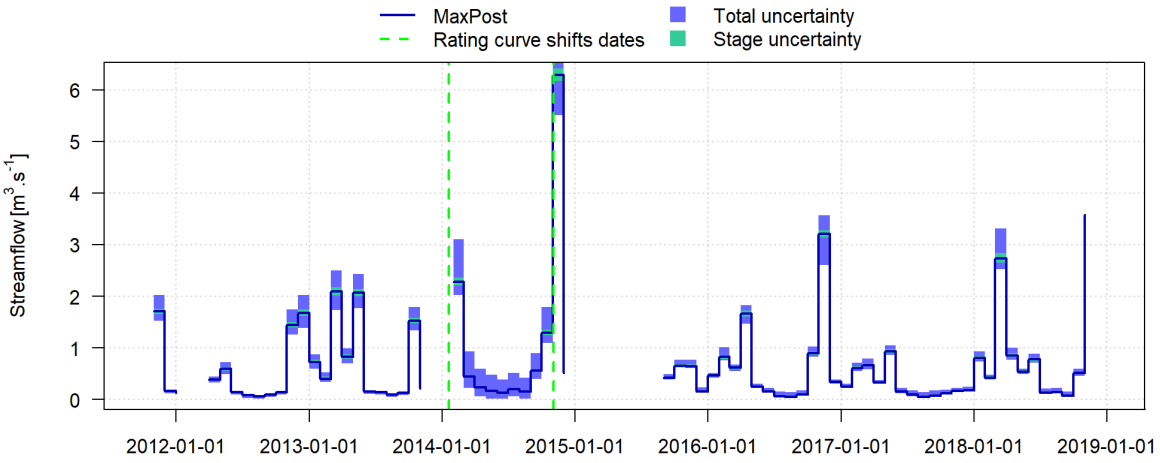

Figure B.21: Monthly average of streamflow from October 2011 to December 2018 in the Cladugne catchment.

Appendix C

Details on the J2000 model and associated tools

C.1 J2000 bug fixes and modifications

A bug was identified in the implementation of the MPS inflow and was corrected (see Figure C.1). Before the bug correction, if the potential inflow into the MPS reservoir, $I_{\mathrm{POT}}(t)$, exceeded the remaining available storage of MPS, the MPS reservoir was completely filled, short-cutting Equation 2.18.

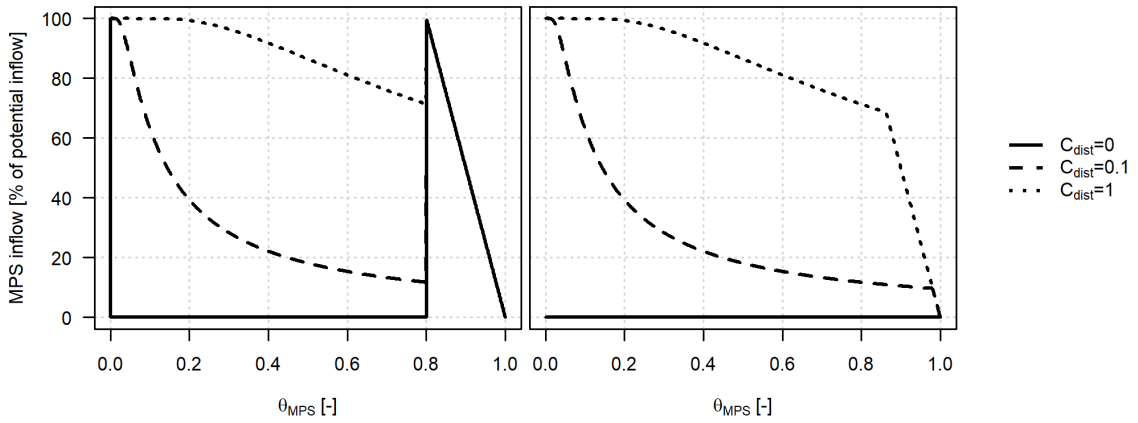

Figure C.1: Effect of the coefficient C_{DIST} on the proportion of $I_{\mathrm{POT}}(t)$ going into the MPS reservoir before (left) and after (right) the bug fix. In this example, the potential inflow $I_{\mathrm{POT}}(t)$ represents 20% of MPS_{max}.

Another bug was identified in the implementation of the diffusion and was corrected (see Figure C.2). As it affected only the case where MPS was empty ($MPS_{\mathrm{act}}(t) = 0$), it arguably had very little effect on the model behavior.

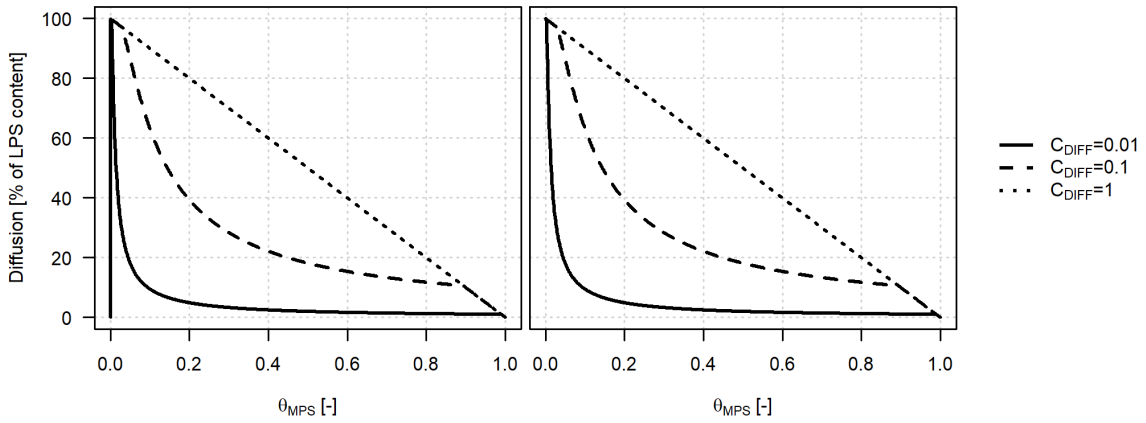

Figure C.2: Effect of the coefficient C_{DIFF} on the proportion of the LPS reservoir content being diffused to the MPS reservoir before (left) and after (right) bug fix. In this example, the LPS reservoir is fully saturated and has the same size than the MPS reservoir.

The impact of the sealing coefficient, K_{sealing}, on the model behavior was also modified. Previously, it was used to choose between only 10 possible values of actual surface sealing. As it was found unnecessary and removed. Parameter K_{sealing} is now used as it the actual surface sealing coefficient.

C.2 Layout of J2000 in JAMS

The general structure or layout of J2000 within JAMS is presented in Figure C.3. It was recreated from scratch based on the structure used in the J2000 Rhône model (Branger et al., 2016). As shown in Figure C.3, the actual hydrological processes represented in the model correspond to only a limited number of modules. The other modules manage forcing inputs, parameters, outputs and internal variables.

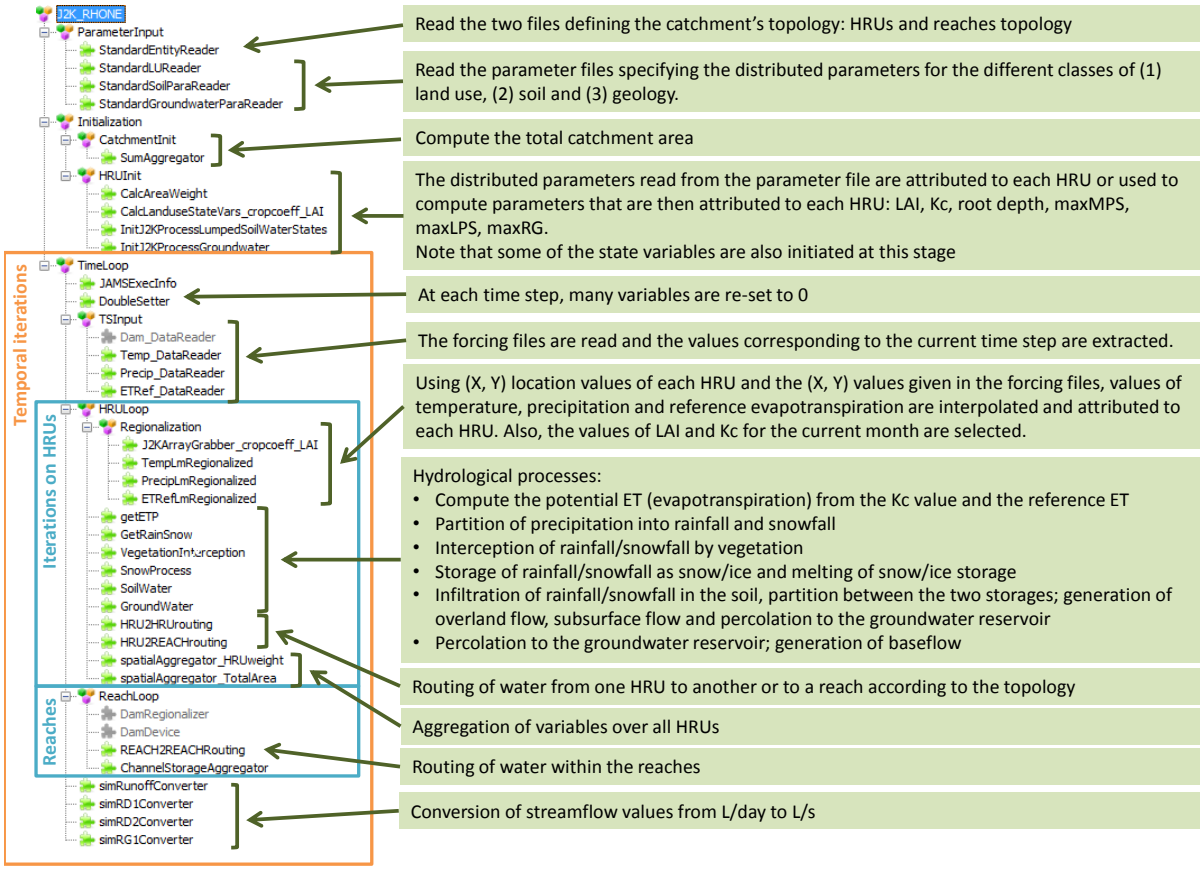

Figure C.3: Structure of the J2000 model within the JAMS platform

The general structure of the J2000 model that was recreated (Figure C.3) is independent of any catchment, i.e. it can be used for any catchment. Only the parameter files (including the topology file) and forcing files need to be modified to adapt the model to a given catchment. Note that some lumped parameters specified within JAMS might also need to be modified depending on the modeler needs. However, specific modules need to be added to output state and/or output variables of sub-catchments within a given catchment. These additional modules are necessary to aggregate the distributed parameters, inputs and state variables at the sub-catchment scale and retrieve the streamflow variables at the outlet of the sub-catchments. This is illustrated in Figure C.4.

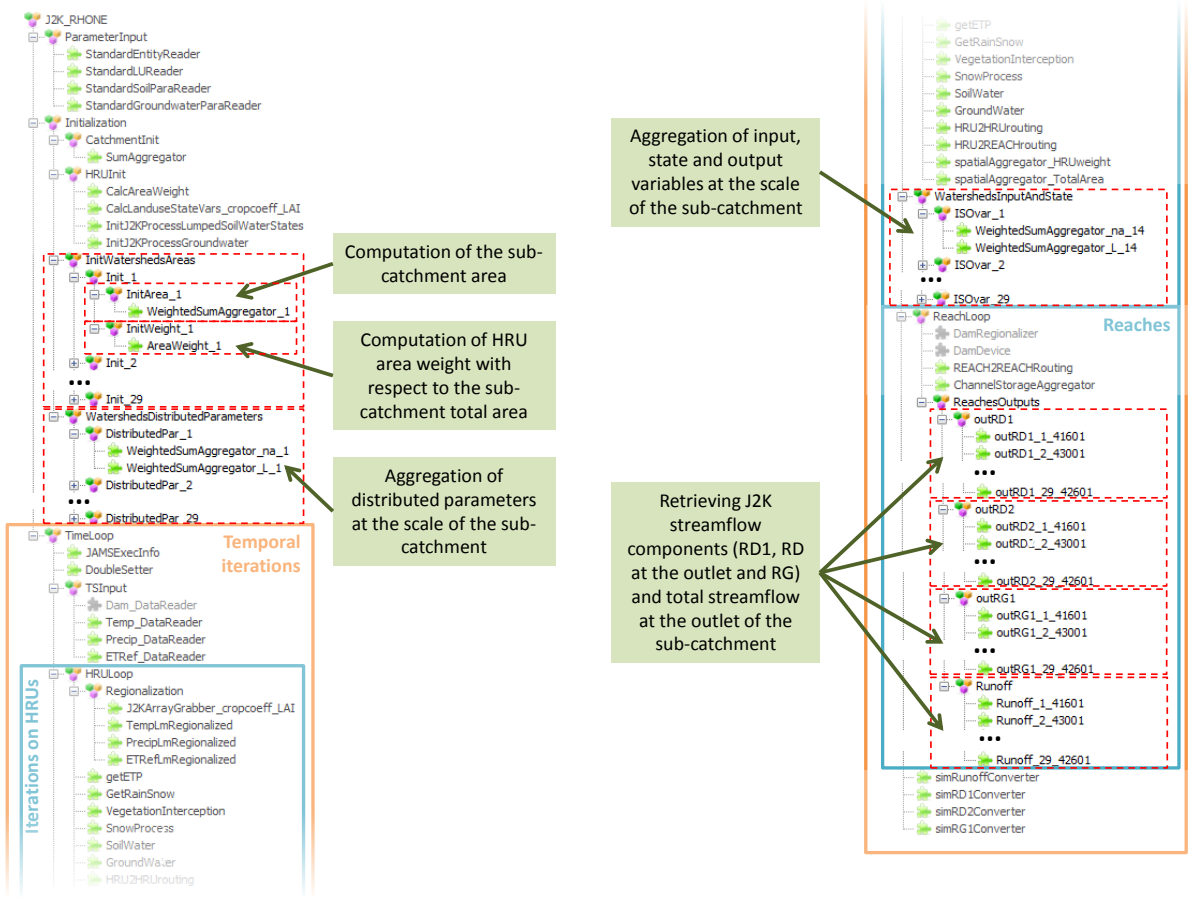

Figure C.4: Additional modules needed in JAMS to get aggregated distributed parameters, inputs and state variables at the sub-catchment scale and to retrieve streamflow variables at the outlet of the sub-catchments.

C.3 J2K-RUI: R tools for automatic edition of a J2000 model

Depending on the number subcatchments, adding these additional modules can become a cumbersome task. As a JAMS model is stored on the hard drive as an XML file, automatic editing using an external software is possible. For the J2000 Rhône model, this was done from R (R Core Team, 2018). However, most of the implemented R code was specific to the Rhône catchment. Therefore, I developed a new set of tools for the automatic edition of a J2000 model (XML file) from R. It was coded in a flexible way to be applicable to any catchments, taking advantage of the XML R package (Lang and The CRAN Team (2019)[1]).

This set of tools is called J2K-RUI (J2000 R User Interface). Its main goals are the automatic addition of the modules necessary to account for subcatchments. However it include other functionalities. The J2K-RUI:

- automates the addition of stations by automatically detecting, for each station, all the upstream HRUs from the topology files (hurs.par files) and shapefiles produced by HRU-Delin.
- set the variables wanted as outputs (for each subcatchment) by creating the modules that either sum (when in volume unit), average (other units) and/or retrieve (flow reach variables) the variable values.
- set the distributed parameters that the user wants to be averaged or summed for each subcatchment.
- creates the forcing files from NCDF Safran data files (automatically detecting the required Safran cells).
- edits the forcing files names and the simulation start and end time.
- extract any sub-catchments from topology files (and optionally shapefiles) creating new topology files (and new shapefiles) thus making it possible to create individual J2000 model for any subcatchment.
- reads/writes parameters files (*.par files) and input/output files (*.dat files).
- reads and plots the result time series after a J2K simulation has been run.

J2K-RUI allows gaining considerable time when setting up a model for any catchment. Moreover, the layout of the model in JAMS is more organized than for the J2000 Rhône model making exploration in the model contexts and components easier (Figure C.4); in the case of the J2000 Rhône model, the number of subcatchment considered and the lack of encapsulating contexts for the added modules made the model exploration within JAMS a long and difficult task.

[1] https://CRAN.R-project.org/package=XML

C.4 HRU-Delin: resulting files and bug fix

C.4.1 HRU and reach parameter files

The contents of the HRU and reach parameter files, *reach.par* and *hru.par*, resulting from HRU-Delin are presented in Tables C.1 and C.2 respectively. In these tables, the J2000 column gives the name of the parameter used in our version of J2000. Note that all these parameters are unique to each entity (HRU or reach) and are directly derived from spatial data. Two exceptions are the width and roughness (Strickler coefficient) of the reach that need to be specified for each reach by the modeler.

In Table C.1, the variables landuseID, soilID and hgeoID refer to the classes of the land-use, soil and geology of each HRU. Additional J2000 parameters files (land-use, soil and geology files) need to be created by the modeler to specify the values of the parameters that are distributed according to the type of land-use, soil or geology. The identification numbers in the HRU parameter files (Table C.1) are used by J2000 to retrieve, for each HRU, the parameter values specified in these additional parameter files. In J2000, each HRU is then associated with the parameters in the HRU parameter files and the parameters retrieved from the additional parameters files. Figure C.5 illustrates this through a fictive minimal example.

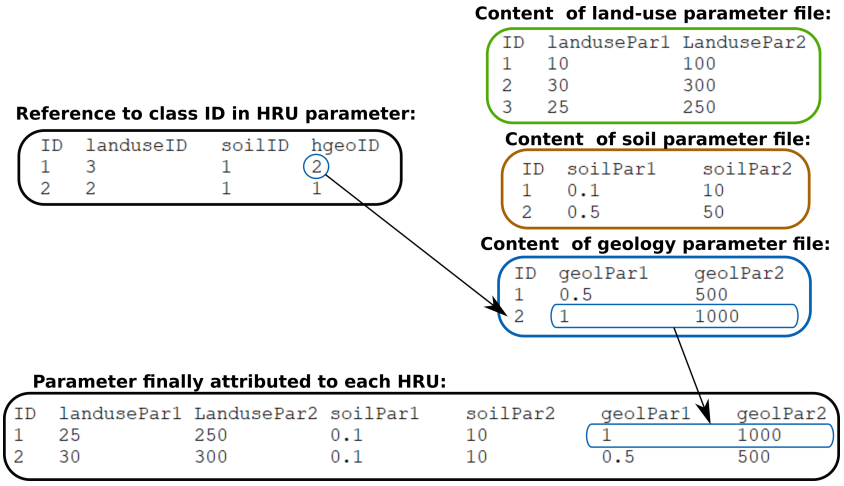

Figure C.5: Parameterization of each HRU according to the land-use, soil and geological class ID specified in the HRU parameter file and the parameter values and associated class ID in the additional parameter files. This is a fictive example for illustrative purposes only.

Table C.1: Content of the HRU J2000 parameter file produced by HRU-Delin. When specified, the J2000 name corresponds to the notation used to refer to the parameter in J2000 in this document.

Name	J2000 Name	Description
ID		Unique identification number of each HRU
area	HRU_{area}	Area, in m^2, infer from DEM
elevation		Average elevation, in m, infer from DEM
slope	HRU_{slope}	Average slope, in degree, infer from DEM
aspect		Average aspect, in degree, infer from DEM
x	X_{HRU}	X location, in m (Lambert93 projection), of centroid
y	Y_{HRU}	Y location, in m (Lambert93 projection), of centroid
watershed		Identification number of the HRU-Delin subcatchment
subbasin		Identification number of the user defined subcatchment
hgeoID		Identification number of the class of geology
landuseID		Identification number of the class of land-use
soilID		Identification number of the class of soil
to_poly†		Identification number of the downhill HRU it is connected to
to_reach†		Identification number of the reach it is connected to

† A HRU can be connected either to one reach or one HRU, not both; a 0 is specified when there is no connection.

Table C.2: Content of the reach J2000 parameter file produced by HRU-Delin. When specified, the J2000 name corresponds to the notation used to refer to the parameter in J2000 in this document.

Name	J2000 Name	Description
ID		Unique identification number of each reach
to-reach		Identification number of the downstream reach
length	L_{reach}	length of the reach, in m
slope	J_{reach}	average slope of the reach, in degree, infer from DEM
sinuosity		sinuosity of the reach, unit-less, infer from DEM
rough	K_{reach}	Roughness, Strickler coefficient of the reach, in $m^{1/3}/s$
width	W_{reach}	width of the reach, in m

C.4.2 HRU-Delin bug fix

HRU-Delin is a tool running on Linux. It is coded in Python and depends on many GIS libraries such as GRASS, GDAL and OGR. The treatment is performed both following raster and polygon approaches to address the challenging task of the GIS overlay, pixel grouping and HRU generation. It relies also on Java and AWK codes for the creation of the J2000 model topology.

The analysis of the J2000 topology resulting from HRU-Delin enabled the identification of a major bug. HRU-Delin creates its own sub-catchments based on the DEM using a GRASS drainage algorithm. Sub-catchments corresponding to the location of hydrometric stations or dams are defined independently using the same algorithms. In the HRU-Delin code, it turned out that these additional sub-catchments were ignored in the HRU delineation process and topology computation. It was visible only for some of the sub-catchments as HRU-Delin sub-catchments and the additional sub-catchments often share the same boundaries. This issue is illustrated in Figure C.6 for the Goulette catchment: water from the sub-catchments located to the East is routed within the Goulette catchment. In this case, the model will overestimate the volume of water at the outlet of the Goulette catchment. In other cases, the water could shortcut the catchment outlet resulting in an underestimation of the simulated streamflow volume at the outlet of the catchment.

HRU-Delin python codes were therefore modified to correct this bug. Figure C.6 shows the topology created by HRU-Delin after the bug correction.

The bug fix consisted mainly in making the part of the code were the HRUs are delineated account for the new constraint imposed by the additional subcatchments. The main modifications are detailed in the next paragraphs.

In step 2: The sub-catchments created in step 1, resulting from the GRASS drainage algorithm (the "subbasins" in the HRU-Delin terminology), and the sub-catchments created in step 2, corresponding the station[2] (the "watersheds" in the HRU-Delin terminology), are merged together: the two raster layers contains the indices of the "subbasins" (I_{subbasin}) and "watersheds" ($I_{\text{watersheds}}$) that are used to compute the new raster layer using the equation $I_{\text{watersheds}} \times 100000 + I_{\text{subbasin}}$. An example of the "subbasins" and "watersheds" is shown in Figure C.7. The resulting raster layer is re-classified according the reaches ids (which have already been cut according to the stations); an example of result is presented in Figure C.8. The results is saved in the intermediate result folder in the file *step2_ subbasins_ 2.tif*.

In step 3: Instead of taking the subbasin raster layer created in step 1 as a constraint in the HRU delineation process, the new subbasin raster layer (see previous paragraph) is used.

In step 4: Similarly to step 3, the new subbasin raster layer is used for looping over the HRUs when creating the topology of the J2000 model.

C.4.3 Other modifictions of HRU-Delin

HRU-Delin was further modified to add minor functionalities or facilitate and improve the user experience. In particular, the reaches are cut at the location of the hydrometric station (or dams) and the reach corresponding to each hydrometric station was previously not recorded. As the reach corresponding to each hydrometric station (dam) is necessary to retrieve the simulated streamflow, the user had to find them afterwards manually or using automatic approaches based on proximity criteria. HRU-Delin code was modified to retrieve this information and store it in the attribute table of hydrometric station (and dam) shapefile. A new (edited) shapefile is saved in the intermediate result folder: *step2_ stations.shp*.

Other modifications of the HRU-Delin codes include (1) computation progress monitoring and (2) polygonization of output raster layers for easy *a posteriori* exploration in a GIS software.

[2] hydrometric stations or dams

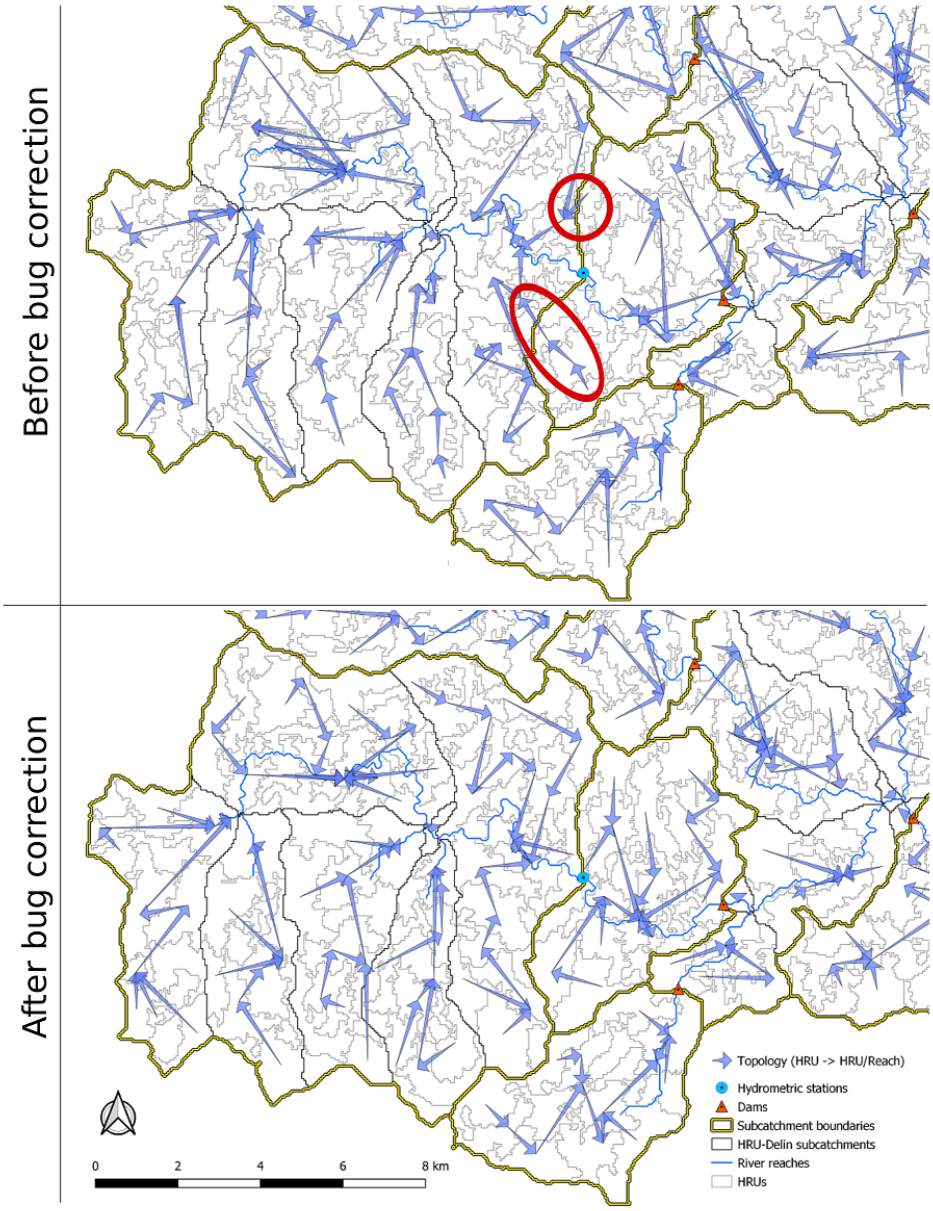

Figure C.6: Topology of J2000 created by HRU-Delin for the Ardèche catchment zoomed on the Goulette catchment, before (top) and after (bottom) the bug correction. The red circles locates examples of topology issues.

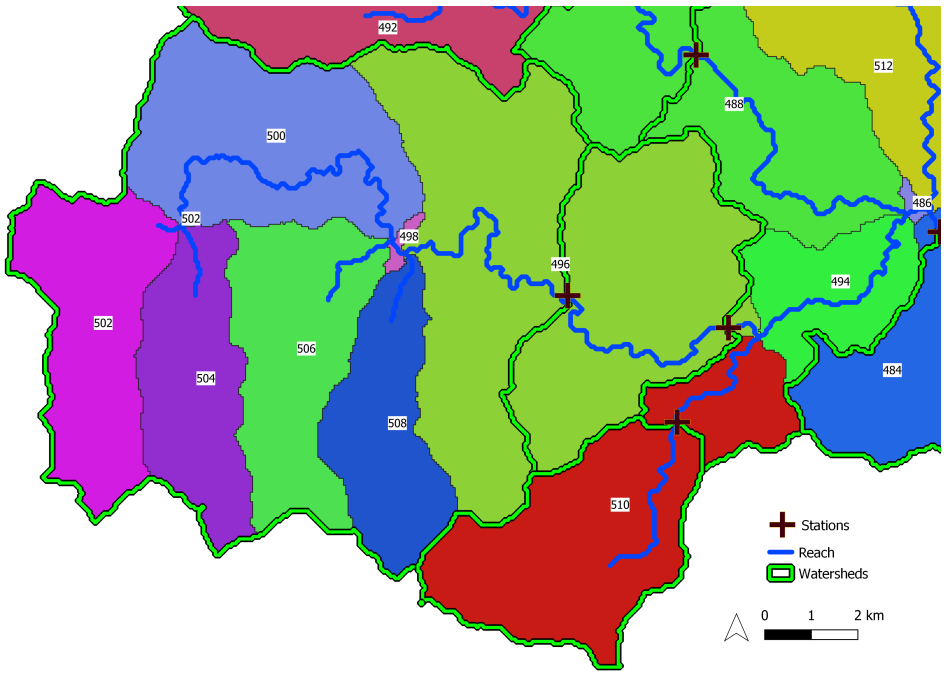

Figure C.7: Examples of "subbasins" (identified by the different colors and labels) and "watersheds" created in Step 1 and 2 of HRU-Delin respectively.

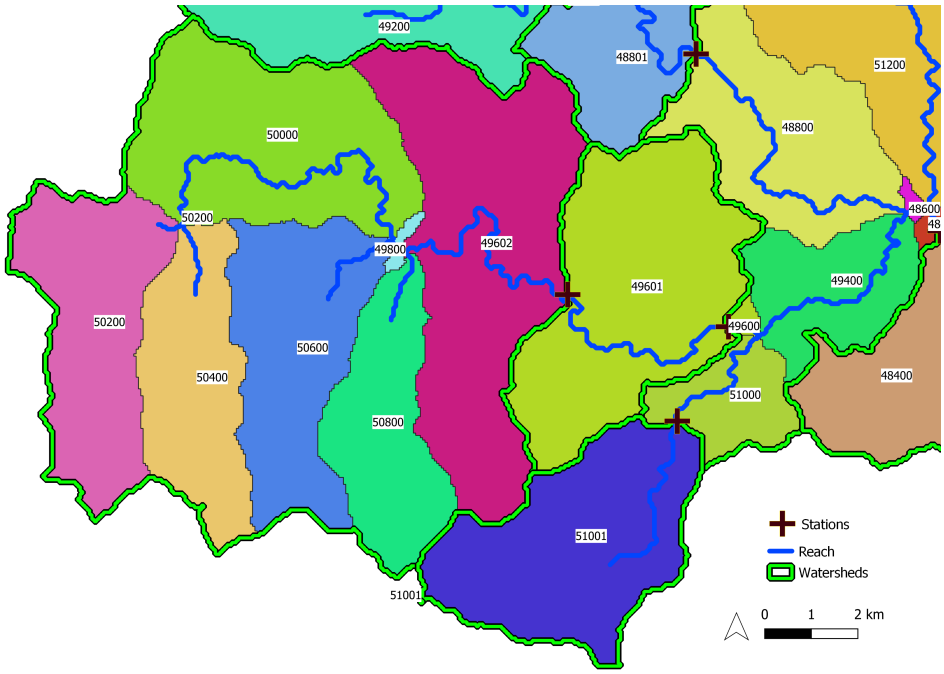

Figure C.8: Examples of the result of the cross product between "subbasins" and "watersheds" (presented in Figure C.7). The resulting new "subbasins" are identified by different colors. The associated labels show the results of the reclassification according to reach ids.

Appendix D

Details on the snow signatures

D.1 Examples of precipitation and streamflow for the Providence and Bull catchments

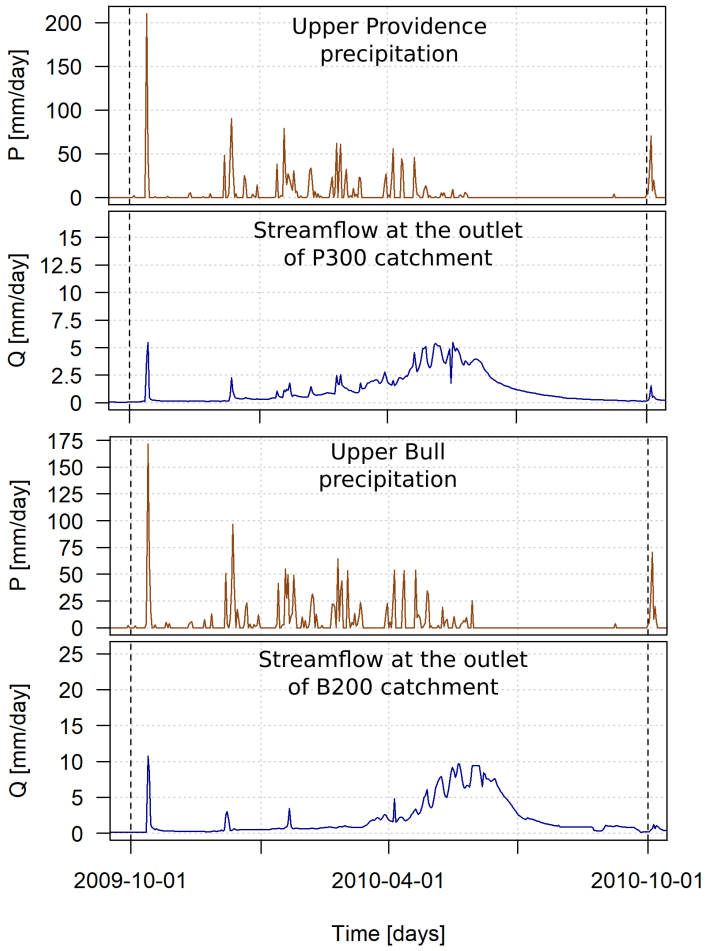

Figure D.1: Precipitation at the Upper Providence and Bull meteorological station and streamflow at the outlet of the Providence P300 and Bull B200 catchments over the hydrological year 2009-2010.

D.2 Details on the Mass Curve Technique approach for the estimation of snow storage

Let's consider inter-annual average of precipitation $\overline{P}$ and streamflow $\overline{Q}$ of each hydrological year calendar day. First, the cumulative precipitation P_{cum} and streamflow Q_{cum} are computed and plotted versus the days of the year. At any given day d of the hydrological year, it is possible to write the following relation:

$$P_{\text{cum}}(d) = Q_{\text{cum}}(d) - E_{\text{cum}}(d) + \Delta S_{\text{subsurface}}(d) + \Delta S_{\text{snow}}(d) \tag{D.1}$$

where E_{cum} is the actual cumulative evapotranspiration and $\Delta S_{\text{subsurface}}$ and ΔS_{snow} are the cumulative variations of soil and snow storage respectively.

The start and end of the high streamflow period corresponds to the inflection points in the sigmoid shape of Q_{cum}. The inflection points in Q_{cum} are found using its second derivative as follows: (1) the first derivative (i.e. streamflow $\overline{Q}$) is first smoothed using a 30-days moving window, then (2) the second derivative is computed and also smoothed using a 30-days moving window; finally (3) the timings of maximum, d_a, of the second derivative are used to derive the inflection points in the cumulative streamflow Q_{cum}.

From Eq. D.1, assuming that the first inflection point correspond to the start of the snow melt season (or the end of the snow accumulation season) and assuming that the actual cumulative evapotranspiration and the cumulative change in subsurface storage are small in front the cumulative change of snow storage a snow estimate, S_{MCT}, can be derived:

$$\begin{aligned} S_{\text{MCT}} &= \Delta S_{\text{snow}}(d_a) \\ &= P_{\text{cum}}(d_a) - Q_{\text{cum}}(d_a) + E_{\text{cum}}(d_a) - \Delta S_{\text{subsurface}}(d_a) \\ &= P_{\text{cum}}(d_a) - Q_{\text{cum}}(d_a) \end{aligned} \tag{D.2}$$

D.3 Additional results

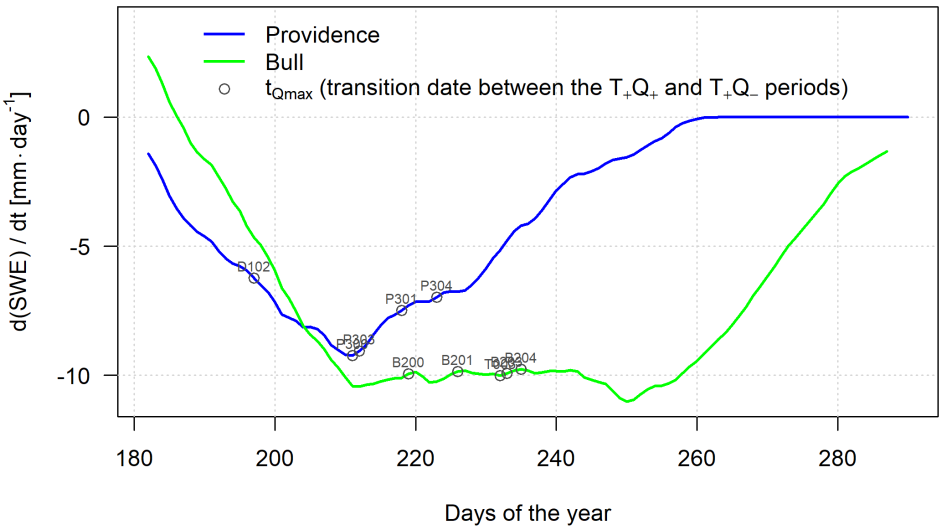

Figure D.2: Variations of SWE regimes dSWE/dt for the Bull (green) and Providence (blue) catchments over the T_+Q_+ and T_+Q_- periods. Circles locate the timings of the streamflow regimes maxima, transition dates between the T_+Q_+ and T_+Q_- periods.

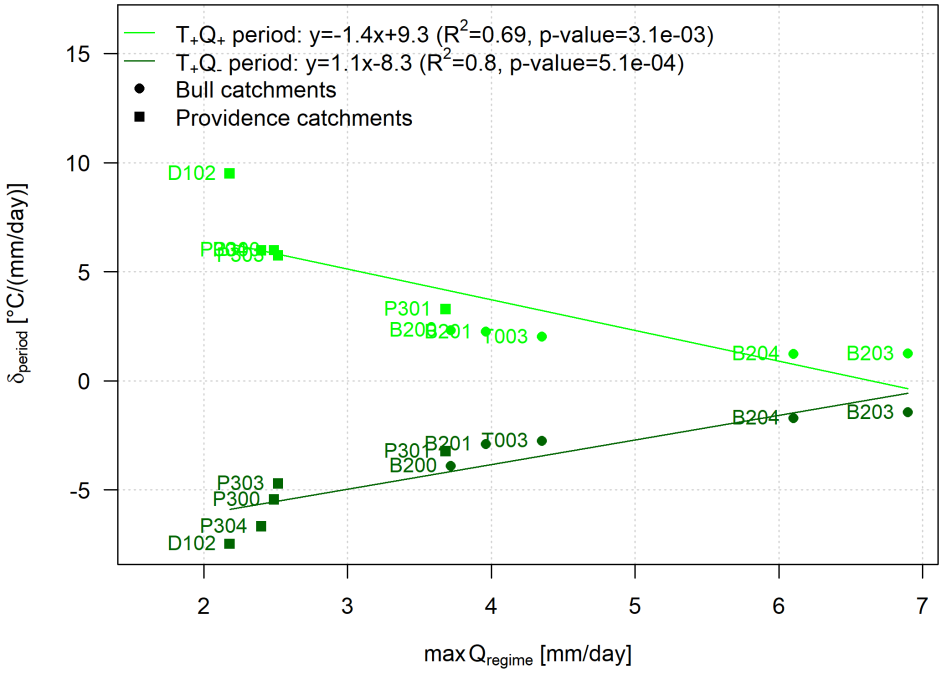

Figure D.3: Relation between the slopes of the T_+Q_+ and T_+Q_- periods and the streamflow regimes maxima for the Providence and Bull catchments.

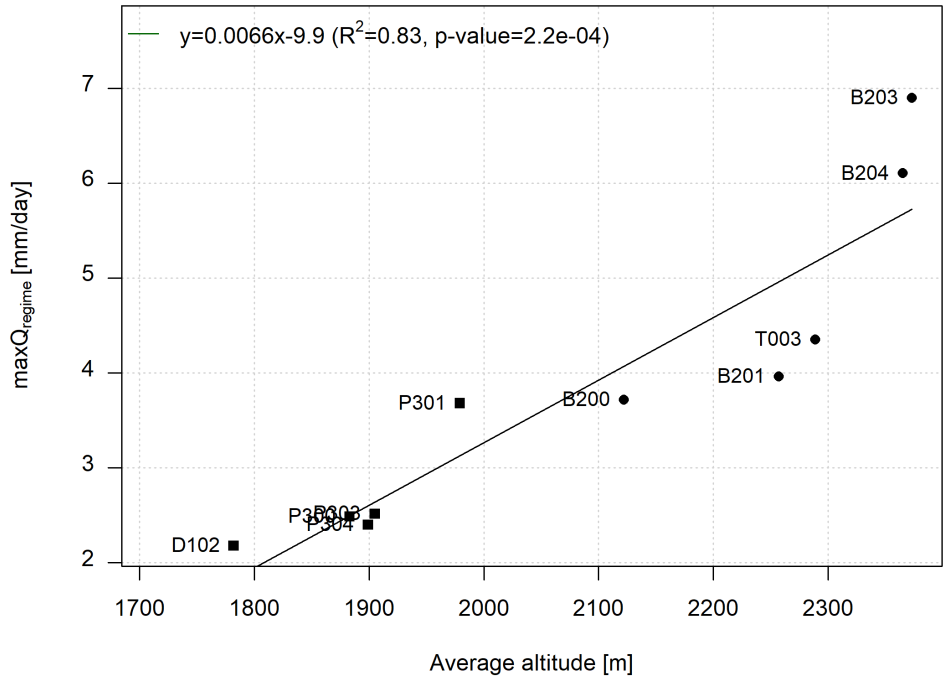

Figure D.4: Relation between the streamflow regimes maxima and the catchments average elevations for the Providence (square) and Bull (dots) catchments.

Appendix E

Details on the streamflow/precipitation based hydrological signatures

E.1 Not retained hydrological signatures

E.1.1 Event-based hydrological signatures

E.1.1.1 Event extraction

Studying the relationship between rainfall and runoff is possible using the whole time series. However, studying events can help to gather additional information on runoff processes such as the influence of rain intensity or antecedent rain (Molina-Sanchis et al., 2016). For such approaches, an event separation procedure is necessary.

Event separation methods are typically based on criterion on rainfall and many extraction procedures have been proposed (e.g. McMillan et al. (2010, 2011, 2014); Pfister et al. (2002); Troch et al. (2009); Zabaleta and Antigüedad (2013); Molina-Sanchis et al. (2016)). For example, McMillan et al. (2010) defined an event as follows: (1) the start of the event is identified when rainfall in a given hour is greater 0.5mm/day and if rainfall in the following 24 hours is greater than 10mm; and (2) the end of the event is identified if the maximum hourly rainfall in the next 36h is less than 0.5mm/day with a maximum duration for the whole event of 5 days.

As succinctly presented in the next subsection, events can be analyzed in terms of volumes (e.g. event runoff coefficient), timing (e.g. rainfall-runoff lag-time) or threshold with respect to precipitation intensity, volume or antecedent catchment wetness conditions.

E.1.1.2 Event runoff coefficient

The event runoff coefficient is a typical hydrological signature used to characterize events. It is the ratio between the event i streamflow volume Q_i and precipitation volume P_i (McMillan et al., 2014):

$$S_{ERC,1,i} = Q_i/P_i \tag{E.1}$$

Instead of total streamflow, the quickflow component, $Q_{QF,i}$, is also often used (Merz et al., 2006; Blume et al., 2007; Zabaleta and Antigüedad, 2013):

$$S_{ERC,2,i} = Q_{QF,i}/P_i \tag{E.2}$$

Using this second equation (Equation E.1) allows investigating the relative importance of quickflow which is closely related to overland flow. Using total streamflow (Equation E.2), McMillan et al. (2014) see the event runoff coefficient as a measure of the *"split between fast and slow runoff processes"*. In practice, the mean or median of all the event runoff coefficient is used.

Another way of approaching the event runoff coefficient is to use the Double Mass Curve (DMC) (Pfister et al., 2002). After separating the rainfall and streamflow time series into individual events, Pfister et al. (2002) plotted the cumulative values of event rainfall versus the cumulative values of event quickflow (extracted using digital filter) of all identified events. This so-called double-mass curve (DMC) showed high variability depending on the season *"with high stormflow values in winter and very low stormflow values in summer"* (Pfister et al., 2002). The slope of such a curve can be directly interpreted as an average runoff coefficient of all the considered events. As the maximum slope value, found in winter, is for period with arguably highly saturated soils, it reflects the maximum runoff coefficient (Pfister et al., 2002). In their study, Wrede et al. (2015) used the DMC to investigate catchment seasonality and catchment storage. They argued that the change of slope in the DMC between summer and winter periods indicated *"that a certain threshold needs to be exceeded before streamflow is initiated"*. They explained this threshold behavior as differences in the *"hydrological connectivity"* that depend on

the saturation of the catchment.

E.1.1.3 Rainfall-runoff lag time

Timing of events have also been used as hydrological signature. A typical approach is to measure the time lag between the center of mass of the event precipitation and event streamflow (e.g. Talei and Chua (2012); McMillan et al. (2011, 2014)). It can be used to asses how fast the water travels within the catchment. Combined with other types of analysis, the event lag time can help understand how the event water travels (e.g. as overland flow, sub surface flow, (McMillan et al., 2011, 2010, 2014)). Similarly to the event runoff coefficient, the mean or median event lag time is often used.

E.1.1.4 Threshold in event streamflow response

Events are also studied to investigate possible threshold behaviors. For example, McMillan et al. (2014) investigated the threshold behavior of runoff coefficients against precipitation and soil moisture. Using precipitation and the quickflow component of streamflow, Tromp-van Meerveld and McDonnell (2006) investigated threshold response at the hill-slope scale. Threshold behaviors seem to be mostly visible at small space scales (hill-slope or small headwater catchments). They are explained following several theory including the *"fill-and-spill"* hypothesis of Tromp-van Meerveld and McDonnell (2006) and/or Lehmann et al. (2007) who hypothesized that *"water flows along preferential flow pathways which may include macropores, bedrock valleys, and free water pounding at the bedrock. [...] As long as these pathways are not connected the runoff at the bottom of the hill-slope will be small but increases dramatically if the flow pathways become connected"*.

E.1.1.5 Irrelevance of event based hydrological signatures when using daily data

Most of the approaches cited above were tested including many automatic event extraction algorithms. However, we were unsuccessful in extracting relevant hydrological signatures that captured meaningful differences between observed and simulated data, or between catchments.

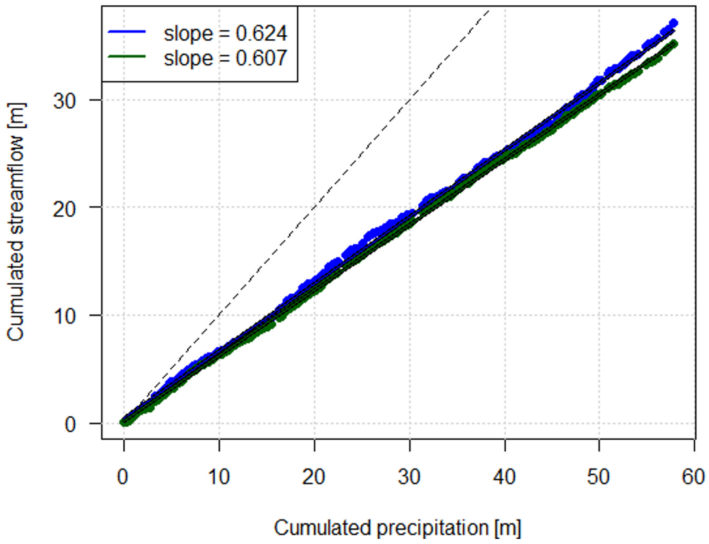

Figure E.1: Example of double mass curve obtained for the Meyras observed (blue) and simulated (green) data. The double mass curve is the plot representing the cumulative event streamflow volume and cumulative event precipitation volumes.

The event runoff coefficient showed differences when taken event by event but the overall difference were small when compared to observed streamflow time series uncertainties. Figure E.1, shows the

double mass curve of all the extracted events of Meyras. It shows that little differences are visible, on average, between observed and simulated event streamflow with respect to event precipitation.

For the catchments that were studied, Meyras, Pont-de-Labeaume and Goulette and Claduègne, timing could not be used probably because the daily temporal resolution is too coarse for the investigated processes: for all the investigated catchments, lag time of zero or one day were obtained for most events.

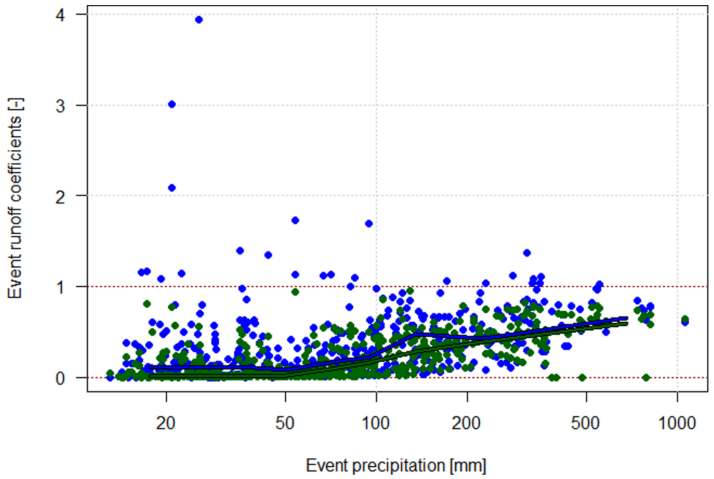

Figure E.2: Observed (blue) and simulated (green) event runoff coefficient against event precipitation volume obtained for the Meyras catchment. The blue and green lines represent the moving median of the observed and simulated runoff coefficient respectively. Note that a log scale is used for the x axis.

Threshold behavior were slightly visible but none of the propose techniques in the literature led to satisfactory results: either no threshold were detected or the results were very similar between observed and simulated data. For example, Figure E.2 shows the event runoff coefficient and their relation to event precipitation extracted for the Meyras catchment. In this example, a moving median shows that a change of trend in the runoff coefficient can be detected for high event precipitation volumes. This change of trend, in addition to being similar between observed and simulated data, could not be detected using automatic approaches (e.g. segmented regression).

E.1.2 Rising/declining limb density

The rising limb density or declining limb density were used in model calibration contexts (e.g. Shamir et al. (2005b)), catchment classification contexts (e.g. Sawicz et al. (2011)) and model structure evaluation (e.g. Euser et al. (2013)). It is defined as the number of peaks N_{pk} divided by the total duration of rising (declining) parts of the streamflow time series T_R (T_D) over either the whole time series (Euser et al., 2013) or on specific time intervals (e.g. months, years) (Shamir et al., 2005b):

$$S_{RLD} = \frac{N_{pk}}{T_R} \tag{E.3}$$

$$S_{DLD} = \frac{N_{pk}}{T_D} \tag{E.4}$$

The rising (declining) limb density is a measure of the *"smoothness of the hydrograph"* that is uncorrelated to flow volumes (Sawicz et al., 2011; Euser et al., 2013). Shamir et al. (2005b) stated that these signatures were hard to relate to specific characteristics of a catchment. Similarly, Sawicz et al. (2011) found that it had little discrimination power between catchment in their classification scheme. Therefore, these hydrological signatures were not kept in our set of hydrological signatures.

E.1.3 Cross and auto-correlation

E.1.3.1 Auto-correlation between precipitation and streamflow time series

The catchment response have also been studied using signal analysis such as auto-correlation analysis, cross-correlation analysis and spectral analysis. These analysis have been widely used in hydrology *"to estimate hydrodynamic parameters and to quantify the relative importance of the different flow components"* (Zabaleta and Antigüedad, 2013).

Using the auto-correlation analysis, the auto-correlation coefficient at a given lag-time can be taken as a hydrological signature (e.g. 1 days as in Euser et al. (2013); Kundu et al. (2016)). As stated by Euser et al. (2013), this auto-correlation coefficient can be used as *"a measure of smoothness of a hydrograph"*. Euser et al. (2013) used it to represent the timing of the peaks. Mangin (1984) used an auto-correlation analysis to assess the *"memory effect"* of a catchment that he defined as the time necessary for the value of the auto-correlation to drop below a certain threshold.

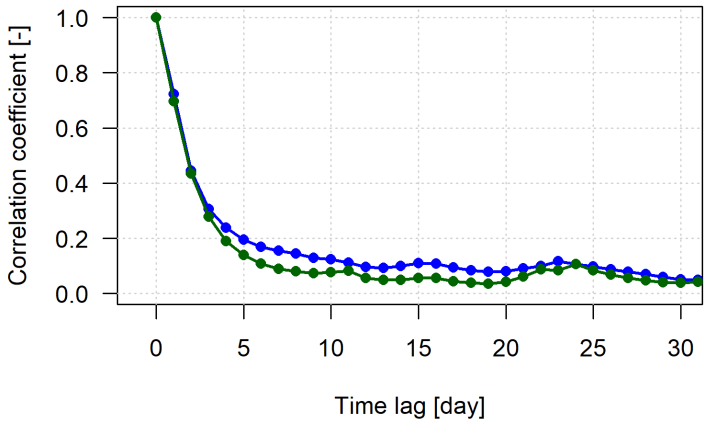

Figure E.3: Observed (blue) and simulated (green) auto-correlation function of the Meyras catchment.

Figure E.3 shows the 30 first days of the auto-correlation function of observed and simulated streamflow of Meyras. At a lag time of 1 day, the difference between the autocorrelation coefficient computed from observed and simulated data is small and does not seem to capture any actual differences between observed and simulated time series. Visible differences are obtained for lag-time larger than 3 days. However, these differences remains small and difficult to relate to actual differences in terms of hydrological processes. Therefore, the auto-correlation analysis was, in the end, not retained in our set of hydrological signatures.

E.1.3.2 Cross-correlation between precipitation and streamflow time series

Cross-correlation of time series study the correlation between the precipitation signal with the streamflow signal. Yilmaz et al. (2008) used such a method to derive a *"rainfall-runoff lag time"*. These methods are often used as they avoid the difficulty and the subjectivity necessarily involved in an event separation procedure (Yilmaz et al., 2008). In practice, the *"time shift at which the cross-correlation between areal rainfall and streamflow time series is maximized"* (Yilmaz et al., 2008) is used to estimate the lag time. They mentioned that such a method assumes a linear relationship between rainfall and runoff. They only use streamflow higher than a certain threshold to increase linearity and because high flows are arguably more representative of overland flow (Yilmaz et al., 2008). Wrede et al. (2015) used a similar method and interpreted the obtained lag time as the *"time to peak"* characteristic of the catchment.

Figure E.4 shows the cross-correlation between observed precipitation and observed streamflow and simulated streamflow for the Meyras catchment. Similarly to the analysis of the lag-time derived from

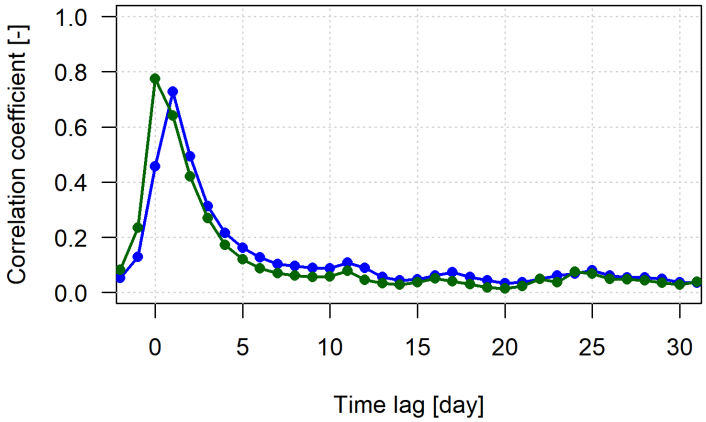

Figure E.4: Observed (blue) and simulated (green) cross-correlation function between precipitation and streamflow of the Meyras catchment.

the analysis of events, no clear differences can be seen between observed and simulated data. This is also a consequence of the too coarse daily temporal resolution used in our analysis. The cross-correlation analysis was, in the end, not used in our set of hydrological signatures.

E.1.3.3 Recession time and recession concavity

A classical approach to study recessions is to plot the variations of streamflow $\mathrm{d}Q(t)/\mathrm{d}t$ against streamflow $Q(t)$ to build the so-called *"recession plot"* (Kirchner, 2009) and then fit a recession model to obtain the parameter values. The logarithm transformation of Equation 4.17 yield a linear relation:

$$\log\left(-\frac{\mathrm{d}Q(t)}{\mathrm{d}t}\right) = \log(a) + b\log(Q(t)) \tag{E.5}$$

Classical fitting procedures can then be used to estimate parameters a and b, such as least-square regression (e.g. Kirchner, 2009; Stoelzle et al., 2013) or quantile regression (e.g. Vannier et al., 2013). In practice the points defined by $(Q(t) - Q(t - \Delta t))/\Delta t$ and $(Q(t-1) + Q(Qt))/2$ are used to fit the recessions. If Δt is often set to 1, other authors used larger time variation (e.g. Rivera-Ramirez et al., 2002). Parameters a and b can also be obtained by fitting the solution of the differential equation (Equation 4.18) with an iterative least squares fitting method (Wittenberg and Sivapalan, 1999).

The two parameters, a and b, of Equation 4.17 (or Equation E.5) can be used as hydrological signatures. The inverse of parameter a , $\tau = 1/a$ is more convenient to use as it is expressed in time unit and can be interpreted as a characteristic recession time. Using the solution of the differential Equation 4.17 (Equation 4.18), it is possible to see how these two parameters are linked to the shape of recessions (see Figure E.5). Figure E.5 shows that these two parameters can be used to describe the shape of the recession, i.e. how fast streamflow decreases over time (parameter τ) and how the rate of streamflow decrease changes over time (parameter b). Parameter b measures the "concavity" of the recession: a high value indicates a very fast decrease in the early part of the recession and a slow decrease in the late part whereas a value of 1 indicates a linear decrease (in log space) for the whole recession.

The recession time τ is likely mostly related to how fast, on average, water stored in the catchment is released. It most likely characterizes groundwater release rates. As the early parts of recessions are also considered here, it also likely characterizes the rate of release from faster catchment water storage (fast and slow soil drainage contributions) and possibly overland flow contributions.

The shape of the recession as described by parameter b can be interpreted in various ways. Its value typically ranges between 1 and 3 (Brutsaert and Nieber, 1977; McMillan et al., 2014; Vannier

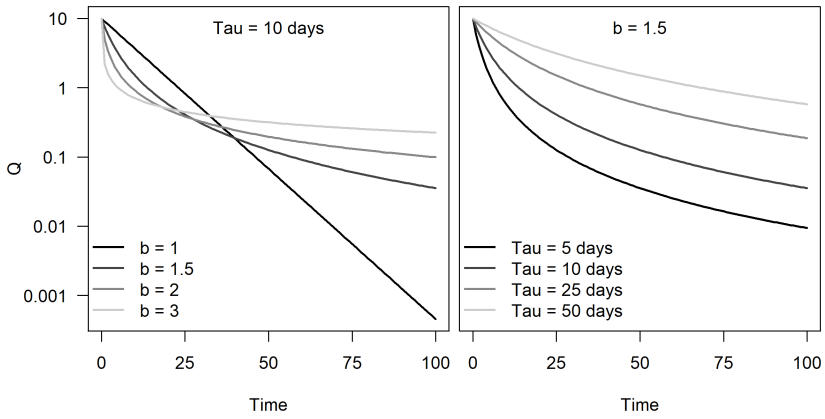

Figure E.5: Synthetic example illustrating the effects of parameter b and τ $(1/a)$ on the shape of recessions.

et al., 2013). McMillan et al. (2014) used the exponent b as a signature of the catchment complexity as there is evidence that increasing b could be related to increasing complexity (Clark et al., 2009). The increasing complexity can be seen as multiple (parallel) reservoirs draining at various rates as a consequence of heterogeneity (1) in stored water at a specific time, (2) water storage capacity and (3) hydraulic properties. Harman et al. (2009) demonstrated that the observed non linearity can be related to the spatial scale considered and hence to heterogeneity of the studied catchment: larger scales necessarily imply higher heterogeneity. Vannier et al. (2013) used the short and long time solutions of the Dupuit-Boussinesq aquifer problem proposed by Brutsaert and Nieber (1977) and demonstrated that parameters τ and b could be linked to physical characteristics or properties of the aquifer.

Parameter b can also be seen as a measure of the temporal dynamics between the fast and slow streamflow generation processes. A large value (large concavity) indicates that fast flow contributions cease quickly to the profit of slow flow contributions whereas a small value (small concavity) indicates a smooth change, if any, between fast flow contributions and slow flow contributions. This interpretation is linked to the temporal dynamics of the relative importance of different flow contributions, i.e. the temporal partitioning between fast and slow soil lateral drainage, vertical drainage and groundwater release rates.

To derive parameters τ and b that best characterize the average shape of a recession in a catchment, Equation E.5 is fitted to each recession event (see an example in Figure E.6). For each recession event i, a pair of values, τ_i and b_i, is obtained. The medians taken over all recession events are computed and used as hydrological signatures: (1) the recession time $S_{\mathrm{REC}.\tau}$ and (2) the recession concavity $S_{\mathrm{REC}.b}$.

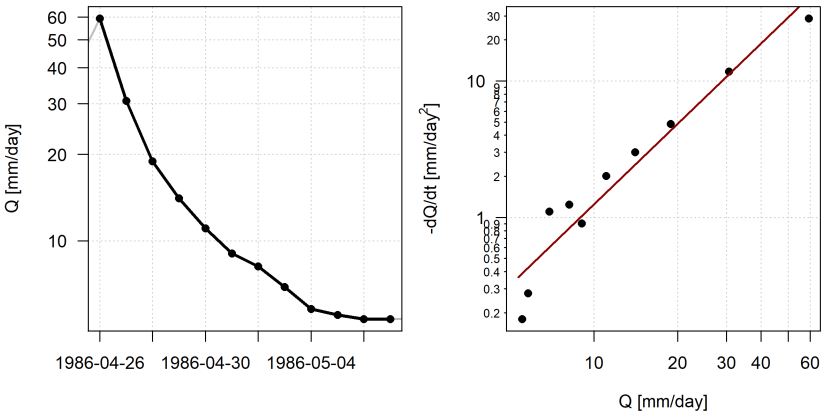

Figure E.6: Example of one recession fitted using Equation E.5 to extract the event recession parameters b and τ. Left: recession time series. Right: recession plot used to fit the recession; the red line is the obtained fit.

Figure E.7 shows the recession times, $S_{\mathrm{REC}.\tau}$, and recession concavity, $S_{\mathrm{REC}.b}$, obtained from the observed and simulated streamflow time series of the four study catchments. Figure E.7 shows simulated

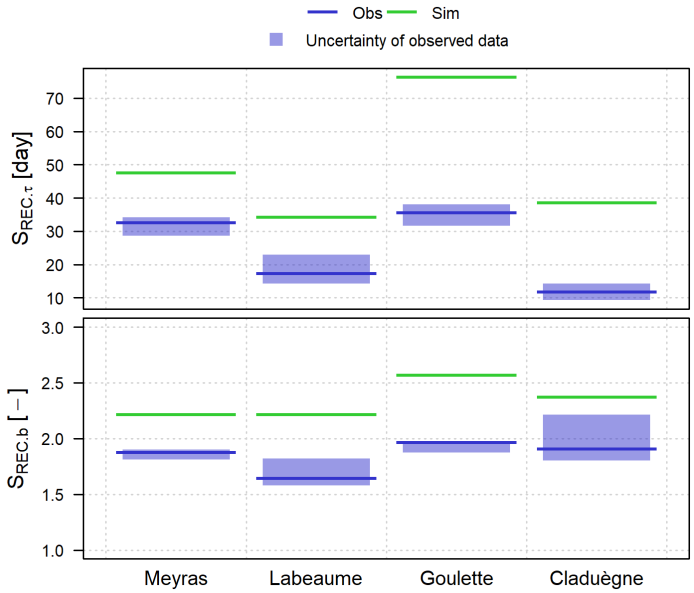

Figure E.7: Observed and simulated hydrological signatures $S_{\mathrm{REC}.\tau}$ and $S_{\mathrm{REC}.b}$ derived from the analysis of recessions. The results are shown for the four study catchments.

recession times and recession concavity are larger than observed ones. It shows that the globally slower recessions in simulated data identified in Figure 4.16 are captured. The larger concavity ($S_{\mathrm{REC}.b}$) in simulated data also reflects the stronger change of trend between the early and late parts of recessions identified in Figure 4.16.

The method used to compute $S_{\mathrm{REC}.\tau}$ and $S_{\mathrm{REC}.b}$ is based on all the individual recessions, i.e. the median of all τ_i and b_i (i = 1, 2, ..., n) estimated for the n recessions. Simple statistics of these n values of the parameter show that the variability of b_i is small: considering the b_i values estimated from observed recessions of Meyras, the median is 2.0, 50% of the values are between 1.5 and 2.9 and 90% of the values are found between 0.42 and 5.5. Although some values are outside of the expected range – between 1 and 3 – the low variability gives confidence into the ability of the extracted median to effectively describe the characteristic shape of the recession for a particular catchment.

On the other hand, the same statistics on τ_i show very large variability: considering the τ_i values estimated from observed recessions of Meyras, the median is 35 days, 50% of the values are found between 22 and 85 days and 90% of the values are found between 8.6 and 340 days. Even larger variability are found when considering simulated recessions. This is likely the consequence of the automatic procedure to extract recessions that sometimes result in almost flat recessions. These results suggest possible issues in the robustness and relevance of this hydrological signatures.

The recession time computed using Equation E.5, presented here, likely lack robustness as suggested by the very large inter recession event variability. Moreover, it is an overall recession time, i.e. it gives an indication how slowly/fast water stored in the catchment is released globally, considering both the early and late part of recessions which are arguably linked to different hydrological processes. Therefore, the approach described here to was not retained four our set of hydrological signatures.

E.2 Recession analysis: details on the storage-discharge power law model

At any given time t, the water mass balance equation at the catchment scale is:

$$\frac{\mathrm{d}S(t)}{\mathrm{d}t} = P(t) - E(t) - Q(t) \tag{E.6}$$

where $P(t)$, $E(t)$ and $Q(t)$ are the precipitation, evapotranspiration and streamflow at time t. $S(t)$ represents the catchment water storage at time t and hence, $\mathrm{d}S(t)/\mathrm{d}t$ is the variation of catchment water storage. In the case where the precipitation $P(t)$ and evapotranspiration $E(t)$ are small compared with streamflow $Q(t)$ ($P(t) << Q(t)$ and $E(t) << Q(t)$), Equation E.6 becomes:

$$\frac{\mathrm{d}S(t)}{\mathrm{d}t} = -Q(t) \tag{E.7}$$

The storage-streamflow relationship of the catchment (Equation E.7) is often investigated considering that the relation between catchment storage $S(t)$ and streamflow $Q(t)$ can be modeled using power-law model (Brutsaert and Nieber, 1977; Wittenberg and Sivapalan, 1999; Kirchner, 2009; Stoelzle et al., 2013; McMillan et al., 2017; Bart and Tague, 2017):

$$S(t) = cQ(t)^d \tag{E.8}$$

Note that if d is set to 1 in Equation E.8, it becomes a linear model:

$$S(t) = cQ(t) \tag{E.9}$$

Combining Equation E.7 and Equation E.8 yields:

$$\frac{\mathrm{d}Q(t)}{\mathrm{d}t} cdQ(t)^{d-2} = -Q(t) \iff -\mathrm{d}t = cdQ(t)^{d-2}\mathrm{d}Q(t) \tag{E.10}$$

Equation E.10 can be integrated between time 0 and t:

$$\int_0^t -\mathrm{d}t = \int_{Q(0)}^{Q(t)} cdQ(t)^{d-2}\mathrm{d}Q(t) \tag{E.11}$$

For $d \neq 1$, Equation E.11 Equation yields:

$$\begin{aligned} -t = \frac{cd}{d-1}Q(t)^{d-1} - Q(0)^{d-1} \quad &\iff \quad -\frac{d-1}{cd}tQ(0)^{1-d} = \left(\frac{Q(t)}{Q(0)}\right)^{d-1} - 1 \\ &\iff \quad Q(t) = Q(0)\left(1 + \frac{(1-d)Q(0)^{1-d}}{cd}t\right)^{1/(d-1)} \end{aligned} \tag{E.12}$$

Similarly, for $d = 1$, Equation E.11 yields:

$$-t = c\left(\ln(Q(t)) - \ln(Q(0))\right) \quad \iff \quad Q(t) = Q(0)\mathrm{e}^{-t/c} \tag{E.13}$$

Both solutions (Equations E.12 and E.13) can be combined to yield a general solution to Equation E.10:

$$Q(t) = \begin{cases} Q(0)\left(1 + \dfrac{(1-d)Q(0)^{1-d}}{cd}t\right)^{1/(d-1)} & \text{if} \quad d \neq 1 \\ Q(0)\mathrm{e}^{-t/c} & \text{if} \quad d = 1 \end{cases} \tag{E.14}$$

For convenience and consistency with the literature, Equation E.10 is reformatted in a simpler form:

$$-\frac{\mathrm{d}Q(t)}{\mathrm{d}t} = aQ(t)^b \tag{E.15}$$

with the following parameter transformations:

$$a = \frac{1}{cd} \tag{E.16}$$

$$b = 2 - d \tag{E.17}$$

Following this parameter transformation, Equation E.14 becomes:

$$Q(t) = \begin{cases} Q(0)\left(1 + a(b-1)Q(0)^{b-1}t\right)^{1/(b-1)} & \text{if} \quad b \neq 1 \\ \\ Q(0)\mathrm{e}^{-at} & \text{if} \quad b = 1 \end{cases} \tag{E.18}$$

Appendix F

Sensitivity analysis: preliminary and detailed results

F.1 Preliminary sensitivity analysis of the J2000 model

F.1.1 Sensitivity analysis setup

Following the SA methodology described in Section 5.2.1, considering 1000 rows in the two input matrices ($N = 1000$), 56000 model runs would be required. Although this number of model runs is manageable (although very long) given the computation time of the J2000 model (which greatly depends on the number of HRUs), a sub set of parameters was first selected.

Guided by the results of previous studies (e.g. Branger et al. (2016); Gouttevin et al. (2017)) and many trial-and-error SA experiments with the J2000 Meyras model (not detailed here), some of the parameters listed in Table 2.5 were not considered in the SA:

- The two parameters modulating the maximum interception storage capacity ($INT_{\max}$), a_{rain} and a_{snow} were not considered.
- Following the result of the sensitivity analysis done by Gouttevin et al. (2017) on the snow module of the J2000 model, most parameters related to snow processes were not considered. Snow is expected to have only little influence on the Ardèche catchment, but the following 3 snow related parameters were however kept in the analysis: the two temperatures controlling the partition between rainfall and snowfall, $T_{\text{snow},1}$ and $T_{\text{snow},2}$, and the temperature factor of the snow melt model, T_{f}.
- As detailed in Section 2.4.1.2, only the field capacity parameters θ_{FC} are considered to compute $MPS_{\max}$. Here, only the resulting value of $MPS_{\max}$ was considered as an input factor for the SA.
- The two parameters controlling the distribution and diffusion of water between the MPS and LPS reservoir, C_{DIST} and C_{DIFF}, were not considered as the way they are currently specified is part of how we want the model to behave (see Section 2.4.1.2).
- The parameter C_{ET} that modulates how plants are able to withdraw water from MPS for transpiration was also not considered.

As a result, 17 parameters were kept for the deployment of the SA including 9 distributed parameters (see Table 5.1).

In addition distributed parameters were handled in a specific strategy to limit the number of actual parameters to investigate in the SA. One possible strategy is to keep the spatial pattern of the distributed parameter and use a multiplier to perturb the parameters (e.g.(Yilmaz et al., 2008)). For a given distributed parameter F taking n_F different values depending on the type of HRU (i.e. land-use, soil or geology class), the latter strategy requires an additional lumped parameter, an adaptation factors F_{AF}, to modify F in the same way for all HRU types. The adaptation factor can affect F_i ($i = 1, 2, ..., n_F$) either through multiplication (as in Yilmaz et al. (2008)) or addition: $F_i \times F_{AF}$ or $F_i + F_{AF}$. Here, additive adaptation factors were used to perturb the distributed parameters. Additive adaptation factor keeps the magnitudes of the inter-class differences in F the same regardless of its value. This property is particularly important when these differences are large as a multiplicative adaptation factor (1) would induce much larger change when F_i is large than when it is small and (2) would require great care in the specification of their range of variation to have resulting distributed parameter value within realistic range for all the classes. Using additive adaptation factors overcome these issues and were thus chosen in our SA. The modules of the J2000 model were modified to include these additive adaptation factors.

The explored range of values for each parameters (or adaptation factor) were chosen to stay within realistic model behaviors. All parameters were sampled in uniform distribution $\mathcal{U}(a, b)$ as no information

could support any more precise distributions. The lower a and upper b specified for each parameter (and each adaptation factor) is reported in Table F.1.

Table F.1: Selected lumped and distributed parameters for the sensitivity analysis: (1) default values and range of variation of lumped parameters and (2) range of variation of the additive adaptation factors used for the distributed model

Name	Unit	Default	Range $\mathcal{U}(a,b)$	
			a	b
Lumped parameters				
$T_{\text{snow},1}$	°C	2	0	3
T_{f}	mm·°C^{-1}	1.84	0.5	4
$I_{\text{max,summer}}$	mm·day^{-1}	40	10	70
$I_{\text{max,winter}}$	mm·day^{-1}	50	10	90
$I_{\text{max,snow}}$	mm·day^{-1}	20	5	35
K_{LPSout}	–	5	1	5
K_{latvert}	–	1	0.5	2
P_{max}	mm·day^{-1}	20	2	30
Adaptation factors for distributed parameters				
LAI	–		-2	2
K_{crop}	–		-0.2	0.2
K_{sealing}	–		-0.15	0.35
MPS_{max}	mm		-20	30
LPS_{max}	mm		-80	80
τ_{RG}	day		-20	50
RG_{max}	mm		-200	200
K_{reach}	m$^{1/3}$·s^{-1}		-2	2
W_{reach}	m		-5	5

Note that large variations were specified for T_f given its influence on the J2000 Ardèche model is expected to be very limited. Small minimal values were specified for $I_{\text{max,summer}}$, $I_{\text{max,winter}}$, $I_{\text{max,snow}}$ and P_{max}. The range of variations of the reach parameter K_{reach} was kept small given the large effect it has on the model flow routing and that its default specification is supported by past hydraulic modeling studies (Section 2.4.1.2).

The range of variation for K_{LPSout} was kept between 1 and 5 to have realistic drainage behavior of the soil according to its saturation (see Figure 2.17). The parameter K_{latvert} controls the importance of the HRU slope in the computation of the proportion of lateral subsurface flow according to Equation 2.26 (see Figure 2.18). The range of variations for this parameter was specified in order to have proportion of lateral subsurface flow ranging betwen 0 and 100% according to the slope of the HRUs of the 4 sub-catchment models (maximum of about 30°).

The range of variation for parameter MPS_{max} was specified according to the largest (resp. smallest) maximum storage capacity of the MPS reservoir of 125 mm (resp. 25 mm). Similarly, the ranges of variation for parameters LPS_{max} and RG_{max} were specified according to the minimum and maximum values these parameter can take (see Tables 2.8 and 2.9). Similarly, for parameters LAI, K_{crop}, K_{sealing} and τ_{RG}, the maximum and minimum values these parameters can take were considered to specify their ranges of variation in the SA. However, particular care was also given so that the resulting parameter values remained within realistic ranges.

F.1.2 Results of the preliminary sensitivity analysis

This preliminary sensitivity analysis of the J2000 model, focused on the the 4 sub-models of the J2000 Ardèche model corresponding to the four study catchments Meyras, Pont-de-Labeaume, Goulette and Claduègne. The model output considered for the computation of first order and total order sensitivity indices, S_M and S_T, are the 16 following hydrological signatures: $S_{\text{FDC.slope}}$, $S_{\text{FDC.Q10}}$, $S_{\text{FDC.Q90}}$,

S_{RC}, S_{BFI}, $S_{\text{BFR.min}}$, $S_{\text{BFR.max}}$, $S_{\text{BFR.mag}}$, $S_{\text{REC.}b}$, $S_{\text{REC.}\tau}$, $S_{\text{REC.}\tau\text{early}}$, $S_{\text{REC.}\tau\text{late}}$, $S_{\text{PQ.dry}}$, $S_{\text{PQ.wet}}$, $S_{\text{PQ.strength}}$ and $S_{\text{PQ.date}}$. Note that the recession concavity $S_{\text{REC.}b}$ and recession time $S_{\text{REC.}\tau}$ are presented in Appendix E.1.3.3 and were not considered in the final sensitivity analysis. Similarly, results for $S_{\text{BFR.min}}$ and $S_{\text{BFR.max}}$ are presented here although only $S_{\text{BFR.mag}}$, computed from $S_{\text{BFR.min}}$ and $S_{\text{BFR.max}}$, was kept in the final sensitivity analysis.

Figure F.1 shows the first and total order sensitivity indices, S_M and S_T, of the 16 hydrological signatures, for the 4 study catchments. Overall, Figure F.1 shows that the results are consistent across the 4 investigated catchments. Only a few notable differences between catchments can be noted for some parameters and some hydrological signatures, showing that mostly the Claduègne catchment differs from the other 3 catchments. In particular, in the case of the Claduègne catchment, the sensitivity of (1) $S_{\text{FDC.Q10}}$ and $S_{\text{REC.}b}$ to parameter τ_{RG} and (2) $S_{\text{BFR.max}}$ and S_{BFI} to $I_{\text{max,winter}}$, are larger than for the other three catchments. Another well visible inter-catchment differences is the sensitivity indices of all the hydrological signatures that are sensitive to parameter K_{latvert} with large sensitivity indices for Meyras, medium for Pont-de-Labeaume, small for Goulette and null for Claduègne. This parameter controls the partitioning of water between lateral and vertical water drainage (i.e. subsurface flow or percolation) by giving more or less weight to the average slope of the HRU. These inter-catchment differences reflect the differences in steepness of the different catchments: Meyras is the steepest catchment whereas Claduègne is the less steep catchment.

Figure F.1 also shows that, for most parameters and most hydrological signatures, the sensitivities of the hydrological signatures to the model parameters are mostly caused by direct influence of the parameter with very only little interaction. Noteworthy exceptions are the hydrological signature $S_{\text{REC.}\tau}$ and $S_{\text{REC.}\tau\text{early}}$. To a lesser extent, the sensitivity indices of hydrological signatures $S_{\text{REC.}b}$, $S_{\text{PQ.wet}}$, $S_{\text{PQ.strength}}$ and $S_{\text{PQ.date}}$ also show significant interaction between model parameters. Note that more interaction leads to more uncertainty in the estimated total sensitivity indices. Large parameter interaction inevitably lead to difficulty in identifying how the model parameters affect the hydrological signatures. In addition, larger parameter interaction can be the sign of low robustness of the considered hydrological signature. Therefore, the more parameter interaction there is, the weaker the diagnostic power of the hydrological signatures is likely to be.

Figure F.1 shows that two of the J2000 model parameters are particularly influential: the maximum infiltration rate in Summer, $I_{\text{max,summer}}$, and the groundwater reservoir depletion time characteristics, τ_{RG}. Other model parameters can be identified as influential: the parameter controlling the partitioning of water between lateral (sub-surface flow) and vertical (percolation) drainage, K_{latvert}, the parameter controlling how fast/easy soils can drain, K_{LPSout}, the maximum soil infiltration rate in Winter, $I_{\text{max,winter}}$, the sealing of surfaces coefficient, K_{sealing} (although through only large interaction), and the crop coefficient, K_{crop}. On the other hand, other parameters are found to have no or insignificant effect for all catchment and all hydrological signatures. This is the case of the leaf area index, LAI, which controls the volume of water that can be intercepted by the vegetation canopy, the size of the MPS reservoir, MPS_{max}, where the water available for plant transpiration is stored as well as the two reach water routing parameters, the roughness, K_{reach}, and width, W_{reach}.

F.1.3 Relevance of preliminary sensitivity analysis

Some of the results of the sensitivity analysis can also be attributed to the way the sensitivity analysis was set up (see Section F.1.1). In particular, the explored parameter space was probably not relevant for some of the parameters. For example, the range of variation specified for $I_{\text{max,summer}}$, between 10 mm/day and 70 mm/day, might include values that are too low to be realistic and induced too large effect on the model behavior. As a consequence, the large sensitivity indices obtained for many hydrological signatures might prevent the identification of other key parameters. Irrelevant parameter range might also explain why some parameters are found to have no influence. This is the case, for

instance, of the very low influence of $P_{\max}$ or of the maximum storage capacities, $MPS_{\max}$ and $RG_{\max}$.

Influence of $P_{\max}$

The very low sensitivity to parameter $P_{\max}$ for all catchments and all hydrological signatures is a consequence of the range of explored values – between 2 mm/day and 30 mm/day (see Table 5.1) – which, given the actual percolation rates, is too high to affect model behavior. This is confirmed by the internal flux variable of the J2000 model: for Meyras, in the default simulation (with $P_{\max}$ = 20 mm/day) 95% (resp. 75%) of the daily percolation rates are below 7.5 mm/day (resp. 1.2 mm/day). Even lower values are obtained in the case of Claduègne. As a consequence, $P_{\max}$ influence model behavior only if specified at a low value (e.g. below about 7.5 mm/day for Meyras).

Influence of $MPS_{\max}$

The lack of effect of $MPS_{\max}$ is due to how the water infiltrating into the soils is partitioned between the MPS and LPS reservoirs (see Subsection 5.3.2.1): soil drainage, from LPS, happens before water is eventually "diffused" to fill the MPS reservoir (with only the size of MPS and the content of LPS limiting the transfer). Investigation of the saturation state variation of the MPS reservoir (results not shown) shows that the MPS reservoir storage capacity is limiting evapotranspiration during the dry months. Therefore, it is unexpected that the the MPS reservoir has so little effect on the hydrological signatures. This might be a consequence of the range of variation specified in the sensitivity analysis as the adaptation factor was set to range between -20 mm and +30 mm which might have affected only the shallower soils.

Influence of $RG_{\max}$

The adaptation factor of $RG_{\max}$ ranges between ±200 mm (Table 5.1) but only in the case of the volcanic rock class (default value of 200 mm) was this range large enough to affect model behavior; for the other dominant geology classes of the study catchments, the default values of $RG_{\max}$ were around 400 mm and 500 mm. As a consequence for the most represented geology classes, the adaptation factor was possibly not large enough to affect model behavior. This clearly questions the relevance of the use of additive adaptation factors rather than multiplicative adaptation factors or the use of adaptation factors altogether.

In the case of $RG_{\max}$, exploring much lower values would have affected model behavior in terms of groundwater release and lateral soil drainage. Given the default parameter values for $RG_{\max}$ (aggregated at the catchment scale in Table 2.10), the groundwater reservoir is never filled: 95% of the time, the RG reservoir is filled at about 38% in the case of Meyras, Pont-de-Labeaume and Goulette and 23% in the case of Claduègne. Much lower $RG_{\max}$ value, e.g. if the current default values are to be 5 times lower, would imply that lateral soil drainage is generated because of a "saturated" RG reservoir. Moreover, such a model behavior is meaningful: it can represent the rise of the deep water table above the bedrock within in the soils where, for example, the combination of preferential flow path ways connections and high hydraulic pressure induce a rise in lateral soil drainage.

F.1.4 Conclusion

These results indicate that the use of additive adaptation factors are inappropriate to investigate the effect of distributed parameters. Given the default values and the large inter-class differences in these values, additive factors could not be specified appropriately for the parameter to have any significant

effect. Such issues probably explain the small sensitivity indices obtained for $RG_{\max}$, $MPS_{\max}$ and $LPS_{\max}$ parameters.

The very large effect of $I_{\max,\text{summer}}$ on most hydrological signatures highlight the importance of the range of variation specified in the sensitivity analysis. This large effect was caused by the very low values specified in the range of $I_{\max,\text{summer}}$ which were clearly unrealistic for the study catchments.

Finally, some parameters considered here in the sensitivity analysis have no or little influence and could therefore be discarded thus reducing computational cost. This is the case of the two reach parameters K_{reach} and W_{reach}, the three snow parameters $T_{\text{snow},1}$, T_{f} and $I_{\max,\text{snow}}$ as well as the interception parameters LAI.

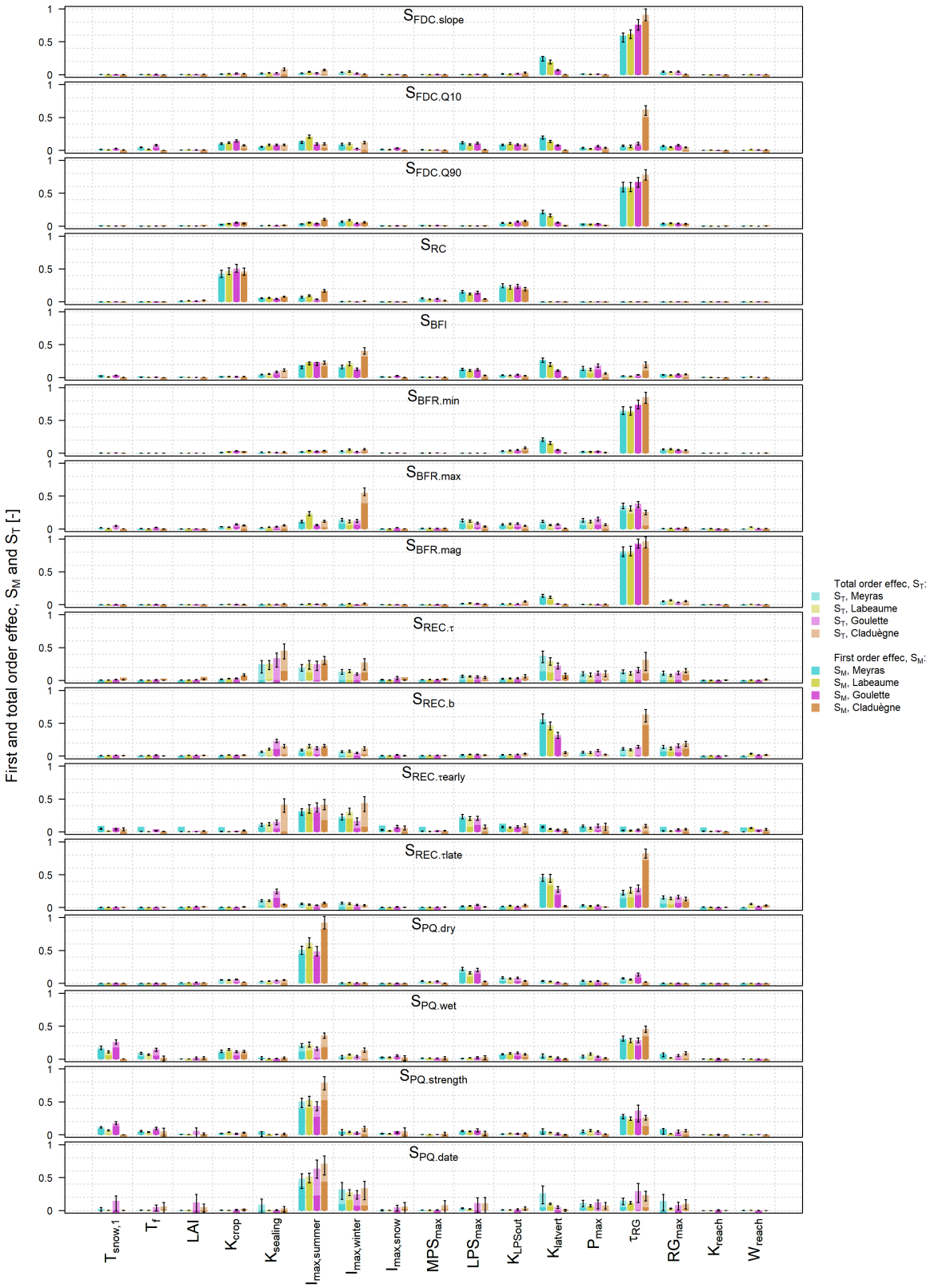

Figure F.1: First and total order sensitivity analysis of the J2000 model parameters for the four study catchments and each hydrological signatures (rows).

F.2 Additional results of the sensitivity analysis of J2000

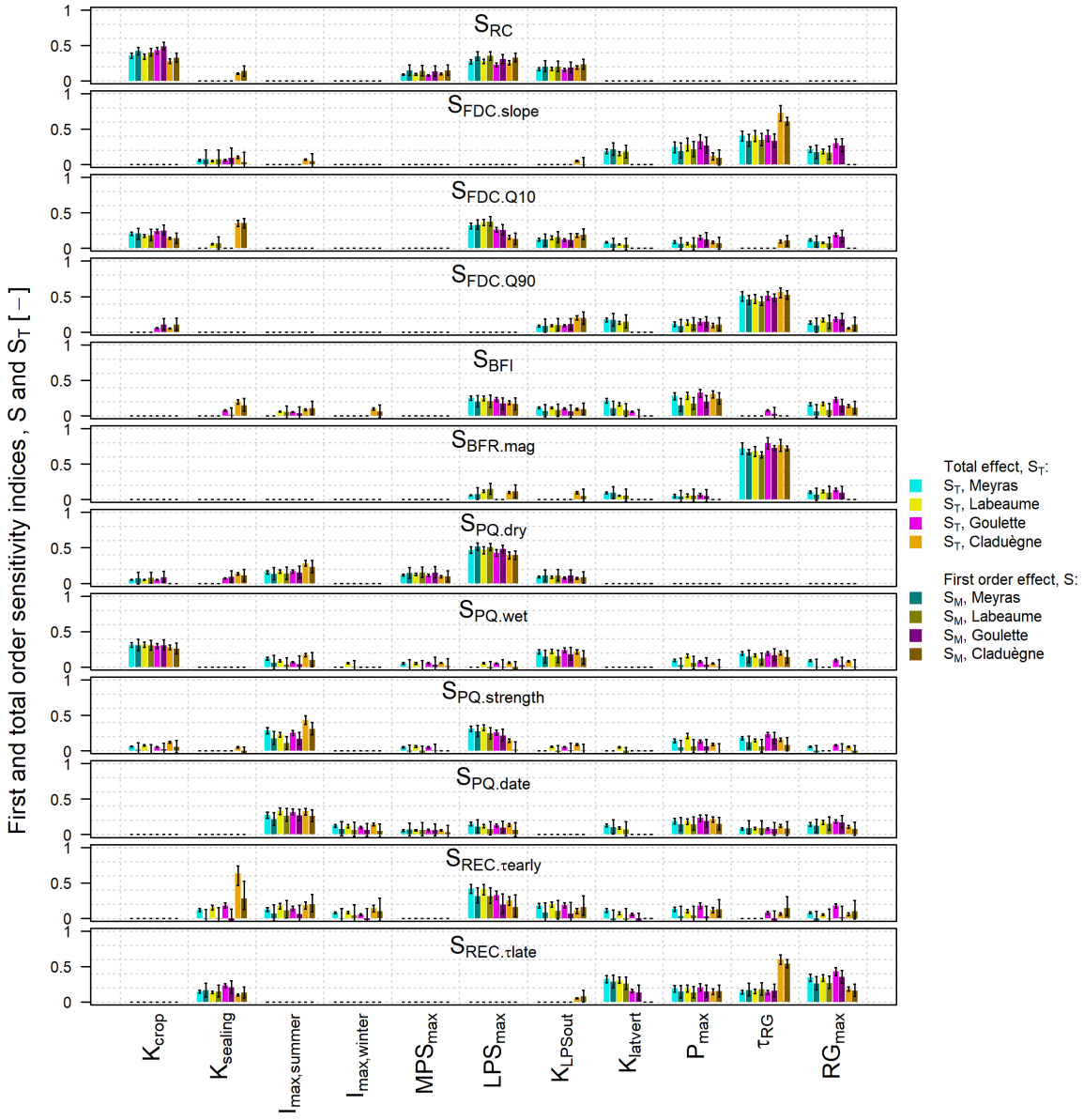

Figure F.2: First and total order sensitivity indices of the J2000 model parameters for the four study catchments and each hydrological signature (rows). Indices indicated a significant effect when above 0.05.

Figure F.2 shows the first and total order sensitivity indices and their associated uncertainties for the four study catchment, the 12 hydrological signatures and the 11 model parameters investigated in the sensitivity analysis. The first order sensitivity indices S_i should be smaller than the total order sensitivity indices S_{Ti}: $S_i \leq S_{Ti}$. The large uncertainties affecting the estimated indices, particularly the first order sensitivity indices, results in some cases to the first order sensitivity indices being larger that the total order sensitivity indices (however, with an overlap of the uncertainty bounds). Therefore, in the main document (Figure 5.8), we chose to show only the lower boundary of the uncertainty of the first order indices to increase the readability of the results.

The consequence of this choice is that, when interpreting the differences between the first and total order sensitivity indices (in Figure 5.8), we have an idea of the maximum interactions: the larger the difference between S_{Ti} and S_i, the larger the maximum interaction. Note that this choice does not affect the analysis or the conclusions.

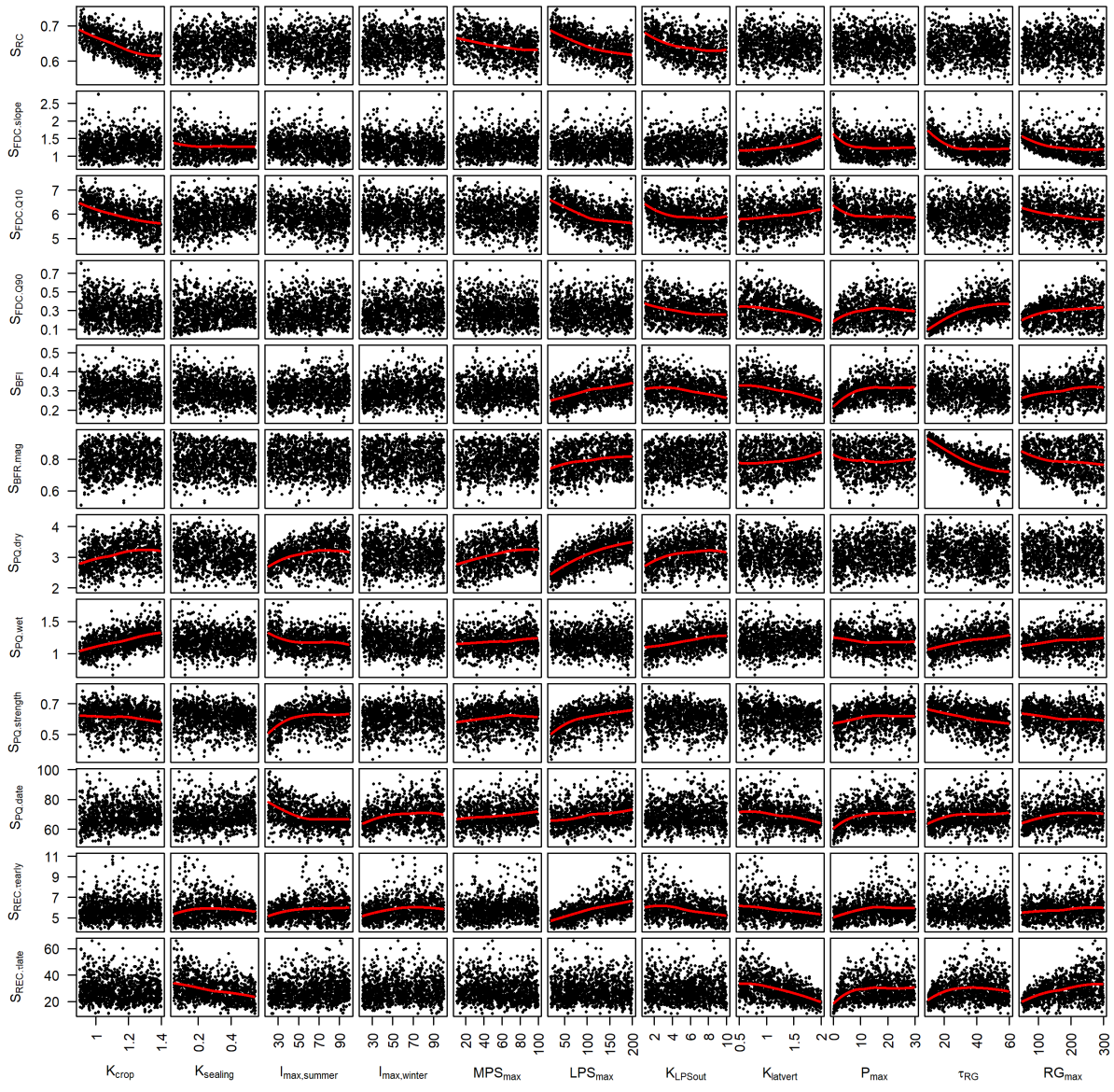

Figure F.3: Scatter plots of the hydrological signatures (y-axis) values versus J2000 model parameter values (x-axis) of a random sub-sample of 500 model runs of the sensitivity analysis experiments of the Meyras catchment. Red lines, shown only when the total effect is above 0.05, are the results of locale polynomial fits providing an estimate of the average parameter-signature relationship.

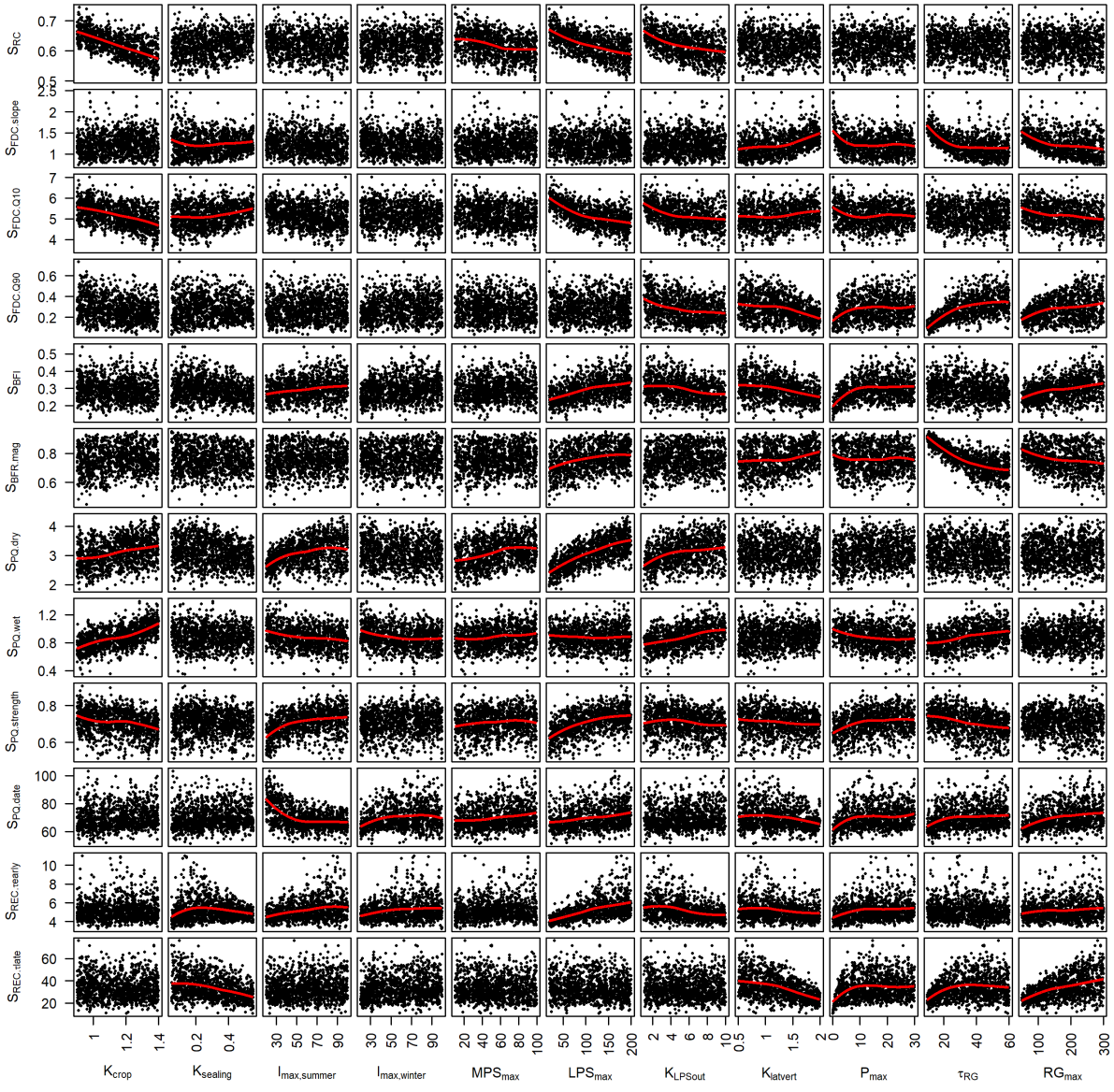

Figure F.4: Scatter plots of the hydrological signatures (y-axis) values versus J2000 model parameter values (x-axis) of a random sub-sample of 500 model runs of the sensitivity analysis experiments of the Pont-de-Labeaume catchment. Red lines, shown only when the total effect is above 0.05, are the results of locale polynomial fits providing an estimate of the average parameter-signature relationship..

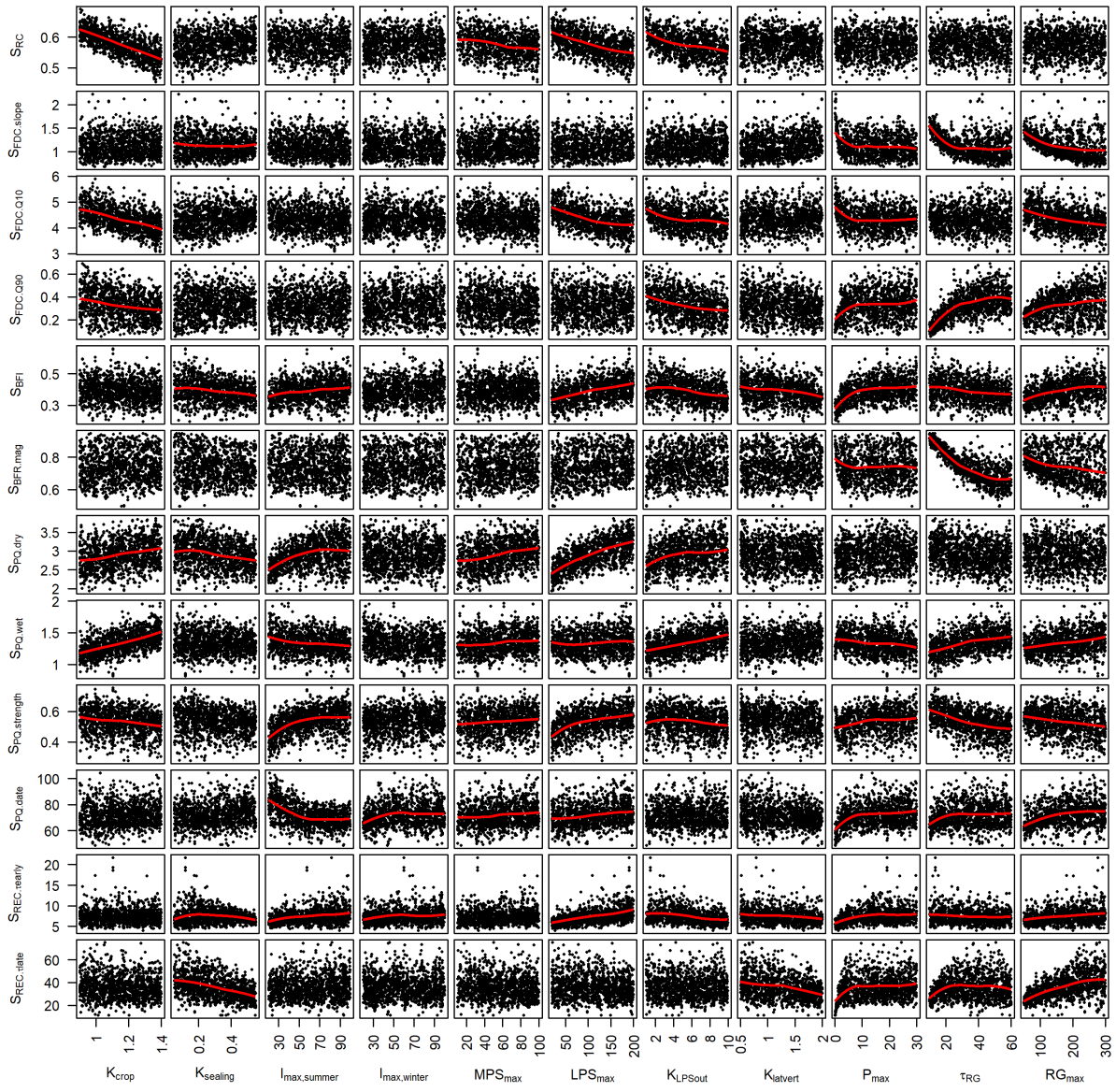

Figure F.5: Scatter plots of the hydrological signatures (y-axis) values versus J2000 model parameter values (x-axis) of a random sub-sample of 500 model runs of the sensitivity analysis experiments of the Goulette catchment. Red lines, shown only when the total effect is above 0.05, are the results of locale polynomial fits providing an estimate of the average parameter-signature relationship..

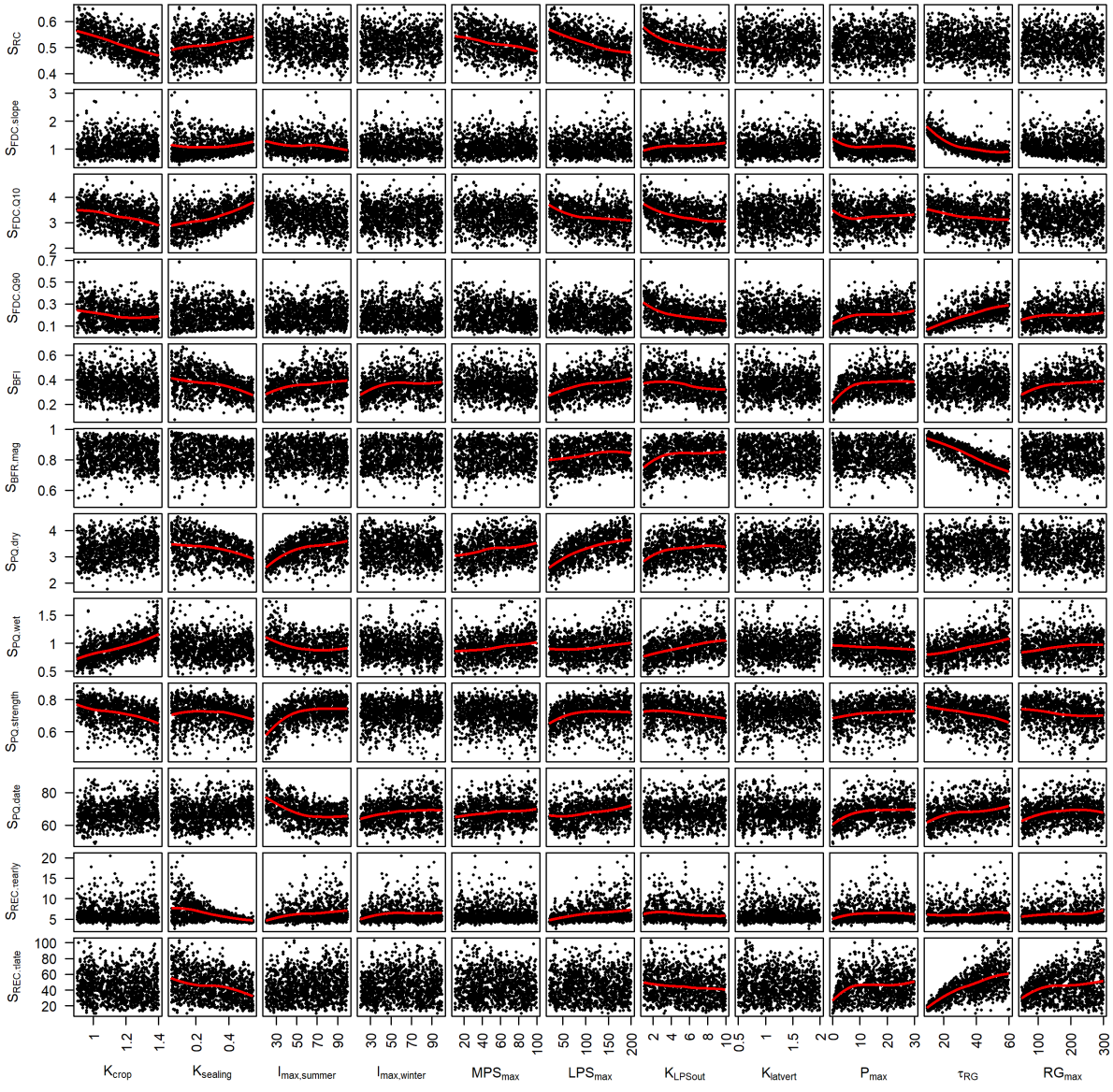

Figure F.6: Scatter plots of the hydrological signatures (y-axis) values versus J2000 model parameter values (x-axis) of a random sub-sample of 500 model runs of the sensitivity analysis experiments of the Claduègne catchment. Red lines, shown only when the total effect is above 0.05, are the results of locale polynomial fits providing an estimate of the average parameter-signature relationship..

Design and evaluation of hydrological signatures for the diagnosis and improvement of a process-based distributed hydrological model

Abstract

The evaluation of hydrological models is typically based on comparisons of observed and simulated streamflow time series using performance metrics such as the Nash-Sutcliffe Efficiency. Although it provides relevant measures of the predictive performance of a model, this type of approach provides very little information on the reasons behind good or bad performance. Instead, Gupta et al. (2008) proposed to use hydrological signatures which are indicators that characterize catchment behaviors. Because they can be related to hydrological processes, using them when comparing observation with simulation enable the evaluation of the model while offering diagnostics, i.e. indications on the hydrological processes that are well or badly represented in the model.

In this PhD thesis, we focus on the interpretations and diagnostic power of hydrological signatures and how they can be used to guide the improvement of a distributed model. We present the building of a set of hydrological signatures, using only widely available data – precipitation, streamflow and air temperature – to characterize the hydrological functioning of 4 Ardèche sub-catchments (South East of France) and 10 snow dominated catchments of the Southern Sierra mountains (California, USA). Already existing and new hydrological signatures are selected and/or designed. Collectively, they can characterize catchment behavior in a wide variety of hydro-climatic contexts. We demonstrate the value of additional snow measurements to evaluate the information content of snow dedicated hydrological signatures. In the context of the Ardèche catchment, we set up the J2000 distributed model and use a sensitivity analysis to understand how the hydrological signatures are linked to the model parameters. This provides insights into how they are to be interpreted in the context of the J2000 Ardèche model and allows the assessment of their diagnostic power. Finally, combining the results of the sensitivity analysis with comparisons between observed and simulated hydrological signatures, we undertake an in-depth diagnostic of the model to provide and test recommendations for its improvement. Deficiencies of the model functioning are identified, mainly related to soil and groundwater storage and fluxes, highlighting issues in the spatial representation of soil and geological properties.

Construction et évaluation de signatures hydrologiques pour le diagnostic et l'amélioration d'un modèle hydrologique distribué

Résumé

L'évaluation des modèles hydrologiques est généralement basée sur des comparaisons des séries de débit observées et simulées à l'aide de critères de performance tels que l'efficience de Nash-Sutcliffe. Bien que cette approche fournisse des mesures pertinentes de la performance prédictive d'un modèle, elle ne fournit que très peu d'informations sur les raisons d'une bonne ou d'une mauvaise performance. Gupta et al. (2008) ont proposé d'utiliser plutôt des signatures hydrologiques, des indicateurs qui caractérisent le comportement d'un bassin versant. Les signatures hydrologiques pouvant être liées aux processus hydrologiques, la comparaison des signatures hydrologiques observées et simulées permet l'évaluation du modèle tout en offrant des diagnostics, i.e. des indications sur les processus hydrologiques qui y sont bien ou mal représentés.

Dans cette thèse de doctorat, nous nous concentrons sur l'interprétation et le pouvoir diagnostique des signatures hydrologiques et comment celles-ci peuvent être utilisées pour guider l'amélioration d'un modèle distribué. Nous présentons la construction d'un jeu de signatures hydrologiques, utilisant uniquement des données largement disponibles – précipitations, débit et température de l'air – pour caractériser le fonctionnement hydrologique de 4 sous-bassins versants de l'Ardèche (Sud-Est de la France) et 10 bassins versants de montagne à influence nivale (Southern Sierra, Californie, États-Unis). Des signatures hydrologiques existantes et des nouvelles sont sélectionnées et/ou développées. Conjointement, elles permettent de caractériser le comportement de bassins versants dans une grande variété de contextes hydro-climatiques. Des mesures de neige supplémentaires sont utilisées afin d'évaluer la pertinence des signatures hydrologiques dédiées aux processus nivaux. Par ailleurs, le modèle distribué J2000 est déployé sur le bassin versant de l'Ardèche et une analyse de sensibilité est réalisée afin de comprendre comment les signatures hydrologiques sont liées aux paramètres du modèle. Cela nous permet de déterminer la façon dont elles doivent être interprétées dans le contexte du modèle J2000 de l'Ardèche et permet l'évaluation de leur pouvoir diagnostique. Enfin, en combinant les résultats de l'analyse de sensibilité avec des comparaisons entre signatures observées et simulées, nous entreprenons un diagnostic approfondi du modèle afin de dériver et tester des recommandations pour son amélioration. Nous identifions des déficiences du modèle, principalement liées au flux et stockage de l'eau souterraine et des sols, mettant en évidence des problèmes de représentation spatiale des propriétés géologiques et pédologiques.